INSTITUT FÜR KONSTRUKTIVEN INGENIEURBAU

LEHRSTUHL FÜR TUNNELBAU, LEITUNGSBAU UND BAUBETRIEB

PROF. DR.-ING. M. THEWES

Doctoral Thesis

RHEOLOGICAL CHARACTERISATION OF EARTH-PRESSURE-BALANCE (EPB) SUPPORT MEDIUM COMPOSED OF NON-COHESIVE SOILS AND FOAM

submitted in fulfilment of the requirements for the degree of Doctor of Engineering (Dr.-Ing.) to the Department of Civil and Environmental Engineering of the Ruhr-Universität Bochum

BY

DIPL.-ING. MARIO GALLI

SFB 837
**Interaction Modeling
Mechanized Tunneling**

**RUB
RESEARCH SCHOOL**

Doctoral Thesis

Rheological Characterisation of Earth-Pressure-Balance (EPB) Support Medium composed of non-cohesive Soils and Foam

submitted in fulfilment of the requirements for the degree of Doctor of Engineering (Dr.-Ing.) to the Department of Civil and Environmental Engineering of the Ruhr-Universität Bochum

BY

Dipl.-Ing. Mario Galli

Reviewers:

Prof. Dr.-Ing. Markus Thewes

Institute for Tunnelling and Construction Management, Ruhr-Universität Bochum (Germany)

Prof. Ing. Daniele Peila

Department of Environment, Land and Infrastructure Engineering, Politecnico di Torino (Italy)

Prof. Dr.-Ing. habil. Holger Steeb

Institute of Applied Mechanics, Chair of Continuum Mechanics, Universität Stuttgart (Germany)

Date of submission: 18 January 2016

Date of oral examination: 20 June 2016

PREFACE

The present study was developed and executed in my time as research assistant at the Institute for Tunnelling and Construction Management ("TLB") of the Ruhr-Universität Bochum between 2010 and 2016 under guidance of Prof. Dr.-Ing. Markus Thewes.

Prof. Dr.-Ing. Markus Thewes supported me incessantly over the last years. He gave me the feeling of trustworthiness at all times and he had confidence in me and my skills even in times of trouble. I will not be able to make up for this act of faith except by carrying the spirit of "TLB" into the world. Thank you for the very instructive times and the many unique opportunities regarding my personal as well as my professional development.

Additionally, I explicitly recognise Prof. Ing. Daniele Peila and Prof. Dr.-Ing. Holger Steeb for their deep interest in my work, the countless fruitful and informative discussions, and their active participation in my examination.

Furthermore, I have to thank my colleagues at the Institute for Tunnelling and Construction Management for outstanding five and a half years. We have been family for one another. Open arms, a cheerful and still productive working environment, internationality, being there for each other, sharing good times and bad, room for constructive discussions, and the insatiability for anything eatable were significant imprints of our community. Keep on this exceptional attitude as you move through life.

The same applies for the comrades of the Collaborative Research Center 837 and in particular for my subproject partner, Aycan Özarmut. Bundling so many different cultural and scientific backgrounds was a great challenge but we established our own little scientific community. In this destined formation, we probably will never come together again. However, I wish you all the best for your various careers.

Experimental work is a big challenge; it can probably never be mastered without a helping hand. The team of the Structural Testing Laboratory of the Ruhr-Universität Bochum was always there, when assistance was needed. Thereof, Yvonne Ueberholz and Dieter Abraham have to be pointed out. All your patience with me and your continuous support is particularly appreciated.

Additionally, the work of numerous students and the support of the student assistants has to be recognised here, too. Especially, I would like to bow to my "EPB crew" consisting of Christopher, Sascha, Karin, Gerrit and Timon. We formed a great team and became dear friends over the years. I would not have come so far without you.

A big thank you goes also to Ingenieurbüro Dipl.-Ing. H. Vössing and the ARGE BOL/BÜ Albaufstieg, who enabled me live experience and active participation in mega tunnelling whilst having all the freedoms to finish this thesis.

Besides the professional environment, there is a private life. Without the continuous encouraging and empathic backing from my girlfriend, Katharina, and my beloved family and friends, I could not have brought up the power of endurance, which is necessary to conquer the doctoral quest. This work is dedicated to you. I owe you – especially time!

Ruhr-Universität Bochum, January 2016   Mario Galli

ACKNOWLEDGEMENTS

ABSTRACT

The flow behaviour of soil-foam mixtures, used as support medium in closed mode tunnelling with EPB shields, is an essential factor for the operation of the TBM. On the one hand, a rather soft consistency is required providing a homogeneous face support pressure transfer to the tunnel face. High accuracy in face support regulation is crucial for settlement control, especially in sensitive environments, such as urban areas. On the other hand, a rather stiff consistency is preferable concerning transportation and disposal of the excavated ground in order to avoid additional treatments for landfilling, tipping or sewage management. Outside the classical application range for EPB shields, which is formed by clayey and silty soils, the addition of conditioning agents is necessary to generate appropriate consistencies, particularly in cohesionless soils below the groundwater table. In such ground conditions, foam is injected to the excavated ground to generate a face-supporting muck and to control water inflows at the tunnel face.

So far, the flow behaviour of soil-foam mixtures has been investigated by index tests. Most notably, the slump test, known from concrete technology, is widely applied on soil-foam mixtures. However, flow is actually a non-static phenomenon and cannot be expressed by a single parameter, which is derived from an equilibrium-state condition at rest. Therefore, this thesis focuses on the rheology of soil-foam mixtures aiming at an extended understanding of the flow behaviour and of the influences the individual components have on it. An experimental programme was elaborated, which dealt with two main scopes: a discussion on the slump test and its value as index test for the flow behaviour of soil-foam mixtures and secondly, the application of rheometer tests to soil-foam mixtures. The method in sample preparation, test conduction and temporal restraints were strictly defined for all tests, ensuring reproducibility and comparability. The initial water content was derived from foam penetration tests depending on the residual (foam-)water content that occurs during excavation.

A large number of slump tests was executed providing information on the slump and spread of the mixture samples when altering the different shares of the sample composition (soil, water, foam). These were evaluated with analytical approaches enabling a derivation of rheological properties from slump tests. The application of the analytical models is dependent on the geometry of the slumped sample. For an application to soil-foam mixtures, the models had to be partially adjusted. The value of the slump test and the applicability of the models to soil-foam mixtures were discussed based on the results.

Rheological tests on various scales were performed with a variety of soil-water-foam mixtures in order to determine flow curves and thus to characterise their flow pattern. Rheometers were equipped with cylinder and ball measuring systems. The findings have been compared with flow curve data from literature determined in micro-scale investigations on particle-foam mixtures. Due to their grain-size, real soil-foam mixtures cannot be investigated in such precise rheological setups. From this multi-scale analysis, it can clearly be shown that the flow behaviour of soil-foam mixtures is very dependent on the particular shearing condition. Each scale provides its own informative value on rheology. On the micro-scale, flow curves of particle-foams could be well described by the Papanastasiou-Herschel-Bulkley model, whereas in macro-scale experiments using a ball measuring system, the results were dominated by yield-stresses, slip effects and the destructive behaviour of foams. Nonetheless, the material possesses a particular behaviour and differences in results from different mixture compositions could be detected. Finally, the findings from slump and ball rheometer tests have been compared to establish a comparable basis between both approaches. Thus, it becomes possible to relate the results of both experiments to each other.

This thesis provides information on the interaction between soil, water and foam during the excavation process in EPB tunnelling. Therefrom, optimisation strategies can be derived in order to design the soil conditioning process with foam more effectively. Moreover, suggestions are presented for an implementation of the ball measuring equipment in the excavation chamber of an EPB-TBM for live analysis of the flow behaviour and the conditioning process.

INDEX

1. INTRODUCTION

1.1 Motivation

Increasing population and economical centralisation in industrialised countries make modern cities become high-density areas, which demands for an optimum in infrastructure. Such a vast agglomeration of people and goods necessitates a transport system not just for passenger and freight conveyance but also of their by-products, which is especially waste and sewage. However, space is limited, which is why today's transport infrastructure is preferably brought subsurface. Tunnels are the most common subsurface infrastructure system offering high flexibility in design and usability. They are used for railway or metro, roads, wastewater, communication, gas and oil.

Due to the unique boundary conditions, subsurface constructions in city areas represent one of the most challenging engineering disciplines. Narrow space, maintenance of traffic flow and the limitation of damnification (e.g. noise, pollution) are just some constraints increasing the project complexity. Of highest priority is the safety of aboveground edifices and humans. Depending on the ground, tunnelling under such restrictions is conducted using full-face excavation machines, so called tunnel boring machines. Regarding surface settlements, the stabilisation of the tunnel face and the tunnel lining are thereby two key factors of the advance influencing ground and surface settlements. Furthermore, these factors distinguish the classification of tunnel boring machines.

The most frequently applied tunnel boring machine in soft soil is the EPB type shield machine. It uses the excavated ground to support the tunnel face and thus to reduce the risk of ground movements and surface settlements. The properties of the supporting medium, which is the excavated ground plus possible additives, are of decisive influence for the advance process and face stability. Since the excavation chamber of those machines is pressurised, a direct evaluation of the essential

characteristics of the support material is not possible while advancing. This is why an interpretation of machine data and testing of the constructing ground is so important to gain information for an effective supporting process. The flow behaviour of the support medium and the permeability ahead of the machine plays thereby an important role.

1.2 Problem statement

The processes going on before, at and behind the face during tunnelling in closed mode are a black box. Not only that geotechnical and hydro-mechanical properties of the construction ground are often not sufficiently described, but the adequacy as support medium of the tunnel face is a priori unrateable. In fact, the machine and ground interaction is the determinant for the whole tunnelling process and particularly for face stability.

In EPB tunnelling, the support medium needs to exhibit specific properties in order to assure face stability. The main factors according to literature and tunnelling practice are the flow behaviour (or consistency) of the support material, its hydraulic conductivity and its compressibility. The interplay with the ground ahead of the machine has also to be regarded. If the support medium in its original condition cannot comply with the demands for effective face support, it needs to be treated with additives to fulfil at least temporarily the requirements. This improvement procedure is called soil conditioning.

Up to now, various researchers in the past 30 years worked on the topic of face support in EPB tunnelling, especially on the application in coarse grounds, which is linked to the matter of soil conditioning. It has become recent practice to use mainly foams as a treater of soil. The addition of foam to soil reduces surface tensions of the grains and thusly decreases inner friction (shear strength) and clogging potential (cohesive soils). Furthermore, the foam – regarded as fluid – awards the soil a flowing behaviour, when a certain amount is injected that suspends the grain-to-grain contacts. Consisting of air, the soil is then converted into a compressible, granular flowing medium. This character can be considered as a complex material behaviour. So far, research was not able to suggest holistic approaches for the qualitative and quantitative description of this material behaviour, but a lot of effort has been put

into testing in order to make an evaluation of the several material properties possible. Works have been conducted on the hydraulic conductivity, the shear strength, the abrasiveness under the consideration of soil conditioning, the compression behaviour and in particular the workability and flow behaviour. Approaches have been made in laboratory studies and numerically. Most of these properties can only be evaluated indirectly by index tests, since no criteria has been defined, yet, or else no standard tests exist. Moreover, the simulation of real boundary conditions is difficult; this includes natural stress-strain and ambient pressure conditions at the tunnel face, the influence of the machine and the realistic conditioning behaviour, which requests for approaches in constitutive modelling.

1.3 Approach

In this study, the processes at the tunnel face in cohesionless soils under the groundwater table shall be analysed in detail. The focus here is on the flow behaviour of the support material in the excavation chamber during tunnelling with EPB shields. Therefore, a literature review is conducted in order to sort and filter the state-of-the-art in EPB research and tunnelling techniques. After that, the current practice in testing and considering soil conditioning with respect to face stability is summarised and evaluated. Based on the basic principles in rheology, flow models, test methods and approaches on granular fluid rheology are presented from various disciplines to demonstrate the complexity in assessing the flow behaviour of such materials experimentally. This review leads to a definition of the own research scope. Aspects like the initial / residual water content and procedural influences of testing (e.g. reproducibility, time-dependency) are narrowed by a sharp description of the experimental approach. The flow behaviour of soil-foam mixtures is then assessed from two sides. Firstly, the slump test, which is commonly used for an evaluation of the workability of soil-foam mixtures, is analysed regarding its value and possible additional information it may possess. Thereafter, the scientific focus is detoured from index testing to fundamental rheology. Two test methods (concentric cylinder rheometry and sphere flow rheology) will be adopted for conditioned soils in order to find a suitable flow description for realistic soil-water-foam proportions, which incorporates basic ground and conditioning parameters. The significance of noth assessments, index tests and rheometry, shall provide new information for the tunnelling practice.

In addition to the rheological investigations, the development of pore water during excavation is dealt with in an excursus chapter. Therein, the residual water content of the excavated ground is assessed by foam penetration tests. A detailed analysis of these tests discusses the expulsion rate of water from the soil skeleton as well as the residual amount of void water within the foam-penetrated zone. Thus, a bandwidth of soil-specific water contents entering the excavation chamber can be determined in dependence of operational parameters (e.g. advance speed, face pressure).

All findings shall lead to new perspectives on the ground-machine interaction under consideration of the soil conditioning process enabling potentials for improved EPB tunnelling.

2. SOIL CONDITIONING IN EPB TUNNELLING

According to the "Recommendations for selecting and evaluating tunnel boring machines" of the German Tunnelling Committee (DAUB e.V.) full face excavation machines in tunnelling can be differentiated into (shielded) tunnel boring machines (TBM, TBM-S), which are applied in rock conditions, and shield machines (SM) that are mainly used in soft ground, see DAUB & ITA-AITES (2010). Thereof, shield machines with fluid support (hydro-shield, SM-V4) and with earth pressure balance support (EPB shield, SM-V5) of the face represent the most frequently applied types of soft ground tunnelling machines. The differentiation is visualised in Figure 2-1.
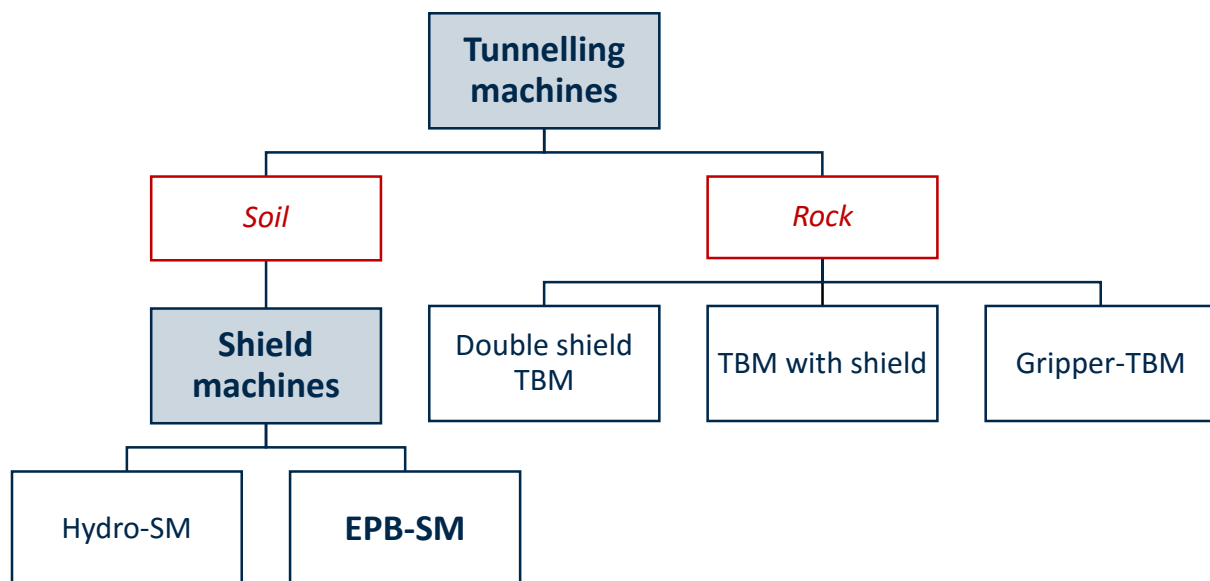
Figure 2-1:   **Simplified differentiation of tunnelling machines related to their prevalent ground of application according to DAUB & ITA-AITES (2010)**

Hydro shields are mostly applied in sandy and gravely grounds. Face support is normally achieved using bentonite slurry as support medium. EPB machines, on the other side, operate usually in cohesive soils. The excavated ground itself serves as support medium. Due to cost-intensive and time-consuming recycling processes in

order to separate and reuse the support medium in hydro shield tunnelling, the application of EPB shield is steadily extended into coarse-grained soils. However, the support medium has to comply with the demands regarding workability, permeability and compressibility so that an extension of the application range into less cohesive soils is linked to several boundary conditions.

This study focuses on EPB tunnelling and its extended application range. Design, functioning and application demands of EPB shields are presented subsequently.

2.1   Design and operation of EPB shields

EPB machines consist of a cutting wheel (1), which the cutting tools are assembled on, an excavation chamber (2), where the ground falls into after excavation and the face support pressure is generated, a screw conveyor (5) for spoil extraction from the excavation chamber and pressure control, thrust jacks (4) pushing the machine head forward and thusly penetrating the cutting tools into the ground, and an erector (6), which is used for positioning the segmental lining (7). The excavation chamber, which usually is under pressure due to face stabilisation, is separated from the atmospheric part behind the machine by the bulkhead (3). The machine is coated by a shield awarding the machine its name. An assembly of a typical EPB shield design is shown in Figure 2-2.

Depending on the tunnelling and ground situations, it might be necessary to stabilise the face area in front of the machine. The excavated ground itself is used as support medium to counter the impulse of ground movement into the tunnel, if the inherent stability of the ground is too low. From the operational view of the machine, three scenarios of face handling are defined: closed mode, open mode and semi-closed mode.

When the tunnel face is stable enough and does not demand for any face support, the machine is run in open mode. This is the case in highly cohesive and poorly permeable grounds with solid consistency ($I_C > 1$) (MAIDL ET AL. (2012)) or in stable (sedimentary) rock conditions. Open mode operation means that the excavation chamber is empty during advance. In fact, the excavated ground falls through the cutting wheel openings into the chamber, but the screw conveyor removes it from there immediately. The filling level is negligibly small.
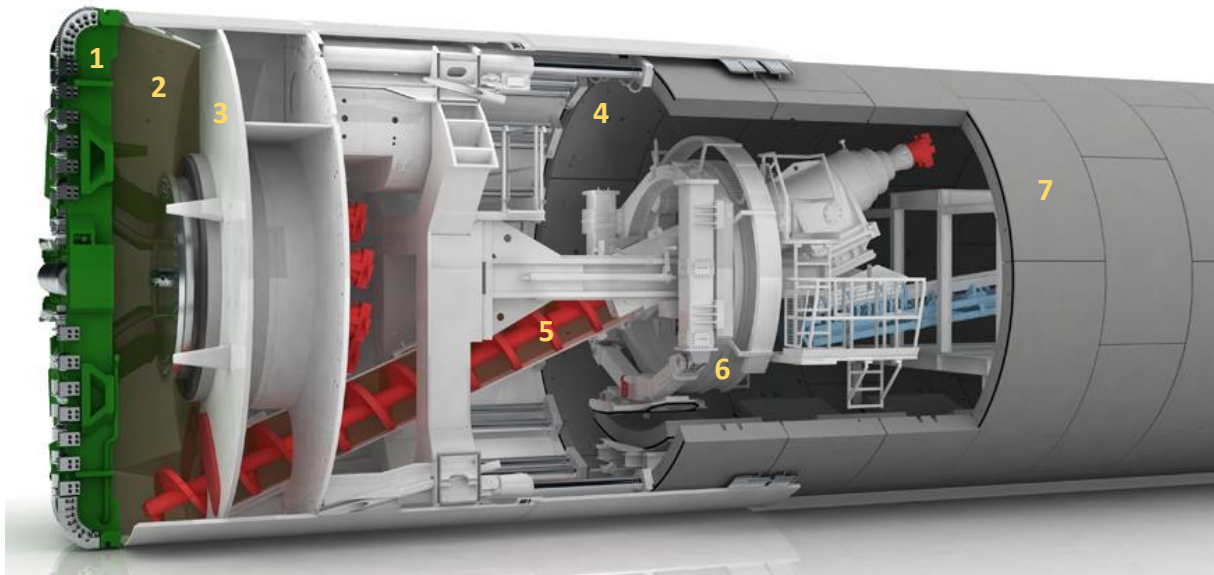
Figure 2-2: Longitudinal cut through an EPB shield (1 cutting wheel, 2 excavation chamber, 3 bulkhead, 4 thrust jacks, 5 screw conveyor, 6 segment erector, 7 segmental concrete lining) (HERRENKNECHT AG (2014))

On the contrary, when the tunnel face (urgently) needs to be stabilised to prevent ground movements and surface settlements or in case of possible gas occurrence, full-face support is applied; so called closed mode. This mode represents the actual earth pressure balance (EPB) mode, because a counter pressure is generated as an equilibrium for the active earth and water pressures on the face. The excavated ground again falls into the excavation chamber but initially remains there until the filling level of the chamber reaches the crown. In dependence of the ground properties, further ground treatments might be necessary for sufficient face support (see chapter 2.3). The semi-closed mode is a mixture of both pre-described operation modes. Here, the excavation is just partially filled with excavated material. This mode often is applied in mixed face conditions or in conditions of a weak layered face, where in the lower part of the tunnel face the acting pressures will be too high in order to maintain face stability.

Besides the advance modes that are linked to the ground conditions, there are two further essential operations of the machine, which are related to the tunnelling situations. In case of maintenance (repair works and inspections), the excavation chamber needs to be accessible. Therefore, the level of supporting muck is reduced to a minimum and replaced by compressed air. Through air locks, interventions are possible for trained personnel. In times of longer periods of stoppage – especially in coarse soils –, it might be required to stabilise the face with (high-density) slurry. In

these situations, the decomposition or degeneration of the support medium, in particular when treated with foam, could lead to inhomogeneity and thusly to local insufficient face support. A slurry then replaces the supporting muck.

In this study, the focus is on closed mode operations as it represents the most frequently applied operation mode of EPB machines. Furthermore, it will be concentrated on cohesionless soils; here usually full-face support is mandatory. The pressure regulation and the essential requirements for the support medium are presented consecutively.

2.2   Face support in closed mode

As mentioned before, face support in closed mode is realised by using the excavated soil to build up a pressure in the excavation chamber countering earth and water pressures acting on the tunnel face (Figure 2-3). The quantum of pressure is regulated via the advance speed (cutting speed), injection of foam (MAIDL (1997)) and the spoil extraction rate of the screw conveyor.

Depending on the ground conditions, in which the advance takes place, the support pressure needs to exhibit specific properties for effective face support (control). These requirements have been summarised by GALLI & THEWES (2014) to the following:
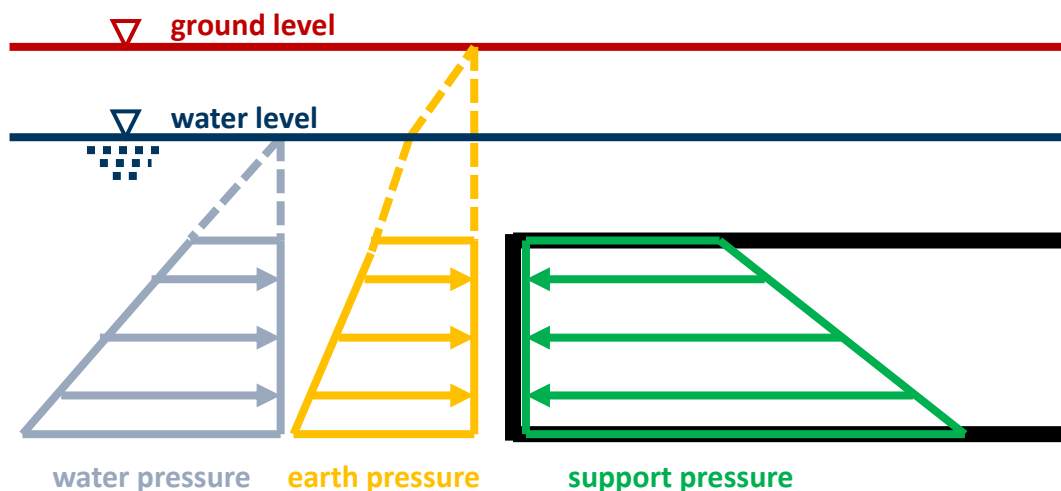
Figure 2-3:   Schematic of the EPB principle – equilibrium of acting and supporting forces

- **Suitable flow behaviour**

  A sufficient flow behaviour of the support medium is relevant to ensure an appropriate material flow in the excavation chamber and in the screw conveyor. So far, recommendations for physical (rheological) flow parameters do not exist; rather values from index testing are used for the evaluation of the material flow. The measure of flow is distinguished regarding the fines content of the support medium. For cohesive soils, the flow is described by the consistency, whereas in non-cohesive, coarse soils the measure is the workability as used in concrete engineering. According to MAIDL (1995), cohesive soils with a consistency index I_C between 0.40 and 0.75 are considered suitable as support medium and do not need any further treatment regarding material flow. In non-cohesive soils, the workability is expressed through the slump test according to DIN EN 12350-2 (2009-08) as an index value for the flow behaviour. Numerous authors describe slumps between 10 and 20 cm as a suitable range for the workability of the support medium, cf. BUDACH & THEWES (2013), VINAI ET AL. (2008). At the same time, the support material should show sufficient stiffness for muck conveyance and landfill or disposal.

- **Homogeneous pressure transfer**

  For effective face support, a uniform pressure transfer to the face is required. Therefore, homogeneous material properties and a minimum rate of compressibility are necessary. At the same time, volume and support pressure fluctuations can thusly be reduced as well as the pressure can be diminished over the extraction length of the screw conveyor towards atmospheric pressure conditions (THEWES & BUDACH (2010b)). The compressibility is determined according to BUDACH (2012), BUDACH & THEWES (2013) depending on the dimensions of the tunnelling machine.

- **Low hydraulic conductivity**

  Another factor is the permeability of the support medium. To prevent uncontrolled inflow of groundwater into the excavation chamber and in order to minimise destabilising forces from seepage flow at the face (cf. ANAGNOSTOU & KOVÁRI (1996), ZIZKA ET AL. (2013)), the hydraulic conductivity should be limited. According to ABE ET AL. (1979), the hydraulic conductivity k_f should be less than

10^{-5} m/s. In gravelly soils (application area 3, see chapter 2.3.1), i.e. in coarse soils, even a boundary value of 10^{-4} m/s would still be suitable (MAIDL ET AL. (2012)).

- **Reduced inner friction**

  The reduction of the inner friction (friction angle) of the support medium leads to reduced torques and power demands for the cutting wheel and the screw conveyor. Furthermore, the friction at solid interfaces is decreased as well reducing material wear to the cutting tools and other machine components, cf. THEWES & BUDACH (2010a).

- **Low clogging potential**

  Clogging is a major reason for standstills in tunnelling. Particularly in fine soils, the tendency to clogging is significant. The clogging potential depends on the plasticity, the consistency and the clay mineralogy, see FEINENDEGEN ET AL. (2011), HOLLMANN & THEWES (2013). Especially clayey, even overconsolidated are very prone to clogging. The plasticity and consistency are dependent of the Atterberg limits and thus it is possible to influence the clogging potential (and the flow behaviour) by adjusting the water content.

- **Sufficient stability**

  Primarily during longer stoppages, the support medium must consist of sufficient sedimentation stability and a slow degeneration behaviour, see LANGMAACK (2004). This is particularly important when foam is used as conditioning agent, because it exhibits only temporary and highly changeable stability, see BABENDERERDE ET AL. (2005). This is due to the drainage processes of the liquid phase. Steadily reoccurring changes in the balance of the internal structure benefits decomposition. When the foam decomposes, the result can be separation of the supporting material into its different phases. This can lead to an uneven support pressure transfer (see above) or, if an air bubble forms in the crown, it can even danger the blowout safety (LANGMAACK (2004)).

These characteristics are usually derived partly from empirical values from practical experience and partly from laboratory testing.

2.3 Application ranges of EPB shields

In the presented operational descriptions of EPB tunnelling, it was occasionally mentioned that specific properties or behaviours are related to the ground of application. Consecutively, the application ranges of EPB shields shall be treated in more detail.

2.3.1 Classical application range

According to MAIDL ET AL. (2012), the classical application range is in soils with a fines content (d ≤ 0.063 mm) of at least 30 wt%. In these conditions, only water and an anti-clogging agent may have to be added to fulfil the forenamed requirements for the support medium. Figure 2-4 shows the typical areas of application for EPB machines depending on grain size, conditioning agent and water pressure, which are based on both laboratory works and tunnelling experience. The limit of the classic application range is shown by line 1.

2.3.2 Extended application ranges

The sections outside the area bordered by line 1 are defined as extended ranges of application for EPB machines. These granulometric areas in large parts are congruent with the main application range for hydro shields. By the use of foams, polymers and
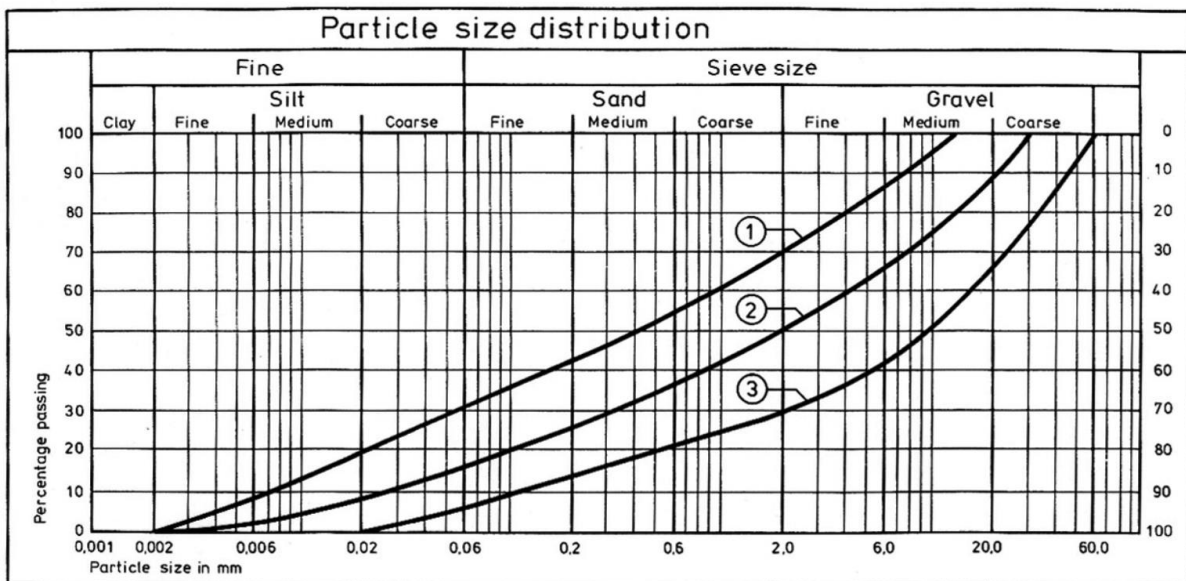
Figure 2-4: Application ranges for EPB shields according to MAIDL ET AL. (2012). Area 1 with $I_C = 0.40 - 0.75$, Area 2 with $k_f < 10^{-5}$ m/s and water pressure < 2 bar, Area 3 with $k_f < 10^{-4}$ m/s and without water pressure

(high-density) slurries, EPB advances even in highly permeable soils are efficiently feasible. The treatment of the ground is called "soil conditioning". In coarse soils, it often is necessary to temporarily improve the properties of the support medium and thusly fulfil the requirements.

BUDACH & THEWES (2013) aimed at affirming the recommendations of application by laboratory testing. Therefore, they conducted series of tests on various soils with a main concentration on the extended area resulting in modified recommendations for the application of EPB shields in coarse-grained soils (Figure 2-5; here shown in comparison to the application ranges from Figure 2-4 according to MAIDL ET AL. (2012)). The diagram shows that tunnelling with EPB machines can be extended into fine-gravelly sands by the use of foam as conditioning agent only. Basic prerequisite therefore is a fines content of about 5 wt% and a limitation of the water pressure to 3 bar. An even reduced fine fraction requests the addition of further additives.

It is significant to bear in mind, that a derivation of any soil conditioning measures from these recommendations alone is however still not possible, see THEWES ET AL. (2010). The recommendations should work as a first estimator of possible additional
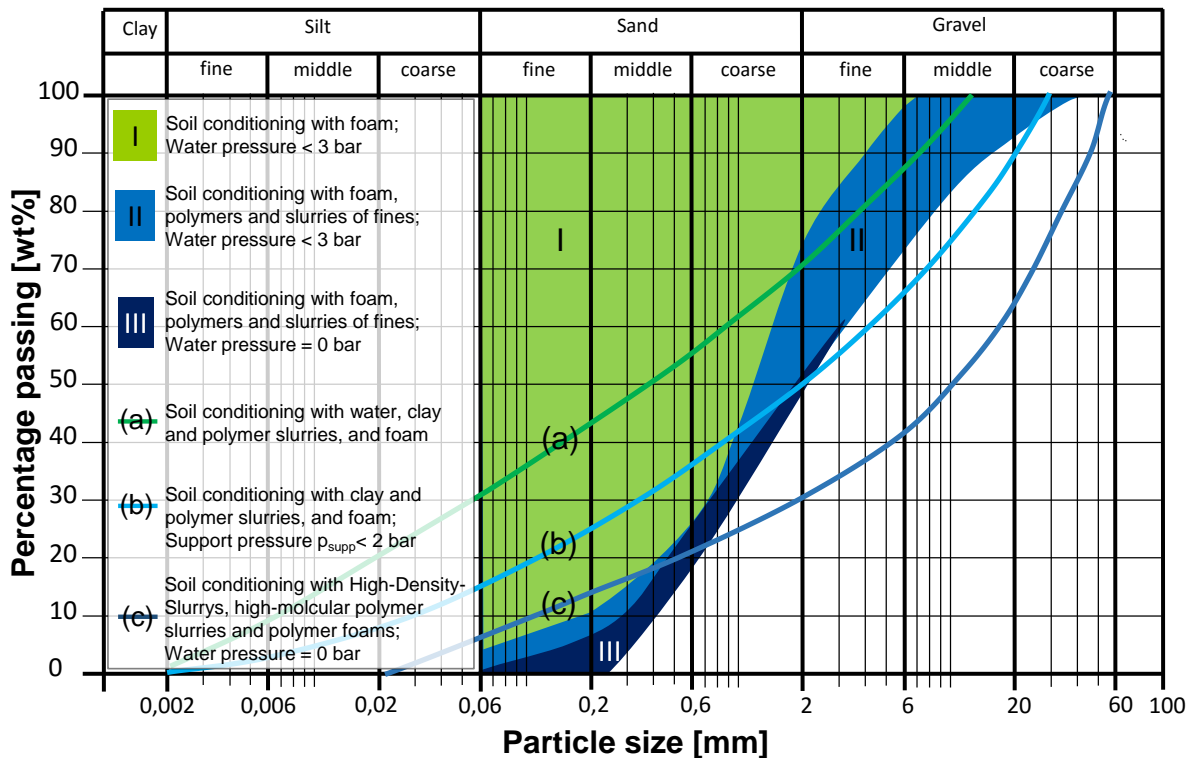
Figure 2-5:   Application ranges for EPB shields in coarse soils in dependence of the conditioning agents according to BUDACH & THEWES (2013) supplemented by application ranges according to MAIDL ET AL. (2012)

treatments of the ground to be projected. Advanced information on the conditioning behaviour or on the properties of conditioning agents and conditioned soils can however be found through laboratory testing.

2.4 Concepts and lab tests for soil conditioning

The recommendations in form of application ranges give a good indication of the necessary treatments to be expected. Actual conditioning parameters for the conditioning process can be determined in laboratory tests. Based on the requirements for the support medium introduced before, lab tests have been defined by various researchers in order to make an evaluation of the conditioning behaviour and the quality of soil conditioning possible. Before the most significant test methods and results from research on soil conditioning are presented, the important basic parameters and facts on soil conditioning are introduced.

2.4.1 Soil conditioning for EPB tunnelling

The term "soil conditioning" describes the treatment of a soil with additives influencing (or changing) its basic properties. Therefore, a number of conditioners is available in practice, which have been proven suitable for the intended application.

The easiest way to influence the soil behaviour is simply to add water. Especially in fine soils, the change in water balance can have significant effects regarding the consistency.

For the extension of the classic application range into coarse soils, foams, polymers and (high-density) slurries are fed into the excavation cycle. The most frequently applied conditioning agent thereof is foam. Foam is an emulsion of water and air. The immiscibility of these fluids is neutralised by a surfactant (surface-active agent), which reduces the surface energy and thus the interfacial tension between the two components, see Stache (1979). Surfactants are hydrocarbon-based molecular chains with one hydrophilic and one hydrophobic end. Hence, the water molecules will bond to the hydrophilic part and the air to the hydrophobic end. In aqueous phases, surfactants form spherical, cylindrical or laminar aggregates (micelles), where the hydrophobic ends frame the core. This explains the bubbly structure of foams, when gas phase and liquid phase are mixed together. In order to define the foam

composition, in tunnelling two descriptive parameters have been defined in the EFNARC GUIDELINES 2001 (2003): the concentration of the foaming liquid c_f and the foam expansion ratio FER. The concentration of the foaming liquid describes the amount of surfactant in the solution of surfactant and water. The definition is shown in Eq. 2.1.

$$c_f = \frac{Q_f}{Q_f + Q_w} \cdot 100 = \frac{Q_f}{Q_L} \cdot 100 \qquad \text{[vol\%]} \qquad \text{Eq. 2.1}$$

with Q_f volume flow of surfactant [l/min], Q_w volume flow of water [l/min], Q_L volume flow of liquid [l/min].

The foam expansion ratio (FER) describes the ratio of the total foam volume Q_F [l/min] and liquid phase volume of the foam Q_L [l/min] (Eq. 2.2); in turn this means, the FER is an indicator for the wetness (or dryness) of a foam. The determining factor in this description is the volume of air Q_A [l/min].

$$\text{FER} = \frac{Q_F}{Q_L} = \frac{Q_L + Q_A}{Q_L} \qquad \text{[-]} \qquad \text{Eq. 2.2}$$

With regard to the conditioning process, one further parameter has to be defined. It is the foam injection ratio FIR, which describes the volume of foam in relation to the volume of soil being excavated Q_S [l/min] (Eq. 2.3), see EFNARC GUIDELINES 2001 (2003).

$$\text{FIR} = \frac{Q_F}{Q_S} \cdot 100 = \frac{Q_F}{v_{Adv} \cdot A_{exc}} \cdot 100 \qquad \text{[vol\%]} \qquad \text{Eq. 2.3}$$

with v_{Adv} advance speed [m/min], A_{exc} face area [m^2].

The less the fines content of the construction ground, the more important other conditioning agents become (MAIDL (1995)). Besides foam, there are two more materials usually applied in EPB tunnelling. One of them is polymers. Polymers are macromolecular chain-configurations, which can be formed in countless variants, see NEUMÜLLER (1987). The length and composition of the molecular chain influence very much the polymer's properties. The field of application for polymers is therefore almost indefinable, but amongst others, they are applied in EPB tunnelling. There, hydrocarbon-based polymers are usually used to influence the rheological properties of the support muck and as water absorber, see BABENDERERDE (1998), MAIDL (1995).

The polymers are concentrated either as additive into the foaming liquid or separately as polymer suspension with its own injection system. The addition of polymers shall help in handling pore water pressures. This is the fact at the tunnel face, when the polymers penetrate into the ground. The water absorbency provides gelling of the penetrated zone and the matrix composed of soil grains and a polymer-water gel reduces the permeability immensely, see MAIDL (1995). This sealing effect is particularly interesting in very permeable grounds. Moreover, polymers can also be applied in the screw conveyor, in order to assist the support medium in reducing pore water pressures.

If the ground is too permeable to treat it with polymers, e.g. in sandy gravel, soil conditioning with slurry might be mandatory. Since the excavation chamber design of EPB shields mostly is different from hydro shield machines, a switch of the construction method to hydro shield tunnelling is not feasible at short notice and without tremendous measures of reconstruction. The addition of slurry to the ground and the usage of the soil-slurry mixture still can fulfil the demands on the support medium. Projects in the past reported this successfully, cf. BOONE ET AL. (2005), KÖNEMANN & TAUCH (2012), MAIDL & PIERRI (2014). Important issue to control in these very coarse soils is the permeability. It exists a real danger of uncontrolled water inflow and of blowouts. The properties of the slurry have to be determined in dependence of the ground properties. Above all, this is the density, the destructuration behaviour and the face sealing behaviour (membrane or penetration zone). These characteristic properties are connected to two operational parameters: the concentration of the slurry, c_{susp}, and the slurry injection ratio, SIR. They are defined according to BUDACH (2012) as follows (Eq. 2.4 and Eq. 2.5):

$$c_{susp} = \frac{Q_{fines}}{Q_{fines}+Q_w} \cdot 100 = \frac{Q_{fines}}{Q_{susp}} \cdot 100 \qquad [vol\%] \qquad \text{Eq. 2.4}$$

with Q_{fines} volume flow of fines [l/min], Q_w volume flow of water [l/min], Q_{susp} volume flow of slurry [l/min].

$$SIR = \frac{Q_{susp}}{Q_S} \cdot 100 = \frac{Q_{susp}}{v_{Adv} \cdot A_{exc}} \cdot 100 \qquad [vol\%] \qquad \text{Eq. 2.5}$$

with Q_{susp} volume flow of slurry [l/min or m³/min].

Based on the soil compositions that will be investigated in this study (see chapter 4.3.1), in the following only foam conditioning is considered without addition of any further ground treaters.

2.4.2   Experience from lab testing and recommendations

Subsequently, test methods and experiences from lab works in the field of soil conditioning are presented. The test methods can be applied to the recommendations given above. Because no standardised tests exist in the context of soil conditioning, any of the experiments can be used as an index test. Regarding reproducibility and comparison of test results between projects and research institutions, some of the tests will be pointed at as recommended standard. The tests will be introduced first on the level of application ranges and second, distributed according to the requirements for the support medium.

1.   Classical application area

The classical application area of EPB shields is predominantly determined by cohesive soils. Water is used as conditioning agent for the alternation of the water content and maybe foam to reduce stickiness. The two essential properties connected to the application range are the consistency and the clogging behaviour. The latter one is evaluated in dependence of the consistency.

The **consistency** of a cohesive soil or a support material predominantly consisting of cohesive soil is described by the consistency index I_C through the water content w and the Atterberg limits (Eq. 2.6). Generally, consistency is denoted as the degree of the firmness of a soil and can be divided into the states "liquid", "very soft", "soft", "stiff", "very stiff" or "hard".

$$I_C = \frac{w_L - w}{w_L - w_P} = \frac{w_L - w}{I_P} \qquad [-] \qquad\qquad \text{Eq. 2.6}$$

with w_L liquid limit [wt%], w water content [wt%], w_P plastic limit [wt%], I_P plasticity index [wt%].

The Atterberg limits, which is the liquid limit and the plastic limit that are used here, are determined with the Liquid Limit Device (Casagrande Cup) and the Plastic Limit Test in accordance to ASTM D4318 (2000-06), DIN 18122-1 (1976-04) or DIN 18122-1

(1976-04). The plasticity and consistency indexes are then calculated from it using Eq. 2.6.

Bearing in mind that MAIDL ET AL. (2012) recommends a suitable consistency for the supporting material in the excavation chamber of $0.4 < I_C < 0.75$, the water content can accordingly modified by the addition of further water (water conditioning).

Furthermore, the **clogging behaviour** can be determined from the same information as above. Taking into account the natural water content, the Atterberg limits and the plasticity index, and thusly the consistency, the risk of clogging can be evaluated with the help of the clogging diagram of HOLLMANN & THEWES (2013), see Figure 2-6.

The difference of the plastic limit w_P and the natural water content w_n is plotted on the X-axis, whereas the difference of the liquid limit w_L and the natural water content is plotted to the Y-axis. Moreover, the water content in steps of 5 wt%, the plasticity and the consistency are inserted in the diagram, too. Hence, it is possible to enter the diagram having determined the natural water content and the Atterberg limits in advance. Strong clogging will occur in soft to stiff consistencies; these areas should be avoided. Again it can be seen, that by adding water, the consistency can be changed and at the same time the clogging behaviour. This has to be taken into account seriously when changing the water content deliberately.

Furthermore, the plot in Figure 2-6 highlights also the recommended consistency range of MAIDL ET AL. (2012). Obviously, the range complies with the highest risk for clogging. This explains, why foam should be added to these grounds, when used as support medium, although the consistency apparently exhibits suitable values; the foam reduces the interfacial tension between the clay minerals and the machine steel structure. Further details on this topic can be found in HOLLMANN (2015), HOLLMANN & THEWES (2013).

Additionally, the clogging behaviour of clays in EPB tunnelling has been assessed experimentally. FEINENDEGEN ET AL. (2010) developed a "cone pull-out test" apparatus, from which the clogging behaviour can be evaluated via the adherence of sticky material. A metal cone is penetrated into the test sample and pulled out. The adhering material on the metal surface is weighted and the ratio of adhering weight and surface area is defined as "adherence". Furthermore, ZUMSTEG & PUZRIN (2012)

conducted mixing tests under certain boundary conditions and measured the amount of adhering material to the mixer. Moreover, they developed an enhanced apparatus for equivalent measurements deriving the adhesion from the resistant torque. Therefore, constant shear load conditions are considered. Besides information on the clogging behaviour, the **shearing behaviour** is analysed, too. The addition of conditioning agents, such as foam or polymers, can significantly reduce both the clogging potential and the shear resistance, see Zumsteg et al. (2013), Zumsteg & Puzrin (2012). Comparative tests using a modified shear vane apparatus by Messerklinger et al. (2011) – see also chapter 3.2.3 – support these findings. Nevertheless, all these experimental approaches can function only as index tests.
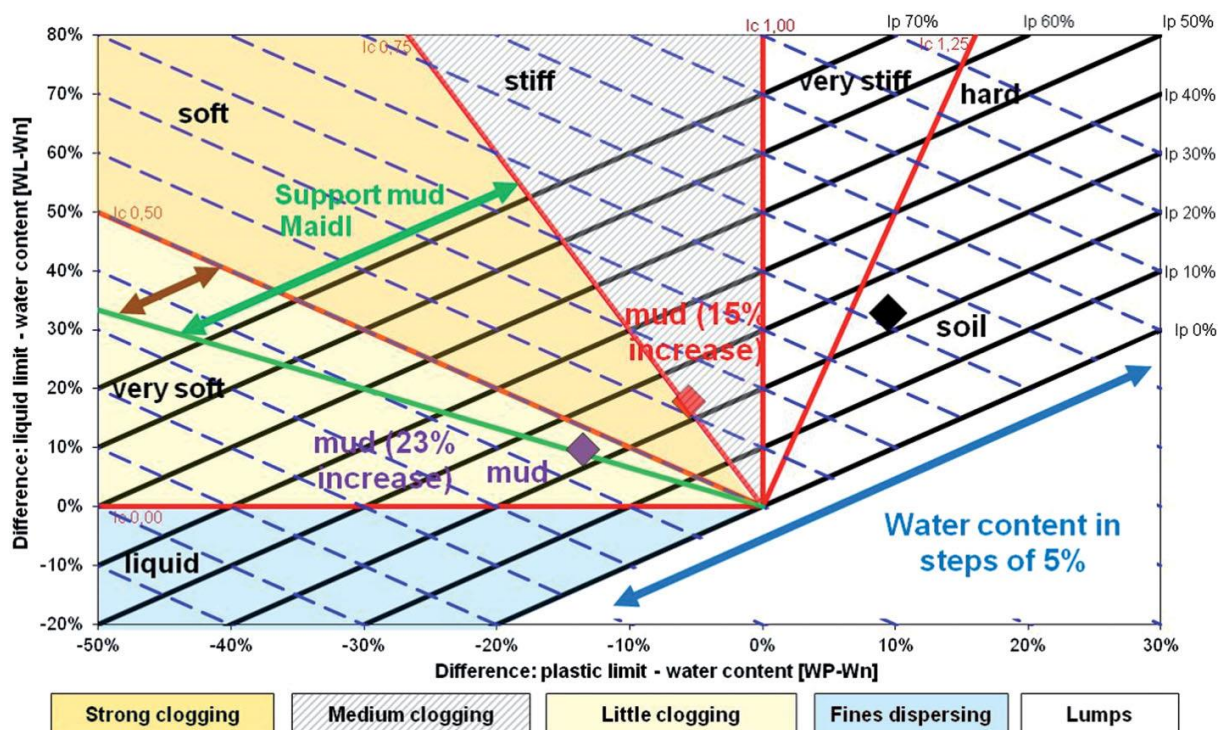
Figure 2-6: Diagram of Hollmann & Thewes (2013) for the evaluation of the clogging potential; dependent of the plasticity (I_P), the Atterberg limits (w_L and w_P) and the natural water content (w_n)

2. Extended application area

(Project-related) Studies showed that lab tests are a helpful tool for the planning of EPB tunnelling and soil conditioning, cf. Borio et al. (2009), EFNARC GUIDELINES 2001 (2003), Maidl & Pierri (2014), Thewes et al. (2010). So far, some approaches exist for the investigation of the foam quality and of the conditioning behaviour of soils (e.g. EFNARC GUIDELINES 2001 (2003)), but not any standards for testing related to soil conditioning. State-of-the-art research on the topic is and was conducted for example

in Bochum (Germany) by Budach (2012), Maidl (1995), in Lyon (France) by Quebaud et al. (1998), in Oxford and Cambridge (Great Britain) by Borghi (2006), Peña Duarte (2007), in Delft (Netherlands) by Bezuijen & Schaminée (2001), in Turin (Italy) by Borio (2010), Peila et al. (2013a), Vinai (2006), and in Aachen (Germany) by Vennekötter (2012). Additionally, applied science is reported by the tunnelling practice and suppliers of conditioning agents. Examples can be found in Babendererde et al. (2011), Langmaack (2000), Langmaack (2004), Maidl et al. (2015), Maidl & Pierri (2014), Merritt et al. (2013), Merritt et al. (2015), Schulkins et al. (2013). Although the research focus in all these and further studies varied, similar test methods and test series were applied. A standardisation of essential properties and testing methods (setup and procedures) however did not take place. Over the time however, approaches became more and more comparable. In Table 2-1 and Table 2-2, the most common approaches and test methods within the frame of soil conditioning are summarised and distinguished by the main properties investigated according to the requirements in chapter 2.2.

Table 2-1: **Characteristic properties and associated recommended tests for foam**

Criteria	Approach / Test method	Main references
Foaming behaviour	Foam density	Borio (2010), Galli (2009), Maidl (1995), Merritt (2004), Peña Duarte (2007), Psomas (2001), Thewes & Budach (2010b), Vennekötter (2012), Vinai (2006)
Foam quality	Drainage test according to EFNARC GUIDELINES 2001 (2003)	Borio (2010), Budach (2012), EFNARC GUIDELINES 2001 (2003), Galli (2009), Merritt (2004), Vennekötter (2012), Vinai (2006)
	Drainage test according to D/DSTAN/ 42/40 (2002-08)	Peña Duarte (2007)
	Bubble-size	Budach (2012), Galli (2009), Peña Duarte (2007)

Table 2-2:   **Characteristic properties and associated recommended tests for assessing the interaction of cohesionless soil/rock and conditioning agents (I/II)**

Criteria	Approach / Test method	Main references
Flow behaviour / workability	Slump test according to DIN EN 12350-2 (2009-08)	Borio (2010), Budach (2012), Leinala et al. (2000), Peila et al. (2013b), Peña Duarte (2007), Quebaud et al. (1998), Vennekötter (2012), Vinai (2006), Wu & Qu (2009)
	Miniature slump test	Malusis et al. (2008)
	Slump flow test according to DIN EN 12350-8 (2009-12)	Budach (2012), Vennekötter (2012)
	V-funnel test according to DIN EN 12350-9 (2010-12)	Vennekötter (2012)
	Flow cone test according to ASTM C939 (2010)	Peña Duarte (2007)
	Rheometer (FANN Model35, Schleibinger Viscomat NT)	Maidl (1995), Vennekötter (2012)
Shear strength / Power consumption	Torque measurements / Mixing tests	Dobashi et al. (2013), Levent et al. (2013), Quebaud et al. (1998)
	(Direct) Shear-box test	Bezuijen et al. (1999), Peña Duarte (2007), Psomas (2001), Wu & Qu (2009)
	Shear vane tests	Bezuijen et al. (1999), Budach (2012), Meng et al. (2011), Messerklinger et al. (2011)

Table 2-3: **Characteristic properties and associated recommended tests for assessing the interaction of cohesionless soil/rock and conditioning agents (II/II)**

Criteria	Approach / Test method	Main references
Hydraulic conductivity / Permeability	Constant head permeameter tests according to ASTM D2434 (2006), DIN 18130-1 (1998-05)	BORIO (2010), BUDACH (2012), MAIDL (1995)
	Consolidation test according to ASTM D2435 (1996)	PEÑA DUARTE (2007), PSOMAS (2001)
Compressibility	Consolidation test according to ASTM D2435 (1996)	PEÑA DUARTE (2007), PSOMAS (2001)
	Compression test	BUDACH (2012), MAIDL (1995), VENNEKÖTTER (2012)
Stability	Drainage tests	MAIDL (1995), PEÑA DUARTE (2007), VINAI (2006)
	Segregation tests	BUDACH (2012)
Penetration behaviour / face impregnation	Foam penetration test	BEZUIJEN ET AL. (1999), MAIDL (1995), MENGÜ (2012), QUEBAUD ET AL. (1998), TORKHANI (2013)
Abrasiveness	Weight loss of metals during mixing	GHARAHBAGH ET AL. (2014), HEDAYATZADEH ET AL. (2015), JAKOBSEN ET AL. (2013), PEILA (2013), WILMS (1995)
Screw conveyor tests / Extraction tests		BEZUIJEN ET AL. (1999), BORIO (2010), JIANG ET AL. (2013), MERRITT (2004), PEÑA DUARTE (2007)

The results from laboratory testing can only function as index values for practice because in the studies, production and application of the conditioning agents mainly takes place under atmospheric conditions. Nevertheless, the tests enable basic understanding of feasibility as well as processes and interactions going on during soil conditioning. Recommendations for standardised and reproducible testing can be found in BUDACH (2012), BUDACH & THEWES (2015), THEWES ET AL. (2012).

BUDACH (2012) defines the **workability**, the **compression behaviour** and the **hydraulic conductivity** as the essential properties of the support medium. In addition, LANGMAACK (2004) emphasises sufficient **stability** of the soil-foam mix as an important requirement. Yet, the most extensive investigations of the interaction between soil and conditioning agents have been performed by using the slump test from concrete engineering according to DIN EN 12350-2 (2009-08). Hence, the greatest experience exists for this test method, although it does not describe the actual **flow behaviour**, rather it represents an index test. Characterisations of the actual flowing of soil-foam mixtures so far have only been attempted by MAIDL (1995), VENNEKÖTTER (2012) and in some extend by GATTERMANN & KIEHL (2004), MENG ET AL. (2011), MESSERKLINGER ET AL. (2011). These approaches will be further analysed in chapter 3.2.3, as they function as a base for a more detailed approach of the flow characterisation within this research study.

2.4.3   Conditioning behaviour of a ground: recommended testing procedure

Project related testing regarding soil conditioning could be conducted on the basis of the test methods and experiences presented in chapter 2.4.2. In order to evaluate the results, a standard procedure should be introduced, which creates a consistent, reproducible and comparable workflow. QUEBAUD & MOREL (1995) and FREIMANN (2013), in their research, developed flow-charts for the testing procedure for investigations on the conditioning behaviour of a soil. In the presented context, the latter one was applied successfully in practice, see MAIDL & PIERRI (2014). Figure 2-7 shows an updated, exemplary version according to their diagrams with respect to pure foam conditioning. This sequence could be seen as a recommendation for such a standardised testing procedure. First, the foam alone is evaluated, then, second, the conditioning behaviour is investigated. The course is as follows:

1. **Parameter estimation for foam production (i.e. c_f, FER, Q_F) considering further influences such as the type of foam gun, conveying pressures, conveying length etc.**

2. **Investigation of the foaming behaviour and the foam density (actual FER) (see chapter 2.4.2)**

    If the actual FER excesses the pre-assigned tolerances from the target value, the production parameters have to be adjusted accordingly, cf. THEWES ET AL. (2012).

3. **Investigation of the drainage behaviour and the foam structure (see chapter 2.4.2)**

    If the drainage times (half-life) are too low or the bubble-sizes too large, the production parameters have to be readjusted.
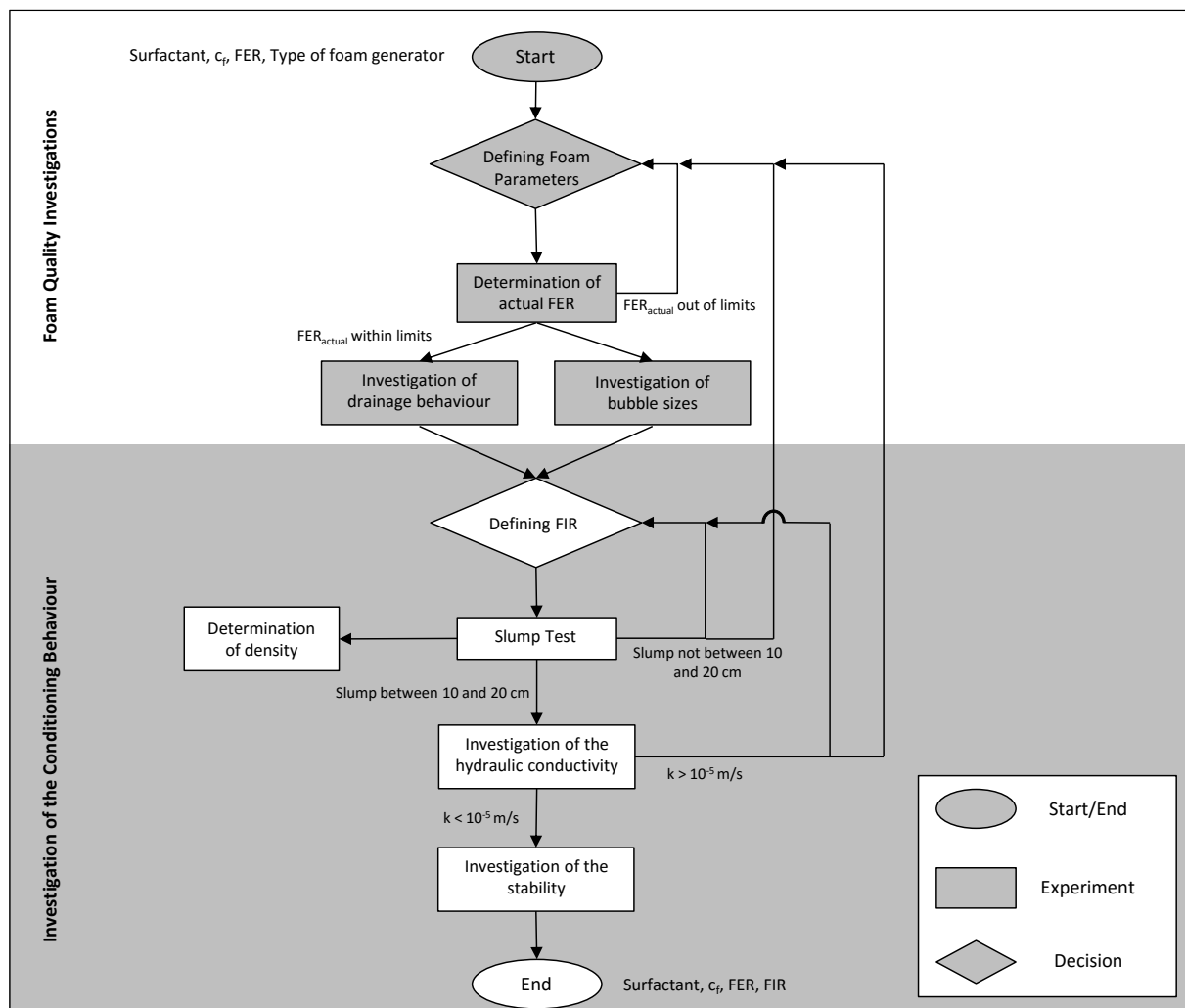
Figure 2-7: **Recommended procedure for testing of the foam conditioning behaviour of coarse soils based on FREIMANN (2013)**

4. **Parameter estimation for foam conditioning (i.e. FIR); grain-size distribution curve and water content are assumed to be known in advance**

5. **Investigation of the workability / flow behaviour (see chapter 2.4.2)**

    If the slump is outside the recommended range of 10 and 20 cm, the FIR has to be changed: slump smaller 10 cm → more foam; slump greater 20 cm → less foam

6. **Investigation of the hydraulic conductivity and the stability (see chapter 2.4.2)**

    If the hydraulic conductivity cannot be reduced to values lower than $k_f = 10^{-5}$ m/s (in very coarse soils $k_f = 10^{-4}$ m/s, see above) and kept below this limit for at least 120 min, the FIR has to be reconsidered. More foam usually reduces the permeability even further, but it is accompanied with the effect of quicker decomposition of the mixture. Eventually, a consideration of further conditioning additives is necessary.

This iterative process is rerun as long as all requirements are fulfilled. When other or multiple conditioning agents are used, it can be proceeded analogously considering the conditioner-dependent parameters.

Particular attention should be given to the various tunnelling situations in highly permeable grounds. During short-term stoppages, e.g. ring build, a sufficient sealing of the face has to be maintained. When required, the application of further conditioning agents might be necessary. During longer standstills, especially for compressed air interventions, face sealing with foam alone is not feasible.

2.5   Face stability

As described in chapter 2.2, face stability is maintained, when an equilibrium state is generated between the acting pressures (earth pressure, water pressure) and the support pressure. In mechanised tunnelling, it is common practice to assess face stability analytically based on the failure model according to HORN (1961). It describes a soil collapse mechanism in the form of a sliding wedge in front of the tunnel face and a prism on top of the wedge. The rupture area is assumed plane and inclined by a sliding angle ϑ, on which the wedge is sliding. The failure model is considered as limit equilibrium method with Mohr-Coulomb failure criterion and was firstly introduced

to mechanised tunnelling by Anagnostou & Kovári (1994) and Jancsecz & Steiner (1994). Based on the works of Janssen (1895) and Terzaghi (1943), the loading by the prism on the wedge can be reduced in certain conditions according to "silo effects". This depends very much on the particular researcher's perspective; examples: consider silo **a.** always (Anagnostou & Kovári (1994)), **b.** when overburden > 3·D (Girmscheid (2008)), **c.** when overburden "several times greater than" D (Terzaghi et al. (1996)) or greater than "a certain minimum cover" (Babendererde & Elsner (2014)), **d.** only for deep tunnels (>2·D) (Maidl et al. (2014)), **e.** when overburden > 1·D (Daub (2005)). A scheme of the impacts on face stability as well as the geometrical boundaries according to the mentioned theories connected to face stability assessment is shown in Figure 2-8.
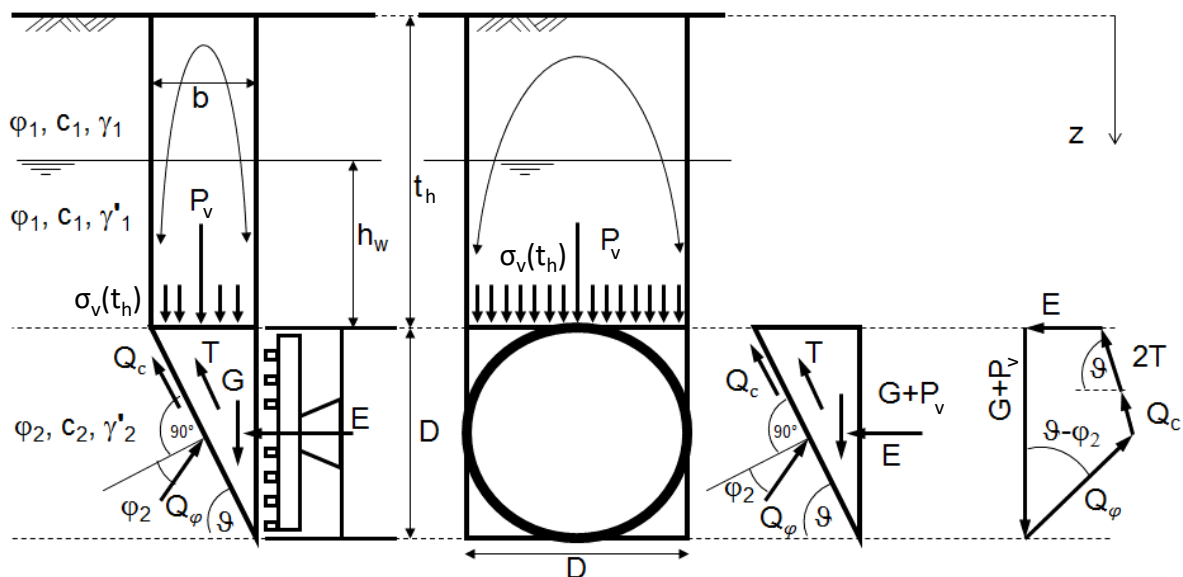
Figure 2-8: Scheme of the failure situation at the tunnel face based on the theories of Horn (1961) and Janssen (1895); modified from Thewes (2009)

The calculation of the acting earth pressure at the face can be conducted based on Figure 2-8 by equilibrium equation. The loads and forces acting on the wedge, that are necessary for the calculation, are the tangential forces at the sides of the wedge T, the friction forces in the sliding plane Q and the loading from the prism on top of the wedge (reduced if applicable) $\sigma_v(t_h)$ (or P_v). Besides, the dead weight of the wedge itself, G, has to be taken into account, too. Equilibrium and transformation lead to the resulting earth pressure E (Eq. 2.7). The friction force Q thereby vanishes.

$$E = \frac{(G+P_v)\cdot(\sin(\vartheta)-\cos(\vartheta)\cdot\tan(\varphi_2))-2\cdot T-c_2\cdot\frac{D^2}{\sin(\vartheta)}}{\sin(\vartheta)\cdot\tan(\varphi_2)+\cos(\vartheta)} \qquad [N] \qquad \text{Eq. 2.7}$$

wherein G is the dead weight of the sliding wedge [N], P_v the vertical loading from the prism on the wedge [N], ϑ the sliding angle [°], φ friction angle of the soil [°], T the lateral shearing force at the sides of the wedge [N], c the cohesion [Pa], and D the diameter of the tunnel [m].

Several authors' works differ in the calculation of the single loads incorporated in Eq. 2.7, which primarily concerns the tangential shear forces T and the surcharge P_v (or $\sigma_v(t_h)$). The value of P_v depends on the consideration of soil arching effects (silo effect; see above). A very common rule of thumb is to consider soil arching, when the overburden's thickness equates at least to twice the dimension of the tunnel diameter (= deep tunnels), cf. MAIDL ET AL. (2014). Furthermore, the coefficient of lateral earth pressure for the silo equation is treated differently in the literature, see e.g. ANAGNOSTOU & KOVÁRI (1994), GIRMSCHEID (2008), JANCSECZ & STEINER (1994), KIRSCH & KOLYMBAS (2005), MAYER ET AL. (2003), MÉLIX (1986). The surcharge from the prism on the wedge without soil arching can be determined by using Eq. 2.8 and with soil arching by Eq. 2.9.

For $t_h \leq 2\cdot D$:

$$\sigma_v(z) = \gamma_1 \cdot z \qquad [Pa] \qquad \text{Eq. 2.8}$$

For $t_h > 2\cdot D$:

$$\sigma_v(z) = \frac{\frac{A_{silo}}{U}\cdot\gamma_1 - c_1}{K_1 \cdot \tan(\varphi_1)} \cdot \left(1 - e^{-\frac{U}{A_{silo}}\cdot K_1 \cdot z \cdot \tan(\varphi_1)}\right) + p_0 \cdot e^{-\frac{U}{A_{silo}}\cdot K_1 \cdot z \cdot \tan(\varphi_1)}$$

$$[Pa] \qquad \text{Eq. 2.9}$$

with γ the unit weight of soil [N/m³], z the depth below surface [m], t_h the overburden height [m], A_{silo} the cross-sectional area of the silo [m²], U the circumference of the silo [m], K the lateral earth pressure coefficient [-], and p_0 the surcharge on the surface [Pa].

Moreover, the lateral forces at the wedge T are assessed in different manners. Again, the consideration of silo effects and the lateral earth pressure coefficient influence the result (see references above) as well as the approach for the distribution of vertical stresses; compare ANAGNOSTOU & KOVÁRI (1994), DIN 4126 (2013-09), GIRMSCHEID (2008) with KIRSCH & KOLYMBAS (2005), cf. BROERE (2001). Here, the definition according to the first group is presented. The total tangential force is composed of a friction (T_R) and a cohesion component (T_C) (Eq. 2.10).

$$T = T_R + T_C \qquad\qquad [N] \qquad Eq.\ 2.10$$

$$\text{with:}\quad T_C = \frac{c_2 \cdot D^2}{2 \cdot \tan(\vartheta_{crit})} \qquad\qquad [N]$$

$$T_R = \tan(\varphi_2) \cdot K_2 \cdot \left(\frac{D^2 \cdot \sigma_v(t_h)}{3 \cdot \tan(\vartheta_{crit})} + \frac{D^3 \cdot \gamma_2}{6 \cdot \tan(\vartheta_{crit})} \right) \qquad [N]$$

wherein K is the lateral earth pressure coefficient [-] according to DIN 4126 (2013-09). The dead weight G (Eq. 2.11), however, is treated commonly.

$$G = \frac{1}{2} \cdot \frac{D^3}{\tan(\vartheta_{crit})} \cdot \gamma_2 \qquad\qquad [N] \qquad Eq.\ 2.11$$

Generally, the sliding angle ϑ is varied until the maximum earth pressure is achieved (worst-case scenario; ϑ_{crit}). The friction angle φ is assumed to be known; the same applies for the cohesion c. For T, the cohesion is accounted only to 2/3 of its value, see DIN 4126 (2013-09).

ANAGNOSTOU & KOVÁRI (1996) researched on the influence of seepage flow in the direction of the excavation chamber on the face stability. A reduction in the hydraulic head towards the face is a sign for a flow potential field from groundwater flow, which is orientated to the excavated tunnel. This groundwater flow is generating flow forces possibly benefitting to erosion of the face. Therefore, destabilising forces from seepage flow should be considered additionally in the earth pressure calculation.

BUDACH (2012) extended the analysis of ANAGNOSTOU & KOVÁRI (1996) by variation of the hydraulic conductivity ahead of the face, in the excavation chamber and in the screw conveyor. He explained this alteration by the soil conditioning processes within the machine. The investigation was done for a single tunnel scenario with different couplings of hydraulic conductivities. FADHEL (2012) then did a similar simulation-

based analysis, but considering different tunnelling conditions (change of overburden, water level, shield diameter etc.). Finally, PAWLIK (2014) added the penetration of conditioning agents to the model. She analysed the foam penetration rate into the ground and thusly influencing the hydraulic conductivity at and ahead of the tunnel face. Moreover, she also took the cutting process of the EPB machine into account. All the studies could conclude, that sufficient soil conditioning and thus, a significant reduction in the support medium's hydraulic conductivity prevent destabilising forces from seepage flow.

Lastly, the acting water force at the face can be calculated according to Eq. 2.12.

$$W = \gamma_w \cdot \left(h_w + \frac{D}{2} \right) \frac{\pi}{4} D^2 \qquad\qquad \text{[N]} \qquad\qquad \text{Eq. 2.12}$$

with γ_w the unit weight of water [N/m³] and h_w the height of groundwater table above tunnel crown [m].

Both forces, earth and water force, weighted by safety factors (η_E: safety factor for earth pressure = 1.50 [-], η_W: safety factor for water pressure = 1.05 [-], see ZTV-ING Part 5 (2012-12)) result in the total support force S on the tunnel axis (Eq. 2.13). By considering the face area and the unit weight of the support medium, γ_S [N/m³], the support pressures in the crown and in the invert respectively are obtained (Eq. 2.14).

$$S = \eta_E \cdot E + \eta_W \cdot W \qquad\qquad \text{[N]} \qquad\qquad \text{Eq. 2.13}$$

$$s_{\text{invert/crown}} = \frac{S}{\frac{\pi \cdot D^2}{4}} \pm \gamma_S \cdot \frac{D}{2} \qquad\qquad \text{[Pa]} \qquad\qquad \text{Eq. 2.14}$$

Eq. 2.14 assumes a linear distribution (gradient) of the support pressure at the tunnel face. Due to possible inhomogeneity of the support material, a non-linear support pressure distribution could be likely – especially when dealing with EPB shields, see ANAGNOSTOU & KOVÁRI (1996), BEZUIJEN ET AL. (2005), BEZUIJEN & TALMON (2014), THEWES & BUDACH (2010b). In situ measurements of actual earth pressures at the bulkhead show this (Figure 2-9), most significantly in the zone of the screw intake. An assumed difference between pressures measured on the bulkhead and acting pressures at the face could not be determined in saturated sandy conditions, cf. BEZUIJEN & TALMON (2014).
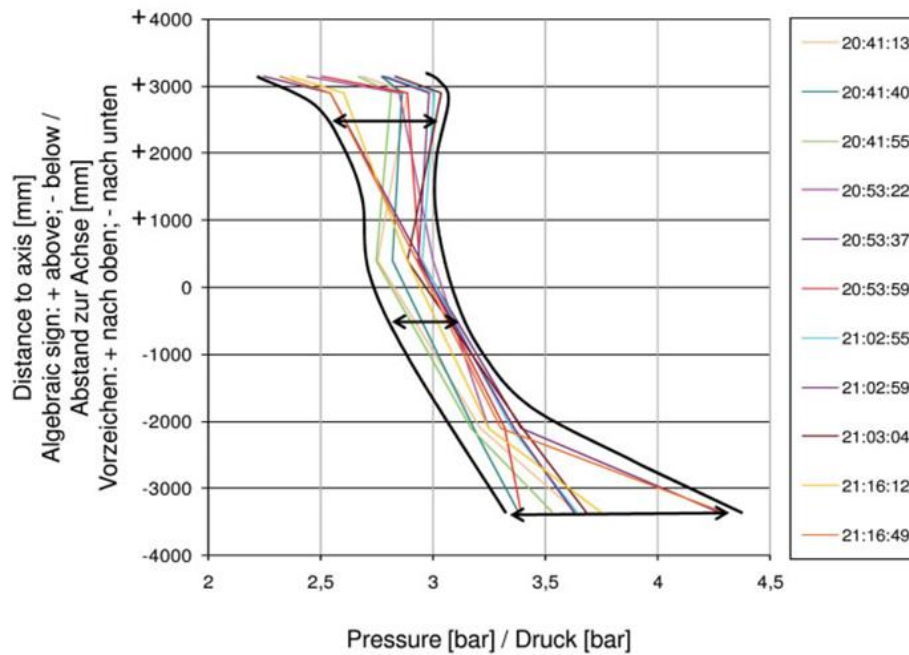
Figure 2-9: Analysis of earth pressure sensors at the bulkhead regarding the actual support pressure distribution of an EPB shield according to THEWES & BUDACH (2010b)

Furthermore, the unit weight of the support medium is yet not specified, neither for slurry nor for earth muck. ANAGNOSTOU & KOVÁRI (1994), SCHWARZ ET AL. (2006) for example assume a unit weight of 12 kN/m³ as for slurry; BABENDERERDE ENGINEERS GMBH (2014) assumes 14 kN/m³ as unit weight for the earth muck. Depending on the approach for the unit weight, the safety margin of face stability differs significantly (ZIZKA & THEWES (2015)).

Another approach for the analytical design of face stability can be made by using active limit state considerations, cf. DAVIS ET AL. (1980), KIRSCH (2009), KIRSCH & KOLYMBAS (2005), LECA & DORMIEUX (1990). Furthermore, besides analytical assessment, empirical (BROMS & BENNERMARK (1967)), numerical (e.g. KIRSCH (2009), VERMEER ET AL. (2002)) and even experimental (e.g. MAIR (1979)) investigations on the tunnel face stability can be conducted. For detailed information on the different assessments, see e.g. ZIZKA (2012).

3. APPROACHES IN NON-NEWTONIAN, GRANULAR FLUID RHEOLOGY

The pressure distribution is linked to the material fluidity. The more fluid the support medium is, the closer it is to the hydrostatic gradient (static limit state). The flow behaviour of the material in the chamber is evaluated by index testing and yet, only by some first more sophisticated rheological assessments. In order to determine a more sophisticated way of describing the flow behaviour of the support medium consisting of cohesionless soil and foam, approaches from related material sciences and fundamentals of flow dynamics and rheology have to be researched and analysed. Subsequently, basic flow patterns of non-Newtonian fluids are presented and discussed with regard to their transfer potential for the material contemplated here.

3.1   Rheology

Rheology is the science of flow of matter. Predominantly, it deals with matter in fluid state conditions, but also materials with solid-like properties showing a plastic flow behaviour under certain circumstances fall in the study of rheology. For the sake of convenience, in the following all types of flowing substances are accounted for "fluids". The fundamentals of rheology and rheological testing as presented subsequently are based on Brummer (2006), Chhabra & Richardson (2008), Mezger (2011).

3.1.1   Rheological parameters

The flow behaviour of fluids is described by the main rheological parameters, which are the shear-induced stress and the shear rate as well as the viscosity. These basic
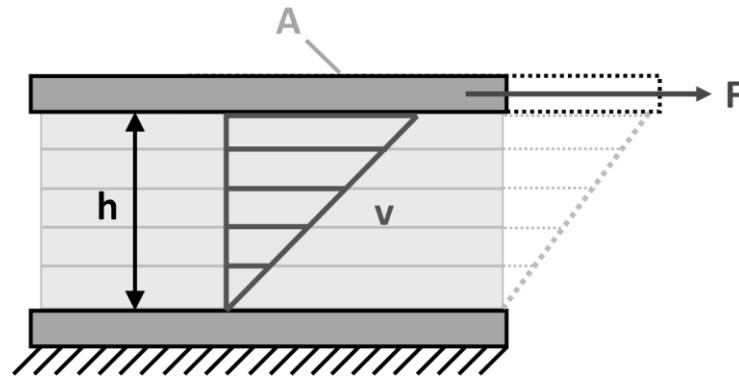
Figure 3-1: Newton's parallel plate model; with: F = shear force, A = plate surface area (shear area), h = gap distance, v = velocity

rheological properties can be best explained by Newton's parallel plate model (Figure 3-1). A fluid appears between two plates (gap distance h [m]). The upper plate with shear area A [m²] is agitated by the shear force F [N] and the resulting velocity v [m/s] is measured or vice versa. The bottom plate is fixed (v=0). The fluid is sheared within the gap restricted through the two plates. The rheological parameters can be derived from this model, when no slip effects on the plates' surfaces occur and the flow condition is laminar. Then, the shear stress τ and the shear rate $\dot{\gamma}$ can be calculated using Eq. 3.1 and Eq. 3.2.

$$\tau = \frac{F}{A} \qquad\qquad [Pa] \qquad\qquad Eq.\ 3.1$$

$$\dot{\gamma} = \frac{v}{h} \qquad\qquad [1/s] \qquad\qquad Eq.\ 3.2$$

The flow resistance the fluid shows towards the external agitation is connected to internal friction forces, which is described through the viscosity. The (shear) viscosity η can be calculated from Eq. 3.3. This equation also represents the Newtonian flow model for ideal viscous fluids, see chapter 3.1.2.

$$\eta = \frac{\tau}{\dot{\gamma}} \qquad\qquad [Pa{\cdot}s] \qquad\qquad Eq.\ 3.3$$

3.1.2 Classification of fluids: flow behaviour and viscosity

The flow behaviour and flow properties of fluids generally are dependent of the shear load, temperature and time. Thusly, fluids can be classed by their load-dependent flow behaviour, which is characterised by its shear rate-shear stress-interaction and its viscosity respectively. Fluid behaviour is distinguished into purely viscous, ideal

elastic and visco-elastic flow behaviour. The ideal viscous fluids can be described by the Newtonian model. Hence, fluids are classified into Newtonian fluids, i.e. ideal viscous fluids with constant viscosity, and non-Newtonian fluids. The latter group exhibits both elastic and viscous shares in the deformation behaviour, which leads to a non-proportional relationship between shear rate and shear stress. Therefore, the non-Newtonian fluids can be divided into shear-thinning and shear-thickening fluids, each with and without yield stress. With increasing shear rate, shear-thinning fluids show a rather reduced increase in shear stress, while shear-thickening fluids would show an increasing incremental growth. The yield stress represents a certain shear stress, which must be overcome first to initiate fluid flow and thusly, plastic or viscous deformation. In other words, it can be seen as shear strength for (soft) solids. Figure 3-2 qualitatively illustrates the stress-strain relationships for the different fluid types as introduced before.
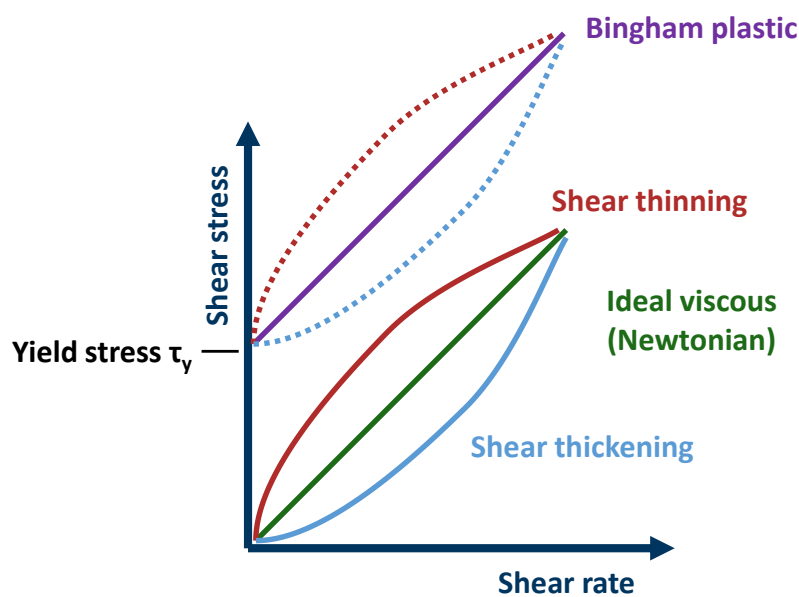
Figure 3-2: **Classification of fluid according to their shear stress-shear rate-relationship**

The shear rate-shear stress-relationship can be determined in rheometer testing through flow curve experiments. The same applies for the shear rate-viscosity-relation (viscosity curve). The data generated in testing usually consists of torque measurements and shear velocities. As described on the Newtonian plate model, the measurements have to be transformed into rheological parameters first. Then, an approximation of the data points by a model function can be conducted. Several constitutive flow models exist in order to describe the different flow patterns.

Ideal viscous fluids are described by the Newtonian model (Eq. 3.4).

$$\tau = \eta \cdot \dot{\gamma} \qquad\qquad [Pa] \qquad\qquad Eq.\ 3.4$$

Fluids without yield stress can be approximated with the model of Ostwald-de Waele (or power-law equation) (Eq. 3.5). Depending on the exponent p (form factor; [-]), the model either describes a shear thinning (p<1) or a Newtonian (p=1) or a shear thickening fluid (p>1).

$$\tau = k \cdot \dot{\gamma}^p \qquad\qquad [Pa] \qquad\qquad Eq.\ 3.5$$

with k the viscosity parameter [Pa·s].

The formulation according to Herschel-Bulkley exhibits the same form, but it is extended by τ_y [Pa], a summand for the yield stress (Eq. 3.6). When the yield stress is zero, the equation is similar to the power-law equation. If p=1, the Herschel-Bulkley model results in the Bingham plastic model.

$$\tau = \tau_y + k \cdot \dot{\gamma}^p \qquad\qquad [Pa] \qquad\qquad Eq.\ 3.6$$

The Bingham plastic model is a very common and simple model for fluids with yield stress (Eq. 3.7) but otherwise constant viscosity. Overcoming the threshold of yield, Bingham fluids show purely plastic flow.

$$\tau = \tau_y + k \cdot \dot{\gamma} \qquad\qquad [Pa] \qquad\qquad Eq.\ 3.7$$

Besides these models, a multitude of other approaches exists from several fields of applications. One of them used later in this study is a modified version of the Herschel-Bulkley model considering an extension by PAPANASTASIOU (1987), also known as Papanastasiou-Herschel-Bulkley model (Eq. 3.8), see MITSOULIS (2007).

$$\tau = a \cdot \dot{\gamma}^p + \tau^* \cdot \left(1 - e^{-m \cdot \dot{\gamma}}\right) \qquad\qquad [Pa] \qquad\qquad Eq.\ 3.8$$

wherein a is the fluid consistency factor [Pa·s^n], τ^* is the yield stress [Pa], and m is a factor controlling the stress growth at low shear rates [s]. p again is a shape parameter [-]. Thus, it is possible to capture courses of shear stress measurements with different performance at low and high shear rates suitably, which features a

description of the material response under shear loading in both the yielded and the unyielded region.

Another flow curve model is the Casson model (Eq. 3.9). It was originally applied to printing pastes and is often used to describe the flow behaviour of foodstuffs (especially chocolate melts), blood and other biological materials.

$$\sqrt{\tau} = \sqrt{\tau_y} + \sqrt{k \cdot \dot{\gamma}} \qquad\qquad [Pa] \qquad\qquad Eq.\ 3.9$$

Further models with and without yield stress consideration can be found for example in MEZGER (2011).

3.1.3   Rotational rheometry

In rheology, various types of tests are being performed in order to gain information about the rheological behaviour of fluids. Mainly it is distinguished into rotational rheometry, creep and relaxation testing and oscillation tests. In creep and relaxation tests (also named step strain test), the visco-elastic behaviour is investigated over a number of shear stress levels (creep test) and deformation levels (relaxation test) respectively. Both tests are applied rather rarely nowadays in applied rheology (MEZGER (2011)). More frequently oscillation tests are performed. The fluid is stimulated as in the Newtonian model (Figure 3-1), though the moving plate is oscillating fore and back. Thusly, a shear rate in waveform is applied and the resonance shear stress can be determined. There are two types of oscillation tests: amplitude sweep tests and frequency sweep tests. In amplitude sweep tests, the amplitude of oscillation is altered while the frequency is maintained constant. Accordingly, in frequency sweep tests, the frequency of stimulation is changed and the amplitude remains the same. From testing, the (complex) shear modulus, the storage modulus and the loss modulus can be derived, which provide information about the substance's (time-dependent) deformation behaviour. The deformation behaviour bears elastic and viscous shares. Furthermore, from the deformation behaviour the yield point can be determined.

In rotational rheometry, the flow behaviour of fluids can be investigated by experimentally determining their flow curves. Rotational rheometry generally means that a rotation is applied onto a testing sample. Often, some kind of shearing body

(rotor) rotates in the material at pre-defined speeds or deformation rates. By doing so, torques are obtained which in turn can be transformed into rheological parameters taking into account the very specific flow conditions. Several test methods and measuring profiles and geometries exist for such flow curve experiments. This is why established procedures and setups shall be introduced in more detail in the following and furthermore, how a conversion of data into rheological parameters can be approached.

3.1.3.1   *Testing procedures*

Flow curve tests can either be conducted stress- or rate-controlled. Thus, the default measuring profile consists of either a predefined velocity (shear rate) or shear stress function over time. Depending on what is aimed at, the testing profile is selected. Determining flow and viscosity curves, the profile usually has the form of a (linear or logarithmic) ramp (Figure 3-3) or a step-like distribution (Figure 3-3). Time-dependent behaviours of fluids often are investigated either at constant values of shear rate or shear stress (Figure 3-4), or by using hysteresis profiles (i.e. first increasing the default value, then decreasing again; Figure 3-4). Restructuring effects under certain loadings are one example for time-dependent patterns that can be evaluated thusly. The temperature in flow curve tests usually is kept constant in order to avoid further influences on the results. An exception are temperature rate-controlled experiments. Table 3-1 summarises common test profiles and their benefits for the different rheological applications.
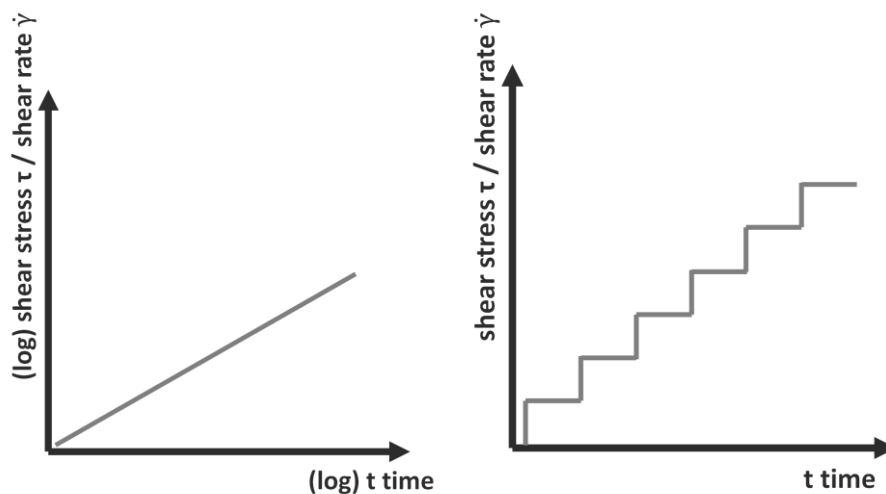
Figure 3-3:   Typical profiles in flow curve experiments I: linear / logarithmic ramp (left) and step-like profile (right)
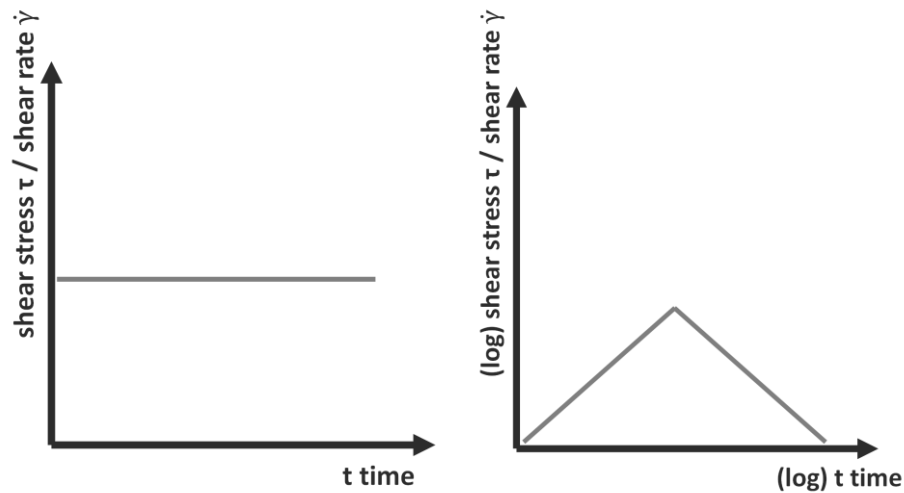
Figure 3-4: Typical profiles in flow curve experiments II: constant shear rate (left) and hysteresis loop (right)

Table 3-1: Typical profiles in flow curve experiments applied in rotational rheometry

Profile	Description	Test outcome
Step-like profile	Shear rate/shear stress is maintained for a certain time and then repeatedly increased to the next level	Flow curve, viscosity curve
Constant value	Shear rate is maintained constant	Time-dependent evolution of the shear stress
Linear ramp	Shear rate/shear stress is continuously increased	Flow curve, yield point (when shear stress is increased)
Logarithmic ramp	Shear rate/shear stress is logarithmically increased	Flow curve
Hysteresis loop	Shear rate/shear stress is increased to a maximum value and then decreased again; step-like or ramp profile possible	Analysis of time-dependent behaviour, evaluation of restructuration effects

Besides the presented profiles, it can be beneficial to implement resting times or a period of pre-shear. Measuring systems dipping into the sample may cause disturbances and the material might require a certain time to relax. Other experiments might need a certain pre-shearing of the material in order to overcome retardation effects, acceleration effects or material inhomogeneity.

Time is an important factor in rheometry. Rheometry is distinguished into low-shear ($\dot{\gamma} < 1$ 1/s) and high-shear ($\dot{\gamma} > 1$ 1/s) testing. Especially when shearing in a low-shear range, a certain time is necessary in order to assign the whole shear gap with the defined shear rate. The retardation of each shear layer to take over the shear rate is defined as transient viscosity effect. Yet, in order to gain significant results, a steady state in viscosity is needed. Hence, the data-sampling rate has to be adjusted. In literature, a minimum data-sampling rate equal the corresponding reciprocal shear rate value is recommended, see e.g. MEZGER (2011). Therefore, in flow curve tests that cover several magnitudes of shear rate or shear stress, it is advantageous to use a logarithmic ramp profile. In this manner, shear responses can be obtained within the low-shear range as well as in the high-shear range. Transient flow effects, which can arise during logarithmic augmentation of shear, have to be countered with variable measuring point durations. Normally, the times between the single measurements during the test is maintained constant for the reason of simplicity.

The temperature in flow curve tests usually is kept constant in order to avoid further influences on the results. An exception are temperature rate controlled experiments.

3.1.3.2   *Measuring systems and conversion of raw data*

In rotational rheometry, mainly three types of measuring systems are applied: concentric cylinder, cone-plate and plate-plate (parallel plate) configurations. These measuring systems are described in DIN 53019-1 (2008-09). Besides those, other measuring systems exist in various designs, very often adopted and modified for countless applications. This group often is referred to as relative measuring systems. The geometry and configurations often are too complex to find a simple conversion approach between measurable data (e.g. torque and rotational speed) and rheological properties (e.g. viscosity, shear stress), to describe the flow in the system and to incorporate all side and boundary effects (slip, fractions of viscous and form

drag etc.). The most commonly used measuring systems and selected relative systems, which are of relevance for this study, are presented subsequently.

1. Plate-plate and cone-plate configuration

Both setups consist of one stationary plate at the bottom and the rotary upper part (plate or cone). The cone exhibits an angle usually between 1° and 4°; the plate is plane and has a smooth surface. The minimum recommended diameter for both is 20 mm. The sample gap between needs to be filled completely. When investigating granular fluids, the maximum particle-size should be limited to one fifth of the gap width between upper device and bottom plate (DIN 53019-1 (2008-09)). In any case, the gap width H should be always much smaller than the rotor radius R. The cone-plate measuring system and the parallel plate measuring system are illustrated in Figure 3-5.

Both systems exhibit advantageous features. Using the cone-plate system, homogenous shear conditions are achieved due to constant shear rates in the entire gap. The plate-plate system does not reach constant shear rate values within the whole gap but it enables measuring fluids containing larger particle-diameters. This however can benefit secondary flow effects.
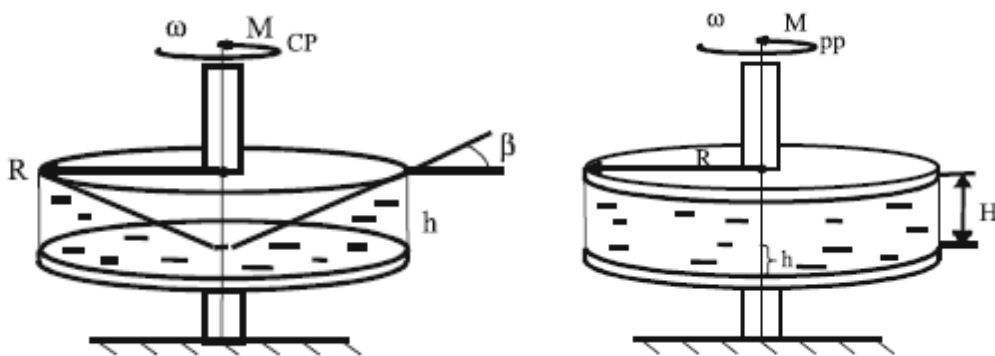
Figure 3-5: Cone-plate system (left) and plate-plate system BRUMMER (2006)

Conversion of raw data (torque M [mNm] and rotational speed N [1/min]) into the rheological parameters τ and $\dot{\gamma}$ can be done by using Eq. 3.10 and Eq. 3.11 for the cone-plate configuration and Eq. 3.12 and Eq. 3.13 for the plate-plate configuration respectively, see DIN 53019-1 (2008-09). The viscosity then can be calculated again according to the Newtonian model as shown in chapter 3.1.1.

Cone-plate configuration:

$$\tau = \frac{3}{2\pi \cdot R_c^3} \cdot M \qquad\qquad [Pa] \qquad\qquad Eq.\ 3.10$$

$$\dot{\gamma} = \frac{6}{\alpha_c} \cdot N \qquad\qquad [1/s] \qquad\qquad Eq.\ 3.11$$

with R_c the cone radius [mm] and α_c the cone angle [°].

Plate-plate configuration:

$$\tau = \frac{4}{3\pi \cdot R_p^3} \cdot M \qquad\qquad [Pa] \qquad\qquad Eq.\ 3.12$$

$$\dot{\gamma} = \frac{\pi \cdot R_p}{45 \cdot h} \cdot N \qquad\qquad [1/s] \qquad\qquad Eq.\ 3.13$$

with R_p the plate radius [mm].

2. Concentric cylinder configuration

The concentric cylinder configuration consists of a cylindrical sample beaker (cup) and an inner cylindrical measuring geometry (bob), both of them with the same rotational axis. The gap between cup and bob needs to be very narrow in order to apply the Newtonian model and its derivation of rheological parameters. Otherwise, secondary flow (Taylor vortices and turbulent flow), transient effects or inhomogeneous deformations may occur. The limitation of the shear gap is defined in DIN 53019-1 (2008-09) especially over the (squared) ratio of the inner and outer cylinder radii: $R_e/R_i = 1.0847$ or $(R_i/R_e)^2 = 0.85$. When using bigger shear gaps, the rheological parameters are often related to the bob surface. The concentric cylinder measuring system and its geometrical definitions are displayed in Figure 3-6.

In general, two modes of operation exist. Either the cup is rotated while the inner cylinder is maintained stationary (Couette method), or the cup is stationary and the bob is at motion (Searle method). The latter one is more commonly practiced.

The biggest advantage of this measuring system is that the testing fluids cannot flow off the shearing gap, as they could in the cone-plate or plate-plate setup; even at high rotational speeds or low viscosities. However, the filling process and especially the
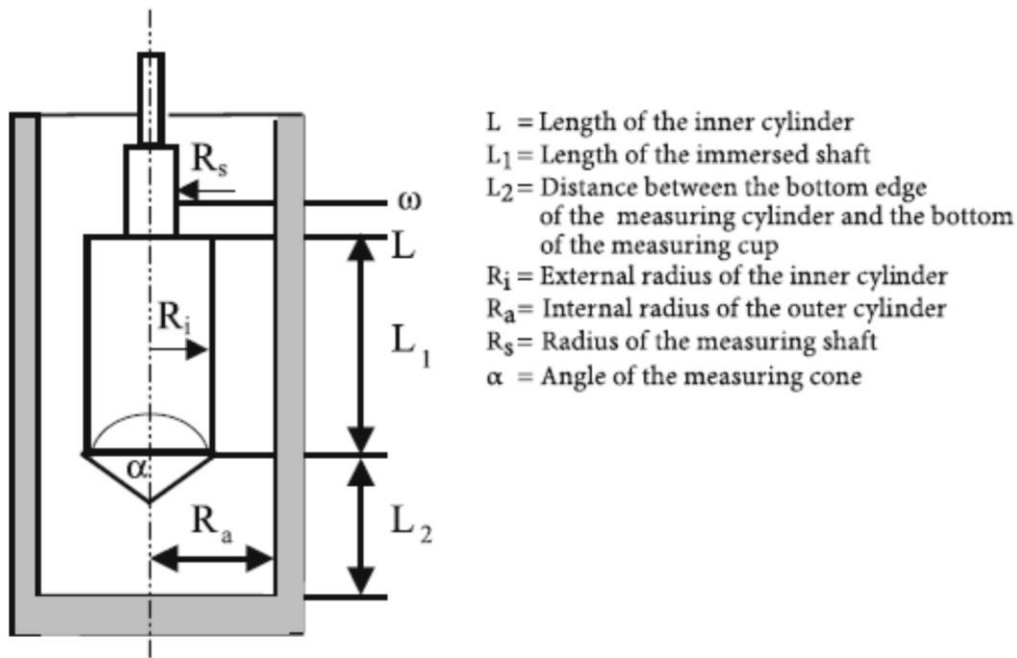
Figure 3-6: **Concentric cylinder system according to DIN 53019-1 (2008-09); taken from** BRUMMER **(2006)**

dipping process of the bob into the sample container is difficult and bears the danger of air entrapments.

The conversion of raw data into the rheological parameters τ and $\dot{\gamma}$ can be done by using Eq. 3.14 and Eq. 3.15 for the narrow gap according to DIN 53019-1 (2008-09) related to the middle of the gap.

$$\tau = \frac{1}{2\pi \cdot L \cdot R_i^2 \cdot c_L} \cdot M \qquad\qquad \text{[Pa]} \qquad\qquad \text{Eq. 3.14}$$

$$\dot{\gamma} = \frac{2\pi \cdot (1 + \frac{R_e^2}{R_i^2})}{60 \cdot (\frac{R_e^2}{R_i^2} - 1)} \cdot N \qquad\qquad \text{[1/s]} \qquad\qquad \text{Eq. 3.15}$$

with L the bob length (height) [mm], R_i the bob radius [mm], R_e the cup radius [mm], and c_L the end-effect correction factor (1.10 for conical shape, for plane shape see annotations in DIN 53019-3 (2008-09)) [-].

Multiphase fluids containing particles of increased size require a larger gap because otherwise the fluid cannot be considered as continuum anymore (BARNES (1995). The particle scale would be much more significant than the liquid scale. DIN 53019-1 (2008-09) recommends a maximum particle-size not exceeding 20% of the present gap distance in the testing device. However, a large gap can lead to unsteady shear

conditions. Therefore, the rheological data usually is related to the bob surface (MEZGER (2011)). Eq. 3.16 and Eq. 3.17 should be used for large gap configurations to calculate the rheological parameters from the measurements.

$$\tau = \frac{1}{2\pi \cdot L \cdot R_i^2} \cdot M \qquad\qquad [Pa] \qquad\qquad Eq.\ 3.16$$

$$\dot{\gamma} = \frac{4\pi \cdot R_e^2}{60 \cdot (R_e^2 - R_i^2)} \cdot N \qquad\qquad [1/s] \qquad\qquad Eq.\ 3.17$$

The viscosity can be calculated again according to the Newtonian model as shown in chapter 3.1.1.

3. Systems with treated surfaces

The concentric cylinder measuring system and the parallel plate system both feature the possibility to modify the shearing surfaces. Smooth surfaces benefit slip effects because of intermediate fluid layers with high velocity gradients between the fluid and the surface material, see BARNES (1995), DENKOV ET AL. (2012); see also chapter 3.1.3.3. This of course depends on the viscosity and the surface material. In order to reduce the occurring slip, the plate and cylinder surfaces are often treated. This can be done by gluing sandpaper with different degrees of roughness to the surface area, compare ÖZARMUT ET AL. (2013), or by sandblasting. Another way is to manufacture plates, bobs and cups with serrated or profiled designs, see MEZGER (2011). The degree of roughness and the serration/profile depth has a significant influence when working with granular fluids, since the grains might enter the uneven surfaces. Furthermore, the laminar flow conditions might be disturbed by treated surfaces leading to turbulent flow and vortices, particularly in the boundary layers.

4. Vanes, paddles and spindles

Relative measuring systems are manifoldly existent by field of application or design. However, the measuring principle remains usually the same. A conversion of the measured parameters (torque, deformation) cannot be done easily, which is why rheological data is specified in relative values (e.g. "relative viscosity"). This data cannot be compared to absolute rheological values obtained in precise rheometry, except for some correlation approaches after many comparative tests. The cause for this lies within the complex flow field generated through the geometrical system design. Spindles, paddles and vanes create secondary flow effects such as local

turbulent flow conditions or vortices. Nevertheless, for the generation of homogeneous shear conditions and thus the application of Newton's plate model and the determination of the rheological parameters, laminar flow conditions are substantial.

For instants, commonly used relative systems for rheological applications in the field of granular fluids (suspensions containing mineral particles, cementitious materials, soils) are:

- **four-bladed or six-bladed vanes (Figure 3-7)**

  Vane impellers have the advantage of immersion into a sample without influencing the sample structure too severely, cf. BARNES & NGUYEN (2001). Once at motion, the failure body acts as a rotating cylinder, particularly in very stiff materials, compare Figure 3-7. Thus, wall slip effects might be prevented in contrast to smooth cylinder surfaces (BARNES (1995), MEZGER (2011)). Shear vanes represent a common field test device in soil mechanics. Based on DIN 4094-4 (2002-01), the shear strength c_{fv} (field vane shear strength) of the soil can be estimated in dependence of the required torque to overcome the material resistance, M_{max}, (Eq. 3.18). Required preconditions of this assumption are an aspect ratio of $H = 2 \cdot d$ (H = vane height, d = vane diameter) and an equally distributed stress distribution on the cylinder surfaces.
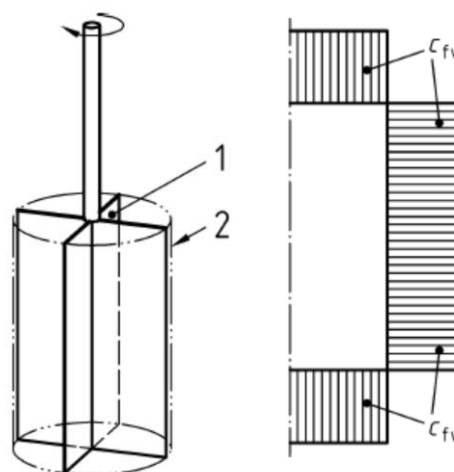
Figure 3-7:   **Shear vane system according to DIN 4094-4 (2002-01): assumption of cylindrical failure body (left), equally distributed shear stress c_{fv} on the lateral and end surfaces of the cylinder**

$$c_{fv} = \frac{6 \cdot M_{max}}{7\pi \cdot d^3} = \tau \qquad\qquad [Pa] \qquad\qquad \text{for H = 2·d} \qquad\qquad \text{Eq. 3.18}$$

- **paste spindles (Figure 3-8)**

  Paste spindles are applied in material sciences for example for the investigation of fresh mortars or other similar pasty materials. An interpretation of the obtained measurements through rheological parameters oftentimes is not feasible or can only be seen as device-specific parameters.

- **paste paddles (Figure 3-8)**

  Lime paddles are widely used for the stirring and the rheological characterisation of dispersions, such as cement limes or plasters, containing only small particles. The lime paddle resembles a two-bladed vane with grand openings. Hence, the testing fluid surrounds the vertical bars from two sides. Furthermore, the gap between these bars and the container wall is designed very narrow. Therefore, the maximum particle-size within the testing fluid is limited.
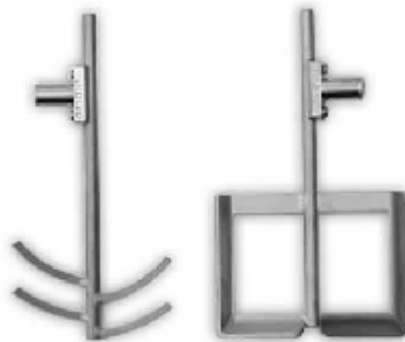
Figure 3-8:   Examples for paste spindles (left) and paddles; both pictures from SCHLEIBINGER GERÄTE TEUBERT U. GREIM GMBH (2015b)

5. Ball measuring system

The ball measuring system is designed in a way that a sphere (diameter d_{Sphere}) is rotating eccentrically (eccentric radius L_{Sphere}) on a circular path in a sample cup (Figure 3-9b). First appearances date in the 1990s, see MÜLLER ET AL. (1999), JP3388621(B2) (2003), JP7229823(A) (1995), with a main field of application for plasters and mortars. Up to now, only few approaches using the ball measuring system have been established, because its rheological interpretation especially in non-Newtonian fluids is quite complex. The analysis of results is not based on laminar flow conditions only, but also on displacement flow. Form drag and viscous drag

appear on the sphere surface, when drawn through the material. Approaching the conversion of raw data into rheological parameters is therefore quite challenging. Moreover, a comparison of the attained values of the ball measuring system with absolute rheological values of setups according to DIN 53019-1 (2008-09), as presented afore, is not feasible. However, the use of this measuring system enables the rheological investigation of granular materials even with large particle-sizes, cf. SCHATZMANN ET AL. (2009). Existing setups consist of sphere diameters d_{Sphere} ranging from 8-20 mm; the cup has a volume of approximately 500 ml. The eccentricity is around 35-40 mm. The theoretical background and the approaches of data conversion for different fluids, which have been developed so far for the ball measuring system, will be presented in detail in chapter 7.3.2.1 in order to highlight the complexity. The experimental procedures, the aims of testing and the attained findings will be presented briefly in chapter 3.2.
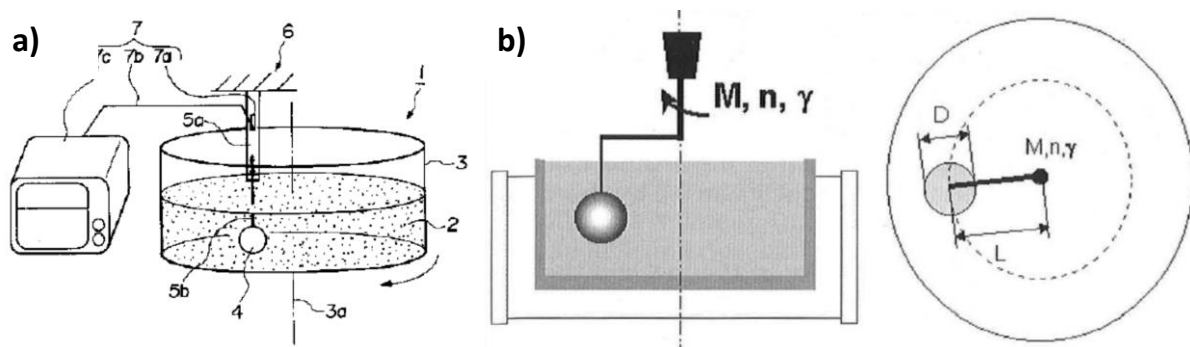
Figure 3-9:   **System sketches of the ball measuring system; a) according to JP3388621(B2) (2003), JP7229823(A) (1995), b) according to MÜLLER ET AL. (1999)**

3.1.3.3   Wall slip

A generally applied boundary condition in fluid dynamics is the so-called no-slip condition. It says that at a solid boundary (wall), the velocity of viscous fluids will be zero, see CHHABRA & RICHARDSON (2008). When investigating flow patterns of non-Newtonian fluids, it is often observed that the no-slip condition is not valid anymore. Small layers exhibiting a reduced viscosity occur between the bulk fluid and the confining wall. This condition is defined as wall depletion or slip effect (BARNES (1995)). Within these small residual layers (boundary layers), high velocity gradients can occur. Hence, the boundary layer can act as lubricant resulting in an increased flow rate of the bulk fluid and it thusly even benefits several engineering applications. This appears particularly for multiphase fluids like colloidal dispersions because the

disperse phase (e.g. particles) is moving away from the solid walls. Furthermore, smooth walls and large shear gaps benefit depletion (BARNES (1995)), which can lead to contradictory design criteria. Looking back on the constraint that the maximum particle-size within a testing fluid should be limited to 20% of the gap width, suspensions containing large-particles require large-gap configurations in order to confirm a continuum description of the material. In contradiction, the gap should be as narrow as possible in order to limit wall slip influences, see BARNES (1995). However, wall slip can influence the results determined in rheological investigations significantly. Applying constant shear rates, wall slip effects result in reduced shear stresses compared to what was expected, cf. CHHABRA & RICHARDSON (2008). Interpretation of data can then produce artefact effects (DENKOV ET AL. (2012)).

Frequent occurrences are encountered between the rotor or container surfaces of the rheometer and the testing fluid. Therefore, adequate contemplations have to be taken into account, which neutralise the error from wall slip. Common counter-acting approaches consider either adjustments in the design of the test equipment (surface treatments; see chapter 3.1.3.2 and BARNES (1995), BARNES & NGUYEN (2001), MEZGER (2011)) or customised correction models. Model developments quantifying the slip usually assume a slip velocity, which is linked to the wall shear stress. This dependency has to be assessed realistically in order to consider the slip effects in the results, cf. CHHABRA & RICHARDSON (2008).

3.2   Investigations on the flow behaviour of colloidal dispersions

Heterogeneous systems containing two usually immiscible media, whereof one is particles or drops, are defined as colloidal dispersions (YARIV & CROSS (1979)). Examples for colloidal dispersions can be foam (gas dispersed in liquid), emulsions (mixture of two liquids), gels (liquids dispersed in solid), suspensions (solids dispersed in liquid), or sols (solids in gas or solids). Approaching the flow behaviour, or rheology, of soil-foam mixtures, one key question is to discuss the type of dispersion. One might consider this material as a foam containing particles or as foam-enriched soil. This probably relies on the different volume fractions, of which the mixture is composed. Therefore, the rheology of selected colloidal dispersions linked to this study is surveyed. A particular review of the rheology of both components, foam and soil, is essential for the methodological approach. Furthermore, experimental

assessments of the flow behaviour of soil-foam mixtures are introduced in more detail compared to chapter 2.4.2. In the last subchapter, investigations of the flow behaviour of cementitious materials are presented because they of similarities in some extend to EPB support material – especially regarding possible maximum grain-sizes. Gaining information on research strategies, on possible challenges and questions of importance, on boundary problems, and on the flow behaviour of these materials, first expectations and limitations of this study might be phrased based upon this literature research. The literature review focuses particularly on experimental approaches. Analytical models are presented occasionally, in case of significance. Numerical attempts are pointed at briefly in chapter 3.2.5.

3.2.1   Rheology of foams

Apart from other essential properties like for instance morphology (see WEAIRE ET AL. (2012)) and drainage behaviour (see KOEHLER (2012)), which are not of main interest in this study, several authors have analysed flow properties of foam. Particularly flow curve tests have been performed to determine the flow behaviour and to find an adequate flow model. KROEZEN ET AL. (1988) used a coaxial Brabender viscometer to investigate foamed aqueous solutions containing lauryl sulphate and different concentrations of thickener. The measuring system consisted of different configurations considering both smooth and profiled surfaces. Two aspects were of main interest for the authors: one aspect was the analysis of the slip effect and a second objective was the investigation of structural change under shear load. The results of the experimental data were obtained using a "hysteresis linear ramp" profile (0 - 500 rpm) and were fitted with a power-law model. KHAN ET AL. (1988) determined the foam viscosity as a function of shear rate for different gas volume fractions by using a plate configuration of the Rheometrics Mechanical Spectrometer RMS7200. In order to minimise slip effects between the foam and the metal plates, sandpaper was glued to the plates. Stress relaxation tests were performed on the different foam samples leading to information on the yield stress in a low shear rate range ($\dot{\gamma}$<1 1/s). Furthermore, they conducted amplitude sweep tests determining the foam viscosity. They found foam to behave like a shear-thinning fluid. DENKOV ET AL. (2012) summarise the foam rheology as follows: under small shear stresses, foams behave like soft solids; beyond the yield stress, foams show a shear-thinning flow behaviour.

Most important in the rheological analysis of foams is the consideration of wall slip effects in the experiment and the maintenance of the foam properties over the duration of testing (HöHLER & COHEN-ADDAD (2005)). Wall slip can be reduced either by roughening the confining walls or by adequate modelling of the slip boundary condition, i.e. the determination of the viscous stress acting on the wall surface under the residual slip shear rate (see 3.1.3.3). Slippage between foam and wall is also a focus of the study of DENKOV ET AL. (2005). By performing rheometer tests on foams using a parallel plate measuring system with both a sandpaper-sandpaper and a sandpaper-glass configuration, they could analyse the viscous friction within the foam and the foam-wall friction. Additionally, they found the Herschel-Bulkley model adequately describing the stress behaviour of foam.

Foams were also investigated by MAIDL (1995). He developed a large-scale capillary viscometer based on SCHULZE ET AL. (1991) in order to determine yield stress properties of foams used in EPB tunnelling. However, a stagnation within the capillary (represented by a hose) was not achieved and thus a determination of a yield stress was not possible. During the extrusion of foam from the hose, a plug flow of the foam on a small fluid film was observed, which means that the no-slip condition at the inner wall seemed not to be valid.

3.2.2   Soil rheology

V̄IALOV (1986) refers the rheology of soils to creeping and consolidation processes. The application of the rheological Kelvin-Voigt model in consolidation theories is a common example in soil mechanics, cf. KRIZEK (1984). MARKGRAF (2011) extends this view to the deformation characteristics of soils. She founds this on a description of soils as viscoelastic material due to elastic and plastic strain behaviour. As mentioned in chapter 3.1.2, viscoelastic fluids possess likewise elastic and plastic fractions of shear responses. According to KRIZEK (1984), the soil deformation behaviour probably benefits from the visco-elastic theory but the degree of enhancement of the outcome may not justify the effort.

A rheometer for the determination of visco-plastic parameters of soils was developed by KARMAKAR & KUSHWAHA (2007). It is based on the principle of a turning shear vane. Investigations were performed at pre-defined constant vane speeds on a soil composition of clay (29%), silt (24%) and sand (47%) with different water contents

and different levels of compaction. The resulting measured torques were translated into shear stresses by the vane shear model as proposed in DIN 4094-4 (2002-01). The peak torque of the single measurements was defined as shear strength. A distribution of the shear strength values over the corresponding shear rates of one sample was fitted with the Bingham model. Thusly, effects of the moisture content and the compaction onto the rheological behaviour could be elaborated. The device is shown in Figure 3-10.
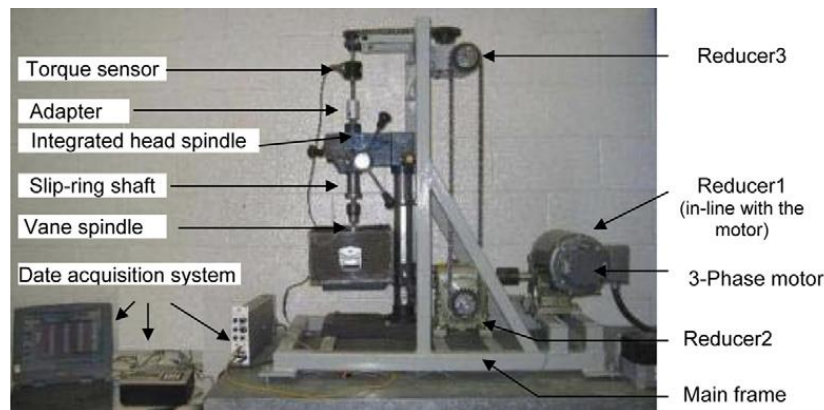
Figure 3-10: Soil rheometer of KARMAKAR & KUSHWAHA (2007)

LUBE ET AL. (2005) performed column failure tests with several dry granular materials (sands, sugar, and rice). Column failure tests to some extend can be linked to slump tests, since at the beginning of the experiment, the material is held in a certain form and then suddenly released from it and its movement is analysed. The basic principle is displayed in Figure 3-11. The aim of LUBE ET AL. (2005) was a two-dimensional description of the movement of the granular column and of the final shape. Therefore, they used acrylic glass containers of different aspect ratios and high-speed video cameras. During movement, they observed that the main flow occurred above the material forming the bottom layer, which – once in contact with the bottom – remained stationary. The kinematics of the flow front could be derived from the camera recordings. Additionally, the run-out distance could be approximated by a power-law function considering the aspect ratio up to certain limitations.

Overall, it is more common to derive stability parameters of pure soils from oedometer, triaxial and shearbox tests. At this point, the applicability of rheometry to soils is more valuable to the study. Nonetheless, these standard procedures from soil mechanical testing will be further considered in the context of conditioned soils (chapter 3.2.3), particularly the transferability of these tests to soil-foam mixtures.
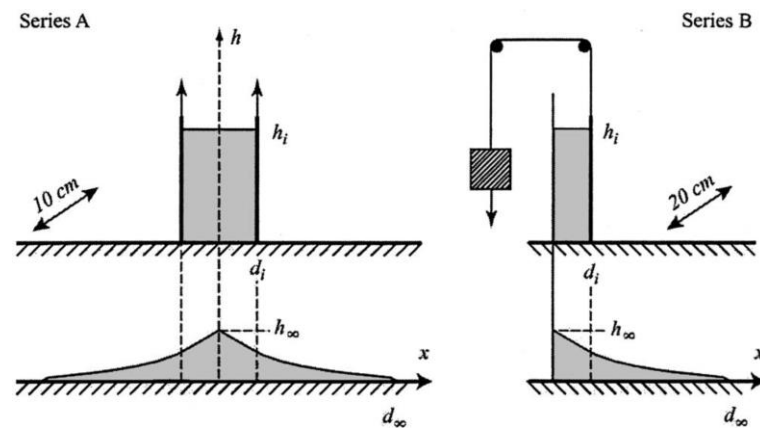
Figure 3-11: Principle of the column failure tests according to LUBE ET AL. (2005)

Yet, the application of rheometry in soil mechanical investigations is uncommon but becoming progressively more important (MARKGRAF & HORN (2005)). More often, it is applied to suspended soils (e.g. clay slurries), to debris flows and to mudflows (highly concentrated suspensions). Experience from rheological testing of these media is presented in the following.

3.2.2.1   *Rheology of mineral-based particle-suspensions*

The rheology of mineral-based particle-suspensions has been assessed widely both in science as in practice. Depending on the distinct properties such as the consistency, suspensions can exhibit several flow patterns but most frequently, the flow behaviour of particle-suspensions are characterised non-Newtonian, see API RECOMMENDED PRACTICE 13D (2010-05), LUCKHAM & ROSSI (1999), YARIV & CROSS (1979). Numerous test methods are applied on various types of suspensions in order to gain information on their flow properties and most of them have become standards in their specific area of application. However, only few of these tests provide quantitative information on the actual flow behaviour. It is more likely to assess properties as the yield stress or the viscosity via index tests. Commonly applied test methods for such suspensions are regulated in norms as for example API RECOMMENDED PRACTICE 13D (2010-05), DIN 4127 (2014-02). One of them is the Marsh cone (Figure 3-12), a flow-out test. From a measurement of specific flow-out times, conclusions can be drawn regarding yield stress or viscosity. Another example is the Ball Harp (Figure 3-12). It gives information on the yield stress of the suspension. A set of spheres with different dimensions and unit weights are dipped into the testing fluid. Based on the fluid surface tension and the fluid yield stress, the last subsiding ball and the first non-sinking ball provide information on the yielding

properties. However, all information gained through these tests are incomparable to each other due to the different shear or flow conditions, which is why the obtained properties should indicate the used testing instrument, cf. MEZGER (2011). There have been some recent assessments determining flow curves from index testing, see GHORBANPOUR AKBARABADI (2013), SCHÖßER & THEWES (2015).

Nevertheless, rheological experiments with rheometers on suspensions are belonging by now to common practice, too. An often-applied rheometer on suspensions is the FANN Model 35a (Figure 3-12), which is based on the recommendations in API RECOMMENDED PRACTICE 13D (2010-05). It is a concentric cylinder type rheometer with mechanical measurement of the torque.

Figure 3-12: Recommended test methods determining flow properties of bentonite slurries: Marsh cone (left), ball harp (middle) and FANN rotational viscometer Model 35a.

HEINZ (2007) summarises several state-of-the-art test methods applied on suspensions, both index tests and rheometers. Furthermore, she conducts experiments using different methods (index tests: Marsh cone, kasumeter according to SCHULZE ET AL. (1991), ball harp; rotational rheometry) for a comparison of the resulting rheological parameters of pure and modified bentonite slurries. In the rheometer experiments, the parallel plate system and the ball measuring system were used. Flow curve tests and amplitude sweep tests were performed in order to obtain the yield stress and the viscosity.

3.2.2.2   Rheology of debris and mudflow material

The rheology of fine-grained debris materials was investigated by JEONG (2006), JEONG ET AL. (2009). The various test samples were composed of different clays and fine soils representing real debris flow materials and highly concentrated suspensions.

Rheological investigations on these samples were executed using a rotational rheometer with concentric cylinder measuring system and a laboratory shear vane. Within a shear rate of 1 - 1,000 1/s the flow behaviour of the investigated soils was found to behave according to the power-law model.

Rheological investigations on suspensions and debris flow materials containing large particles (up to 25 mm) were conducted by SCHATZMANN (2005), SCHATZMANN ET AL. (2009) through a comparative experimental study. The flow behaviour was assessed with index tests (slump test, inclined plane/channel test and a capillary rheometer) as well as with rheometry (BML Viscometer, Large-scale Coaxial Cylinder Rheometer and MCR Rheometer with ball measuring system (Figure 3-9)). An analysis of the results should provide information of the applicability of the different test methods to complex colloidal suspensions. As will be introduced in chapter 7.3.2.1, the adaption and calibration of the ball measuring system was one key issue in the investigation. Flow curve tests were performed on debris flow material with the ball measuring system and the resulting shear stress distributions, which are based on the developed approach, were compared to the results of the other rheometers. The flow curves obtained with the three rheometers were all in the same range of shear stress and could be fitted adequately by the Herschel-Bulkley model. Furthermore, the yield stress was derived from index tests for different concentrations of particles. The inclined plane/channel test was conducted as proposed by COUSSOT & BOYER (1995), the capillary rheometer (kasumeter) followed SCHULZE ET AL. (1991) and the slump test was performed according to PASHIAS ET AL. (1996) with a slump cylinder instead of a cone. The determination of the single yield stresses of each tests followed the approaches of the correspondent authors. Deviations were less than 30% compared to the yield stresses from the flow curve approximations.

COUSSOT & BOYER (1995) investigated the flow behaviour of mudflow materials resembling clay-water mixtures. Therefore, they used an inclined plane test depicting an open channel, in which the flow profile of the testing material was determined after the fluid reached the final position and was at rest. From the final geometrical heights of the profile (see Figure 3-13) and the channel aspect ratio, assuming a Herschel-Bulkley fluid behaviour, and based on the theory of steady free surface flow, COUSSOT & BOYER (1995) could develop an approach of obtaining the fluid yield stress. Considering a variation of the channel inclination, different shear rates could be
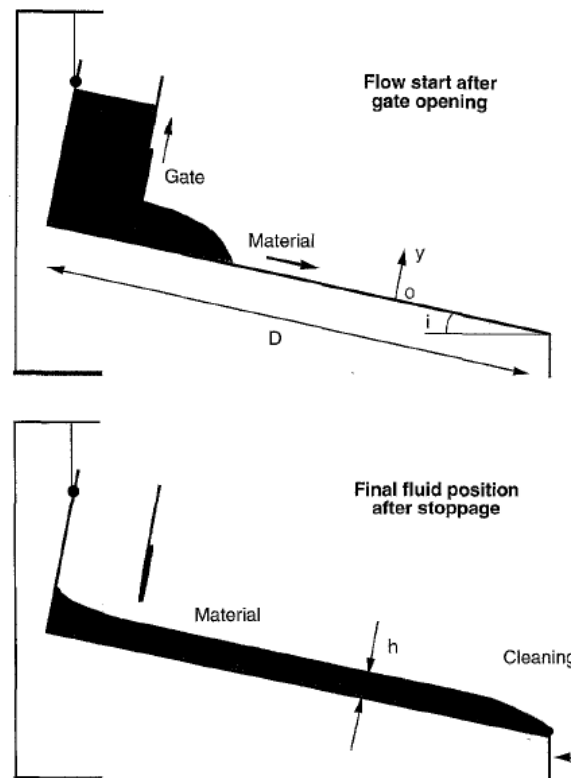
Figure 3-13: Principle of the inclined plane test according to Coussot & Boyer **(1995) showing the fluid state just after beginning to flow (top) and in the final position at rest**

generated. Comparative tests were performed using a rotational rheometer with plate-plate and cone-plate configurations. Fitting the data was possible with the Herschel-Bulkley model. Thusly, a comparison of the flow curves attained with both devices was possible.

3.2.3   Rheology of conditioned soils

The experience from lab testing of conditioned soils (chapter 2.4.2) showed that there are some approaches to describe the flow behaviour, or the workability, of conditioned soils. The mostly applied method to describe the material flow is the slump test according to DIN EN 12350-2 (2009-08), which can only work as index test because actually no flow properties are being determined. A summary of various investigations on the workability of conditioned soils using the slump test and resulting recommended slump ranges can be found in Budach (2012), Vinai (2006). Thereof, slumps between 10 and 20 cm have been reported as suitable workability for EPB applications, which goes along with slump classes S3 and S4 according to DIN

EN 206 (2014-07), see 3.2.4. Besides these common approaches, other assessments of the flow behaviour of conditioned soils shall be presented in the following.

However, there is actually not much known about the rheological behaviour of particle/soil-foam mixtures and the application of rheometry so far is rare. COHEN-ADDAD ET AL. (2007) investigated viscoelastic properties of particle-laden foams in amplitude sweep tests using a rheometer with both cone-plate and plate-plate measuring system. The contact surfaces were profiled in order to reduce slip effects. The testing mixture consisted of shaving foam (Gillette) and glass or carbon particles of varying volume fractions. Increasing contents of particles influence the rheological parameters but not the basic flow pattern up to a certain volumetric ratio.

Based on the work of KARMAKAR & KUSHWAHA (2007), MENG ET AL. (2011) designed a pressure cell enabling rheological testing of conditioned sandy silts under backpressure. The pressure cell consists of a four-bladed vane, which is connected to and which is agitated by the motor drive (Figure 3-14). The material consisting of silt and sand, water, foam, and bentonite slurry is prepared in advance under ambient pressure conditions and then filled into the testing apparatus. After closing of the cell, a gasbag is inflated and thusly increasing the pressure within the device up to 400 kPa for 10 minutes as pre-compression. After that, testing is performed at different constant turning speeds of the vane between ranging from approximately
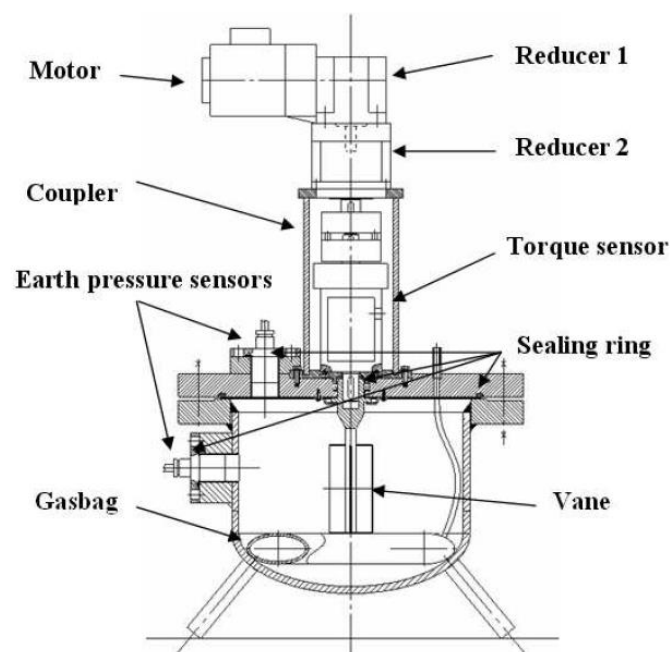
Figure 3-14: Cross sectional sketch of the shear vane apparatus of MENG ET AL. (2011)

0.03 to 0.3 rpm and at different confining pressure conditions of 0 to 400 kPa. Data conversion is performed according to the proposed model of DIN 4094-4 (2002-01) and the resulting, pressure dependent flow curves are approximated by the Bingham plastic model.

MESSERKLINGER ET AL. (2011) developed a similar shear vane apparatus. It was applied for the analysis of the effect of conditioning agents on the shearing behaviour of clays under realistic confining pressure conditions (Figure 3-15). Although they focus in their research on clays, their experience from testing with foams most probably is beneficial to this study. Generally, the advantage of vanes is that no slip effects can occur within the interfacial shear zone between testing material and vane. Especially the use of foam increases the danger of slip effects even more. The surfactants within the foam reduce the interfacial tension. In addition, MESSERKLINGER ET AL. (2011) used a rectangular sample container reducing the risk of slip between the testing material and the container wall, too. The vane is turned at constant angular speed and the resistant torque is measured. Data conversion into rheological parameters is just done for the measured torque based on the model presented in DIN 4094-4 (2002-01), see also chapter 3.1.3.2. Thus, the shear stress behaviour over the degree of vane rotation could be determined. One key interest to study was the development of shear strength in dependence of the injected volume of conditioning agent and the influence of backpressure on the results. They found out, that the shear strength
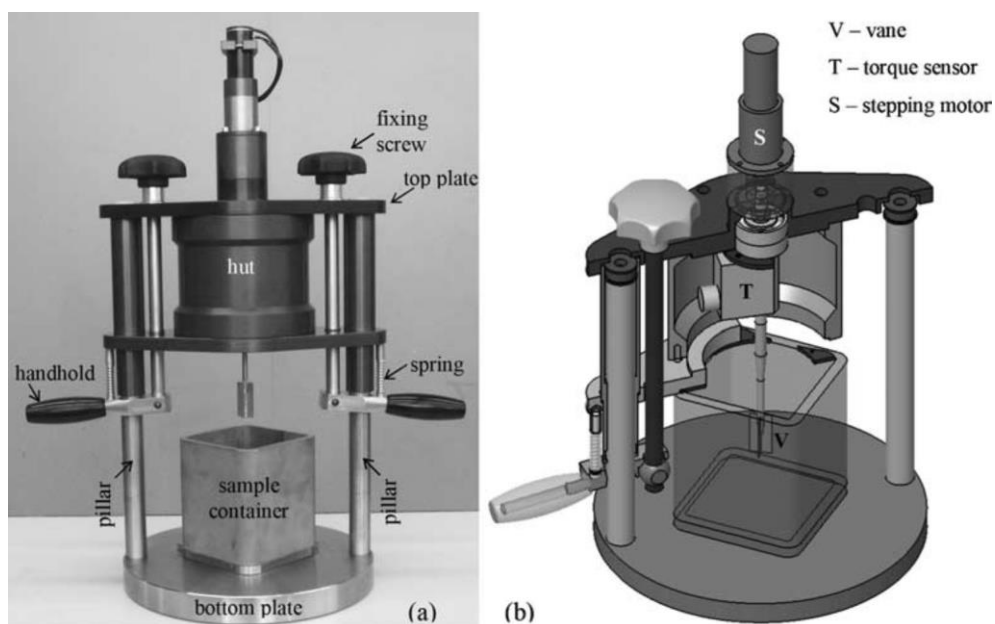
Figure 3-15: Photograph (left) and 3d cross section of the shear vane apparatus of MESSERKLINGER ET AL. (2011)

decreases with increasing FIR and increases with increasing backpressure. Data fitting of flow curves as described above was not part of the study but a following work of ZUMSTEG ET AL. (2012) later fitted data of conditioned clays obtained with the modified shear vane apparatus with a Herschel-Bulkley model.

VENNEKÖTTER (2012) investigated the pumping behaviour of foam-conditioned sands in the context of microtunnelling. He developed a model, realistically picturing the pressure gradient in the pumping line, which he verified in large-scale pumping experiments. Therefore, it was necessary to determine in advance also rheological properties (viscosity, yield stress) that were part of the analytical approach. The parameters were derived from flow curve tests performed with the rotational viscometer Schleibinger Viskomat NT. This device is usually applied for the rheological investigation of mortars or cement limes in concrete engineering. The shearing geometry was a six-bladed vane, which was accelerated constantly from 0 to 30 rpm and back to 0 rpm ("hysteresis linear ramp"). The system design was a compromise of the recommended radii ratios for homogeneous concentric cylinder rheometry and the recommended minimum gap width depending on the maximum grain-size, compare DIN 53019-1 (2008-09). Data conversion into rheological parameters (shear rate, shear stress) was based on coupling the Reiner-Rivlin equation for Couette flow in the vertical shear gap with a description of the flow in the bottom shear gap as concentrically rotating circular plates according to GIESEKUS (1994). A priori, a Bingham fluid was assumed. Applying the method of equating the coefficients, the conversion factors for the rotational speed and the measured torque were determined. Regression analysis was conducted for recorded pair values above a rotational speed of 2 rpm. It is assumed that in this range, laminar flow conditions were achieved and the threshold of yielding was overcome. The residual converted data samples from the experiments showed a Bingham plastic flow behaviour, which complies with the pre-defined model assumptions.

The use of standardised soil mechanical test methods in order to characterise the EPB material as mentioned before (chapter 3.2.2) has yet not become common practice. Shear box tests (direct shear tests), oedometer tests and vane shear tests have been applied to a limited extent for the analysis of the shearing behaviour of conditioned soil samples most notably by BEZUIJEN ET AL. (1999), BUDACH (2012), PEÑA DUARTE (2007), PSOMAS (2001), WU & QU (2009), cf. chapter 2.4.2. It was observed that the shear

strength is generally significantly reduced by foam conditioning. These observations comply with the findings from rheometric testing, see MENG ET AL. (2011), MESSERKLINGER ET AL. (2011). In addition, triaxial tests were conducted on conditioned sands but neither with any detailed description of the methodical approach nor with any information on the influence of the conditioning agent on the soil properties, see SHANGGUAN ET AL. (2010).

In a project-related study, MERRITT ET AL. (2015) associated the vane shear strength to slump measures. Shear strength values of 1 to 5 kPa corresponded to slump measures of 10 to 20 cm.

3.2.4 Rheology of cementitious materials

The rheology of cementitious materials is a wide field of research, which is too large to mention in its single branching here. However, selected scopes of research shall be introduced because of similarities in the material properties and of course, because of the standardised methods in concrete engineering, which are already applied on soil-foam mixtures, compare chapters 2.4.2 and 3.2.3.

Extensive works of FERRARIS (1996), FERRARIS & DE LARRARD (1998), deal with the rheological analysis of concretes and cement pastes. FERRARIS (1996) discusses different approaches determining rheological parameters of cement pastes, mortars and concretes. She explains the advantages and disadvantages of index tests and the application of rheometers based on the various existent definitions for the flow behaviour of the cementitious materials. As in EPB technology, the terms for the material flow are indefinably and similarly used in concrete engineering, too; i.e. the workability, consistency and plasticity. Nevertheless, the description of the flow can be either qualitative or quantitative empirical or quantitative fundamental, see TATTERSALL (1976). Furthermore, the experimental approaches to determine quantitative parameters can be distinguished in single point tests (determining single values) and two point tests (determining two related values).

Thereof, the slump test represents one of the most commonly used one-factor tests (index tests), which furthermore has been applied widely in EPB research. It is a standard measure to evaluate the workability of fresh concrete and it is regulated in DIN EN 12350-2 (2009-08). The slump value determines the slump class according to

DIN EN 206 (2014-07), which ranges from C1 to C5 and classes the workability of the material. Since slumping is induced by the dead weight, the material starts to flow, when its dead weight is sufficiently high to overcome the yield stress. Slumping terminates again, when the loading per area is below the yield stress. Many researchers developed empirical dependencies between rheological parameters and slump values, see chapter 3.3. The slumping principle is demonstrated in Figure 3-16.
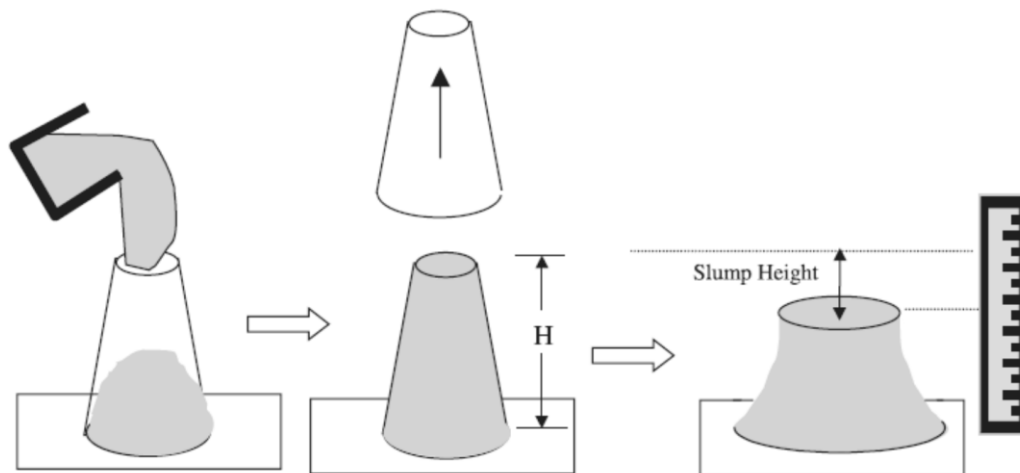
Figure 3-16: Principle of the slump test according to DIN EN 12350-2 (2009-08); taken from CLAYTON ET AL. **(2003)**

In contrast to the large application of index tests, BANFILL (2006) summarises the inadequacy of single-point tests for absolute evaluation of rheological behaviour picturing the complexity of the flow and material conditions. He underlines the necessity for fundamental rheological testing. Tests determining rheological information of fresh concrete and mortar are performed with rheometers or measuring systems of different types (see chapter 3.1.3.2). Pioneering work has been carried out by Tattersall, who developed the Two-point Apparatus, a four-bladed or H-shaped impeller rotating in a sample bowl, for rheological testing of concretes (see TATTERSALL (1991)). Upgrades of this device are the IBB Rheometer (BEAUPRÉ (1994)) and the BML Viscometer (WALLEVIK & GJORV (1990)). The latter one resembles a Couette measuring system with ripped coaxial cylinders. Another established device is the BTRHEOM parallel plate rheometer for fresh concrete with a maximum particle-size of 25 mm of DE LARRARD ET AL. (1997). A first large-scale rheometry approach has been conducted by COUSSOT & PIAU (1995). They developed a concentric cylinder rheometer for about 500 L of concrete (Large-scale Coaxial Cylinder Rheometer). The outer cylinder wall was equipped with blades, while the inner

cylinder consisted of a roughened surface. It was originally designed for mudflow investigations.

Comparative testing of all instruments (devices shown in Figure 3-17 and Figure 3-18) determined similar flow patterns of the same testing materials, although different ranks of rheological data were obtained, see BROWER & FERRARIS (2003), FERRARIS & BROWER (2001), FERRARIS & BROWER (2004). These differences may be addressed to several influences, most probable slip and sedimentation effects, secondary flow
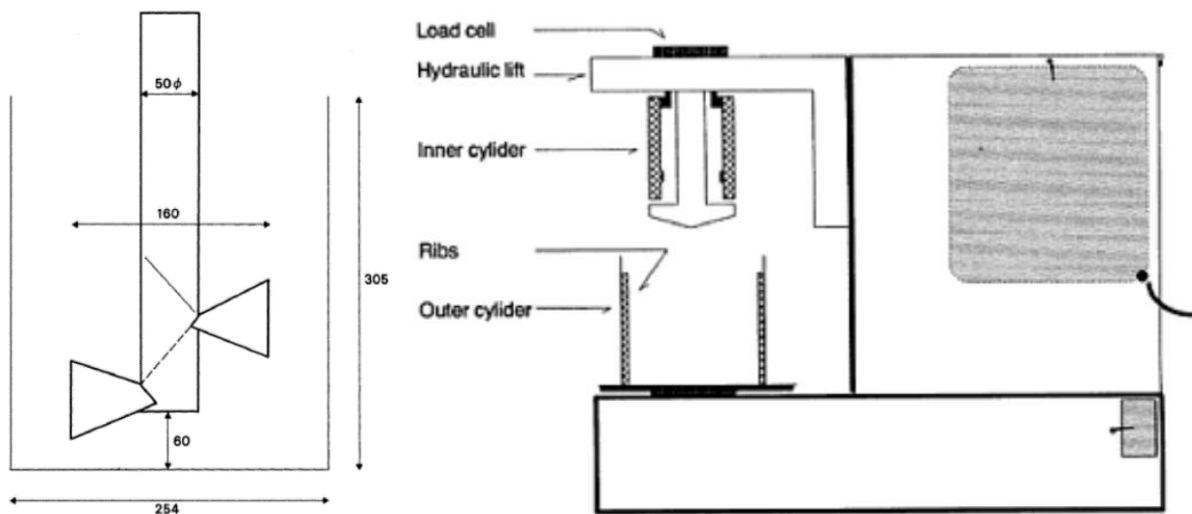
Figure 3-17: left: Two-point workability test equipped with interrupted-helix impeller (TATTERSALL (1991)), right: BML Viscometer (WALLEVIK & GJORV (1990))
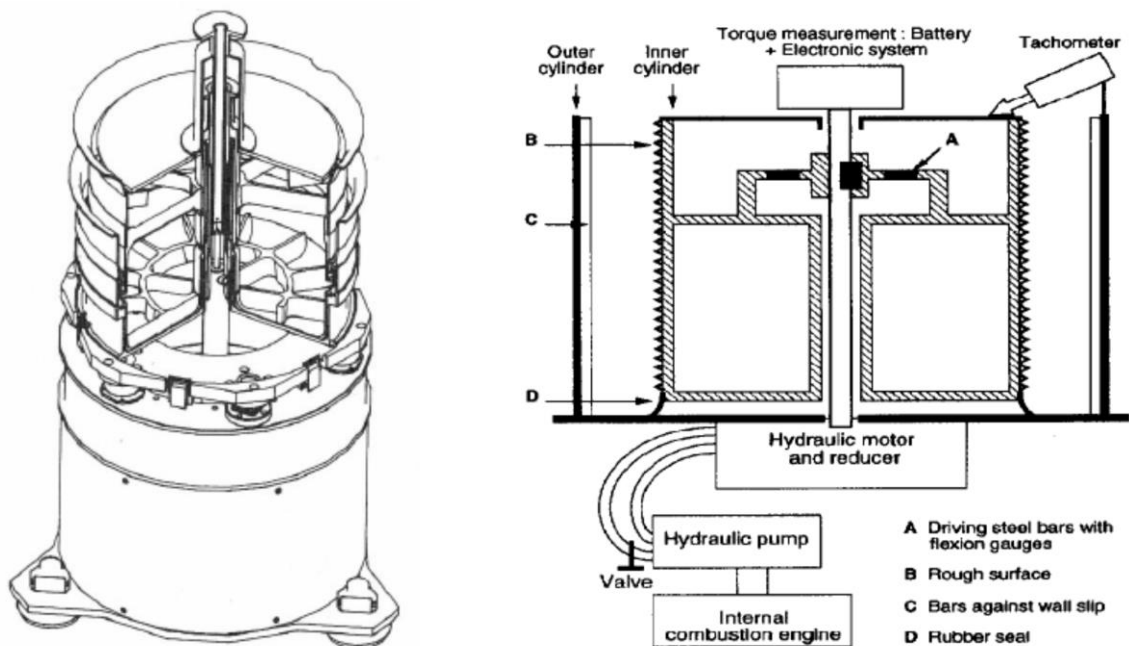
Figure 3-18: left: BTRHEOM (DE LARRARD ET AL. (1997)), right: Large-scale Coaxial Cylinders Rheometer (COUSSOT & PIAU (1995))

effects, and different generations of the shear flow field. However, partially significant correlations between the apparatuses could be found.

THIENERT (2011) investigated different compositions of annular gap grout for tunnelling. In order to evaluate the effect of stabilisers on the mortars, the cement pastes were rheologically examined. Therefore, he used a Searle type rheometer (Haake Stress 600) with profiled container walls and a lime paddle as rotor (Figure 3-19) and performed amplitude sweep tests. From these tests, he derived the storage and loss moduli. A conversion of raw data into rheological parameters did not take place due to inhomogeneous shear field conditions.
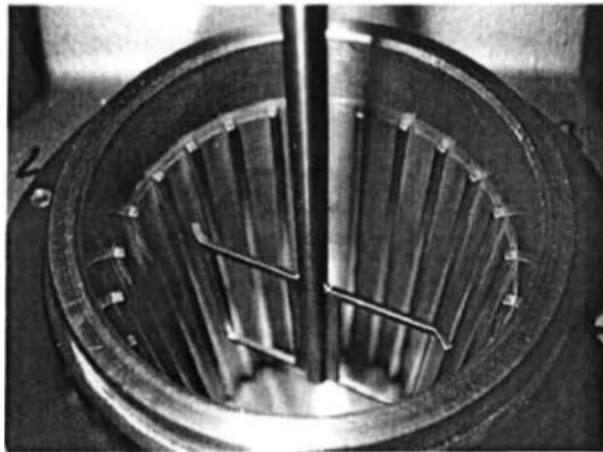
Figure 3-19: Profiled sample container and lime paddle (THIENERT (2011))

MÜLLER ET AL. (1999), TYRACH (2000) applied a different measuring system, the ball measuring system as described in detail in chapter 3.1.3. They applied this method for cementitious plasterings. Possible boundary effects (container restraints, surface slip, particle settling etc.) were discussed very basically, if at all. Curve fitting of test results was not conducted with established approximation models but with a fifth order polynomial function. Different investigations were compared by an integration parameter describing the area underneath the polynomial distribution.

BLASK (2002) studied the influence of plasticisers on the rheology of various types of cementitious materials, such as mortars, plasters or adhesives for tiles. For the determination of rheological parameters, he applied different measuring techniques (shear rate- and strain rate-controlled flow curves, oscillatory tests) using both the ball measuring system and the coaxial cylinder system. The shear stress results of cylinder measurements appeared significantly less compared to the ball measuring

system. BLASK (2002) related this phenomenon to wall slip effects in the cylinder configuration. Furthermore, he compared the results to several standardised index tests.

LOWKE (2013) focuses in his work on stability properties of self-compacting concretes on different scales in order to analyse and improve the material robustness. Most notably, the sedimentation behaviour – particularly the particle interactions – and its influence on the structural mechanics were of interest for him. Besides theoretical and experimental assessments of particle interdependencies and particle sedimentation, LOWKE (2013) analyses the rheology of the cement paste in a rheometer with ball configuration. The ball measuring system should simulate the dispersed aggregates in the cement paste and lead to information on the thixotropic behaviour (time-dependent shear stress development). Additionally, he determines the yield stress of the cement paste through the Haegermann slump tests (DIN EN 1015-3 (2007-05)) and an empirical approach of ROUSSEL ET AL. (2005).

Based on the previous works of BLASK (2002), SCHATZMANN (2005), TYRACH (2000), FLEISCHMANN (2013), FLEISCHMANN (2014) developed a large-scale ball measuring system for the investigation of rheological properties of self-compacting concrete in concrete mixers (Figure 3-20). Thusly, it shall be possible, to gain in-mixer information on the rheology of the concrete and based on these, to adjust the recipe during the production process.

Figure 3-20: RheoCT: Prototype of a large-scale ball measuring system for rheological in-mixer measurements (FLEISCHMANN (2013))

Several researchers investigated the flow behaviour of cementitious materials not only in rheometers but also in pipes. Especially the pumping behaviour of concrete and mortars is yet a rather empirical issue of research. Recent studies assessing the pumping behaviour provide approaches enabling a quantification of the material-wall friction (wall slip effects). One of them is the Tube Viscometer for Concrete (TVC) according to ROSHAVELOV (2005), which reminds of a modified and large-scaled version of the V-funnel test or the Marsh cone test (Figure 3-21). The TVC is based on the principle of Bingham-fluid flow through a pipe. About 30 L of fresh fluid concrete is inserted into the testing system and surcharged with weight discs on a piston determining the shear load. The piston displacement is recorded, while it is pushing the material through the vertical pipe at constant load. Considering the Buckingham-Reiner equation, which describes the pipe flow of a Bingham plastic fluid (GIESEKUS (1994)), the shear rate can be calculated. After the passage of the pipe, the material falls into a cylindrical container. This container represents a cylindrical slump test. Lifting the cylinder enables a yield stress estimation in dependence of the material spread similar to other approaches (e.g. PASHIAS ET AL. (1996), see above). Different load conditions in repeated experiments lead to further shear conditions and thus to additional flow curve points.

Enhancing the idea of ROSHAVELOV (2005), KASTEN (2010) developed the Sliding Pipe Rheometer ("SLIPER"; Figure 3-21) enabling a determination of flow properties of high-consistency substances in pipes. One of his main motivations was a consideration of the pressure gradients occurring during pumping of the fresh concrete. Based on the model assumption of plug flow, he setups a pressure calculation for Bingham fluids in pipes, wherein two parameters (a and b) represent equivalent parameters of yield stress and plastic viscosity. These parameters can be determined using the Sliding Pipe Rheometer. In addition, also the slip condition can be evaluated using the SLIPER, see MECHTCHERINE ET AL. (2014).

At last, BUCHENAU & HILLEMEIER (2005) reported of an application of a Falling Sphere Viscometer for self-compacting concrete. They adopted the method for this type of materials and developed a test stand, which was of increase dimensions due to the particle-sizes (d_{Sphere} = 9 cm, $V_{Container} \approx 8$ L). A ball is released into the sample medium and the sinking process is recorded (distance-velocity distribution). From the measured data, flow curves can be processed.
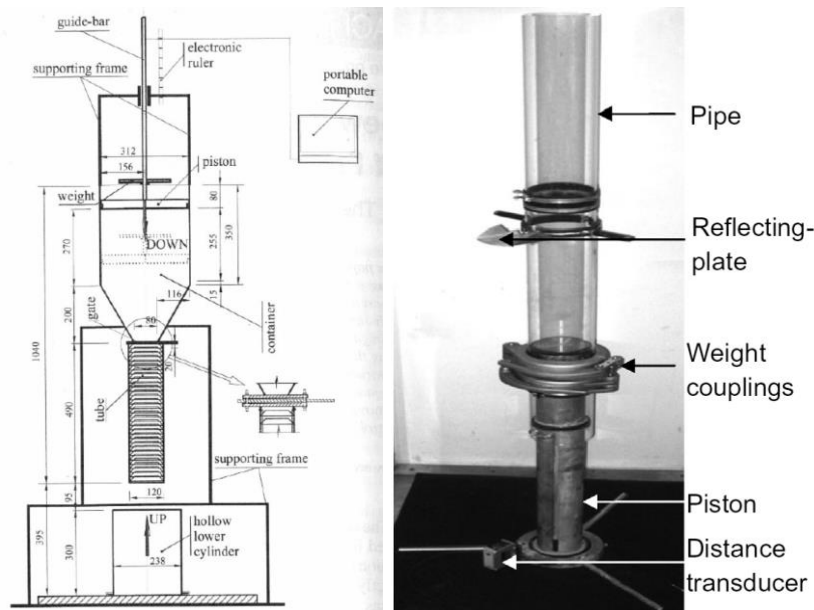
Figure 3-21: left: Tube Viscometer for Concrete (Roshavelov (2005)); right: Sliding Pipe Rheometer (Mechtcherine et al. (2014))

3.2.5   Numerical assessments of granular flows

Aiming at a numerical simulation of the flow behaviour of the column failure tests of Lube et al. (2005), see chapter 3.2.2, Bandara (2009) applied different methods from computational mechanics. One was the material point method (MPM) and the other the smooth particle hydrodynamics (SPH). The MPM is a finite element method-based particle method in computational mechanics. The advantage of this method is that single particles can be traced in the simulation without re-meshing. The SPH method represents a computational Lagrangian mesh-free method commonly applied in fluid dynamics. Each particle owns distinct properties with influence on the flow conditions. Bandara (2009) finally found the MPM less computationally expensive than the SPH for granular problems and the shape functions were more consistent.

Roussel & Coussot (2005) did an analysis of results from single point tests (slump test) and two point tests (rheometer, HAAKE ViskoTester 550 with vane geometry) on cementitious or mineral-based pastes and suspensions in comparison to a numerical simulation (commercial software Flow3D) of these materials (Figure 3-22). They found a good correlation between the yield stress-slump distribution from the experimental data and the numerical analysis (Figure 3-23).
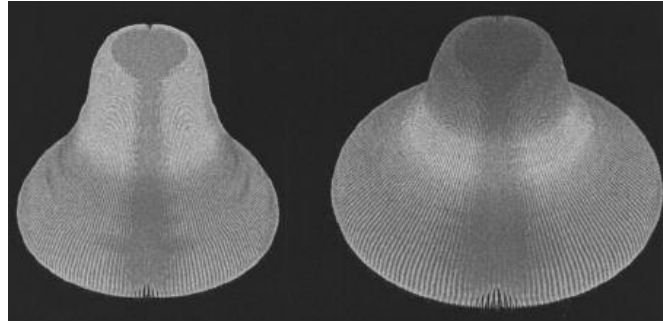
Figure 3-22: 3d-simulation of slump test: material density=2.5 kg/m³ (both), different yield stresses (left: 2,600 Pa, right: 2,000 Pa) (ROUSSEL & COUSSOT (2005))
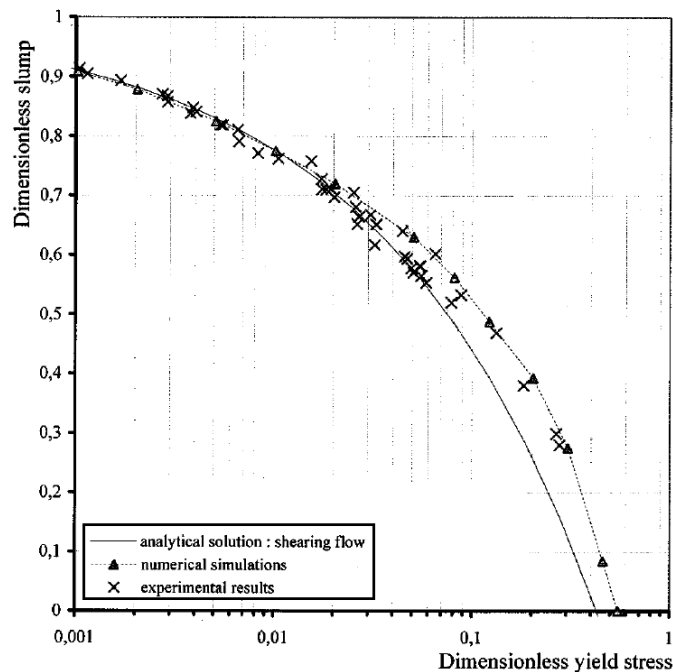
Figure 3-23: Comparison of experimental, analytical and numerical yield stress - slump distributions (ROUSSEL & COUSSOT (2005))

The simulation of such flow experiments with conditioned soils has been undertaken numerically already by few researchers. WU & QU (2009) performed a discrete element analysis (DEM) on foam-conditioned sands simulating slump tests and shearbox tests. Other related numerical works are still in the development, e.g. THEWES & STEEB (2014). Therein, the flow behaviour of conditioned soils in rheological experiments shall be simulated using the SPH method based on works as e.g. by SIVANESAPILLAI ET AL. (2014).

Besides the presented examples, additional details on numerical investigations of granular flow could be taken from the pertinent technical literature but it is not introduced any further here.

3.3 Correlation of slump tests and rheometrically determined parameters

Since most index tests are cheap and feature the ease of on-site conduction and comparative evaluation within a short time, their application will maintain popular throughout engineering practice. In order to describe the physics behind the occurring phenomena in these tests, many researchers aimed at establishing a link between index tests and rheology. Several assessments have been raised to find a correlation between slump tests and rheometry, most notably in concrete engineering. Either the different concretes were investigated using a rheometer and the obtained rheological values (yield stress, viscosity) were correlated with the slump / spread, or the slumping process was evaluated over time and it was derived a rheological relationship. This methodology was later also applied for suspensions and other materials. Some significant researches are presented in the following.

MURATA (1984) initiated the research of deriving rheological parameters from the slump test based on a simple equilibrium consideration. The material in a slump cone of the total height in the initial state H experiences a non-linear shear stress distribution due to its dead weight (Figure 3-24). If the shear stress is sufficient large to overcome the material's yield stress, it is responsible for vertical mobilisation, when the cone is lifted. Idealising the slump figure as body composed of horizontal slices, the single lamellae are squeezed in thickness and thus – assuming incompressibility – tend to elongate horizontally. The slump process terminates when an equilibrium state is achieved. The result is a rotationally symmetric slump body, which can be reduced to a two-dimensional flow phenomenon. The slumped material consists of a deformed and an undeformed shape part, which by MURATA (1984) was described through the slump value S_L and the height of the undeformed shape h_0, see Figure 3-24. In equilibrium state, the deformed part has reached a uniform shear stress distribution equal to the yield stress value ($\tau_y = \tau_0$). The material remains undeformed in the region of $0 < z < h_0$, since the vertical stress was not sufficient to overcome the yield stress ($\tau_y \leq \tau_0$). Integration of the stress behaviours over all lamellae makes a geometry-dependent calculation of the yield stress possible.
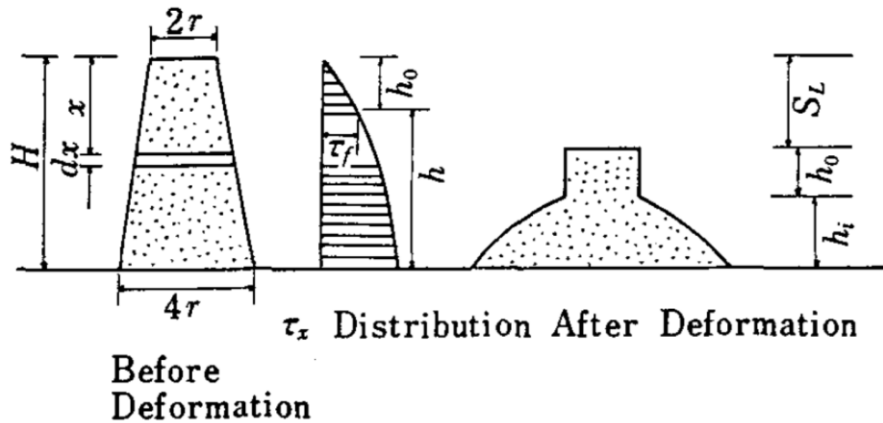
Figure 3-24: Description of the deformation behaviour of a slump sample (MURATA (1984))

The friction between material and bottom plate is taken into account in a simplified manner as it is equated to the yield stress (MURATA (1984)), whereas "perfect slip" (CLAYTON ET AL. (2003)) is assumed to act between material and mould surface. The stress distribution after completion of the slump process is visualised in Figure 3-25.
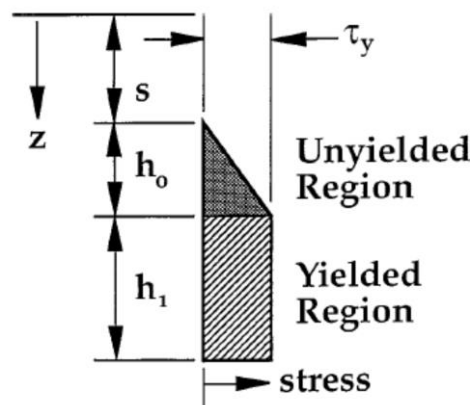
Figure 3-25: Shear stress distribution within the slumped material (SCHOWALTER & CHRISTENSEN (1998))

Similar approaches have been made for example by PASHIAS ET AL. (1996), who transferred the approach of MURATA (1984) to cylindrical slump mould shapes and mineral suspensions. Yield stress measurements from vane shear tests corresponded quite well with the analytical approach. SCHOWALTER & CHRISTENSEN (1998) determined some little integration error in the work of MURATA (1984), but still found a good correlation of the approach in general with measurements obtained in testing. Furthermore, they stated, *"the potential for characterization of fresh concrete or other rheologically complex materials goes far beyond the simple measurement of slump height. The profile of the final mound of material as well as the dynamics by*

which the final shape is attained are governed by the rheology. Finite element solutions of the free boundary problem should allow a richer interpretation of the slump test than has been possible heretofore." (Schowalter & Christensen (1998)). Results from their own FE simulations however showed deviations in the same range of the simplified analytical approach.

Clayton et al. (2003) and Saak et al. (2004) propose two generalised cone theories allowing for a consideration of varying geometrical proportions. Thereof, Clayton et al. (2003) conducted comparative slump experiments on mineral suspensions with both cylindrical and cony moulds and applied their generalised cone theory and the cylinder approach of Pashias et al. (1996). Comparing the yield stress results from vane tests with the analytical models, better agreement was found for the cylinder test as for the cone tests. Therefore, Clayton et al. (2003) recommend to apply the cylinder slump test as standard test in practice. Saak et al. (2004) compared the results of their theory with experimental data obtained from slump tests on cement pastes and with yield stresses determined in a rheometer with vane measuring system. They also found the results from cylindrical slump tests correlating better than the results from slump cone testing. Both research groups imply that one reason for the divergence might reside in rather big slump spreads.

Roussel et al. (2005), Roussel & Coussot (2005) took on this aspect and explained the explored discrepancies by the presence of two possible flow regimes: one that is determined by a large height-diameter ratio (small slump values), and the other that is determined by a large diameter-height ratio (large slump values). In other words, they state that materials with a small slump value behave solid-like whereas large slump values refer to a more fluid-like behaviour. Furthermore, the selection of an adequate yield criterion would be crucial. According to Roussel & Coussot (2005), the Tresca yield criterion is not passable to capture the flow pattern realistically. They recommend using the van Mises yield criterion. In addition, the initial height and the total volume have to be regarded, too. Thusly, they proposed two equations depending on the respective appearing flow behaviour (slump- or spread-determined flow). Verification of the approach was performed with measurements on different cement pastes using a coaxial cylinders rheometer. The data was fitted with the Herschel-Bulkley model, from which the yield stress was taken and compared to the analytically calculated yield stress. Additionally, Roussel et al. (2005), Roussel &

COUSSOT (2005) advised to account for surface tension effects that can affect the results, which depend on the contact angle between testing fluid and solid plane.

PIAU (2005) pointed in a similar direction. He also supported that choosing an adequate approach for describing the flow characteristic in the slump test is based on the material characteristic (solid or fluid). Linked to this is the selection of the yield criterion. According to PIAU (2005), the yield criterion again depends on the failure mode in the experiment and cannot be covered generally by one stress hypothesis. For the solid-like behaving materials, he introduces an adjustable variable λ representing the yield criterion. Furthermore, PIAU (2005) derives several formulae for the different possible material and testing conditions.

FLATT ET AL. (2006) incorporated the remarks of ROUSSEL ET AL. (2005), ROUSSEL & COUSSOT (2005) and applied the models proposed by MURATA (1984) and successors, and ROUSSEL ET AL. (2005), ROUSSEL & COUSSOT (2005) to own experimental data. Surface tension effects were also taken into account. They found out, that both approaches have a destined range of application. Between, it might be necessary to find an intermediate range model, which they did by best-fit interpolation. Furthermore, surface tension effects have to be considered for large spreads.

PIERRE ET AL. (2013) focused on finding an adequate intermediate range model for cylindrical moulds by combining the approaches for slump and spread regime models as presented by ROUSSEL & COUSSOT (2005) and PASHIAS ET AL. (1996), which they applied successfully to self-obtained experimental data. However, the application still demands for an undeformed section of the slump body at the end of flowing.

Further studies have been carried out by FERRARIS & DE LARRARD (1998). They modified a global relationship from literature that links the slump measure to the yield stress based on numerical investigations.

4. EXPERIMENTAL APPROACH

Based on the presented works in the different areas of research, the flow behaviour shall be approached from two sides. In order to maintain a rather simple assessment of the flow behaviour, slump tests should still be considered as indicators of the workability. Therein, the shape of the material after slumping shall be analysed in more detail and the applicability of models for a rheological parameter identification as presented in chapter 3.3 shall be evaluated. Furthermore, rheological investigations using rotational rheometry shall be conducted. Therefore, a suitable testing procedure and a proper measuring device are necessary. Subsequently, the materials used in this study are introduced and the experimental approach is described in more detail. Furthermore, basic assumptions are made with respect to tunnelling narrowing the focus of this research. Thus, the placement of this work in the scientific context shall be pointed out.

4.1 Multi-scale approach

This research was performed within subproject A4 of the Collaborative Research Center 837 "Interaction models for mechanised tunnelling" at the Ruhr-Universität Bochum. Aim of this project is the development of a complex continuum-based multiphase flow model, which is realistically describing the support medium in the excavation chamber of an EPB shield under backpressure, see MESCHKE & KRUSCHWITZ (2009). A first step of this project was the material characterisation on different scales, dealing mainly with conditioned non-cohesive soils. Therefore, index laboratory tests were executed by BUDACH (2012) on various mixtures of sands and gravels using different conditioning agents. One key issue in the characterisation was also the workability. Moreover, the rheology of such materials was approached by ÖZARMUT ET AL. (2013), ÖZARMUT & STEEB (2015), THEWES & STEEB (2014) in small-scale experiments. In their works, they used a rheometer (Anton Paar MCR 301) with different configurations (plate-plate, cone-plate, cup-bob) to assess the flow behaviour of the supporting mix. Precise rheometry, considering very small shearing

gaps, limits the investigation of rather granular materials like the sandy or even gravelly support medium, which is why ÖZARMUT & STEEB (2015), THEWES & STEEB (2014) introduced as a first approach synthetic materials simulating the real material. The synthetic materials were shaving foam and (wetted) glass beads and mixtures of both. Main advantages of these materials were first the extraordinary long drainage durability of the shaving foam, cf. GALLI (2009), and second the inert and almost ideal-shaped surface of the glass particles. Thusly, it was possible to determine a basic flow pattern, which could be described best by applying the Papanastasiou-Herschel-Bulkley model.

The transfer of the findings from the micro-scale investigations towards the real scale (realistic materials, realistic loading conditions) is here defined as multi-scale approach. Figure 4-1 illustrates this approach: precise rheometry on the micro-scale leads to substantiated results on the rheological properties but of synthetic materials; index tests and rheological investigations using more complex test configurations (e.g. geometries), which take certain restraints and inhomogeneous boundary conditions into account but however realistic materials, can be used for basically understanding the material behaviour. A comparison of the findings through the scales is achieved by an overlap of the materials. This means, that the synthetic materials, which are well understood on the small scale, are also investigated in the heterogeneous experiments on the large scale. Thus, the tests with realistic materials can be referenced qualitatively and perhaps quantitatively to the flow behaviour of the synthetic materials.

The macro-scale investigations and the transfer of findings are main aspects of this study. They will be presented in the following chapters with varying emphasis (pre-study / main study focus) for the heterogeneous experiments (cylindrical, vane and ball geometries; chapter 7) and for index tests ((modified) slump (flow) tests; chapter 6).
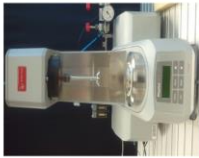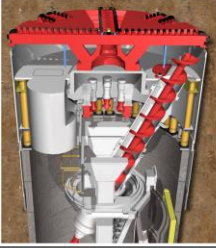
Measuring system	MICRO-SCALE		MACRO-SCALE			Real scale
	plate-plate / cone-plate	cylinder, vanes (material cells)	ball	slump (flow) tests	large-scale tests	machine data
	Anton Paar MCR 301	Anton Paar MCR 301, Anton Paar Rheolab QC, Schleibinger Viskomat NT	Anton Paar Rheolab QC		COSMA	EPB shield
Sample volume	ca. 1 ml	ca. 16 - 350 ml	ca. 0,25 - 20 l	ca. 20 l	ca. 500 l	> 500 l
Preciseness	HOMOGENEOUS EXPERIMENTS	HETEROGENEOUS EXPERIMENTS			INDEX TESTS, BACK ANALYSIS	
Material		foam + micro-particles				real conditioned soils
			foam + clay / silt / sand			
			foam + clay / silt / sand / gravel			
			foam + rock cuttings			

Figure 4-1: **Multi-scale approach: investigation of the flow behaviour of synthetic and realistic EPB support materials with different experimental methods and configurations**

4.2   Assumptions

Narrowing the large influences occurring in tunnelling, certain assumptions are made, which have to be clearly stated once, to demonstrate the restraints of this research. As mentioned before, only cohesionless soils within the extended range of EPB tunnelling according to Budach (2012) are considered here, that show a qualitatively good conditioning behaviour with just foam. Furthermore, the EPB advance is regarded below groundwater table, so that groundwater is present and thusly fully saturated ground conditions (saturation S = 1.0). No groundwater flows occur. All influences (loadings, streaming, mixing, advance etc.) take place in steady state conditions.

The most important simplification is, that at this level of research, ambient pressures are assumed and backpressures, as they would exist in the excavation chamber as well as pressure gradients, are neglected. These conditions shall be part of future investigations and is now knowingly taken into account.

4.3   Materials and quality control

Since this research work focusses on foam conditioned non-cohesive soils, two cohesionless soils were selected as reference soils and one foam was chosen as reference foam. Results and findings gained with other materials are later related to the main materials.

In the following, all the materials are introduced and their compositions and basic properties are described. Additionally, the preparations of some of the materials is presented as well as the accuracy in preparing them with respect to reproducibility.

4.3.1   Soils

The soils were selected based on the work of Budach (2012). He investigated the conditioning behaviour of a wide set of non-cohesive soils. The soils, which show a good conditioning behaviour with only foam, range from fine sand to fine gravelly sand. Therefrom, the poorly graded lower bound soil (fine sand; Soil 1) and a well-graded "average" soil (sand; Soil 2) were chosen for the present investigation. The grain-size distribution curves of the reference soils are shown in Figure 4-2.
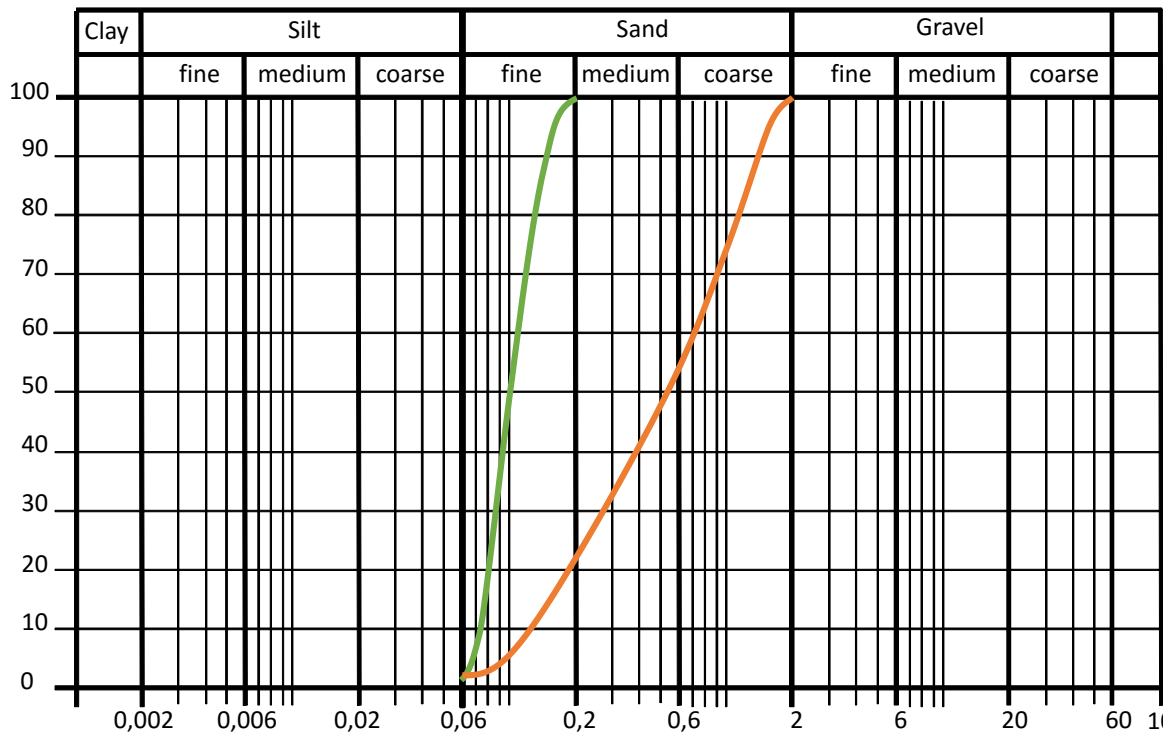
Figure 4-2:   **Grain-size distribution curves of the main soils used in the investigations: Soil 1 (green) and Soil 2 (orange)**

The soils were composed manually by special dry laboratory quartz sands (Euroquarz Siligran, see EUROQUARZ GMBH (2015) for details) with well-determined grain-size distributions and deviations supporting a high level in reproducibility. The fine sand (Soil 1) consists of only one soil fraction (0.063 – 0.250 mm), whereas the sand (Soil 2) is composed of four evenly distributed soil fractions (0.063 – 0.250, 0.2 – 0.6, 0.5 – 1.0, 1.0 – 2.0 mm).

4.3.2   Foam

The foam was produced with two laboratory foam generators according to FREIMANN (2012) and GALLI (2009), which both were calibrated to a realistic foam generator on EPB shields, such as in THEWES & BUDACH (2010b). The target FER was set to 15 in all experiments. The production rate was 26.25 l/min for foam generator 1 ("TLB Mini Foam Generator"; Figure 4-3 left) and 60 l/min for foam generator 2 ("TLB Laboratory Foam Generator"; Figure 4-3 right). The surfactant used was Condat CLB F5/TM, which is recommended to use predominantly in highly permeable sands, in a concentration of 3.0%, see CONDAT LUBRIFIANTS (2015). The production parameters are summarised in Table 4-1.

Figure 4-3:   Foam generator 1 ("TLB mini foam generator"; left), Foam generator 2 ("TLB Laboratory Foam Generator"; equipped on real-scale foam generator) (THEWES & BUDACH (2010b))

Assuring a limited deviation in the actual foam quality, immediately after foam production the foaming behaviour – i.e. the foam density and the actual FER – was evaluated prior each test. Experience shows, that using foam generator 1 with the presented targeted values, the actual FER ranges between 13.0 and 15.0, and using foam generator 2 the actual FER lies between 14.0 and 16.0. If the actual FER was within this defined range, the foam was used for testing; otherwise, the foam production had to be adjusted.

The foam is expected to exhibit a drainage behaviour characterised by a half-life time ranging between approximately 10 and 15 minutes and to possess maximum cell-sizes of 0.2 to 0.6 mm within this time, compare BUDACH (2012), FREIMANN (2012), GALLI (2009).

Table 4-1: **Targeted foam production parameters**

	Property	Value / Type
Foaming liquid	Surfactant	Condat CLB F5/TM
	Solution c_f	3.0%
Foam	Target FER	15
	Flowrate foam Q_F	26.25 l/min and 60.0 l/min
	Flowrate liquid Q_L	1.75 l/min and 4.0 l/min
	Flowrate air Q_A	24.5 l/min and 56.0 l/min
Foam generator 1	Design	"TLB Mini Foam Generator" with filled foam gun
	Bluff body	Glass pearls (d=5mm)
	Flowmeters	Rotameters (by Krohne)
	Flow regulation	manually
	Supplying pressure air/liquid	4 bars
Foam generator 2	Design	"TLB Laboratory Foam Generator" for reduced flow rates with filled foam gun
	Bluff body	Glass pearls (d=5mm)
	Flowmeters	Electromagnetic and thermal mass flowmeters (by Endress+Hauser)
	Flow regulation	manually
	Supplying pressure air/liquid	5 bars

4.3.3   Soil-foam mixtures

The preparation of the foam conditioned soil samples followed a strict procedure with temporal restrictions. Foam exhibits time-dependent properties, especially its drainage behaviour influences the stability and thusly the lifetime. Therefore, a precise production procedure was necessary in order to warrant comparable ages of the foam and of the mix of foam and soil respectively. This procedure is demonstrated in Table 4-2 as well as remarks on the accuracy of measuring the amount of the different ingredients to add.

Water is added to the soil, which was composed in advance as described in chapter 4.3.1, in dependence of the required water content w [wt%] (Eq. 4.1). Approaches of realistic water contents are going to be discussed in chapter 5.

$$w = \frac{m_W}{m_{S,dry}} \cdot 100 \qquad\qquad \text{[wt\%]} \qquad\qquad \text{Eq. 4.1}$$

with m_W the mass of water [kg] and $m_{S,dry}$ the mass of dry soil [kg].

After its production, the FIR-dependent amount of foam m_F is poured manually to the moistened soil according to Budach (2012) using Eq. 4.2 and following the descriptions in chapter 4.3.2 and Table 4-2.

$$m_F = \frac{\rho_W}{\rho_{S,wet}} \cdot \frac{FIR}{FER_{actual}} \cdot (m_{S,dry} + m_W) \qquad\qquad \text{[kg]} \qquad\qquad \text{Eq. 4.2}$$

with ρ_W the density of water (simplified for foaming liquid) [kg/m³], $\rho_{S,wet}$ the density of wetted soil [kg/m³], FIR the foam injection ratio [vol%], and FER_{actual} the actual foam expansion ratio [-].

The use of a concrete bowl mixer has been found suitable in other studies; see e.g. Budach (2012), Merritt (2004), Peila et al. (2011), Vennekötter (2012). However, small amounts of conditioned soils should be mixed by hand because the efficiency of mixing in a bowl mixer would be too low and the loss of material too high. Mixtures containing more than 3 kg of soil are suitable for mixing in a concrete mixer. The mixing time is limited to one minute in order to prevent probable re-foaming effects due to the introduction of mixing energy. Thusly, the actual FER within the mix is changed and furthermore the density of the mixture is influenced, too.

Table 4-2: **Procedure for production of soil-foam mixtures and test preparations including remarks regarding the measuring accuracy**

Step no.	Time	Duration	Task	Accuracy
I	---	---	Test preparations	
II	---	---	Compose soil according to recipe	±1.0 wt%, max. ±1.0 g
III	---	01:00	Mix soil until homogenised	
IV	---	---	Measure water in dependence of water content w	±1.0 wt%, max. ±1.0 g
V	---	01:00	Mixing of water and soil until homogenised	
1	00:00	03:30	Foam production and sampling, determination of actual FER and measuring FIR-dependent amount of foam for the mixture	±10.0 wt%, max. ±1.0 g
2	03:30	01:00	Mixing of foam and wetted soil until homogenized; small samples (< 3 kg) by hand, large samples (3 – 24 kg) with concrete bowl mixer	
3	04:30	04:00	Preparation of testing sample(s); further test preparations, if necessary	
4	08:30	---	Start of testing	

4.3.4   Further materials

For calibration issues of the rheometers, further materials are used. Additionally, other materials should be tested on the different scales providing information about the transfer of findings using different rheological test methods. Therefore, the following materials were also investigated:

1. Silicon oil

Silicon oil represents a Newtonian fluid with constant viscosity. They are widely applied in fluid rheology for the calibrations of rheometers. Silicon oils are available with different viscosities at different temperatures. Testing a silicon oil with a certain measuring profile under constant temperature conditions, the resulting viscosity should comply with the given viscosity. Deviations are allowed within a manufacturer's defined range. The silicon oil, which was chosen for this research, is the BROOKFIELD Viscosity Standard 1000 calibration oil. It exhibits a viscosity of 990 mPa·s at a temperature of 25°C considering a precision of ±1.0%; see BROOKFIELD ENGINEERING LABORATORIES VERTRIEBS GMBH (2015) for further details.

2. Bentonite slurry

Bentonite slurries consist of clay particles suspended in water. Often, they exhibit the feature of swelling, which is why they are commonly applied in geotechnical engineering as transport, lubricating or supporting fluid. Many rheological investigations have been performed on bentonite slurries determining the flow behaviour and adequate flow models. Most often, bentonite slurries are described in a simplified manner by the Bingham model. Other researchers found good correlations with more sophisticated models, such as the Herschel-Bulkley model. However, both models represent a non-Newtonian fluid type. By applying both fluids, silicon oil and bentonite slurry, a holistic calibration of the rheometers for Newtonian and non-Newtonian fluids is possible.

The bentonite slurry used in this study consists of sodium bentonite type "W" (Wyoming Bentonite; see PHRIKOLAT DRILLING SPECIALTIES GMBH (2015)), concentrated in water by 25 g/l (c_{susp} = 2.5 vol%). The bentonite powder is poured to the water while mixed with a coaxial dissolver mixer at 1,500 rpm. Mixing is processed for ten minutes. After that, the mixture undergoes a swelling phase at rest for 24 hours in a

sealed container before it is mixed again for another ten minutes in the dissolver mixer at 1,500 rpm.

3. Glass beads

As described in chapter 4.1, the multi-scale approach is based on realistic and synthetic materials. The synthetic EPB mixtures are composed of (wetted) glass beads and shaving foam. The glass beads used are 3M™ Glass Bubbles K1, which are hollow and have a mean diameter of 64.5 μm, or SiLibeads Glass beads Type S, which are solid and exhibit a mean diameter of 48.5 μm. In geotechnical terms, both their particle-size distributions can be compared to a silt, but in contrast to minerals, they are fully inert and of round shape. For further details on their characterisation, see 3M (2015), ÖZARMUT ET AL. (2013), SIGMUND LINDNER GMBH (2012).

Mixes of glass beads, water and foam are only generated in very small amounts (max. 0.5 L) because especially the glass beads are very cost expensive. Mixing is performed by hand, but otherwise analogously to Table 4-2.

4. Gillette shaving foam

In order to neglect short-term time-effects in the micro-scale experiments and to generate a particle-foam mixture with almost monodisperse particles and cells, shaving foam is used. The cell-size distribution was found Gaussian for the shaving foam, which was selected here, cf. ÖZARMUT ET AL. (2013). The mean cell-diameter corresponds approximately to the mean particle-diameter of the glass beads. This type of foam has been used not only for foam analyses in other research (cf. chapter 3.2.1), but also for rheological investigations. This is a fundamental advantage for the scientific comparison of results.

5. EXCURSUS: ASSESSMENT OF THE RESIDUAL WATER CONTENT OF EXCAVATED SOIL IN EPB TUNNELLING

The amount of moisture of the excavated soil in EPB tunnelling steers the demand for additional treatments of the material in the excavation chamber. All the main process parameters (conditioning, wear, support pressure etc.) are affected by the water content. With respect to foam conditioning, this means that the less water enters the chamber the drier the actual mix of soil and foam at constant foam properties. Especially in cohesionless soils below groundwater-table, the magnitude of free pore water is quite high. Ground decompaction resulting from the cutting process, the acting pressure state and the usage of conditioning agents can cause a displacement of water from the pore space at the face. Thus, only a residual moisture content is present, when the soil is entering the chamber. The question of how much water enters the excavation chamber has not been answered satisfactorily, yet.

In order to simulate the material conditions in the excavation chamber of an EPB shield in laboratory experiments, it is necessary to assess the initial water content of the test soils realistically. Earlier studies on soil conditioning dealt with the initial water content, too. BUDACH (2012) derived the required amount of water to be added to the dry soils, which he used in his experiments, from the retention porosity for sands. He globally applied a water content of 10 wt% for all investigated cohesionless soils. VENNEKÖTTER (2012) determined the water content for his investigations of conditioned silty sands from the maximum Proctor density. The resulting water contents were 8.3 wt% and 7.2 wt%. BORIO ET AL. (2009), PEILA ET AL. (2009), PEÑA DUARTE (2007) varied the initial water content showing its influence on the

conditioning behaviour but did not explicitly determine a residual water content for particular soils.

Based on observations on the pore fluid behaviour during hydro-shield tunnelling, BEZUIJEN ET AL. (1999), BEZUIJEN & SCHAMINÉE (2001) investigated fluid infiltration processes at the face more closely and their influence on the pore water ahead of the machine, when tunnelling with EPB shields. Therefore, they simulated the drilling process in sands experimentally considering foam conditioning through a small-scale cutter head. Although a determination of the residual water content was not a primary purpose of their study, the analysis of the void water behaviour during tunnelling provided the oppotunity for a derivation of the remaining moist volume. Therefore, BEZUIJEN (2002) established an interaction between the groundwater expulsion and the foam injection. He defined an expel rate of pore water based on a three-dimensional flow situation in porous media and thus, he could provide information on the residual water content entering the excavation chamber.

A more simplified approach by MAIDL (1995) focuses on the penetration behaviour of foam into coarse soil. Under a constant pressure head, foam was forced to infiltrate into saturated soils and the long-term penetration rate was analysed in order to gain information on the foam stability within the grain skeleton and the foam rheology.

Both approaches enable a measurement of water expulsion from the void matrix. Details and findings from the studies will be presented in the following chapter. It will be discussed, whether the approaches can lead to information on the residual water content and how it can be assessed.

5.1   Assessments on fluid flows at the tunnel face

Dealing with the flow mechanisms occurring at the tunnel face, one has to contemplate fluid dynamics in porous media. In many engineering applications, the knowledge of the particular hydrogeological situation is essential preventing groundwater influx or hydraulic failure. An elementary description of ground water flow through aquifer strata is governed by the law of Darcy, which incorporates the characteristic fluid and soil properties. The flow through the soil is induced by the piezometric head ($\Delta h = h_1 - h_2$) across the regarded aquifer length L, which is also defined as the hydraulic gradient. It includes the pressure and energy states of the

fluid. The loss in energy is due to friction, which the fluid is exposed to during the passage through the soil (BEAR (1988)).

Regarding the fluid flows at the face, two assessments have been executed to investigate the foam-groundwater interaction in cohesionless soils during tunnelling with EPB shields.

5.1.1   Analytical approach by Bezuijen

According to BEZUIJEN (2002), in permeable conditions, the overpressure in the excavation chamber regarding the in-situ pore water will result in a displacement of the pore fluid and in a replacement by foam. Consequently, groundwater flow is initiated away from the tunnel face. That way, the amount of moisture in the excavated soil is reduced compared to the natural soil moisture state. The less permeable the ground, the less pore water is expelled.

BEZUIJEN (2002) assumes the specific discharge at the tunnel face to be uniformly distributed over the excavation area considering quasi-static conditions. At any location x ahead of the tunnel face on the tunnel axis, the discharge q_x in direction of advance can be determined using Eq. 5.1, when the soil permeability k_f [m/s], the tunnel radius R_T [m] and the change in piezometric head Φ [m] are known and when the soil is saturated. Φ is defined by Eq. 5.2, wherein Φ_0 [m] can be approximated by the pressure head acting at the tunnel face. The subsequent equations were taken from BEZUIJEN (2002).

$$q_x = \frac{\phi \cdot k_f}{\sqrt{x^2 + R_T^2} - x} \qquad\qquad \text{[m/s]} \qquad\qquad \text{Eq. 5.1}$$

$$\phi = \phi_0 \cdot \left(\sqrt{1 + \left(\frac{x}{R_T}\right)^2} - \frac{x}{R_T} \right) \qquad \text{[m]} \qquad\qquad \text{Eq. 5.2}$$

Validation of the flow formulation ahead of the face was performed on field data from the Botlek Rail Tunnel in the Netherlands, see BEZUIJEN (2002). With x = 0 m, the gradient at the tunnel face is calculated. In turn, the specific discharge of expelled pore water q_0 [m/s] is received (Eq. 5.3).

$$q_0 = \frac{\phi_0 \cdot k_f}{R_T} \qquad\qquad\qquad \text{[m/s]} \qquad\qquad \text{Eq. 5.3}$$

By foam injection, the porosity of the excavated soil should be increased to reduce grain-to-grain stresses, which for instants directly affects the potential for wear or the required driving torque. Hence, the actual porosity of the mix in the excavation chamber, n_m [-], is bigger than the void ratio in the soil's natural state, n_p [-]. In saturated conditions, when the groundwater flow rate at the face q_0 is slower than the cutting speed v_{adv} [m/s] of the machine, the residual pore water content $\theta_{residual}$ [vol%] is reduced from n_p (fully saturated pore volume) to a residual liquid content composed of the residual pore water and the injected liquid foam phase (Eq. 5.4). If the expulsion rate is greater than the advance speed of the TBM, all pore water is suppressed and replaced by foam.

$$\theta_{residual} = \begin{cases} \left(n_p - \dfrac{q_0}{v_{adv}} + \dfrac{FIR}{100 \cdot FER} \right) \cdot 100, & \dfrac{q_0}{v_{adv}} < n_p \\[2em] \dfrac{FIR}{FER}, & \dfrac{q_0}{v_{adv}} \geq n_p \end{cases} \quad \text{[vol\%]} \qquad \text{Eq. 5.4}$$

BEZUIJEN (2012) relates the water content in the excavation chamber to the actual foam properties instead to the soil by introducing a FER_m-value. This parameter is defined as the regular FER (volume of foam divided by volume of foaming liquid) but now considering also the incoming residual pore water. Therefore, the present FER_m within the muck is much less compared to the design value – if not all pore water is expelled. Regarding other material parameters within the excavation chamber (e.g. hydraulic conductivity, density, shear strength; see chapter 2.4.2), the additional water has also to be taken into account because it may significantly influence the properties (BEZUIJEN (2013)).

Model experiments by BEZUIJEN & SCHAMINÉE (2001) aimed at a simulation of the EPB drilling process. Foam penetration or even a penetration of conditioned soil into the tunnel face throughout the course of advancement were not observed. During standstill, little penetration was determined. Main factors of influence limiting the foam penetration were the low permeabilities of the sands and the pressure gradients. Hence, the excess pore water pressures and the corresponding groundwater flow at the tunnel face as proposed by BEZUIJEN (2002) do not result from penetration of foam into the face but from expulsion of void water when being conditioned while entering the chamber.

5.1.2   Experimental approach by Maidl

Aware of the fact that the tunnel face is not covered solely by foam, MAIDL (1995) simplified the situation at the tunnelling front and assumed sufficient excess pressure making the foam penetrate into the ground. In order to investigate this phenomenon, MAIDL (1995) performed foam penetration tests on two non-cohesive soils: a sand and a gravelly sand. For the studies, he used a test stand consisting of two communicating cylinders (Figure 5-1). The soil is inserted and compacted in cylinder 1 before it is saturated. The water balance in both cylinders is the same. Foam is produced and injected under constant backpressure conditions into cylinder 1. Opening the bottom valve connecting cylinders 1 and 2, the time count is started and the foam penetration depth is recorded. At the same time, the water level rises in cylinder 2 because of the pressure difference between the two cylinders. MAIDL (1995) worked with two pressure gradients of 0.2 and 0.5 bar at a base pressure of 2.0 bar simulating augmented pore water pressures.

In his tests, he observed an infiltration behaviour, which he distinguished into two phases. At the beginning of phase 1, after opening the bottom valve, the foam entered the soil sample rapidly due to the large pressure gradient that acted between the cylinders. The penetration rate decreased with diminished pressure head until
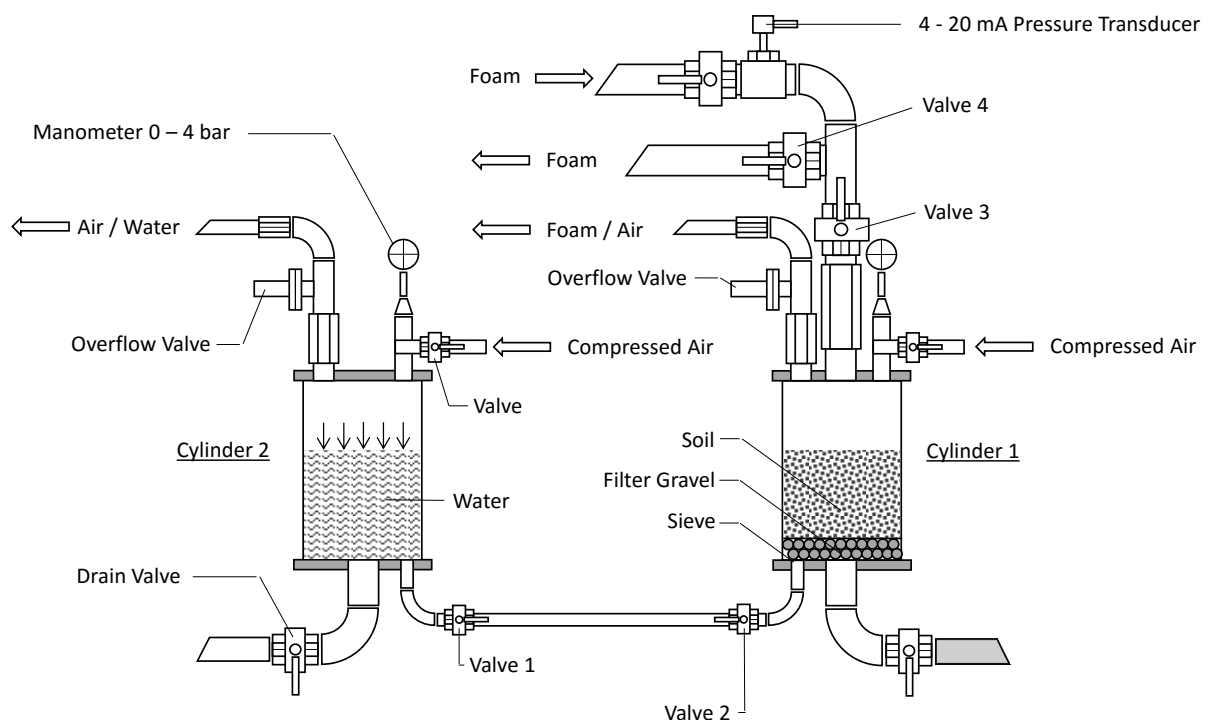

Figure 5-1:   Rig for foam penetration tests according to MAIDL (1995)

the penetration front converged apparently to a limit value. Under ideal conditions, MAIDL (1995) expected the foam to stagnate at a certain state of penetration, since the residual pressure level would not be sufficient large to overcome the foam yield stress. Although at small values, the penetration rate however maintained constant in phase 2. Furthermore, phase 2 was characterised by foam degeneration effects, which additionally influenced the penetration behaviour. According to MAIDL (1995), the transit to phase 2 depended on the foam recipe, the pressure difference and the design grain-diameter d_{10}.

Generally, he observed the foam moving through the soil with a planar front and expulsing the void water completely. MAIDL (1995) compared his measurements with expected values, which he derived from the water inclination in cylinder 2. The relationship between the penetration depth and the water inclination should be the void ratio n_p of the soil sample. However, the expected values exceeded the actual recordings. MAIDL (1995) attributed the additional water to a destruction of foam while passing through the grain matrix. Hence, free foam water from the destroyed foam would have to be additionally considered in the expelled void water.

5.2   Foam penetration tests

From their experiments, BEZUIJEN ET AL. (1999), BEZUIJEN & SCHAMINÉE (2001) concluded that a penetration of pure foam does not take place in practice. Nevertheless, the foam is of significant relevance to pore water expel. The foam injection together with the soil properties (k_f, n_p) and the acting pressure steers the suppression of pore water when the excavated soil is entering the mixing chamber. MAIDL (1995) also stated that a coverage of the tunnel face solely by foam is not expectable. The occurrence of foam penetration would depend on the density of the support mix in the excavation chamber and on the distribution of injection points. Most probable, the penetration of foam into the soil is a local phenomenon and it appears only within a couple of centimetres (MAIDL (1995)). Whether the foam penetration takes place overall, only locally, e.g. in front of the injection nozzle at the cutting wheel, or globally over the full cutting face area cannot be justifiable answered for reality. It has also to be considered that there is a considerable gap between the steel structure, on which the foam injection points are installed, and the actual face, which is filled already with excavated soil. However, it is assumed here that the soil

mechanical and procedural conditions at the tunnel face provide a sufficient level to allow foam penetration. Hence, the experimental approach of MAIDL (1995) is consulted for an assessment of the residual water content of excavated soil entering the excavation chamber of an EPB shield combined with a comparative analysis with respect to the approaches of BEZUIJEN (2002). Figure 5-2 shows the supposed principle of foam penetration at the tunnel face. Thereupon, the foam penetration is discussed on the background of BEZUIJEN (2002), BEZUIJEN (2012), BEZUIJEN & SCHAMINÉE (2001), MAIDL (1995). The fundamental assumptions, boundary conditions and materials described in chapter 4 are still respected here, unless specified otherwise. Prior to the main tests, pre-studies have been guided within the framework of this research, which contributed to the development of the final testing procedure.

1 Foam injection at the cutting wheel

2 Foam penetration into face

3 Pore water expell
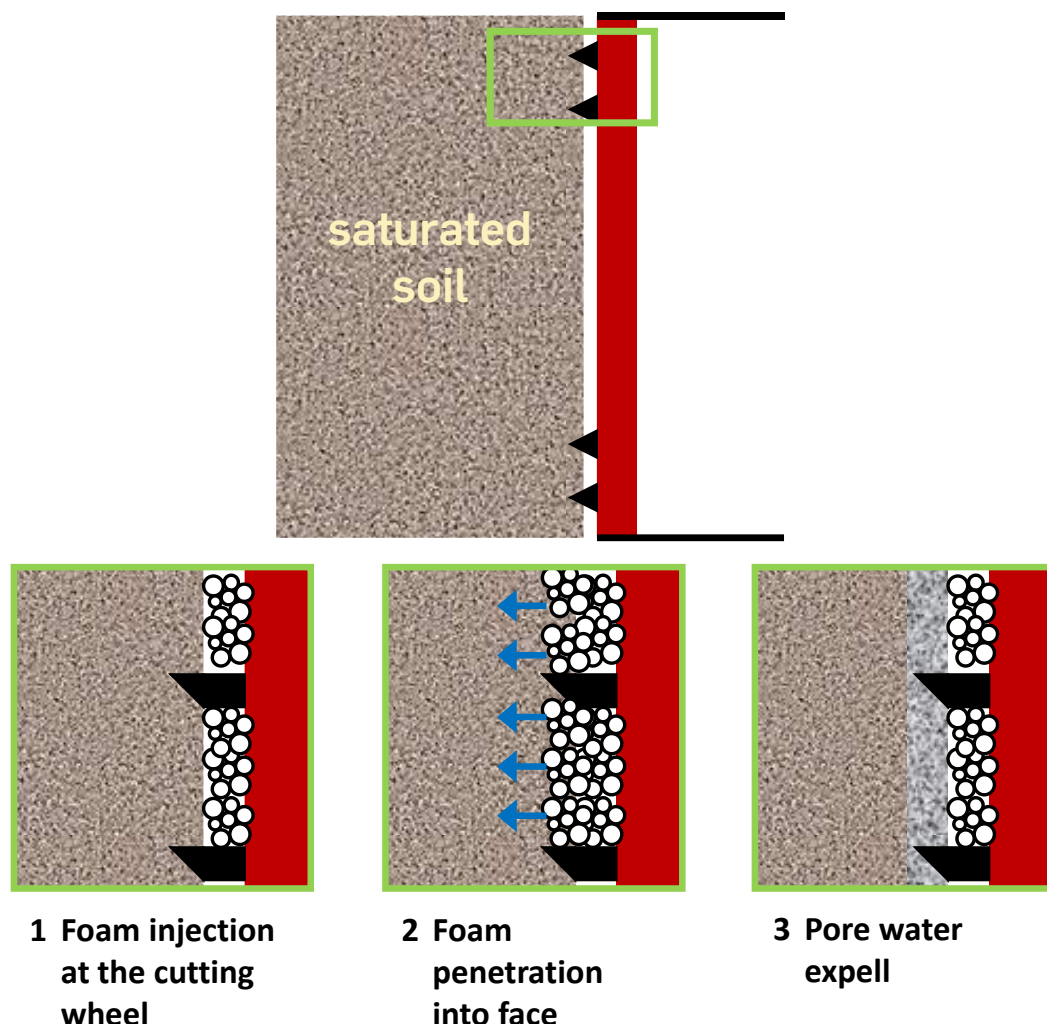
Figure 5-2:   Supposed principle of foam penetration and pore water replacement

5.2.1   Pre-studies

In small-scale experiments on the phenomenology of foam penetration into particle matrices, a Hele-Shaw setup was used in order to achieve pseudo-2d flow conditions (Figure 5-3), see DENTER (2012). Aiming at reducing effects from the test materials on the basic penetration pattern, real materials (i.e. tunnelling foam and soil) were simulated through synthetic materials (shaving foam, glass particles). The artificial materials provided a long-term stability due to an increased content of stabilisers (polymers) and a rounded particle-shape. During testing, a compact planar foam penetration front was observed over the penetration process (Figure 5-4) as it was also described by MAIDL (1995). When drainage effects became more significant, surface and boundary effects occurred.

In large-scale tests on the penetration behaviour of tunnelling foam into cohesionless soils according to MAIDL (1995), the test setup was redesigned several times in order to meet the requirements for the aim of the study, see MENGÜ (2012), TORKHANI (2013). Main steps in the development were the use of video recording of the penetration process and the installation of an outlet valve in order to weigh the
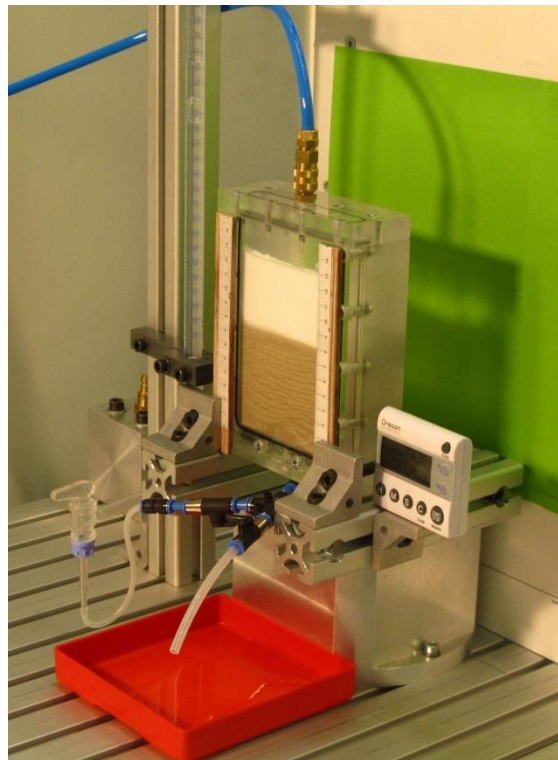
Figure 5-3:   Setup for small-scale 2d-infiltration experiments (modified Hele-Shaw cell) (DENTER (2012))
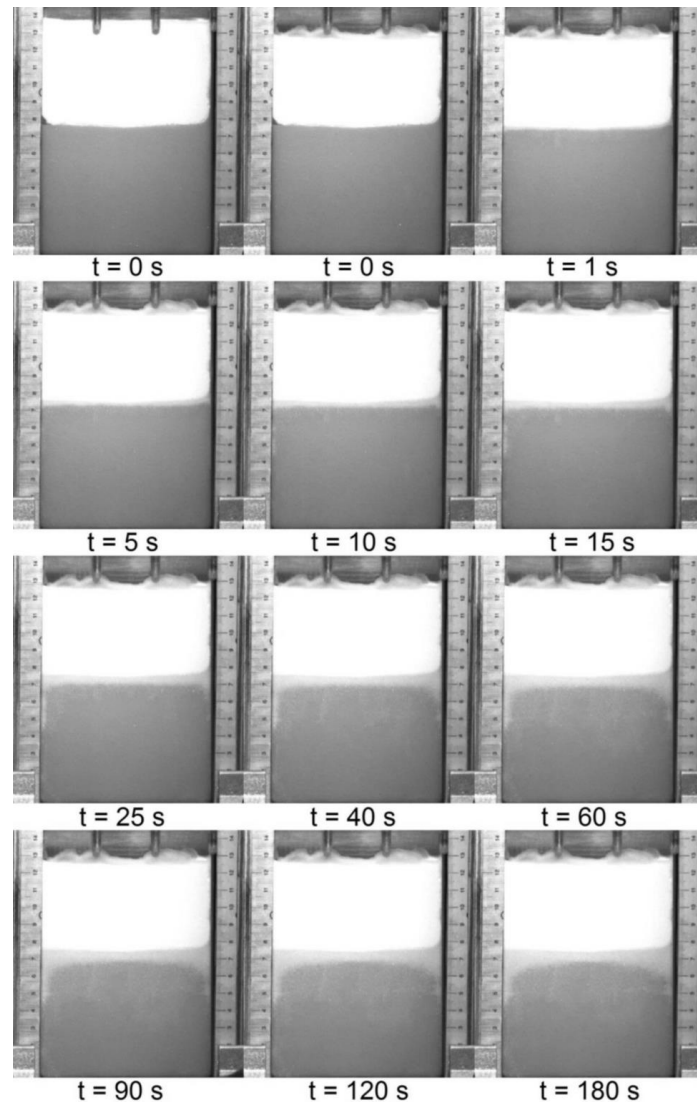
Figure 5-4:   Foam penetration into water-saturated glass particles in a Hele-Shaw cell under pressure load of 0.2 bar at different time steps (DENTER (2012))

expelled void water instead of measuring a water inclination. With reference to the testing programme of BUDACH (2012), a variety of different non-cohesive soils was chosen for investigation. The resulting foam penetration behaviour depended significantly on the soil composition, see TORKHANI (2013).

5.2.2   Setup, testing procedure and experimental programme

The test setup was designed according to the studies of MAIDL (1995). However, it involved some significant differences (Figure 5-5), which were based on experience from the pre-studies, see chapter 5.2.1. Since it was not intended to investigate excess pore pressure conditions, a spillway was installed on the height of 25 cm in cylinder 2. Balancing of the water level in both cylinders can be achieved by elevation
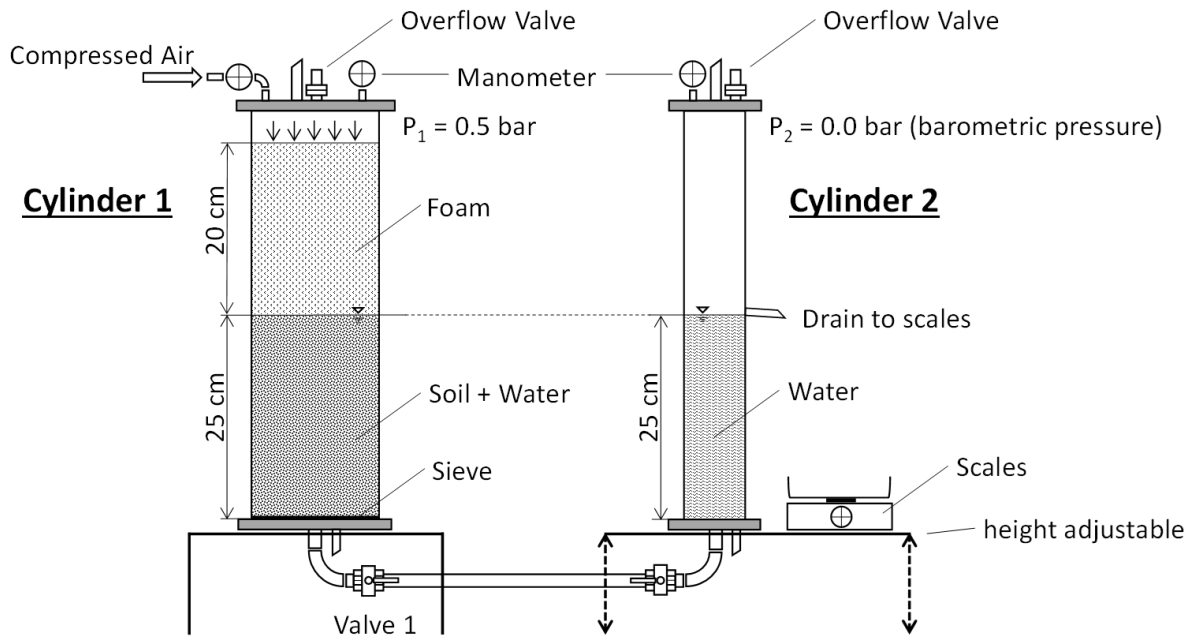
Figure 5-5:   **Scheme of rig for foam penetration tests**

adjustment of cylinder 2. Thus, it is possible to record the actual weight of the expelled water, which flows from the drain of cylinder 2 into a container on scales.

Another change in the test compared to the original procedure of MAIDL (1995) was the insertion of soil. From the pre-studies, where an installation procedure was considered similar to MAIDL (1995), it was found that a penetration of foam can occur prior to start of testing, see TORKHANI (2013). Based on experience of LINS (2009), the saturation of soil after insertion and compaction benefits air entrapments. Air bubbles, once bound in the grain matrix, might not be able to vanish during the saturation process. Therefore, the filling process was conducted as follows: water is filled into cylinder 1 for a couple of centimetres and then soil is dribbled into the water. This happens stepwise until a level of 25 cm is reached. Preliminary tests on this setup procedure have shown that additional compaction is not necessary to achieve maximum compactness. Thus, a saturation S close to 1.0 was realised.

Generally, the foam penetration is examined top-down in a vertical setup. A foam injection from the bottom was not feasible ensuring a steady contact face between soil and foam. Sieves or comparable filter layers maintaining the soil in position would have influenced the penetration process. A horizontal test setup was precluded from the outset because pressure gradients could have occurred which should be avoided at this stage of research.

After introduction of the soil, foam is produced and placed on the soil at atmospheric conditions. The consideration of placing the foam at ambient pressure into the test setup was due to procedural restraints. This is an eminent simplification and the results as presented in the following need to be reassessed based on pressurised foam injection. By recompression, drainage processes might be accelerated and the bubble structure might be affected.

Once the test stand was hermetically sealed, it is pressurised with compressed air to a reference pressure of 0.5 bar (50 kPa). This pressure was chosen according to the pressure differences used by MAIDL (1995). TORKHANI (2013) did an analytical variation study on the pressure differences to be expected at the tunnel face and chose 0.5 bar to be on the safe side. When pressurised, the bottom valve was then opened and testing started at the same time. Details on the test setup and a precise description of the testing procedure can be found in chapter A.2.1.

The experiments were conducted according to this testing procedure for a variety of non-cohesive soils with different gradation according to BUDACH (2012), see Table 5-1 and Figure 5-6. Soils 1 and 2 equal the reference soils in the main parts of this study (chapter 4.3.1); details on the compositions of the other soils (dashed grain-size distribution curves) and their characteristic properties can be found in BUDACH (2012).

Table 5-1: **Grain-sizes of test soils used in foam penetration tests**

Soil	Grain-size range [mm]
Soil 1 (Fine sand)	0.063 - 0.250
Soil 2 (Sand)	0.063 - 2.000
Soil 3 (Middle sand)	0.2 - 0.6
Soil 4 (Coarse sand)	0.5 - 1.0
Soil 5 (Fine and middle sand)	0.063 - 1.000
Soil 6 (Middle and coarse sand)	0.5 - 2.0
Soil 7 (Middle sand to fine gravel)	0.5 - 4.0
Soil 8 (Fine sand to fine gravel)	0.063 - 4.000
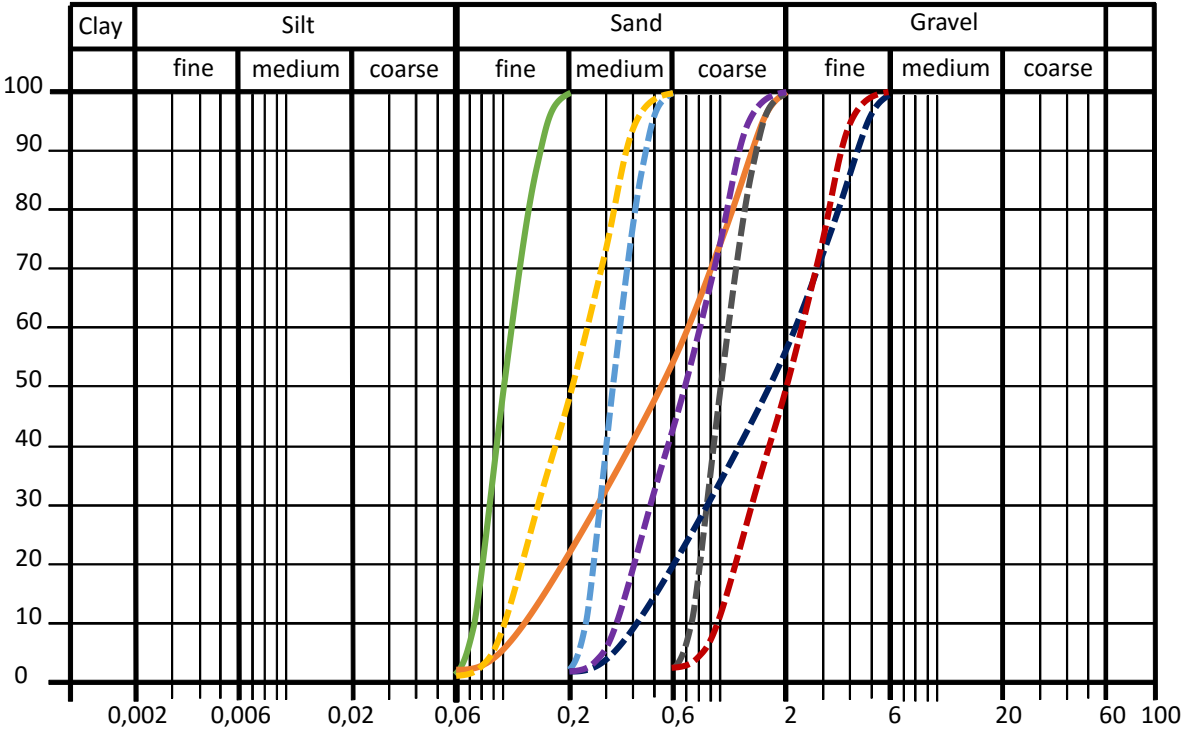
Figure 5-6:   Scheme of grain-size distribution curves of the soils used in the foam penetration study; green: reference soil 1, orange: reference soil 2

The foam properties were maintained constant as described in chapter 4.3.2. The test duration was limited to three minutes because it was aimed at the short-term penetration behaviour during advance and not the long-term conditions during standstills. Typically, the experiments were conducted only once. In case of irregularities or unexpected events, the tests were repeated for comparison reasons.

5.2.3   Test results and analysis of the penetration process

The test results of the foam penetration as described afore (i.e. the penetration depth z_p over time t) are visualised in Figure 5-7. Therein, the penetration depth is displayed over time. Recordings were taken every second over the first thirty seconds by video camera. Additionally, the foam depths were measured every thirty seconds visually from tape measures on the test cylinders up to a total time of 180 seconds. Thus, the final measurements (data points) every thirty seconds represent the mean value of two visual readings and one camera recording. Interim values are single values from the video camera.

In all experiments, the foam penetration occurred quickly at large infiltration rates within the first seconds before it reduced to a lower penetration speed. Basically, the

penetration process behaved similarly to the observations by MAIDL (1995). The penetration depth into soil 1 is less than into soil 2. It seems likely that this is mainly determined by the soil gradation. The same conclusion can be drawn with respect to all other soils. Contrary to MAIDL (1995), the emphasis was on the short-term foam infiltration behaviour during advance.

An application of a flow model for porous media to the foam penetration process would provide a sound description of the dynamics. However, the development of an adequate model is complex and exceeds the aim of the present study. Therefore, the penetration process is evaluated qualitatively by regression analysis. Over the observed period, the penetration behaviour can be well described for all samples by a power-law model with intercept zero ($z_p(t) = a \cdot t^b$). Through linear regression analysis applying the least-squares method and considering the concept of linearisation, best-
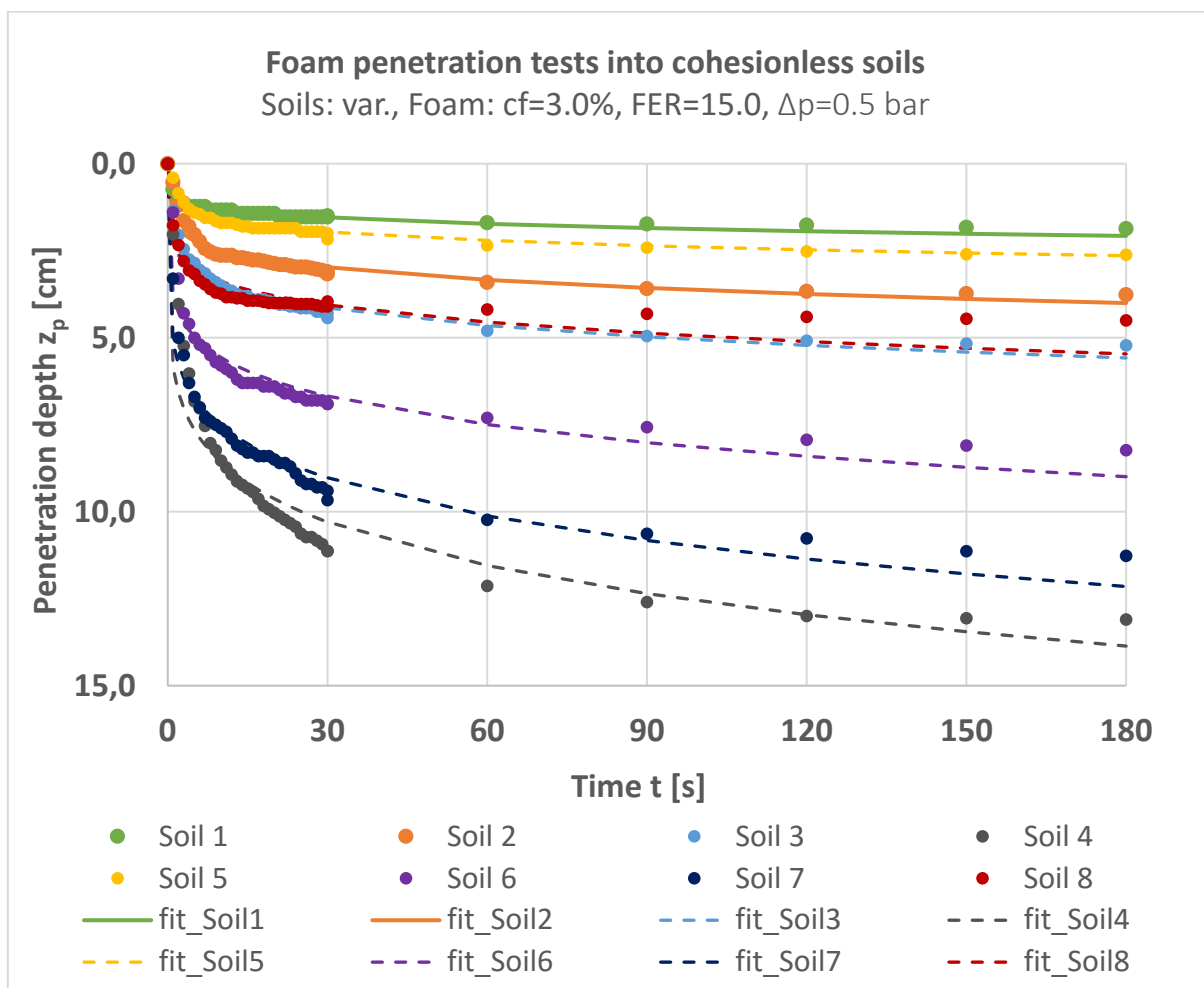
Figure 5-7: Penetration depths of tunnelling foam into different cohesionless soils (data points) including reference soils 1 (green) and 2 (orange) and power-law functions (continuous lines) fitted to the data; see Table 5-2 for details

Table 5-2:   Regression analysis of foam penetration data: best-fit equations and coefficients of determination

Soil	Best-fit equation	Coefficient of determination
Soil 1 (Fine sand)	$z_p(t) = 0.88 \cdot t^{0.166}$	$R^2 = 0.946$
Soil 2 (Sand)	$z_p(t) = 1.69 \cdot t^{0.166}$	$R^2 = 0.848$
Soil 3 (Middle sand)	$z_p(t) = 2.36 \cdot t^{0.166}$	$R^2 = 0.929$
Soil 4 (Coarse sand)	$z_p(t) = 5.85 \cdot t^{0.166}$	$R^2 = 0.827$
Soil 5 (Fine and middle sand)	$z_p(t) = 1.12 \cdot t^{0.166}$	$R^2 = 0.880$
Soil 6 (Middle and coarse sand)	$z_p(t) = 3.80 \cdot t^{0.166}$	$R^2 = 0.882$
Soil 7 (Middle sand to fine gravel)	$z_p(t) = 5.13 \cdot t^{0.166}$	$R^2 = 0.949$
Soil 8 (Fine sand to fine gravel)	$z_p(t) = 2.31 \cdot t^{0.166}$	$R^2 = 0.853$

fit equations could be found for the different soils with adequate coefficients of determination, see Table 5-2. In Figure 5-7 the fitting curves of the soils of reference, soils 1 and 2, are highlighted by continuous green and orange lines compared to the other soils (dashed lines). The main soil property influencing the fluid discharge through the soil is the intrinsic permeability, which depends on the pore ratio and an effective grain-diameter. Other properties influencing the fluid passage like of the foam were maintained constant in all tests and therefore, do not play a weighty role in a comparative analysis. Multivariate data analysis determined the exponent b to be close for all soils (0.11 … 0.20). Therefore, in a second calculation, this factor was maintained constant (b = 0.166). Thus, a significant correlation of the remaining regression coefficient a was revealed with both the representative grain diameter at 30% passage, d_{30} [mm] (linear; Figure 5-8), and the mass-specific surface area, S_m [cm²/g] (power-law correlation; Figure 5-9). Later, in chapter 5.3.1, it will be shown, that both parameters can be linked together.

Foam penetration tests into cohesionless soils
Correlation analysis of regressors and soil properties

$a = 7.04 \cdot d_{30} + 0.24$
$R^2 = 0.983$

Regression coefficient a

d_{30} [mm]
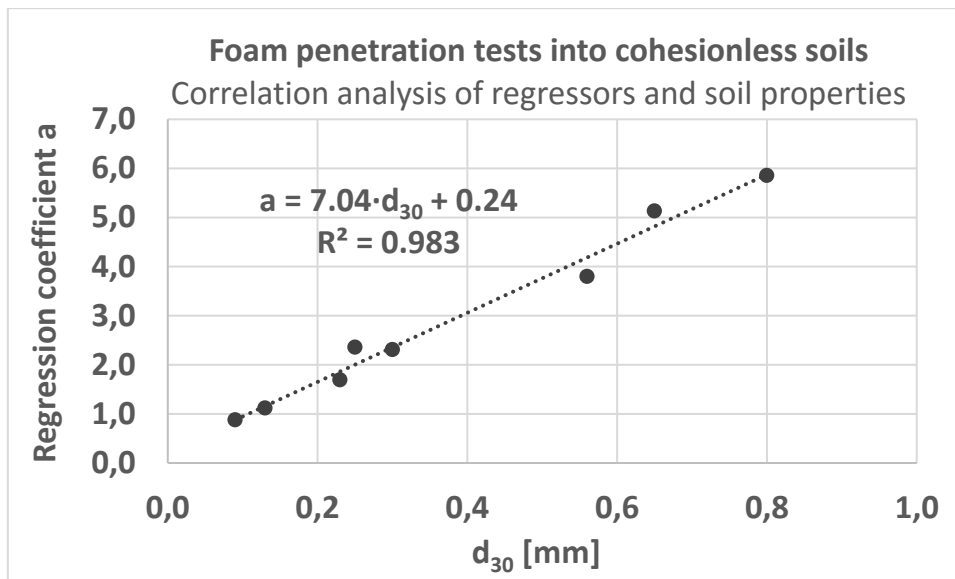
Figure 5-8:   Linear correlation of regressor a and representative grain diameters d_{30}

Foam penetration tests into cohesionless soils
Correlation analysis of regressors and soil properties

$a = 0.047 \cdot S_m^{-0.92}$
$R^2 = 0.983$

Regression coefficient a

S_m [cm²/g]
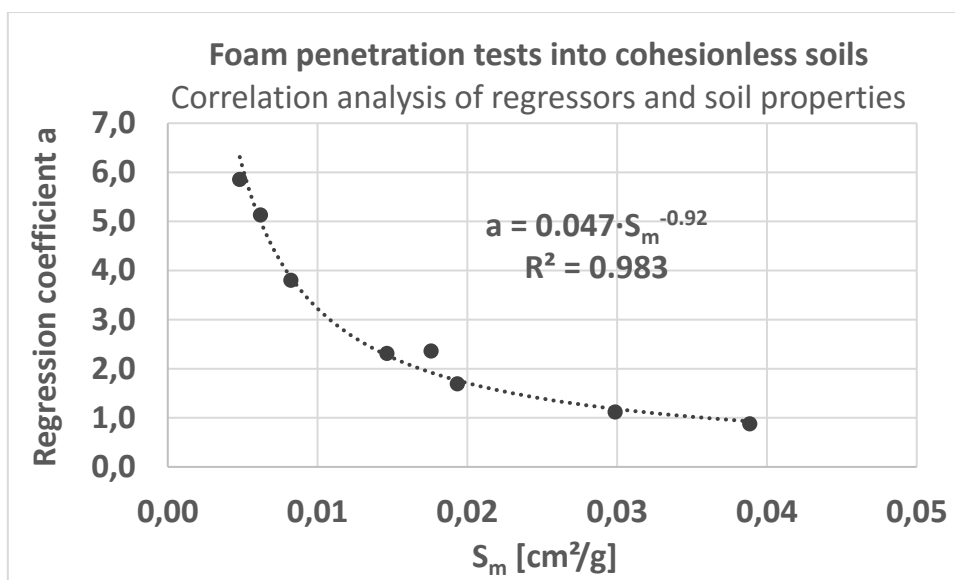
Figure 5-9:   Power-law correlation of regressor a and the mass-specific surface areas of the soils S_m

5.2.4   Analysis of the residual water content in the excavated soil

The foam penetration tests should provide an access to approach the residual water content within the zone of excavation covered by the cutting depth of the excavating tools. Figure 5-10 shows a representative excavated volume element (REVE) indefinite in its extent except for its length, which equals the excavation depth of the cutting tool (tool penetration h_{tool}). The REVE may show three conditions:
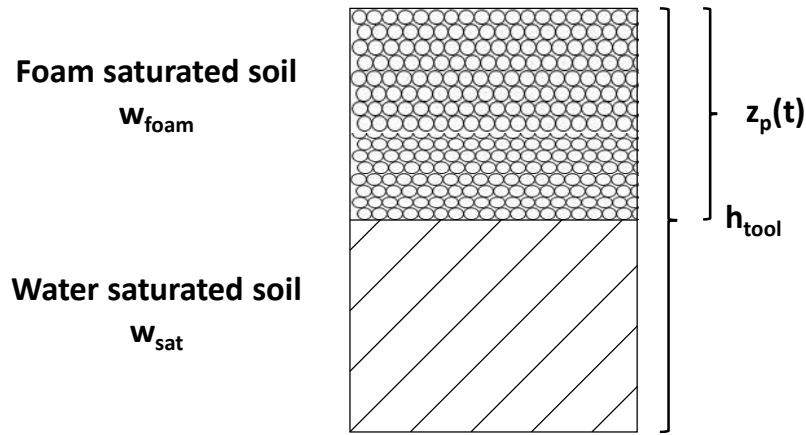
Figure 5-10: Representative excavated volume element (REVE) showing the proportions in water content depending on the degree of foam penetration $z_p(t)$

a. **fully saturated by foam ($z_p(t) \geq h_{tool}$)**

b. **fully saturated by water ($z_p(t) = 0$)**

c. **one part saturated by foam ($z_p(t)$) and one part saturated by water (h_{tool} - $z_p(t)$)**

Assuming initially a complete expel of pore water from the voids in the foam-penetrated region, the water content in the foam-penetrated zone consists only of the foam liquid, which can be described by the parameter w_{foam} [wt%]. The water content of a soil in its water-saturated state, w_{sat} [wt%], can be derived considering the soil's bulk density ρ_d [kg/m³]. Depending on the time-dependent foam penetration depth $z_p(t)$ (condition a., b., or c.), the proportions in water content over tool penetration h_{tool} form the residual excavated water content w_{exc} according to Eq. 5.5.

$$w_{exc}(t) = \frac{\left(h_{tool} - z_p(t)\right) \cdot w_{sat} + z_p(t) \cdot w_{foam}}{h_{tool}} \cdot 100 \qquad [wt\%] \qquad \text{Eq. 5.5}$$

$$\text{with:} \quad w_{foam} = \frac{\frac{n_p}{FER} \cdot \rho_w}{\rho_d} \cdot 100 \qquad [wt\%]$$

wherein ρ_w is the density of water [kg/m³] and n_p is the void ratio [-].

Supposing a certain tool penetration, the change in water content over time due to foam penetration can be calculated. The resulting development of water content for the investigated soils based on Eq. 5.5 is shown in Figure 5-11 for a cutter depth of 20 mm. It can be seen that the residual water content very quickly reaches the lower
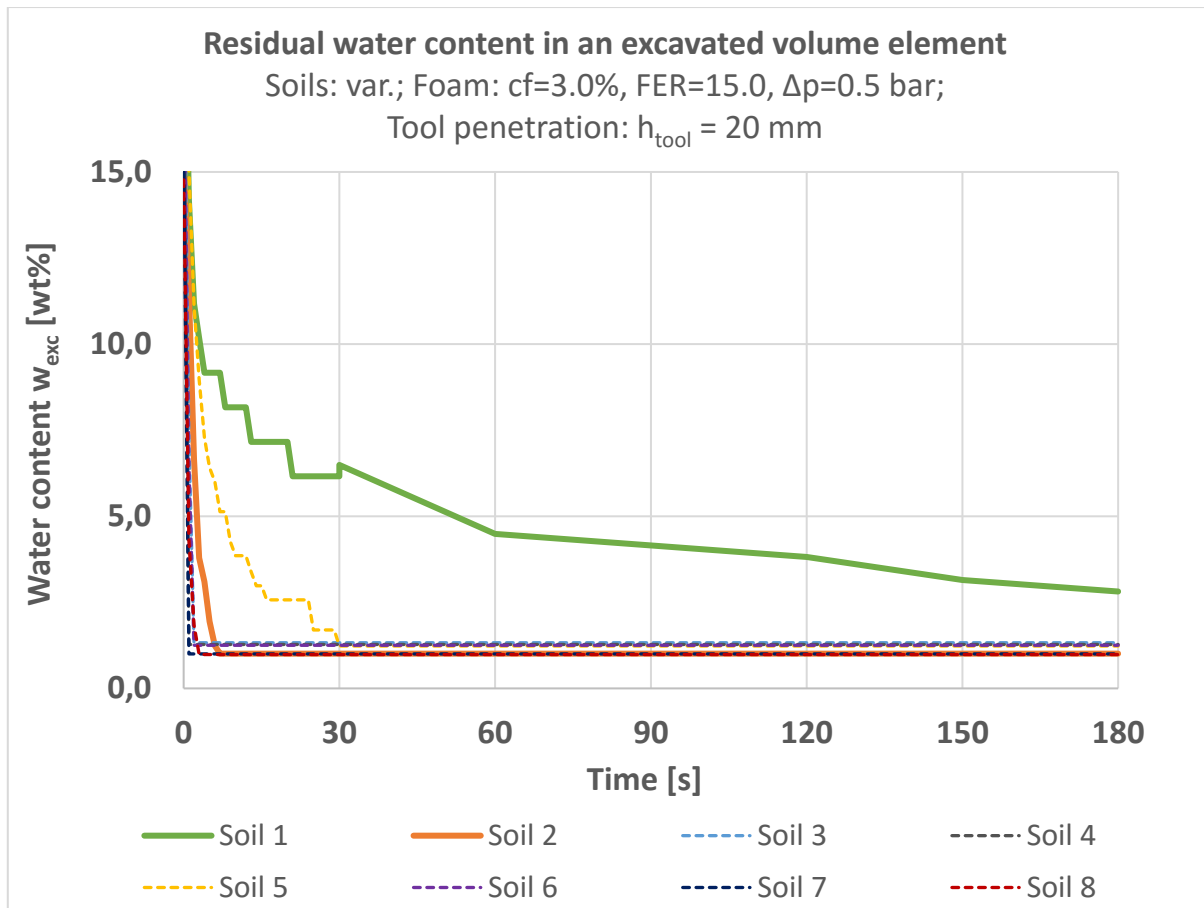
Figure 5-11: Development of the water content of an excavated volume element based on foam penetration tests

boundary limit, which is the foam-water content. A distinct excavated water content can be determined, when the time t is expressed by the procedural parameters turning speed of the cutting wheel N_{CW} [1/min] and the tool stocking per track n_{tool} [-], representing the duration between two cutters passing, t_{tool} [s] (Eq. 5.6). An insertion of Eq. 5.6 into Eq. 5.5 enables a calculation of the residual water content of the excavated material considering advance-dependent parameters.

$$t_{tool} = \frac{60}{N_{CW} \cdot n_{tool}} \qquad\qquad [s] \qquad\qquad Eq. 5.6$$

Except for the very first 1-2 seconds and for the rather fine soils 1 (fine sand) and 5 (fine and middle sand), the determined water contents from the experiments are so low (≈ 1.0 wt%), that neglecting the proportion of residual moist seems grave. At least, a thin film of surface moistening water must actually remain in the foam-penetrated section; otherwise, grains would become dry during the penetration process. Consequently, the suppression of water from the soil in the tests needs to be

evaluated in order to determine how much water stays in the foam-penetrated soil and whether its magnitude needs to be taken into account or not.

5.2.5   Analysis of the residual water in the foam-penetrated soil

Besides the foam penetration, also the water efflux from the drain was recorded in the experiments (Figure 5-12). The outflow rate of expelled water showed the same pattern as the foam infiltration rate (Figure 5-7). From a theoretical point of view, the expected amount of outflow water should equal the pore volume, which was filled by foam. Thus, the relation of water volume and penetrated soil volume should be the void ratio n_p. Table 5-3 shows this (maximum) ratio ($n_{p,test}$) compared to actual values present in the setup ($n_{p,setup}$), which were determined from the soil and water volumes utilised in the tests. In most cases, the actual amount of water is greater than it was expected from the setup. Therefore, the ratio of expelled water and foam penetration depth is larger than estimated. These deviations arise from drained foam water, which needs to be considered in the total amount of outflow water. The same conclusion was drawn by MAIDL (1995). They occur most notably in soils containing
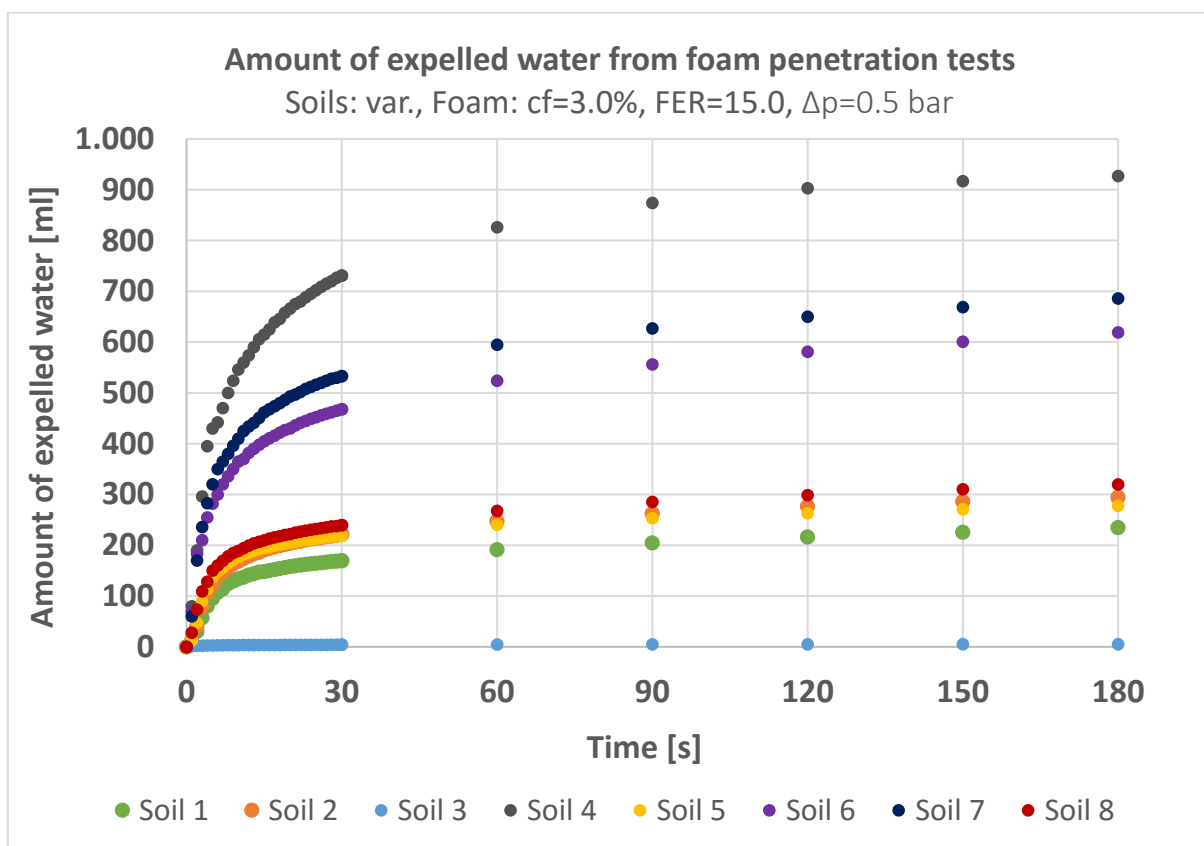
Figure 5-12: Outflow rate of expelled water from foam penetration tests on different cohesionless soils including reference soils 1 (green) and 2 (orange)

Table 5-3:   Void ratios $n_{p,setup}$ of different test samples compared to volumetric ratios of expelled water and foam penetration depth with ($n_{p,corrected}$) and without ($n_{p,test}$) consideration of displaced foam water

Soil	$n_{p,setup}$ [–]	$n_{p,test}$ [–]	$n_{p,corrected}$ [–]
Soil 1 (Fine sand)	0.363	0.596	0.571
Soil 2 (Sand)	0.289	0.370	0.351
Soil 3 (Middle sand)	0.345	0.411	0.388
Soil 4 (Coarse sand)	0.335	0.335	0.313
Soil 5 (Fine and middle sand)	0.337	0.540	0.519
Soil 6 (Middle and coarse sand)	0.332	0.356	0.334
Soil 7 (Middle sand to fine gravel)	0.298	0.288	0.270
Soil 8 (Fine sand to fine gravel)	0.276	0.337	0.318

fine sands. In these soils, the pores are less in size compared to the foam bubbles that usually have diameters around 0.3 - 0.5 mm (GALLI (2009)). Forcing the bubbles to enter the pore space, the foam cells might be destroyed and the interlamellar liquid has to be assigned to the void water. The air will stay entrapped within the soil skeleton. The comparative ratio results then in a corrected value, $n_{p,corrected}$. However, deviations remain partially significant. Presumably, the additional outflow water originates from drainage of the foam sample on top of the soil, which permeates through the penetrated zone. Thus, the magnitude of residual water cannot be measured in a reproducible manner.

In fact, smaller ratio values would have been expected compared to the setup values. There are effects to be regarded, which result from remaining water within the foam-penetrated zone (Figure 5-13). These affect the residual water content obversely as the drainage processes. On the one hand, a moisture film will remain on the grain surfaces (adsorption). Hence, the available pore space for a passage of the liquid is reduced to an effective void volume represented by the index ratio $n_{p,eff}$. On the
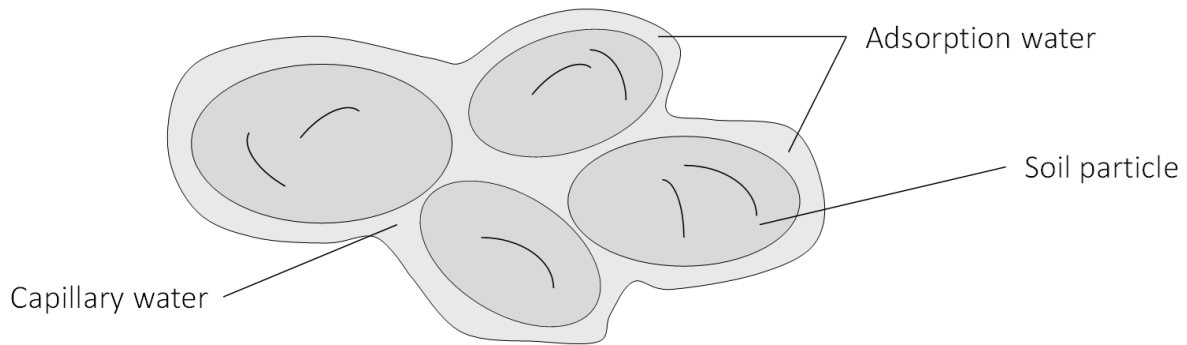
Figure 5-13: Binding form of water in soils (PAWLIK (2014))

other hand, water in capillaries experiences large molecular forces, which can be higher than the applied pressures acting within the grain matrix. Thus, the capillary water might not be able to move as quickly as the foam travels through the grain skeleton. It is then entrapped. In the tests, only soil 7 (middle sand to fine gravel) exhibits a lower test value as it would have been expected, which probably is due to sufficiently large void-sizes for the foam bubbles to pass without any damage.

5.3   Estimation of the remaining soil saturation after foam penetration

The residual water content within the foam-penetrated zone was not sustainably quantifiable over the water outflow rate of the experiments described above. Consequently, a qualitative investigation of the amount of remaining water is conducted estimating the magnitude of absorption and capillary water in the tests. One investigation is based on a physical model (MK model; chapter 5.3.1), into which typical soil parameters are incorporated. The results of its application to the present boundary conditions are compared to simple drainage tests (chapter 5.3.2). If comparable, the findings from both approaches shall provide information on whether the residual water is a weighty factor to be regarded or not.

5.3.1   Soil-water characteristic curve ("MK model")

Depending on the grain-size distribution, the density, the pore space structure and the actual arrangement of particles, soils obtain a very own characteristic relation between saturation (or volumetric water content) and occurring (matric) suction in the soil skeleton. This relation can be described by so-called "soil-water characteristic curves" (SWCC), which are usually determined in experiments like drainage tests. The

matric suction is a negative pressure that results from combined effects of adsorption and capillarity within the soil skeleton. Differences in the suction potential induce flow in unsaturated soils from wet soils (low matric suction) to dry soils (high matric suction). Typical SWCCs for sands, silts and clays are shown in Figure 5-14. As one can easily imagine, the water content decreases with increasing suction from the fully saturated state (S = 1) to dry conditions (S = 0). For coarse soils like sand, the SWCC shows a rather steep course compared to fine soils.
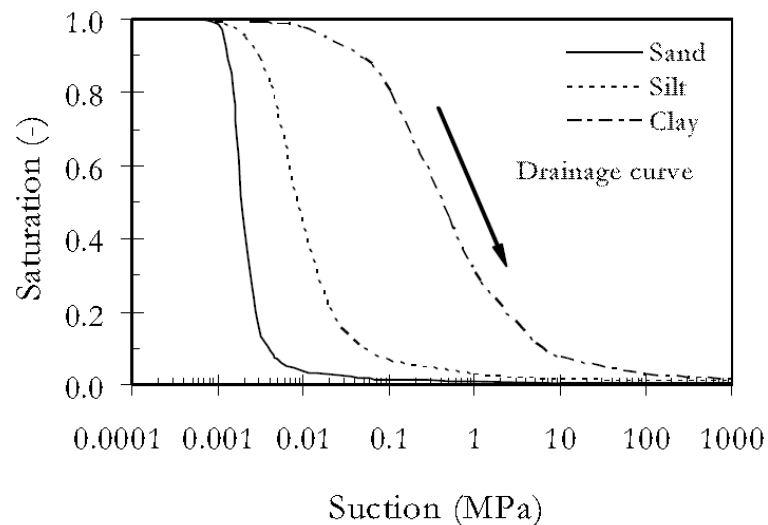
Figure 5-14: Exemplary SWCCs (drainage path) for sand, silt and clay (modified from Lɪɴs (2009))

Characteristic points on the SWCC are the "air entry value" (AEV), which defines the crossing from saturated conditions to partially saturated conditions, and the "residual water content". Beyond the suction that corresponds to the residual water content, adsorption forces become more responsible for the retention of water (Sɪʟʟᴇʀs ᴇᴛ ᴀʟ. (2001)). Water is then transported only by vapour diffusion. The shape and the slope of the SWCC are mainly affected by the pore-size distribution (Lɪɴs (2009)). An exemplary drainage curve for a sand with typical curve parameters and zones is shown in Figure 5-15.

A determination of SWCCs can be done with empirical models, which demand for experimental data. These data can be found in flow experiments of different kind. A quite recent overview of the state-of-the-art, experimental techniques and common approaches, and more issues on this topic can be found in Lɪɴs (2009), which should be consulted for further details. The determination of SWCCs with appropriate techniques is time-consuming and laborious. Since the assumptions considered so far
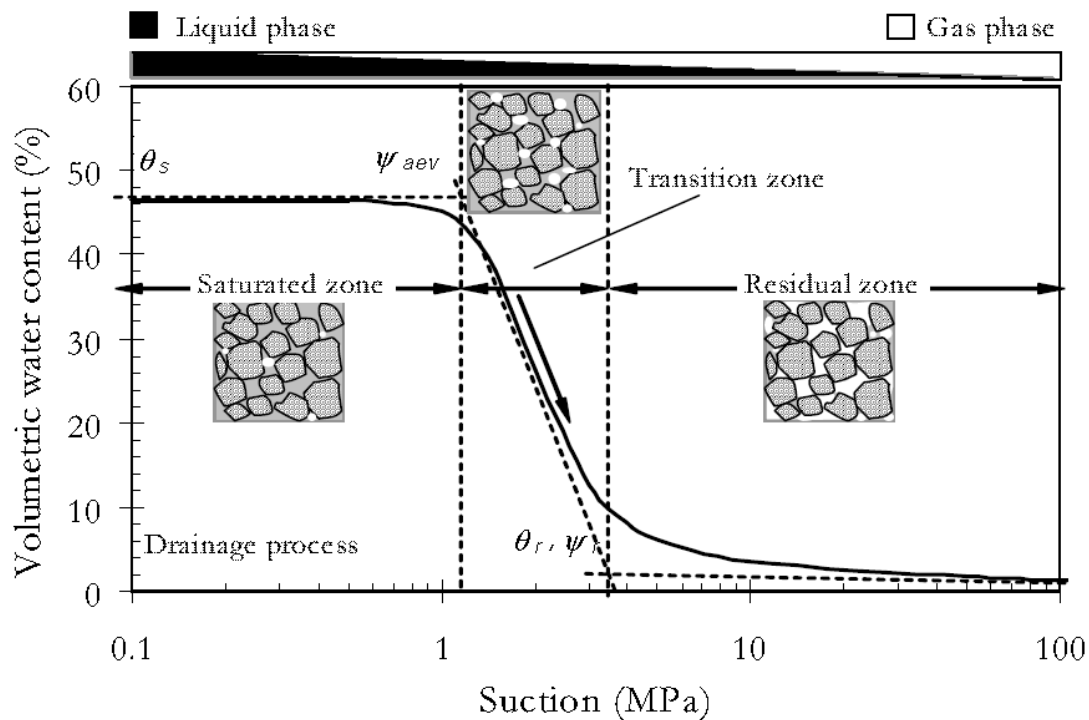
Figure 5-15: **Typical drainage path as part of an SWCC for a sand; with characteristic parameters (saturated volumetric water content, AEV, residual water content) and saturation states (saturated, transition and residual zone) (LINS (2009))**

most likely dominate the precision of these methods, here a physical model (namely "MK model") of AUBERTIN ET AL. (2003) is used to estimate the SWCCs for soils 1 and 2. The MK model is based on soil properties and geometrical parameters and is not dependent of any experimental data. The model bases on the model developed by KOVÁCS (1981) considering some adjustments making the model generally applicable to porous media. It is presented in the following.

The relationship between saturation and matric suction is established through a reference parameter defined as the equivalent capillary rise of water in a porous medium. The equivalent capillary rise is expressed in terms of hydraulic head and is closely defined to capillary rise of water in a capillary tube. Just the representative tube diameter is replaced either by an equivalent pore diameter or, in coarse-grained soils, by an equivalent particle diameter, D_H (Eq. 5.8). Hence, the equivalent capillary rise expressed by h_{co} [cm] can be determined using Eq. 5.7, wherein the second fraction factor represents an approximation of the mass-specific surface area S_m [cm²/g]. According to KOVÁCS (1981), the shape factor α [-] is set to 10.

$$h_{co} = \frac{\sigma_w \cdot \cos \beta_w}{\gamma_w} \cdot \frac{\alpha}{e_p \cdot D_H} = \frac{\sigma_w \cdot \cos \beta_w}{\gamma_w} \cdot \frac{\rho_s \cdot S_m}{e_p} \qquad \text{[cm]} \qquad\qquad \text{Eq. 5.7}$$

$$\text{with:} \quad D_H = [1 + 1.17 \cdot \log C_U] \cdot d_{10} \qquad \text{[cm]} \qquad\qquad \text{Eq. 5.8}$$

wherein σ_w is the fluid surface tension (0.073 N/m for water at 20°C) [N/m], β_w is the contact angle between water and the capillary surface [-], γ_w is the unit weight of water [kN/m³], D_H is the equivalent particle diameter [cm], e_p is the void number [-], ρ_s is the solid grain density [kg/m³], C_U is the coefficient of uniformity [-], and d_{10} is the effective grain diameter at 10 wt% passage [cm].

By Eq. 5.7, a linear relationship is established between a representative grain diameter (here D_H) and the mass-specific surface are S_m. Reconsidering the analysis of the foam penetration tests in chapter 5.2.3, a linear correlation can also be found between h_{co} and the regressor variable a, compare appendix A.2.3.2.

Eq. 5.9 relates volumetric water content θ to soil saturation. The saturation is considered composed of two fractions: in the transition zone (i.e. between the air entry value (AEV) and the residual suction limit), the water is retained by capillary forces, while at higher suction values, the saturation is ruled by adhesive forces (van der Waals interaction). Towards the original model, AUBERTIN ET AL. (2003) reformed the adhesion component of soil saturation. The two components of the saturation, S_a^* and S_c, can be calculated with the help of Eq. 5.10 and Eq. 5.11.

$$\theta = n_p \cdot \left(S_c + S_a^* \cdot (1 - S_c)\right) \qquad \text{[-]} \qquad\qquad \text{Eq. 5.9}$$

$$S_c = 1 - [(h_{co}/\psi)^2 + 1]^{m_p} \cdot e^{-m_p \cdot (h_{co}/\psi)^2} \; \text{[-]} \qquad\qquad \text{Eq. 5.10}$$

with ψ the matric potential [cm], m_p a pore-size distribution parameter [-], and e the Euler number [-].

$$S_a^* = \begin{cases} S_a, & S_a < 1 \\ 1, & S_a \geq 1 \end{cases} \qquad \text{[-]} \qquad\qquad \text{Eq. 5.11}$$

$$\text{with:} \quad S_a = a_c \cdot C_\psi \cdot \frac{(h_{co}/\psi_n)^{2/3}}{e_p^{1/3} \cdot (\psi/\psi_n)^{1/6}} \qquad \text{[-]}$$

wherein S_a is the pristine adhesion component of soil saturation [-], ψ_n is a normalisation parameter [cm], a_c is an adsorption coefficient [-], C_ψ is a correction

factor [-], e_p is the void number [-]. The pore-size distribution parameter m_p can be fairly approximated by the inverse of the uniformity coefficient: $m_p = 1/C_U$ (AUBERTIN ET AL. (2003)). The absorption coefficient a_c can be considered approximately constant for coarse soils, with $a_c = 0.01$ (AUBERTIN ET AL. (2003)). Furthermore, a correction factor has to be considered in order to force the water content to zero (Eq. 5.12), when the matric suction reaches a hydrostatic head of 10^7 cm. This value is commonly defined as ultimate matric potential ψ_0 of the SWCC.

$$C_\psi = 1 - \frac{\ln(1+\psi/\psi_r)}{\ln(1+\psi_0/\psi_r)} \qquad\qquad [-] \qquad\qquad\qquad \text{Eq. 5.12}$$

The residual suction ψ_r can be estimated by Eq. 5.13, wherein e_p [-] is the void number.

$$\psi_r = \frac{0.42}{(e_p \cdot D_H)^{1.26}} \qquad\qquad [cm] \qquad\qquad\qquad \text{Eq. 5.13}$$

Thus, the SWCCs based on the MK model of AUBERTIN ET AL. (2003) (Eq. 5.7 to Eq. 5.13) can be determined for all soils, which are here exemplarily depicted in Figure 5-16 only for the soils of reference, 1 and 2. SWCCs of all soils can be found in appendix
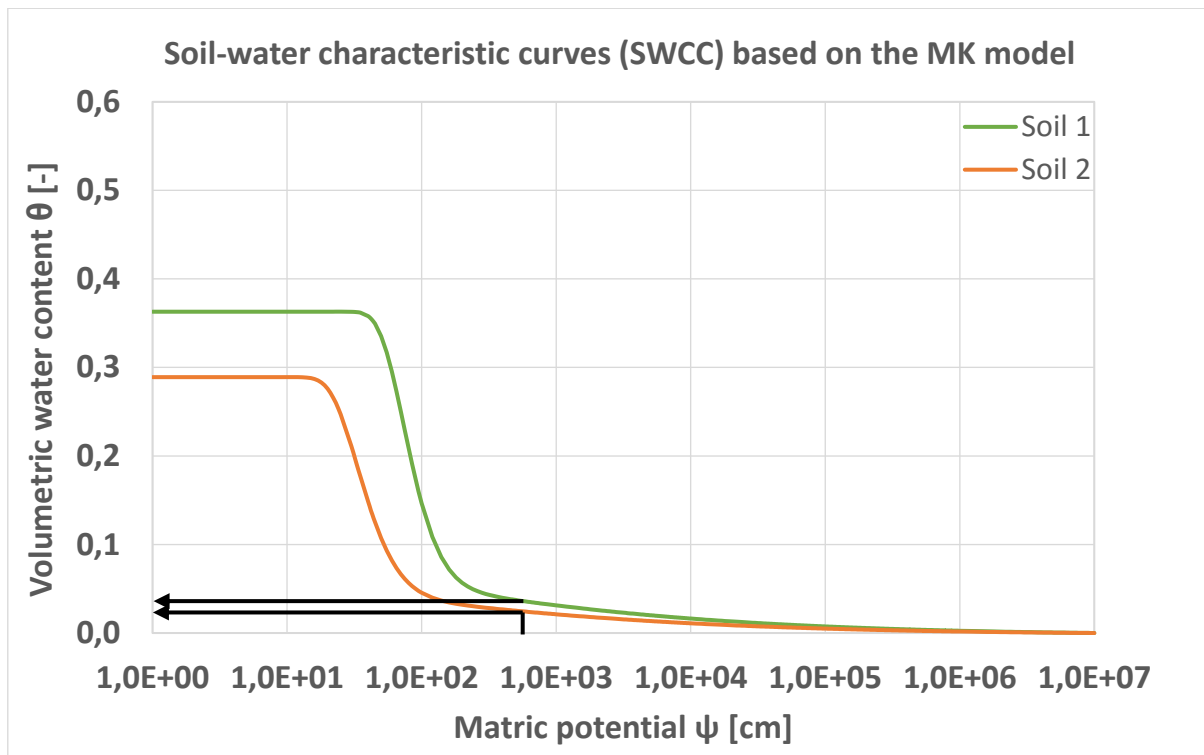
Figure 5-16: Water content-suction relationship for soils 1 and 2 based on the MK model according to AUBERTIN ET AL. (2003); residual water contents are highlighted for an assumed suction of 500 cm occurring in the foam penetration tests

A.2.3.3. Assuming now that the occurring suction at the foam penetration front within the soil matrix equals the applied pressure in the penetration tests (50 kPa = 500 cm), the resultant saturation can be detected. The same applies for the volumetric water content respectively. This actually is a significant simplification, because the pressure decreases along the foam penetration depth. The gradient however is not known. Bearing this in mind, conversion into the gravimetric water content results then in the values $w_{res,SWCC}$ summarised in Table 5-4 (see section 5.3.3) representing the residual moisture within the foam penetrated section. The applied pressure obviously corresponds to a suction beyond the residual suction.

5.3.2   Drainage test

PAWLIK (2014) conducted drainage tests (DT) under a constant pressure load of 50 kPa. She prepared the tests similarly to the foam penetration tests as described in chapter 5.2.2 using only cylinder no. 1 (Figure 5-17). Pressurisation by compressed air for 180 seconds forced the pore water to emit from the saturated soils. Thus, she aimed at determining the residual water content in the penetration zone, where void water was suppressed. The method applied by PAWLIK (2014) to some extent represents one step in a multi-step experiment to determine the soil-water characteristic curve, where several suction levels are applied one after another. In pre-tests, the amount of water was determined filling gussets of the setup, which can
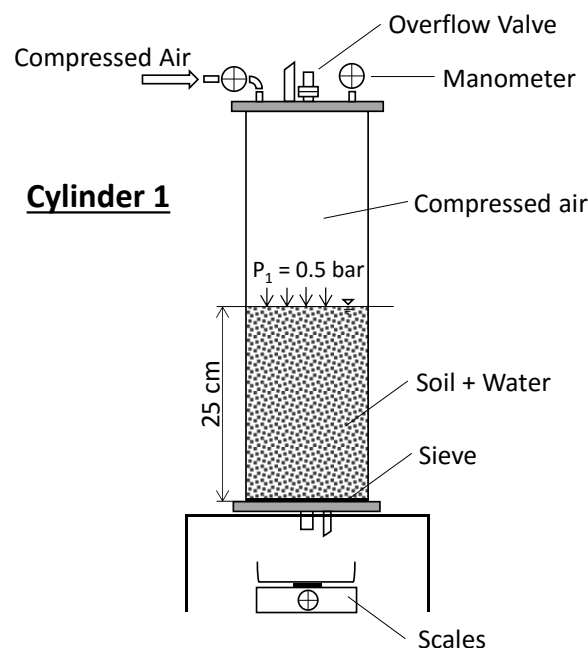
Figure 5-17: Scheme of rig for drainage tests

be treated as a standard error and which needs to be subtracted from the residual water in the cylinder when balancing the test results. As the work of PAWLIK (2014) was conducted within the scope of this study, she used the same soils. The resulting gravimetric water contents $w_{res,DT}$ from the drainage tests for the different soils are summarised in Table 5-4 (see section 5.3.3). Furthermore, PAWLIK (2014) detected a reasonable dependence between the resulting water contents and the soil characteristics, especially the specific surface area.

5.3.3   Results and conclusion

The results of the SWCC approach and of the experimental approach (drainage tests) are summarised in Table 5-4. As for the MK model, the results from the drainage tests show that the amount of residual soil water in the foam-penetrated zone has a significant portion in the total amount of residual moist. Except for soil 8, the findings from the SWCCs and the drainage tests are very close to each other (±0.9 wt%).

Table 5-4:   Residual water contents of test soils 1 - 8 determined in drainage tests ($w_{res,DT}$) and from the characteristic SWCCs ($w_{res,SWCC}$) based on the MK model according to AUBERTIN ET AL. (2003) without considering foam water

Soil	$w_{res,DT}$ [wt%]	$w_{res,SWCC}$ [wt%]
Soil 1 (Fine sand)	7.4	6.3
Soil 2 (Sand)	4.4	4.8
Soil 3 (Middle sand)	4.3	3.6
Soil 4 (Coarse sand)	1.1	1.4
Soil 5 (Fine and middle sand)	6.3	5.7
Soil 6 (Middle and coarse sand)	1.3	2.2
Soil 7 (Middle sand to fine gravel)	2.2	2.0
Soil 8 (Fine sand to fine gravel)	4.3	2.4

The small differences in residual water content between results of the drainage tests and the MK model might result from several factors. Higher residual water contents in the tests may be explained by the test duration. Since the tests lasted only 180 seconds, additional water might have flown out over a longer period of testing. A higher residual moisture from the physical model than determined in the tests may result from the principle assumptions of the model. One of them is the hypothesis that the matric potential accords the backpressure. A further factor of influence might be the surface tension. As the foam penetrates, the groundwater gets in touch with the surfactants and its surface tension reduces depending on the concentration, see STACHE (1979). As defined in Eq. 5.7, this affects the equivalent capillary rise decisively. The surface tension of foams used by BEZUIJEN & SCHAMINÉE (2000) was 0.0215 N/m, which is only one third of the characteristic value for water. Considering this value, the residual water contents reduce by approximately 55%. However, the actual concentrations of foaming liquid in groundwater in the particular sections during testing are not known. The actual amount of foaming liquid coming from foam on top of the soil or from other sections is indefinable. Therefore, the influence of surface tension is disregarded.

Nonetheless, the findings underline the necessity in regarding the residual soil water, although the approaches certainly consider different physical interrelations. Compared to the residual water contents, when neglecting the remaining soil water, the differences are significantly high.

5.4   Water content of the excavated soil

Regardless of the accuracy in its value, the necessity of taking into account the remaining soil moisture in addition to the foam water was clearly emphasised in chapter 5.3. There is a big, non-negligible difference between the free void water, which is replaced by foam, and the total void water content. It is supposed that the lower value of the two residual water contents for each soil (Table 5-4) may serve as a minimum residual soil moisture in the foam-penetrated zone $w_{res,i}$ [wt%] (with i = DT or SWCC) to be considered when assessing the total excavated water at the tunnel face. Adding the residual moisture to the foam-water and reconsidering the approach made in chapter 5.2.4, the excavated water content of a representative volume element can be determined over time using Eq. 5.14.

$$w_{exc}(t) = \frac{\left(h_{tool} - z_p(t)\right) \cdot w_{sat} + z_p(t) \cdot \left(w_{foam} + w_{res,i}\right)}{h_{tool}} \cdot 100 \qquad [wt\%] \qquad \text{Eq. 5.14}$$

$$\text{with:} \quad w_{foam} = \frac{\frac{n_p}{FER} \cdot \rho_L}{\rho_d} \cdot 100 \qquad\qquad\qquad [wt\%]$$

wherein $z_p(t)$ [m] is the time-dependent foam penetration from the foam penetration tests in chapter 5.2.3. The density of the foaming liquid, ρ_L [kg/m³], is approximated by the density of water ($\rho_W = 1{,}000$ kg/m³).

The updated courses of the change in water content for all soils are shown in Figure 5-18, again for a tool penetration h_{tool} of 20 mm.

From the considerations above, water contents for the design of soil conditioning concepts can be determined for specific tunnelling situations. The two master soils of
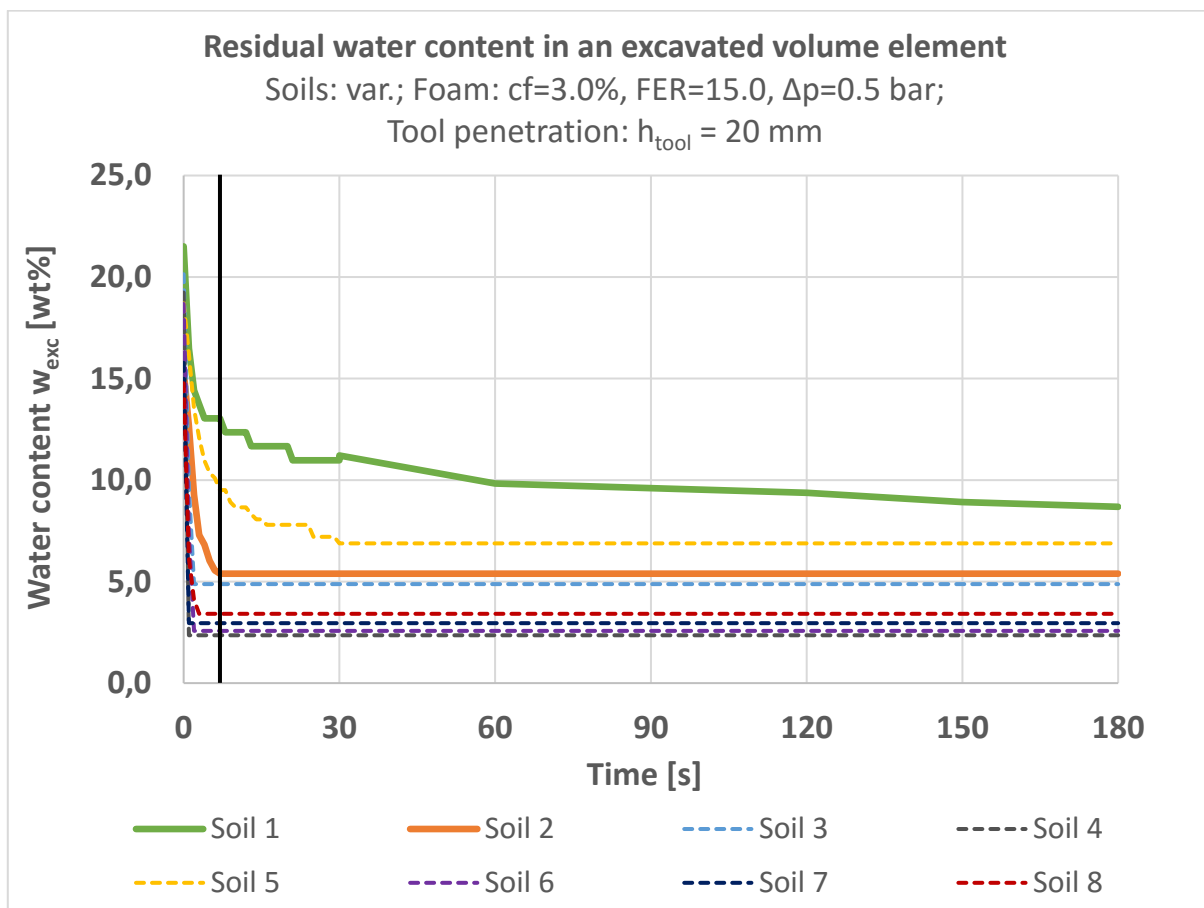

Figure 5-18: Change in water content over time for volume elements composed of the different test soils 1 – 8 to be excavated by cutting tools with a penetration of 20 mm; the vertical black line indicates water contents for a typical tunnelling situation (N_{CW}=1.0 rpm, n_{tool}=8, h_{tool}=20 mm)

the present study shall function as a reference to illustrate the procedure. The following operational parameters are chosen for a tunnel with diameter D_T = 10 m: N_{CW} = 1.0 rpm and n_{tool} = 8. Insertion of these values into Eq. 5.6 and introducing the consequential penetration time (t_{tool} ≈ 8 s) into Eq. 5.14 results in the reference water contents of $w_{exc,soil1}$ = 12 wt% and $w_{exc,soil2}$ = 6 wt% for a tool penetration h_{tool} = 20 mm.

The bandwidth in water contents at these specific typical tunnelling conditions ranges from 2 wt% to 12 wt%. Therefore, the water contents within the experimental work in the main sections of this study are varied between 2 wt% and 12 wt%.

Comparing the approach with the considerations of BEZUIJEN (2002), BEZUIJEN (2012), BEZUIJEN & SCHAMINÉE (2001) as presented before, the obtained water contents are much larger. Using the same (operational) boundary parameters as input values, taking into account the required soil properties and considering that the FIR in the tests equals the pore ratio n_p (i.e. no volume increase due to foam injection), the residual water contents can be determined according to Eq. 5.4. All significant input values as well as the resulting volumetric and gravimetric water contents for the test soils are summarised in Table 5-5. In any case, the residual water content is only dependent of the foam water because the expel rate is expressively larger than the advance rate. Most probably, this is caused by the excessive difference in pressure head. The results go along with the first hypothesis of total void water replacement in chapter 5.2.4, i.e. without consideration of the residual void water.

Table 5-5:   Residual water contents of test soils 1 to 8 according to model of Bezuijen (2002), Bezuijen (2012) and necessary input values

Input	Soil 1	Soil 2	Soil 3	Soil 4	Soil 5	Soil 6	Soil 7	Soil 8
Void ratio n_p [-]	0.363	0.289	0.345	0.333	0.337	0.332	0.298	0.276
FER_{actual} [-]	14.9	15.2	15.0	14.9	15.6	15.0	16	14.6
Soil density ρ_d [kg/m³]	1,688	1,884	1,735	1,762	1,758	1,769	1,860	1,919
Hydraulic conductivity k [m/s]	1.6e-4	1.7e-4	2.2e-4	2.8e-4	1.5e-4	2.5e-4	2.2e-4	5.2e-5
Hydraulic head at tunnel face ϕ_0 [m]	5	5	5	5	5	5	5	5
Specific discharge of expelled pore water at tunnel face q_0 [m/s]	1.6e-4	1.7e-4	2.2e-4	2.8e-4	1.5e-4	2.5e-4	2.2e-4	5.2e-5
Tunnel radius R_T [m]	5	5	5	5	5	5	5	5
Tool penetration h_{tool} [m]	0.02	0.02	0.02	0.02	0.02	0.02	0.02	0.02
Turning speed cutting wheel N_{CW} [rpm]	1	1	1	1	1	1	1	1
Advance rate v_{adv} [m/s]	3.3e-4	3.3e-4	3.3e-4	3.3e-4	3.3e-4	3.3e-4	3.3e-4	3.3e-4
Output	Soil 1	Soil 2	Soil 3	Soil 4	Soil 5	Soil 6	Soil 7	Soil 8
Residual water content (volumetric) $\theta_{residual}$ [vol%] according to Eq. 5.4	2.44	1.90	2.30	2.25	2.17	2.22	1.86	13.87
Residual water content (gravimetric) $w_{exc,Bezuijen}$ [wt%]	1.44	1.01	1.33	1.28	1.23	1.25	1.00	7.23

6. INDEX TESTS ON SOIL-FOAM MIXTURES USING THE SLUMP TEST

Index tests are frequently used in practice in order to gain information on material properties in a simple and low-cost manner. They represent a compromise between quality of the information to be obtained and the complexity of the test method. In EPB tunnelling, the slump test from concrete engineering according to DIN EN 12350-2 (2009-08) is one often-applied index test to evaluate the conditioning behaviour of soils. Studies have been performed also in research very extensively, see chapter 2.4.2. An analysis of the obtained results regarding rheological parameters has yet not taken place.

In order to establish a link between slump tests and rheology, the analytical models that were presented in chapter 3.3 needed to be reconsidered and adjusted to be applicable to a test series on foam-conditioned soils. Therefore, an extensive experimental program was completed. Test setup and test procedure were closely aligned to the normative regulations. Experience from pre-studies, however, disclosed some significant influences from the test proceeding on the results. As far as possible, these influences were considered through enhancements in design and temporal constraints. The analytical slump models could then be applied to the test data. Finally, the value of information the models provided was analysed.

6.1 Pre-studies

Slump tests have been used for qualitative and quantitative assessment of the conditioning behaviour of soils in both EPB tunnelling practice and research. Standardised procedures do not exist with respect to EPB-related material (conditioned soils), although all applicants used similar test setups, which are either

related to DIN EN 12350-2 (2009-08) or comparable international / national standards.

PEILA ET AL. (2008), VINAI (2006) show that time is a demanding factor in slump testing. Drainage and restructuring effects occur within the foam leading to pre-consolidation over time, see Figure 6-1. Hence, test results are less comparable and less reproducible when working with nonuniform reference times. PEILA ET AL. (2008), VINAI (2006) use this behaviour as quality index for the stability of the soil-foam mix over time. The final slump result is affected by the time-dependent changes of the material properties and thus, it reduces over time. VINAI (2006) found a logarithmic approximation suitable to describe the slump development (Figure 6-2).

Figure 6-1:   **Water outflow due to drainage effects (left), consolidation effects due to structural changes in the material (GESING (2013))**
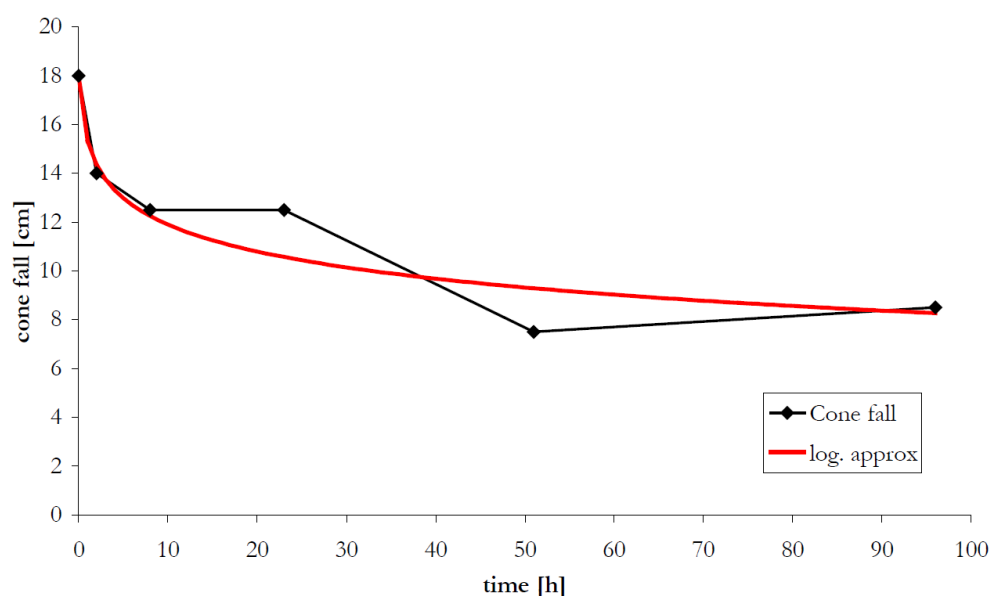

Figure 6-2:   **Slump development of one soil-foam mixture over time and logarithmic approximation (VINAI (2006))**

Recent research on the expressiveness of this test for EPB material and on possible faults deriving from the test execution, which were conducted by GESING (2013), KAYSER (2015) as pre-tests for the present study, revealed significant results. GESING (2013) used a slump test setup, which was amended with guide rails (Figure 6-3). Thus, lifting of the cone is performed vertically. Furthermore, he used a plate that could be fit into the guide rail system containing a coordinate system as shown in Figure 6-3. From a defined spot, photographs were taken for photo-optical measurement and analysis respectively. Thus, it enables analysing the slump shape not only by the slump value and the spread but also in every single location of the spline. Sketches of the setup can be found in the appendix chapter A.3.1.
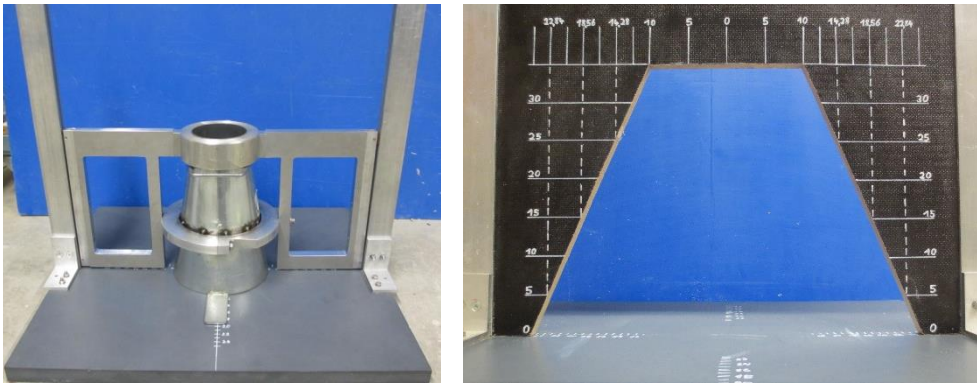
Figure 6-3:   Realised version of the modified slump test (left; GESING (2013)); 2-d coordinate measuring plate (right)

As PEILA ET AL. (2008), VINAI (2006), GESING (2013) found the time to be a factor of severe influence in slump testing, too. Therefore, a specific testing procedure was setup considering precise temporal constraints as well as an alignment of the single steps of the test preparations (Figure 6-4). It establishes the basis of the principle temporal testing procedure as presented in chapter 4.3.3.

KAYSER (2015) conducted tests with other flow-out tests that are founded on the basic principle of cone lifting such as the flow table test cone (DIN EN 12350-5 (2009-08)), the mortar cone (DIN EN 1015-3 (2007-05); with Haegermann Table) and a miniature slump cone according to MALUSIS ET AL. (2008), see chapter 3.3. KAYSER (2015) tried to elaborate further ranges for a recommended workability with the other test methods because on the one hand the flow table test represents the mainly applied test to determine the consistency of fresh concrete in Germany, whereas on the other hand possible savings in the required sample volume would be favourable. However, he found out that the materials exhibiting the same slump values in the standard slump

Beginning of time count:

Foam production $t_0 = 0$min

		time

1 Determination of FER, filling foam into mixer
2 Mixing
3 Homogenization of the mixture with scraper
4 Mixing, meanwhile pre-moistening of
   bottom plate and cone
5 Filling the cone in three layers
6 Lifting of the cone
7 Photo from in front
8 Surveying the sample

step no.

0 1 2 3 4 5 6 7 8 9 10 [min]

1 — 210 sec
2 — 15 sec
3 — 30 sec
4 — 15 sec
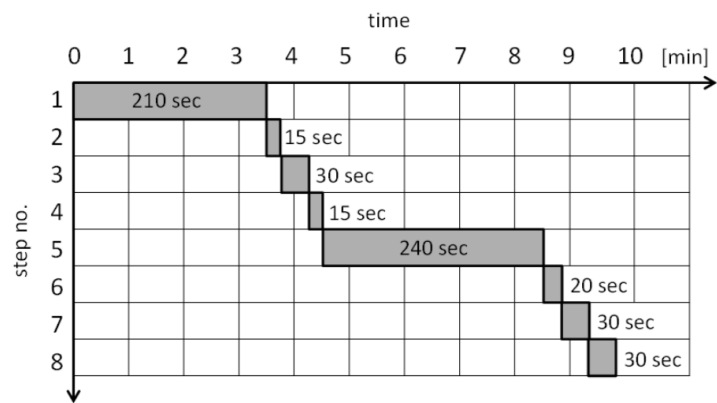5 — 240 sec
6 — 20 sec
7 — 30 sec
8 — 30 sec

Figure 6-4:   Standard procedure for slump tests

test according to DIN EN 12350-2 (2009-08) showed different patterns of workability using the other established tests – all of them considering the procedural influences and affections from the design as elaborated by GESING (2013). One explanation for this phenomenon could be that the materials actually do not possess the same flow behaviour. KAYSER (2015) also took the work of MALUSIS ET AL. (2008) into account, which considers a scaling of the geometrical slump proportions. The resulting shapes of the materials owning the same slump value actually look different, especially regarding the undeformed part.

ALTUN (2011) investigated the applicability of the prognosis model of CLAYTON ET AL. (2003) to soil-foam mixtures. He had little success in finding a good correspondence between real slumps and the theoretically expected values. Instead of the material yield stress and the unit weight, ALTUN (2011) used undrained shear strength measurements from a laboratory shear vane and the material density. Hence, the applicability of the prognosis model to slump tests on soil-foam mixtures could yet not been demonstrated correctly.

6.2   Setup, testing procedure and experimental programme

The test setup consists of the equipment as demanded in DIN EN 12350-2 (2009-08), except for the guide rail extension for perpendicular lifting and the coordinate plane as proposed in chapter 6.1. The test procedure is aligned to the general testing schedule described in chapter 4.3.3 and to the elaborated sequence of GESING (2013) mentioned above. After preparation of the probe (step no. 2 in Table 4-2), step no. 3 incorporates the filling of the test preparations, i.e. the filling of the cone. Filling and densifying of the inserted material are performed according to DIN EN 12350-2

(2009-08) in three layers of equal height. After filling of each layer, the material is compacted by equally distributed immersions of a steel bar within the layer. Photographs are taken for later verification of possible errors in recording the measurements. Besides the slump measure S in the planar reference, also the average slump flow SF of depth and width is recorded as well as occurring heights h_0 of the undeformed section of the original conical shape after lifting. The recorded parameters are depicted in Figure 6-5. Details on the test setup and a precise description of the testing procedure can be found in chapter A.3.1.

The testing programme is based on a parametric study considering a variation of single sample properties. According to current literature, a suitable flow behaviour of soil-foam mixtures is determined by slump values ranging between 10 and 20 cm. The reference FIR leading to a slump of 10 cm (FIR_{10}) and of 20 cm (FIR_{20}) of the foam-conditioned soils 1 and 2 were found in preliminary tests and are indicated separately in Figure 6-6. The reference water contents for soils 1 and 2 were determined from the foam penetration tests as described in details in chapter 5.2.4. The experimental programme for the index tests and the variation parameters for both soils are presented in Figure 6-6.
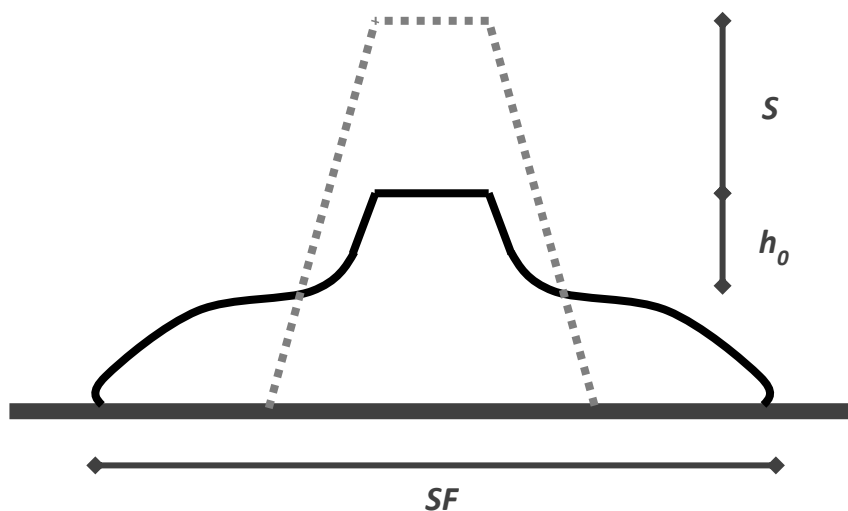
Figure 6-5:   **Recorded values in slump experiments**
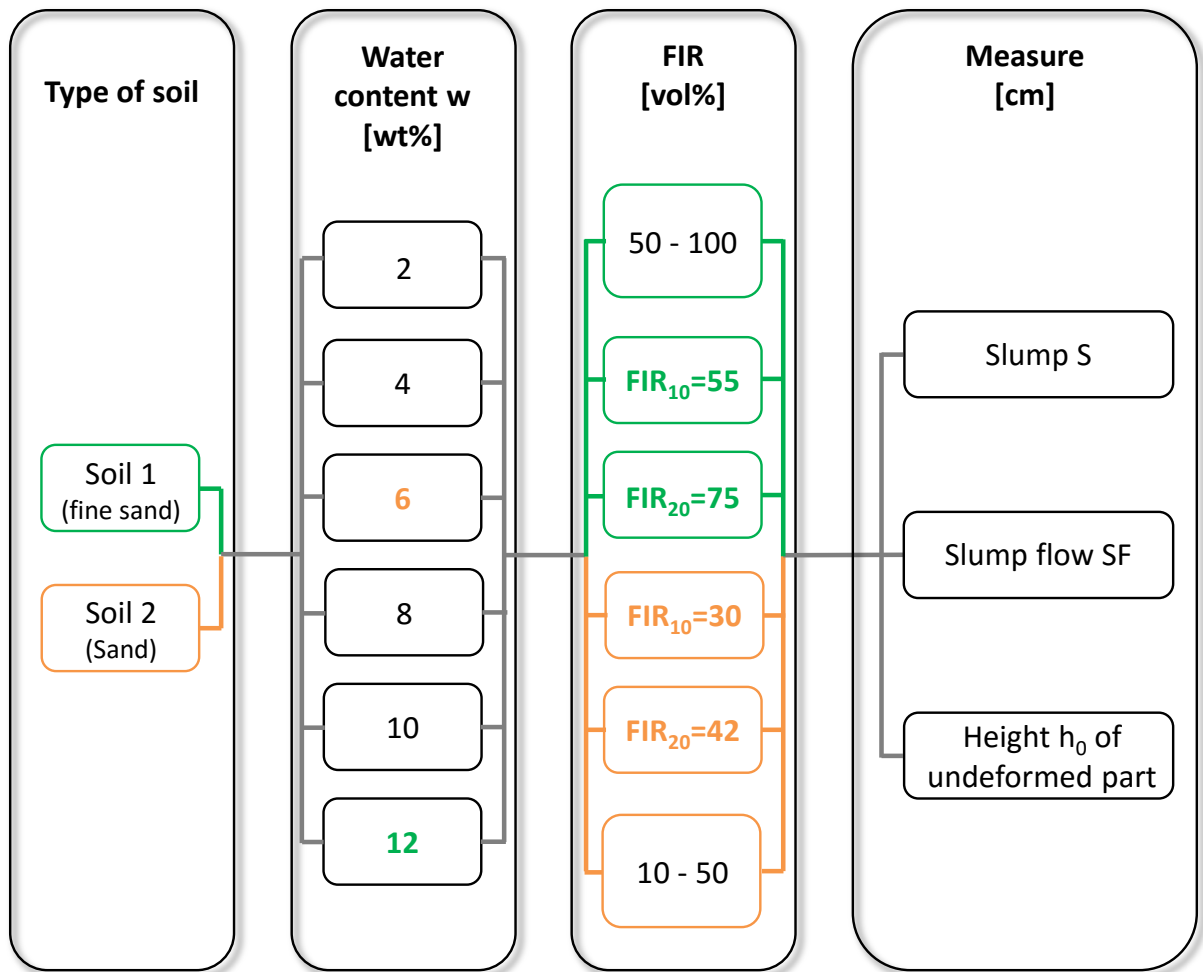
Figure 6-6: Experimental programme for index tests and variations of material parameters: black boxes for both soils, coloured boxes only for corresponding soil; coloured water contents represent reference water contents for FIR_{10} and FIR_{20}

6.3   Test results

The slump test results of the different soil-foam mixtures act as one might expect: the more water or foam the soils contain the bigger the resulting slump measure. The same applies for the slump flow measure respectively. Furthermore, both soils with each water content can be conditioned to a suitable flow behaviour in terms of recommended slump values of 10 and 20 cm. The value of h_0, i.e. the height of the undeformed shape, reduces with increasing FIR. However, the systematic test series provides more information as probably can be seen at a first glance. Consequently, the results are processed in more detail separately for each measuring parameter.

6.3.1   Slump S

The test results of the slump test are depicted in Figure 6-7. A diagram showing the slump data in dependence of the water content can be found in chapter A.3.3.1. Each data point represents the mean value of at least three tests with one soil-foam mixture. Additionally, the standard deviation of the slump measures of the single mixtures is attached to the data points as well. The connecting lines between the data points shall support the legibility of the data only. The colours signify one variation of the water content, dashed lines stand for Soil 2 (sand) and continuous lines for Soil 1 (fine sand). The constant black horizontal borderlines highlight the recommended range for a suitable flow behaviour (compare chapter 3.2.3).
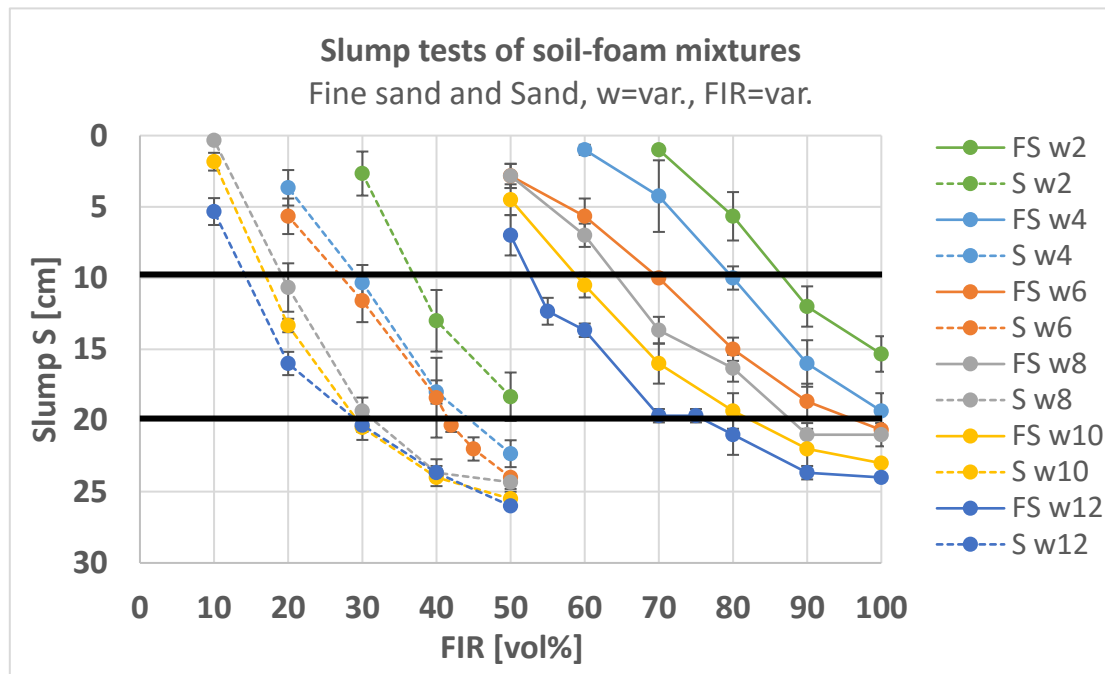
Figure 6-7:   **Mean slump values S and standard deviations from experiments on different soil-foam mixtures over foam injection ratio FIR; colours represent water contents, type of line stands for type of soil (continuous: soil 1/fine sand, dashed: soil2/sand). Black lines indicate recommended range of suitable workability.**

The course of the lines might indicate a possible correlation between the main variation parameters (soil, water content, foam injection ratio) and the test measures (slump). Therefore, a statistical analysis is performed in order to investigate truly existing relationships between the independent variables (= variation parameters) and the dependent variables (= measures). Since multiple independent variables are involved, a multivariate data analysis is required. The aim of the analysis is to find a

significant functional relationship. The classical method for these types of data analysis is the multiple linear regression, see HENRION & HENRION (1995). Establishing a basic functional relationship between the independent variables and the one dependent variable forms the starting point of the regression analysis, which contains additional regression coefficients.

From Figure 6-7, a non-linear trend can be estimated describing the slumping behaviour best. A similar conclusion can be drawn from the results when outlined over the water content (see chapter A.3.3.1). Therefore, the estimated function describing the dependency between the Slump and the water content w and the FIR is chosen to be a polynomial equation of the second order (Eq. 6.1). An inclusion of a third independent variable as representative for the soil type was consciously excluded because the number of alterations in the experiments was too small to expect a reliable dependency. The usage of more soils in similar experiments in future variation studies would allow for an implementation of an additional parameter. The soil could be considered for example by the representative grain-diameter at 60% passage in the sieve analysis (d_{60}), the uniformity coefficient C_u or the curvature coefficient C_c.

$$S(w, FIR) = b_0 + b_1 \cdot w + b_2 \cdot FIR + b_3 \cdot w \cdot FIR + b_4 \cdot w^2 + b_5 \cdot FIR^2$$

<div align="right">[cm]   Eq. 6.1</div>

wherein the parameters b_i represent the regression coefficients. By applying the linear least-squares methodology to the present data, the regression coefficients b_i can be found that lead to the best fit of the model to the sampled data, which actually represents a three-dimensional fitting plane. The method of least squares is a calculation process, which minimises the sum of squared deviations between the actual measured slump values $S_{measured}$ and the predicted slump values $S_{predicted}$, which underlie Eq. 6.1, by alteration of the regression coefficients b_i. In multiple linear regression, it is based on matrix algebra. It is substantial to mention that this method considers only the vertical deviations between the data points and the implicit function to fit.

The final resulting equations describing the behavioural dependency between the slump and the water content and the FIR for the two investigated soils are Eq. 6.2

and Eq. 6.3. Comparative analyses have been conducted with polynomial functions of third order. The fitting was not significantly increased. It was also considered to restrict the iteration process through boundary conditions in order to produce only meaningful results, such as positive outcomes for S ($b_i \geq 0$) or a crossing of the origin ($b_0 = 0$) are musts. However, the complexity would have increased unreasonably.

Soil 1:

$$S_{FS}(w, FIR) = -64.126 + 4.112 \cdot w + 1.147 \cdot FIR - 0.019 \cdot w \cdot FIR$$

$$-0.088 \cdot w^2 - 4.0 \cdot 10^{-3} \cdot FIR^2 \qquad [cm]$$

$$\overline{R}^2 = 0.968 \qquad \text{Eq. 6.2}$$

Soil 2:

$$S_S(w, FIR) = -41.344 + 4.609 \cdot w + 1.713 \cdot FIR - 0.040 \cdot w \cdot FIR$$

$$-0.131 \cdot w^2 - 12.5 \cdot 10^{-3} \cdot FIR^2 \qquad [cm]$$

$$\overline{R}^2 = 0.970 \qquad \text{Eq. 6.3}$$

Having obtained the equations above, the multiple regression analysis demands for some tests, determining the goodness of fit of the overall model on the one hand and the significance of the regression variables on the other. The goodness of fit of the regression model can be described by two factors: one is the coefficient of determination, R^2; and the other is the F-test. Generally, the coefficient of determination describes the ratio of the explained sum of squares SS_E and the total sum of squares SS_T [here: cm²]. In multivariate data analysis, the coefficient of determination is defined slightly different from single variable conditions because the pure addition of further explanatory variables to the regression model increases causelessly the quality of fit, cf. MONTGOMERY (2005). Therefore, it is adjusted to $\overline{R}^2$ by considering the present degrees of freedom and can be rewritten to Eq. 6.4.

$$\overline{R}^2 = 1 - \frac{SS_R/(n-p_r-1)}{SS_T/(n-1)} \qquad [-] \qquad \text{Eq. 6.4}$$

with SS_R the residual sum of squares [cm²], n the sample size [-], and p_r the number of regression variables without the intercept [-]. Due to its values close to one, the

coefficient of determination manifests a strong relationship between the regression models and the present data here (Table A-2 in appendix A.3.4).

However, it is still to prove, if an overall functional relationship exists between the independent and dependent variables, see MONTGOMERY (2005). This can be determined through an F-test, which approves or refuses the hypothesis of a dependency of the regression coefficients. Furthermore, multiple regression analysis demands for a significance test. It might occur that some of the independent variables are statistically insignificant for the overall functional description. Then, a reduction of variables is advantageous. This is achieved through statistical hypothesis testing of the regression coefficients by a t-test, see MONTGOMERY (2005). If the regression coefficients are insignificant, they can be neglected, and thus, the corresponding independent variables vanish, too. The final function is reduced to significant terms only and by this, the scope for interpretation is enhanced.

The elimination of variables happens stepwise, which is why the fitting process with the least squares method has to be repeatedly executed. The procedure is as follows: A t-value t_i is established for each determined regression coefficient b_i using Eq. 6.5, which is compared to the two-tailored Student distribution (t-distribution) value at a probability level of 95%, considering the present degrees of freedom

$$t_i = |b_i| \cdot \sqrt{\frac{n - p_r - 1}{\sum_{i=1}^{n}(S_{measured,i} - S_{predicted,i})^2 \cdot c_{i+1}}} \qquad [-] \qquad \text{Eq. 6.5}$$

with b_i the regression coefficient [-], $n-p_r-1$ the degrees of freedom [-], $S_{measured}$ the measured slump [cm], $S_{predicted}$ the prognosed slump value from the model [cm], and c_{i+1} the value from main diagonal of the matrix operation [-]

If the test value t_i exceeds the tabulate value $t_{0.95}$ of the Student distribution, the probability that the corresponding regression coefficient exhibits a value unequal zero is 95%; i.e. it is significant. In turn, this means, that a test value is insignificant, when it is smaller than the reference t-value $t_{0.95}$. If one or more test values are smaller than the reference t-value, the regression coefficient exhibiting the smallest test value t_i is excluded from the regression analysis and regression is performed again. This procedure is repeated until all regression coefficients are tested significant.

At last, confidence intervals have to be calculated for the coefficients of regression in order to provide a range of confidence, in which the true values can appear.

Table A-2 in appendix A.3.4 gives a summary of the output values of the regression analyses and corresponding tests (F-test, t-test, confidence levels, and coefficients of determination). The results of t-test and F-test show that a dependency between the variables exists and that the regressors are statistical significant. Eq. 6.2 and Eq. 6.3 represent already the models in the final form after applying all statistical testing. Further details on the statistical analysis of engineering experiments can be found in HENRION & HENRION (1995), LIPSON & SHETH (1973), MONTGOMERY (2005), MYERS (1986).

Figure 6-8 exemplarily shows the course of the final equations for soil 1 in the two-dimensional FIR-S-plane. The distribution of mean values as shown in Figure 6-7 is plotted into the diagram, too, in order to visualise the fitting behaviour. An equivalent diagram showing the functional relationship towards the water content can be found in appendix A.3.3.1 as well as both illustrations for soil 2.

In order to validate the functional relationship, the formulas shall be applied to data from literature. BUDACH (2012) and KAYSER (2015) also performed systematic slump experiments with similar soils. The application of Eq. 6.2 and Eq. 6.3 ("Model Galli 2016") to their data is shown in Figure 6-9 and Figure 6-10.
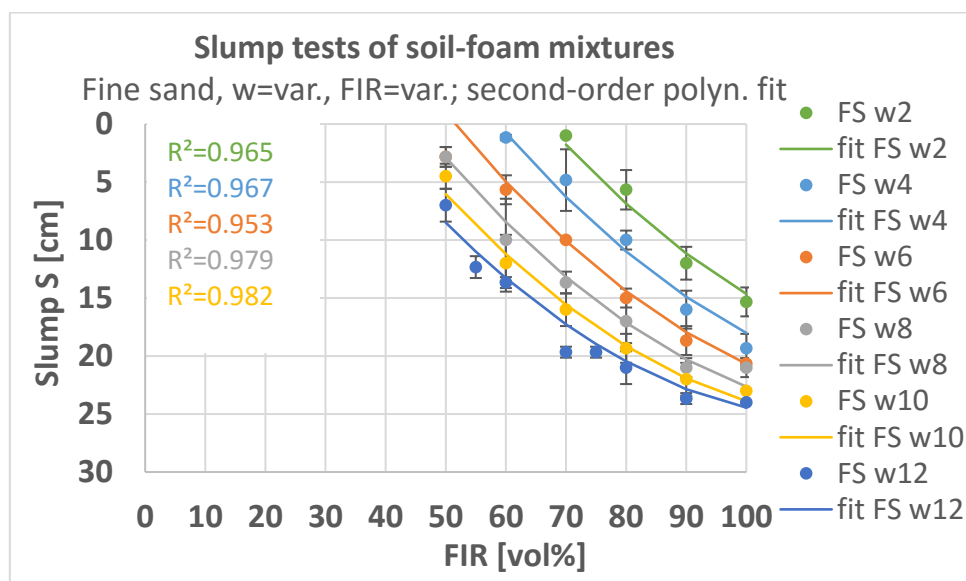
Figure 6-8:   **Mean slump values S (dots) and standard deviations from experiments on fine sand-foam mixtures over foam injection ratio FIR fitted by a second-order polynomial equation (continuous lines)**
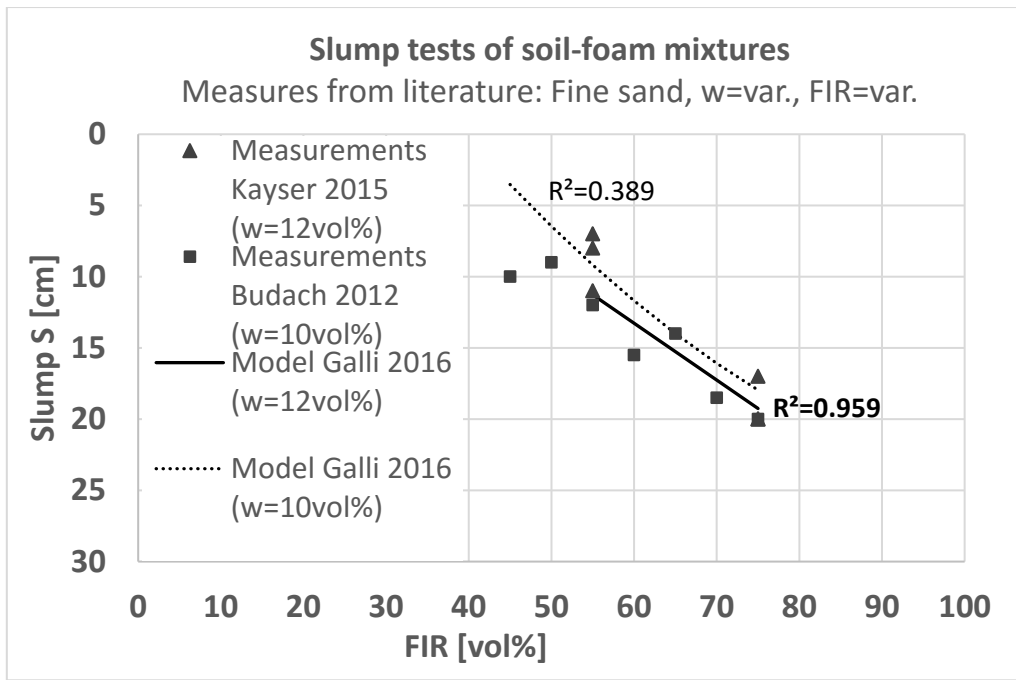
Figure 6-9: Application of model function to slump measures on fine sand-foam mixtures from literature
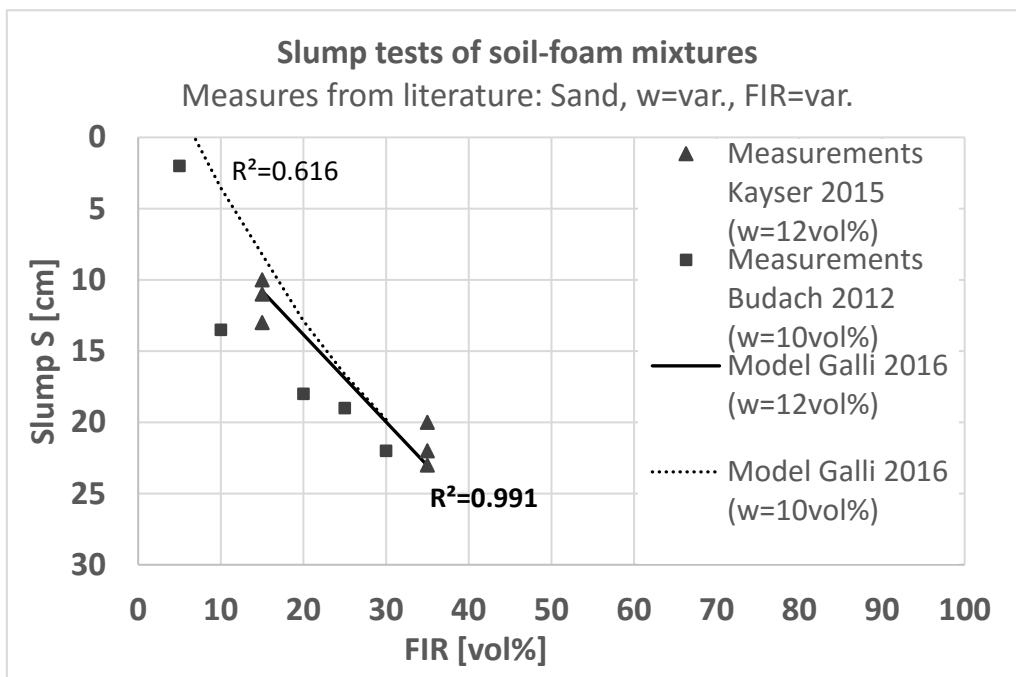
Figure 6-10: Application of the model function to slump measures of sand-foam mixtures from literature

The data of KAYSER (2015) is approximated well by the equations ($R_{FS}{}^2 = 0.959$, $R_S{}^2 = 0.951$), however, the population of data is very low. A description of the measures of BUDACH (2012) by the equations is not successful ($R_{FS}{}^2 = 0.389$, $R_S{}^2 = 0.616$); the slump values are underpredicted. An additional factor to bear in

mind can be differences in the testing or sample preparation procedures that influence the goodness of fit. These differences are not present in comparison to the experiments of KAYSER (2015). An application to further data would enhance the applicability of the generated model.

6.3.2 Slump flow SF

The results of slump flow measurements are shown in Figure 6-11. Again, additional diagrams can be found in the appendix (chapter A.3.3.2). The format is the same as for the slump data. As described before for the slump test in chapter 6.3.1, the same data analysis process could now be repeated for the measures of the slump flow. However, the slump flow test usually is performed in one with the slump test. It is worth contemplating, if there is a correlation between the slump and the slump flow. BUDACH (2012) and KAYSER (2015) tried to correlate the results from their experiments and independently found a quite good correlation of the slump with the slump flow using a logarithmic function, see Table 6-1. However, the standard measure referred to in EPB technology is the slump value. Therefore, a correlation of the slump flow on the slump would be more reasonable. A conversion of their formulas leads to an exponential relationship of the slump flow and the slump (Table 6-1). In comparison
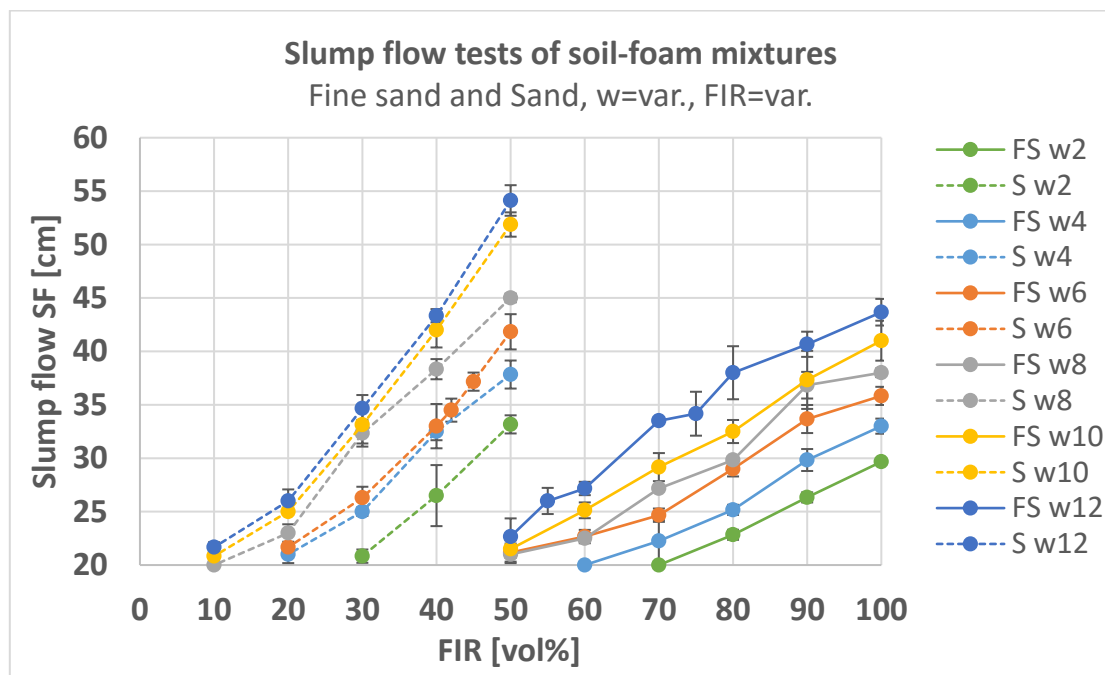
Figure 6-11: Mean slump flow values SF and standard deviations from experiments on different soil-foam mixtures over foam injection ratio FIR; colours represent water contents, type of line stands for type of soil (continuous: soil 1/fine sand, dashed: soil2/sand)

Table 6-1:   Models of Budach (2012) and Kayser (2015) describing the functional relationship between slump S [cm] and slump flow SF [cm]

	Original fitting equations	Converted equations
Budach (2012)	$S(SF) = 22.227 \cdot \ln(SF) - 60.253$	$SF(S) = e^{\frac{(S+60.253)}{22.227}}$
Kayser (2015)	$S(SF) = 23.105 \cdot \ln(SF) - 63.076$	$SF(S) = e^{\frac{(S+63.076)}{20.105}}$

to Budach (2012), the number of tests in this study, that can be used for such a correlation, is much larger and is performed following a strict temporal testing procedure. However, this study is limited to two types of soil compositions only. In comparison to Kayser (2015), the number of variations in water content and injection ratio of foam applied here exceeds his scope in testing. The mean measures of slump and slump flow of all soil-foam mixtures as presented above are summarised in Figure 6-12.

Quite surprisingly, all data seem to coincide with a functional relation regardless of
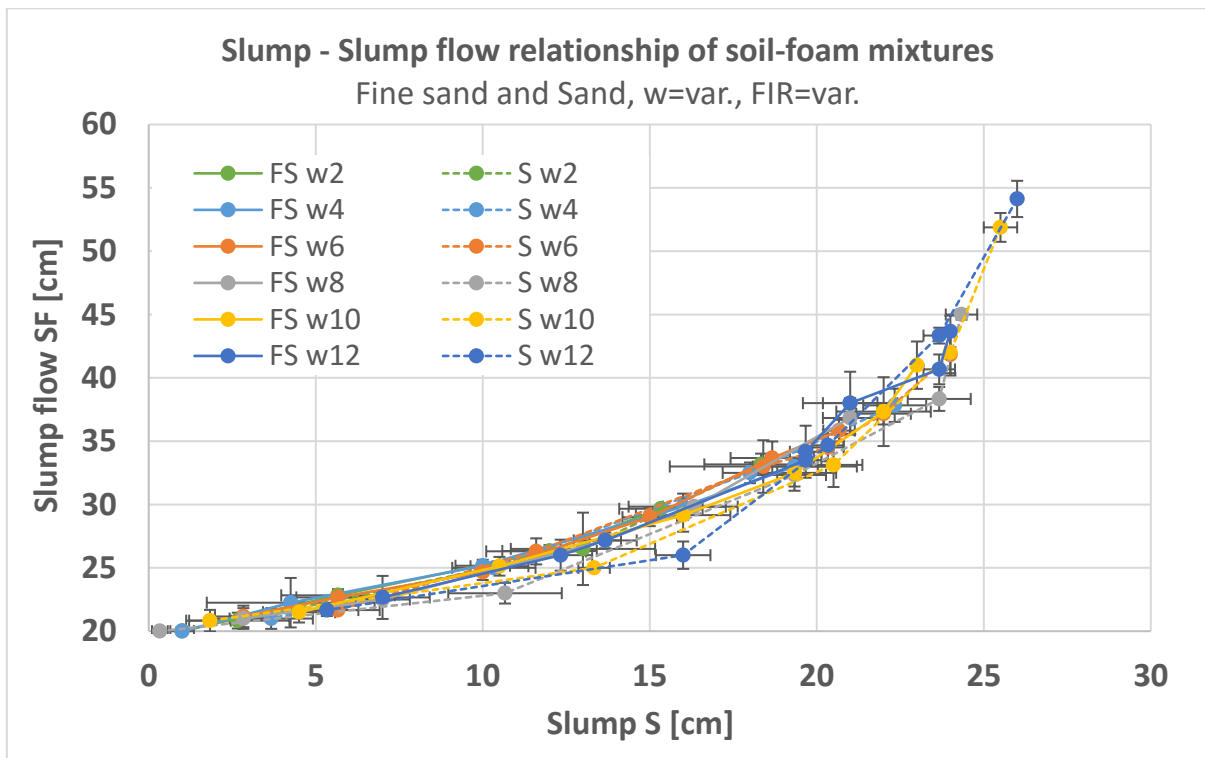

Figure 6-12: Mean slump flow values SF over corresponding mean slump values S and standard deviations from experiments on different soil-foam mixtures

their composition. Therefore, a correlation analysis is performed again using the methods of linear regression and least squares. Due to its coinciding appearance, the single constituent fractions of the different mixtures are neglected at first for the regression analysis. Once more, a non-linear basic function is assumed of second polynomial order, which after application of the least square process results for the present data in Eq. 6.6 (R^2 = 0.951). The constant term was pre-defined to the initial bottom diameter of the slump cone (20 cm), which is the least possible slump flow value. The regression coefficients need to be positive in order to assure values of SF greater or even 20 cm. Eq. 6.6 simply describes a wide parabola. If the analysis is conducted separately for each of the soils, the difference in the resulting formula is almost negligible: the parabola shape-factor is 0.038 for soil 1 and 0.040 for soil 2. It is necessary to mention two limits of this function: First, if mixes that were more fluid were being investigated, the data would show an asymptotic behaviour towards a limit value of slump flow. Since only a certain volume of material is available, this limit slump flow is reached at infinitesimal small fluid thickness. Second, the maximum slump value that can theoretically occur is 30 cm, which restricts the obtained function to this boundary value of S.

$$SF(S) = 20 + 0.039 \cdot S^2 \qquad\qquad [cm] \qquad R^2 = 0.951 \qquad Eq.\ 6.6$$

Figure 6-13 shows the course of Eq. 6.6 in combination with all measurements. Furthermore, the converted equations of BUDACH (2012) (R^2 = 0.884) and KAYSER (2015) (R^2 = 0.901) are complemented to the data, too. As one can see, the latter models underestimate the data in the small-slump regime. This can be traced back to the violated boundary condition of the minimum possible slump flow value of 20 cm.

As validation, Eq. 6.6 is applied to the data of BUDACH (2012) and KAYSER (2015). From Figure 6-14 and Table 6-2, it can clearly be seen that the model found in the present study complies well with the foreign data and even exceeds slightly the goodness of fit, although the testing procedures, sample preparations and mixture compositions might be diverse. Especially in the range of small slumps, the developed model seems to be more accurate to the actual measures.
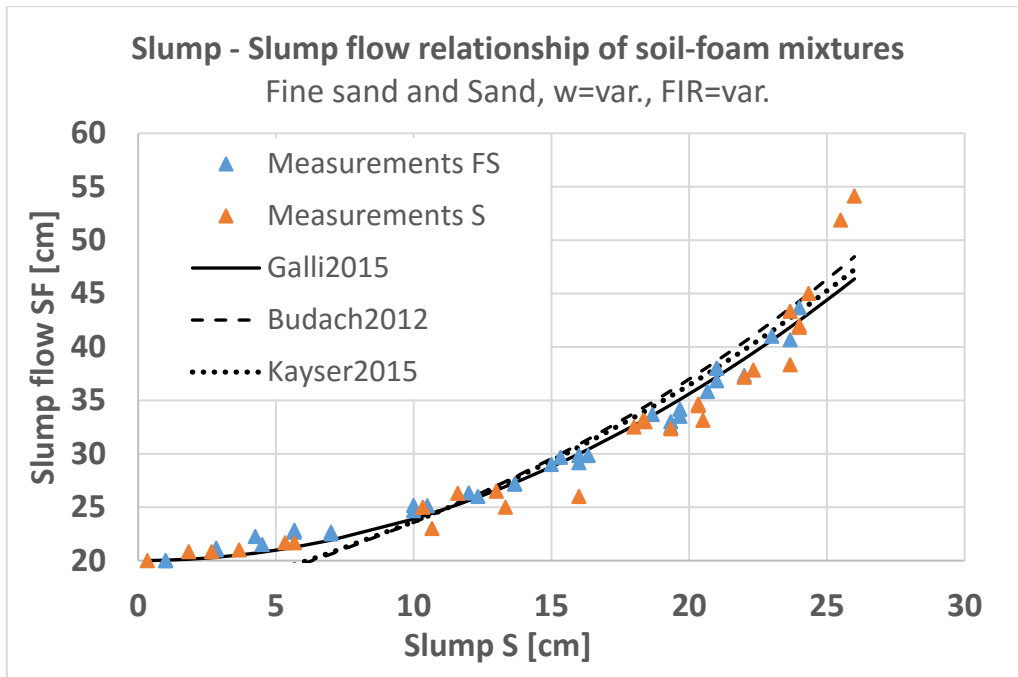
Figure 6-13: Mean slump flow values SF over corresponding mean slump values S from experiments on different soil-foam mixtures (data points), regression models according to Galli (continuous line), Budach (2012) (dashed line) and Kayser (2015) (dotted line)

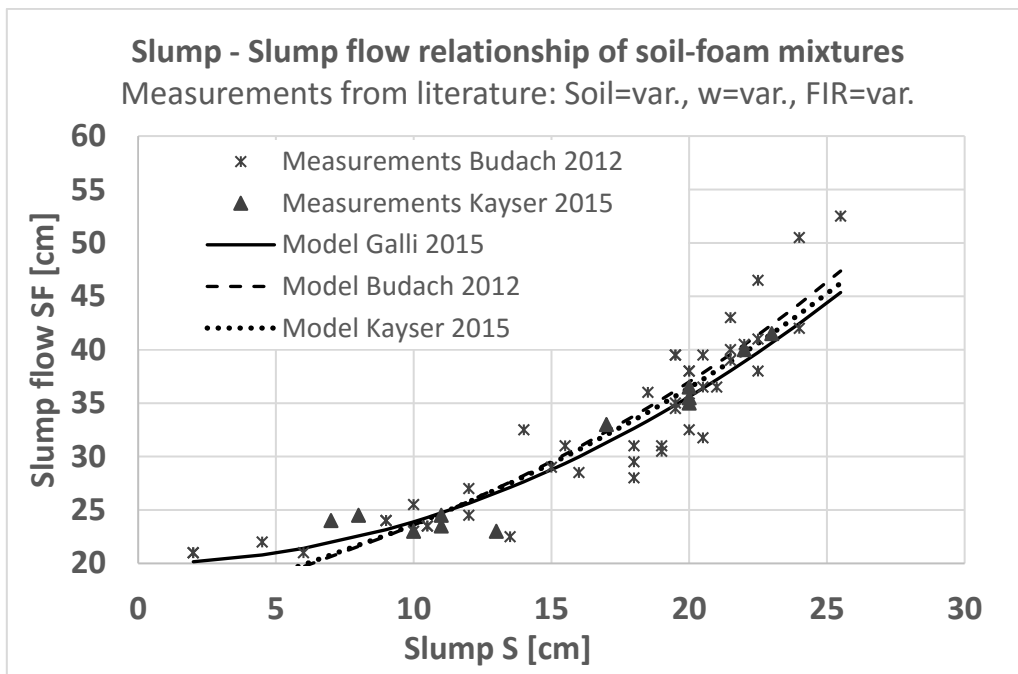**Figure 6-14:** Slump flow measures SF over corresponding slump values S from experiments on different soil-foam mixtures conducted by Budach (2012) (stars) and Kayser (2015) (triangles), regression model according to Eq. 6.6 (continuous line)

Table 6-2: Models of BUDACH (2012), KAYSER (2015) and Galli (present study) describing the functional relationship between slump S and slump flow SF

R^2	Data Budach 2012	Data Kayser 2015	Data present study
Budach model	0.845	0.920	0.884
Kayser model	0.845	0.931	0.901
Present model	0.853	0.948	0.951

Considering the restrictions mentioned above, it is now also possible to combine the formulas for the prediction of the slump flow (Eq. 6.6) and the slump (Eq. 6.2 and Eq. 6.3) to an expression for the slump flow depending on the water content and the FIR (Eq. 6.7 and Eq. 6.8).

Soil 1:

$$SF_{FS}(w, FIR) = 180.374 - 20.569 \cdot w - 5.735 \cdot FIR + 0.4632 \cdot w \cdot FIR$$

$$+ 1.0996 \cdot w^2 + 0.0712 \cdot FIR^2 - 13.986 \cdot 10^{-3} \cdot w^2 \cdot FIR$$

$$- 2.982 \cdot 10^{-3} \cdot w \cdot FIR^2 - 28.223 \cdot 10^{-3} \cdot w^3 - 0.356 \cdot 10^{-3} \cdot FIR^3$$

$$+ 41.498 \cdot 10^{-6} \cdot w^2 \cdot FIR^2 + 130.880 \cdot 10^{-6} \cdot w^3 \cdot FIR$$

$$+ 5.920 \cdot 10^{-6} \cdot w \cdot FIR^3 + 301.938 \cdot 10^{-6} \cdot w^4$$

$$+ 0.618 \cdot 10^{-6} \cdot FIR^4 \qquad\qquad [cm] \qquad\qquad Eq. 6.7$$

Soil 2:

$$SF_S(w, FIR) = 86.663 - 14.864 \cdot w - 5.525 \cdot FIR + 0.745 \cdot w \cdot FIR$$

$$+ 1.2524 \cdot w^2 + 0.1548 \cdot FIR^2 - 31.995 \cdot 10^{-3} \cdot w^2 \cdot FIR$$

$$- 9.863 \cdot 10^{-3} \cdot w \cdot FIR^2 - 47.245 \cdot 10^{-3} \cdot w^3 - 1.672 \cdot 10^{-3} \cdot FIR^3$$

$$+ 191.103 \cdot 10^{-6} \cdot w^2 \cdot FIR^2 + 411.529 \cdot 10^{-6} \cdot w^3 \cdot FIR$$

$$+ 39.181 \cdot 10^{-6} \cdot w \cdot FIR^3 + 673.428 \cdot 10^{-6} \cdot w^4$$

$$+ 6.104 \cdot 10^{-6} \cdot FIR^4 \qquad\qquad [cm] \qquad\qquad Eq. 6.8$$

Application of the equations to the different mixture compositions leads to the distributions of the slump flow measures over the FIR as depicted in Figure 6-15. Therein, also the data from Figure 6-11 is plotted. In a similar manner, this can be shown for soil 2 and for the dependency with the water content, see appendix chapter A.3.3.2. The fitting throughout all the experimental data of soils 1 and 2 shows a good correlation (Soil 1: R_{min}^2 = 0.962 for w = 6.0%, R_{max}^2 = 0.989 for w = 4.0%).
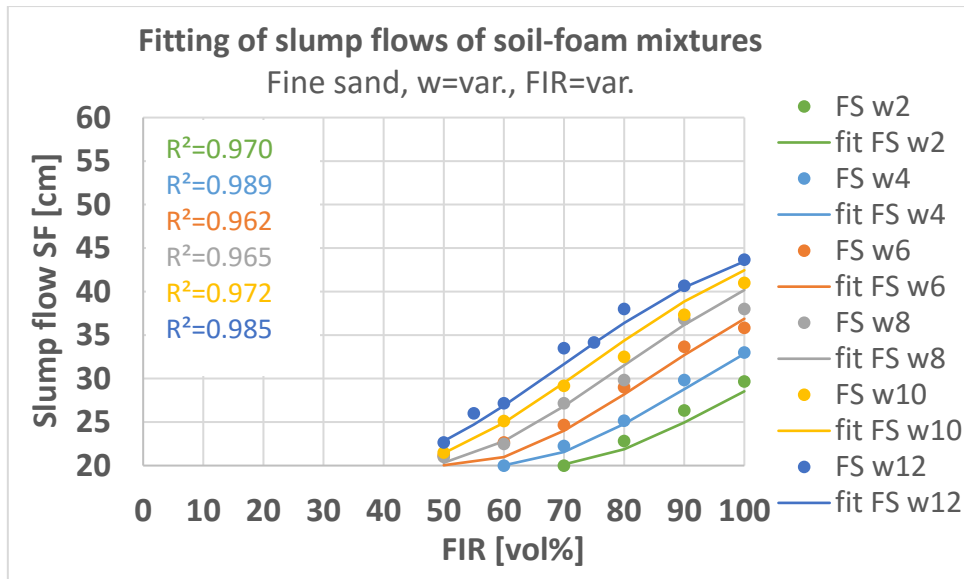
Figure 6-15: Application of prognosis model to slump flow measurements for soil 1 (fine sand) in dependence of different water contents and FIRs

6.3.3   Height h_0 of the undeformed section

The measurements of the undeformed section h_0 has not been an issue, so far. The relevance of this measure is emphasised in the following chapter. For the sake of completeness, Figure 6-16 is introduced here, containing the mean h_0-values from at least three tests of each mixtures. In addition, the corresponding standard deviations are included in the diagram. The undeformed height of the material body reduces with increasing water and foam content. Mixtures that were reported of above and that are missing here did not possess an undeformed part in their outer shape. The interpretation whether the shape is deformed or not is not always easy. In some tests, the resulting figure consists of a part, which apparently seems undeformed but it does actually not have the original dimensions (Figure 6-17). The samples containing low amounts of water and foam tend to dump in the upper part. This is

expressed by the high standard deviations. It impedes precise and reproducible testing at such stiff mixture compositions.
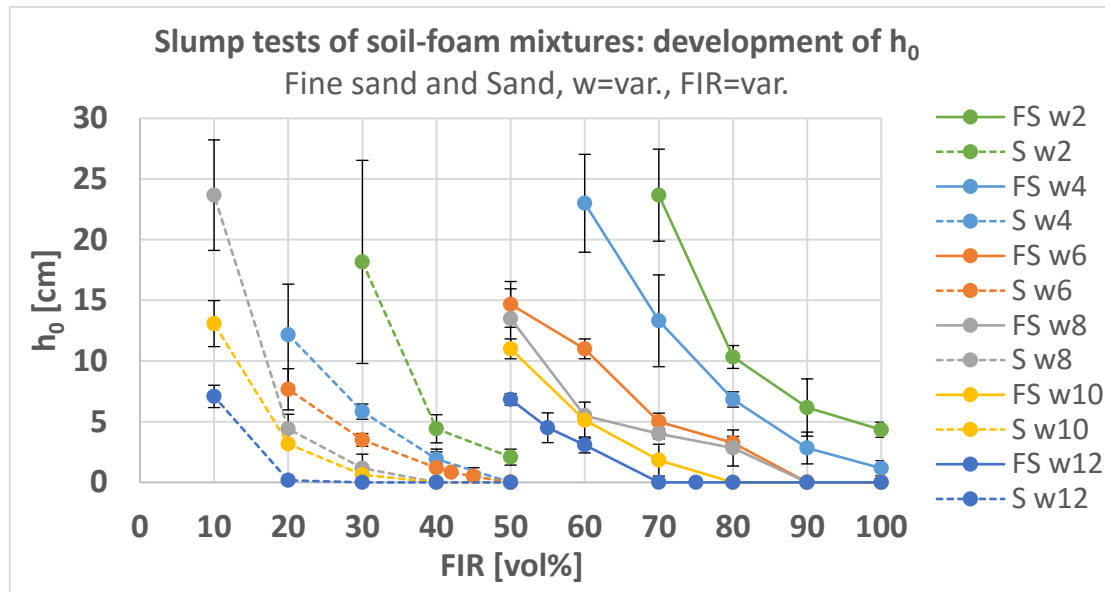
Figure 6-16: Development of the undeformed height h_0 of the slump body depending on water content w and FIR and standard deviations
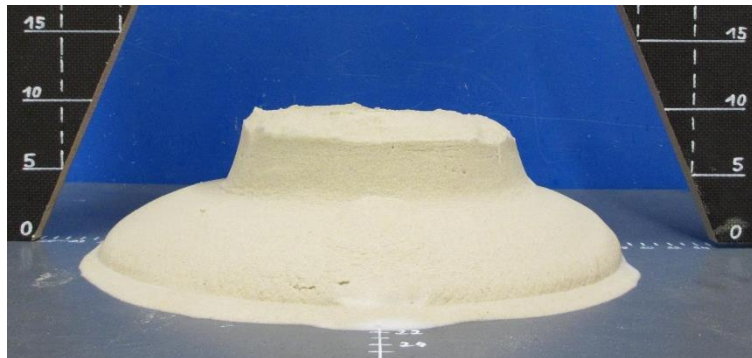
Figure 6-17: Slumped sample body consisting two different <u>deformed</u> shapes. Upper part does not exhibit initial dimensions.

6.4 Analytical derivation of rheological parameters from slump tests

According to PIAU (2005), ROUSSEL ET AL. (2005), ROUSSEL & COUSSOT (2005), a derivation of rheological parameters from slump tests is possible, however, the model deduction is highly dependent on the flow pattern. For low-viscosity fluids (i.e. large spread and large slump) a different analytical approach is necessary than for high-viscosity fluids (i.e. low slump and small spread). As presented in chapter 3.3, the derivation of rheological parameters from the slump test in literature was founded

on two different flow regimes: the "slump regime", which is characterised by both an undeformed and a deformed section in shape, and the "spread regime", which is dominated by the slump flow measure and usually does not exhibit any undeformed shape. Basic assumptions for the analytical model in either case are:

- **Three-dimensional free surface flow**

- **Rotation-symmetric around vertical axis**

- **Inertia effects and influences from cone lifting are neglected**

- **Material incompressibility and mass conservation**

The friction at the surfaces (cone, bottom plate) is dealt with individually.

Since experience showed that – depending on the FIR – both regimes can be encountered in slump testing of soil-foam mixtures, models are presented covering the two possible flowout principles. First, an analytical approach is developed based on the works of CLAYTON ET AL. (2003), MURATA (1984), ROUSSEL & COUSSOT (2005), SAAK ET AL. (2004), SCHOWALTER & CHRISTENSEN (1998). It will be shown, that this model is mathematically not applicable for the whole range of expected slumps, particularly in the fully developed flow regime. This is why, the model according to ROUSSEL ET AL. (2005), ROUSSEL & COUSSOT (2005) is presented for the "spread regime" afterwards. Finally, the applicability of the models to soil-foam mixtures is reviewed and evaluated in chapter 6.4.2. Therefore, the experimental data is used, which was presented above.

6.4.1 Theoretical models

6.4.1.1 *Slump regime*

Considering the material prior of slumping in shape of a conical frustum composed of cylindrical slices with thickness dz [m] and radius $r_x(z)$ [m], the single slices experience a particular loading state from the vertical stress on top, compare Figure 6-19. The underlying scheme with the origin of coordinates defined at the top and essential parameters for the approach are shown in Figure 6-18. The vertical stress $p_z(z)$ [Pa] on any horizontal layer at depth z of the conical frustum can be calculated from the dead weight $W_z(z)$ [N] acting on the circular plane $A_{xy}(z)$ [m²] (Eq. 6.9). The dead
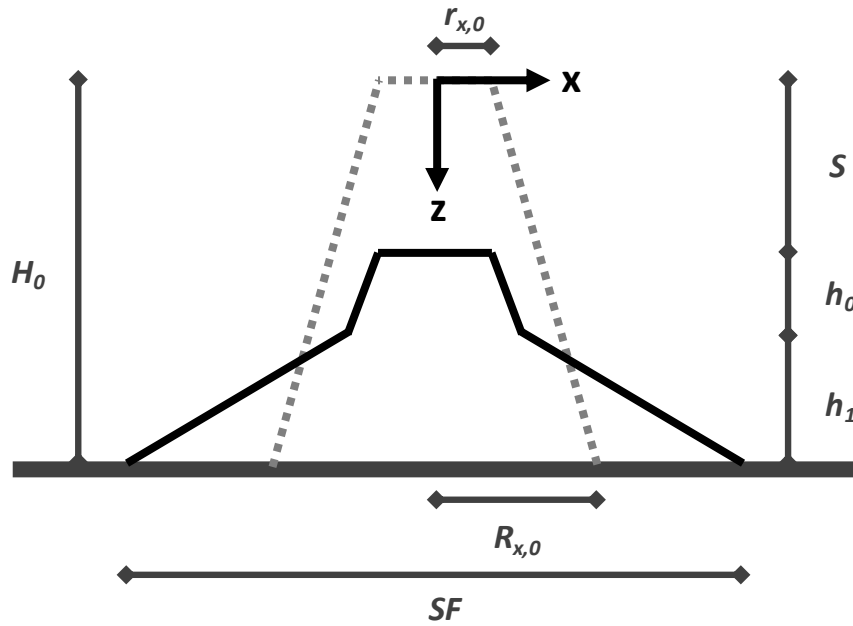
Figure 6-18: Schematic principle and relevant parameters for the rheological model development

weight is dependent on the material volume V(z) [m³] and the material density ρ [kg/m³].

$$p_z(z) = \frac{W_z(z)}{A_{xy}(z)} = \frac{\rho \cdot g \cdot V(z)}{\pi \cdot r_x(z)^2} \qquad \text{[Pa]} \qquad \text{Eq. 6.9}$$

with g the gravitational acceleration [m/s²]. The regarded volume of the conical frustum can be determined using Eq. 6.10 considering an increasing radius with increasing depth (Eq. 6.11).

$$V(z) = \frac{\pi}{3} \cdot z \cdot \left(r_x(z)^2 + r_x(z) \cdot r_{x,0} + r_{x,0}^2 \right) \quad \text{[m³]} \qquad \text{Eq. 6.10}$$

$$r_x(z) = \frac{z}{H_0} \cdot \left(R_{x,0} - r_{x,0} \right) + r_{x,0} \qquad \text{[m]} \qquad \text{Eq. 6.11}$$

with the initial measures H_0 [m] (height of the conical frustum), $r_{x,0}$ [m] (top radius), and $R_{x,0}$ [m] (bottom radius). Insertion of Eq. 6.10 into Eq. 6.9 leads then to Eq. 6.12.

$$p_z(z) = \frac{\rho \cdot g}{3} \cdot z \cdot \left[1 + \frac{r_{x,0}}{r_x(z)} + \frac{r_{x,0}^2}{r_x(z)^2} \right] \qquad \text{[Pa]} \qquad \text{Eq. 6.12}$$

Depending on the quantity of load, the material response will be either an elastic deformation or, if the stress state is high enough, plastic yielding. In rheology, this threshold is defined as yield stress. Multiple theories exist determining the yield

stress from a yield criterion, which relate the yield point to the stress condition. Depending on the presence of stresses, i.e. the stress state, the corresponding stress tensor can contain multiple stresses acting in several directions. For uniaxial stress (simple tension / compression) or pure shear conditions, the stress tensor can reduce to particular relationships between the yield stress and the present stresses in the regarded situation. All slump regime models present in the literature assume pure shear flow conditions. The models of MURATA (1984) and successors consider the yield criterion of Tresca. ROUSSEL & COUSSOT (2005) recommend using the yield criterion according to von Mises. The latter choice is supported also by FLATT ET AL. (2006). They approximated experimental data with models considering both yield theories and received a better fit with the von Mises yield criterion. PIAU (2005) generalised the selection of the yield criterion by introducing a parameter λ, which can be determined through experiments or numerical analysis. According to PIAU (2005), the yield behaviour has to be defined discretely for each material and its initial shape from which it is released to slump. Therefore, a general parameter λ is introduced here as proposed by PIAU (2005), too, resulting in a dependency of vertical and tangential stresses according to Eq. 6.13.

$$\tau_z(z) = \lambda \cdot p_z(z) \qquad\qquad \text{[Pa]} \qquad\qquad \text{Eq. 6.13}$$

For $\lambda = \frac{1}{2}$, it complies with the theory of Tresca; $\lambda = 1/\sqrt{3}$ considers the von Mises criterion. However, at small shear stresses, the material behaves as elastic and does not show any perceptible deformations. If the yield criterion is overcome by the present shear stress, plastic flow is induced. After deformation, the material shape can be approximated by a bilinear form, which is described by the corresponding heights h_0 [m] and h_1 [m] for each section (Figure 6-18). h_0 describes the height of an undeformed part (i.e. original cony shape), in which it can be assumed that the shear stresses induced by self-weight were not sufficiently large to initiate flow. The deformed section at the end of slumping is described by its height h_1. The thickness of the slices in the yielded part will reduce to dz' [m] at termination of the slumping process while the radius increases to $r_x(z')$ [m] until an equilibrium state is achieved (Figure 6-19).
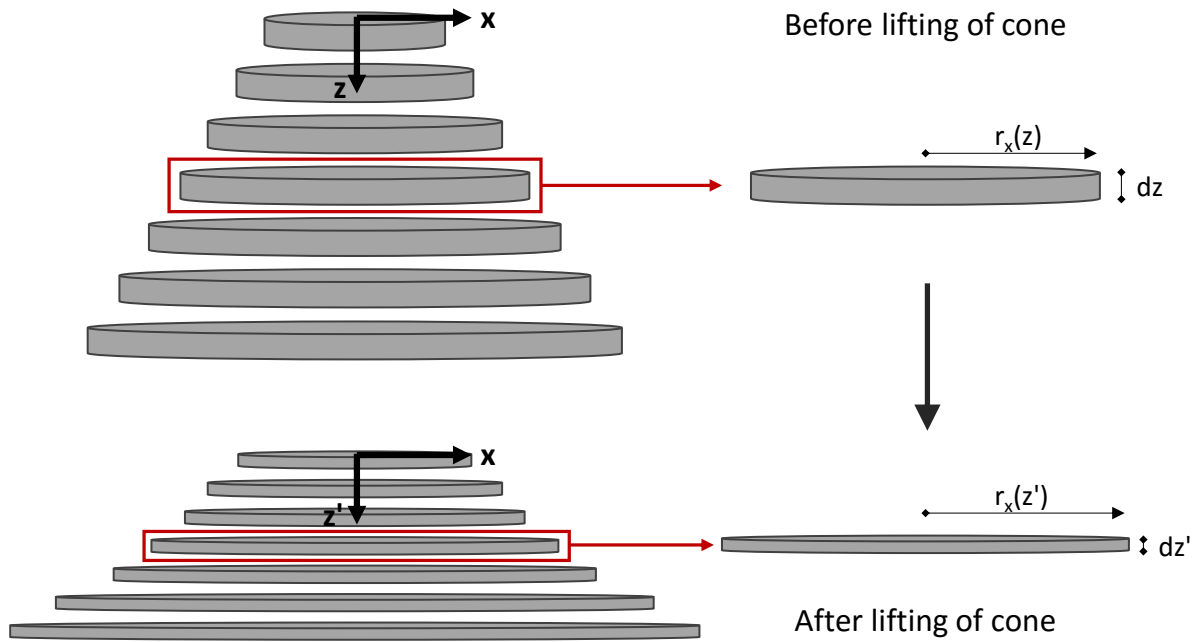
Figure 6-19: Sliced slumping behaviour: mass conservation before and after lifting of the cone due to incompressibility assumed

Due to the assumptions of mass conservation and incompressibility as presented in the introduction above, the volume of a slice will remain constant (Eq. 6.14).

$$dz \cdot \pi \cdot r_x(z)^2 = dz' \cdot \pi \cdot r_x(z')^2 \Leftrightarrow dz' = \frac{r_x(z)^2}{r_x(z')^2} dz \qquad [m] \qquad Eq. 6.14$$

Integration over all slices of the height dz' in the deformed regime, which means between z = h_0 and z = H_0, leads to the height of the deformed section h_1 (Eq. 6.15).

$$h_1 = \int_{h_0}^{H_0} dz' = \int_{h_0}^{H_0} \frac{r_x(z)^2}{r_x(z')^2} dz \qquad [m] \qquad Eq. 6.15$$

However, the shear stress acting on each slice will reduce continuously, which is due to the increasing circular area. An equilibrium state is reached again when the shear stress reduces to the yield stress τ_0 [Pa].

$$\tau_z(z) \cdot \pi \cdot r_x(z)^2 = \tau_0 \cdot \pi \cdot r_x(z')^2 \Leftrightarrow \frac{r_x(z)^2}{r_x(z')^2} = \frac{\tau_0}{\tau_z(z)} \qquad Eq. 6.16$$

Replacing the ratio of radii in Eq. 6.15 by the transformed expression of Eq. 6.16 and integration over dz results in the antiderivative computing the height h_1 of the deformed part of the slump body (Eq. 6.17). It is dependent of the material density, its yield stress and geometrical parameters.

$$\Rightarrow h_1 = \int_{h_0}^{H_0} \frac{\tau_0}{\tau_z(z)} \cdot dz = \frac{3 \cdot \lambda}{\rho \cdot g} \cdot \tau_0 \int_{h_0}^{H_0} \frac{1}{z \cdot \left[1 + \frac{r_{x,0}}{r_x(z)} + \frac{r_{x,0}^2}{r_x(z)^2}\right]} \cdot dz$$

$$= \frac{\lambda}{\rho \cdot g} \cdot \tau_0 \cdot [\ln(r_{x,0}^2 \cdot H_0^3 + R_{x,0} \cdot r_{x,0} \cdot H_0^3 + R_{x,0}^2 \cdot H_0^3)$$

$$- \ln(3 \cdot r_{x,0}^2 \cdot H_0^2 \cdot h_0 - 3 \cdot r_{x,0}^2 \cdot H_0 \cdot h_0^2 + 3 \cdot R_{x,0} \cdot r_{x,0} \cdot H_0 \cdot h_0^2$$

$$+ (R_{x,0} - r_{x,0})^2 \cdot h_0^3)] \qquad\qquad \text{[m]} \qquad \text{Eq. 6.17}$$

For the slump cone geometry according to DIN EN 12350-2 (2009-08), the following relations apply: $r_{x,0} = \frac{1}{6} \cdot H_0$ and $R_{x,0} = \frac{2}{6} \cdot H_0$. Introduced into Eq. 6.17, the formula for the height of the deformed region simplifies to Eq. 6.18.

$$\Rightarrow h_1 = \frac{\lambda}{\rho \cdot g} \cdot \tau_0 \cdot [\ln(7 \cdot H_0^5) - \ln(3 \cdot H_0^4 \cdot h_0 + 3 \cdot H_0^3 \cdot h_0^2 + H_0^2 \cdot h_0^3)]$$

$$\text{[m]} \qquad \text{Eq. 6.18}$$

The main reference parameter recorded in slump tests however is the slump value S. It is the differential height between initial sample height H_0 and residual height ($h_0 + h_1$) after termination of slumping (Eq. 6.19). The residual height needs to consist an undeformed section described by h_0, otherwise the analytical model is not applicable; the second ln-term in Eq. 6.18 demands for a value of h_0 unequal zero ($h_0 \neq 0$).

$$S = H_0 - h_0 - h_1 \Leftrightarrow h_1 = H_0 - h_0 - S \qquad\qquad \text{[m]} \qquad \text{Eq. 6.19}$$

Insertion of Eq. 6.18 into Eq. 6.19 and conversion to the yield stress τ_0 results in the final equation (Eq. 6.20) linking the recorded slump test parameters (S and h_0) to rheological parameters (i.e. yield stress).

$$\tau_{0,\text{slump}} = \frac{\rho \cdot g \cdot (H_0 - h_0 - S)}{\lambda} \cdot [\ln(7 \cdot H_0^5) - \ln(3 \cdot H_0^4 \cdot h_0 + 3 \cdot H_0^3 \cdot h_0^2 + H_0^2 \cdot h_0^3)]^{-1}$$

$$\text{[Pa]} \qquad \text{Eq. 6.20}$$

According to ROUSSEL & COUSSOT (2005), surface tension between the bottom plate and the material is only important when the friction forces are bigger than the yield stress. This is particularly important when dealing with low-yield stress fluids, which form a large spread and exhibit a great contact face with the solid plane. CHAMBERLAIN ET AL. (2003) assume the friction to be of Coulombic nature.

6.4.1.2 *Spread regime*

The analytical model presented in the following was developed by ROUSSEL ET AL. (2005), ROUSSEL & COUSSOT (2005). A similar approach was considered also by PIAU (2005). Originally, this model was applied for cementitious pastes, but it shall be analysed whether an application on soil-foam mixtures with large slump values (fully deformed shape) is considerable, too. The relevant data, on which the approach is based, is shown in Figure 6-20. The origin of coordinates lies in the bottom centre.
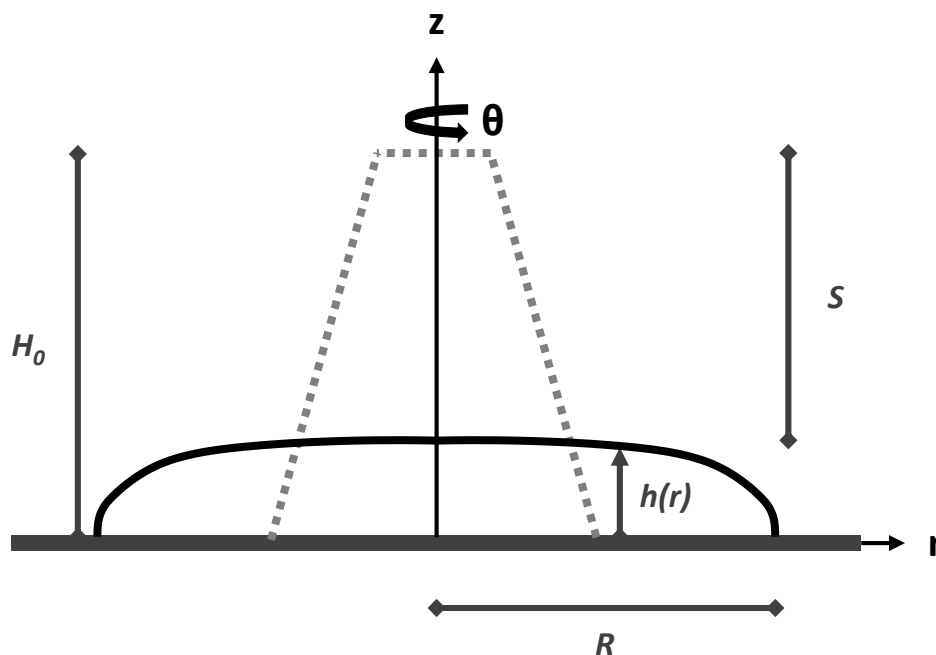
Figure 6-20: Underlying cone shape and relevant parameters for the analytical "spread regime" model of ROUSSEL & COUSSOT (2005)

ROUSSEL ET AL. (2005), ROUSSEL & COUSSOT (2005) use the lubrication theory to describe the flow behaviour in the spread regime. This theory takes into account a rather low thickness h of the flowing material but a large extent in the flow distance R ($h/R \ll 1$). Considering pure shear flow conditions and of course, the other assumptions named above, the flow description thusly can be simplified to a one-

dimensional flow problem. It is governed by the two equilibrium momentum equations Eq. 6.21 and Eq. 6.22, see BATCHELOR ET AL. (2000), PANTON (1984) for details.

Equilibrium equation of momentum in z-direction:

$$0 = -\rho \cdot g - \frac{\partial p}{\partial z} \qquad\qquad [\text{N/m}^3] \qquad\qquad \text{Eq. 6.21}$$

Radial equilibrium equation of momentum:

$$0 = -\frac{\partial p}{\partial r} + \frac{\partial \tau_{rz}}{\partial z} \qquad\qquad [\text{N/m}^3] \qquad\qquad \text{Eq. 6.22}$$

with h(r) the sample height distribution at stoppage [m], p the vertical pressure [Pa], and τ_{rz} the shear tress acting on the r-z-plane [Pa], here defined according to Eq. 3.6.

The slumped material at stoppage is described by the run-out distance R [m] (or slump flow SF = 2·R) and the sample height h(r) as a function of r [m]. It is assumed that the equilibrium conditions deduced from the lubrication theory are valid also for yield-stress fluids – soil-foam mixtures are hypothesised to exhibit yield-stress fluid behaviour here – and the pressure distribution is hydrostatic. The pressure is then obtained through integration of Eq. 6.21 and results in Eq. 6.23.

$$p(z) = \rho \cdot g \cdot (h(r) - z) \qquad\qquad [\text{Pa}] \qquad\qquad \text{Eq. 6.23}$$

Introducing Eq. 6.23 into Eq. 6.22 and integration over the fluid depth z leads to Eq. 6.24 considering an equilibrium state of shear stress and yield stress at termination of flow ($\tau_{rz} = \tau_0$, because $\dot\gamma = 0$).

$$\rho \cdot g \cdot h(r) \frac{d\,h(r)}{dr} = \tau_0 \qquad\qquad [\text{Pa}] \qquad\qquad \text{Eq. 6.24}$$

Repeated integration, now over r, gives an equation describing the material height (Eq. 6.25).

$$h(r) = \left(\frac{2 \cdot \tau_0 (R-r)}{\rho \cdot g}\right)^{\frac{1}{2}} \qquad\qquad [\text{m}] \qquad\qquad \text{Eq. 6.25}$$

Because of axis-symmetry, the form described by Eq. 6.25 represents a solid of revolution. Its volume can be calculated from volume integral over the maximum spread radius (r = 0 … R) and the circumference (θ_c = 0 … 2π). Thus, an expression for

the yield stress in dependence of the spread radius R (or the slump flow measure SF) can be found (Eq. 6.26) as well as a formulation considering the slump measure S (Eq. 6.27), when h(r=0) is replaced by (H_0 - S).

$$\tau_{0,spread,SF} = \frac{225 \cdot \rho \cdot g \cdot V^2}{128 \cdot \pi^2 \cdot R^5} = \frac{225 \cdot \rho \cdot g \cdot V^2}{4 \cdot \pi^2 \cdot SF^5} \qquad [Pa] \qquad\qquad \text{Eq. 6.26}$$

$$\tau_{0,spread,S} = \sqrt{\frac{2\pi}{15 \cdot V}} \cdot \rho \cdot g \cdot (H_0 - S)^{\frac{5}{2}} \qquad [Pa] \qquad\qquad \text{Eq. 6.27}$$

with V the sample volume [m³] and H_0 the initial sample height prior to slumping [m].

As mentioned in the previous subchapter, frictional effects have to be regarded especially with fluids possessing a large boundary layer with the solid bottom plane and low yield stress. Hence, the actual yield stress is smaller than calculated Eq. 6.28. The difference is associated with changes in the interfacial energies between the different phases and depends on the factor β [-], which incorporates surface tension and the contact angle, see ROUSSEL ET AL. (2005).

$$\tau_{0,spread,SF,corrected} = \frac{225 \cdot \rho \cdot g \cdot V^2}{4 \cdot \pi^2 \cdot SF^5} - \beta \cdot \frac{\pi \cdot SF^2}{4 \cdot V} \qquad [Pa] \qquad\qquad \text{Eq. 6.28}$$

6.4.2 Application of the models to the test data

As mentioned in chapter 6.4.1, the application of the analytical model for the slump regime is only valid for slump bodies that exhibit an undeformed section. Due to the containment of h_0 in the ln-term, the mathematical model is otherwise undefined. However, the model for the slump regime shall be applied in the first place to the measurements from section 6.3. In cases where h_0 equals zero (compare Figure 6-16), the model of the spread regime is used instead. Later, the validity of its application is checked.

Figure 6-21 shows the calculated yield stresses from the analytical models for all investigated mixtures. λ is chosen to equal $1/\sqrt{3}$ (von Mises yield criterion); the discussion of adequacy is again revived in chapter 8.1.2. The slump values and slump flow values respectively introduced into the equations Eq. 6.20, Eq. 6.26 and Eq. 6.27 are the mean values of the measurements for each soil-foam mix as already presented in chapter 6.3. Surface tension effects were neglected (β = 0) because the bottom plate was moistened for testing. Furthermore, the containment of
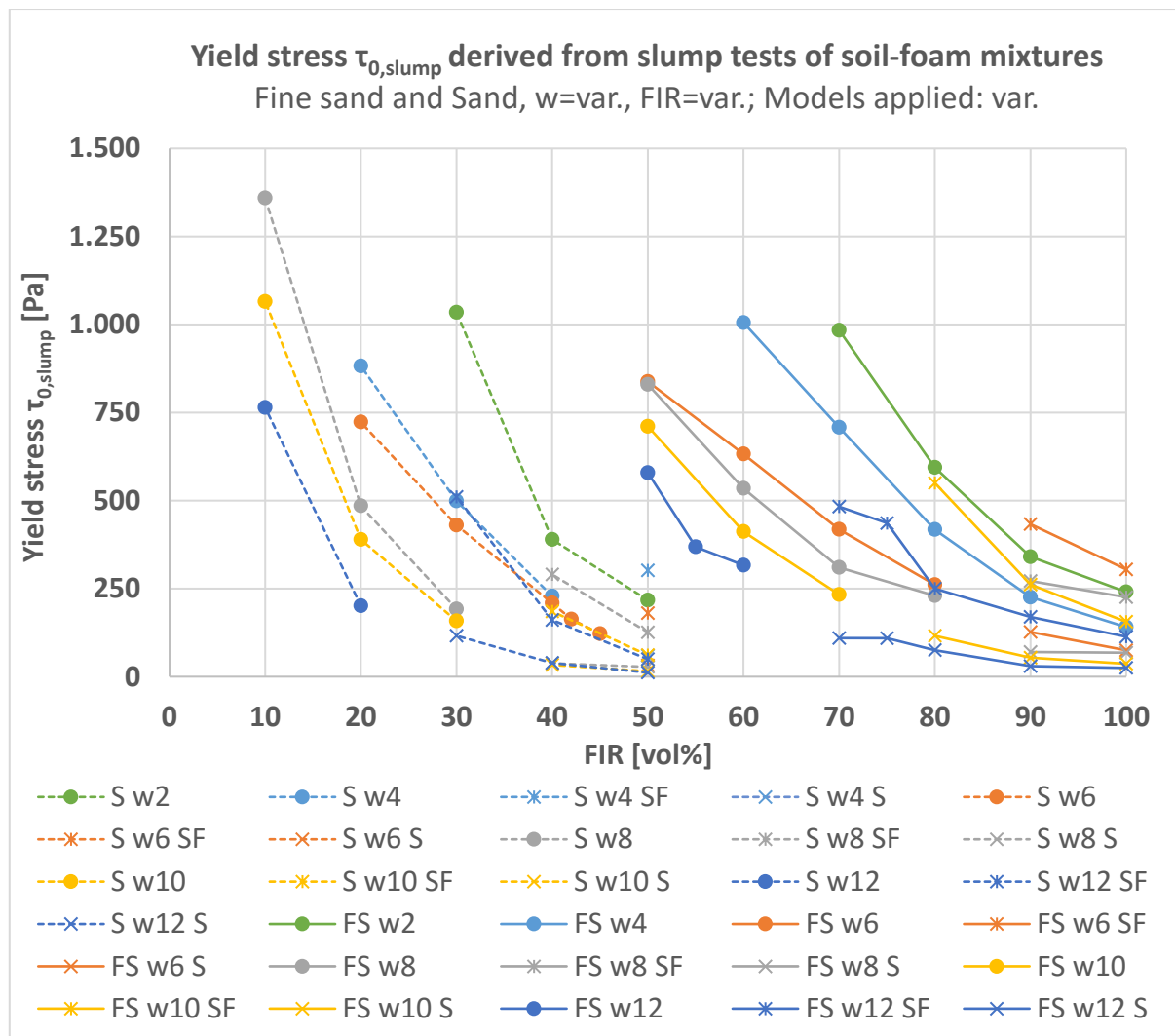
Figure 6-21: Yield stresses $\tau_{0,slump}$ derived from analytical slump models for different soil-foam-mixtures; no attribute: slump regime model (Eq. 6.20), attribute "SF": spread regime model based on slump flow measure (Eq. 6.26), attribute "S": spread regime model based on slump measure (Eq. 6.27)

surfactants within the liquid phase is assumed to benefit the assumed perfect slip condition.

Again, the results are depicted over the foam injection ratio. Dashed lines represent soil 2 (sand) and the continuous lines soil 1 (fine sand). The colouring stands for the different water contents. Data points in the shape of a star (*) and of a cross (ˣ) were determined using the spread regime model. Dots represent outcomes from the slump regime model. In the range, where the slump regime model was applicable, the results from the spread regime model were left out. The differences between stars and crosses result from the fact, that the yield stresses calculated with the spread regime model depend on the formula applied; i.e. Eq. 6.26, in which the slump flow

SF is inserted, gives different results in comparison to Eq. 6.27, which incorporates the slump S. In the following, only the formulation based on the slump flow value is considered if not stated differently. Nevertheless, it is obvious that the calculated yield stresses decrease with increasing FIR for both soils. The same applies with respect to the water content. In the transition region between the application ranges of the two analytical models, a distinct offset in the course of the yield stresses is noticeable considering the stars. If some values within this section were left out for some reason, the evolution would shape continuous. In contrast, the crosses comply more with the ideal expectation for the further development.

FLATT ET AL. (2006) did a comparative analysis of the approaches of MURATA (1984) and ROUSSEL ET AL. (2005), ROUSSEL & COUSSOT (2005). They applied the analytical models to experimental results flowout tests of cement pastes from cylindrical geometries (different aspect ratios). They found the approach of MURATA (1984) valid only for small spread values (SF ≤ 3·R_0; R_0: initial bottom radius of the mould), while the results based on the model of ROUSSEL ET AL. (2005), ROUSSEL & COUSSOT (2005) were acceptable for spread values SF ≥ 4·R_0. The residual interim range of spread values was fitted empirically by an exponential function.

The results in the present study show, that in most cases, when an undeformed section was present, the slump flow was smaller than 3·R_0 = 30 cm. The fundamental assumption in the analytical approach of ROUSSEL ET AL. (2005), ROUSSEL & COUSSOT (2005) is the application of the lubrication theory. This theory considers flow conditions with a considerable large radial extent while the thickness of the flowing medium is much smaller h (h/R << 1). Therefore, subsequently the ratio of material thickness h_{max} and radial extent R_{max} at termination of the slumping process is analysed. Figure 6-22 shows this ratio h_{max}/R_{max} for all mean measurements. The black borderline represents the limit ratio h_{max}/R_{max} = 1. If actually the borderline ratio of h_{max}/R_{max} = 1 is considered as recommended criterion of adequacy of the two models, the plot of yield stresses is the same as in Figure 6-21 because all measures without an undeformed section exhibit a ratio smaller than 1. However, the ratio should actually be much smaller than one according to theory. A reasonable course would be established, when h_{max}/R_{max} ≤ 0.34 for soil 1 or even smaller with respect to soil 2. Corresponding slump flows are greater than 4·R_0. Thus, the findings of FLATT ET AL. (2006) could be confirmed.
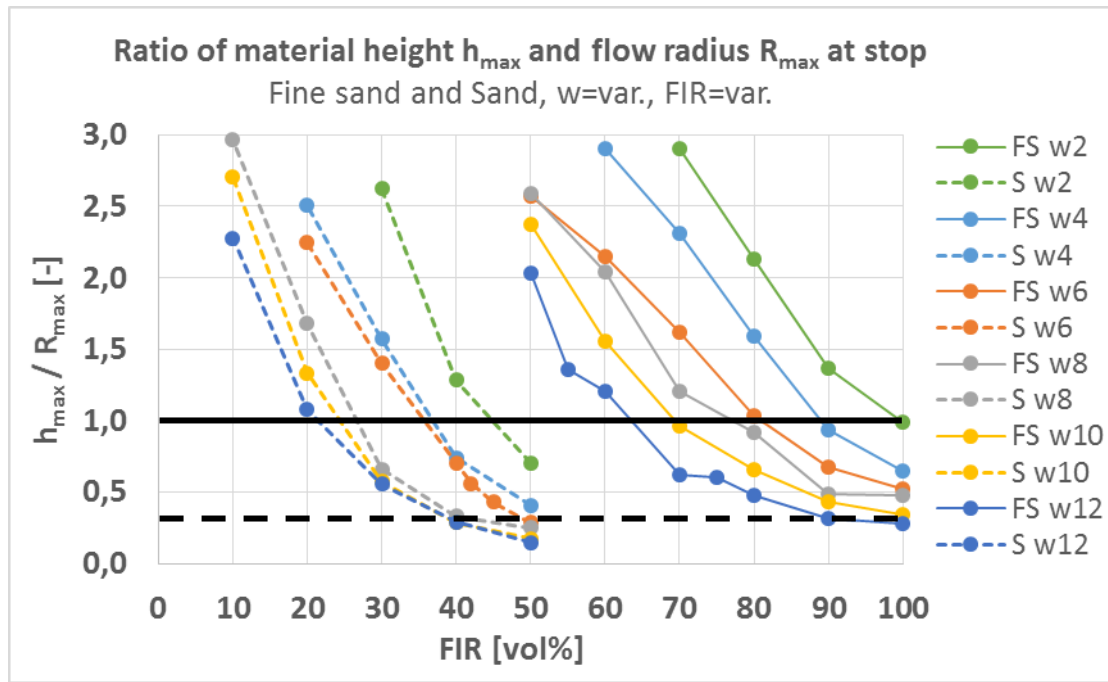
Figure 6-22: **Development of maximal material height h_{max} and maximum outflow radius R_{max} after slumping; continuous benchmark: ratio of 1.0, dashed benchmark: ratio of 0.33**

Nevertheless, the gap in the interim range has to be closed, compare data points in Figure 6-23. Therefore, a mathematical formulation would have to be found, which adequately covers the range between values that were determined with the slump regime model and slump flow values greater than 40 cm. The exponential function as proposed by FLATT ET AL. (2006) cannot be assigned to the present data since it was developed for very low viscous cement pastes that were tested in the ASTM miniature cone. An application would lead to unreal values of τ_0. This implies that an approximation function is material and geometry dependent. The function found most suitable for an interim range ($h_0 = 0$ cm and $h_{max}/R_{max} \geq 0.34$) for soil-foam mixtures is still of exponential character as formulated in Eq. 6.29.

$$\tau_{0,\text{interim,SF}} = 3,479.5 \cdot e^{-0.078 \cdot \text{SF}} \qquad\qquad [\text{Pa}] \qquad\qquad \text{Eq. 6.29}$$

Figure 6-23 shows the yield stresses calculated with the slump regime model (Eq. 6.20) and/or the spread regime model (Eq. 6.26) within the range of their application over the corresponding slump flows. As it can be seen from Figure 6-23, the calculated yield stresses apparently coincide with one trend irrespective of the mixture composition.

Figure 6-23: **Yield stresses derived from slump models and empirical approximation for closing the interim division outside the range of applicability (h_0 = 0 cm and $h_{max}/R_{max} \geq 0.34$) based on slump flow**

Besides the discussion of model applicability conducted above, there is still the outcome of yield stresses from the spread regime model based on the slump value S. All values for τ_0 determined with the S-based formula lead to a reasonable trend without any sudden jumps. However, the yield stresses are significantly smaller than for the SF-based equation. However, if these values are considered, the empirical model for the interim range based on the slump S results in Eq. 6.30, which is a second-order polynomial equation. Based on the coefficient of determination, R^2, the goodness of fit seems to be better (Figure 6-24).

$$\tau_{0,interim,S} = 1.5069 \cdot S^2 - 81.523 \cdot S + 1{,}126.4 \qquad [Pa] \qquad \text{Eq. 6.30}$$

Another aspect of discussion is the fundamental model assumption of incompressibility. When a compressible medium is considered, a volume expansion has to be regarded. Because of the decreasing acting stress on a layer during slumping, the material experiences relaxation. The expansion will take place in radial and vertical direction and thusly influence the slump and the spread measure. Hence, the presumed slices in the model at rest consist of a larger volume than in their initial state. In order to establish a relationship between the initial and ultimate state, the final volume has to be reduced by factor incorporating the fraction of expansion. Here, the simplification is assumed that the volume expansion occurs only in radial
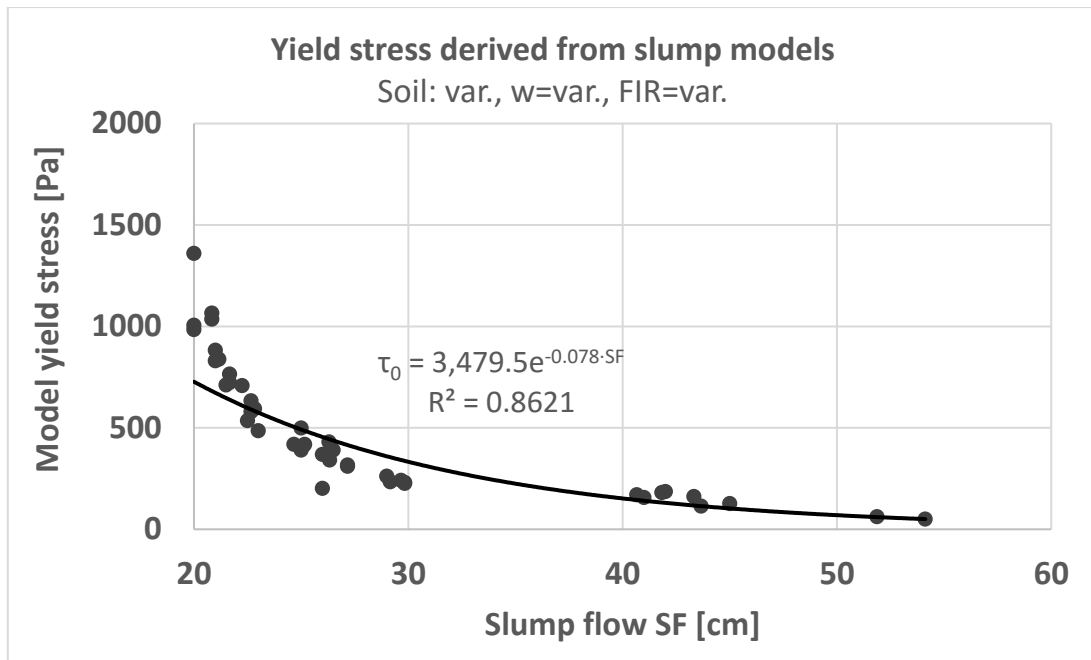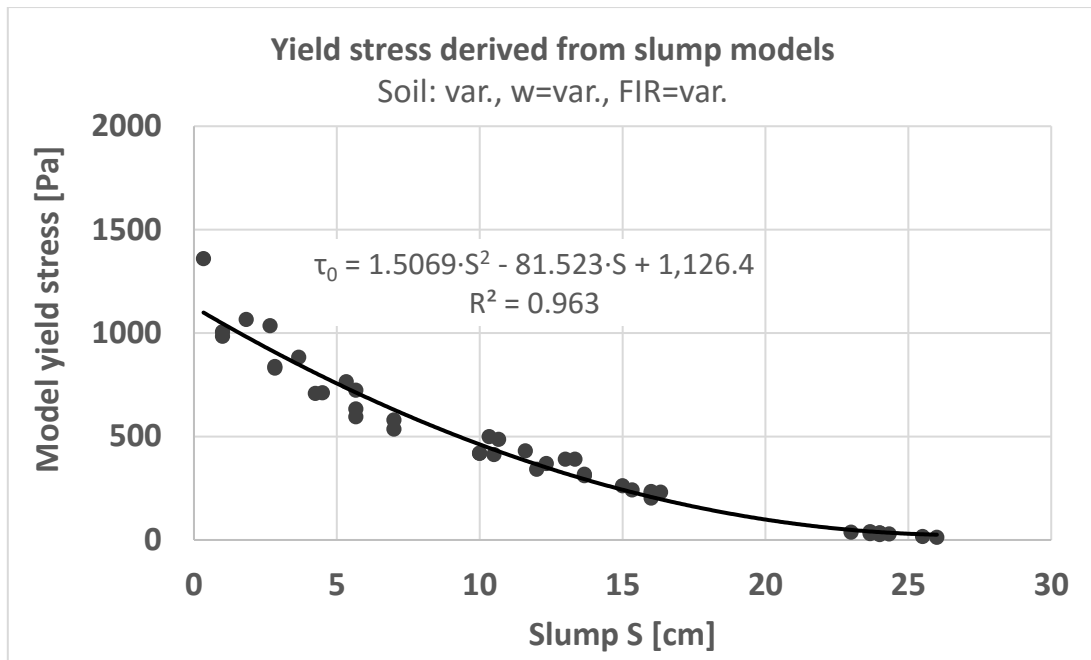
Figure 6-24: Yield stresses derived from slump models and empirical approximation for closing the interim division outside the range of applicability (h_0 = 0 cm and $h_{max}/R_{max} \geq 0.34$) based on slump

direction. Hence, solely the radius is charged with the expansion factor α_{exp} [-] and thusly, it is reduced to maintain volume balance as in Eq. 6.14. Volume equilibrium of layers before slumping (with thickness dz) and at the end of the slump process (with thickness dz') considering expansion is expressed by Eq. 6.31.

$$dz \cdot \pi \cdot r_x(z)^2 = dz' \cdot \pi \cdot r_x(z')^2 \cdot \left(1 - \alpha_{exp}\right) \Leftrightarrow dz' = \frac{r_x(z)^2}{r_x(z')^2 \cdot (1 - \alpha_{exp})} dz$$

$\qquad\qquad\qquad\qquad\qquad\qquad\qquad\qquad$ [m] $\qquad\qquad$ Eq. 6.31

The volume growth is dependent on the volume of the compressible phase and the pressure difference before and after slumping. With respect to foam and foam-conditioned soils, it can be determined based on Boyle's Law with Eq. 6.32 taking into account the conditioning parameters FER [-] and FIR [vol%]. However, the ultimate acting pressures $p_z(z')$ [Pa] are a priori not known.

$$\alpha_{exp} = \frac{FER - 1}{FER \cdot \left(1 + \frac{1}{FIR}\right)} \cdot \frac{\left(p_z(z) - p_z(z')\right)}{p_0}$$

$\qquad\qquad\qquad\qquad\qquad\qquad\qquad\qquad$ [-] $\qquad\qquad$ Eq. 6.32

with p_0 the atmospheric pressure (100,000 Pa). Back analysis – after calculating the yield stress – showed that the volume expansion ranges around 0.4 vol% for the

worst case scenario of the present samples (FER=15, FIR=80%) and is therefore considered negligibly small. The calculation is documented in the appendix chapter A.3.5.

7. RHEOLOGICAL TESTING OF SOIL-FOAM MIXTURES USING ROTATIONAL RHEOMETRY

Main goal of the present study is the rheological characterisation of soil-foam mixtures as used as EPB support material. In chapter 6, the focus was to derivate rheological parameters from simple index tests. In this chapter, information on the flow behaviour shall be gained through experiments that are more complex. The choice of adequate experiments requires both research on similar studies and a discussion on a sound description of necessary boundary conditions. Moreover, the potential for a well-grounded analysis of these experiments as well as the degree in complexity needs to be weighted from preliminary tests. Consequently, based on the extensive literature research in chapter 3.2, a set of pre-studies has been undertaken in order to find a suitable experiment permitting an assessment of the soil-foam rheology. Micro-scale investigations on similar materials will be consulted as benchmark for the analysis. Thereupon, suitable test methods, a testing programme and necessary boundary conditions will be defined for the main test series, that were ultimately selected. Test results will be presented and comprehensively analysed. Lastly, findings on the rheology of particle-foam mixtures from the several scales of investigation are compared and evaluated.

7.1   Pre-studies

As presented in chapter 3.2, a lot of experience on the rheology of colloidal suspensions could be found in literature from related disciplines. In various experimental approaches, emphases were diversified with respect to the different rheological characteristics. These approaches exhibited either a quantitative or a qualitative character, determining single parameters or overall flow attributes.

Generally, the type of material, particularly its grain-size distribution, determines the necessary setup regarding shearing gap, motor drive and surface texture. Aiming at modelling the flow pattern in the experiment, the applied model is very dependent on these physical factors. When assessing the flow behaviour of soil-foam mixtures, it is most likely that a suitable experiment needs to have a large gap distance (due to the grain-size; compare chapter 3.1.3.2) and rough surfaces in order to diminish slip effects (particularly with respect to the foam; see chapters 3.1.3.3 and 3.2.1). Additionally, a large volume of soil (i.e. low FIR) probably requires a drive, which is capable of producing high torques. At the same time, the motor should accurately transduce low shear rates to the material and the torque sensors should provide precise measurements even at low torques. It is expected that soil-foam mixtures cover a wide range of shear stresses depending on the shear range and the material composition. Thus, the best possible compromise has to be found between the applicability of the experiment to such granular material and the aspired flow field condition necessary for modelling its rheology.

Within the research related to this thesis, two pre-studies were performed in order to gain first experience on the flow behaviour in rheometer setups and to develop a suitable experimental approach on the rheology of soil-foam mixtures.

Under guidance of the author of this thesis, ALTUN (2011) worked with a rheometer of the type Schleibinger BT2 (Figure 7-1), see SCHLEIBINGER GERÄTE TEUBERT U. GREIM GMBH (2012a). This type of concrete rheometer works with a displacement flow, instead of a shear gap flow. It is composed of the rheometer unit and a bowl (volume of 20 L) with a shaft in its centre, into which the rheometer device is placed. The rheometer
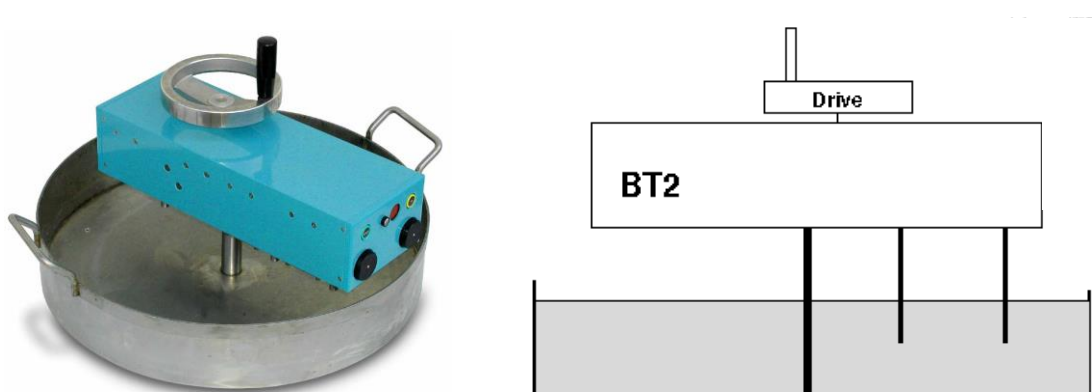
Figure 7-1: **Concrete rheometer Schleibinger BT2; photograph (left) and system sketch taken from SCHLEIBINGER GERÄTE TEUBERT U. GREIM GMBH (2012a)**

unit is turned by a hand rod on top. Thereby, two pins, which are connected to the unit and which dip into the testing sample, rotate on their distinct radial position through the material (Figure 7-1). The resisting force is measured at the pins at one hundred locations over one revolution (SCHLEIBINGER GERÄTE TEUBERT U. GREIM GMBH (2002)). In this way, considering the two different radii, two point clouds of torque data are generated. Based on SCHLEIBINGER GERÄTE TEUBERT U. GREIM GMBH (2002), the apparent rheological parameters can be estimated from the data by applying the Bingham model to the measurements (Figure 7-2).
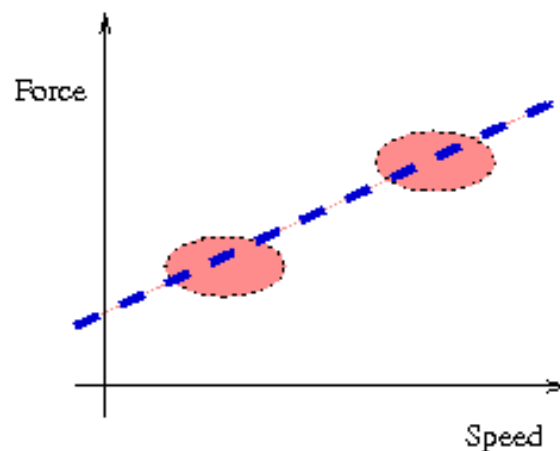
Figure 7-2:   **Principle of determining the Bingham flow curve from the data scatter (SCHLEIBINGER GERÄTE TEUBERT U. GREIM GMBH (2012a))**

According to the manual, the turning speed of the hand rod is irrelevant for the determination of the flow curve. However, ALTUN (2011) showed a definite dependence in the results by synchronising the turning speed to several measuring profiles, i.e. different constant speeds. Nevertheless, ALTUN (2011) developed a testing procedure for an application of the rheometer device to soil-foam mixtures facilitating to some extent reproducible and comparative testing, which however did not contain any target times. He investigated a sand similar to soil 2 from the present study. The water content and the foam injection ratio were varied (w = 0…25 wt%, FIR = 0…40 vol%). Two reference mixtures were defined to w = 10 wt%, FIR_{10} = 10 vol% and w = 10 wt%, FIR_{20} = 25 vol% respectively. He filled 15 litres of material into the bowl and placed the bowl for 30 seconds on a vibrating table (50 Hz) for compaction. After positioning the rheometer unit on the bowl and initialising the device, ALTUN (2011) turned the hand rod manually and best possibly according to the profile shown in Figure 7-3. Over one quarter of the measuring revolution, he kept
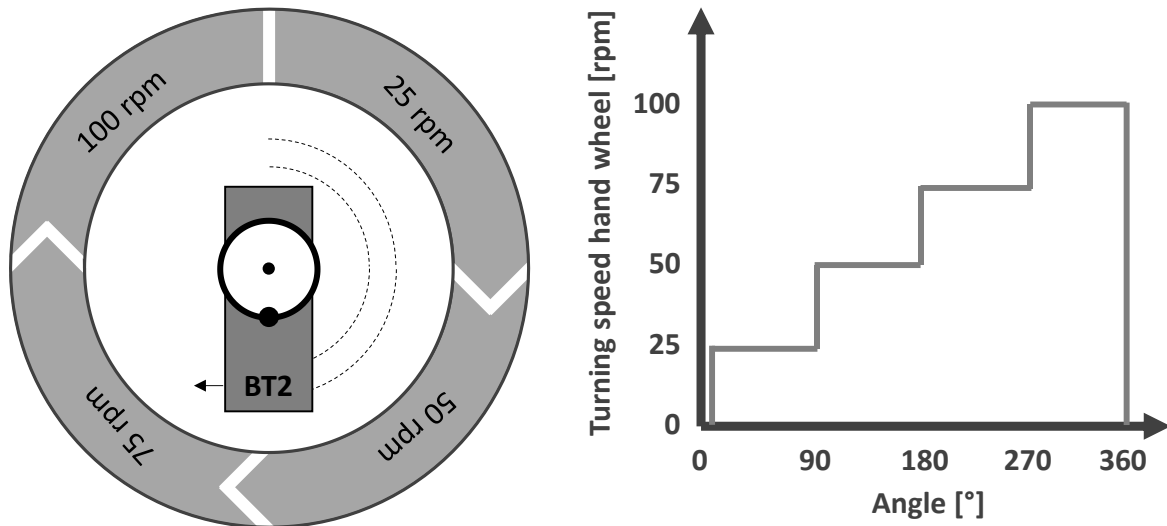
Figure 7-3:   Standard operation procedure of Schleibinger Concrete Rheometer BT2 according to ALTUN (2011)

the turning speed of the hand wheel constant at 25, 50, 75 and 100 rpm with the help of a metronome. Thus, he achieved multiple point clouds representing further significant marks of a potential flow curve. Moreover, the circumferential velocities of the pins could be maintained within the range of application according to the provided evaluation spread sheet, i.e. 0.01 to 0.15 m/s.

Although ALTUN (2011) did not analyse the conversion of raw data into rheological parameters, some qualitative information on the rheology could be derived. The FIR and the concentration c_f had a significant influence on the resisting torque (see Figure 7-4 and Figure 7-5), which was measured in a range between 60 mNm (FIR = 40 vol%) and 3,000 mNm (FIR = 0 vol%; upper gaugeable limit). Furthermore, the data seemed to exhibit a constant slope in the torque-speed diagram. Thinking further, the latter information could indicate a constant shear stress-shear rate relationship and thus a Bingham fluid behaviour, compare chapter 3.1.2. However, the scatter is too big for an adequate fit of the data.

In the meanwhile, the manual concrete rheometer was withdrawn from the market and it was replaced by an electronic version ("eBT-2", see SCHLEIBINGER GERÄTE TEUBERT U. GREIM GMBH (2013)). Thus, it should be possible to drive explicit measuring profiles. It can be equipped with either cylinders or a ball measuring system, cf. FLEISCHMANN & KUSTERLE (2014).
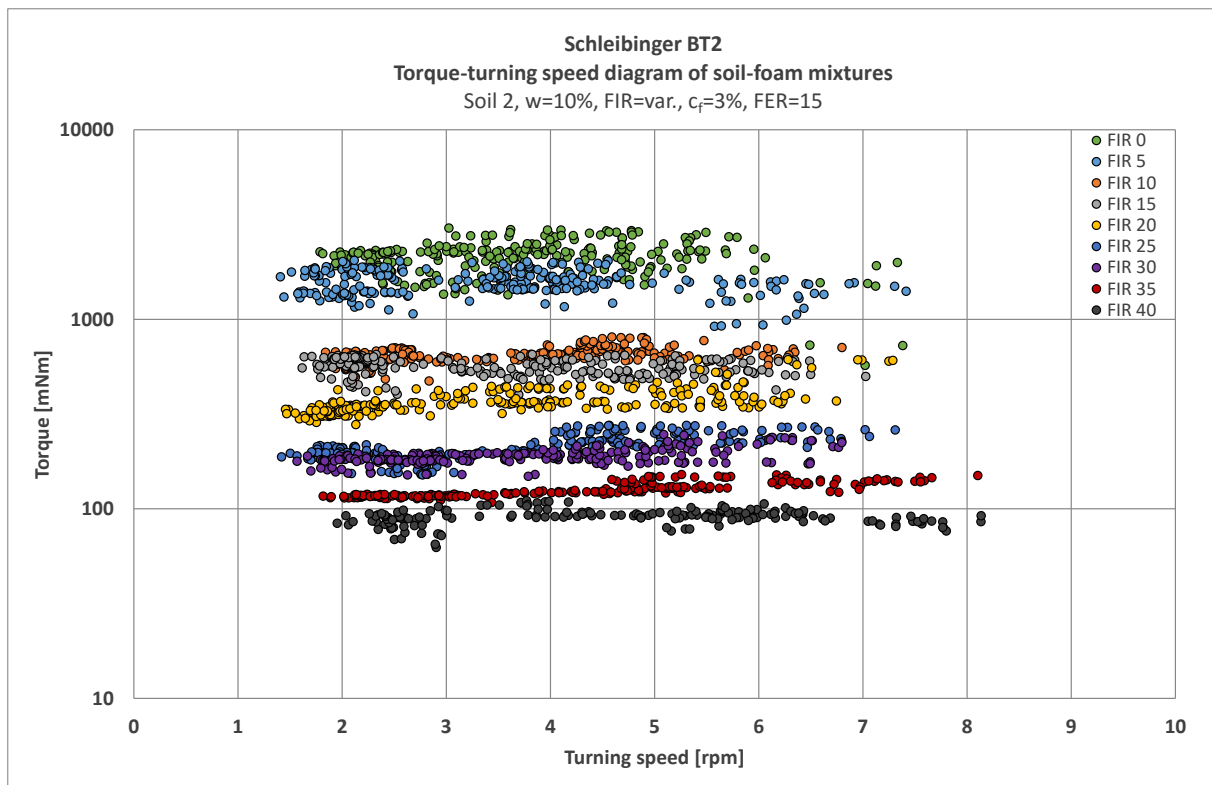
Figure 7-4:   Torque-speed diagram of sand-foam mixtures with different FIR determined with the concrete rheometer Schleibinger BT2
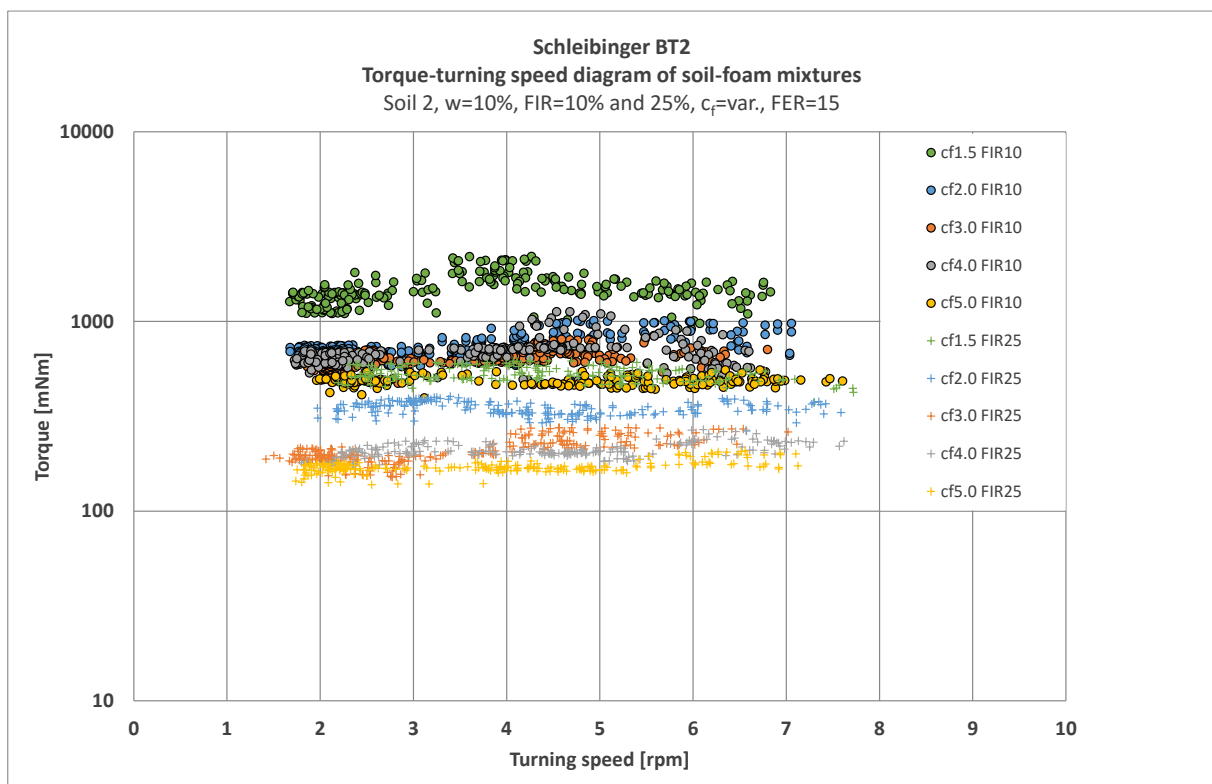
Figure 7-5:   Torque-speed diagram of sand-foam mixtures with different surfactant concentrations c_f determined with the concrete rheometer Schleibinger BT2

In another thesis under guidance of the author, GESING (2013) used two rheometers, which are commonly applied in material science. One of them is the Fann® Model 35 Viscometer (Figure 7-6; see FANN INSTRUMENT COMPANY (2013)). Its main field of application is in the drilling industry. Usually, oils or mud suspensions are investigated regarding their rheological parameters. It consists of a sample beaker with a volume of approximately 350 cm³, a cylinder-shaped rotor and a cylindrical bob with smooth surface within the rotor. Both rotor and bob are fixed to the rheometer and dip into the sample container. Thus, the testing material fills the gap between rotor and bob. The measuring principle is mechanical. The rotor moves at six destined speeds (3, 6, 100, 200, 300, 600 rpm). Hence, it is only possible to test at constant shearing speeds, which can be varied stepwise, compare chapter 3.1.3.1. The shear force is transferred via the testing liquid to the measuring bob. The bob is deflected by means of taking over shear force. A dial shows the degree of deflection, from which the resisting torque and the shear stress respectively can be calculated according to FANN INSTRUMENT COMPANY (2013). The measurements have to be read visually and recorded manually. The working principle is illustrated in Figure 7-6.

The same soils as in the present thesis were investigated both with a water content of 12 wt% and their respective FIR_{10} and FIR_{20}. Besides a smooth cylindrical bob with reduced diameter, two additional bobs in shapes of a four- and a six-bladed vane were fabricated. Conversion of the raw data from the new measuring geometries into
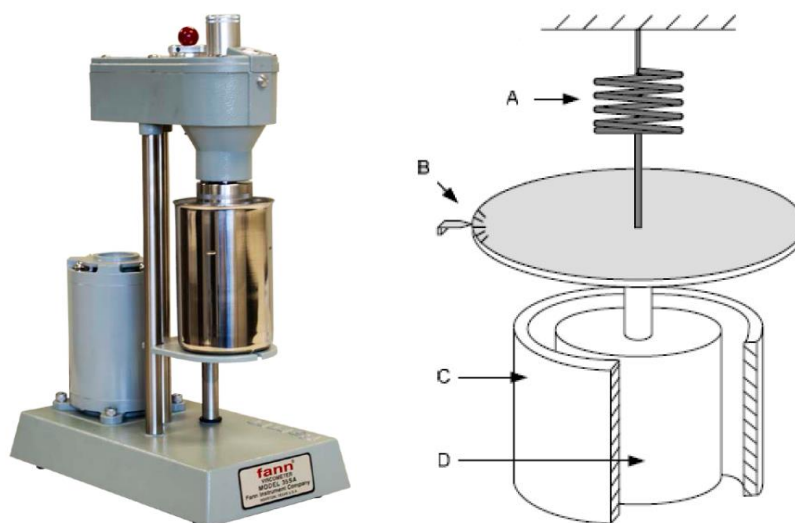
Figure 7-6: **Fann® Model 35 Viscometer (left; FANN INSTRUMENT COMPANY (2013)) and schematic illustration of the working principle (API RECOMMENDED PRACTICE 13D (2010-05)); with: A: torsion spring, B: dial of deflection, C: rotating cylinder (rotor), D: measuring bob**

rheological parameters was established based on DIN 4094-4 (2002-01). In general, the application of sand-foam mixtures in this rheometer was feasible. However, it has to be questioned, whether the gap distances of approximately 6 mm are large enough for the present soils to avoid significant grain-to-grain interactions. Furthermore, slip effects might occur on the smooth surfaces of the rotor and the cylindrical bob. It is uncertain, if the shear rate is applied appropriately to the material in the gap or if there are any losses. Nonetheless, shear stress data for the different materials at different shear rates was determined based on the measuring profile displayed in Figure 7-7. Thus, it was possible to generate rudimental flow curves.
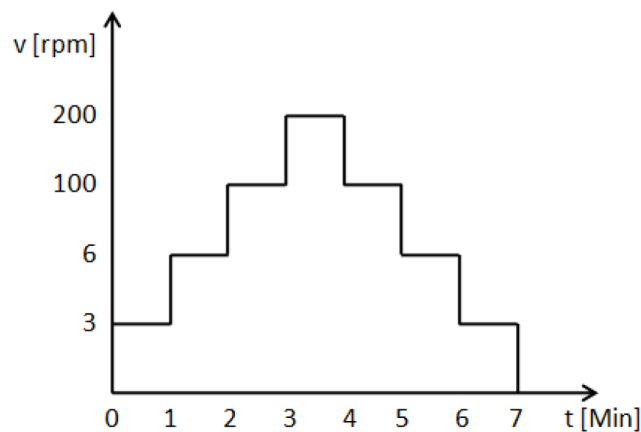
Figure 7-7:   **Measuring profile "Fann viscometer" for flow curve measurements with the Fann® Model 35 Viscometer according to GESING (2013)**

In spite of probable side effects, some basic information on the rheology of soil-foam mixtures could be gained. Therefore, only the measurements from the ascending part of the profile were analysed. Exemplary results are shown in Figure 7-8 and Figure 7-9. Therein, the connecting lines are for better reading of the data. The general course of the data confirms the findings of the BT2 investigations as they followed largely a linear trend over the investigated shear range. The flow curves of soil 1 and 2 covered a shear stress range between 0 and 200 Pa. The shear stresses of the vanes are lower compared to the shear stresses of the cylindrical bob. During testing, foaming effects were observed, which might be ascribed to the appearing shear energy.
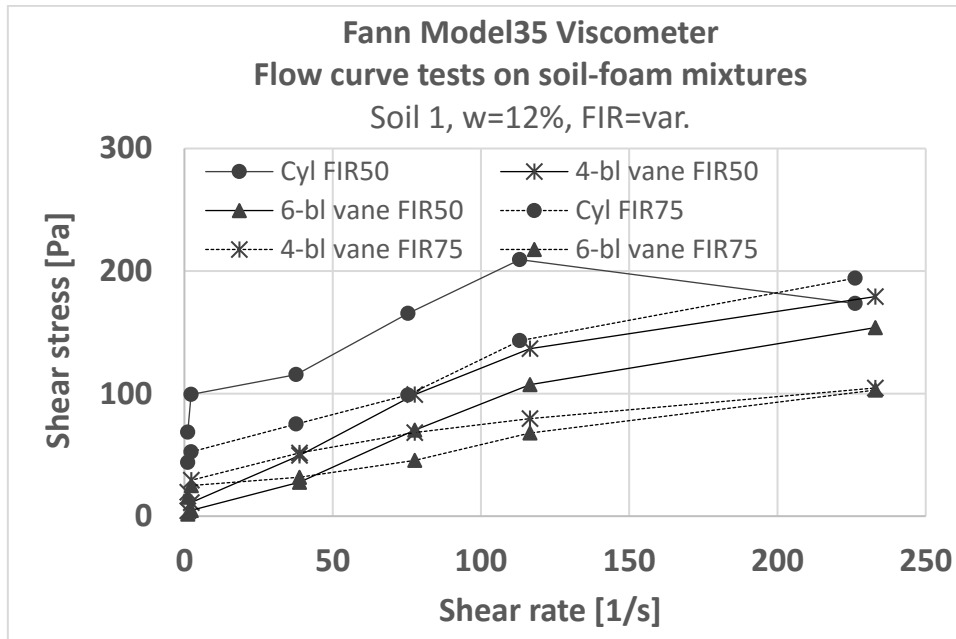
Figure 7-8: Flow curves of fine sand-foam mixtures determined in the Fann® Model 35 Viscometer with different measuring systems: cylindrical bob with smooth surface (Cyl), four-bladed vane (4-bl vane), six-bladed vane (6-bl vane)
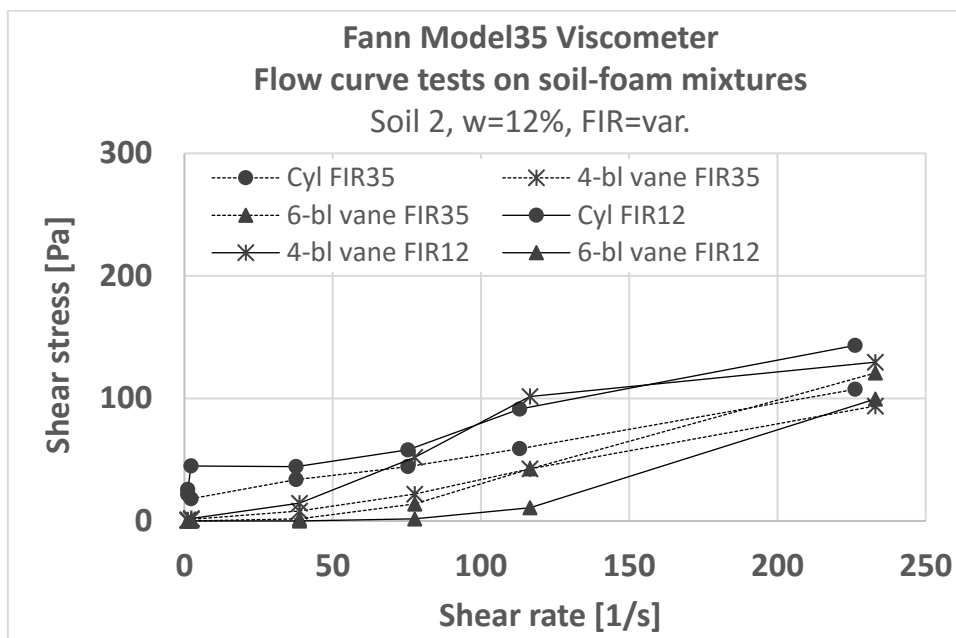
Figure 7-9: Flow curves of sand-foam mixtures determined in the Fann® Model 35 Viscometer with different measuring systems: cylindrical bob with smooth surface (Cyl), four-bladed vane (4-bl vane), six-bladed vane (6-bl vane)

The second rheometer used in the thesis of GESING (2013) was the concrete rheometer Schleibinger Viskomat NT (Figure 7-10; see SCHLEIBINGER GERÄTE TEUBERT U. GREIM GMBH (2012b)). It is mainly applied to mortars and cement pastes in concrete engineering. The apparatus resembles a rotational rheometer of the Couette type (see chapter 3.1.3.2), where the sample cup rotates and the measuring system takes over the shear force but is not in motion (Figure 7-10). The rheometer features a liquid cooling system. Due to the geometries of the measuring systems, the appearing flow field is intricate and conversion of raw data into shear stresses and shear rates is not trivial. The analysis software of the manufacturer supports relative evaluation (e.g. torque over rotational speed) and absolute evaluation (e.g. shear stress over shear rate). For the lime paddle system, it is recommended to conduct only relative analyses for comparative testing (SCHLEIBINGER GERÄTE TEUBERT U. GREIM GMBH (2015a)). The setting of input values allows for numerous specifications. The tests can be steered either stress- or rate-dependent over a large value domain (torque: 0 to 200 mNm, speed: 0.001 to 200 rpm; SCHLEIBINGER GERÄTE TEUBERT U. GREIM GMBH (2009)). Otherwise, the measurements and corresponding recordings are operated automatically.

The same mixtures were investigated under the same temporal restraints and with the same measuring profile as in the previous investigations. Furthermore, (logarithmic) ramp profiles were applied to the testing materials in order to measure

Figure 7-10: Schleibinger Viskomat NT (left) and working principle (SCHLEIBINGER GERÄTE TEUBERT U. GREIM GMBH (2012b))

the resisting torque at continuously increasing rotational speed. However, it was hardly possible to examine soil-foam-mixtures with foam injection ratios smaller than 100 vol%. In these cases, the resulting torques became too high and the rheometer aborted the measurements. Therefore, additional experiments were performed on tunnelling foam and increasing volume fractions of fine sand particles (FIR = 100, 200, 300, 400, 500 vol%, and pure foam) maintaining the water content steady at 12 wt%. Even though possible conversion approaches of the raw data were not studied at that point, the torque measurements were assessed by apparent flow curve analysis. The FIR was determined to be a factor of high influence to the resting torque, which again complies with the BT2 tests and of course with several experiences from other soil conditioning research, compare chapter 3.2.3. And yet, a non-linear relationship was found between the torque and the applied rotation speeds. Due to the detailed setting options, it was possible to gain more responses at low turning speeds and at smaller intervals of data sampling than in the other pre-studies. The results had been approximated in multiple ways and resulting in good agreement between models and data, when applying a power-law description of the Ostwald-de Waele type (Figure 7-11). If only the torques belonging to rotational speeds between 1 rpm and 10 rpm
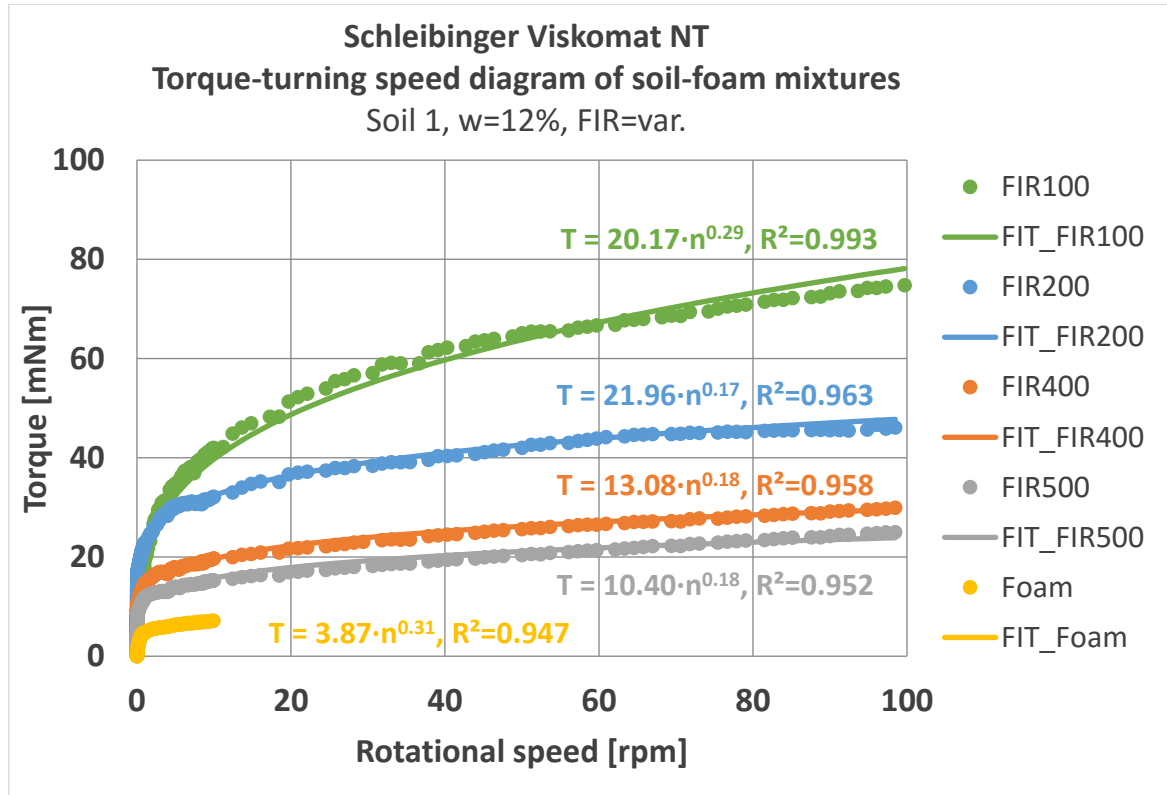
Figure 7-11: Relative flow curves (torque-rotational speed diagram) of fine sand-foam mixtures with changing particle content determined in the Schleibinger Viskomat NT
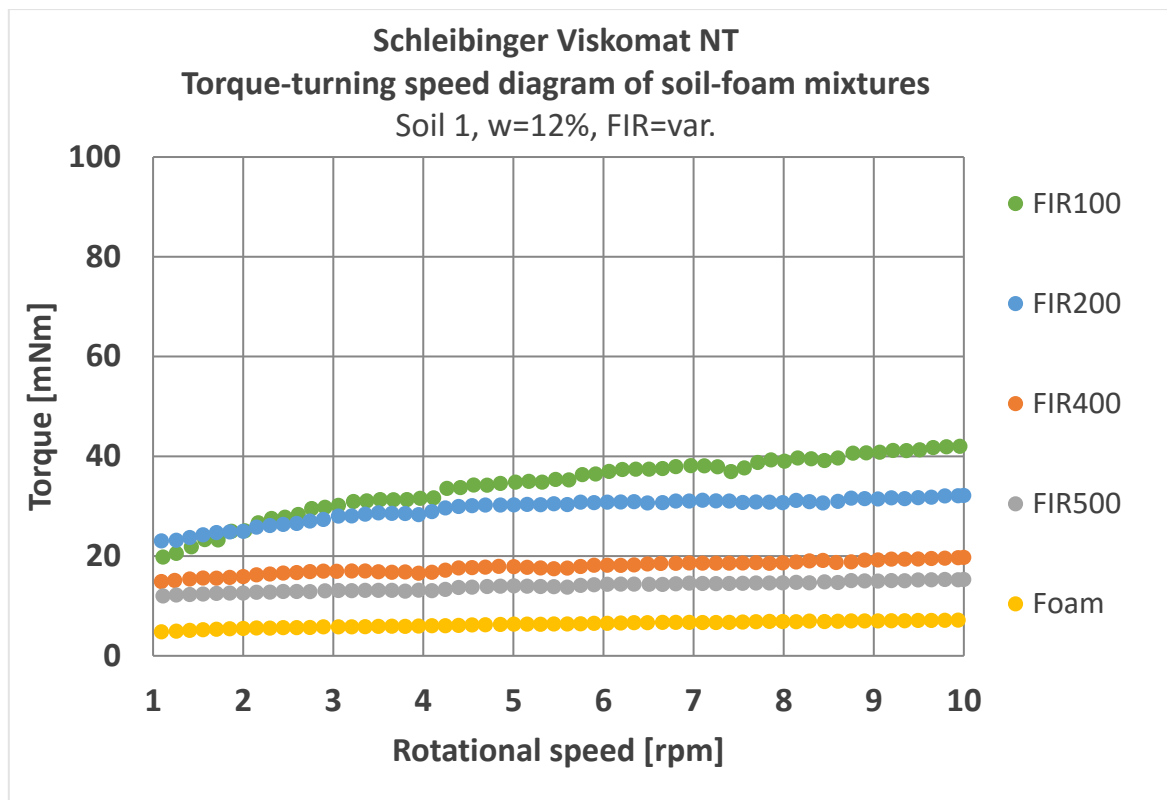
Figure 7-12: Extract (turning speed 1-10 rpm) from the torque measurements on fine-sand-foam mixtures shown in Figure 7-11

were considered, the mixtures exhibit a constant slope (Figure 7-12) similar to the results of the Schleibinger BT2 examinations. A linear description would here be more suitable for data fitting.

In extended preliminary tests, the influence of particles on the rheology of foam was investigated using the Schleibinger Viskomat NT, too. Different types of particles (hollow and solid glass particles as described in chapter 4.3.4 and fine sand (soil 1)) were saturated with water and then mixed with shaving foam considering a foam injection ratio of 100%. These tests should provide general information on the rheological comparability of different particle-foam mixtures. Shaving foam was used in the experiments in order to ensure very limitedly altering foam quality parameters. The flow behaviour of all mixtures showed a similar, non-Newtonian, shear-thinning flow behaviour. However, the particular torque range depended on the respective type of particles. The fine sand-foam mixture exhibited the highest torques, while the glass particle-foam mixtures showed lower torques than the pure foam. This character is determined by the additional water (see chapter 7.2 for details). The results of the pre-study are shown in Figure 7-13.
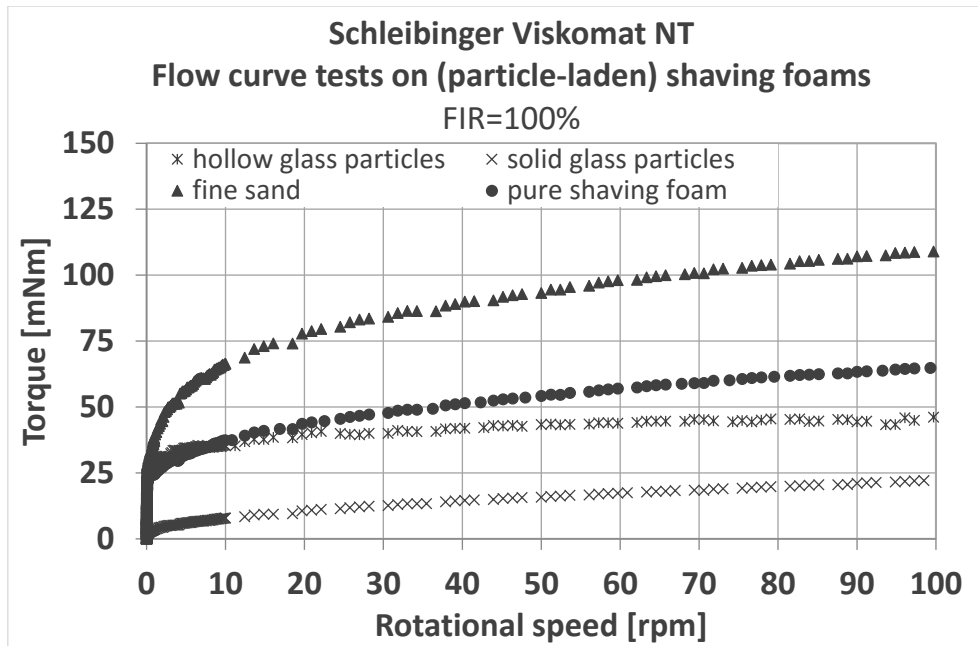
Figure 7-13: **Torque-rotational speed diagram of different particle-foam mixtures (FIR=100%) determined with the Schleibinger Viskomat NT (logarithmic ramp profile 0.001-100 rpm)**

Summarising the pre-studies, some significant findings could be determined in the experiments on the general flow pattern of soil-foam mixtures under the particular flow conditions. In all experiments, a non-Newtonian flow behaviour could be observed, although an adequate transformation of raw data into rheological parameters was not always accomplished. Furthermore, all setups exhibited advantages and disadvantages for an extensive and substantial application to soil-foam mixtures (e.g. gap width, slip, torque range etc.). Nevertheless, differences in results could clearly be seen apart from any uncertainties that may have influenced them. Apparently, the material responds differently at low and high shear ranges. In order to gain basic information on the fundamental flow behaviour under different shearing conditions, the rheology of particle-foam mixtures shall be studied in micro-scale investigations. Micro-scale rheometry features homogeneous shear conditions, which means that only laminar flow effects are present and the shear rate is steadily transferred to the material sample. Thus, a benchmark shall be found for the further study on the rheology of soil-foam mixtures and for a sustainable comparative analysis.

7.2   Micro-scale investigations on the flow behaviour of synthetic EPB support material

Advanced rheological investigations are necessary for physically comprehending the rheological influence of adding foam to the soil. So far, the rheological behaviour of particle-foam mixtures has not been investigated intensely, compare chapter 3.2.3, particularly in the context of EPB tunnelling. The pre-studies on tunnelling-related soil-foam mixtures provided a first insight on the general flow pattern (chapter 7.1). However, a sound description of the rheology could not be established with the applied methods. Micro-scale experiments have been performed by ÖZARMUT ET AL. (2013), ÖZARMUT & STEEB (2015), THEWES & STEEB (2014) investigating the effective rheological parameters (yield stress, viscosity) of particle-foam mixtures. Taking the results of the micro-scale investigations as a reference flow behaviour, they are the foundation for later comparative analyses. The transfer of findings in the basic flow pattern through the different experiments and the comparison of the flow behaviour of the diverse material compositions represent the main objectives of the analysis.

Micro-scale experiments require homogeneous testing configurations, most notably a small gap size ensuring purely laminar shear flow conditions. Because of their grain-sizes, real soil-foam mixtures, which hitherto had been considered here, apparently cannot be investigated under these required conditions. Therefore, ÖZARMUT & STEEB (2015) used polymer-stabilised shaving foam (Gillette™) and solid glass particles (SiLibeads Glass beads Type S, see SIGMUND LINDNER GMBH (2012)) instead, see also chapter 4.3.4. Due to the foam's increased lifetime and its characteristic length scales of the microstructure, it is a suitable replacement for the tunnelling foam in the experiments. The glass beads likewise exhibit adequate characteristic length scales and in addition, they possess uniform shapes and sizes. Since the morphology, i.e. the microstructure of the (particle-laden) foams, is important for effective rheological properties, it was characterised by applying light microscopy. The mean bubble diameter of the foam was determined to 51.80 µm and had a Gaussian-like distribution, cf. ÖZARMUT ET AL. (2013). The size of glass particles was chosen according to the mean diameter of the foam, see chapter 4.3.4 for details. Thus, the particle-foam mixtures consist of a monodisperse microstructure.

The rheological tests performed on the substitute materials by ÖZARMUT & STEEB (2015), THEWES & STEEB (2014) were flow curve tests and oscillation tests. The particles in the mixtures were either dry or wetted to a certain saturation prior of mixing with foam. The different volume fractions of the constituents used in the experiments for both cases (dry / wet) are shown in Table 7-1 and Table 7-2. The tests were conducted using an Anton Paar MCR301 rheometer (Figure 7-14) equipped with a parallel plate measuring system, to which fine-grained sandpaper (P320) was glued reducing wall slip effects (see below). The gap width was set to 1.5 mm in all experiments. The rheological experiments were conducted at room temperature around 23.27 ± 1°C. Shear stresses were measured over a shear rate range between 0.001 and 10 1/s with a logarithmic ramp profile. The test duration was 8 minutes.
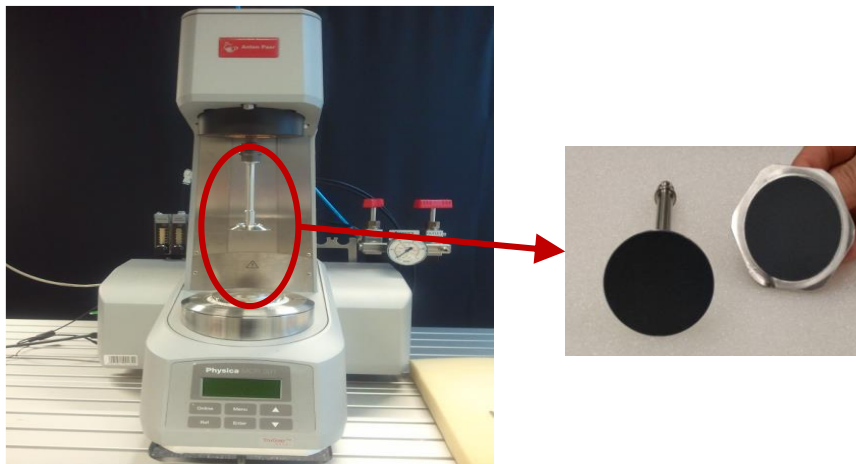
Figure 7-14: **Rheometer Anton Paar MCR301 with plate-plate measuring system and sandpaper surface**

Table 7-1:   **Volume fractions of the constituents foam and dry glass particles used in flow curve tests with plate-plate configuration (modified from ÖZARMUT (2014))**

	1	2	3	4	5	6	7
$dv_0^f [ml]$	40	38	36	34	32	30	28
$dv_0^s [ml]$	0	2	4	6	8	10	12
$FIR [\%]$	∞	1900	900	566	400	300	233
$n_0^s [1]$	0	0.05	0.1	0.15	0.20	0.25	0.30
$n_0^f [1]$	1	0.95	0.9	0.85	0.80	0.75	0.70

Table 7-2:   **Volume fractions of the constituents foam and wet glass particles used in flow curve tests with plate-plate configuration (modified from ÖZARMUT (2014))**

	1	2	3	4	5
$dv_0^f[ml]$	40	20	20	20	20
$dv_0^{w+s}[ml]$	0	6	10	20	36
$FIR[\%]$	∞	333	200	100	67
$n_0^{w+s}[1]$	0	0.23	0.33	0.5	0.64
$n_0^f[1]$	1	0.76	0.67	0.5	0.26

The average results from flow curve testing of three samples are shown in Figure 7-15 for the mixes containing dry particles and saturated particles. Rheological experiments could not be performed for high solid volume fractions. At volume fractions of greater 30%, the mechanical response of the mixture changed to a solid-like material behaviour. ÖZARMUT & STEEB (2015) explained this with occurring adsorption processes of the liquid foam phase at the surface of the glass beads destroying the foam morphology and thusly, the particle-foam mixture. To overcome the adsorption phenomenon, the particles must be wetted prior of mixing with foam. The wetted particle mixes could be investigated up to a volume fraction of particles and water of 64% reflecting a foam injection ratio of 67%. The remark on "no yield stress" is linked to the non-sharp transition from unyielded to yielded conditions covered by the Herschel-Bulkley-Papanastasiou equation.
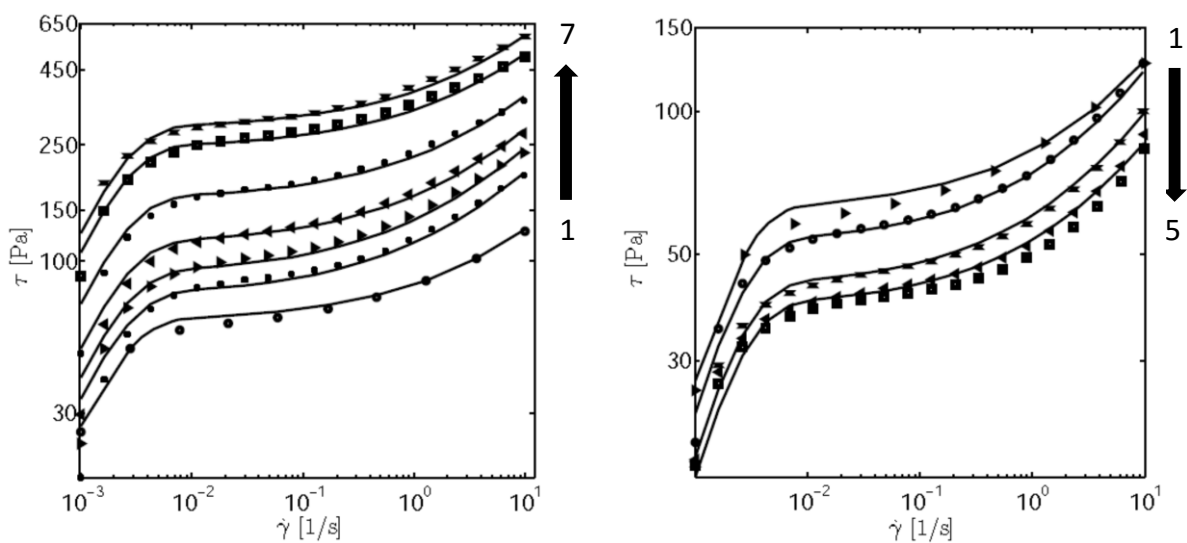
Figure 7-15: **Data of flow curve experiments on particle-foam mixtures (left) and particle-water-foam mixtures (right) fitted with the Papanastasiou-Herschel-Bulkley model (modified from ÖZARMUT (2014), THEWES & STEEB (2014))**

The flow curve experiments on foams led to results similar to findings from former studies as presented in chapter 3.2.1; a non-Newtonian behaviour was determined. A similar behaviour appeared for the particle-foams. Interestingly, the tested mixtures exhibited a shear-thinning behaviour at low shear rates and a shear-thickening behaviour at high shear rates. The standard deviations were so small that the results could be rated material specific (THEWES & STEEB (2014)). Fitting of the obtained data was possible with models of the Herschel-Bulkley type but also of the power-law type, since the yield stress is generally very difficult to capture with high precision in flow curve experiments, see ÖZARMUT ET AL. (2013). However, the best possible fit was achieved using the modified Herschel-Bulkley model according to PAPANASTASIOU (1987) (see Eq. 3.8; ÖZARMUT & STEEB (2015), THEWES & STEEB (2014)). Thus, both shear ranges, low shear and high shear, could be well approximated. The resulting model parameters from regression analysis are summarised in Table 7-3 and Table 7-4. The fits were plotted as continuous lines into Figure 7-15.

The regression coefficients show significant behaviours. The shape parameters m and p (p = 0.5) were constant for all experimental data sets. The Papanastasiou yield stress factor τ* decreases with increasing solid volume fraction and with decreasing foam content (FIR). ÖZARMUT (2014) established a functional relationship between τ* and the volumetric content of particles n_0^s [-] as depicted in Figure 7-16.

Table 7-3:   **Adjusted parameters of the Papanastasiou-Herschel-Bulkley model from regression analysis for particle-foam mixtures of different volume fractions (ÖZARMUT (2014))**

n_0^s	1	2	3	4	5	6	7
$a[\mathrm{Pas}^{-1/2}]$	21	40	49	54	66	86	98
$\tau^*[\mathrm{Pa}]$	61.81	75.55	89.47	113.3	161.9	242.8	283.3
$m[\mathrm{s}]$	560	560	560	560	560	560	560

Table 7-4:   **Adjusted parameters of the Papanastasiou-Herschel-Bulkley model from regression analysis for particle-water-foam mixtures of different volume fractions (THEWES & STEEB (2014))**

n_0^s	1	2	3	4	5
$a[\mathrm{Pas}^{-1/2}]$	21	22	18	15	15
$\tau^*[\mathrm{Pa}]$	61.81	52.30	42.50	38.64	38.64
$m[\mathrm{s}]$	560	560	560	560	560

$$\tau^* = A \cdot (n_0^s)^{3.2} + B$$
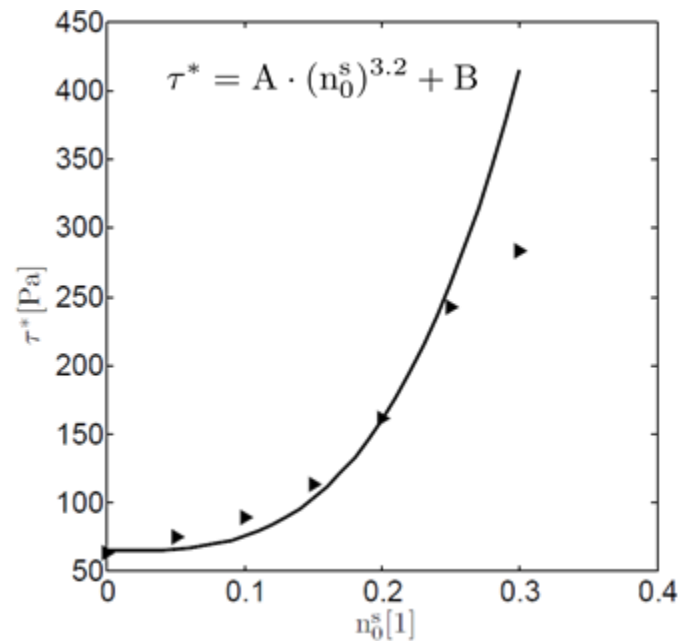
Figure 7-16: Functional relationship of yield stress parameter τ* according to PAPANASTASIOU **(1987) and particle volume fraction in the flow curve experiments (ÖZARMUT (2014))**

Wall slip was investigated prior of the main test series through varying surface asperities of the plates. Based on the findings, later, the main tests were conducted with sandpaper-treated plates exhibiting a particle-size in the order of the mean bubble diameter (sandpaper type P320). Thus, the continuity of flow could be re-established significantly, which results in increased shear stresses compared to smooth plates, see Figure 7-17.

Currently, the experimental programme is extended in order to consider different conditions of backpressure (0 - 400 kPa), cf. THEWES & STEEB (2014). Therefore, a Searle type cup-and-bob configuration is installed into the rheometer with different surface asperities. The measuring system can be pressurised. Thus, the real conditions in the EPB excavation chamber shall be simulated.

The findings from micro-scale flow curve tests on synthetic EPB material supported the observations of the pre-investigations of the present study. The material widely behaved like a non-Newtonian and shear-thinning fluid; it was described best by the generalised Papanastasiou-Herschel-Bulkley formulation. Depending of the degree of saturation, the immersion of particles into the foam affected the level of shear stress, but the general flow behaviour seemed to remain the same.
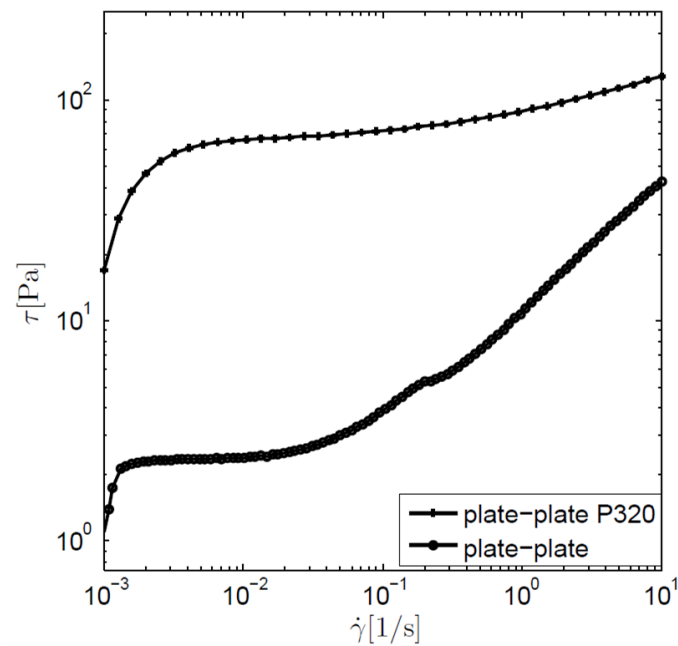
Figure 7-17: Flow curves of shaving foam from experiments with plate-plate system with and without sandpaper surface (ÖZARMUT (2014))

7.3 Macro-scale investigations on the flow behaviour of realistic EPB support material

Based on the outcomes of the pre-studies and of the micro-scale investigations, the rheology of realistic tunnelling foam and of realistic soil-foam mixtures was investigated. The assessment is going to be described in detail in the following sections.

The investigations were conducted using the rotational rheometer Anton Paar RheolabQC (Figure 7-18). Taking into account the state-of-the-art in testing colloidal suspensions and other granular media and considering the experience from the own pre-studies, two measuring configurations were chosen for the main rheological test series. First, the flow behaviour was assessed using the rheometer with concentric cylinder configuration (chapter 7.3.1) and then, the testing programme was extended by measurements with a ball measuring system (chapter 7.3.2). After that, a comparative analysis will be conducted considering the results of the multiple scales and experiments (chapter 7.4).

7.3.1   Concentric cylinder system

7.3.1.1   Setup and calibration

The coaxial cylinder system used was of the Searle type and consisted of the cylinder "CC27" (diameter of 26.7 mm) and the corresponding cup (diameter 28.9 mm). Hence, the present gap width between the sample container and the measuring system was 1.1 mm. The system dimensions accorded to the recommendations given in DIN 53019-1 (2008-09). The testing temperature could be regulated very precisely using a Peltier cooling system. All components are shown in Figure 7-18.

The calibration of the device was checked with a special calibration oil (see chapter 4.3.4 for details). Furthermore, comparative tests were executed on the rheometer applied in the micro-scale experiments and the present rheometer using the same fluids (calibration oil, bentonite slurry, high-density limestone slurry, shaving foam) and measuring systems (CC27). All measurements were congruent with each other. In this way, it was ensured that obtained data was reliable.
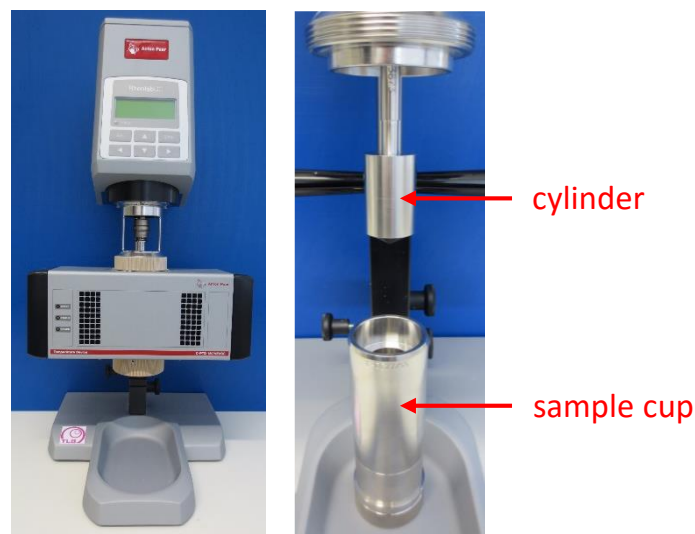
Figure 7-18: Rheometer Anton Paar RheolabQC with Peltier cooling system; right: concentric cylinder system CC27

7.3.1.2   Testing procedure and experimental programme

Aim of this investigation was a comparative analysis of synthetic materials and realistic (particle-laden) foams. Therefore, pure foams (shaving foam and tunnelling foam) and mixtures consisting of both substitute and realistic foams had been tested under the same conditions. However, the investigation of soil-foam mixtures was constrained. According to DIN 53019-1 (2008-09), the particle-size should be limited

to one fifth of the gap size in order to maintain homogeneous shear flow conditions. Considering the present gap width of the concentric cylinder system, this meant that the maximum allowance for the grain-size was 0.22 mm. With respect to the soils regarded in this study, only soil 1 with a maximum grain-size of around 0.25 mm was acceptable. The mixtures that were intended for investigation with both shaving foam and tunnelling foam are displayed in Figure 7-19. The material compositions were chosen identically to the study in chapter 6.

Testing was executed applying a logarithmic ramp profile with shear rate increases from 0.01 to 1,000 1/s. The reference temperature in the Peltier cooling system was defined to 20±0.1°C.
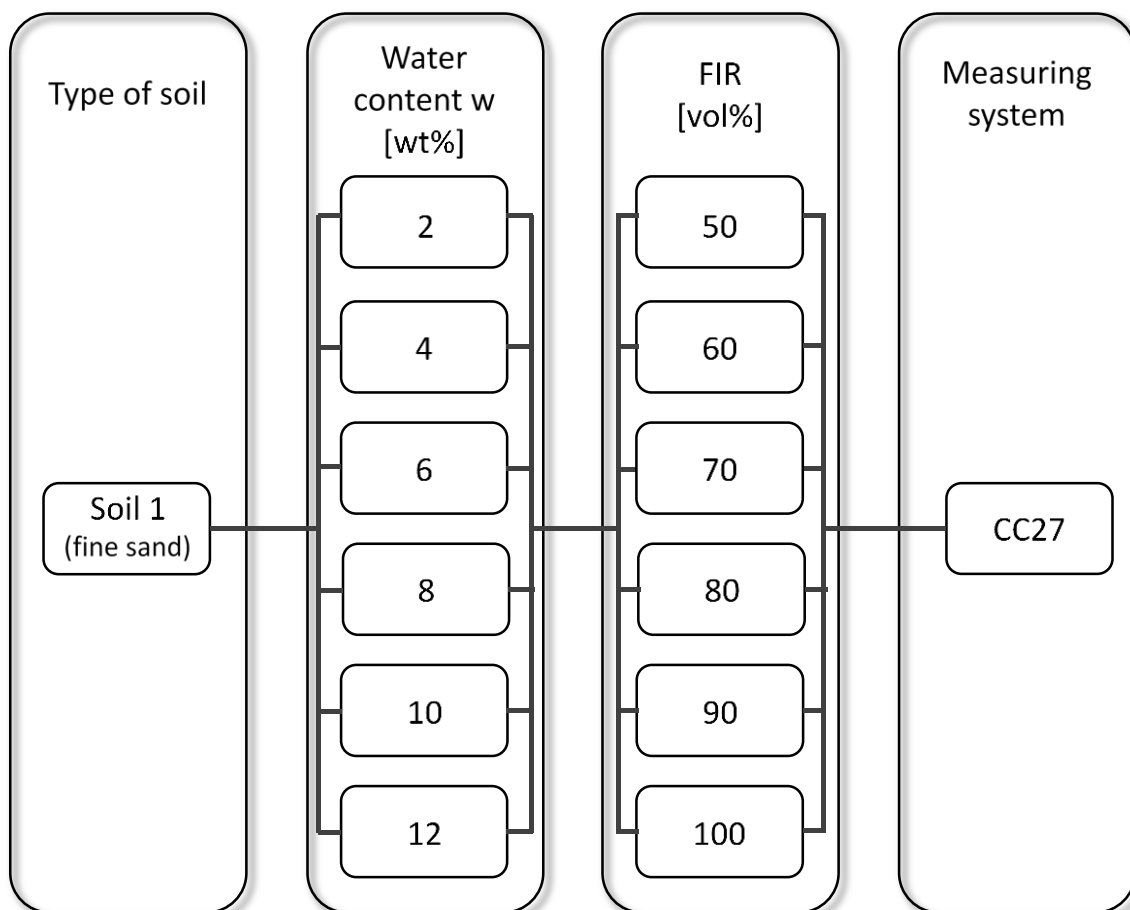
Figure 7-19: Experimental programme for flow curve tests on fine sand-foam mixtures using a concentric cylinder measuring system

7.3.1.3   *Test results and analysis*

▪ **Foams**

Looking at the flow curves of the pure foams (Figure 7-20), a similar flow behaviour could be determined for shaving and tunnelling foam, although pure shaving foam evokes higher shear stresses than the pure tunnelling foam at same shear rates. This difference certainly results from the basic constitutions of the foams. Compared to tunnelling foam, shaving foam consists of a considerably higher share of stabilisers. Cells and lamellae are also much smaller, which hinders destabilising effects.
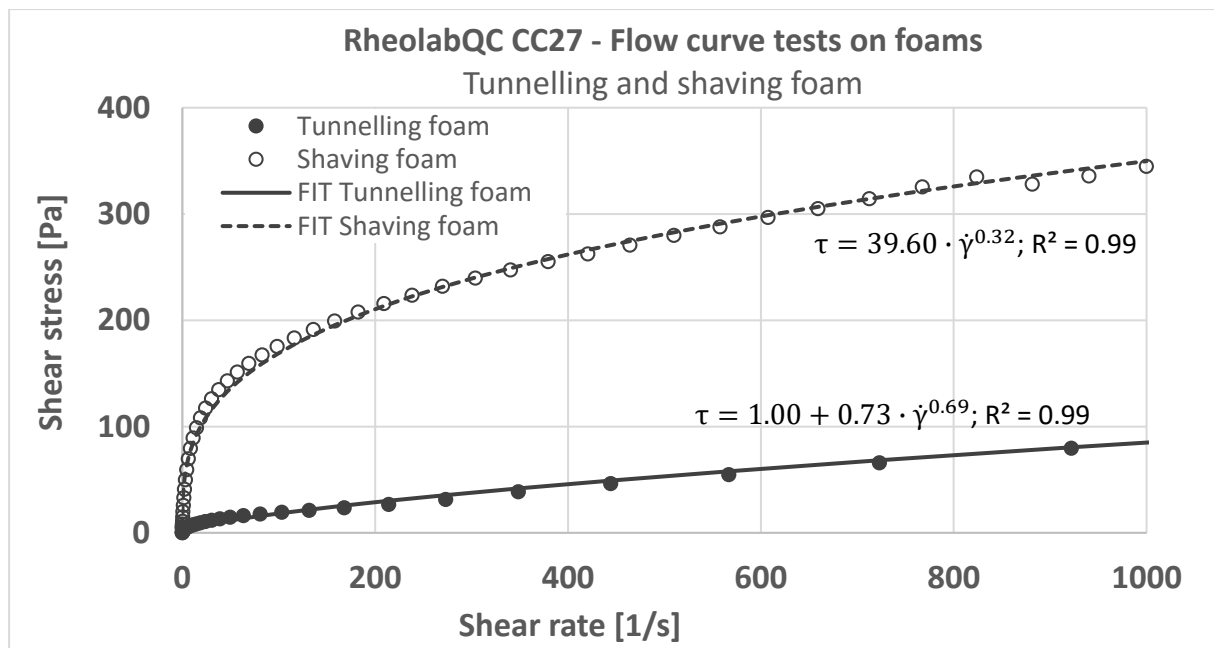
Figure 7-20: Flow curve data of shaving foam and tunnelling foam using a concentric cylinder configuration

Curve fitting was possible using the established non-Newtonian model functions. The application of the Papanastasiou-Herschel-Bulkley model as proposed by ÖZARMUT & STEEB (2015) led not to a significant melioration in fitting the flow curve data in comparison to the simple Herschel-Bulkley model. The coefficients of determination from the regression analysis were very similar to each other. Curve fitting for the shaving foam resulted in a zero yield-stress condition, while for the tunnelling foam, an inclusion of a small yield stress value enhanced the data fit slightly (higher R^2). The resulting formulas describe the flow curves of shaving foam (Eq. 7.1) and tunnelling foam (Eq. 7.2) in the concentric cylinder setup.

$$\tau = 0.73 \cdot \dot{\gamma}^{0.69} + 1.00 \qquad \text{[Pa]} \qquad R^2 = 0.99 \qquad \text{Eq. 7.1}$$

$$\tau = 39.60 \cdot \dot{\gamma}^{0.32} \qquad \text{[Pa]} \qquad R^2 = 0.99 \qquad \text{Eq. 7.2}$$

- **Soil-foam mixtures**

The first and most significant result for the particle-foam mixtures was detected already during the test preparations. Fine sand-foam mixtures with foam injection ratios lower than 70% could not be investigated in the concentric cylinder system independent of the type of foam. Once the material was inserted into the cup, it was impossible immersing the measuring cylinder into the sample because it was too stiff. Mixtures containing less water were not investigable even at higher FIR. With respect to the experience from slump testing on the same mixtures in chapter 6.3.1, fine sand-foam mixtures suitable as support material in EPB tunnelling (i.e. slump range of 10 and 20 cm) cannot be investigated in the standard cylinder measuring system as it was intended using here. Nevertheless, the remaining mixtures should still be analysed in order to make a comparison between the micro-scale and the macro-scale findings possible.

Generally, the flow curves of all mixtures showed a non-linear relation between shear stress and shear rate. Thus, the materials can be classed non-Newtonian. At high shear rates, the flow pattern was similar to the observations made in the pre-studies and in the micro-scale investigation. However, the flow behaviour differed greatly from the micro-scale observations at low shear-rates. Additionally, the flow curves revealed important impacts from the setup due to slip effects, especially for the fine sand-foam mixtures. A treatment of the bob and cup surfaces similar to the plate-plate configuration was not feasible, which is why a quantitative recognition of present slip effects was not possible so far. Nevertheless, it seemed obvious that slip effects were present in the experiments. Comparing the present flow curve data and the findings from the micro-scale investigations, a flow behaviour like the one obtained with the plate-plate geometry without sandpaper (Figure 7-17) was determined. The results are shown in Figure 7-21 (shaving foam) and Figure 7-22 (tunnelling foam). Therein, the flow curves of the pure foams are also depicted again. The behaviour of the different mixtures are presented in the following in more detail.
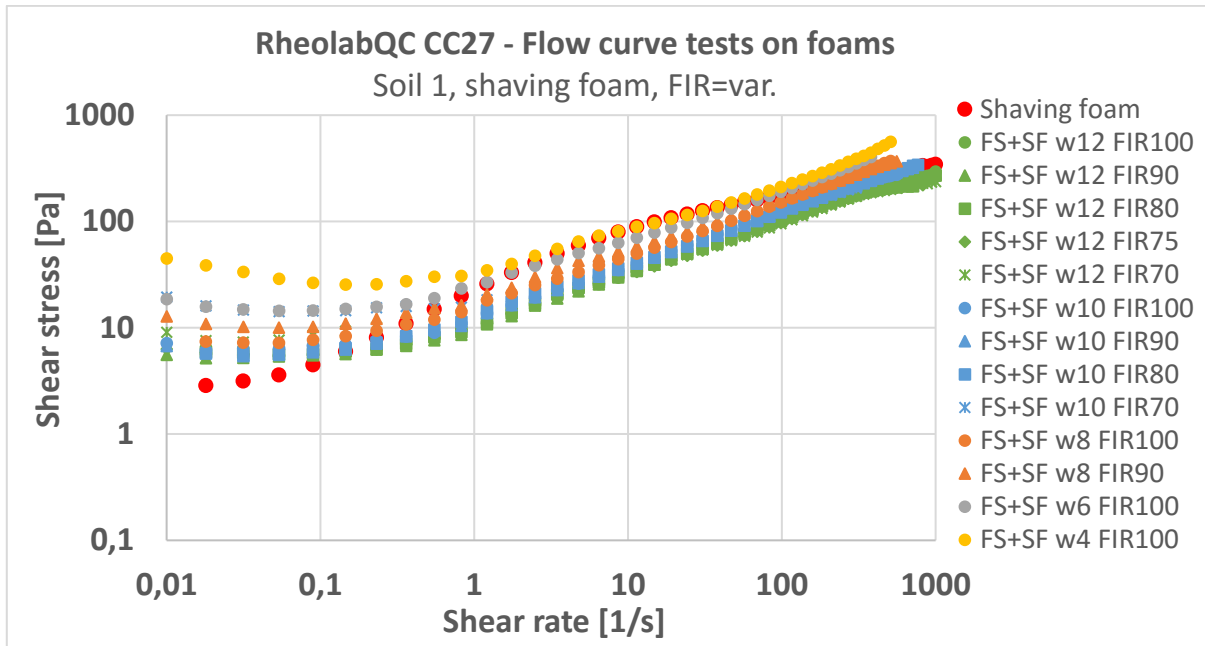
Figure 7-21: Flow curve data of shaving foam and fine sand-shaving foam mixtures with different water contents and foam injection ratios using a concentric cylinder configuration
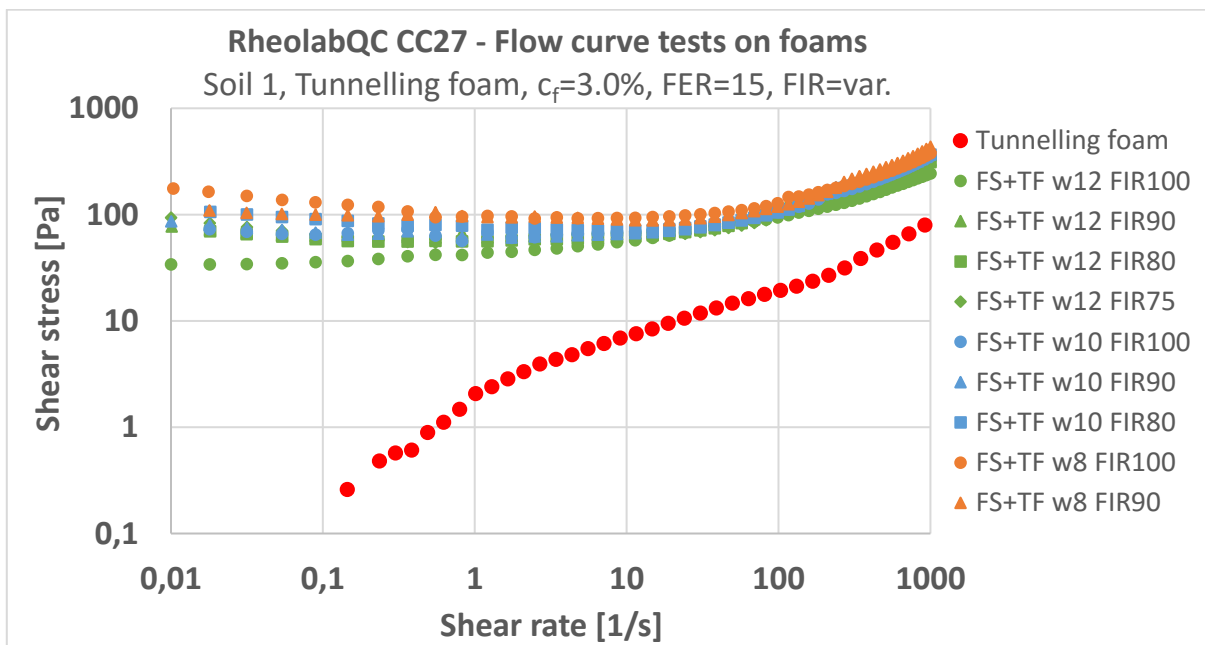
Figure 7-22: Flow curve data of tunnelling foam and fine sand-tunnelling foam mixtures with different water contents and foam injection ratios using a concentric cylinder configuration

Among the particle-foam mixtures, the flow behaviour was comparable, too. For shear rates larger than 10 1/s, even the magnitude of shear stresses was to some extent the same for both foams. Below this shear rate, the flow behaviour in fact was still similar, but the shear stresses of the shaving foam-based sand mixtures were considerably smaller. Additionally, a decrease in shear stress was observable over the low-shear range before shear stresses increased again for all mixtures. The filling process of the rather small cup, the homogeneity of the mix and air entrapments could be comprehensible reasons for this initial fall in shear stress. Air entrapments cannot completely be avoided as well as settling of the material once the rotor accelerates. Although this course probably would reduce the quality of fit of established flow curve models, this data was considered in the analysis because it seemed characteristic for all mixtures. At shear rates > 300 1/s, a sudden drop was observable for some shaving foam-based mixtures. Most probably, this effect can be explained by wall slip at the material-system interface. A minimum interlink is required to perpetuate sufficient friction and by this, to enable an adequate force transmission. Affected data beyond this extraordinary drop was excluded from the analysis. Both effects did not occur for the pure foams.

Comparing the flow curves of foams and particle-laden foams, another significant difference was found out. While the flow curve of pure tunnelling foam ranges considerably below its corresponding fine sand-tunnelling foam mixtures, the shaving foam ranges within the whole bandwidth covered by the fine sand-shaving foam mixtures. The influence of soil particles and water is opposing with respect to the shaving foam's material behaviour. The soil moisture reduces the shaving foam's viscosity, while the particles support its rigidity. At a particular composition, the particles had a greater influence as the water content. This effect was not detectable for the tunnelling foam.

Independent of the type of foam, the influences of water and foam on the test results were of different degrees. A comprehensive difference in results from altered FIR at constant water contents was not observable, which was contrary for the influence of the water content. The small sample volumes that had to be used in the experiments can explain this effect. A change in FIR of 10 vol% made a weight-specific difference of approximately 0.4 g of foam. Alterations in the foam quality and the measuring preciseness of the scales (0.1 g) are much more significant at such small volumes. For

comparison: a change in water content by 2 wt% equalled a difference of 2 g. For further analyses, the FIR was excluded from the examination and for comparison, only the mixtures with a FIR of 100% were considered. The flow curves for both foam types are shown in Figure 7-23. Thus, the flow curves can be compared more easily. The data course was not as strongly of sigmoidal character as it was determined in the micro-scale investigations. Therefore, again, curve fitting was conducted using the Herschel-Bulkley model instead of the generalised Papanastasiou-Herschel-Bulkley model, since there was no benefit in applying a mathematically more complex model.

The formulation describing the whole data family resulting from non-linear regression analysis is shown in Eq. 7.3. The influence of FIR is neglect as mentioned above. The application to the data is shown in Figure 7-24.

$$\tau_{CC27} = (185.583 - 11.015 \cdot w)$$

$$+(-2.074 + 0.302 \cdot w) \cdot \dot{\gamma}^{(1.492-0.064 \cdot w)} \qquad [Pa] \qquad \text{Eq. 7.3}$$
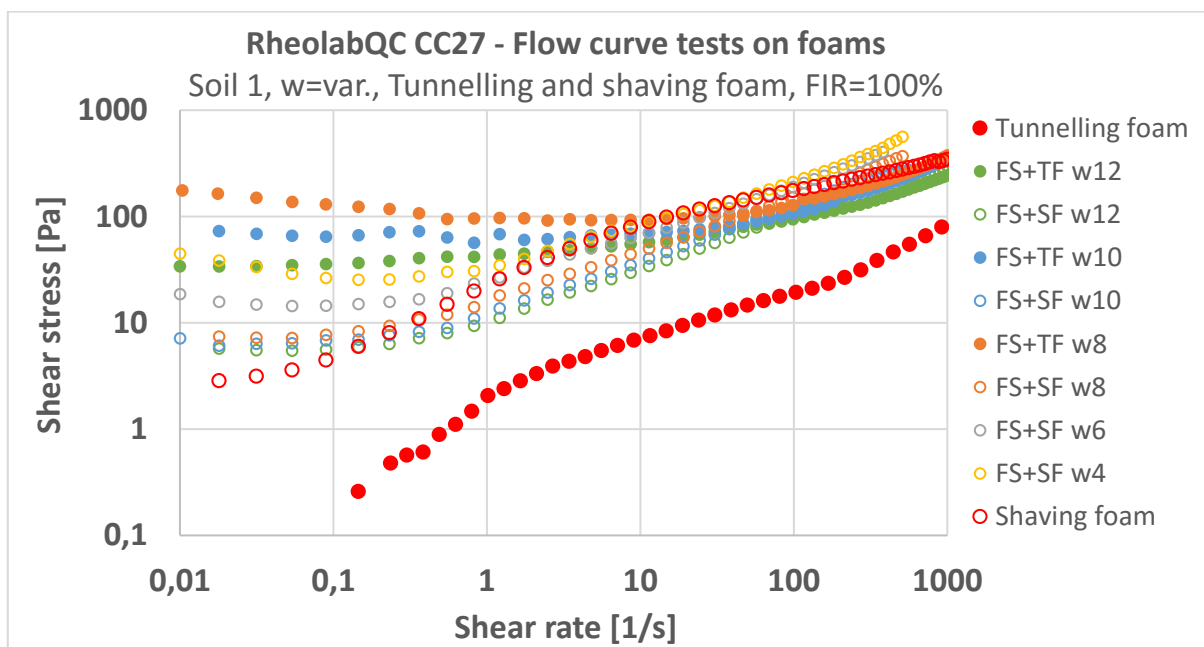
Figure 7-23: **Flow curve data of tunnelling foam and shaving foam and fine sand-foam mixtures with different water contents and FIR=100% using a concentric cylinder configuration**
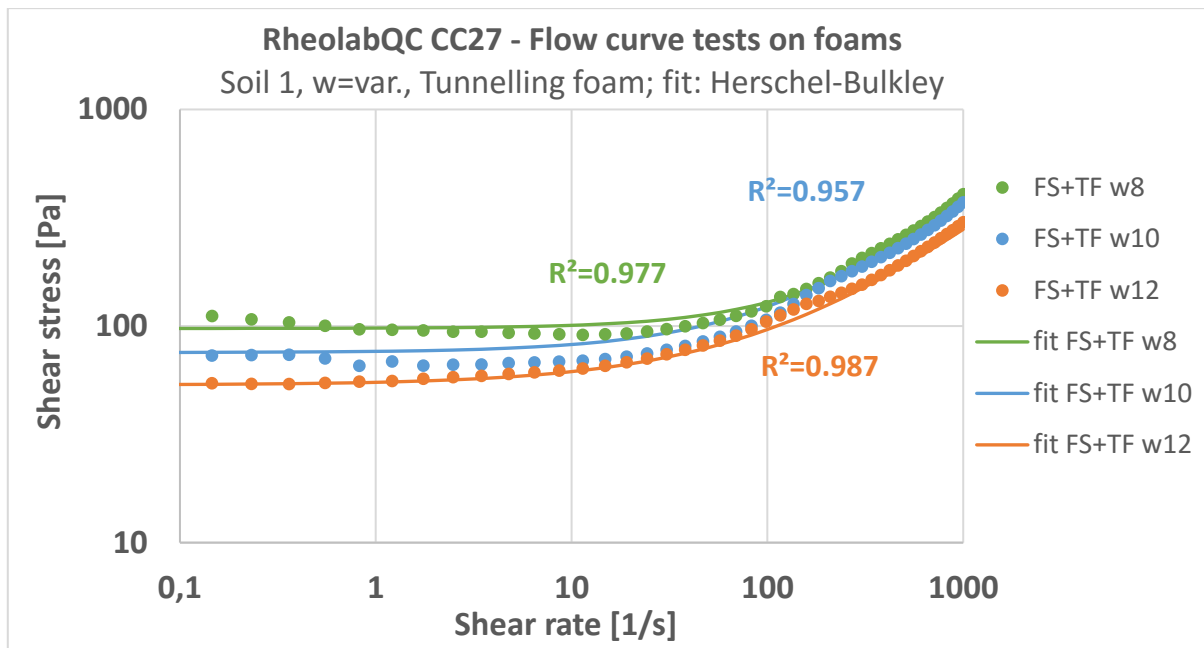
**Figure 7-24:** **Average flow curves from concentric cylinder rheometry on fine sand-foam mixtures and fitting with Herschel Bulkley model considering the water content w**

7.3.2   Ball measuring system

The ball measuring system (BMS) was developed for rheological investigations on suspensions consisting large particles. MÜLLER ET AL. (1999) applied the BMS to cementitious pastes like plasterings in order to perform flow curve tests on granular media. SCHATZMANN ET AL. (2009) investigated the flow behaviour of debris flow material. An investigation of this material in standard rheometers is not feasible. Therefore, they studied the application of the BMS to debris material in comparison to other large-scale rheometers. In the process of developing a suitable conversion theory of the system parameters into effective rheological parameters, MÜLLER ET AL. (1999) and SCHATZMANN ET AL. (2009) chose different approaches. In the following, the theoretical background shall be explained, before the application of the BMS to the own investigations is discussed.

7.3.2.1   Theoretical background

MÜLLER ET AL. (1999), TYRACH (2000) assessed the rheological parameters by a dimensional analysis of the flow occurring in the BMS by means of the Buckingham-Pi theorem (BUCKINGHAM (1914)). All essential system parameters are shown in Figure 7-25. Based on the sphere Reynolds number Re (Eq. 7.4) and a dimensionless drag
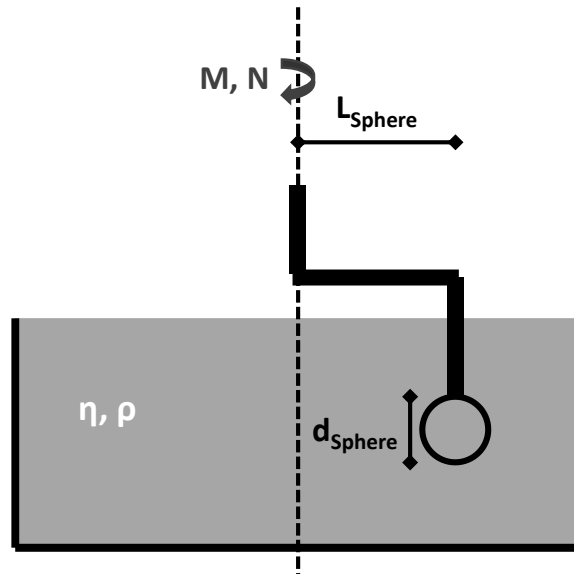
Figure 7-25: System sketch of the ball measuring system according to TYRACH (2000)

coefficient c_D (Eq. 7.5), which consider a projected area A_{sphere} [m²] of the sphere with diameter d_{Sphere} [m], they determined a system number C (Eq. 7.6).

$$Re = \frac{\rho \cdot v \cdot d_{Sphere}}{\eta} = \frac{\rho \cdot 2\pi \cdot L_{Sphere} \cdot N \cdot d_{Sphere}}{\eta} \qquad [-] \qquad Eq. \ 7.4$$

$$c_D = \frac{F_D}{\frac{1}{2} \cdot \rho \cdot v^2 \cdot A_{sphere}} = \frac{M/L_{Sphere}}{\frac{1}{2} \cdot (2\pi \cdot L_{Sphere} \cdot N)^2 \cdot \frac{\pi \cdot d_{Sphere}^2}{4} \cdot \rho} = \frac{2}{\pi^3 \cdot L_{Sphere}^3 \cdot d_{Sphere}^2 \cdot \rho} \cdot \frac{M}{N^2}$$

$$[-] \qquad Eq. \ 7.5$$

$$C = Re \cdot c_D = \frac{4}{\pi^2 \cdot L_{Sphere}^2 \cdot d_{Sphere} \cdot \eta} \cdot \frac{M}{N} \qquad [-] \qquad Eq. \ 7.6$$

The drag coefficient incorporates the force F_D [N], the fluid density ρ [kN/m³], the fluid viscosity η [Pa·s], the radius of the circular path (eccentricity of the sphere from the axis) L_{Sphere} [m], and the trajectory sphere velocity v [m/s] (or the turning speed N [1/s] respectively). For Newtonian fluids in creeping flow conditions (Re < 1), Stokes derived a solution for C equal to 24. Thus, the system-dependent torque (M_1) can be determined. TYRACH (2000) considers an additional torque due to self-rotation of the sphere (M_2) as proposed by BERKER (1963). Due to its diameter, the drag force acts on the sphere with a slight eccentricity from the circular path. Hence, it might be reasonable to take into account this share of the torque. However, BERKER (1963) considered this torque originally for a free falling sphere in a liquid. The total torque M affecting the sphere can be calculated by using (Eq. 7.7).

$$M = M_1 + M_2 = 6 \cdot \pi^2 \cdot d_{Sphere} \cdot L_{Sphere}^2 \cdot \eta \cdot N + 2 \cdot \pi^2 \cdot d_{Sphere}^3 \cdot \eta \cdot N$$

[-]   Eq. 7.7

Because of the additional torque, the system number C changes in its solution from 24 to Eq. 7.8.

$$C = 24 + 8 \cdot \frac{d_{Sphere}^2}{L_{Sphere}^2}$$

[-]   Eq. 7.8

For the conversion of raw data into rheological parameters, a linear relationship was assumed between torque and shear stress and between turning speed and shear rate. The conversion factors were determined from calibration tests on silicon oil with pre-defined viscosity and taking into account Eq. 7.6 and Eq. 3.3. In the calibration tests, deviations from the theoretically expected system number occurred. TYRACH (2000) explained this deviation with the influence of the sphere holder, which was neglected in the analytical approach. Overall, the approach was limited to laminar flow conditions (Re < 1.0).

SCHATZMANN (2005), SCHATZMANN ET AL. (2009) developed another approach for the same system because they wanted to involve flow conditions of higher Reynolds numbers (Re > 1) into the approach. Using the same measuring device, they approached the system number for the flow pattern around the sphere by the Metzner-Otto theory (see METZNER & OTTO (1957)). The research of METZNER & OTTO (1957) dealt with the agitation of fluids by mixing rods (propellers). That means, this assessment does not see the sphere as resistant body within a streaming fluid, but the sphere agitates the fluid. This behaviour is summarised in the Newton number Ne (Eq. 7.9) instead of the drag coefficient as before. Finally, again a system number (now C_1) was determined considering the product of the sphere Reynolds number (Eq. 7.4) and the Newton number similar to the approach of TYRACH (2000), see (Eq. 7.10).

$$Ne = \frac{P}{\rho \cdot d_{Sphere}^5 \cdot N^3} = \frac{2 \cdot \pi}{\rho \cdot d_{Sphere}^5} \cdot \frac{M}{N^2}$$

[-]   Eq. 7.9

where P is the stirring power [Nm/s].

$$C_1 = \text{Re} \cdot \text{Ne} = \frac{4 \cdot \pi^2 \cdot L_{\text{Sphere}}}{d_{\text{Sphere}}^4 \cdot \eta} \cdot \frac{M}{N} \qquad\qquad [-] \qquad \text{Eq. 7.10}$$

In calibration tests, using a Newtonian silicon oil, the system number C_1 was determined empirically. It was constant for $\text{Re} < 1.0$ as by TYRACH (2000), and for $\text{Re} > 1$, the system number occurred non-constant. SCHATZMANN (2005) described this range by a polynomial function.

In addition, the approach of SCHATZMANN (2005), SCHATZMANN ET AL. (2009) was intended to be valid also for non-Newtonian fluids. Therefore, the calibration had to be carried out on non-Newtonian fluids, too. This demanded a modification of Eq. 7.10. As mentioned in chapter 3.1.2, the viscosity of these types of fluids is usually not constant; it is shear rate-dependent. By replacing η with the Ostwald-de Waele viscosity (compare Eq. 3.5), a non-Newtonian relationship was established between the BMS turning speed and the rheological parameters k [Pa·s] (viscosity parameter) and p [-] (shape factor), see Eq. 7.11.

$$\dot{\gamma} = \left(\frac{4 \cdot \pi^2 \cdot L_{\text{Sphere}}}{C_1 \cdot d_{\text{Sphere}}^4 \cdot k} \cdot \frac{M}{N} \right)^{\frac{1}{p-1}} \qquad\qquad [-] \qquad \text{Eq. 7.11}$$

The calibration was achieved by determining effective rheological parameters (i.e. yield stress, viscosity, and shape parameter) in cone-plate and plate-plate rheometers and introducing them into the modified equation above. For this purpose, SCHATZMANN (2005) used a polymer solution as power-law fluid and suspensions of debris with different grain-sizes as yield stress fluids. However, in this way, the system number was a priori still not known because the Reynolds number was not identified for the effective shear rate. Hence, first, an estimation for an initial Reynolds number was necessary, which SCHATZMANN (2005) selected based on the work of ATAPATTU ET AL. (1995), followed by an iterative post-process until the Reynolds number either achieved a value smaller 1.0 (C_1 is constant there) or converged to a specific value, see SCHATZMANN (2005) for details. Additionally, for yield stress fluids, it was necessary to check, if yielding was induced. Therefore, a yield criterion was introduced verifying if the acting forces were sufficient to overcome the yield stress.

In this manner, fluid-dependent relationships were found between the measurements (torque, rotational speed) and the shear rate. Finally, a conversion

factor for the torque into shear stress had to be found from the calibration tests by data fitting. The conversion factors were determined dependent on both the fluid type and the Reynolds number.

The BMS available for the Anton Paar RheolabQC, which was used in this study, founds its conversion factors on the approach of SCHATZMANN (2005), SCHATZMANN ET AL. (2009). The standard setup factors CSR (shear rate) and CSS (shear stress) in the rheometer system are the ones for yield stress fluids. The default testing profile for the BMS incorporated in the operating software is defined according to the procedure used by MÜLLER ET AL. (1999), TYRACH (2000).

7.3.2.2   Setup and calibration

The rheometer used for the investigations was the same as described before. The ball measuring systems were similar to those used by MÜLLER ET AL. (1999), SCHATZMANN (2005), SCHATZMANN ET AL. (2009), TYRACH (2000). The BMS consisted of a sample cup with a volume of approximately 500 ml and of an eccentrically positioned ball with the following diameters: d_{BMS08} = 8, d_{BMS12} = 12, d_{BMS15} = 15 mm as rotor (Figure 7-26). The eccentricity depended on the system used: L_{BMS08} = 38 mm, L_{BMS12} = 37 mm, L_{BMS15} = 35 mm. The immersion depth could vary based on the altitude of the sample container, which the user could regulate manually. Here, the depth of immersion was selected to equal the middle height of the container. Temperature regulation was not possible.
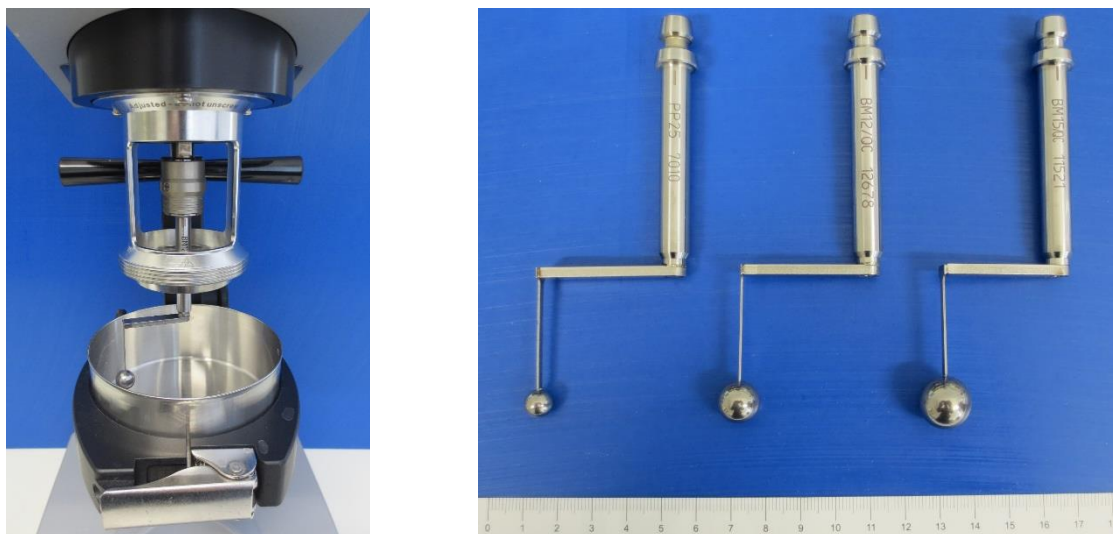
**Figure 7-26: Rheometer with ball measuring system (BMS); right: BMS with different ball-
sizes and eccentricities**

Calibration was performed with several different fluids (calibration oil, bentonite slurry, shaving foam; see chapter 4.3.4) based on concentric cylinder flow curve tests. The conversion factors for the calculation of shear rate and shear stress in the different BMS were determined for the different fluids based on the procedure of SCHATZMANN (2005), see above. Contrary to his investigations, the system number was not found to be constant for the calibration oil for Reynolds numbers smaller 0.1 (Figure 7-27) but within the range of 0.1 to 2.91 (BMS08) / 4.13 (BMS12) / 4.94 (BMS15).

In the same range, the relationships between shear stress and torque was constant, too, which again corresponds to the observations of SCHATZMANN (2005). Therefore, only this range was later referred to for analysing suitable fluid-dependent conversion factors. The detected conversion factors are summarised in Table 7-5. Partially significant deviations occurred compared to the factors of SCHATZMANN (2005). Moreover, the conversion factor CSS was almost the same for all fluids. Regarding the ease of application of the BMS in rheometrical studies, average CSS values were created and applied in the tests.
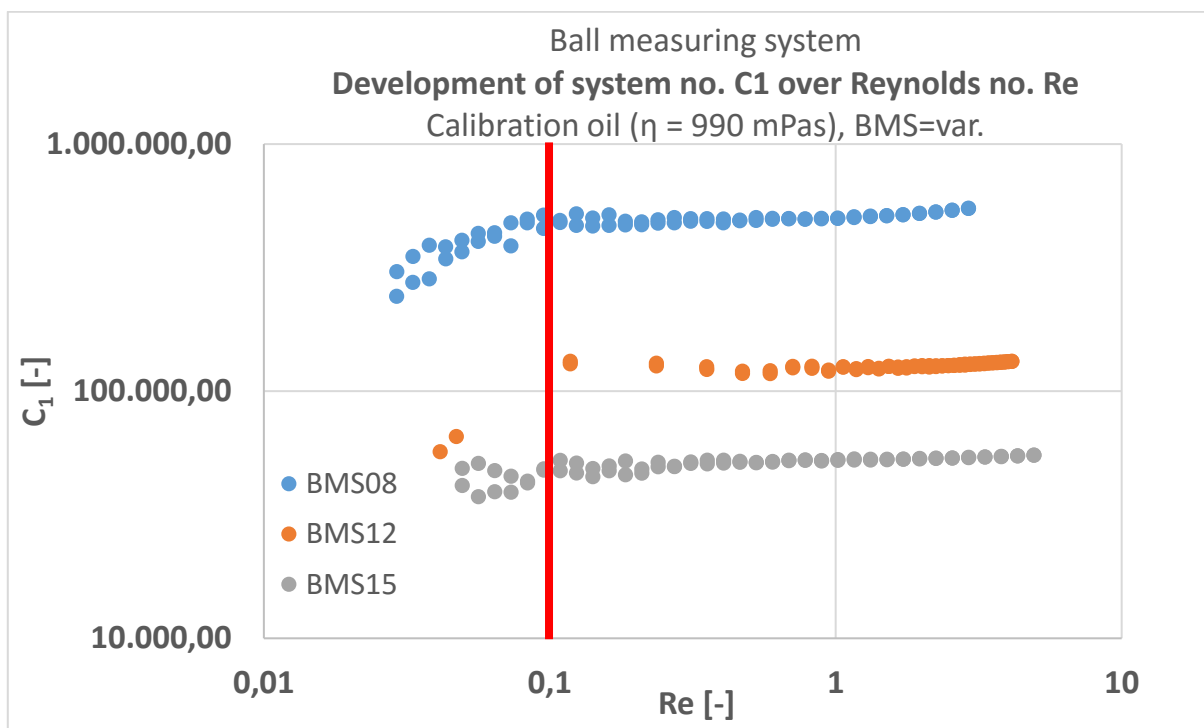
Figure 7-27: Relation of the system number C_1 and Re for the three different BMS for calibration oil; C_1 was detected constant for Re > 0.1 (red borderline)

Table 7-5:   Conversion factors determined in BMS calibration tests; *conversion factors according to SCHATZMANN (2005)

Fluid type		CSR [-]	CSR* [-]	CSS [-]	CSS* [-]
Newtonian fluid (calibration oil)	BMS08	28.7	25.6	16.4	18.5
	BMS12	18.1	25.6	9.3	14.9
	BMS15	13.8	22.8	6.9	12.6
Power-law fluid (shaving foam)	BMS08	28.7	25.6	16.4	18.5
	BMS12	18.1	25.6	9.3	14.9
	BMS15	13.8	22.8	6.9	12.6
Yield-stress fluid (bentonite slurry)	BMS08	28.7	25.6	16.4	22.8
	BMS12	18.1	25.6	9.3	15.0
	BMS15	13.8	22.8	6.9	10.7

7.3.2.3   Testing procedure and experimental programme

The operating software of the rheometer provides a default testing routine, which is based on the works of SCHATZMANN (2005), TYRACH (2000). The shear rate is logarithmically increased over three decades of shear rate within one revolution (345°). For instance, for the BMS08, the shear rate range is from 0.1 to 100 1/s. This routine was revised for the present study. Firstly, the testing profile should allow several rounds to turn and secondly, the region, where the ball was immersed, should be spaciously excluded from data sampling. The material structure is disturbed by the sphere immersion. Hence, the measuring profile had to be adjusted in such a way, that the ball finishes one complete revolution (360°) avoiding measurements in a certain range close to the point of immersion (Figure 7-28). This zone was defined to one diameter before and after. The repeated turning through the material, should provide information on the development of the flow curve from unsheared to sheared material conditions. The total measurement consists of six revolutions,
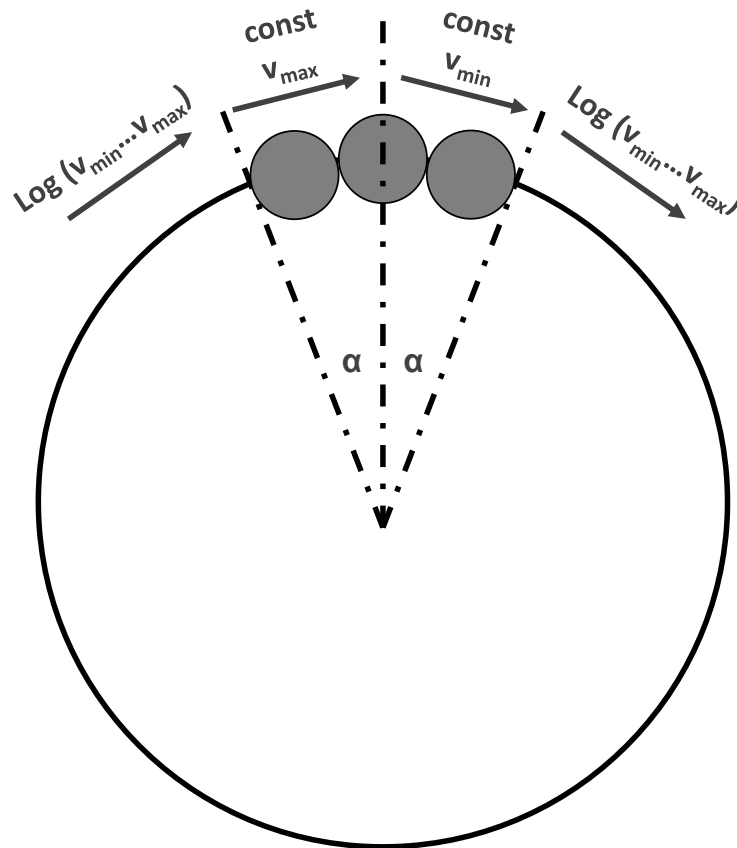
Figure 7-28: Scheme of the adjusted testing profile for BMS-measurements

whereof the first round (unsheared condition) is compared to a representative average flow curve of rounds 2 - 6 (sheared conditions). The relevant information on the final operation procedures for the different BMS (BMS08, BMS12, BMS15) are summarised in Table 7-6 to Table 7-8.

The testing programme was the same as for the slump tests presented in chapters 6.2 (Figure 6-6). All mixtures were investigated with the three ball systems. The sample preparation was as proposed in chapter 4.3.3. Once the soil-foam mixture was generated, the material was filled into the sample cup. The cup was then placed on a Haegermann table and impacted by 15 hits for compaction purposes. After that, the surface was cut straight with the aid of a ruler and the sample was positioned in the rheometer. The ball was immersed into the sample 60 seconds before start of testing (Step no. 4 in Table 4-2). Details on the test setup and a precise description of the testing procedure can be found in chapter A.4.1.

Table 7-6: Relevant information on the adjusted BMS08 testing profile

	Section 1	Section 2 (measuring range)	Section 3
No. of data points	4	31	1
Speed [1/min]	N_{min} = 0.0678 (const.)	N = 0.0678 ... 67.8 (log. ramp)	N_{max} = 67.8 (const.)
Sampling time [s]	11.52 (const.)	4...0.78 (log.)	0.046 (const.)

Table 7-7: Relevant information on the adjusted BMS12 testing profile

	Section 1	Section 2 (measuring range)	Section 3
No. of data points	4	31	1
Speed [1/min]	N_{min} = 0.0647 (const.)	N = 0.0647 ... 64.7 (log. ramp)	N_{max} = 64.7 (const.)
Sampling time [s]	19.32 (const.)	4...0.78 (log.)	0.077 (const.)

Table 7-8: Relevant information on the adjusted BMS15 testing profile

	Section 1	Section 2 (measuring range)	Section 3
No. of data points	4	31	1
Speed [1/min]	N_{min} = 0.061 (const.)	N = 0.061 ... 61.0 (log. ramp)	N_{max} = 61.0 (const.)
Sampling time [s]	25.61 (const.)	4...0.78 (log.)	0.102 (const.)

7.3.2.4   *Test results and analysis*

▪ **Soil-foam mixtures**

Reconsidering the experiences from the pre-studies and the concentric cylinder investigations, either methods were not suitable to test EPB-relevant soil-foam mixtures or conversion of raw data into rheological parameters was difficult. With respect to the resulting torques, all soil-foam mixtures could be investigated with the ball measuring system, except for a rather small number of samples. The mixtures, which could not be tested in the rheometer, were of minor interest to the study, since they exhibited slumps outside the range of suitable workability (slump < 10 cm). Considering the conversion approaches of TYRACH (2000) and SCHATZMANN (2005) for the BMS data, the BMS setup apparently meets the requirements for testing and analysing the rheology of EPB-related soil-foam mixtures.

The material in the excavation chamber of an EPB shield is continuously impacted and agitated by the construction elements of the machine such as the cutting wheel, the cutting tools, mixing elements (stators, rotors) or the screw conveyor. This material state is represented by the average flow curve from the measurements of rounds 2 - 6, which is compared to the flow curve resulting from the first ball revolution representing the material condition at rest. In Figure 7-29, the course of shear rate is exemplarily shown for a soil-foam mixture consisting of soil 2 with a water content w = 6% and a foam injection ratio FIR = 20% for all six rounds. Clearly, the resulting shear stress was the highest for round number one. After that, the shear stress response was less. Then, the differences between the single rounds (2 - 6) were much smaller. This pattern can be explained with the material flow after the passage of the sphere. The sphere path was not completely filled anymore once the measuring system passed. Hence, in the next round, the ball actually struck a disturbed material zone.

For mixtures consisting of higher contents of water and foam, the discrepancy between round number 1 and the other rounds became comparatively less significant, compare Figure 7-30. For further analysis, only the average flow curves of rounds 2 - 6 will be considered because the corresponding material condition is closer to the physical state in the EPB excavation chamber. The spread of data will be represented by the standard deviation.
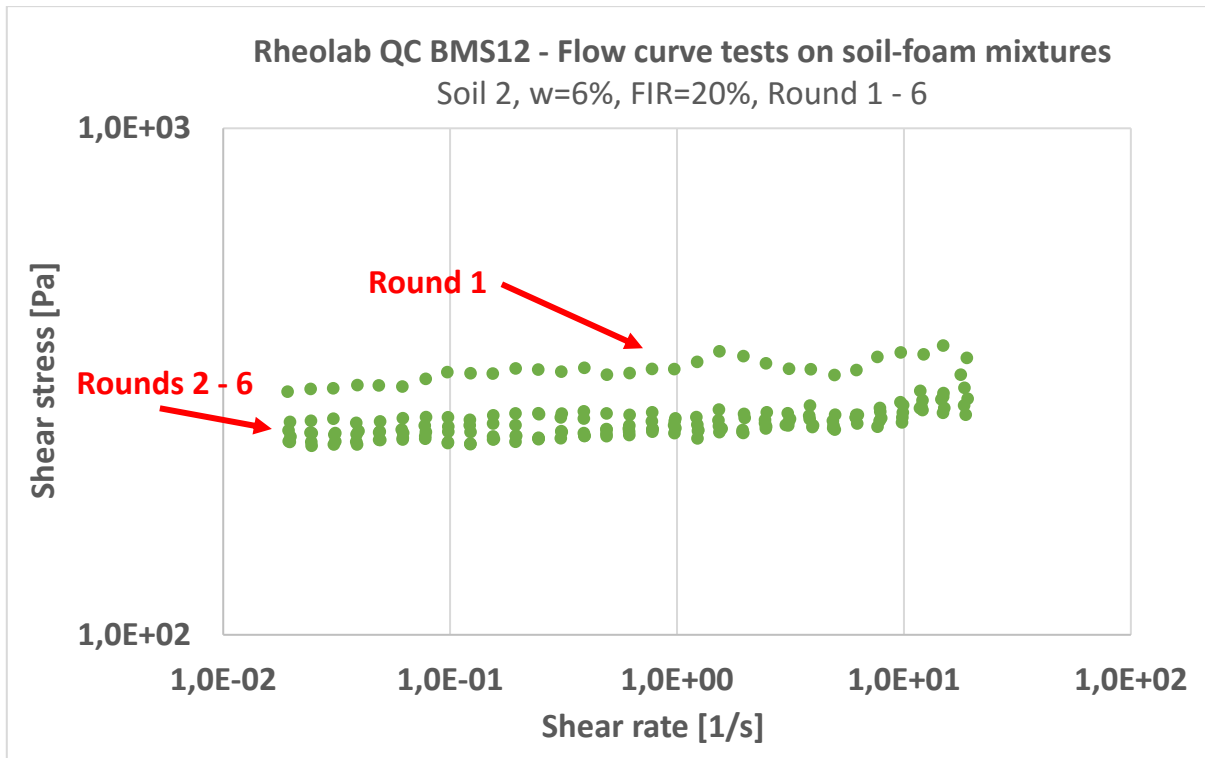
Figure 7-29: Flow curve data of a sand-foam mixture with w = 6% and FIR = 20% in the BMS 12: difference in shear stress magnitude between round 1 and rounds 2 - 6
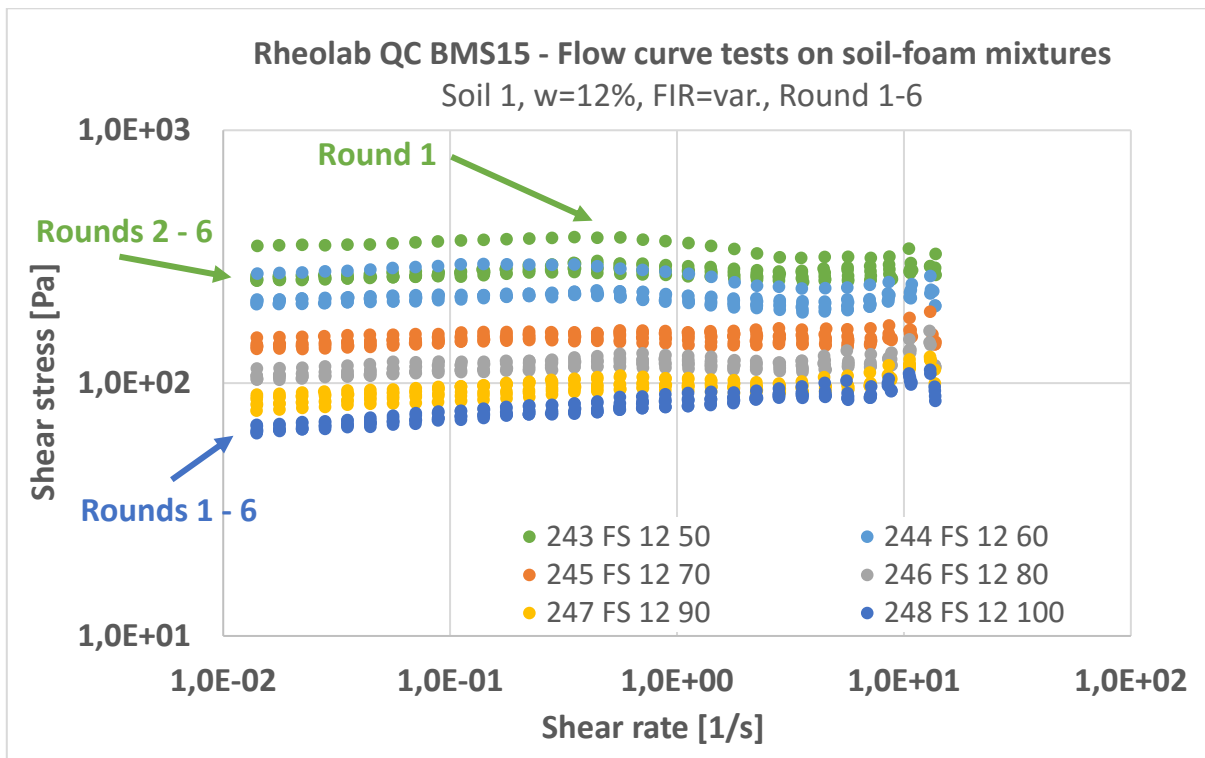
Figure 7-30: Flow curve data of fine sand-foam mixtures with w = 12% and increasing FIR (50% - 100%) in the BMS 15: difference in shear stress magnitude between single ball revolutions

Results are exemplarily shown for soil 1 and BMS 12 in Figure 7-31 to Figure 7-36. Data of all other experiments can be found in the appendix in chapter A.4.3.1. Qualitatively, the course of data was the same for all samples. The increase in shear stress was very small at low shear rates. Only at high shear rates, the increase was a little more significant. Water content and foam injection ratio had a major influence on the magnitude in shear stress. Analysis of the flow behaviour was conducted based on the findings from the concentric cylinders system with both the Herschel-Bulkley model and the Bingham model. Of course, data fitting was improved using the Herschel-Bulkley model compared to the Bingham model because the number of regression variables is larger. However, analysis of the main regression parameters τ_0 and k was enhanced with respect to rheology. Thus, the Herschel-Bulkley model described the data mathematically more suitably while the Bingham model enhanced physical interpretation (plausibility) of the data. For detailed analysis of the results, the Bingham model was chosen again for an evaluation of the viscosity and the yield stress depending on the characteristic material parameters w and FIR. Similar assumptions for the flow behaviour of soil-foam mixtures were made by MENG ET AL. (2011), VENNEKÖTTER (2012).
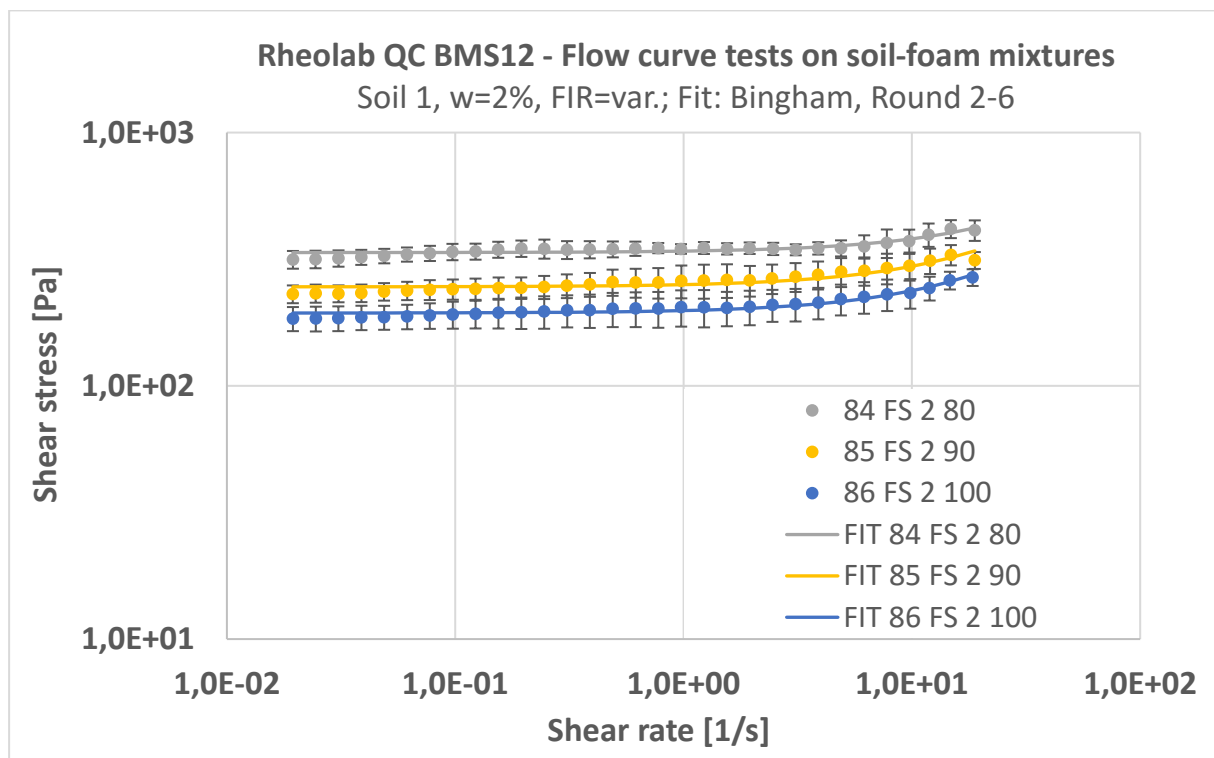
Figure 7-31: Average flow curve data of fine sand-foam mixtures with water content w = 2% and increasing foam content (BMS12, rounds 2 - 6); curve fitting with Bingham model
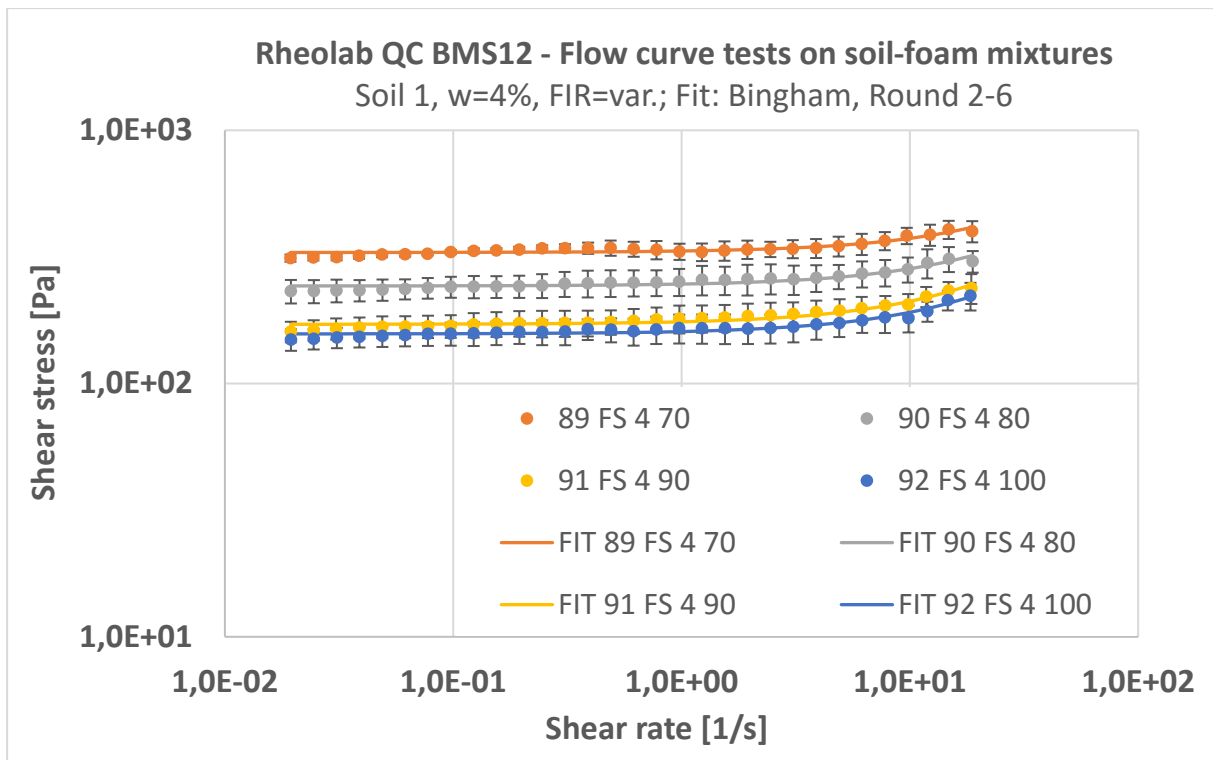
Figure 7-32: Average flow curve data of fine sand-foam mixtures with water content w = 4% and increasing foam content (BMS12, rounds 2 - 6); curve fitting with Bingham model
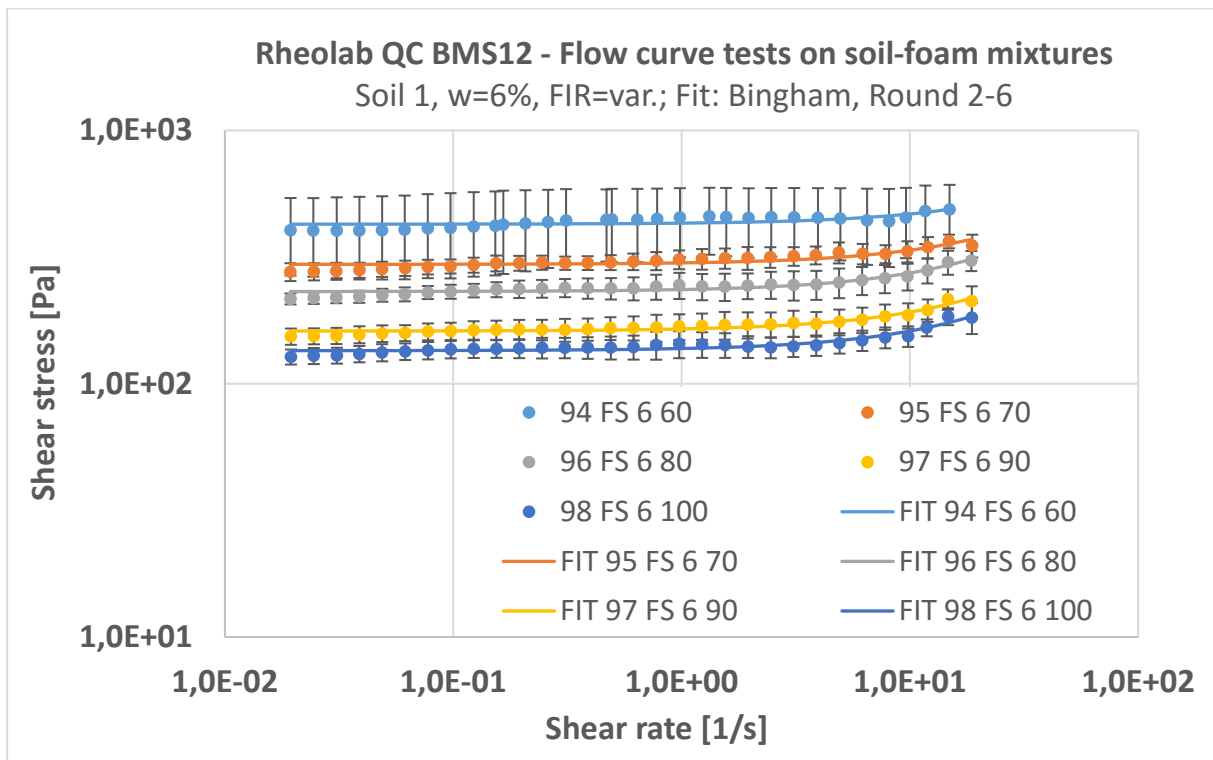
Figure 7-33: Average flow curve data of fine sand-foam mixtures with water content w = 6% and increasing foam content (BMS12, rounds 2 - 6); curve fitting with Bingham model
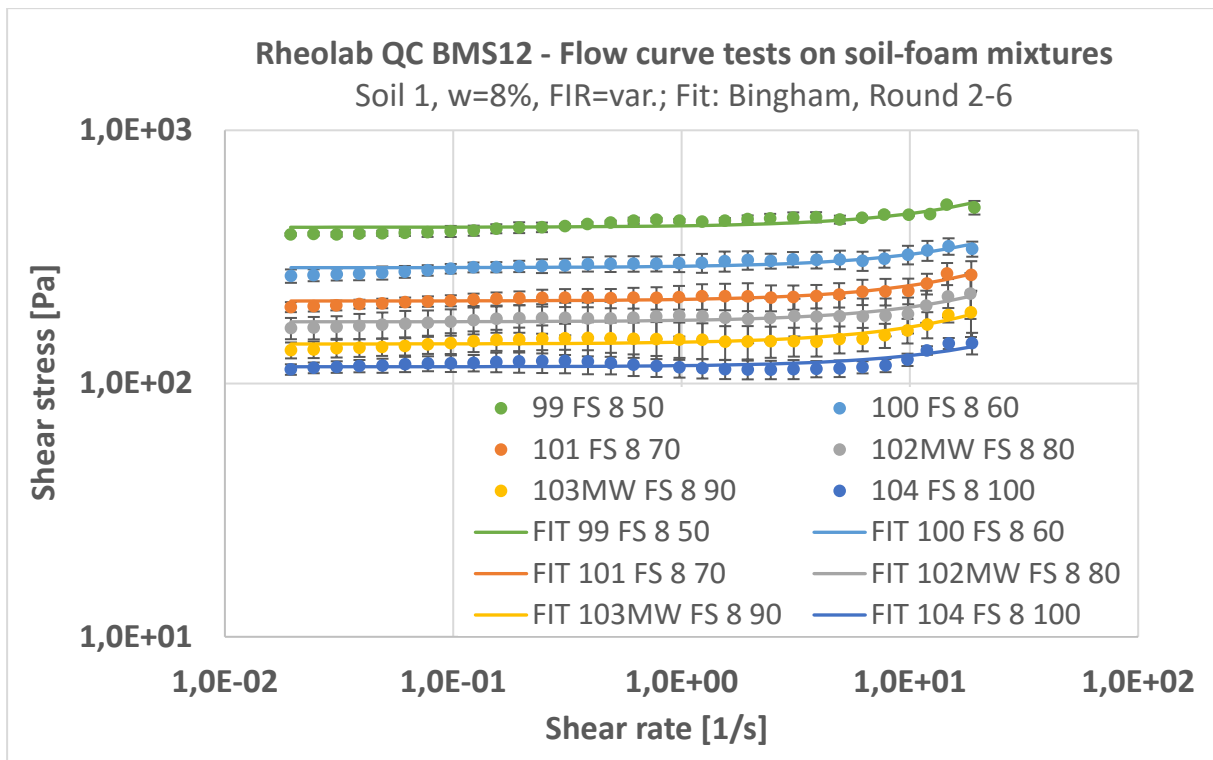
Figure 7-34: Average flow curve data of fine sand-foam mixtures with water content w = 8% and increasing foam content (BMS12, rounds 2 - 6); curve fitting with Bingham model
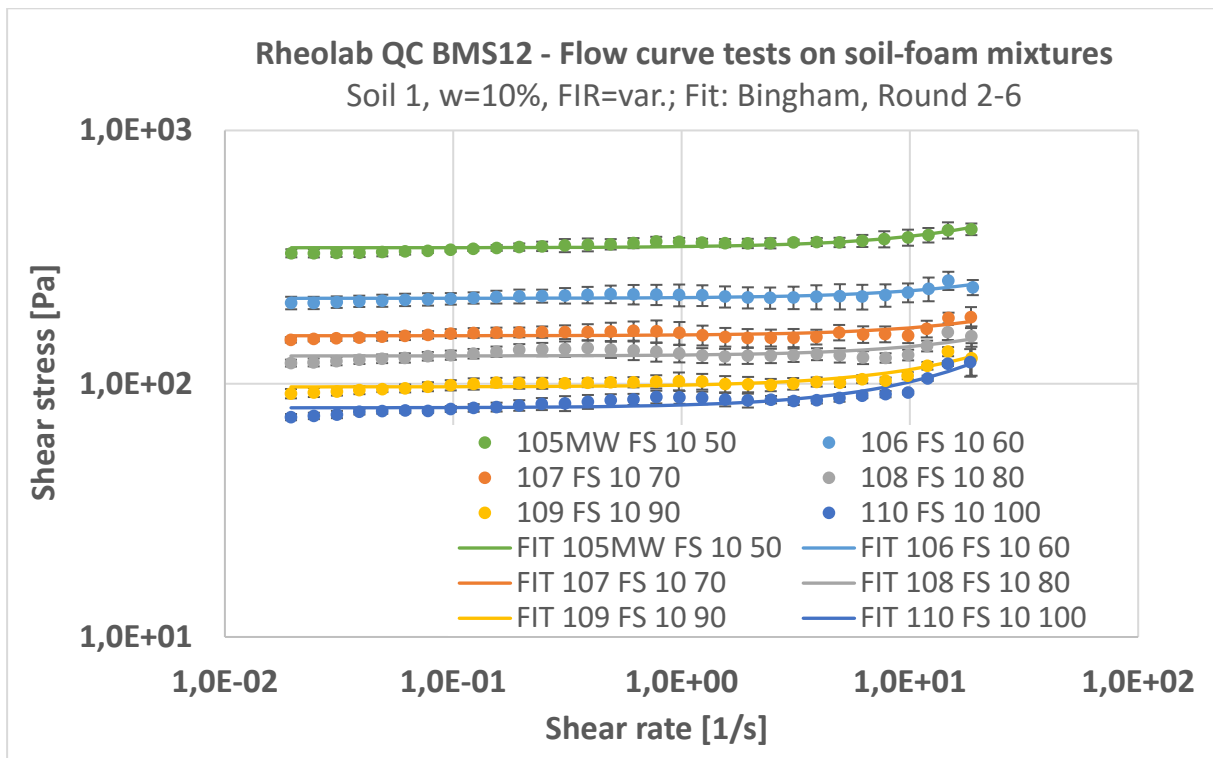
Figure 7-35: Average flow curve data of fine sand-foam mixtures with water content w = 10% and increasing foam content (BMS12, rounds 2 - 6); curve fitting with Bingham model
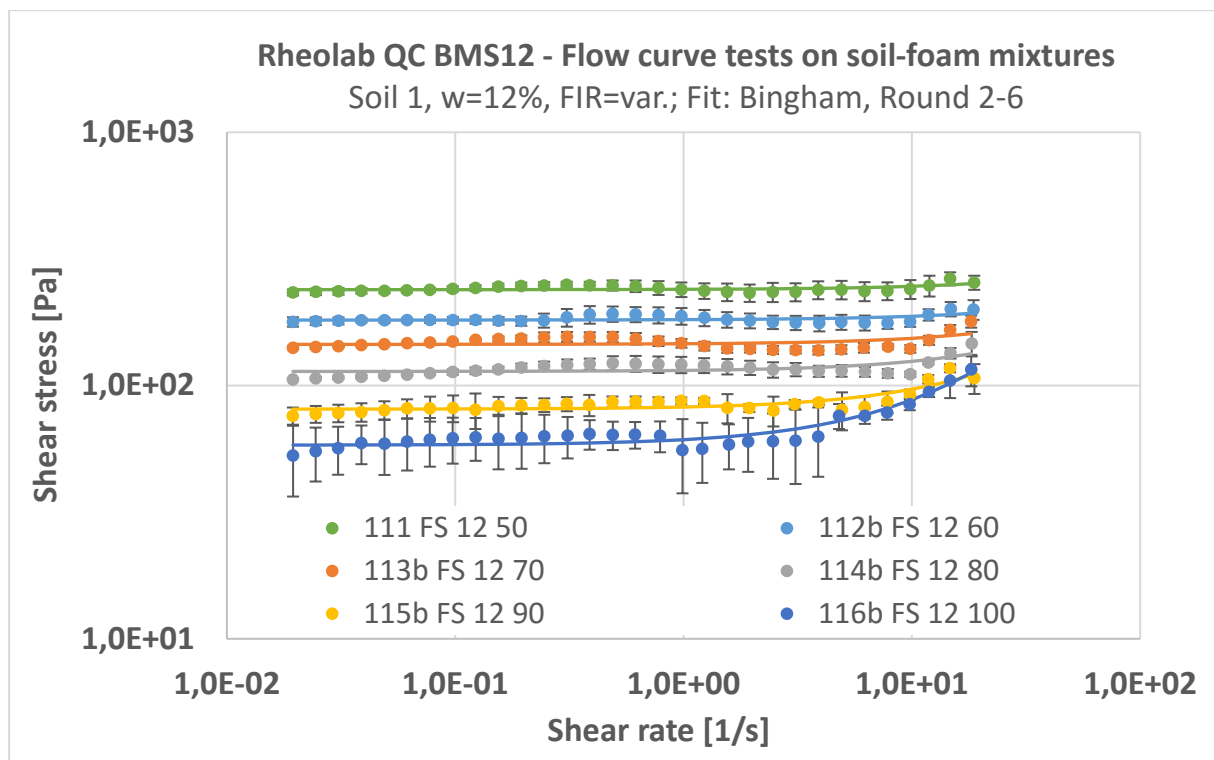
Figure 7-36: **Average flow curve data of fine sand-foam mixtures with water content w = 12% and increasing foam content (BMS12, rounds 2 - 6); curve fitting with Bingham model**

The flow curves of the soil-foam mixtures in almost any test were rather flat. The increase in shear stress compared to the yield stress was small. This would imply that the shear stress is independent of the shear rate. Most probably, this effect has to do with the actual flow behaviour in the BMS.

Comparing soil-foam mixtures to other materials such as mortar or high-density slurries, the viscosity of soil-foam mixtures was expected high. An examination of the viscosity parameter k from the regression analysis showed however remarkably small values for k (0-10 Pas). An example for soil 1 is shown in Figure 7-37. Due to the small values for k, a significant trend in dependence of the water content or the foam injection ratio cannot be established. Such small values are significantly affected by the fitting quality of the flow curve data.

The drag force exerted on the sphere consists of two parts: form drag and viscous drag. In the case of a sphere passing through a Newtonian fluid, the proportion of the two shares equals approximately 2:1, cf. CHHABRA & RICHARDSON (2008). With increasing degree of shear-thickening behaviour, this ratio usually further increases and with increasing degree of pseudoplasticity, the ratio reduces. A significant factor
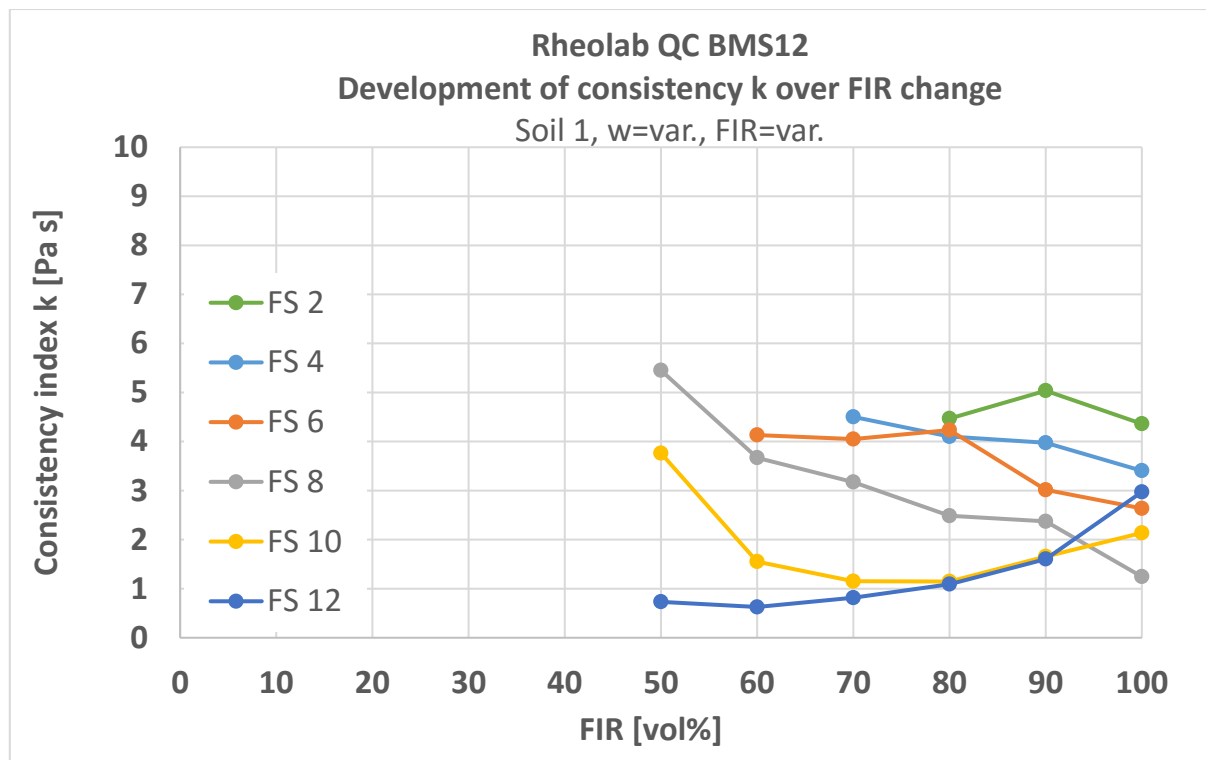
Figure 7-37: Development of Bingham viscosity parameter k from BMS flow curve tests on soil-foam mixtures containing soil 1 and different amounts of water and foam

of influence on the viscous share is wall slip. In order to capture the slip condition on the sphere surface realistically, the boundary layer between the solid surface and the material needs to be described accurately on a micro-scale. Here, the general qualitative course of the material response shall be investigated with regard to the expected behaviour identified in former researches on similar materials. The stress-strain behaviour shown in Figure 7-38 is very characteristic for solid cellular structures. It consists of three regimes: a linear elastic regime, a plastic plateau and a zone, where densification effects become larger due to cell destruction and restructuration of the foam morphology, see GIBSON & ASHBY (1997). While an elastic (or unyielded) response was not determined in the present experiments, the plateau regime was present in the flow curves very dominantly. The region of densification was not determined very vastly. Therefore, shear rates might have been too low. However, densification effects were observed by the differences in stresses from one revolution to the next. Hence, a compressive destruction mechanism was actually determined in the experiments instead of an ideal shear flow around the sphere. Nonetheless, the tests are analysed based on the Bingham approximation (or linearity) referring to the yield stress parameter ("BMS yield stress") as reference
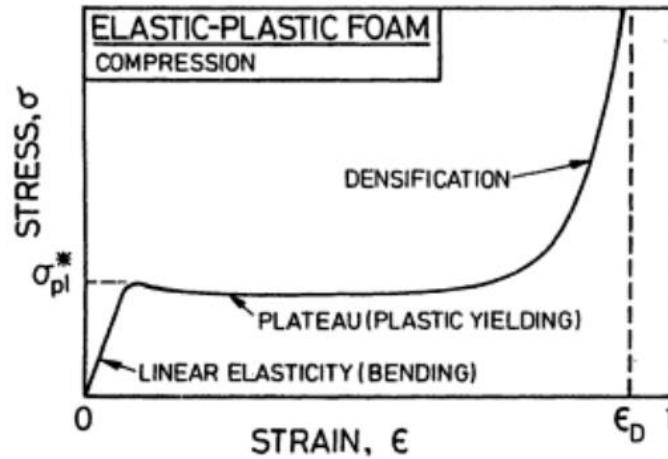
Figure 7-38: Schematic compressive stress-strain curves for elastic-plastic foams showing the three characteristic regimes: linear elasticity, plastic yielding and densification (GIBSON & ASHBY (1997))

value for the soil-foam rheology. Therefore, a prognosis model is developed for the yield stress but a family function of the flow whole flow curve is not determined.

Figure 7-39 shows the development of BMS yield stress of the BMS12 data in dependence of water content and FIR for soil 1. The yield stress reduces for both increasing w and increasing FIR. Multivariate data analysis alike the procedure in chapter 6.3.1 reveals a second-order polynomial function for the yield stress (Eq. 7.12) incorporating the two characteristic parameters for water and foam. The same applies for soil 2 (Figure 7-40, Eq. 7.13) and the other ball systems (BMS08, BMS15; cf. appendix chapter A.4.3.2).

$$\tau_{0,FS,BMS12} = 1732.975 - 68.934 \cdot w - 24.798 \cdot FIR$$

$$+0.578 \cdot w \cdot FIR + 0.095 \cdot FIR^2 \qquad [Pa]$$

$$R^2 = 0.957 \qquad Eq.\ 7.12$$

$$\tau_{0,S,BMS12} = 699.385 - 40.012 \cdot w - 16.114 \cdot FIR$$

$$+0.339 \cdot w \cdot FIR + 0.851 \cdot w^2 + 0.121 \cdot FIR^2 \qquad [Pa]$$

$$R^2 = 0.965 \qquad Eq.\ 7.13$$
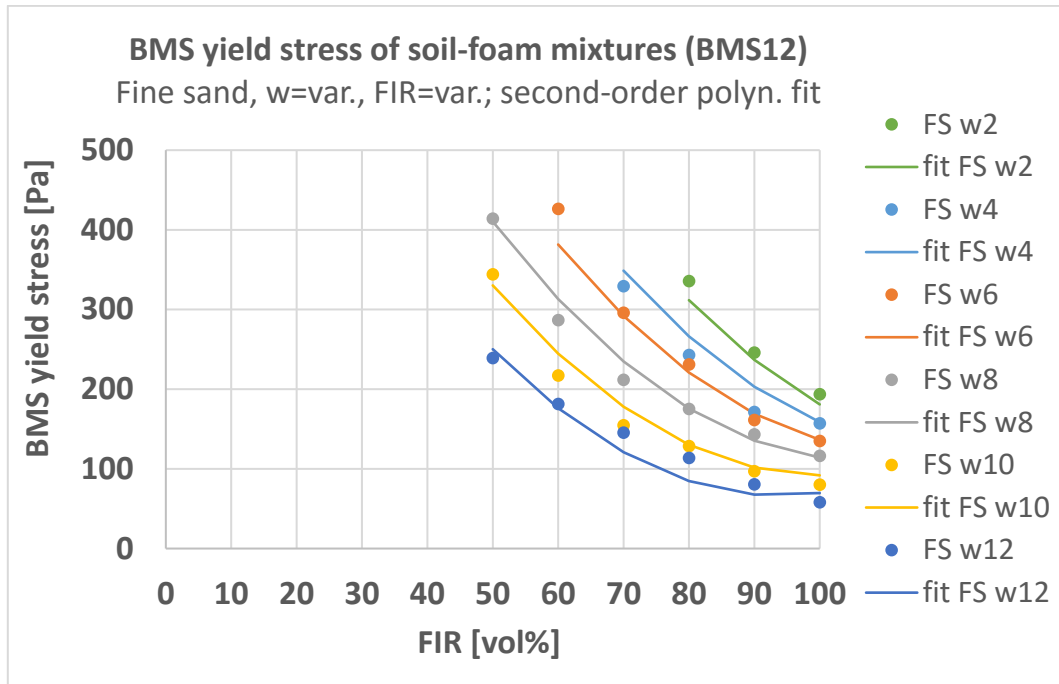
Figure 7-39: Development of "BMS yield stresses" (Bingham) from flow curve tests on fine sand-foam mixtures; data fitting with second-order polynomial function
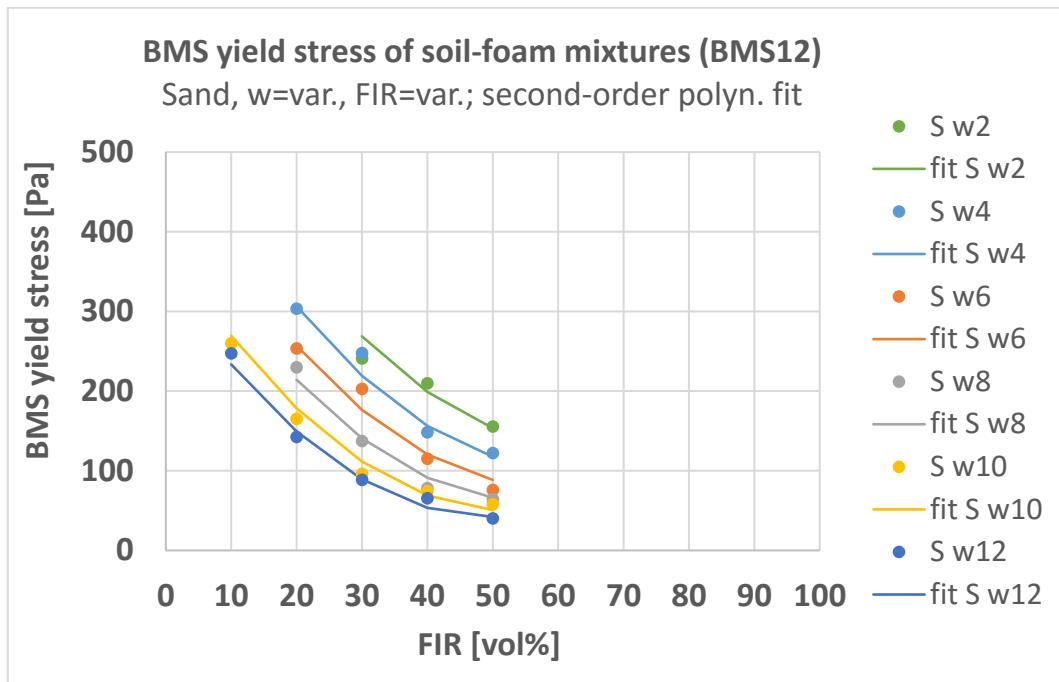
Figure 7-40: Development of "BMS yield stresses" (Bingham) from flow curve tests on sand-foam mixtures; data fitting with second-order polynomial function

Besides the water content and the foam injection ratio, the soil itself has an influence on the rheology, too, of course. As explained along with the analysis of the slump tests (chapter 6), the number of soils investigated in the present study was too small in order to incorporate a characteristic parameter of the soil. Nonetheless, a superordinate comparison of different conditioned soils can take place when considering the densities. The density in the sample container is a good reference value presupposing the same procedural impacts on the sample. This value incorporates influences from water and foam but also from soil. Figure 7-41 shows the yield stresses of fine sand-foam mixtures with different water and foam contents. With increasing material density, the ball yield stress increases, too. This behaviour can roughly be approximated by a linear trend, which applies for all ball systems. For sand-foam mixtures, the basic tendency is the same but the data scatter is higher.
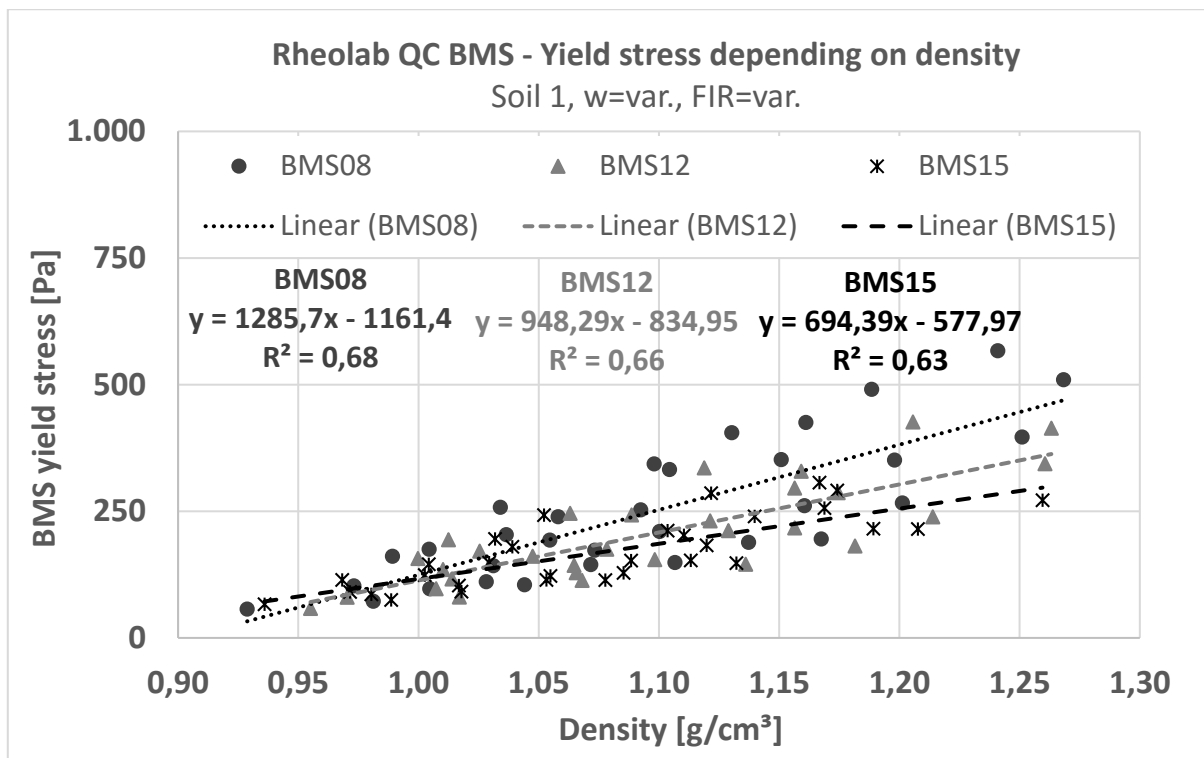
Figure 7-41: **Development of BMS yield stresses with increasing material density**

▪ **Foam**

The pure tunnelling foam had been investigated in the different BMS, too. The average results of three measurements with each BMS are shown in Figure 7-42. The results of all three BMS are almost congruent with each other. The course in shear stress over shear rate is steadily increasing and is largely similar to the behaviour determined with the concentric cylinder measuring system. The flow behaviour

appears mainly shear thinning. At shear rates of approximately 10 1/s, the data of the BMS12 and 15 suddenly increases. This effect again could denote the destruction behaviour of foams, see Figure 7-38. In the cup and bob configuration, this effect was not determined.

Curve fitting was conducted with the Herschel-Bulkley model in order to capture this increase in shear stress realistically. Due to its domination, the resulting formulas appear with a form factor p describing a shear-thickening flow behaviour (p > 1), see Table 7-9. Exclusion of the few outliers significantly increases the quality of fit and clearly turns the characteristic into a shear-thinning behaviour (Table 7-10). The magnitude in yield stress is comparable to the cylinder results, cf. Eq. 7.1. The consistency index and the shape factor deviate slightly but not meaningfully.
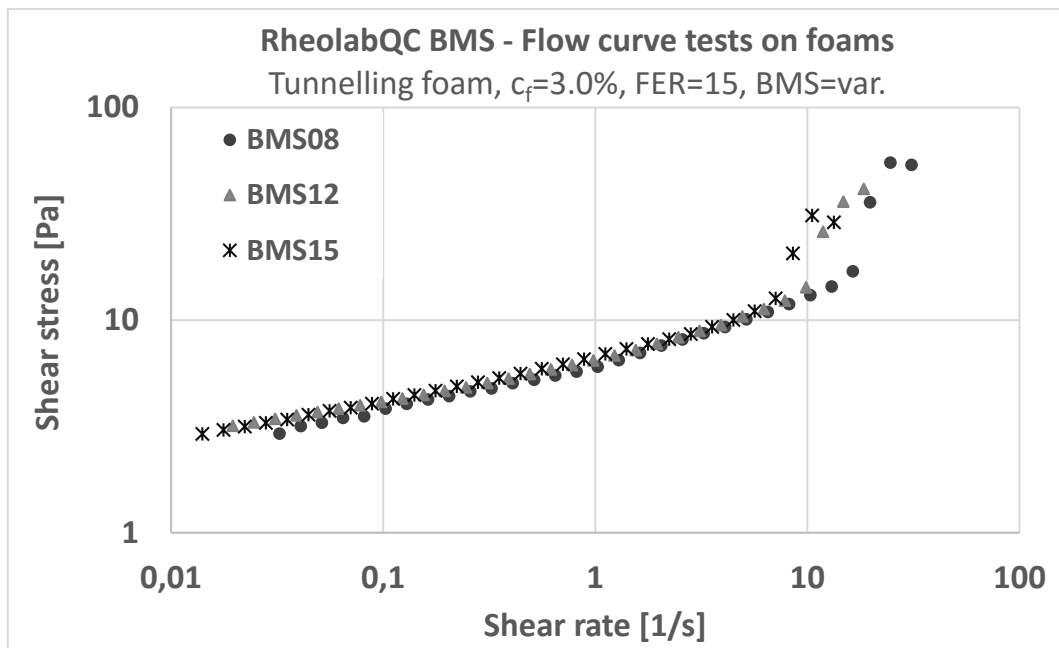
Figure 7-42: BMS flow curves of tunnelling foams with different BMS; data fitting with Herschel-Bulkley model

Table 7-9:   Rheological parameters from curve fitting of BMS flow curve data of tunnelling foam

BMS	τ_0	k	p	R^2
BMS 08	4.76	0.31	1.51	0.938
BMS 12	4.77	0.45	1.57	0.983
BMS 15	4.27	1.13	1.23	0.972

Table 7-10:   Rheological parameters from curve fitting of BMS flow curve data of tunnelling foam excluding suddenly increasing shear stresses at higher shear rates from the analysis

BMS	τ_0	k	p	R^2
BMS 08	2.77	3.25	0.51	0.9997
BMS 12	2.93	3.51	0.49	0.9997
BMS 15	2.35	4.36	0.40	0.9993

7.3.2.5   Evaluation of the different BMS

All BMS tests have been performed using three sphere sizes. So far, the intention of the different dimensions was not discussed. Figure 7-43 and Figure 7-44 show flow curves of the same soil-foam mixtures from all three BMS. One mixture consists of soil 1 (fine sand; Figure 7-43) and the other of soil 2 (sand; Figure 7-44). For soil 1, the flow curves of all BMS are very close. For soil 2, the level in shear stress decreases
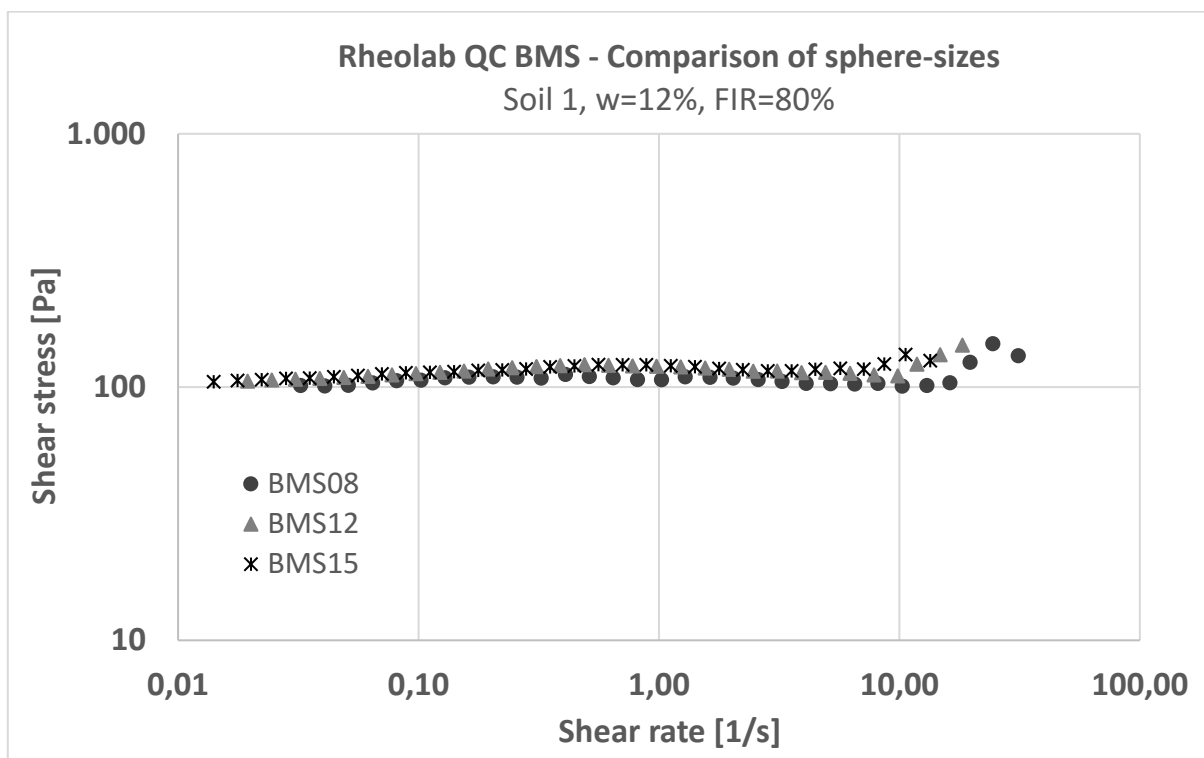
Figure 7-43:   Flow curves of soil-foam mixtures consisting of soil 1 (fine sand; d_{max} = 0.25 mm) with w=12% and FIR=80% determined with different BMS (d_{BMS} = 8, 12, 15 mm)
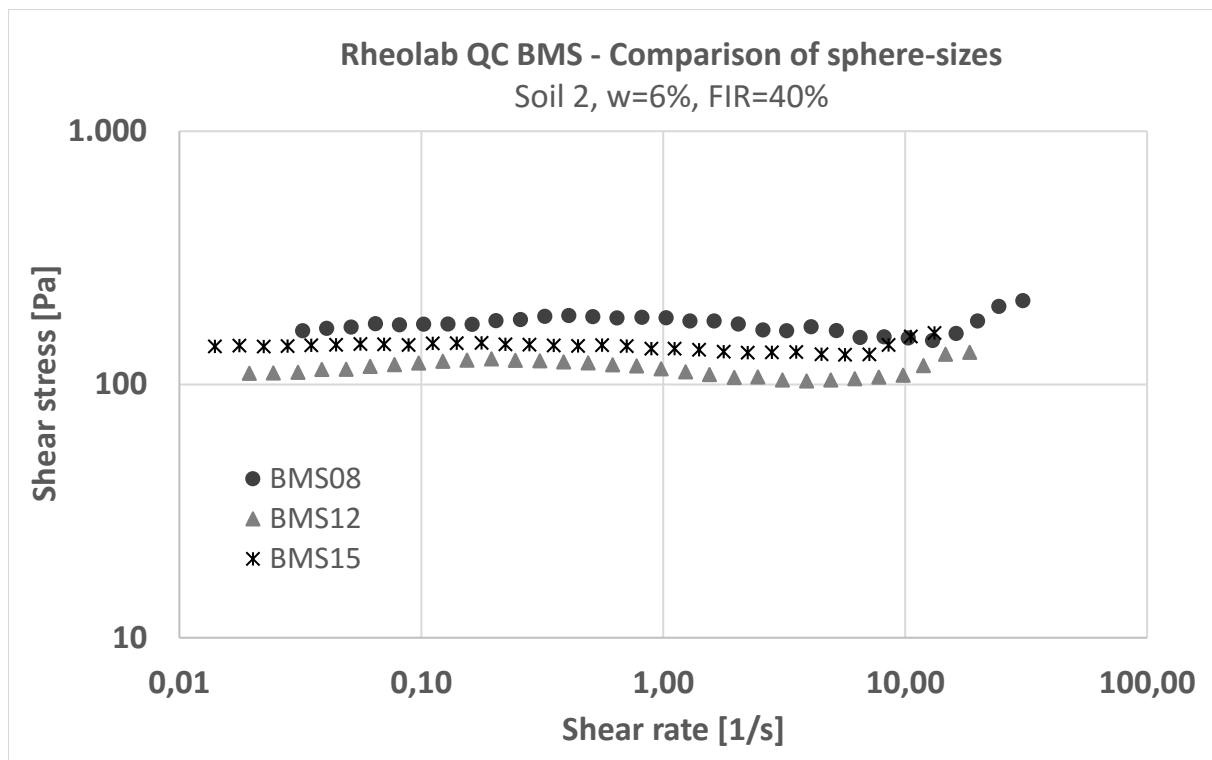
Figure 7-44: Flow curves of soil-foam mixtures consisting of soil 2 (sand; d_{max} = 2.0 mm) with w=6% and FIR=40% determined with different BMS (d_{BMS} = 8, 12, 15 mm)

with increasing sphere-size. These appearances are exemplary for a large number of the results. The cause for these phenomena is the interaction of particle-size and sphere diameter. Large particles exert a higher impact on the spheres than small particles. The larger the sphere, the less it is affected by the same particle size. Therefore, the shear rates of the BMS15 are lower than of the BMS08 or the BMS12. SCHATZMANN (2005) drew similar conclusions from his observations. Additionally, the influence of the sphere holder on the results reduces with increasing sphere diameter. However, the drag force is smaller on smaller spheres because both the projected sphere area transversely to the stream and the sphere surface are smaller. This increases the accuracy of the theory behind the BMS model (e.g. reduced slip surface).

According to FLEISCHMANN (2014), the maximum particle-size should be limited to 1/5 to 1/10 of the sphere diameter (reference value 1/8, see FLEISCHMANN (2013)) in order to reduce the impact from the large particles on the shear stress. In the present study, the maximum grain-size is 0.25 mm for soil 1 and 2 mm for soil 2. Hence, the relation of the particle diameter to the sphere diameter is insignificant for soil 1

(BMS08: 1/32, BMS12: 1/48, BMS15: 1/60), but it is not negligible for soil 2 (BMS08: 1/4, BMS12: 1/6, BMS15: 1/7.5). Thus, the deviations in results for soil 2 can be explained. The recommended particle-sphere diameter ratio can be approved and should be considered when designing experiments using BMS rheometers.

7.4   Transferability of findings through the scales

Testing of soil-foam mixtures in several rheological devices considering different sample volumes, measuring systems, types of foams and particles, boundary conditions, and testing profiles showed that the rheological behaviour reacts very sensitively to all these influencing parameters.

In micro-scale investigations on synthetic EPB material using plate-plate configurations, flow curve tests could be conducted very precisely and reproducible flow curves of the Herschel-Bulkley-Papanastasiou type were determined. A dependency was found between the material volume fractions and the model parameters. A treatment of the plate surfaces changed the stress response significantly.

Coaxial cylinder systems were found not suitable for a rheological investigation of realistic EPB material. Slip effects and the geometric limitations in grain-size made a reliable analysis of the results difficult. Soil-foam mixtures containing realistic tunnelling foam contents were determined to exert high torques onto the rheometric device, which confined the experiments, too. Flow curves of fine sands with high contents of foam (FIR) could be described by the Herschel-Bulkley model. Furthermore, a mathematical formulation was found for both investigated soils by linear regression linking the material parameter w to the model parameters τ_0, k and p. Due to the small sample volumes, a valid dependency could only be shown for the yield stress τ_0 and the water content.

Experience from literature on similarly coarse materials issued the possibility for a trustworthy application of the ball measuring system to soil-foam mixtures of interest with respect to EPB tunnelling. The material response to flow curve tests was similar to the compressive material behaviour of foams as known from literature. The flow curve data showed discontinuities resulting from side effects contradicting the basic assumptions made in the flow field definition. Therefore, the BMS test was evaluated

as index test referring to the ball yield stress as reference value, which was derived from a fitting model of the Bingham type. Influences from foam and water contents on the reference parameter were elaborated.

The findings from the multiple experiments show that the interpretation of the flow behaviour of foams and soil-foam mixtures depends on the very particular scale of observation. Homogeneous small-scale experiments provide an accurate and sensitive analysis capturing also small deviations in the flow pattern precisely. The Herschel-Bulkley-Papanastasiou model possesses a high quality for modelling the small-scale flow curve tests. Realistic soil-foam mixtures however demand for robust test equipment and make simplifications in the analysis necessary. Therefore, a model with less quality (i.e. less degrees of freedom) is advantageous in order to prevent over-interpretation of results maintaining plausibility.

A comparison of magnitudes of rheological parameters (yield stress, viscosity) between the rheological setups is difficult because the materials that were investigated in the devices differ substantially from each other. Therefore, flow curve experiments on one material on all scales should support the findings mentioned before and enable a "trans-scale comparison". Hence, experiments have been performed on synthetic particle-foam mixtures composed of shaving foam, water and glass particles (w = 35 wt%, FIR = 100 vol%). This mixture could be applied to all rheometers. Figure 7-45 shows the flow curve data of all experiments (plate-plate with sandpaper surface, concentric cylinders and three ball measuring systems). The data shows very unambiguously that the flow behaviour is very much dependent on the setup. The BMS results are quite overlaying each other. At high rotational speeds, the characteristic sudden increase in shear stress is determinable as it was mentioned above. In the concentric cylinders measuring system, the shear stresses are smaller than the shear stresses of the BMS for shear rates ≤ 1 1/s. Here, the slope in viscosity is not as developed as for higher shear rates (Figure 7-46), too. For higher shear rates, the shear stresses approach the shear stress and viscosity ranges of the BMS. Compared to the micro-scale investigations (plate-plate system), the shear stresses of both the concentric cylinder system and the BMS are significantly smaller. The influence of the sandpaper surface on the results is clearly observable.
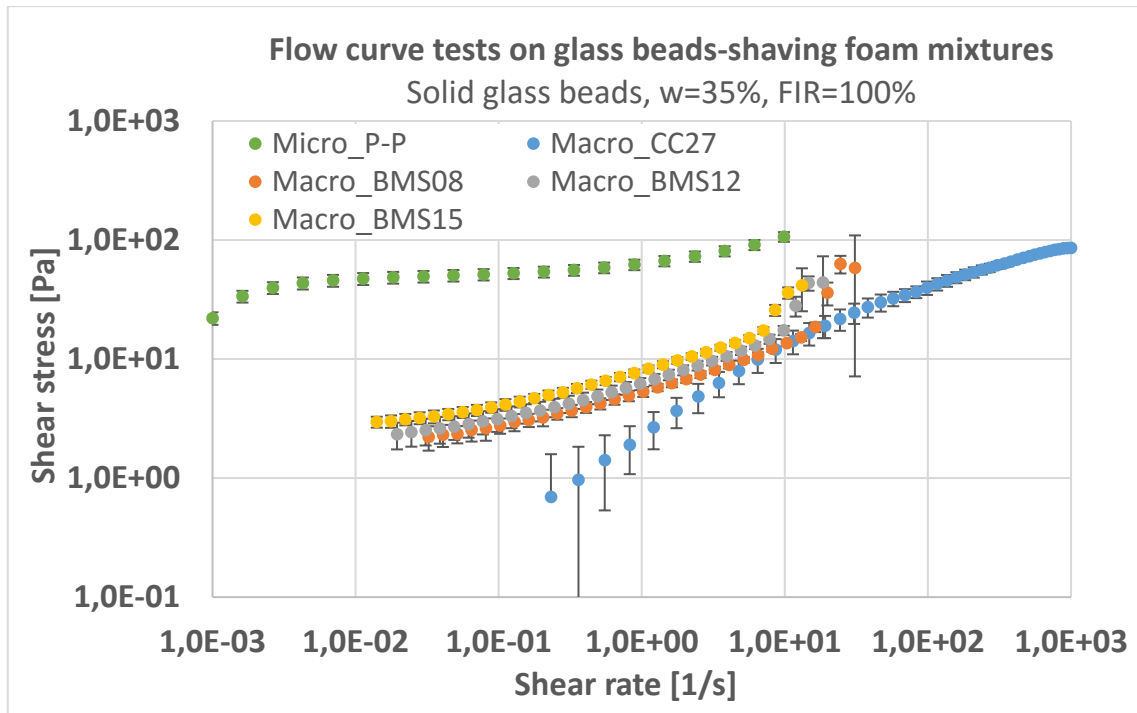
Figure 7-45: Micro-scale and macro-scale flow curves of glass particle-shaving foam mixtures of similar composition. Determination with different measuring systems: plate-plate system with sand paper surface (P-P), concentric cylinders system (CC27), ball measuring systems with different sphere sizes (BMS08, BMS12, BMS15)
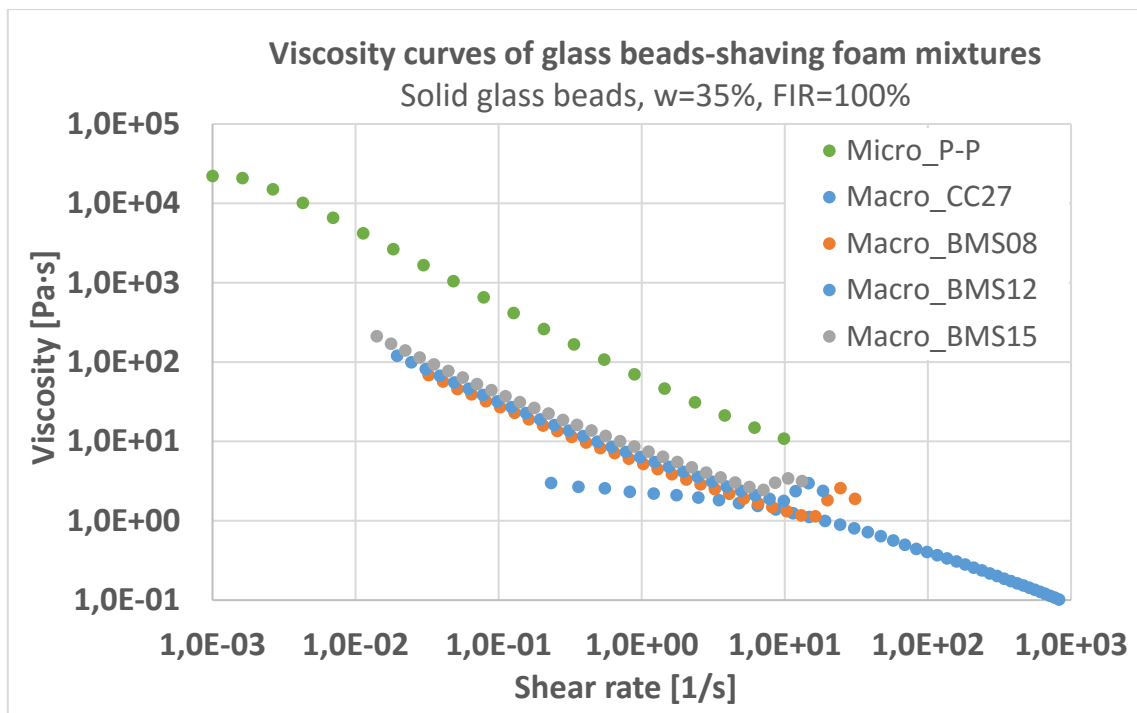
Figure 7-46: Viscosity curves of glass particle-shaving foam mixtures with similar composition. Determination with different measuring systems: plate-plate system with sand paper surface (P-P), concentric cylinders system (CC27), ball measuring systems with different sphere sizes (BMS08, BMS12, BMS15)

Overall, the flow behaviour of soil-foam mixtures was determined non-Newtonian in all experiments and it could be approximated quite well with established rheological models, from which characteristic rheological parameters could be derived. Table 7-11 summarises the adequacies each scale provides with respect to application, modelling and experimental pros and cons.

Table 7-11: Comparison of scales of investigation: rheological value and suitability for EPB relevant mixtures

Scale	Fitting model	Real soil-foam mixtures?	Range	Pro	Contra
Micro-scale (plate-plate)	Papanastasiou-Herschel-Bulkley	no	-	Precision, laminar flow field, handling of slip	Gap width
Macro-scale (coaxial cylinders)	Herschel-Bulkley	very limited	$\tau_0 = 0 \dots 110$ Pa $k = 0 \dots 5$ Pa·s $p = 0.5 \dots 1.0$	Standardised system, sample size	Geometrical dimensions, wall slip, filling
Macro-scale (BMS)	Bingham	yes	$\tau_0 = 0 \dots 570$ Pa $k = 0 \dots 10$ Pa·s	Applicability to coarse materials	Compressive / destructive impact, τ_0 as BMS index value

8. RHEOLOGY OF SOIL-FOAM MIXTURES: DISCUSSION AND APPLICATION

The most common practice to determine the suitable conditioning of a soil with foam is by evaluating the workability of the mixture. Therefore, usually, the slump test is used indicating the flow behaviour based on predefined workability ranges. From an actual flow analysis, much more information could be gathered possessing additional value for tunnelling processes. In chapter 6, the derivation of such additional flow information from slump tests was analysed. In chapter 7, an approach was followed initiated by rheological investigations and the trial of subsequent upscaling of the gained flow information. Both assessments exhibit advantages and disadvantages regarding reliability of the outcome. This is discussed both separately and comparatively for the two approaches within the present chapter. Additionally, indications for tunnelling practice and future research are going to be discussed.

8.1 Evaluation of rheological approaches

8.1.1 Rotational rheometry

Rotational rheometry has proven to be a useful approach in order to analyse the flow behaviour of fluids. In the present study, the application of rotational rheometry to soil-foam mixtures was investigated. It has been shown, that it is difficult to find a suitable setup and test conduction leading to reliable rheological data. The model behind data conversion requires a well-founded description of the physics developing in the experiments. Hence, simplifications and assumptions had to be made in order to establish a conversion of raw data into realistic rheological parameters.

The rheology of soil-foam mixtures was approached through BMS rheometry. Calibration was realised with different fluids based on similar approaches from literature on diverse granular media. The application to soil-foam mixtures showed that an investigation of a wide range of mixtures, as used in EPB tunnelling, is feasible. However, weaknesses in the approach have to be taken into account. Slip effects on the sphere surface as well as the flow field around the sphere probably are not fully incorporated. Particle sedimentation, the interaction of particle-size and sphere-size, and the distances to the boundary box defined by the sample container walls play also an influencing role when interpreting the data.

The rheometrical approach should be supported by a transfer of findings through experiments on different scales. However, the investigation of realistic soil-foam mixtures on all scales was not possible. In micro-scale experiments on synthetic EPB material using a plate-plate measuring system, a turnaround was detected in the basic material response. Depending on the containment of particles, both a fluid-like and a solid-like behaviour could be observed. From a rheological point of view, the realistic mixtures as tested in the BMS most certainly are closer to the solid-like type of mix. The investigation of the synthetic reference mixture, which could be tested on all scales, showed that the magnitude in rheological numbers between the rheological devices is close but the actual flow behaviour differs for the different rheometer setups.

8.1.2   Slump tests

The slump test represents a commonly accepted tool for evaluating the workability of pastes, mortars, fresh concrete, slurries and similar media. In the past, researchers aimed at a deduction of rheological parameters from this rather simple test, cf. chapter 3.3. Such a parameter deduction demands for a realistic approximation of the rheology. Since the slump test was not analysed during the process of slumping but at termination of motion, the viscosity was of minor concern. The equilibrium state at the end of slumping was associated with the initial condition prior to slumping (but after lifting the slump cone). The model representation emanates from a sliced body. Therein, the leading force is the dead weight, which initiates flow due to gravity. As several authors stated, this approach is very sensitive to the consideration of the several frictional boundaries. On the one hand, the friction

between the single slices has to be considered, and on the other hand, the friction between the bottom slice and the substrate needs to be accounted for. Both frictional forces are of different magnitude and degree of influence to the model. Furthermore, internal friction within the material layers is acting, too. All these effects were simplified. Perfect slip was assumed for the boundary between the bottom plate and the material. The friction between the slices was not regarded. The internal friction was considered by the yield stress, which was arrived in the equilibrium state. For the application of the slump models, the consideration of friction at all external interfaces has to be investigated more deeply. Certainly, the contact face between material and bottom plate surface is decisive on the prognosis of the slumping process. Furthermore, the internal friction acting between the infinitesimal small layers and the material yielding behaviour (yield point) of particle-foams plays an important role in the analytical analysis. The discussions on suitable laws (Tresca, von Mises) for the slumping process were conducted by FLATT ET AL. (2006), PIAU (2005), ROUSSEL & COUSSOT (2005) (see chapter 6.4.1) but they have to be extended in future researches based on the presented considerations.

As it was found out in the micro-scale experiments, soil-foam mixtures can exhibit both fluid-like and solid-like behaviours; different approaches were established based on the material behaviour (slump regime, spread regime). Both approaches were discussed extensively. A generalised best-fit approximation was found capturing well the trend between slump measures and yield stresses, which are founded on the different slump models, cf. Eq. 6.30. However, the mechanical and geometrical parameters are thusly neglected.

8.1.3   Correlation of BMS and slump yield stresses

The derivation of rheological parameters from the slump tests features the ease of test conduction while providing substantial information on the flow behaviour, if the resulting values are reliable. The trustworthiness in results can only be acknowledged by rheometry. Therefore, the findings from rotational rheometry using the BMS function as calibration measures. In the best case, yield stresses from the analytical slump models and the BMS experiments would be identical. If there is some deviation in results between the yield stresses, the slump model values have to be adjusted by a conversion model.
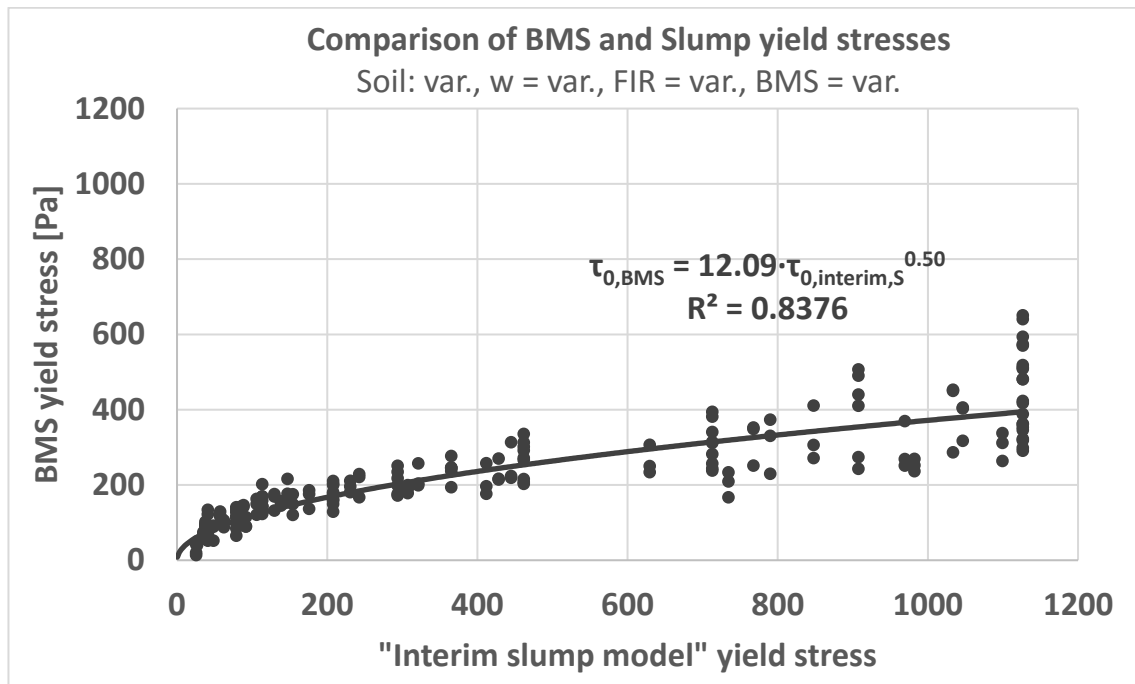
Figure 8-1: BMS yield stresses of fine sand-foam mixtures plotted over Slump yield stresses based on the superordinate interim model according to Eq. 6.30

Figure 8-1 shows yield stresses from BMS experiments and the interim range slump model (Eq. 6.30), which adequately covered the yield stress results of all mixtures, see chapter 6.4.2. Therefrom, it can clearly be seen that a linear dependency is not existent but rather a non-linear relationship. However, the magnitudes in yield stress are close. As discussed in chapter 7.3.2.5, the influences from the different sphere sizes on the results are again obvious; BMS15 gives reduced results compared to the other two. The influence from the particular testing soils are marginal, which is why Figure 8-1 shows the results of both soils. Indeed, the relationship between slump yield stresses and BMS yield stresses are of non-linear character. The final conversion model between slump yield stress and BMS yield stress is expressed by Eq. 8.1. This formula does not differentiate between the actual BMS but incorporates average values from all BMS.

$$\tau_{0,BMS} = 12.09 \cdot \tau_{0,interim,S}^{0.5} \qquad [Pa] \qquad Eq.\ 8.1$$

Applying Eq. 6.30 to Eq. 8.1 results in Eq. 8.2, which finally can be used to determine yield stresses of soil-foam mixtures from slump experiments according to DIN EN 12350-2 (2009-08).

$$\tau_0(S) = (220.26 \cdot S^2 - 11{,}916.06 \cdot S + 164{,}643.75)^{0.5} \qquad [Pa] \qquad Eq.\ 8.2$$

8.1.4   Discussion of models and approaches

The approaches of BMS rheometry and slump testing for an analysis of the flow behaviour of soil-foam mixtures actually deal with different flow states. In slump experiments, the material is evaluated, when coming to an equilibrium state at termination of flow (at rest). Therefore, the yield stress is the factor of relevance in the rheological analysis. In the BMS, the material is investigated in its condition during flow. Once in motion, the yield stress is overcome and the viscosity becomes the main factor of relevance in this test. However, it was shown, that the viscosity could not be determined as dominating as it was expected. Nevertheless, from the BMS experiments, the apparent yield stress was derived. Thus, a comparison with the slump yield stress was enabled. This is necessary in order to validate the slump approach. A validation of the slump approach was only possible by rotational rheometry. The reliability of the BMS data was achieved through calibration tests with other materials (oil, slurry, shaving foam) and through fine rheometry (plate-plate measuring system).

Both models behind the rheological data consider the density of the mixture and the distinct geometries from the experiments (slump test geometry, sphere diameter, sphere eccentricity). Due to the flowing state and the acceleration of the system, the BMS approach also considers the motion through the Reynolds number Re and the Newton number Ne and the shares of form drag and viscous drag. On the contrary, the slump model takes into account gravitation, which is the impulse initialising motion.

The preciseness in capturing the occurring slip phenomena realistically deserves further discussion in future. A calibration of the slump model through slump test with other materials did not take place.

8.2   Influences from constituents

To conclude the discussion on the rheology of soil-foam mixtures, the influence of the single constituents of the mixes on the flow behaviour shall be analysed. Prior to deeper discussion, it can already be stated that the basic flow pattern is not affected by the three integral parts.

8.2.1   Soil

Analysis of the influence from the soil type on the flow behaviour is limited because only two soils have been investigated. The range in FIR was chosen soil-specifically covering a realistic bandwidth of workability. A real comparison is only possible for the soil-foam mixtures with FIR = 50% and the same water content because it is the only overlap in the experimental program. Figure 8-2 shows flow curve data from BMS12-measurements for soil 1 and 2 with different water contents but same FIR. The same amounts of water and foam with fine sand evoke higher shear stresses than with sand. The requirement in lubrication of the single grains is higher for fine sand because its specific surface and the porosity are significantly higher compared to sand. Hence, to achieve a similar fluidisation for both soils, the water and/or foam content of fine sand needs to be increased. This fact is already known from slump testing, too, compare e.g. BUDACH (2012), BUDACH & THEWES (2015).
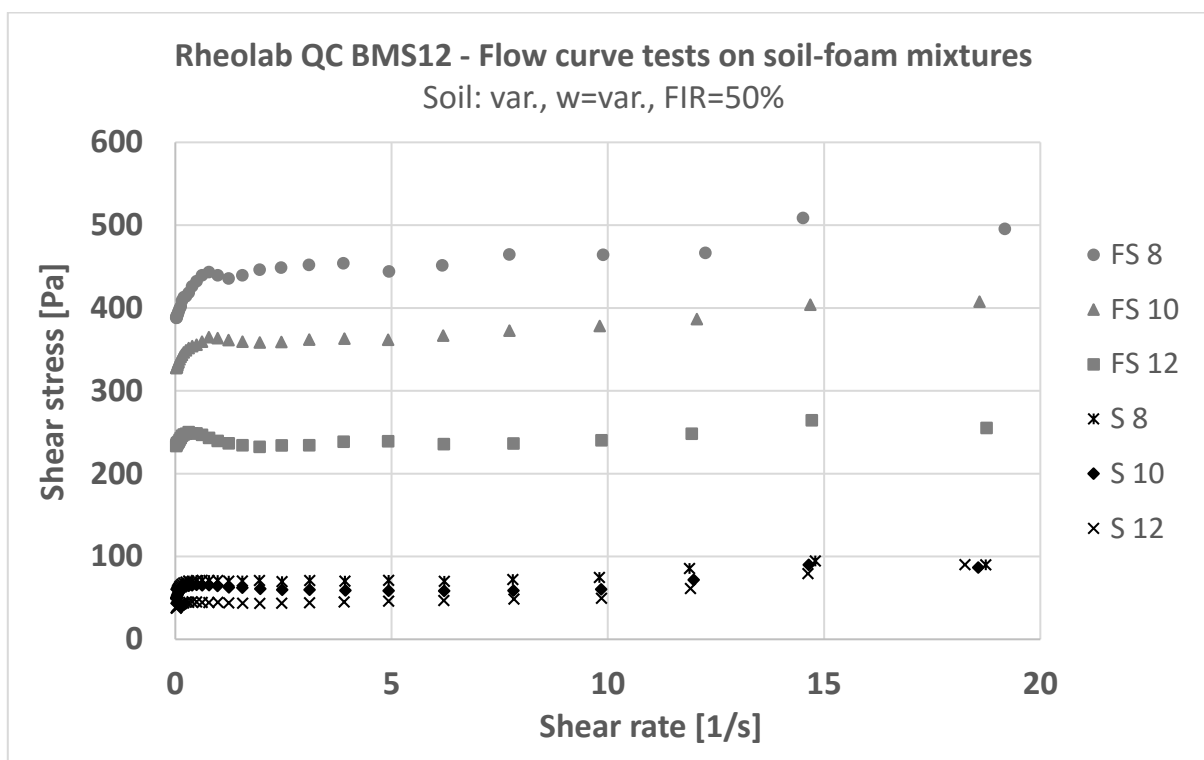
Figure 8-2:   Flow curve data from BMS12 of fine sand and sand with FIR=50% and varying water content. Fine sand-foam mixtures (grey) evoke higher shear stresses compared to sand-foam mixtures (black).

8.2.2   Water

The residual water content of soils entering the excavation chamber during tunnelling was matter of discussion in chapter 5. The water content of a soil has a significant

influence on the conditioning behaviour. The required foam injection ratio is very dependent of this prerequisite, see also PEILA ET AL. (2009), VINAI ET AL. (2008).

Data from BMS flow curve tests is depicted in Figure 8-3 for different water contents and FIR for soil 1. Principally, shear stress is increasing with decreasing water content when maintaining the FIR steady. In many tests, it could be determined that the increase in water content by 2 wt% resulted in very similar flow curves as for an increase in FIR by 10 vol%. The mixture density is then very close although the actual amount of liquid is not the same. The necessity of knowing the residual water content in the excavation chamber is again supported by the results. Little fluctuations in moisture may influence significantly the required conditioning.

On the other hand, this means also, that conditioning agent can be spared by adding water instead. However, this conclusion is valid only to a limited extent. Besides the flow behaviour, foam is injected to respond to abrasion processes. Yet, the addition of water can even intensify abrasion, especially in sandy soils, cf. GHARAHBAGH ET AL. (2014), NATSIS ET AL. (1999).
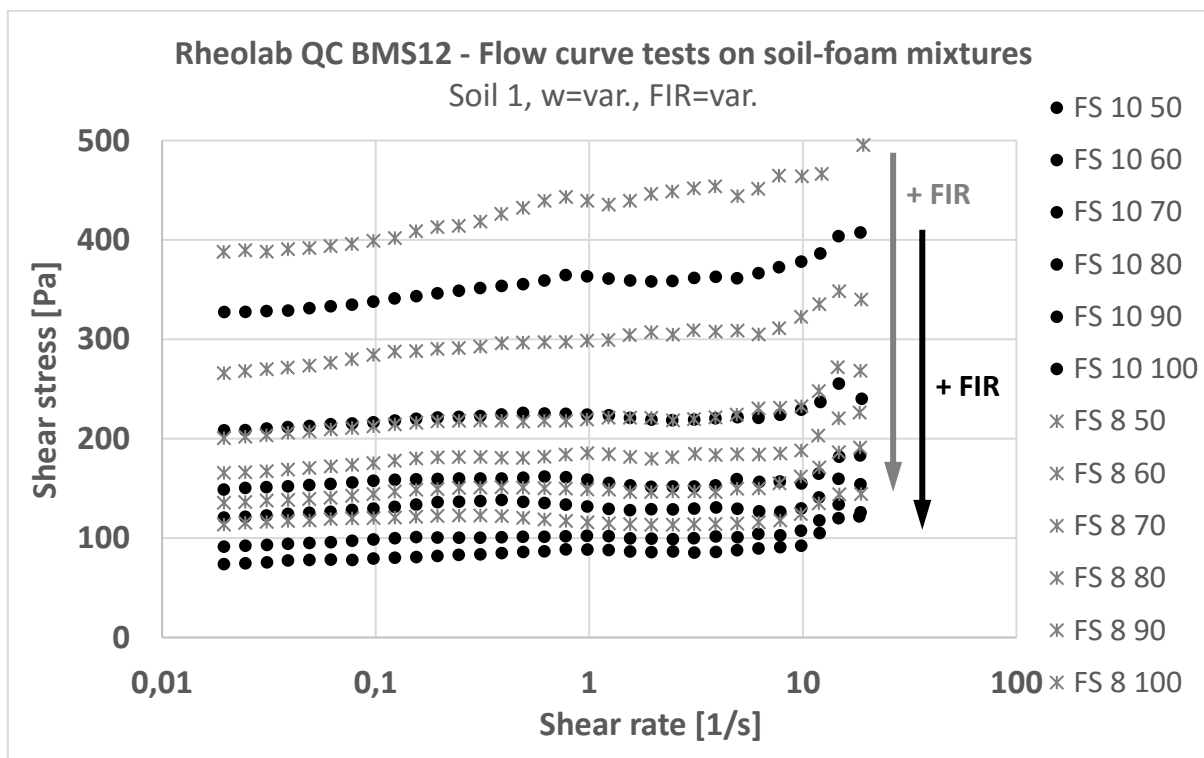
Figure 8-3:   **Flow curve data from BMS12 of fine sand-foam mixtures with different water contents (w=8% grey stars, w=10% black dots) and FIR (increasing top down). Shear stress is increasing with decreasing water content and/or decreasing FIR.**

8.2.3   Foam

Figure 8-3 gives also information on the influence of foam on the rheology of soil foam mixtures. The influence of the foam injection ratio is similar to the water content. Foam fluidises the soil. The higher the FIR is the less the shear stresses.

8.3   Indications for the tunnelling practice

Research in the construction sector aims at enhancements for practice. Reconsidering the origin of this study, the scope was an investigation of the flow behaviour of foam-conditioned soils as used in EPB tunnelling as support medium. Main issues during the elaboration were the analysis of the flow behaviour under different shearing conditions (slump test, rheometry) considering different material compositions (soil, water, foam) and an evaluation of the results from testing regarding probable process improvements to EPB tunnelling. Such enhancements could be related to the soil conditioning process like an online conditioning evaluation tool or recommendations for suitable simulation models of the support medium in face pressure calculations. In the following, some indications are given for the tunnelling practice, which can be derived from the present study.

8.3.1   Calculation of required foam injection ratios

From index testing, estimations on the rheology of soil-foam mixtures were determined in chapter 6. The numerous test executions opened the possibility to establish a prognosis model for a calculation of the slump depending on the soil, the water content and the foam injection ratio (eq. 6.2/6.3). Rearranging these formulas, a calculation of required FIR_{10} and FIR_{20} values leading to slumps of 10 and 20 cm (recommended range of suitable workability) can take place with given soil and water content. In this way, a probable range of required foam contents can be determined prior to advance (e.g. design phase) in order to create a support material with effective workability. Higher foam contents than the calculated may be required to meet further process demands (lubrication, wear reduction, temperature control, etc.).

As explained already in chapter 6.3.1, incorporating a third independent variable as a representative for the soil type could not be established because the number of

alterations in the experiments was too small to expect a reliable dependency. Hence, it is not possible to cover different types of soils by one general model. A consideration of additional soils in similar future experiments is therefore needed.

8.3.2 Calculation of yield stresses

Viscosity and yield stress are essential parameters influencing the processes going on in the excavation chamber. The required cutting wheel torque is not only designed for loosening the ground but also for overcoming the shear forces exerted on the cutting wheel by the support material in the excavation chamber, cf. DÜLLMANN ET AL. (2014). The latter share is necessary for mixing, moving and kneading the material. These shear forces are composed of the yield force and the viscous force, of which the yield force possesses the much larger share. Considering the suitable range of workability (10 and 20 cm slump), corresponding yield stresses can be determined from the ball rheometer tests. Figure 8-4 and Figure 8-5 show the ball yield stresses for all BMS for soil-foam mixtures consisting of slumps of 10 and 20 cm. The yield stresses for the same slump results are very close to each other with average values of 250 Pa for FIR_{10} and 130 Pa for FIR_{20} independent of the ball size and the type of soil.
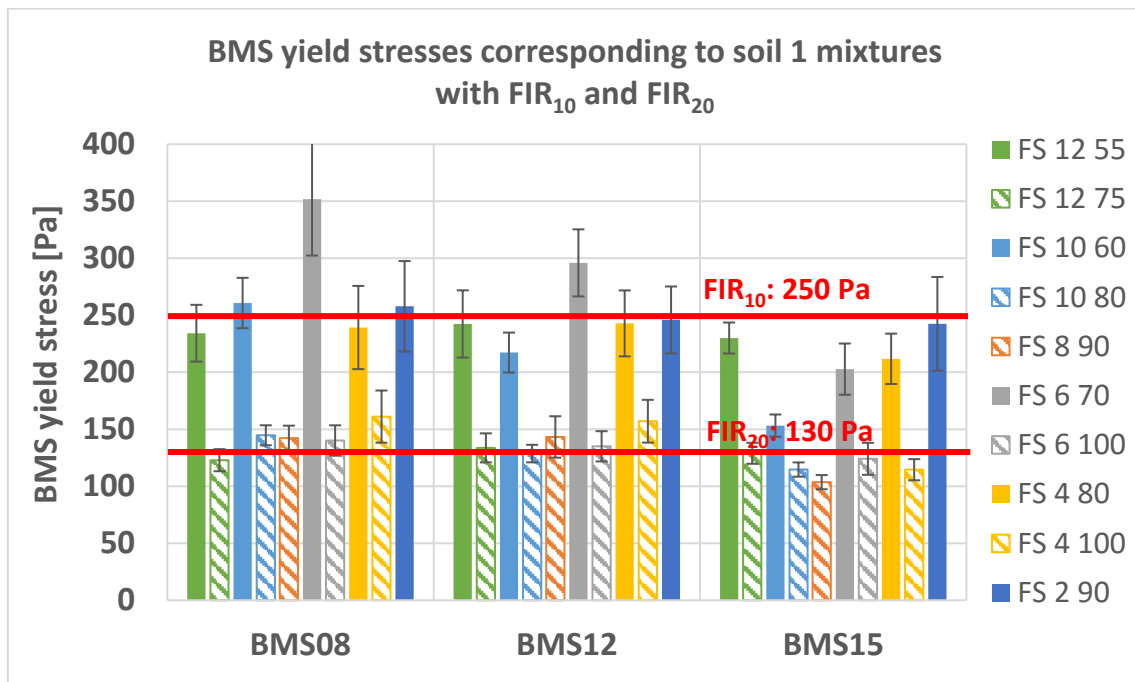
Figure 8-4: Average BMS yield stresses and standard deviations of fine sand-foam mixtures with slumps of 10 and 20 cm. Recommended range of BMS yield stresses: 130 - 250 Pa
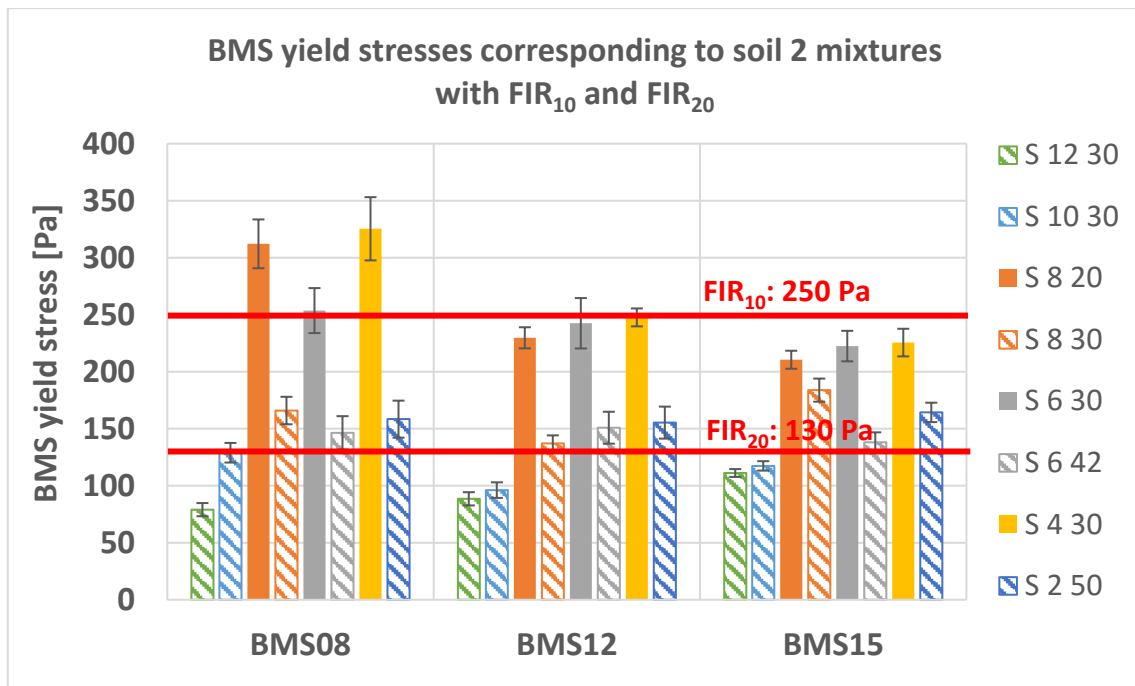
Figure 8-5:   Average BMS yield stresses and standard deviations of sand-foam mixtures with slumps of 10 and 20 cm. Recommended range of BMS yield stresses: 130 - 250 Pa

8.3.3   Sensitivity of test methods

In this study, two methods (Slump test, BMS) were presented for an experimental approach of the workability of soil-foam mixtures. The question one could arise is which test gives the most trustworthy results? The motive behind this question is of course which test equipment to hold available on the job site or in laboratories.

A look at the sensitivities of the test results should provide an answer. Therefore, the standard deviations were determined for each test. Since the range and the scale of the test results are diverse, the standard deviations have to be set into a relative perspective. The criterion to compare is the dimensionless ratio ξ of standard deviation s and recommended value range Δ indicating suitable workability (Slump test: $\Delta = 10$ to 20 cm $= 10$ cm; BMS: $\Delta = 130$ to 250 Pa $= 110$ Pa). It is referred to as the relative standard deviation, see Eq. 8.3.

$$\xi = \frac{s}{\Delta} \qquad\qquad\qquad [-] \qquad\quad Eq.\ 8.3$$

The minimum number of slump tests for each mixture was three. The BMS tests had only been repeated for the reference mixtures. Analysis of the main test measures "slump" and "BMS yield stress" and their corresponding standard deviations reveals

that the standard deviations of less fluid mixtures (low water content, low FIR) are generally higher than for more fluid mixtures (high water content, high FIR). This perception applies likewise for the slump test and the BMS. The relative standard deviations ξ are close for each test method: for the slump test, ξ was 9.3% and for the BMS, ξ was 8.7%. This actually appoints approximately the same precision to both test methods. However, the BMS tests provide further advantageous information on the conditioning or other tunnelling processes besides on the workability, see also chapter 8.3.4. The higher initial costs (acquisition) could then pay out compared to the slump test, which gives only one-dimensional information under atmospheric conditions.

8.3.4   Online evaluation tool for soil conditioning and face pressure

A further beneficial application for the tunnelling practice would be an installation of a suitable setup in the excavation chamber providing information on

- **the efficiency of soil conditioning,**

- **the filling level,**

- **and the flow behaviour.**

Closely aligned to the ball system, such an agile setup would need to be very robust dealing with high impacts from temperature, shock loads of the excavated material, fluids (water, conditioning agents, oils) and adhesion. Furthermore, little space is available in the excavation chamber. A thinkable scenario for an installation is shown in Figure 8-6; the actual two (or more) devices are sketched in an inflated way compared to the other components. The ball system needs to be installed on multiple heights considering different pressure conditions over the vertical axis. The most favourable place probably is on the bulkhead. An installation on the cutting wheel implies a non-permanent position for the measurement. In certain intervals, measurements can take place by turning all devices at the same time for several rounds through the material. From the resistant torque, information can then be derived on the rheological properties. Considering the findings from the present study, a relationship can be established between the material parameters (water content, conditioning parameters), the rheological parameters (yield stress, viscosity) and the measurements (torque, rotational speed). If the yield stresses are lower than
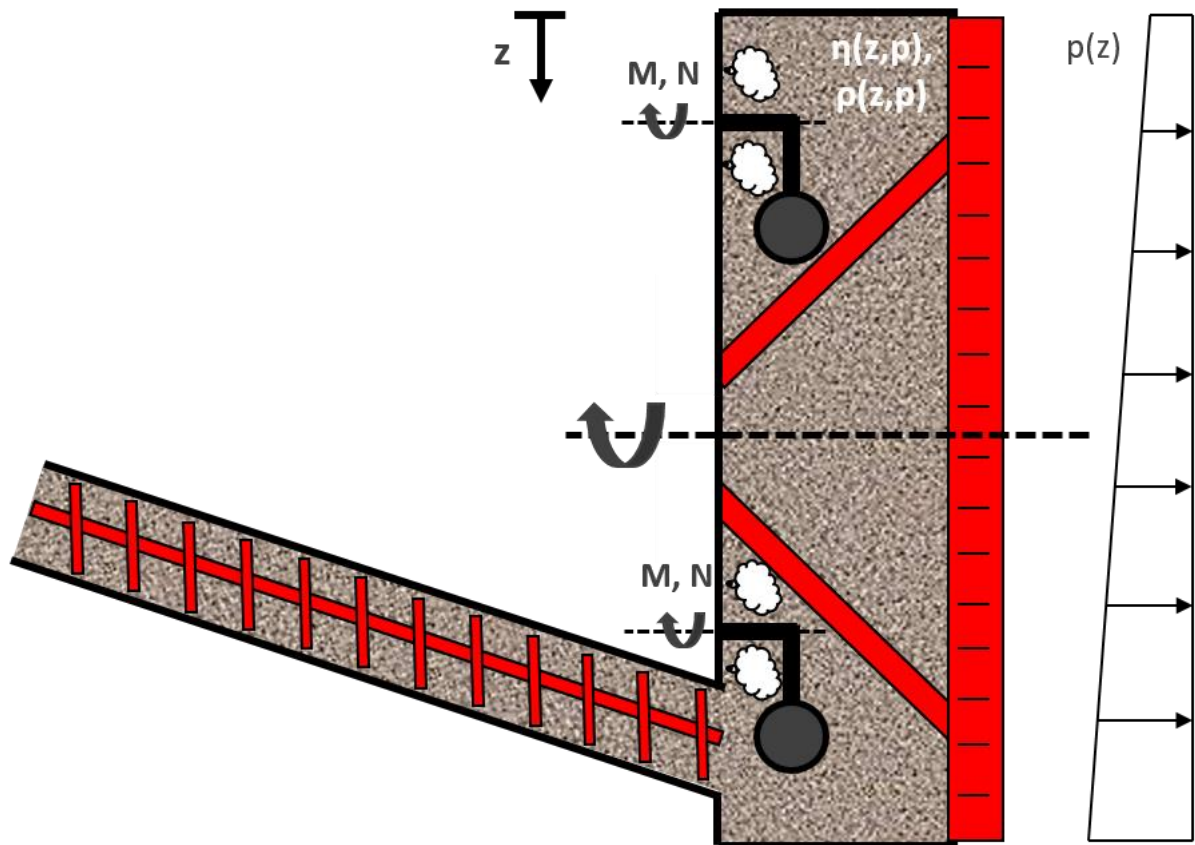
Figure 8-6: Installation of BMS-like systems (inflated design) for an estimation of the current workability of the support material and the filling level in the excavation chamber

the reference yield stress range (lower level), less conditioning agent has to be injected, and vice versa.

Additionally, a similar but smaller device could be kept available on the construction site for preliminary testing and testing during advance. Thus, comparisons between the in situ measurements and design values from the laboratory can be established. A calibration between both devices before is prerequisite.

An installation of one system in the crown could provide additional information on the filling level. If the resistance is very low (close to the intrinsic moment), the chamber probably is not filled completely. In this way, suitable counter actions could be implemented and potential blowouts could thusly be prevented.

Similar developments have been made by DOBASHI ET AL. (2005), DOBASHI ET AL. (2007a), DOBASHI ET AL. (2007b), DOBASHI ET AL. (2013) in the form of a one-bladed vane ("flapper"; Figure 8-7). The "flapper" is intended to be used as a muck flow control in

the excavation chamber. Multiple "flappers" are installed at several locations on the bulkhead (Figure 8-7). The devices are rotated continuously at constant speeds (2 rpm) and the torque is recorded. In laboratory tests, a calibration was established based on a flow behaviour, which was founded on the Casson flow model (cf. Eq. 3.9 and chapter 3.1.2), allowing for data conversion into shear stresses, cf. DOBASHI ET AL. (2013). Interpolation between the measuring spots is realised by linear interpolation. Thus, a three-dimensional visualisation of the fluid state over time can be generated, see Figure 8-8.
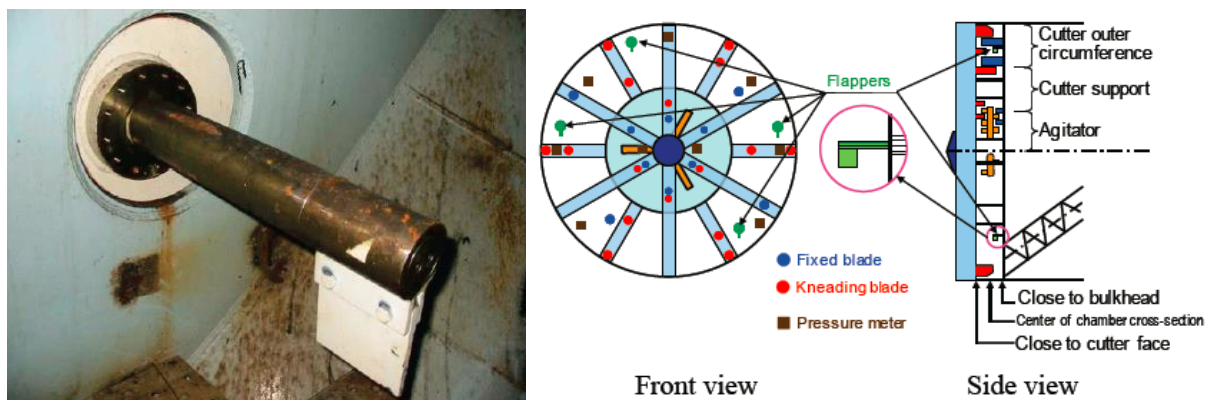
Figure 8-7: Muck Flow Control System "Flapper" according to DOBASHI ET AL. (2013); picture of an installation in an EPB TBM excavation chamber (left) and drawing of installation positions (DOBASHI ET AL. (2013))
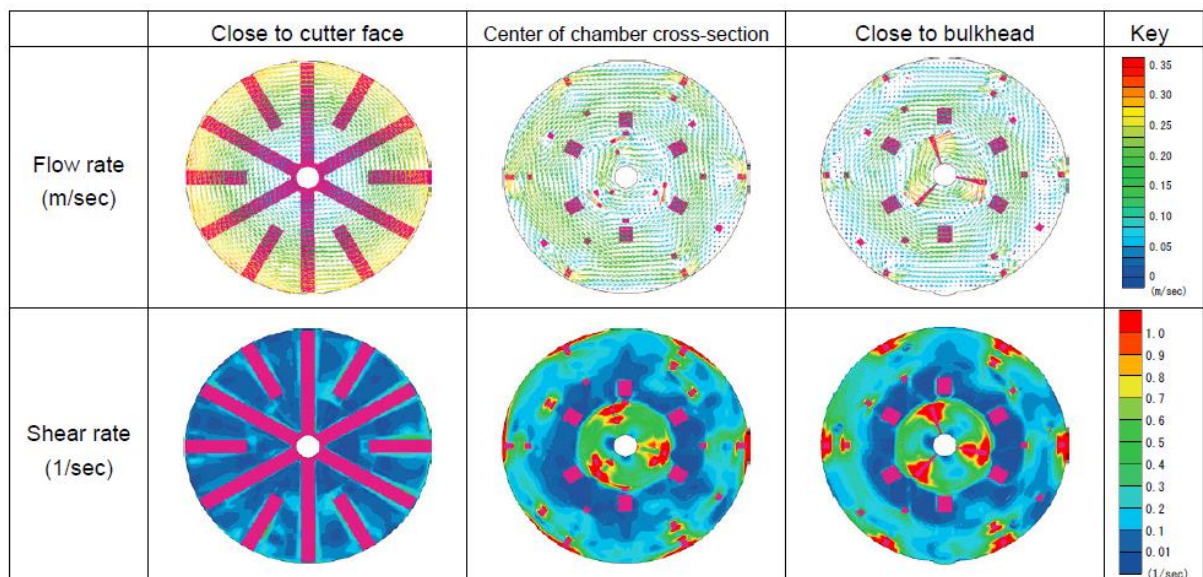
Figure 8-8: Visualisations of flow rates and shear rates at a certain time in several cross-sections of the excavation chamber based on "flapper" measurements and fluid-dynamics (DOBASHI ET AL. (2013))

Although the required driving torque of a comparable ball device would probably much higher, the ball system features less adhesion potential and thusly requires less cleaning effort.

8.3.5   Face pressure calculations

As mentioned in chapter 2.5, the calculation of the support pressure incorporates the unit weight of the support medium. A common standard for the unit weight does not exist so far regarding EPB shield tunnelling. The material density is pressure-dependent due to its compressible habit. The material's flow properties (yield stress, viscosity) depend also very much on the density, compare chapter 7.3.2.4. As mentioned before, a certain flow behaviour is required to ensure material flow in the excavation chamber, which can be described either by index test values (slump test) or by apparent yield stresses from ball rheometry. The range of yield stresses indicating a suitable flow behaviour was defined afore between 130 and 250 Pa. Depending on the particular ground and ground properties, treatments for soil conditioning can be predefined (FIR) in order to generate a proper support material density. This density should then be considered under distinct boundary conditions (pressure) within the support pressure calculation.

8.4   Outlook for future research

In future works, investigations should concentrate on the characterisation of essential properties of soil-foam-mixtures under backpressure conditions. The actual ambient pressure conditions of the support medium in most cases are different from atmospheric pressure. Prior to complex rheological investigations, a characterisation of soil-foam mixtures should take place with tests similar to the series of BUDACH (2012). Thus, a comparison in the material response towards his results is possible. Therefore, adjustments and additional adaptions of the test equipment are necessary because a conduction of slump tests under backpressure without any further contemplations will not be possible.

Additionally, the testing programme should be stretched also to non-cohesive soils and additional conditioning agents. The spectrum of EPB application covers a far greater range than treated in the present study. Thus, the calculations and models developed in this study (e.g. required $FIR_{10/20}$-calculation as introduced above) could

be further summarised by introducing a characteristic soil parameter like a representative grain-size parameter (d_{10}, d_{60}) or the uniformity index C_u.

Moreover, the scaling process of rheological information on soil-foam mixtures should be extended to even larger applications. Therefore, a large-scale test rig for the simulation of excavation and mixing process under backpressure was developed at Ruhr-Universität Bochum (Figure 8-9). Therein, an online ball system as proposed in chapter 8.2 could be installed for calibration purposes and comparison to the small-scale (micro/macro) experiments.

A further step would be the analysis of real machine data. Considering the actual machine design – especially the cutting wheel and chamber designs –, a simplified model of the impacting forces can be established acting on the support material. Incorporating machine data and corresponding boundary conditions (e.g. ground conditions, overburden, surface loads, machine diameter etc.), material properties could be determined from back analysis. First approaches are being made in subsequent studies, cf. THEWES & STEEB (2014).

Furthermore, the rheological information gained from rheometrical testing can be implemented in numerical flow simulations of the material in the excavation chamber. Thus, material streaming, conditioning processes and actual support pressure distributions can be analysed under different boundary conditions. The
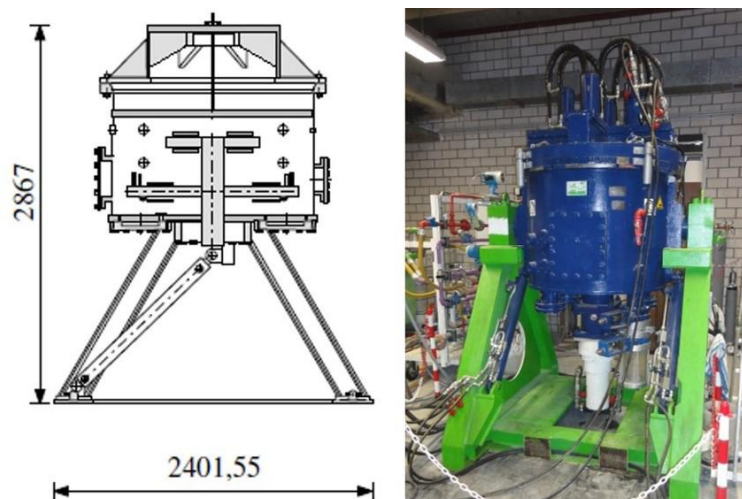
Figure 8-9:   **Large-scale test stand COSMA at Ruhr-Universität Bochum for simulation of mixing processes in the EPB excavation chamber and moreover, production, sampling and testing of conditioned soils under backpressure conditions (THEWES & STEEB (2014))**

application and efficiency of conditioning agents or other treatments could be evaluated in advance. Assessments on this topic were elaborated e.g. by DANG & MESCHKE (2014), WESSELS ET AL. (2013) and are still in progress. From this examinations, information on wear and tear or adhesion can be gained in terms of "where is the highest exposure?".

Although fundamental processes are different in hydro-shield tunnelling, some questions are similar. Infiltration processes at the tunnel face are a demanding factor for effective support pressure transfer in permeable soils. Here, a necessary transient perspective of ongoing processes make the scientific problem even more complex. Additionally, the change in rheology of the support medium (i.e. bentonite suspension) by the addition of particles (particle concentration) is decisive for material transport and face support. Ongoing research is conducted by SCHÖßER & SCHANZ (2014), ZIZKA ET AL. (2015).

The analysis of the infiltration processes of the slurry into the ground may lead to a more comprehensive analysis of the residual water content also for the foam penetration processes at the face in EPB tunnelling. Pressure distributions over the depth of the soil skeleton and the incorporation of rheological foam parameters would enable the modelling of the void water expulsion. Thus, the water content that is excavated could be determined more precisely.

At last, as frequently discovered in the rheological experiments, slip was a big issue of influence to the test results. Therefore, the slip phenomena need to be described more accurately in order to find a suitable consideration of slip in the rheology. In this way, rheological parameters will be approached more realistically. This investigation requires a micro-scale perspective.

9. CONCLUSION

EPB tunnelling in coarse soils requires soil conditioning of the excavated material in order to fulfil the necessary properties for effective support of the tunnel face. The determination of adequate conditioning agents and conditioning parameters can be achieved through lab tests. Soil conditioning not only influences the properties of the excavated ground, moreover it has an effect on face stability. Both, the reduction in hydraulic conductivity of the support material as well as the penetration of foam into the face, reduce seepage flow towards the machine. Thus, an additional support pressure against excess pore pressures is not required. The theoretical pressure distribution assumes a linear course over the vertical axis. However, the value for the unit weight is usually not determined case-dependently and the actual distribution of the support pressure at the tunnel face is unknown. One influencing factor on the pressure distribution certainly is the material fluidity: the more fluid the support medium, the closer the pressure distribution to the hydrostatic gradient. The flow behaviour of the material in the chamber can be affected by soil conditioning. It is usually evaluated by index testing and yet only by some first more sophisticated rheological assessments. Therefore, the topic of rheology, especially regarding granular media, was widely studied and discussed in this work.

The application of index tests in practice is very popular due to inexpensiveness and the ease of conduction. However, the obtained results often are of qualitative character. An assessment of the flow behaviour on a physical scale enables a quantitative evaluation and can found the basis for the development of simulation and prognosis models. In fluid dynamics, the flow behaviour and corresponding rheological parameters such as the viscosity or the yield stress of a fluid are determined through rheometer experiments. Flow curves represent a common technique for describing the flow pattern by applying established constitutive equations, from which rheological parameters can be derived. Therefore, homogeneous conditions are required, which is a laminar flow regime without any transient or surface effects.

As experience from several studies from related material disciplines shows, maintaining homogeneous shear conditions is hardly feasible when investigating EPB support material. Therefore, devices that feature an investigation of cohesionless soils have to be used and heterogeneous flow conditions like turbulences, vortices, slip effects, or time-dependent behaviours have to be tolerated. Hence, these effects can be considered to some extent in the test setup or in the analysis. Measuring systems of different designs have been applied satisfactorily for coarse-grained materials such as cylinder, vane and sphere configurations. Nevertheless, it is not possible to eliminate every potential source of error.

Conditioned soils have been formerly investigated with vane geometries and the flow behaviour was characterised by the Bingham plastic model. However, an interpretation of the applied flow models with respect to the investigated soils, the conditioning parameters or equivalent characteristic material parameters was not performed; it was more the influence of certain boundary conditions on the effective parameters that were investigated. Otherwise, slump tests are commonly performed to evaluate the flow behaviour. For this test, analytical models have been established to determine rheological parameters of yield stress fluids from the slump test. For concretes and suspensions, it could be shown that these models correlate suitably with rheometer-obtained data.

Starting point of the elaboration was a distinct description of the materials used in this study. This was necessary with respect to reproducibility. Without essential material specifications, a reconsideration of test results is generally not feasible. Two soils were chosen as a reference for this study. In future, the number of soils needs to be increased. The variation of foam parameters was limited, too, because otherwise the number of tests would have been exorbitantly high. The question of how much water needs to be added to the soil was formerly assessed by other researchers based on different perspectives. In this study, the initial water content was linked to an analysis of the residual water content entering the excavation chamber during advance (chapter 5). Therefore, the fluid interactions (foam and groundwater) at the tunnel face were investigated experimentally based on the theory of pore water replacement by foam penetration. It was found that not only the foam water needed to be regarded but also residual water, which is captured within the soil matrix due to capillary and/or adhesive forces. Thus, the determination of the water content of the

excavated soil was approached by considering different theories, trying to assess the residual amount of pore water due to groundwater displacement by foam more realistically. One approach followed a model enabling a derivation of the soil-water characteristic curve from physical properties. Information on the residual water content can then be found depending on the acting suction within the soil skeleton. Here, it was estimated to equal the applied backpressure. The second approach was again of experimental origin, which should provide information on the drainage behaviour of soils under a certain backpressure load. Both assessments led to significant and quite similar values to be taken into account additionally to the foam water. In future investigations, the process of groundwater displacement needs to be analysed during testing with the help of additional equipment (e.g. pore pressure gauges) as it was done for instance by BEZUIJEN & SCHAMINÉE (2001). Thus, the actual pressure distribution within the soil skeleton could be determined. Furthermore, the residual water content within the foam-penetrated zone could be researched using direct measurement techniques such as TDR (time domain reflectometry). However, since the actual penetration depths of the investigated soils are very small (< 15 cm), the applicability of these methods (e.g. regarding the required minimum distance of the sensors) has to be checked in the forefront. Nonetheless, a bandwidth of realistic water contents in the excavated ground could be elaborated for different tunnelling scenarios, which was used in the rheological experiments.

Furthermore, a detailed statement of the basic research approach and associated assumptions, that had to be made to particularise the scope, was given. Here, a multi-scale approach was suggested that considers homogeneous rheological testing on synthetic materials in order to characterise the flow behaviour of simulated soil-foam mixtures on the micro-scale. Additionally, these mixes were analysed in heterogeneous index tests and in large-gap rheometry as well as selected other test configurations (macro-scale). Furthermore, realistic soil-foam mixtures were investigated extensively with these test methods, too. Based on the definition of scales, the experimental programme was developed, which was divided into index tests (chapter 6) and rheometer tests (chapter 7).

Chapter 6 dealt with recommendations for and experience from testing using the slump (flow) test. Therein, testing conditions, findings and the significance for tunnelling were presented. An extensive experimental programme was carried out in

form of a variation study of single material components. A variety of soil-foam mixtures was investigated with the slump test according to DIN EN 12350-2 (2009-08). It was able to condition all mixtures to an index range of workability represented by slumps between 10 and 20 cm. Furthermore, an explicit relationship between the slump and the slump flow measures was found. In addition, equations were developed based on multivariate data analysis modelling the slump in dependence of the main conditioning parameters w and FIR. A linkage between index values and rheological parameters could be established based on analytical model representations from literature, which seem to be widely applicable also for soil-foam mixtures. Certain restraints have to be consciously taken into account like material incompressibility or neglecting surface friction. However, it could be shown that this was valid to some extent. An interim range, in which the models are not applicable, could be covered by an empirical model based on linear regression (data fitting).

The rheological investigations using rotational rheometry were described in chapter 7. Flow curve tests on soil foam mixtures were conducted using several rheometers. Thereof, the ball measuring system appeared most suitably for systematic determination of yield stress and viscosity of soil-foam mixtures. However, the viscosities of numerous mixtures were determined low, while the yield stress was high – depending on the foam and water contents. The experimental data showed the classical compressive behaviour of foams. The yield stress was referred to as reference value ("BMS yield stress"). Due to the magnitudes in yield stress, this parameter appeared to provide the most expressive rheological information. As could be shown in the trans-scale analysis on synthetic soil-foams, the basic flow pattern and the magnitude in results can be detected through the scales. However, the adequacy and the quality of the rheological models varies from scale to scale. An investigation of realistic soil-foam mixtures on all scales was not feasible.

The validation of the presented models (BMS and slump test) was matter of discussion in chapter 8. The results from rotational rheometry were compared to the findings of the slump tests. The interaction between the two indicating factors (BMS yield stress, slump yield stress) is of non-linear character. The composition of the mixes does not have an influence on the basic flow behaviour, but the soil gradation, the water content and the FIR affect the magnitudes in shear stress.

The slump test and the BMS rheometer provide an analysis of the workability of soil foam mixtures. As the range from 10 to 20 cm indicates suitably workability when using the slump test, the corresponding recommendation for the BMS rheometer ranges from 130 to 250 Pa. Both methods provide similar precision in reproducibility.

From testing, several indications for the tunnelling practice and future research could be given. Besides small calculation tools, which can be helpful e.g. in the design phase of soil conditioning, suggestions were made enabling online evaluation and online steering of the conditioning process during excavation. Furthermore, contemplations for an optimisation of face pressure calculations were proposed.

This study did not aim at a global solution for effective application of EPB shields. It should provide helpful considerations for improvements of soil conditioning processes, especially in challenging grounds. The approaches that were followed should inspire other researchers from similar disciplines to pick up, continue, and enhance the present work.

LITERATURE

3M: *3M™ Glass Bubbles K1 for Cryogenic Insulation Applications.* http://multimedia.3m.com/mws/media/536541O/3mtm-glass-bubbles-k1-for-cryogenic-insulation-app-prod-info.pdf, 23.01.2015.

ABE, T.; SUGIMOTO, Y.; ISHIHARA, K.: *Development and application of environmentally acceptable new soft ground tunnelling method.* In: Tunnelling under difficult conditions. Proceedings of the International Tunnel Symposium, Tokyo, 1978. Kitamura, I.; Kyokai, Nihon Tonneru Gijutsu; Gakkai, D. (Ed.), Pergamon Press, Oxford, New York 1979, pp. 315–320. ISBN: 0080242375.

ALTUN, J.: *Untersuchung rheologischer Eigenschaften von schaumkonditioniertem Lockergestein.* Diploma Thesis, Ruhr-Universität Bochum, Institute for Tunnelling and Construction Management 2011. ***Unpublished***.

AMERICAN PETROLEUM INSTITUTE (API): *Rheology and hydraulics of oil-well drilling fluids.* API RECOMMENDED PRACTICE 13D (2010-05), Washington, DC.

AMERICAN SOCIETY FOR TESTING AND MATERIALS (ASTM): *Test Methods for One-Dimensional Consolidation Properties of Soils Using Incremental Loading.* ASTM D2435 (1996), West Conshohocken, PA, USA. ***Superseded.***

AMERICAN SOCIETY FOR TESTING AND MATERIALS (ASTM): *Test Methods for Liquid Limit, Plastic Limit, and Plasticity Index of Soils.* ASTM D4318 (2000-06), West Conshohocken, PA, USA.

AMERICAN SOCIETY FOR TESTING AND MATERIALS (ASTM): *Standard Test Method for Permeability of Granular Soils (Constant Head).* ASTM D2434 (2006),, West Conshohocken, PA, USA. ***Withdrawn.***

AMERICAN SOCIETY FOR TESTING AND MATERIALS (ASTM): *Test Method for Flow of Grout for Preplaced-Aggregate Concrete (Flow Cone Method).* ASTM C939 (2010), West Conshohocken, PA, USA.

ANAGNOSTOU, G.; KOVÁRI, K.: *The Face Stability of Slurry-shield-driven Tunnels*. In: Tunnelling and Underground Space Technology 9 (1994) No. 2, pp. 165–174.

ANAGNOSTOU, G.; KOVÁRI, K.: *Face Stability Conditions with Earth-Pressure-Balanced Shields*. In: Tunnelling and Underground Space Technology 11 (1996) No. 2, pp. 165–173.

ATAPATTU, D. D.; CHHABRA, R. P.; UHLHERR, P.: *Creeping sphere motion in Herschel-Bulkley fluids: flow field and drag*. In: Journal of Non-Newtonian Fluid Mechanics 59 (1995) No. 2-3, pp. 245–265. DOI: 10.1016/0377-0257(95)01373-4.

AUBERTIN, M.; MBONIMPA, M.; BUSSIÈRE, B.; CHAPUIS, R. P.: *A model to predict the water retention curve from basic geotechnical properties*. In: Canadian Geotechnical Journal 40 (2003) No. 6, pp. 1104–1122. DOI: 10.1139/T03-054.

BABENDERERDE, L.: *Developments in polymer application for soilconditioning in EPB-TBMs*. In: Tunnels and metropolises. Proceedings of the World Tunnel Congress'98 on tunnels and metropolises : Sao Paulo, Brazil, 25-30 april 1998. Negro, A.; Ferreira, A. A. (Ed.), A.A. Balkema, Rotterdam 1998. ISBN: 905410936X.

BABENDERERDE, S.; HOEK, E.; MARINOS, P. G.; CARDOSO, A. S.: *EPB-TBM Face Support Control in the Metro do Porto Project, Portugal*. In: Rapid Excavation and Tunneling Conference. 2005 proceedings. Hutton, J. D.; Rogstad, W. D. (Ed.), Society for Mining, Metallurgy, and Exploration Inc., Littleton, Colo. 2005. ISBN: 9780873352437.

BABENDERERDE, T.; ELSNER, P.: *Face support and stabilisation in soft ground TBM tunnelling*. In: Tunnels for a better life. Proceedings of the World Tunnel Congress; Iguassu Falls, Brazil, May 9th - 15th, 2014. Negro, A. (Ed.), Brazilian Tunnelling Committee CBT, São Paulo 2014. ISBN: 9788567950006.

BABENDERERDE, T.; HENSEL, W.; BINAYAK, S.: *Additive zur Beherrschung starker Durchlässigkeiten bei EPB- und Slurry-TBM*. In: Tunnel (2011) No. 3, pp. 35–40.

BABENDERERDE ENGINEERS GMBH: *Sample Project with EPB TBM according to DIN 4085.*

http://www.facesupport.org/documents/40416/40682/01_EPB__DIN_factor _EN.pdf, 25.11.2014.

BANDARA, S.: *Meshfree Methods to simulate Fluidization Problems in Fluid-saturated Granular Medium.* First Year Report, University of Cambridge, Department of Engineering 2009. ***Unpublished***.

BANFILL, P.: *Rheology of fresh cement and concrete*. In: Rheology Reviews 2006. The British Society of Rheology (Ed.)2006, pp. 61–130. ISBN: 0-9547414-4-7.

BARNES, H. A.: *A review of the slip (wall depletion) of polymer solutions, emulsions and particle suspensions in viscometers: its cause, character, and cure*. In: Journal of Non-Newtonian Fluid Mechanics 56 (1995), pp. 221–251.

BARNES, H. A.; NGUYEN, Q. D.: *Rotating vane rheometry — a review*. In: Journal of Non-Newtonian Fluid Mechanics 98 (2001) No. 1, pp. 1–14. DOI: 10.1016/S0377-0257(01)00095-7.

BATCHELOR, G. K.; MOFFATT, H. K.; WORSTER, M. G.: *Perspectives in fluid dynamics. A collective introduction to current research.* 1st pbk. ed, Cambridge University Press, Cambridge 2000. ISBN: 9780521531696.

BEAR, J.: *Dynamics of fluids in porous media.* Dover Publications, Inc., New York 1988. ISBN: 9780486656755.

BEAUPRÉ, D.: *Rheology of high performance shotcrete.* Ph.d. Thesis, University of British Columbia, Department of Civil Engineering 1994.

BERKER, R.: *L'integration des equations du mouvement d'un fluide visqueux incompressible*. In: Encyclopedia of Physics. Fluid Dynamics II. Flügge, S.; Truesdell, C. A. (Ed.), Springer-Verlag, Berlin, Heidelberg, New York 1963, pp. 1–384. ISBN: 3-540-02997-4.

BEZUIJEN, A.: *The influence of soil permeability on the properties of a foam mixture in a TBM*. In: Geotechnical aspects of underground construction in soft ground. Kastner, R.; Emeriault, F.; Dias, D. (Ed.), Spécifique, Lyon 2002, pp. 221–226. ISBN: 2951041632.

BEZUIJEN, A.: *Foam used during EPB tunnelling in saturated sand, parameters determining foam consumption*. In: Proceedings of World Tunnel Congress 2012. Tunneling and Underground Space for a Global Society, Bangkok,

Thailand 21-23 May 2012. Phen-Wej, N.; Boonyatee, T. (Ed.), Engineering Institute of Thailand, Bangkok 2012. ISBN: 9789747197785.

BEZUIJEN, A.: *Foam parameters in saturated sand, theory and model tests*. In: Underground. The way to the future, proceedings of the World Tunnel Congress, Geneva, Switzerland, May 31-June 7, 2013. Anagnostou, G.; Ehrbar, H. (Ed.)2013, pp. 1336–1343. ISBN: 978-1-138-00094-0.

BEZUIJEN, A.; JOUSTRA, J. F. W.; TALMON, A. M.; GROTE, B.: *Pressure gradients at the tunnel face of an Earth Pressure Balance shield*. In: Underground space use. Analysis of the past and lessons for the future: proceedings of the 31st ITA-AITES World Tunnel Congress, 7-12 May 2005, Istanbul, Turkey. Erdem, Y.; Solak, T. (Ed.), A.A. Balkema Publishers, Leiden 2005, pp. 809–814. ISBN: 0415374529.

BEZUIJEN, A.; SCHAMINÉE, P. E. L.: *Model Experiments Using Foam simulating the drilling with an EPB shield.* Report no. BF 51010, Delft Geotechnics (Ed.), Delft 2000.

BEZUIJEN, A.; SCHAMINÉE, P. E. L.: *Simulation of the EPB-shield TBM in model tests with foam as additive*. In: Modern tunneling science and technology. Proceedings of the International Symposium on Modern Tunneling Science and Technology (IS-Kyoto 2001) Kyoto, Japan, 30 October-1 November 2001. Adachi, T.; Tateyama, K.; Kimura, M. (Ed.), A.A. Balkema, Lisse, Netherlands, Exton, PA 2001, pp. 157–263. ISBN: 9026518609.

BEZUIJEN, A.; SCHAMINÉE, P. E. L.; KLEINJAN, J. A.: *Additive testing for earth pressure balance shields*. In: Geotechnical engineering for transportation infrastructure. Theory and practice, planning and design, construction and maintenance proceedings of the Twelfth European Conference on Soil Mechanics and Geotechnical Engineering, Amsterdam, Balkema, Rotterdam 1999, pp. 1991–1996. ISBN: 9058090485.

BEZUIJEN, A.; TALMON, A. M.: *Soil pressures on both sides of the cutter wheel of an EPB-shield*. In: Tunnels for a better life. Proceedings of the World Tunnel Congress; Iguassu Falls, Brazil, May 9th - 15th, 2014. Negro, A. (Ed.), Brazilian Tunnelling Committee CBT, São Paulo 2014. ISBN: 9788567950006.

BLASK, O.: *Zur Rheologie von polymermodifizierten Bindemittelleimen und Mörtelsystemen.* Doctoral Thesis, Universität-Gesamthochschule Siegen, Institute for Buildings and Materials Chemistry 2002.

BOONE, S. J.; ARTIGIANI, E.; SHIRLAW, J. N.; GINANNESCHI, R.; LEINALA, T.; KOCHMANOVA, N.: *Use of ground conditioning agents for earth pressure balance machine tunnelling*. In: Les tunnels, clé d'une Europe durable. Compte-rendu du congrès international; Chambéry du 10 au 12 octobre 2005 = Tunnelling for a sustainable Europe : proceeding of an international congress. Association Française des Travaux en Souterrain (AFTES) (Ed.), Spécifique, Lyon 2005, pp. 313–319. ISBN: 2951041667.

BORGHI, F. X.: *Soil conditioning for pipe-jacking and tunnelling.* Ph.D. Thesis, University of Cambridge, Department of Engineering 2006.

BORIO, L.: *Soil conditioning for cohesionless soils.* Ph.D. Thesis, Politecnico di Torino, Department of Environment, Land and Infrastructure Engineering 2010.

BORIO, L.; PEILA, D.; OGGERI, C.; PELIZZA, S.: *Effects of foam on soil conditioned behaviour*. In: Safe tunnelling for the city and for the environment. Proceedings ITA-AITES world tunnel congress 2009, Budapest, Hungary, May 23-28, 2009. Kocsonya, P. (Ed.), Hungarian tunnelling association, Budapest 2009. ISBN: 978-963-06-7239-9.

BRITISH MINISTRY OF DEFENCE: *Foam Liquids, Fire Extinguishing (Concentrates, Foam, Fire Extinguishing).* D/DSTAN/ 42/40 (2002-08), Defence Procurement Agency, Glasgow.

BROERE, W.: *Tunnel face stability & new CPT applications.* Ph.d. Thesis, Technische Universiteit Delft, Geotechnical Laboratory. DUP Science, Delft 2001. ISBN: 90-407-2215-3.

BROMS, B. B.; BENNERMARK, H.: *Stability of clay in vertical openings*. In: Journal of the soil mechanics and foundations division: proceedings of the American Society of Civil Engineers (1967) No. 193, pp. 71–94.

BROOKFIELD ENGINEERING LABORATORIES VERTRIEBS GMBH: *Silikonstandards.* http://www.brookfield.eu/products/kalibrierstandards/general-purpose-silicone-fluids.asp#specifications, 23.01.2015.

BROWER, L. E.; FERRARIS, C. F.: *Comparison of Concrete Rheometers*. In: Concrete International 25 (2003) No. 8, pp. 41–47.

BRUMMER, R.: *Rheology essentials of cosmetic and food emulsions. 18 tables.* Springer, Berlin, Heidelberg 2006. ISBN: 3540255532.

BUCHENAU, G.; HILLEMEIER, B.: *Kugelfallrheometer zur Prüfung von Selbstverdichtendem Beton*. In: Beton- und Stahlbetonbau 100 (2005) No. 2, pp. 139–147.

BUCKINGHAM, E.: *On Physically Similar Systems; Illustrations of the Use of Dimensional Equations*. In: Physical Review 4 (1914) No. 4, pp. 345–376. DOI: 10.1103/PhysRev.4.345.

BUDACH, C.: *Untersuchungen zum erweiterten Einsatz von Erddruckschilden in grobkörnigem Lockergestein.* Doctoral Thesis, Ruhr-Universität Bochum, Institute for Tunnelling and Construction Management. Shaker, Aachen 2012. ISBN: 9783844008456.

BUDACH, C.; THEWES, M.: *Erweiterte Einsatzbereiche von EPB-Schilden*. In: geotechnik 36 (2013) No. 2, pp. 96–103. DOI: 10.1002/gete.201200012.

BUDACH, C.; THEWES, M.: *Application ranges of EPB shields in coarse ground based on laboratory research*. In: Tunnelling and Underground Space Technology 50 (2015), pp. 296–304. DOI: 10.1016/j.tust.2015.08.006.

BUNDESANSTALT FÜR STRAßENWESEN (BaSt): *Zusätzliche Technische Vertragsbedingungen und Richtlinien für Ingenieurbauten - Teil 5 Tunnelbau.* ZTV-ING Part 5 (2012-12).

CHAMBERLAIN, J. A.; CLAYTON, S.; LANDMAN, K. A.; SADER, J. E.: *Experimental validation of incipient failure of yield stress materials under gravitational loading*. In: Journal of Rheology 47 (2003) No. 6, pp. 1317. DOI: 10.1122/1.1619376.

CHHABRA, R. P.; RICHARDSON, J. F.: *Non-Newtonian flow and applied rheology. Engineering applications.* 2nd ed, Butterworth-Heinemann/Elsevier, Amsterdam, Boston 2008. ISBN: 9780750685320.

CLAYTON, S.; GRICE, T. G.; BOGER, D. V.: *Analysis of the slump test for on-site yield stress measurement of mineral suspensions*. In: International Journal of

Mineral Processing 70 (2003) No. 1-4, pp. 3–21. DOI: 10.1016/S0301-7516(02)00148-5.

COHEN-ADDAD, S.; KRZAN, M.; HÖHLER, R.; HERZHAFT, B.: *Rigidity Percolation in Particle-Laden Foams*. In: Physical Review Letters 99 (2007) No. 16, pp. 1–4. DOI: 10.1103/PhysRevLett.99.168001.

CONDAT LUBRIFIANTS: *New high-tech foaming agent for TBM.* http://www.condat-lubricants.com/communiques/CLB%20F5_NewFoamingAgent-for-tunneling-and-ground-treatment.pdf, 23.01.2015.

COUSSOT, P.; BOYER, S.: *Determination of yield stress fluid behaviour from inclined plane test*. In: Rheologica Acta 34 (1995) No. 6, pp. 534–543. DOI: 10.1007/BF00712314.

COUSSOT, P.; PIAU, J.-M.: *A large-scale field coaxial cylinder rheometer for the study of the rheology of natural coarse suspensions*. In: Journal of Rheology 39 (1995) No. 1, pp. 105. DOI: 10.1122/1.550693.

DANG, T. S.; MESCHKE, G.: *An ALE–PFEM method for the numerical simulation of two-phase mixture flow*. In: Computer Methods in Applied Mechanics and Engineering 278 (2014), pp. 599–620. DOI: 10.1016/j.cma.2014.06.011.

DAVIS, E. H.; GUNN, M. J.; MAIR, R. J.; SENEVIRATNE, H. N.: *The stability of shallow tunnels and underground openings in cohesive material*. In: Géotechnique 30 (1980) No. 4, pp. 397–416.

DE LARRARD, F.; HU, C.; SEDRAN, T.; SZITKAR, J. C.; JOLY, M.; CLAUX, F.; DERKX, F.: *A New Rheometer for Soft-to-Fluid Fresh Concrete*. In: ACI Materials Journal 94 (1997) No. 3, pp. 234–243.

DENKOV, N. D.; SUBRAMANIAN, V.; GUROVICH, D.; LIPS, A.: *Wall slip and viscous dissipation in sheared foams: Effect of surface mobility*. In: Colloids and Surfaces A: Physicochemical and Engineering Aspects 263 (2005) No. 1-3, pp. 129–145. DOI: 10.1016/j.colsurfa.2005.02.038.

DENKOV, N. D.; TCHOLAKOVA, S. S.; HÖHLER, R.; COHEN-ADDAD, S.: *Foam Rheology*. In: Foam engineering. Fundamentals and applications. Stevenson, P. (Ed.), John Wiley & Sons, Chichester, West Sussex, UK 2012, pp. 91–120. ISBN: 9780470660805.

DENTER, R.: *Experimentelle Untersuchungen des Infiltrationsverhaltens von Schaum-Boden-Fluidgemischen.* B.Sc. Thesis, Ruhr-Universität Bochum, Chair for Continuum Mechanics 2012. ***Unpublished***.

DEUTSCHER AUSSCHUSS FÜR UNTERIRDISCHES BAUEN E. V.: *Recommendations for static Analysis of Shield Tunnelling Machines*. In: Tunnel (2005) No. 7, pp. 44–59.

DEUTSCHER AUSSCHUSS FÜR UNTERIRDISCHES BAUEN E. V. (DAUB); GERMAN TUNNELLING COMMITTEE (ITA-AITES): *Empfehlungen zur Auswahl von Tunnelvortriebsmaschinen.* http://www.daub-ita.de/uploads/media/gtcrec14.pdf, 2010.

DEUTSCHES INSTITUT FÜR NORMUNG E.V. (DIN): *Soil, Investigation and testing - Consistency limits - Part 1: Determination of liquid limit and plastic limit.* DIN 18122-1 (1976-04), Beuth Verlag GmbH, Berlin.

DEUTSCHES INSTITUT FÜR NORMUNG E.V. (DIN): *Soil, investigation and testing - Determination of the coefficient of water permeability - Part 1 : Laboratory tests.* DIN 18130-1 (1998-05), Beuth Verlag GmbH, Berlin.

DEUTSCHES INSTITUT FÜR NORMUNG E.V. (DIN): *Subsoil - Field testing - Part 4: Field vane test.* DIN 4094-4 (2002-01), Beuth Verlag GmbH, Berlin.

DEUTSCHES INSTITUT FÜR NORMUNG E.V. (DIN): *Methods of test for mortar for masonry – Part 3: Determination of consistence of fresh mortar (by flow table); German version EN 1015-3:1999+A1:2004+A2:2006.* DIN EN 1015-3 (2007-05), Beuth Verlag GmbH, Berlin.

DEUTSCHES INSTITUT FÜR NORMUNG E.V. (DIN): *Viscometry – Measurement of viscosities and flow curves by means of rotational viscometers – Part 1: Principles and measuring geometry.* DIN 53019-1 (2008-09), Beuth Verlag GmbH, Berlin.

DEUTSCHES INSTITUT FÜR NORMUNG E.V. (DIN): *Viscometry – Measurement of viscosities and flow curves by means of rotational viscometers – Part 3: Errors of measurement and corrections.* DIN 53019-3 (2008-09), Beuth Verlag GmbH, Berlin.

DEUTSCHES INSTITUT FÜR NORMUNG E.V. (DIN): *Testing fresh concrete – Part 2: Slump-test.* DIN EN 12350-2 (2009-08), Beuth Verlag GmbH, Berlin.

DEUTSCHES INSTITUT FÜR NORMUNG E.V. (DIN): *Testing fresh concrete – Part 5: Flow table test; German version EN 12350-5:2009.* DIN EN 12350-5 (2009-08), Beuth Verlag GmbH, Berlin.

DEUTSCHES INSTITUT FÜR NORMUNG E.V. (DIN): *Testing fresh concrete – Part 8: Self-compacting concrete – Slump-flow test.* DIN EN 12350-8 (2009-12), Beuth Verlag GmbH, Berlin.

DEUTSCHES INSTITUT FÜR NORMUNG E.V. (DIN): *Testing fresh concrete – Part 9: Self-compacting concrete – V-funnel test.* DIN EN 12350-9 (2010-12), Beuth Verlag GmbH, Berlin.

DEUTSCHES INSTITUT FÜR NORMUNG E.V. (DIN): *Stability analysis of diaphragm walls.* DIN 4126 (2013-09), Beuth Verlag GmbH, Berlin.

DEUTSCHES INSTITUT FÜR NORMUNG E.V. (DIN): *Earthworks and foundation engineering - Test methods for supporting fluids in the construction of diaphragm walls and their constituent products.* DIN 4127 (2014-02), Beuth Verlag GmbH, Berlin.

DEUTSCHES INSTITUT FÜR NORMUNG E.V. (DIN): *Concrete – Specification, performance, production and conformity; German version EN 206:2013.* DIN EN 206 (2014-07), Beuth Verlag GmbH, Berlin.

DOBASHI, H.; MATSUDA, M.; MATSUBARA, K.; KITAYAMA, A.: *Controlling muck flow in a TBM cutting chamber*. In: World Tunnelling (2007a) December Issue, pp. 23–24.

DOBASHI, H.; MATSUDA, M.; MATSUBARA, K.; KITAYAMA, A.: *Design and construction of a tunnel using the technology for controlling muck flow in the cutting chamber of an earth pressure balance shield of large cross section*. In: Underground space. The 4th dimension of metropolises : proceedings of the 33rd ITA-AITES World Tunnel Congress, Prague, Czech Republic, 5-10 May 2007. Barták, J. (Ed.), Taylor & Francis, London, New York 2007b, pp. 427–433. ISBN: 978-0-415-40807-3.

DOBASHI, H.; MATSUDA, M.; MATSUBARA, K.; YAMAMOTO, A.; KONDO, Y.; HINO, Y.; KONDA, T.: *Development of technology to control and manage muck flow inside EPB shield chamber*. In: Journal of JSCE 1 (2013), pp. 90–101.

DOBASHI, H.; SAKURAI, Y.; KONISHI, Y.; OUCHI, S.; MATSUBARA, K.; KITAYAMA, A.; TAKAHASHI, H.: *Visualizing excavated soil flow in the cutter chamber of a large earth pressure balanced shield*. In: Underground space use. Analysis of the past and lessons for the future: proceedings of the 31st ITA-AITES World Tunnel Congress, 7-12 May 2005, Istanbul, Turkey. Erdem, Y.; Solak, T. (Ed.), A.A. Balkema Publishers, Leiden 2005, pp. 377–388. ISBN: 0415374529.

DÜLLMANN, J.; HOLLMANN, F. S.; THEWES, M.; ALBER, M.: *Practical TBM excavation data processing*. In: Tunnels and Tunnelling International (2014) May, pp. 53–66.

EUROPEAN FEDERATION OF NATIONAL ASSOCIATIONS REPRESENTING FOR CONCRETE (EFNARC): *Specification and Guidelines for the use of specialist products for Soft Ground Tunnelling.* EFNARC GUIDELINES 2001 (2003), Farnham, Surrey, UK.

EUROQUARZ GMBH: *Silica   sand   and   quartz   gravel   (0-16mm)   dry.* http://www.euroquarz.com/products/silica-sand-and-gravel-dry0/, 23.01.2015.

FADHEL, H.: *Investigation of the influence of soil conditioning on the calculation of the effective face support pressure in EPB-tunnelling using seepage analysis.* M.Sc. Thesis, Ruhr-Universität Bochum, Institute for Tunnelling and Construction Management 2012. ***Unpublished***.

FANN   INSTRUMENT   COMPANY: *Model   35   Viscometer   Instruction   Manual.* http://www.fann.com/public1/pubsdata/Manuals/Model%2035%20Viscome ter.pdf, 25.05.2015.

FEINENDEGEN, M.; ZIEGLER, M.; SPAGNOLI, G.; AZZAM, R.; FERNÁNDEZ-STEEGER, T. M.: *Ein neues Verfahren zur Bewertung des Verklebungspotenzials beim maschinellen Tunnelvortrieb mit Erddruckschilden.* In: 31. Baugrundtagung. Vorträge. Deutsche Gesellschaft für Geotechnik e. V. (DGGT) (Ed.), Wecom Gesellschaft für Kommunikation, Hildesheim 2010, pp. 103–109. ISBN: 9783981395303.

FEINENDEGEN, M.; ZIEGLER, M.; WEH, M.; SPAGNOLI, G.: *Clogging during EPB Tunnelling: Occurrence, classification and new manipulation methods.* In: Proceedings World Tunnel Congress 2011 Helsinki. Proceedings [of the]

World Sustainable Building Conference, 18-21 October, 2011 Helsinki, Finland, Finnish Association of Civil Engineers RIL; VTT Technical Research Centre of Finland, Helsinki 2011, pp. 767–776. ISBN: 978-951-758-531-6.

FERRARIS, C. F.: *Measurement of Rheological Properties of High Performance Concrete: State of the Art Report.* NIST Interagency/Internal Report (NISTIR) 5869, National Institute of Standards and Technology (NIST) (Ed.), Gaithersburg, MD 1996.

FERRARIS, C. F.; BROWER, L. E.: *Comparison of concrete rheometers: International tests at LCPC (Nantes, France) in October, 2000.* NIST Interagency/Internal Report (NISTIR) 6819, National Institute of Standards and Technology (NIST) (Ed.), Gaithersburg, MD 2001.

FERRARIS, C. F.; BROWER, L. E.: *Comparison of Concrete Rheometers: International Tests at MB (Cleveland, OH, USA) in May, 2003.* NIST Interagency/Internal Report (NISTIR) 7154, National Institute of Standards and Technology (NIST) (Ed.), Gaithersburg, MD 2004.

FERRARIS, C. F.; DE LARRARD, F.: *Testing and modelling of fresh concrete rheology.* NIST Interagency/Internal Report (NISTIR) 6094, National Institute of Standards and Technology (NIST) (Ed.), Gaithersburg, MD 1998.

FLATT, R. J.; LAROSA, D.; ROUSSEL, N.: *Linking yield stress measurements: Spread test versus Viskomat*. In: Cement and Concrete Research 36 (2006) No. 1, pp. 99–109. DOI: 10.1016/j.cemconres.2005.08.001.

FLEISCHMANN, F.: *Die Bestimmung der rheologischen Eigenschaften Selbstverdichtender Betone mit dem Kugelmesssystem*. In: Beiträge zur 1. DAfStb-Jahrestagung mit 54. Forschungskolloquium. Deutscher Ausschuss für Stahlbeton (DAfStb) (Ed.), Ruhr-Universität Bochum2013, pp. 442–448.

FLEISCHMANN, F.: *Ein Beitrag zur Bestimmung der Rheologischen Eigenschaften Selbstverdichtender Betone mit dem Kugel-Messsystem.* Doctoral Thesis, Ruhr-Universität Bochum, Lehrstuhl für Baustofftechnik 2014.

FLEISCHMANN, F.; KUSTERLE, W.: *Neues Rheometer zur Bestimmung der Frischbetoneigenschaften von selbstverdichtenden Betonen*. In: Beton (2014) No. 9, pp. 330–337.

FREIMANN, S.: *Entwicklung einer Laborschaumanlage für reduzierte Volumenströme zur realitätsnahen Produktion von Konditionierungsmitteln für den EPB-Tunnelbau.* B.Sc. Thesis, Ruhr-Universität Bochum, Institute for Tunnelling and Construction Management 2012. ***Unpublished***.

FREIMANN, S.: *Entwicklung eines Konditionierungskonzepts für grobkörnige Böden mit geringem Feinanteil und Verifizierung anhand eines Beispielprojekts.* M.Sc. Thesis, Ruhr-Universität Bochum, Institute for Tunnelling and Construction Management 2013. ***Unpublished***.

GALLI, M.: *Untersuchungen zur Nutzung von Tensidschäumen für die Konditionierung von kohäsionslosen Lockergesteinsböden bei EPB-Vortrieben unter realitätsnahen Randbedingungen.* Diploma Thesis, Ruhr-Universität Bochum, Institute for Tunnelling and Construction Management 2009. ***Unpublished***.

GALLI, M.; THEWES, M.: *Investigations for the application of EPB shields in difficult grounds*. In: Geomechanics and Tunnelling 7 (2014) No. 1, pp. 31–44. DOI: 10.1002/geot.201310030.

GATTERMANN, J.; KIEHL, J. R.: *EPB-Vortriebe im Fels - Verbreiung des Gesteins, erforderliches Drehmoment und Verrollung*. In: geotechnik 27 (2004) No. 2, pp. 208–213.

GESING, C. B.: *Korrelationsuntersuchung zum Fließverhalten von Partikel-Schaum-Gemischen unter Verwendung verschiedener Bewertungsverfahren.* M.Sc. Thesis, Ruhr-Universität Bochum, Institute for Tunnelling and Construction Management 2013. ***Unpublished***.

GHARAHBAGH, E. A.; ROSTAMI, J.; TALEBI, K.: *Experimental study of the effect of conditioning on abrasive wear and torque requirement of full face tunneling machines*. In: Tunnelling and Underground Space Technology 41 (2014), pp. 127–136. DOI: 10.1016/j.tust.2013.12.003.

GHORBANPOUR AKBARABADI, A.: *Bestimmung der Fließgrenze von Bentonitsuspensionen mit dem Marsh-Trichter in Abhängigkeit vom aktuellen Fließzustand.* B.Sc. Thesis, Ruhr-Universität Bochum, Institute for Tunnelling and Construction Management 2013.

GIBSON, L. J.; ASHBY, M. F.: *Cellular solids. Structure and properties.* 2nd ed, Cambridge University Press, Cambridge, New York 1997. ISBN: 9780521495608.

GIESEKUS, H.: *Phänomenologische Rheologie. Eine Einführung.* Springer-Verlag, Berlin, New York 1994. ISBN: 9783540575139.

GIRMSCHEID, G.: *Baubetrieb und Bauverfahren im Tunnelbau.* Ernst & Sohn, Berlin 2008. ISBN: 978-3433018521.

HEDAYATZADEH, M.; ROSTAMI, J.; PEILA, D.: *Experimental investigation on effect of ambient pressure of conditioned soil on tool wear in earth pressure balance (EPB) shield tunneling.* In: SEE Tunnel - Promoting Tunnelling in SEE Region. Proceedings of the ITA-AITES World Tunnel Congress 2015. Kolic, D. (Ed.), HUBITG, Zagreb 2015, pp. 3. ISBN: 978-953-55728-5-5.

HEINZ, A.: *Modifizierte Bentonitsuspensionen für geotechnische Bauverfahren in Böden hoher Durchlässigkeit.* Doctoral Thesis, ETH Zürich, Chair of Underground Construction. Vdf Hochschulverlag AG an der ETH Zürich, Zürich 2007. ISBN: 9783728131126.

HENRION, R.; HENRION, G.: *Multivariate datenanalyse. Methodik und Anwendung in der Chemie und verwandten Gebieten.* Springer-Verlag, Berlin [etc.] 1995. ISBN: 978-3540581888.

HERRENKNECHT AG: *Website der Herrenknecht AG.* http://www.herrenknecht.de/, 11.9.2014.

HÖHLER, R.; COHEN-ADDAD, S.: *Rheology of liquid foam.* In: Journal of Physics: Condensed Matter 17 (2005) No. 41, pp. R1041–R1069. DOI: 10.1088/0953-8984/17/41/R01.

HOLLMANN, F. S.: *Bewertung von Boden und Fels auf Verklebungen und Feinkornfreisetzung beim maschinellen Tunnelvortrieb.* Doctoral Thesis, Ruhr-Universität Bochum, Institute for Tunnelling and Construction Management. Shaker, Aachen 2015. ISBN: 978-3-8440-3379-3.

HOLLMANN, F. S.; THEWES, M.: *Assessment method for clay clogging and disintegration of fines in mechanised tunnelling.* In: Tunnelling and Underground Space Technology 37 (2013), pp. 96–106. DOI: 10.1016/j.tust.2013.03.010.

HORN, M.: *Horizontaler Erddruck auf senkrechte Abschlussflächen von Tunnelröhren*. In: Landeskonferenz der ungarischen Tiefbauindustrie November 1961 in Budapest. Referate zum Thema: "Unterirdische Bauwerke". Deutsche Übersetzung, fachmännische Überarbeitung und Vorwort im Auftrage der Studiengesellschaft für unterirdische Verkehrsanlagen e.V. Studiengesellschaft für unterirdische Verkehrsanlagen e.V. (STUVA) (Ed.), Düsseldorf 1961, pp. 7–16.

JAKOBSEN, P. D.; LANGMAACK, L.; DAHL, F.; BREIVIK, T.: *Development of the Soft Ground Abrasion Tester (SGAT) to predict TBM tool wear, torque and thrust*. In: Tunnelling and Underground Space Technology 38 (2013), pp. 398–408. DOI: 10.1016/j.tust.2013.07.021.

JANCSECZ, S.; STEINER, W.: *Face Support for a large Mix-Shield in heterogeneous ground conditions*. In: Tunnelling '94. Papers presented at the seventh international symposium, 'Tunnelling'94'. Arthur, L. J.; Darby, A. W. et al. (Ed.), Springer US, Boston, MA 1994, pp. 531–550. ISBN: 978-1-4613-6136-7.

JANSSEN, H. A.: *Versuche über Getreidedruck in Silozellen*. In: Zeitschrift des Vereines deutscher Ingenieure 39 (1895) No. 35, pp. 1045–1049.

JEONG, S. W.: *Influence of physico-chemical characteristics of fine-grained sediments on their rheological behavior.* Ph.d. Thesis, Université Laval, Département de génie civil 2006.

JEONG, S. W.; LEROUEIL, S.; LOCAT, J.: *Applicability of power law for describing the rheology of soils of different origins and characteristics*. In: Canadian Geotechnical Journal 46 (2009) No. 9, pp. 1011–1023. DOI: 10.1139/T09-031.

JIANG, H. T.; GONG, Q. M.; LI, Z.: *Earth Pressure Balanced Machine Model Design and Validation Tests on Soil Conditioning Evaluation and Earth Pressure Transformation*. In: Tunnelling and Underground Space Construction for Sustainable Development. Proceedings of International Symposium on Tunnelling and Underground Space Construction for Sustainable Development: TU-SEOUL 2013, Seoul, Korea, 18-20 March 2013. Kim, S.-H.; Yoo, C. et al. (Ed.), CIR PUBLISHING CO2013, pp. 39–43. ISBN: 978-89-97776-59-7 (95530).

KARMAKAR, S.; KUSHWAHA, R. L.: *Development and laboratory evaluation of a rheometer for soil visco-plastic parameters*. In: Journal of Terramechanics 44 (2007) No. 2, pp. 197–204. DOI: 10.1016/j.jterra.2006.10.002.

KASTEN, K.: *Gleitrohr-Rheometer. Ein Verfahren zur Bestimmung der Fließeigenschaften von Dickstoffen in Rohrleitungen.* Doctoral Thesis, Technische Universität Dresden, Institute of Construction Materials. Shaker, Aachen 2010. ISBN: 9783832292652.

KAYSER, T.: *Vergleich verschiedener Indexversuche zur Verarbeitbarkeitsbewertung von konditionierten Böden.* B.Sc. Thesis, Ruhr-Universität Bochum, Institute for Tunnelling and Construction Management 2015. **Unpublished**.

KHAN, S. A.; SCHNEPPER, C. A.; ARMSTRONG, R. C.: *Foam Rheology: III. Measurement of Shear Flow Properties*. In: J. Rheol. Journal of Rheology 32 (1988) No. 1, pp. 69–92.

KIRSCH, A.: *On the face stability of shallow tunnels in sand.* Doctoral Thesis, University of Innsbruck, Division of Geotechnical and Tunnel Engineering. Logos-Verlag, Berlin 2009. ISBN: 9783832521493.

KIRSCH, A.; KOLYMBAS, D.: *Theoretical investigation of face stability*. In: Bautechnik 82 (2005) No. 7, pp. 449–456.

KOEHLER, S. A.: *Foam Drainage*. In: Foam engineering. Fundamentals and applications. Stevenson, P. (Ed.), John Wiley & Sons, Chichester, West Sussex, UK 2012, pp. 27–58. ISBN: 9780470660805.

KÖNEMANN, F.; TAUCH, B.: *Neuer Kaiser-Wilhelm Tunnel – Schildvortrieb im Locker- und Festgestein unter schwierigsten Randbedingungen*. In: Taschenbuch für Tunnelbau 2013. Deutsche Gesellschaft für Geotechnik e. V. (DGGT) (Ed.), VGE Verlag GmbH, Essen 2012, pp. 119–162. ISBN: 3867971382.

KOVÁCS, G.: *Seepage hydraulics.* Elsevier Scientific Pub. Co.; Distribution for the U.S.A. and Canada, Elsevier/North-Holland, Amsterdam, New York 1981. ISBN: 0444997555.

KRIZEK, R. J.: *Rheology, Soil and Rock*. In: Encyclopedia of applied geology. Finkl, C. W. (Ed.), Springer, Berlin [u.a.] 1984, pp. 465–467. ISBN: 0442225377.

KROEZEN, A.; GROOT WASSINK, J.; SCHIPPER, C.: *The flow properties of foam*. In: Journal of the Society of Dyers and Colourists 104 (1988) No. 10, pp. 393–400. DOI: 10.1111/j.1478-4408.1988.tb01138.x.

LANGMAACK, L.: *Advanced Technology of Soil Conditioning in EPB Shield Tunnelling*. In: Proceedings of North American Tunneling 2000. Conference and exhibition : underground construction: "the revolution continues" : Boston, 6-11, June 2000. Ozdemir, L. (Ed.), A.A. Balkema, Rotterdam, Netherlands, Brookfield, VT 2000, pp. 525–540. ISBN: 9058091627.

LANGMAACK, L.: *EPB-Vortrieb in inhomogenen Böden. Möglichkeiten neuer Konditionierungsmittel*. In: Tagungsband Tunnel- und Tiefbautagung Györ 20042004, pp. 121–125.

LECA, E.; DORMIEUX, L.: *Upper and lower bound solutions for the face stability of shallow circular tunnels in frictional material*. In: Géotechnique 40 (1990) No. 4, pp. 581–606.

LEINALA, T.; GRABINSKY, M.; DELMAR, R.; COLLINS, J. R.: *Effects of foam soil conditioning on EPBM performance*. In: Proceedings of North American Tunneling 2000. Conference and exhibition : underground construction: "the revolution continues" : Boston, 6-11, June 2000. Ozdemir, L. (Ed.), A.A. Balkema, Rotterdam, Netherlands, Brookfield, VT 2000. ISBN: 9058091627.

LEVENT, K. Y.; AKSU, F.; TOKCAN, S.; GUMUS, U.; YAZICI, A.; AKDEMIR, S.: *Studies on rock conditioning for hard rock tunnelling by a mobile laboratory*. In: Underground. The way to the future, proceedings of the World Tunnel Congress, Geneva, Switzerland, May 31-June 7, 2013. Anagnostou, G.; Ehrbar, H. (Ed.)2013, pp. 1352–1359. ISBN: 978-1-138-00094-0.

LINS, Y.: *Hydro-mechanical Properties of Partially Saturated Sand.* Doctoral Thesis, Ruhr-Universität Bochum, Lehrstuhl für Grundbau, Boden- und Felsmechanik 2009.

LIPSON, C.; SHETH, N. J.: *Statistical design and analysis of engineering experiments.* McGraw-Hill, New York 1973. ISBN: 9780070379916.

LOWKE, D.: *Sedimentationsverhalten und Robustheit Selbstverdichtender Betone. Optimierung auf Basis der Modellierung der interpartikulären*

Wechselwirkungen in zementbasierten Suspensionen. Doctoral Thesis, TU München, Lehrstuhl für Baustoffkunde und Werkstoffprüfung 2013.

LUBE, G.; HUPPERT, H.; SPARKS, R.; FREUNDT, A.: *Collapses of two-dimensional granular columns*. In: Physical Review E 72 (2005) No. 4, pp. 1–10. DOI: 10.1103/PhysRevE.72.041301.

LUCKHAM, P. F.; ROSSI, S.: *The colloidal and rheological properties of bentonite suspensions*. In: Advances in Colloid and Interface Science 82 (1999), pp. 43–92.

MAIDL, B.; HERRENKNECHT, M.; MAIDL, U.; WEHRMEYER, G.: *Mechanised shield tunnelling.* 2nd ed, Ernst & Sohn, Berlin 2012. ISBN: 978-3433029954.

MAIDL, B.; THEWES, M.; MAIDL, U.: *Handbook of tunnel engineering II. Basics and additional services for design and construction.* First English edition, Ernst & Sohn, Berlin 2014. ISBN: 9783433030493.

MAIDL, U.: *Erweiterung der Einsatzbereiche der Erddruckschilde durch Bodenkonditionierung mit Schaum.* Doctoral Thesis, Ruhr-Universität Bochum, AG Leitungsbau und Leitungsinstandhaltung 1995.

MAIDL, U.: *Aktive Stützdrucksteuerung bei Erddruckschilden*. In: Bautechnik 74 (1997) No. 6, pp. 376–380.

MAIDL, U.; PIERRI, J. C. D. D.: *Innovative hybrid EPB tunnelling in Rio de Janeiro*. In: Geomechanics and Tunnelling 7 (2014) No. 1, pp. 55–63. DOI: 10.1002/geot.201400006.

MAIDL, U.; TUROLLA MAIA, C. H.; COMULADA, M.; MAHFUZ, A.; COUTINHO, A. d. A.: *First experiences gained with the hybrid EPB technology in the Rio de Janeiro sands*. In: SEE Tunnel - Promoting Tunnelling in SEE Region. Proceedings of the ITA-AITES World Tunnel Congress 2015. Kolic, D. (Ed.), HUBITG, Zagreb 2015, pp. 3. ISBN: 978-953-55728-5-5.

MAIR, R. J.: *Centrifugal modelling of tunnel construction in soft clay.* Ph.d. Thesis, University of Cambridge, Department of Engineering 1979.

MALUSIS, M. A.; EVANS, J. C.; MCLANE, M. H.; WOODWARD, N. R.: *A Miniature Cone for Measuring the Slump of Soil-Bentonite Cutoff Wall Backfill*. In: Geotechnical Testing Journal 31 (2008) No. 5, pp. 373–380.

MARKGRAF, W.: *Rheology in Soils*. In: Encyclopedia of agrophysics. Gliński, J.; Horabik, J.; Lipiec, J. (Ed.), Springer, Dordrecht 2011, pp. 700–705. ISBN: 978-90-481-3584-4.

MARKGRAF, W.; HORN, R.: *Rheology in soil mechanics. Structural changes in soils depending on the salt- and water content*. In: Annual Transactions of the Nordic Rheology Society 13 (2005), pp. 149–154.

MAYER, P.-M.; HARTWIG, U.; SCHWAB, C.: *Face stability analysis by means of an analytical failure mass model and FEM*. In: Bautechnik 80 (2003) No. 7, pp. 452–467.

MECHTCHERINE, V.; NERELLA, V. N.; KASTEN, K.: *Testing pumpability of concrete using Sliding Pipe Rheometer*. In: Construction and Building Materials 53 (2014), pp. 312–323. DOI: 10.1016/j.conbuildmat.2013.11.037.

MÉLIX, P.: *Modellversuche und Berechnungen zur Standsicherheit oberflächennaher Tunnel.* Doctoral Thesis, Universität Fridericiana Karlsruhe, Institut für Bodenmechanik und Felsmechanik 1986.

MENG, Q.; QU, F.; LI, S.: *Experimental investigation on viscoplastic parameters of conditioned sands in earth pressure balance shield tunneling*. In: Journal of Mechanical Science and Technology 25 (2011) No. 9, pp. 2259–2266. DOI: 10.1007/s12206-011-0611-9.

MENGÜ, K.: *Untersuchung des Penetrationsverhaltens von Tensidschäumen in kohäsionslose Böden beim Tunnelvortrieb mit Erddruckschildmaschinen.* B.Sc. Thesis, Ruhr-Universität Bochum, Institut für Geologie, Mineralogie und Geophysik 2012. ***Unpublished***.

MERRITT, A.: *Conditioning of clay soils for tunnelling machine screw conveyors.* Ph.D. Thesis, University of Cambridge, Department of Engineering 2004.

MERRITT, A.; JEFFERIS, S.; STORRY, R.; BRAIS, L.: *Soil conditioning laboratory trials for the Port of Miami Tunnel, Miami, Florida, USA*. In: Underground. The way to the future, proceedings of the World Tunnel Congress, Geneva, Switzerland, May 31-June 7, 2013. Anagnostou, G.; Ehrbar, H. (Ed.)2013, pp. 1328–1335. ISBN: 978-1-138-00094-0.

MERRITT, A.; STORRY, R.; BRAIS, L.: *Soil conditioning testing and monitoring for the Port Miami Tunnel*. In: SEE Tunnel - Promoting Tunnelling in SEE Region.

Proceedings of the ITA-AITES World Tunnel Congress 2015. Kolic, D. (Ed.), HUBITG, Zagreb 2015, pp. 3. ISBN: 978-953-55728-5-5.

Meschke, G.; Kruschwitz, J. (Ed.): *Sonderforschungsbereich 837: Interaktionsmodelle für den maschinellen Tunnelbau. Finanzierungsantrag 2010-2014,* Ruhr-Universität Bochum 2009.

MESSERKLINGER, S.; ZUMSTEG, R.; PUZRIN, A. M.: *A New Pressurized Vane Shear Apparatus*. In: Geotechnical Testing Journal 34 (2011) No. 2, pp. 1–10. DOI: 10.1520/GTJ103175.

METZNER, A. B.; OTTO, R. E.: *Agitation of Non-Newtonian Fluids*. In: American Institute of Chemical Engineers (AIChE) Journal 3 (1957) No. 1, pp. 3–10.

MEZGER, T. G.: *The rheology handbook. For users of rotational and oscillatory rheometers.* 3rd rev. ed, Vincentz Network, Hanover, Germany 2011. ISBN: 9783866308640.

MITSOULIS, E.: *Flows of viscoplastic materials: models and computations*. In: Rheology Reviews (2007), pp. 135–178.

MONTGOMERY, D. C.: *Design and analysis of experiments.* 6th ed, John Wiley & Sons, Hoboken, NJ 2005. ISBN: 9780471487357.

MÜLLER, M.; TYRACH, J.; BRUNN, P. O.: *Rheological characterization of machine-applied plasters*. In: ZKG International 52 (1999) No. 5, pp. 252–258.

MURATA, J.: *Flow and deformation of fresh concrete*. In: Materiaux et Constructions 17 (1984) No. 98, pp. 117–129.

MYERS, R. H.: *Classical and modern regression with applications.* Duxbury Press, Boston, Mass. 1986. ISBN: 0871509466.

NATSIS, A.; PAPADAKIS, G.; PITSILIS, J.: *The Influence of Soil Type, Soil Water and Share Sharpness of a Mouldboard Plough on Energy Consumption, Rate of Work and Tillage Quality*. In: Journal of Agricultural Engineering Research 72 (1999) 2, pp. 171–176. DOI: 10.1006/jaer.1998.0360.

NEUMÜLLER, O.-A.: *Römpps Chemie-Lexikon. Band 5, PI-S.* 8., neubearb. u. erw. Aufl, Franckh, Stuttgart 1987. ISBN: 3440045153.

ÖZARMUT, A. Ö.: *Rheology of Particle-Foam Mixture.* Rheologie-Workshop 4.6.2014, Sonderforschungsbereich 837, Ruhr-Universität Bochum 2014.

http://sfb837.sd.rub.de/downloads/rheologie_vortraege/RHEOVortrag_Oeza
rmut_04_06_2014.pdf.

ÖZARMUT, A. Ö.; GALLI, M.; STEEB, H.; THEWES, M.: *Two-scale investigations on the rheological properties of foam and particle-laden foams*. In: EURO:TUN 2013. Proceedings of the Third International Conference on Computational Methods in Tunneling and Subsurface Engineering, Ruhr University Bochum, April 17-19, 2013. Meschke, G. (Ed.), Aedificatio Publishers, Freiburg 2013, pp. 687–698. ISBN: 9783942052016.

ÖZARMUT, A. Ö.; STEEB, H.: *Rheological Properties of Liquid and Particle Stabilized Foam*. In: Journal of Physics: Conference Series 602 (2015), pp. 1–6. DOI: 10.1088/1742-6596/602/1/012031.

PANTON, R. L.: *Incompressible flow.* John Wiley & Sons, New York 1984. ISBN: 9781118013434.

PAPANASTASIOU, T. C.: *Flows of Materials with Yield*. In: Journal of Rheology 31 (1987) No. 5, pp. 385–404. DOI: 10.1122/1.549926.

PASHIAS, N.; BOGER, D. V.; SUMMERS, J.; GLENISTER, D. J.: *A fifty cent rheometer for yield stress measurement*. In: Journal of Rheology 40 (1996) No. 6, pp. 1179–1189. DOI: 10.1122/1.550780.

PAWLIK, K.: *Untersuchungen zu Fluidströmungen an der Ortsbrust und deren Einfluss auf die Ortsbruststabilität beim EPB-Vortrieb unter Berücksichtigung der Schaumkonditionierung in grobkörnigen Böden.* M.Sc. Thesis, Ruhr-Universität Bochum, Institute for Tunnelling and Construction Management 2014. ***Unpublished***.

PEILA, D.: *Soil Conditioning for EPB Shield Tunnelling*. In: Tunnelling and Underground Space Construction for Sustainable Development. Proceedings of International Symposium on Tunnelling and Underground Space Construction for Sustainable Development: TU-SEOUL 2013, Seoul, Korea, 18-20 March 2013. Kim, S.-H.; Yoo, C. et al. (Ed.), CIR PUBLISHING CO2013, pp. 10–13. ISBN: 978-89-97776-59-7 (95530).

PEILA, D.; BORIO, L.; PELIZZA, S.; DAL NEGRO, E.; BOSCARO, A.; SCHULKINS, R.: *Lab test for EPB ground conditioning*. In: Tunnels and Tunnelling International (2011) September Issue, pp. 48–50.

PEILA, D.; OGGERI, C.; BORIO, L.: *Influence of Granulometry, time and temperature on soil conditioning for EPBS applications*. In: Proceedings of the World Tunnel Congress-2008, Agra, India, 22 to 24 September 2008: Underground Facilities for Better Environment and Safety. Kanjlia, V. K. (Ed.), Central Board of Irrigation & Power2008, pp. 881–891.

PEILA, D.; OGGERI, C.; BORIO, L.: *Using the Slump Test to Assess the Behavior of Conditioned Soil for EPB Tunneling*. In: Environmental & Engineering Geoscience XV (2009) No. 3, pp. 167–174.

PEILA, D.; PICCHIO, A.; CHIEREGATO, A.: *Earth pressure balance tunnelling in rock masses: Laboratory feasibility study of the conditioning process*. In: Tunnelling and Underground Space Technology 35 (2013a), pp. 55–66. DOI: 10.1016/j.tust.2012.11.006.

PEILA, D.; PICCHIO, A.; CHIEREGATO, A.: *Laboratory Tests for EPB Tunnelling in Rock Masses Feasibility Study*. In: Tunnelling and Underground Space Construction for Sustainable Development. Proceedings of International Symposium on Tunnelling and Underground Space Construction for Sustainable Development: TU-SEOUL 2013, Seoul, Korea, 18-20 March 2013. Kim, S.-H.; Yoo, C. et al. (Ed.), CIR PUBLISHING CO2013b, pp. 134–137. ISBN: 978-89-97776-59-7 (95530).

PEÑA DUARTE, M. Á.: *Foam as a soil conditioner in tunnelling: physical and mechanical properties of conditioned sands.* Ph.d. Thesis, University of Oxford, Department of Engineering Science 2007.

PHRIKOLAT DRILLING SPECIALTIES GMBH: *Bentonit Typ W.* http://www.phrikolat.de/index.php/wissenscenter/downloadcenter/downloadcenter/category/1-produktinfo?download=20%3Abentonittypw, 23.1.2015.

PIAU, J.-M.: *Axisymmetric slump and spreading of cohesive plastic soft materials: a yield stress measurement by consisto-rheometry*. In: Journal of Rheology 49 (2005) No. 6, pp. 1253–1276. DOI: 10.1122/1.2048747.

PIERRE, A.; LANOS, C.; ESTELLÉ, P.: *Extension of spread-slump formulae for yield stress evaluation*. In: Applied Rheology 23 (2013) No. 6, pp. 1–22. DOI: 10.3933/ApplRheol-23-63849.

PSOMAS, S.: *Properties of foam/sand mixtures for tunnelling applications.* M.Sc. Thesis, University of Oxford, Department of Engineering Science 2001.

QUEBAUD, S.; MOREL, E.: *Use of foams in microtunnelling.* In: International NO DIG '95. 19. - 22.9.1995, Dresden: conference documentation. International Society for Trenchless Technology (Ed.), Hamburg Messe und Congress GmbH, Hamburg 1995, pp. 375–398.

QUEBAUD, S.; SIBAI, M.; HENRY, J.-P.: *Use of chemical foam for improvements in drilling by earth-pressure balanced shields in granular soils.* In: Tunnelling and Underground Space Technology 13 (1998) No. 2, pp. 173–180. DOI: 10.1016/S0886-7798(98)00045-5.

ROSHAVELOV, T. T.: *New Viscometer for Measuring Flow Properties of Fluid Concrete.* In: ACI Materials Journal 102 (2005) No. 6, pp. 397–404.

ROUSSEL, N.; COUSSOT, P.: *"Fifty-cent rheometer" for yield stress measurements: From slump to spreading flow.* In: Journal of Rheology 49 (2005) No. 3, pp. 705–718. DOI: 10.1122/1.1879041.

ROUSSEL, N.; STEFANI, C.; LEROY, R.: *From mini-cone test to Abrams cone test: measurement of cement-based materials yield stress using slump tests.* In: Cement and Concrete Research 35 (2005) No. 5, pp. 817–822. DOI: 10.1016/j.cemconres.2004.07.032.

SAAK, A. W.; JENNINGS, H. M.; SHAH, S. P.: *A generalized approach for the determination of yield stress by slump and slump flow.* In: Cement and Concrete Research 34 (2004) No. 3, pp. 363–371. DOI: 10.1016/j.cemconres.2003.08.005.

SCHATZMANN, M.: *Rheometry for large particle fluids and debris flows.* Doctoral Thesis, Eidgenössische Technische Hochschule ETH Zürich, Versuchsanstalt für Wasserbau, Hydrologie und Glaziologie 2005.

SCHATZMANN, M.; BEZZOLA, G. R.; MINOR, H.-E.; WINDHAB, E. J.; FISCHER, P.: *Rheometry for large-particulated fluids: analysis of the ball measuring system and comparison to debris flow rheometry.* In: Rheologica Acta 48 (2009) No. 7, pp. 715–733. DOI: 10.1007/s00397-009-0364-x.

SCHLEIBINGER GERÄTE TEUBERT U. GREIM GMBH: *Rheometer for fresh concrete BT-2. User   Manual.*

http://schleibinger.com/cmsimple/en/?download=BT2_Userman.pdf, 24.05.2015.

SCHLEIBINGER GERÄTE TEUBERT U. GREIM GMBH: *Viskomat NT - Rheometer f. Mörtel und Leim. Datenblatt.* http://www.schleibinger.com/cmsimple/?download=viskomatdatenblatt_D.pdf, 25.05.2015.

SCHLEIBINGER GERÄTE TEUBERT U. GREIM GMBH: *SCConcrete Rheometer BT2. Technical sheet.* http://www.schleibinger.com/cmsimple/en/?download=bt2_us.pdf, 24.05.2015.

SCHLEIBINGER GERÄTE TEUBERT U. GREIM GMBH: *Viskomat NT. Data sheet.* http://www.schleibinger.com/cmsimple/en/?download=vntblatt.pdf, 25.05.2015.

SCHLEIBINGER GERÄTE TEUBERT U. GREIM GMBH: *Concrete Rheometer eBT2. Technical sheet.* http://www.schleibinger.com/cmsimple/en/?download=ebt2_us.pdf, 24.05.2015.

SCHLEIBINGER GERÄTE TEUBERT U. GREIM GMBH: *Schleibinger Viskomat NT and Viskomat XL. User manual.* http://www.schleibinger.com/cmsimple/en/?download=vntsw_us.pdf, 25.05.2015.

SCHLEIBINGER GERÄTE TEUBERT U. GREIM GMBH: *Viskomat NT - Rheometer f. Mortar and Paste. Accessories.* http://www.schleibinger.com/cmsimple/en/?Rheometers%26nbsp%3B:Viskomat_NT_-_Rheometer_f._Mortar_and_Paste:Accessories, 21.05.2015.

SCHÖßER, B.; SCHANZ, T.: *Lokal instationäre Suspensionsstützung bei Flüssigkeitsschilden.* In: Inderaktionsmodelle für den maschinellen Tunnelbau. SFB 837 Broschüre 2014. Meschke, G.; Sahlmen, J. (Ed.), Bochum 2014, pp. 129–148.

SCHÖßER, B.; THEWES, M.: *Marsh funnel testing for rheology analysis of bentonite slurries for slurry shields.* In: SEE Tunnel - Promoting Tunnelling in SEE Region.

Proceedings of the ITA-AITES World Tunnel Congress 2015. Kolic, D. (Ed.), HUBITG, Zagreb 2015, pp. 262–263. ISBN: 978-953-55728-5-5.

SCHOWALTER, W. R.; CHRISTENSEN, G.: *Toward a rationalization of the slump test for fresh concrete: Comparisons of calculations and experiments*. In: Journal of Rheology 42 (1998) No. 4, pp. 865–870. DOI: 10.1122/1.550905.

SCHULKINS, R.; ALTUNA, A.; BOSCARO, A.: *Ground Conditioning for Mechanized Tunnelling: Analysis of the Correspondences Between Laboratory Tests and Results During Excavation with EPB*. In: Tunnelling and Underground Space Construction for Sustainable Development. Proceedings of International Symposium on Tunnelling and Underground Space Construction for Sustainable Development: TU-SEOUL 2013, Seoul, Korea, 18-20 March 2013. Kim, S.-H.; Yoo, C. et al. (Ed.), CIR PUBLISHING CO2013, pp. 138–140. ISBN: 978-89-97776-59-7 (95530).

SCHULZE, B.; BRAUNS, J.; SCHWALM, I.: *New test device for on-site determining the yield stress of suspensions*. In: geotechnik 14 (1991) No. 1, pp. 125–131.

SCHWARZ, J.; SCHMIDT, J.; MAIDL, R.; HANDKE, D.: *Stützdruckberechnung beim Hydroschildvortrieb – Stand der Technik, dargestellt am City-Tunnel-Leipzig*. In: Geotechnik beim Verkehrswegebau: Beiträge zum 5. Geotechnik-Tag in München, 24.02.2006. Vogt, N. (Ed.), München 2006.

SHANGGUAN, Z.; LI, S.; SUN, W.; LUAN, M.: *Estimating Model Parameters of Conditioned Soils by using Artificial Network*. In: Journal of Software 5 (2010) No. 3, pp. 296–303. DOI: 10.4304/jsw.5.3.296-303.

SIGMUND LINDNER GMBH: *SiLibeads Glass beads Type S, Microglass beads. Product Data Sheet*. http://www.sigmund-lindner.com/fileadmin/user_upload/downloads/pds_en/PDS_en_SiLibeads_Type_S__Microglass_01.pdf, 27.05.2015.

SILLERS, W. S.; FREDLUND, D. G.; ZAKERZAHEH, N.: *Mathematical attributes of some soil-water characteristic curve models*. In: Geotechnical and Geological Engineering 19 (2001) No. 3-4, pp. 243–283. DOI: 10.1023/A:1013109728218.

SIVANESAPILLAI, R.; STEEB, H.; HARTMAIER, A.: *Transition of effective hydraulic properties from low to high Reynolds number flow in porous media*. In:

Geophysical Research Letters 41 (2014) 14, pp. 4920–4928. DOI: 10.1002/2014GL060232.

STACHE, H.: *Tensid-Taschenbuch.* Hanser, München, Wien 1979. ISBN: 9783446125810.

TANIGAWA, Y.; MORI, H.; KUROKAWA, Y.; WATANABE, K.; TERANISHI, K.: *Method and Apparatus for Testing Fluidity of fresh Mortar.* Patent no.: JP3388621(B2), Japan 2003. **Granted patent with preceding publication**.

TANIGAWA, Y.; MORI, H.; KUROKAWA, Y.; WATANABE, K.; TERANISHI, K.: *Method and Apparatus for Testing Fluidity of fresh Mortar.* Patent no.: JP7229823(A), Japan 1995. **Published unexamined patent application**.

TATTERSALL, G. H.: *The workability of concrete.* [Cement and Concrete Association], [Slough, Eng.] 1976. ISBN: 0721010326.

TATTERSALL, G. H.: *Workability and quality control of concrete.* Spon1991. ISBN: 0419148604.

TERZAGHI, K.: *Theoretical soil mechanics.* J. Wiley and Sons, Inc., New York, London 1943. ISBN: 0-471-85305-4.

TERZAGHI, K.; PECK, R. B.; MESRI, G.: *Soil mechanics in engineering practice.* 3rd ed, Wiley, New York 1996. ISBN: 0471086584.

THEWES, M.; BUDACH, C.: *Schildvortrieb mit Erddruckschilden: Möglichkeit und Grenzen der Konditionierung des Stützmediums*. In: 7. Kolloquium Bauen in Boden und Fels 26. und 27. Januar 2010. Technische Akademie Esslingen (Ed.)2010a.

THEWES, M.; BUDACH, C.: *Soil conditioning with foam during EPB tunnelling*. In: Geomechanics and Tunnelling 3 (2010b) No. 3, pp. 256–267. DOI: 10.1002/geot.201000023.

THEWES, M.; BUDACH, C.; GALLI, M.: *Laboratory Tests with various conditioned soils for tunnelling with Earth Pressure Balance shield machines*. In: Tunnel (2010) No. 6, pp. 21–30.

THEWES, M.; BUDACH, C.; GALLI, M.: *Vortrieb mit Erddruckschilden: Empfehlungen für Laboruntersuchungen zur Bestimmung wesentlicher Eigenschaften von Konditionierungsmitteln und konditionierten Lockergesteinen*. In: Bauen in

Boden und Fels. 8. Kolloquium, 17. und 18. Januar 2012, [Ostfildern]; [Tagungshandbuch 2012]. Vogt, C. (Ed.), TAE, Ostfildern 2012. ISBN: 3924813957.

THEWES, M.; STEEB, H.: *Modellbildung für das Stützmedium aus konditioniertem Lockergestein beim Vortrieb mit Erddruckschilden. Bericht und Antrag zum Teilprojekt A4*. In: Sonderforschungsbereich 837: Interaktionsmodelle für den maschinellen Tunnelbau. Finanzierungsantrag 2014-2018. Meschke, G.; Thewes, M.; Sahlmen, J. (Ed.), Ruhr-Universität Bochum 2014, pp. 95–112.

THIENERT, C.: *Zementfreie Mörtel für die Ringspaltverpressung beim Schildvortrieb mit flüssigkeitsgestützter Ortsbrust.* Doctoral Thesis, Bergische Universität Wuppertal, Lehr- und Forschungsgebiet Geotechnik. Shaker, Aachen 2011. ISBN: 978-3-8440-0167-9.

TORKHANI, J.: *Penetrationsverhalten von Tensidschäumen in kohäsionslose Böden beim Tunnelvortrieb mit Erddruckschildmaschinen.* Diploma Thesis, Ruhr-Universität Bochum, Institute for Tunnelling and Construction Management 2013. ***Unpublished***.

TYRACH, J.: *Rheologische Charakterisierung von zementären Baustoffsystemen.* Doctoral Thesis, Universität Nürnberg-Erlangen. 2000.

VENNEKÖTTER: *Separationsfreier Mikrotunnelbau durch Pumpförderung schaumkonditionierter Böden.* Doctoral Thesis, RWTH Aachen, Chair and Institute of Construction Business and Project Management. Shaker, Aachen 2012. ISBN: 3844015329.

VERMEER, P. A.; RUSE, N.; MARCHER, T.: *Tunnel Heading Stability in Drained Ground*. In: Felsbau 20 (2002) No. 6, pp. 8–18.

VIALOV, S. S.: *Rheological fundamentals of soil mechanics.* Elsevier; Distributors for the United States and Canada, Elsevier Science Pub. Co., Amsterdam, New York, New York, N.Y. 1986. ISBN: 0-444-42223-4.

VINAI, R.: *A contribution to the study of soil conditioning techniques for EPB TBM applications in cohesionless soils.* Ph.D. Thesis, Politecnico di Torino, Department of Environment, Land and Infrastructure Engineering 2006.

VINAI, R.; OGGERI, C.; PEILA, D.: *Soil conditioning of sand for EPB applications: A laboratory research*. In: Tunnelling and Underground Space Technology 23 (2008) No. 3, pp. 308–317. DOI: 10.1016/j.tust.2007.04.010.

WALLEVIK, O. H.; GJORV, O. E.: *Development of a coaxial cylinders viscometer for fresh concrete*. In: Properties of fresh concrete. Proceedings of the colloquium organized on behalf of the Coordinating Committee for Concrete Technology of RILEM … by Institut für Baustoffkunde und Materialprüfung der Universität Hannover … : Hanover, October 3-5, 1990. Wierig, H.-J. (Ed.), Chapman and Hall, London, New York 1990, pp. 191–200. ISBN: 0412374307.

WEAIRE, D.; TOBIN, S. T.; MEAGHER, J.; HUTZLER, S.: *Foam Morphology*. In: Foam engineering. Fundamentals and applications. Stevenson, P. (Ed.), John Wiley & Sons, Chichester, West Sussex, UK 2012, pp. 7–26. ISBN: 9780470660805.

WESSELS, N.; DANG, T. S.; HACKL, K.; MESCHKE, G.: *Cutting and Material Transport in EPB Shield Machines: A Coupled Simulation Approach*. In: EURO:TUN 2013. Proceedings of the Third International Conference on Computational Methods in Tunneling and Subsurface Engineering, Ruhr University Bochum, April 17-19, 2013. Meschke, G. (Ed.), Aedificatio Publishers, Freiburg 2013, pp. 599–609. ISBN: 9783942052016.

WILMS, J.: *Zum Einfluß der Eigenschaften des Stützmediums auf das Verschleißverhalten eines Erddruckschildes.* Doctoral Thesis, Gesamthochschule Essen, Fachgebiet Baubetrieb u. Bauwirtschaft 1995.

WU, L.; QU, F.-z.: *Discrete element simulation of mechanical characteristic of conditioned sands in earth pressure balance shield tunneling*. In: Journal of Central South University of Technology 16 (2009) No. 6, pp. 1028–1033. DOI: 10.1007/s11771-009-0170-8.

YARIV, S.; CROSS, H.: *Geochemistry of colloid systems for earth scientists.* Springer-Verlag, Berlin, New York 1979. ISBN: 3540089802.

ZIZKA, Z.: *Untersuchungen zum Einfluss von außergewöhnlich großen Durchmessern auf die Ortsbruststabilität bei Schildvortrieben mit Flüssigkeitsstützung am Beispiel Orlovskij-Tunnel, St. Peterburg.* M.Sc. Thesis, Czech Technical University Prague, Department of Geotechnics 2012.

ZIZKA, Z.; SCHÖßER, B.; THEWES, M.: *Face Stability Assessment of Large-diameter Slurry Shields*. In: EURO:TUN 2013. Proceedings of the Third International Conference on Computational Methods in Tunneling and Subsurface Engineering, Ruhr University Bochum, April 17-19, 2013. Meschke, G. (Ed.), Aedificatio Publishers, Freiburg 2013, pp. 663–674. ISBN: 9783942052016.

ZIZKA, Z.; THEWES, M.: *Excavations with a Slurry Shield Deploying High Sensity Slurry – Consequences for the Face Stability*. In: International Conference and Exhibition on Tunnelling & Underground Space 2015 (ICETUS 2015). Sustainable Transportation in Underground Space Development. Ooi Teik Aun; Ooi Lean Hock (Ed.)2015, pp. 112–116.

ZIZKA, Z.; THEWES, M.; POPOVIC, I.: *Analysis of Slurry Pressure Transfer on the Tunnel Face during Excavation*. In: SEE Tunnel - Promoting Tunnelling in SEE Region. Proceedings of the ITA-AITES World Tunnel Congress 2015. Kolic, D. (Ed.), HUBITG, Zagreb 2015. ISBN: 978-953-55728-5-5.

ZUMSTEG, R.; PLÖTZE, M.; PUZRIN, A.: *Reduction of the clogging potential of clays: new chemical applications and novel quantification approaches*. In: Géotechnique 63 (2013) No. 4, pp. 276–286. DOI: 10.1680/geot.SIP13.P.005.

ZUMSTEG, R.; PLÖTZE, M.; PUZRIN, A. M.: *Effect of Soil Conditioners on the Pressure and Rate-Dependent Shear Strength of Different Clays*. In: Journal of Geotechnical and Geoenvironmental Engineering 138 (2012) No. 9, pp. 1138–1146. DOI: 10.1061/(ASCE)GT.1943-5606.0000681.

ZUMSTEG, R.; PUZRIN, A. M.: *Stickiness and adhesion of conditioned clay pastes*. In: Tunnelling and Underground Space Technology 31 (2012), pp. 86–96. DOI: 10.1016/j.tust.2012.04.010.

LIST OF FIGURES

LIST OF TABLES

LIST OF SYMBOLS

a	$[Pa \cdot s^n]$	fluid consistency factor
A, A_{xy}	$[m^2]$	cross-sectional area
a_c	$[-]$	adsorption coefficient
A_{exc}	$[m^2]$	face area
a_i, b_i	$[-]$	regressor variables
A_{silo}	$[m^2]$	cross-sectional area of the silo
A_{sphere}	$[m^2]$	projected area of the sphere
C	$[-]$	system number
c	$[Pa]$	cohesion
C_1	$[-]$	system number
C_c	$[-]$	curvature coefficient
c_D	$[-]$	drag coefficient
c_f	$[vol\%]$	concentration of the foaming liquid
c_{fv}	$[Pa]$	field vane shear strength
c_{i+1}	$[-]$	value from main diagonal of the matrix operation
c_L	$[-]$	end-effect correction factor
CSR	$[-]$	conversion factor shear rate

CSS	[-]	conversion factor shear stress
c_{susp}	[vol%]	concentration of the slurry
C_U	[-]	coefficient of uniformity
C_ψ	[-]	correction factor
d	[m]	diameter
D, D_T	[m]	tunnel diameter
d_{10}	[mm]	representative grain-diameter at 10% passage
d_{30}	[mm]	representative grain-diameter at 30% passage
d_{60}	[mm]	representative grain-diameter at 60% passage
D_H	[cm]	equivalent particle diameter
d_{Sphere}, d_{BMS}	[mm]	sphere diameter
dz, dz'	[m]	thickness
e	[-]	Euler's number = 2.718
E	[N]	earth pressure
e_p	[-]	void number
F	[N]	(shear) force
F_D	[N]	drag force
FER	[-]	foam expansion ratio
FER_{actual}	[-]	actual foam expansion ratio
FER_m	[-]	foam expansion ratio in the excavation chamber considering residual pore water
FIR	[vol%]	foam injection ratio

FIR_{10}	[vol%]	foam injection ratio leading to a slump of 10 cm
FIR_{20}	[vol%]	foam injection ratio leading to a slump of 20 cm
g	[m/s²]	gravitational acceleration
G	[N]	dead weight of the sliding wedge
h	[m]	height, gap distance, thickness
h_0	[cm]	height of undeformed section of the slump figure
H_0, H	[m]	initial height of the slump cone
h_1	[m]	height of deformed section of the slump figure
h_{co}	[cm]	equivalent capillary rise
h_{tool}	[mm]	tool penetration, cutter depth
h_W	[m]	height of groundwater table above tunnel crown
I_C	[-]	consistency index
I_P	[wt%]	plasticity index
K	[-]	lateral earth pressure coefficient
k	[Pa·s]	viscosity parameter
k_f	[m/s]	hydraulic conductivity
L	[m]	length
L_{sphere}, L_{BMS}	[-]	BMS eccentricity, radius of circular path
M	[Nm]	torque
m	[s]	factor controlling the stress growth at low shear rates
m_F	[kg]	mass of foam

M_{max}	[Nm]	maximum torque
m_p	[-]	pore-size distribution factor
$m_{S,dry}$	[kg]	mass of dry soil
m_W	[kg]	mass of water
n	[-]	sample size
N	[1/s]	turning speed
N_{cw}	[rpm]	turning speed of cutting wheel
Ne	[-]	Newton number
n_m	[-]	soil porosity in the excavation chamber
n_p	[-]	void ratio
$n_{p,corrected}$	[-]	maximum ratio of expelled pore water and foam-penetrated soil volume considering displaced foam water
$n_{p,eff}$	[-]	effective void ratio
$n_{p,setup}$	[-]	void ratio in foam penetration test setup
$n_{p,test}$	[-]	maximum ratio of expelled pore water and foam-penetrated soil volume
n_0^s	[-]	volumetric content of particles
n_{tool}	[-]	tool stocking per track
p	[-]	form factor
P	[Nm/s]	stirring power
p_0	[Pa]	the surcharge on the surface

p_r	[-]	number of regression variables without intercept
P_v	[N]	vertical loading from prism (surcharge) on wedge
p_z	[Pa]	vertical stress
q	[m/s]	volumetric discharge
Q	[N]	shear force on inclined wedge face
Q_A	[l/min]	volume flow of air
Q_F	[l/min]	volume flow of foam
Q_f	[l/min]	volume flow of surfactant
Q_{fines}	[l/min]	volume flow of fines
Q_L	[l/min]	volume flow of liquid
Q_S	[l/min]	volume flow of soil
Q_{susp}	[l/min]	volume flow of slurry
Q_w	[l/min]	volume flow of water
r, R, r_x	[m]	radius
$R_0, R_{x,0}$	[m]	initial bottom radius of slump cone
R^2	[-]	coefficient of determination
$\overline{R^2}$	[-]	adjusted coefficient of determination
R_c	[mm]	cone radius
Re	[-]	Reynolds number
R_e	[mm]	inner cup radius
R_i	[mm]	cylinder or bob radius

R_p	[mm]	plate radius
R_T	[m]	tunnel radius
$r_{x,0}$	[m]	initial top radius of slump cone
S	[-]	soil saturation (chapter 5)
S	[cm]	slump
S	[N]	support force (chapter 2.5)
s	var.	standard deviation
$S_a{}^*$	[-]	adhesion component of soil saturation
S_c	[-]	capillary component of soil saturation
SF	[cm]	slump flow
$S_{invert/crown}$	[Pa]	support pressure in the crown / invert
SIR	[vol%]	slurry injection ratio
S_m	[cm²/g]	mass-specific surface area
$S_{measured}$	[cm]	measured slump value
$S_{predicted}$	[cm]	predicted slump value
SS_E	var.	explained sum of squares
SS_R	var.	residual sum of squares
SS_T	var.	total sum of squares
T	[N]	lateral shearing force at the sides of the sliding wedge
t	[s]	time
$t_{0.95}$	[-]	tabulate value of the Student distribution

T_C	[N]	lateral shearing force at the sides of the sliding wedge due to cohesion
t_h	[m]	overburden height
t_i	[-]	t-value for t-testing
T_R	[N]	lateral shearing force at the sides of the sliding wedge due to friction
t_{tool}	[s]	duration between two cutters passing
U	[m]	circumference of silo
v	[m/s]	velocity
V	[m³]	volume
v_{Adv}	[m/min]	advance speed of the TBM
w	[wt%]	water content
w_{exc}	[wt%]	excavated water content
w_{foam}	[wt%]	water content of soil in foam-saturated state
w_L	[wt%]	liquid limit
w_n	[wt%]	natural water content
w_P	[wt%]	plastic limit
$w_{res,DT}$	[wt%]	residual gravimetric water content based on the drainage test approach
$w_{res,SWCC}$	[wt%]	residual gravimetric water content based on the SWCC approach
w_{sat}	[wt%]	water content of soil in water-saturated state
W_z	[N]	dead weight

x	[m]	coordinate
z, z'	[m]	coordinate, e.g. depth below surface
z_p	[cm]	foam penetration depth
α	[-]	shape factor
α_c	[°]	cone angle
α_{exp}	[-]	expansion factor
β	[-]	factor considering frictional effects
β_W	[-]	contact angle between water and capillary surface
γ	[N/m³]	unit weight of soil
$\dot{\gamma}$	[1/s]	shear rate
γ_S	[N/m³]	unit weight of the support medium
γ_W	[N/m³]	unit weight of water
Δ	var.	reference value range (e.g. slump test: $\Delta = 10$ to 20 cm = 10 cm; BMS: $\Delta = 140$ to 250 Pa = 110 Pa)
η	[Pa·s]	viscosity
η_E	[-]	safety factor for earth pressure = 1.50
η_W	[-]	safety factor for water pressure = 1.05
ϑ	[°]	sliding angle
θ	[vol%]	volumetric water content
θ_c	[rad]	circumference
ϑ_{crit}	[°]	critical sliding angle
$\theta_{residual}$	[vol%]	residual pore water content

λ	[-]	friction factor, yield criterion
ξ	[-]	relative standard deviation
ρ	[kg/m³]	density
ρ_d	[kg/m³]	bulk density
ρ_L	[kg/m³]	density of liquid
ρ_s	[kg/m³]	solid grain density
$\rho_{S,wet}$	[kg/m³]	density of wetted soil
ρ_W	[kg/m³]	density of water
σ_V	[Pa]	vertical loading from prism (surcharge) on wedge
σ_W	[N/m]	fluid surface tension
τ	[Pa]	shear stress
τ_y, τ_0, τ^*	[Pa]	yield stress
φ	[°]	friction angle
Φ	[m]	change in piezometric head
Φ_0	[m]	initial piezometric head at the tunnel face
ψ	[cm]	matric suction, matric potential
ψ_0	[cm]	ultimate matric potential
ψ_n	[cm]	normalisation parameter
ψ_r	[cm]	residual suction

LIST OF ABBREVIATIONS

AEV   air entry value (representative point on soil-water characteristic curve)

BMS   ball measuring system

CC   concentric cylinders measuring system

cf.   confer, compare

CSR   conversion factor shear rate

CSS   conversion factor shear stress

DT   drainage test

e.g.   exempli gratia, for example

EPB   earth-pressure-balance

$FIR_{10/20}$ foam injection ratio leading to a slump of 10 / 20 cm

FS   fine sand

i.e.   id est, that is

L   litre, litres

max   maximum

min   minimum

no.   number

PP   parallel plates measuring system

REVE   representative excavated volume element

rpm   rounds per minute = 1/min

S   sand

SWCC   soil-water characteristic curve

TBM   tunnel boring machine

var.   varying

vol%   volume percent

wt%   weight percent

CURRICULUM VITAE

Personal Information

Name:	Mario Galli
Title:	Dipl.-Ing.
Date and Place of Birth:	22 October 1983, Essen (Germany)
Nationality:	German-Italian
E-mail:	m.galli@gmx.de

Professional Experience

Since 07/2015	Technical Assistant at ARGE BOL/BÜ Albaufstieg Ingenieurbüro Dipl.-Ing. H. Vössing GmbH, Düsseldorf (Germany)
01/2010 – 06/2015	Research Assistant Institute for Tunnelling and Construction Management, Ruhr-Universität Bochum (Germany)

Education

10/2003 – 09/2009	Civil Engineering, Ruhr-Universität Bochum (Germany)
09/2006 – 03/2007	Civil Engineering, Università degli Studi di Firenze, Florence (Italy)
08/1994 – 07/2003	Bischöfliches Gymnasium am Stoppenberg (Highschool), Essen (Germany)

APPENDIX

In this section, the detailed testing procedures and the protocols of the experiments conducted in the frame of this study are attached as well as all relevant diagrams and additional information, to which it was addressed in the main chapters.

A. INDEX

A.1   Standard testing procedure of soil-foam mixtures

Table A-1:   **Procedure for production of soil-foam mixtures and test preparations including remarks regarding the measuring accuracy**

Step no.	Time	Duration	Task	Accuracy
I	---	---	Test preparations	
II	---	---	Compose soil according to recipe	±1.0 wt%, max. ±1.0 g
III	---	01:00	Mix soil until homogenised	
IV	---	---	Measure water in dependence of water content w	±1.0 wt%, max. ±1.0 g
V	---	01:00	Mixing of water and soil until homogenised	
1	00:00	03:30	Foam production and sampling, determination of actual FER and measuring FIR-dependent amount of foam for the mixture	±10.0 wt%, max. ±1.0 g
2	03:30	01:00	Mixing of foam and wetted soil until homogenized; small samples (< 3 kg) by hand, large samples (3 − 24 kg) with concrete bowl mixer	
3	04:30	04:00	Preparation of testing sample(s); further test preparations, if necessary	
4	08:30	---	Start of testing	

A.2   Foam penetration tests

A.2.1   Setup and testing procedure
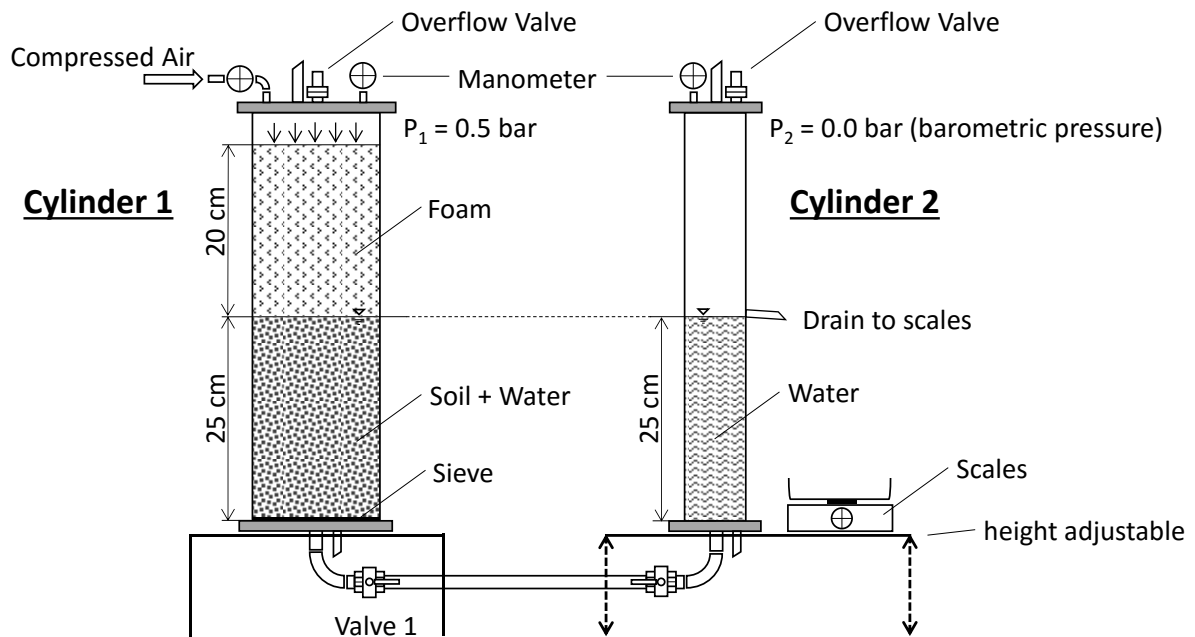
<u>Test stand</u>

Figure A-1:   Scheme of rig for foam penetration tests

<u>Equipment</u>

- 2 buckets

- 1 shovel

- 1 tamper

- 1 scales

- 1 bowl

- 1 stop watch

- 2 video cameras + tripods

Preparations

1. Preparation of test stand, fixing the cameras to tripods, positioning of scales: Position one camera in order to document scales and stop-watch and position the other camera to record the foam penetration zone, a measuring tape and the second stop-watch

2. Prepare 12 kg of soil according to soil gradation

3. Homogenisation of soil for 2 minutes in a gravity mixer

4. Fill soil into a bucket after mixing, weigh and record its mass

5. Fill water into the soil cylinder up to the 5 cm-marking and dripple soil in 5 cm layers into water afterwards

6. Compact soil with tamper in a spiral shaped manner

7. Repeat steps 5 to 6 until a height of 25 cm is reached

8. Adjust the height of the water cylinder so that the overrun has same height as the filled-in soil in cylinder 1; if necessary add/drain water

9. Record the residual masses of water and soil

10. Calculate and record the mean height of the soil level with the help of three measuring scales at the outer cylinder walls

11. Produce and fill foam onto the soil to a height of 15 cm, record foam mass and actual heights afterwards

12. Place the O-rings and close the soil cylinder with its lid by using screws

13. Connection of compressed air to cylinder 1, open the overpressure valve and close the outlet valve on the top

14. Adjust to the desired, constant air pressure in the soil cylinder using the installed manometer

Procedure

15. Start of experiment by simultaneously opening the ball valve at the bottom side of the soil cylinder and starting stop-watches and recordings

16. Record penetration depths in steps of 30 second up to a total of 180 seconds on the basis of two measuring tapes, which are not caught by the camera

Remarks

Close the compressed air supply after finishing the experiment and carefully diminish the pressure in the cylinder.

A.2.2   Testing protocols

Date	03.09.2013		
Soil	Fine sand		
Mass of water [g]	3512,3	Water content w [wt%]	21,5
Mass of soil [g]	8890,7	Void ratio n [-]	0,363
FER	14,9	Density of soil [g/cm³]	1,688
		Saturated density [g/cm³]	2,051
Measurements			
time [s]	Water outflow [g]	Position of foam front [cm]	
0	0,0	24,9	
1	10,0	24,2	
2	30,0	23,9	
3	57,0	23,8	
4	80,0	23,7	
5	95,0	23,7	
6	107,0	23,7	
7	114,0	23,7	
8	124,0	23,6	
9	129,0	23,6	
10	134,0	23,6	
11	137,0	23,6	
12	141,0	23,6	
13	144,0	23,5	
14	147,0	23,5	
15	148,0	23,5	
16	150,0	23,5	
17	152,0	23,5	
18	154,0	23,5	
19	156,0	23,5	
20	158,0	23,5	
21	159,3	23,4	
22	161,1	23,4	
23	162,1	23,4	
24	163,6	23,4	
25	164,3	23,4	
26	165,4	23,4	
27	166,8	23,4	
28	167,9	23,4	
29	168,6	23,4	
30	169,6	23,4	
30	169,6	23,433	
60	191,1	23,233	
90	204,4	23,200	
120	216,0	23,167	
150	225,7	23,100	
180	234,7	23,067	

Date	04.09.2013		
Soil	Middle sand		
Mass of water [g]	3364,2	Water content w [wt%]	19,2
Mass of soil [g]	9209,3	Void ratio n [-]	0,342
FER	15,0	Density of soil [g/cm³]	1,744
	20	Saturated density [g/cm³]	2,078
Measurements			
time [s]	Water outflow [g]	Position of foam front [cm]	
0	0,0	25,0	
1	22,7	24,1	
2	92,2	23,0	
3	145,0	22,5	
4	213,0	22,1	
5	213,0	22,0	
6	230,0	21,7	
7	240,0	21,6	
8	255,0	21,5	
9	266,0	21,4	
10	274,0	21,3	
11	280,0	21,2	
12	287,0	21,2	
13	292,0	21,1	
14	298,0	21,1	
15	302,0	21,1	
16	307,0	21,0	
17	310,0	21,0	
18	314,0	21,0	
19	318,0	21,0	
20	320,0	20,9	
21	324,0	20,9	
22	326,4	20,9	
23	329,1	20,9	
24	331,5	20,9	
25	333,9	20,9	
26	336,6	20,9	
27	338,8	20,9	
28	341,3	20,8	
29	343,5	20,8	
30	345,3	20,7	
30	345,3	20,667	
60	384,5	20,233	
90	408,8	20,033	
120	428,2	19,867	
150	444,2	19,733	
180	457,5	19,633	

Date	13.02.2014		
Soil	Middle sand		
Mass of water [g]	3510,6	Water content w [wt%]	21,1
Mass of soil [g]	9044,8	Void ratio n [-]	0,348
FER	15,3	Density of soil [g/cm³]	1,727
	20	Saturated density [g/cm³]	2,091

Measurements

time [s]	Water outflow [g]	Position of foam front [cm]	
0	0,0	24,8	
1	48,9	23,0	
2	104,9	22,7	
3	148,9	22,4	
4	159,8	22,2	
5	178,9	22,1	
6	203,0	22,0	
7	216,5	21,9	
8	228,3	21,7	
9	238,5	21,6	
10	248,4	21,5	
11	254,5	21,4	
12	263,5	21,3	
13	268,5	21,2	
14	278,4	21,1	
15	283,5	21,1	
16	290,8	21,0	
17	296,8	21,0	
18	300,9	21,0	
19	306,8	20,9	
20	310,9	20,9	
21	316,9	20,8	
22	320,9	20,8	
23	324,5	20,7	
24	327,5	20,7	
25	330,4	20,6	
26	334,8	20,6	
27	338,5	20,6	
28	343,0	20,5	
29	345,5	20,5	
30	350,4	20,5	
30	350,4	20,267	
60	400,5	19,967	
90	409,4	19,867	
120	430,0	19,767	
150	437,6	19,733	
180	447,5	19,733	

Date	05.09.2013		
Soil	Coarse sand		
Mass of water [g]	3392,5	Water content w [wt%]	19,2
Mass of soil [g]	9317,9	Void ratio n [-]	0,335
FER	14,9	Density of soil [g/cm³]	1,762
	20	Saturated density [g/cm³]	2,101
Measurements			
time [s]	Water outflow [g]	Position of foam front [cm]	
0	0,0	25,0	
1	80,0	23,0	
2	190,0	21,0	
3	296,0	19,8	
4	395,0	19,0	
5	430,0	18,2	
6	442,0	18,0	
7	470,0	17,5	
8	500,0	17,0	
9	524,0	16,8	
10	546,0	16,5	
11	560,0	16,3	
12	574,0	16,1	
13	590,0	15,9	
14	606,0	15,8	
15	615,0	15,7	
16	625,0	15,6	
17	639,0	15,4	
18	646,0	15,2	
19	658,0	15,1	
20	666,0	15,0	
21	675,0	14,9	
22	680,0	14,8	
23	688,0	14,7	
24	695,0	14,6	
25	702,0	14,4	
26	709,0	14,3	
27	715,0	14,3	
28	720,0	14,2	
29	727,0	14,1	
30	731,0	13,9	
30	731,0	13,900	
60	826,0	12,900	
90	874,0	12,433	
120	903,0	12,033	
150	917,0	11,967	
180	927,0	11,933	

Date	10.10.2013		
Soil	Fine sand - Middle sand		
Mass of water [g]	3240,4	Water content w [wt%]	17,4
Mass of soil [g]	9409,5	Void ratio n [-]	0,333
FER	15,6	Density of soil [g/cm³]	1,768
	20	Saturated density [g/cm³]	2,076
Measurements			
time [s]	Water outflow [g]	Position of foam front [cm]	
0	0,0	25,2	
1	12,0	25,0	
2	45,0	24,6	
3	92,0	24,3	
4	116,0	24,0	
5	138,0	23,9	
6	153,0	23,8	
7	163,0	23,7	
8	176,0	23,7	
9	183,0	23,6	
10	190,0	23,5	
11	196,0	23,5	
12	200,0	23,5	
13	204,0	23,5	
14	208,0	23,4	
15	210,0	23,4	
16	213,0	23,3	
17	216,0	23,3	
18	218,0	23,3	
19	220,0	23,3	
20	222,0	23,3	
21	224,0	23,3	
22	226,0	23,3	
23	227,5	23,3	
24	229,0	23,3	
25	230,0	23,2	
26	232,0	23,2	
27	233,5	23,2	
28	235,0	23,2	
29	236,1	23,2	
30	237,5	23,2	
30	237,5	22,933	
60	261,0	22,700	
90	275,0	22,700	
120	286,4	22,600	
150	295,4	22,533	
180	303,0	22,500	

Date	27.02.2014		
Soil	Fine sand - Middle sand		
Mass of water [g]	3443,9	Water content w [wt%]	20,0
Mass of soil [g]	9231,8	Void ratio n [-]	0,340
FER	15,5	Density of soil [g/cm³]	1,748
	20	Saturated density [g/cm³]	2,097
Measurements			
time [s]	Water outflow [g]	Position of foam front [cm]	
0	0,0	25,0	
1	13,1	24,4	
2	49,6	23,9	
3	87,4	23,7	
4	110,9	23,6	
5	135,1	23,5	
6	143,5	23,5	
7	149,0	23,4	
8	154,0	23,4	
9	159,5	23,3	
10	164,4	23,3	
11	169,4	23,3	
12	170,8	23,3	
13	174,6	23,2	
14	176,5	23,2	
15	179,6	23,2	
16	180,2	23,2	
17	182,6	23,2	
18	184,6	23,2	
19	186,1	23,2	
20	188,1	23,2	
21	189,0	23,2	
22	192,0	23,2	
23	193,0	23,2	
24	193,2	23,2	
25	195,7	23,1	
26	196,8	23,1	
27	198,3	23,1	
28	198,6	23,1	
29	198,8	23,1	
30	200,0	23,0	
30	200,0	22,933	
60	219,8	22,800	
90	231,3	22,680	
120	239,7	22,567	
150	246,5	22,467	
180	252,7	22,467	

Date	23.10.2013		
Soil	Middle sand - Coarse sand		
Mass of water [g]	3365,8	Water content w [wt%]	18,7
Mass of soil [g]	9454,6	Void ratio n [-]	0,332
FER	15,0	Density of soil [g/cm³]	1,769
	20	Saturated density [g/cm³]	2,099

Measurements

time [s]	Water outflow [g]	Position of foam front [cm]	
0	0,0	25,3	
1	70,0	23,9	
2	183,0	22,0	
3	210,0	21,0	
4	255,0	20,7	
5	282,0	20,3	
6	300,0	20,1	
7	320,0	20,0	
8	336,0	19,8	
9	350,0	19,6	
10	365,0	19,5	
11	370,0	19,4	
12	382,0	19,3	
13	390,0	19,1	
14	398,0	19,0	
15	405,0	19,0	
16	411,0	19,0	
17	416,0	19,0	
18	422,0	18,9	
19	427,0	18,9	
20	430,0	18,9	
21	436,0	18,8	
22	441,0	18,7	
23	445,0	18,7	
24	449,0	18,6	
25	452,0	18,6	
26	456,0	18,5	
27	459,0	18,5	
28	462,0	18,5	
29	465,0	18,5	
30	468,0	18,4	
30	468,0	18,400	
60	524,0	18,000	
90	556,0	17,733	
120	581,0	17,367	
150	601,0	17,200	
180	619,0	17,067	

Date	15.10.2013		
Soil	Sand		
Mass of water [g]	3080,8	Water content w [wt%]	14,7
Mass of soil [g]	10056,0	Void ratio n [-]	0,281
FER	15,2	Density of soil [g/cm³]	1,904
	20	Saturated density [g/cm³]	2,185

Measurements

time [s]	Water outflow [g]	Position of foam front [cm]	
0	0,0	25,0	
1	6,0	24,7	
2	45,0	24,0	
3	80,0	23,6	
4	105,0	23,4	
5	123,0	23,1	
6	136,0	22,9	
7	147,0	22,8	
8	156,0	22,6	
9	166,0	22,5	
10	170,0	22,5	
11	176,0	22,5	
12	183,0	22,5	
13	188,0	22,4	
14	192,0	22,4	
15	196,0	22,4	
16	198,0	22,4	
17	201,0	22,4	
18	204,0	22,3	
19	207,0	22,3	
20	209,0	22,3	
21	212,0	22,3	
22	214,0	22,3	
23	216,0	22,2	
24	218,0	22,2	
25	220,0	22,2	
26	221,0	22,2	
27	223,0	22,2	
28	225,0	22,1	
29	226,0	22,1	
30	228,0	22,1	
30	228,0	21,900	
60	258,0	21,733	
90	275,0	21,633	
120	288,5	21,533	
150	299,0	21,400	
180	308,0	21,333	

Date	29.10.2013		
Soil	Sand		
Mass of water [g]	3135,0	Water content w [wt%]	15,1
Mass of soil [g]	10199,0	Void ratio n [-]	0,283
FER	15,0	Density of soil [g/cm³]	1,901
	20	Saturated density [g/cm³]	2,187

Measurements

time [s]	Water outflow [g]	Position of foam front [cm]	
0	0,0	25,4	
1	20,0	24,9	
2	40,0	24,5	
3	80,0	24,0	
4	104,0	23,9	
5	118,0	23,7	
6	132,0	23,5	
7	140,0	23,1	
8	148,0	23,0	
9	155,0	23,0	
10	159,0	23,0	
11	166,0	23,0	
12	170,0	23,0	
13	174,0	23,0	
14	177,0	23,0	
15	181,0	22,9	
16	184,0	22,9	
17	187,0	22,9	
18	189,0	22,9	
19	190,0	22,9	
20	193,0	22,8	
21	195,0	22,8	
22	197,0	22,8	
23	200,0	22,8	
24	202,0	22,8	
25	203,0	22,8	
26	204,0	22,8	
27	206,0	22,8	
28	207,0	22,8	
29	209,0	22,7	
30	210,0	22,7	
30	210,0	22,533	
60	236,0	22,333	
90	252,0	22,200	
120	265,0	22,067	
150	276,0	22,000	
180	286,0	21,967	

Date	30.01.2013		
Soil	Sand		
Mass of water [g]	3194,8	Water content w [wt%]	16,3
Mass of soil [g]	9755,6	Void ratio n [-]	0,303
FER	15,4	Density of soil [g/cm³]	1,847
	20	Saturated density [g/cm³]	2,149

Measurements

time [s]	Water outflow [g]	Position of foam front [cm]	
0	0,0	25,0	
1	9,4	24,2	
2	37,4	23,3	
3	75,3	22,9	
4	108,4	22,7	
5	122,9	22,5	
6	147,7	22,3	
7	152,7	22,2	
8	160,9	22,2	
9	167,9	22,1	
10	175,3	22,0	
11	178,8	22,0	
12	182,1	22,0	
13	186,7	21,9	
14	190,0	21,9	
15	195,2	21,9	
16	199,4	21,8	
17	201,9	21,8	
18	204,3	21,8	
19	206,6	21,7	
20	209,2	21,7	
21	211,0	21,6	
22	212,6	21,6	
23	215,0	21,6	
24	216,9	21,5	
25	218,0	21,5	
26	219,6	21,5	
27	220,9	21,4	
28	222,1	21,4	
29	224,2	21,4	
30	226,4	21,3	
30	226,4	21,367	
60	248,4	21,100	
90	258,9	20,800	
120	275,9	20,800	
150	283,6	20,800	
180	289,2	20,800	

Date	22.10.2013		
Soil	Middle sand - Fine gravel		
Mass of water [g]	3167,9	Water content w [wt%]	15,8
Mass of soil [g]	9939,8	Void ratio n [-]	0,298
FER	16,0	Density of soil [g/cm³]	1,860
	20	Saturated density [g/cm³]	2,153

Measurements

time [s]	Water outflow [g]	Position of foam front [cm]	
0	0,0	25,3	
1	60,0	22,0	
2	170,0	20,3	
3	236,0	19,8	
4	283,0	19,0	
5	320,0	18,6	
6	350,0	18,3	
7	365,0	18,0	
8	380,0	17,9	
9	396,0	17,8	
10	410,0	17,7	
11	425,0	17,6	
12	434,0	17,4	
13	441,0	17,2	
14	451,0	17,1	
15	462,0	17,0	
16	468,0	17,0	
17	474,0	16,9	
18	480,0	16,9	
19	486,0	16,9	
20	493,0	16,8	
21	497,0	16,7	
22	502,0	16,7	
23	508,0	16,6	
24	512,0	16,4	
25	516,0	16,2	
26	520,0	16,1	
27	524,0	16,1	
28	528,0	16,0	
29	530,0	16,0	
30	533,0	15,9	
30	533,0	15,633	
60	595,0	15,067	
90	627,0	14,667	
120	650,0	14,533	
150	669,0	14,167	
180	686,0	14,033	

Date	22.10.2013		
Soil	Fine sand - Fine gravel		
Mass of water [g]	3020,2	Water content w [wt%]	13,7
Mass of soil [g]	10341,5	Void ratio n [-]	0,270
FER	15,1	Density of soil [g/cm³]	1,935
	20	Saturated density [g/cm³]	2,201

Measurements

time [s]	Water outflow [g]	Position of foam front [cm]	
0	0,0	25,3	
1	18,0	24,4	
2	45,0	23,7	
3	95,0	23,0	
4	113,0	22,8	
5	139,0	22,8	
6	150,0	22,6	
7	161,0	22,5	
8	169,0	22,3	
9	177,0	22,1	
10	181,0	22,1	
11	187,0	22,0	
12	192,0	22,0	
13	197,0	21,9	
14	200,0	21,9	
15	204,0	21,9	
16	208,0	21,9	
17	210,0	21,9	
18	212,0	21,8	
19	215,0	21,8	
20	217,0	21,8	
21	220,0	21,8	
22	222,0	21,8	
23	224,0	21,8	
24	227,0	21,8	
25	228,0	21,8	
26	230,0	21,8	
27	232,0	21,8	
28	234,0	21,8	
29	235,0	21,7	
30	237,0	21,7	
30	237,0	21,333	
60	268,0	21,000	
90	287,0	20,833	
120	301,0	20,733	
150	313,0	20,700	
180	323,0	20,700	

Date	13.02.2014		
Soil	Fine sand - Fine gravel		
Mass of water [g]	3088,3	Water content w [wt%]	14,9
Mass of soil [g]	9994,5	Void ratio n [-]	0,277
FER	14,7	Density of soil [g/cm³]	1,916
	20	Saturated density [g/cm³]	2,201

Measurements

time [s]	Water outflow [g]	Position of foam front [cm]	
0	0,0	24,7	
1	50,0	21,9	
2	98,8	21,5	
3	113,8	21,2	
4	129,9	20,9	
5	149,9	20,8	
6	156,9	20,5	
7	163,8	20,4	
8	171,3	20,3	
9	176,9	20,3	
10	180,4	20,3	
11	185,5	20,2	
12	190,5	20,2	
13	193,9	20,2	
14	196,8	20,2	
15	198,8	20,1	
16	202,0	20,1	
17	204,9	20,1	
18	206,4	20,1	
19	208,8	20,1	
20	210,4	20,1	
21	212,9	20,1	
22	214,9	20,1	
23	216,9	20,1	
24	218,0	20,1	
25	218,9	20,1	
26	220,5	20,1	
27	221,5	20,1	
28	223,4	20,1	
29	224,4	20,1	
30	225,6	20,1	
30	225,6	20,933	
60	252,6	20,800	
90	269,9	20,800	
120	282,6	20,700	
150	293,5	20,633	
180	303,5	20,533	

Date	27.02.2014		
Soil	Fine sand - Fine gravel		
Mass of water [g]	3192,4	Water content w [wt%]	15,7
Mass of soil [g]	10149,7	Void ratio n [-]	0,281
FER	14,1	Density of soil [g/cm³]	1,907
	20	Saturated density [g/cm³]	2,206

Measurements

time [s]	Water outflow [g]	Position of foam front [cm]	
0	0,0	25,2	
1	16,4	23,6	
2	76,7	23,0	
3	119,2	22,6	
4	142,1	22,3	
5	161,8	22,1	
6	173,8	22,0	
7	184,1	21,9	
8	194,4	21,8	
9	201,3	21,7	
10	205,7	21,6	
11	210,8	21,5	
12	216,2	21,5	
13	220,8	21,5	
14	224,1	21,5	
15	227,0	21,4	
16	230,3	21,4	
17	232,9	21,4	
18	235,3	21,4	
19	237,6	21,3	
20	239,3	21,3	
21	241,6	21,3	
22	243,6	21,3	
23	245,5	21,3	
24	247,1	21,2	
25	249,8	21,2	
26	250,6	21,2	
27	252,1	21,2	
28	253,9	21,1	
29	254,2	21,1	
30	256,2	21,1	
30	256,2	21,067	
60	282,7	20,833	
90	299,1	20,633	
120	312,8	20,567	
150	324,4	20,500	
180	333,3	20,467	

A.2.3   Diagrams

A.2.3.1   Analysis of foam penetration tests
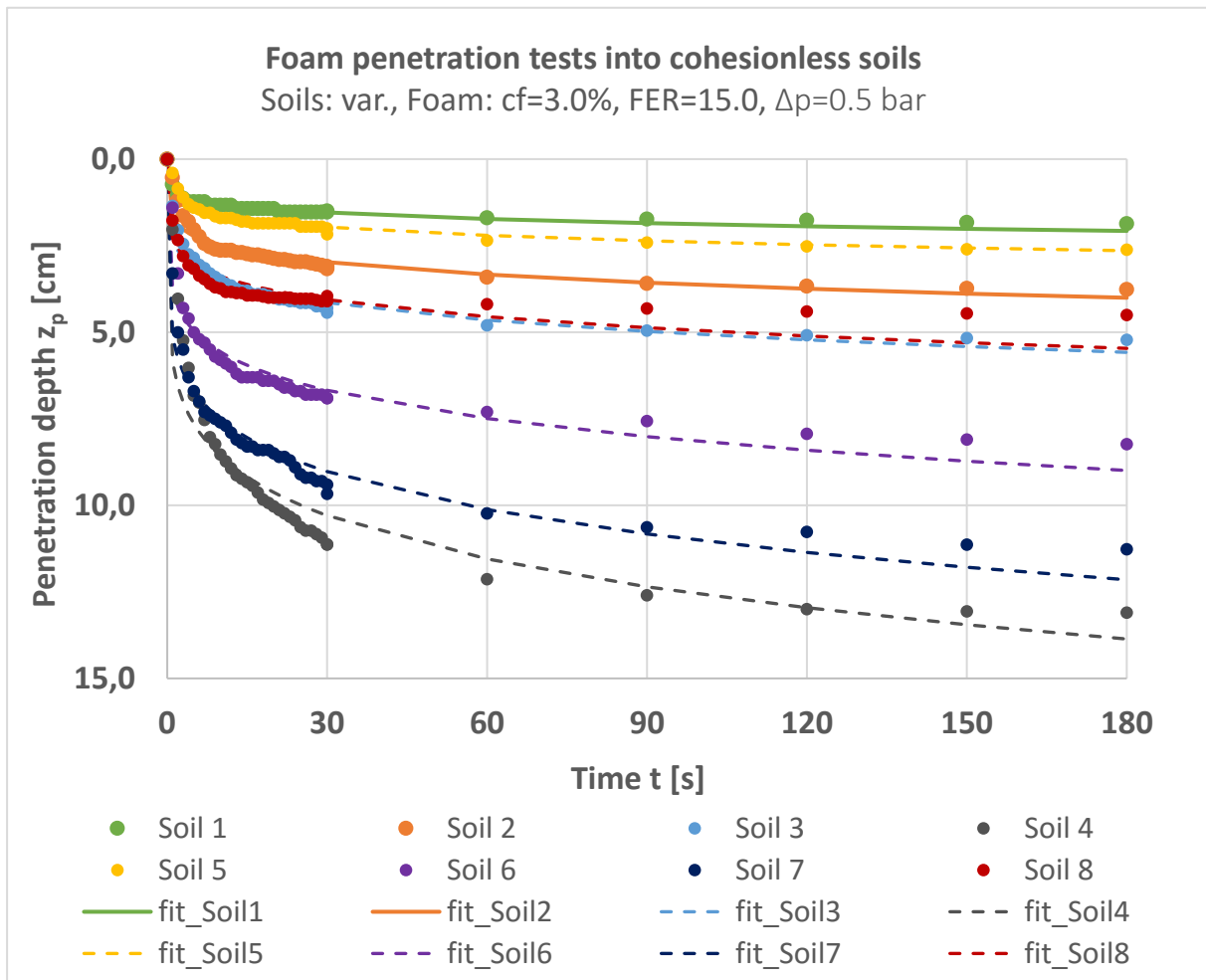
Figure A-2:   **Penetration depths of tunnelling foam into different cohesionless soils (data points) including reference soils 1 (green) and 2 (orange) and power-law functions (continuous lines) fitted to the data**
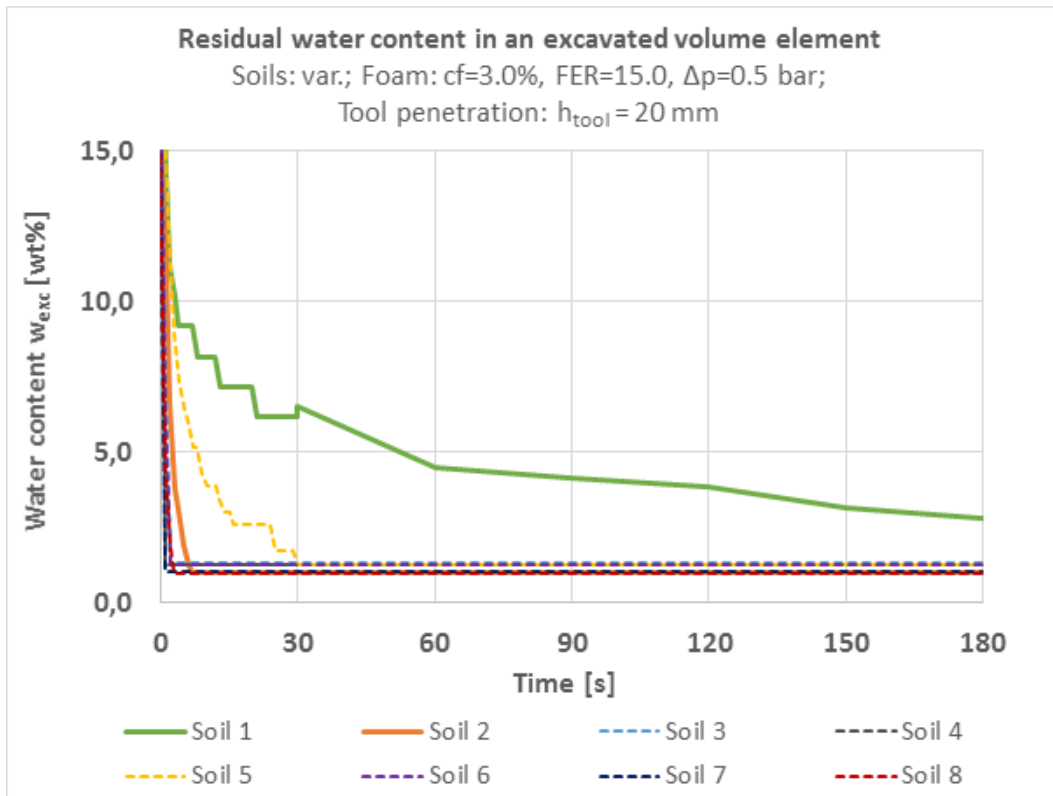
Figure A-3: Development of the water content of an excavated volume element based on foam penetration tests
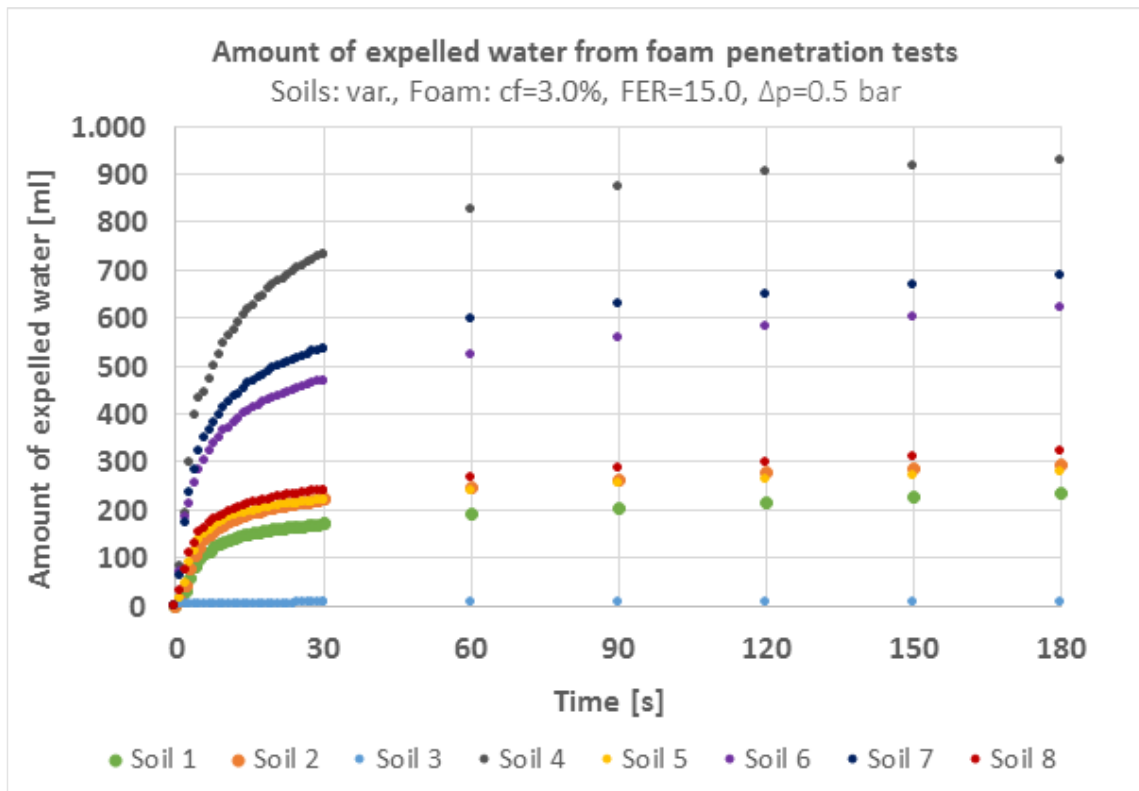
Figure A-4: Outflow rate of expelled water from foam penetration tests on different cohesionless soils including reference soils 1 (green) and 2 (orange)

A.2.3.2   Diagrams on correlations between regressor variables and soil parameters

Foam penetration tests into cohesionless soils
Correlation analysis of regressors and soil properties

$$a = 7.04 \cdot d_{30} + 0.24$$
$$R^2 = 0.983$$
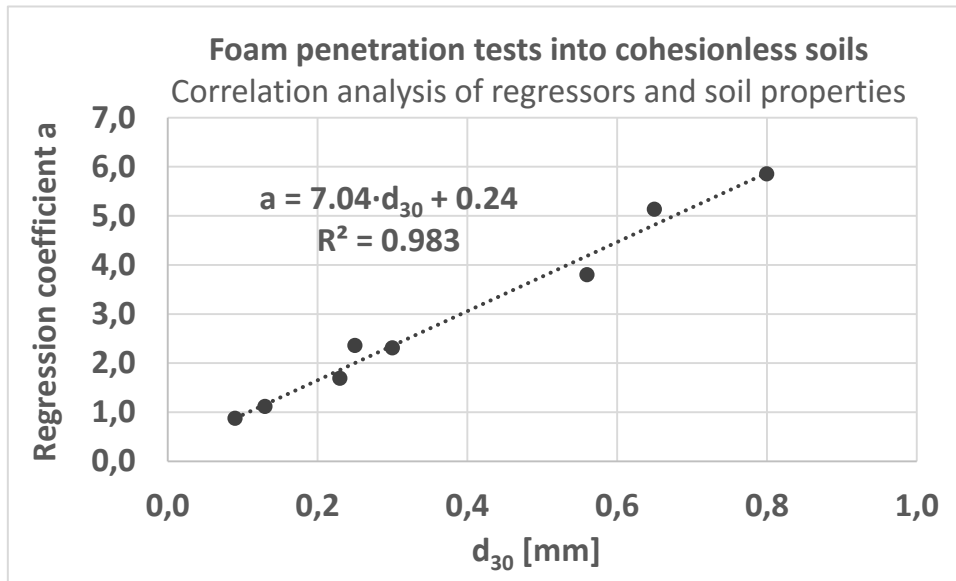
Figure A-5: Linear correlation of regressor a and representative grain diameters d_{30}

Foam penetration tests into cohesionless soils
Correlation analysis of regressors and soil properties

$$a = 0.047 \cdot S_m^{-0.92}$$
$$R^2 = 0.983$$
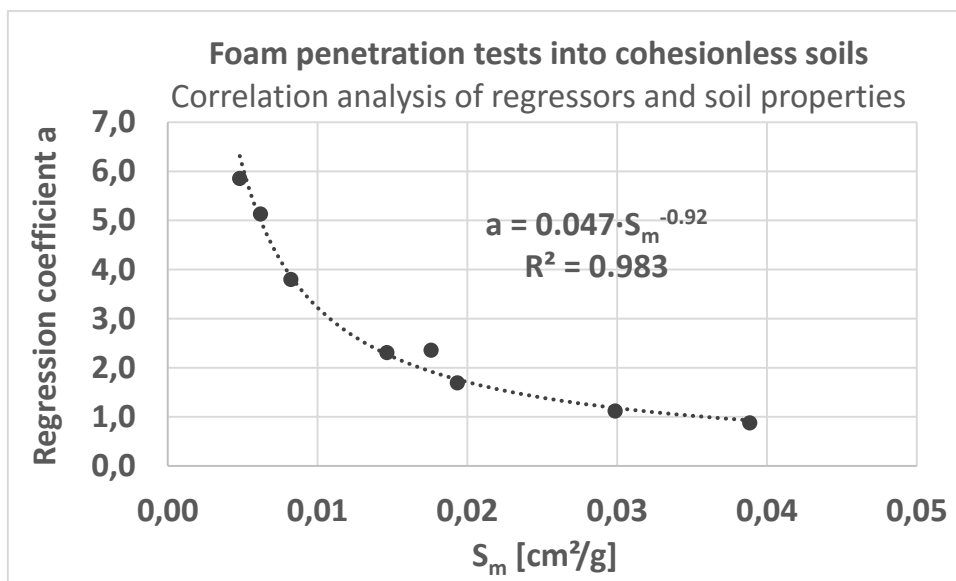
Figure A-6: Power-law correlation of regressor a and the mass-specific surface areas of the soils S_m

Foam penetration tests into cohesionless soils
Correlation analysis of regressors and soil properties

$a = -0.05x + 5.79$
$R^2 = 0.864$

Regression coefficient a

h_{co} [cm]
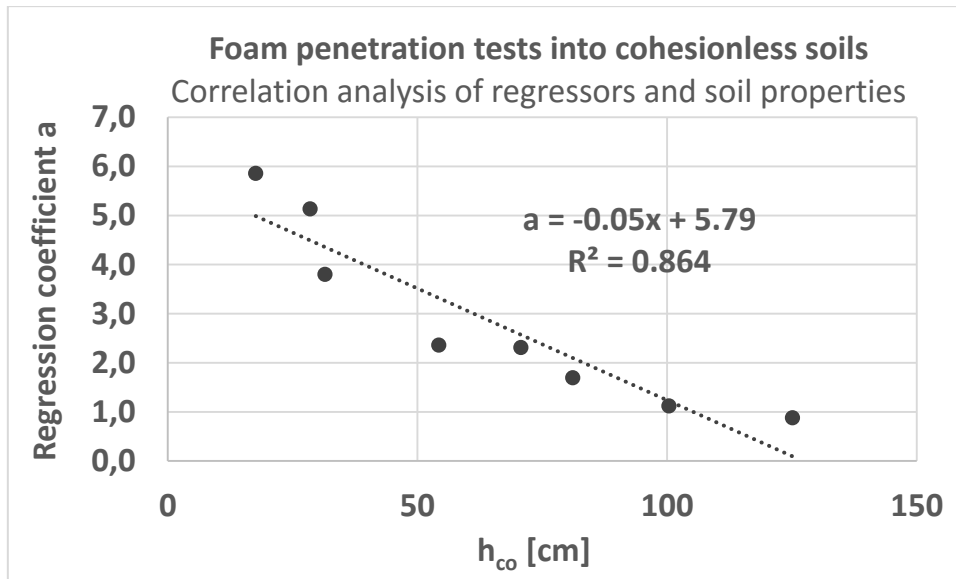
Figure A-7:   Linear correlation of regressor a and the equivalent capillary rise hco according to the "MK model", see section 5.3.1

A.2.3.3   Soil-water characteristic curves according to MK model
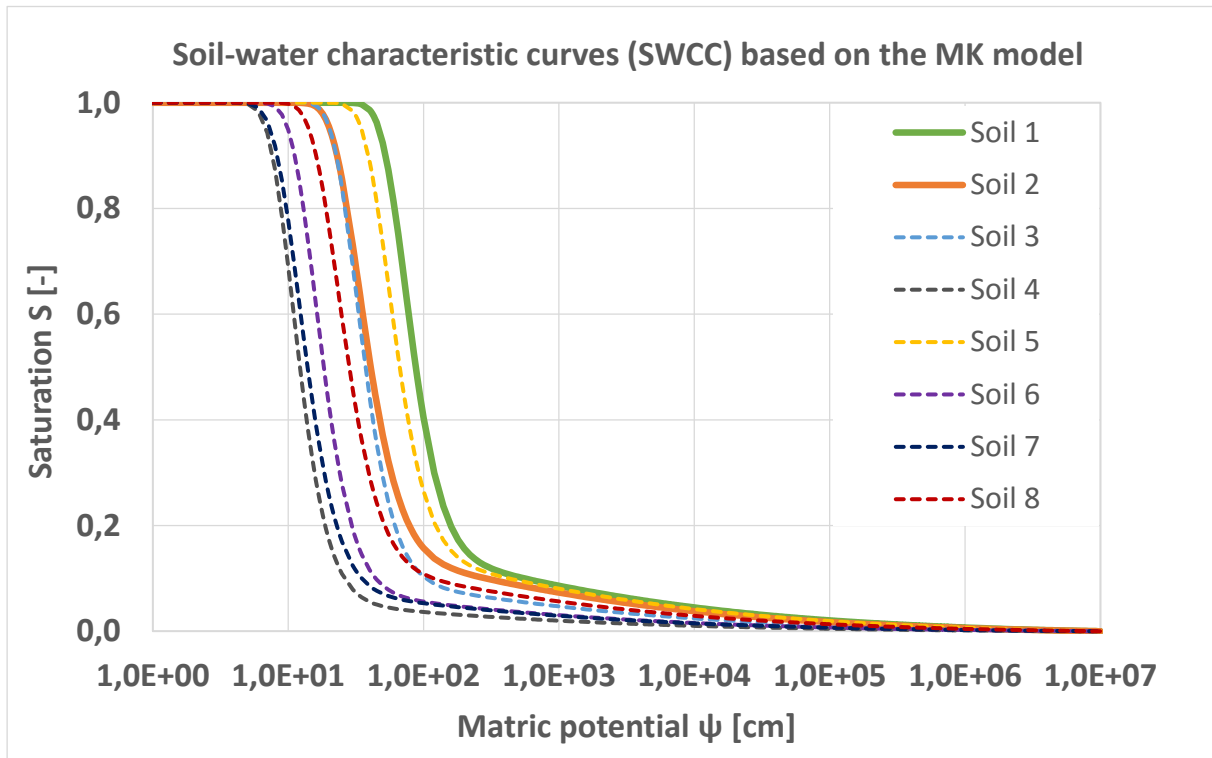
Figure A-8:   Soil-water characteristic curves determined with the MK model according to AUBERTIN ET AL. (2003) for all test soils
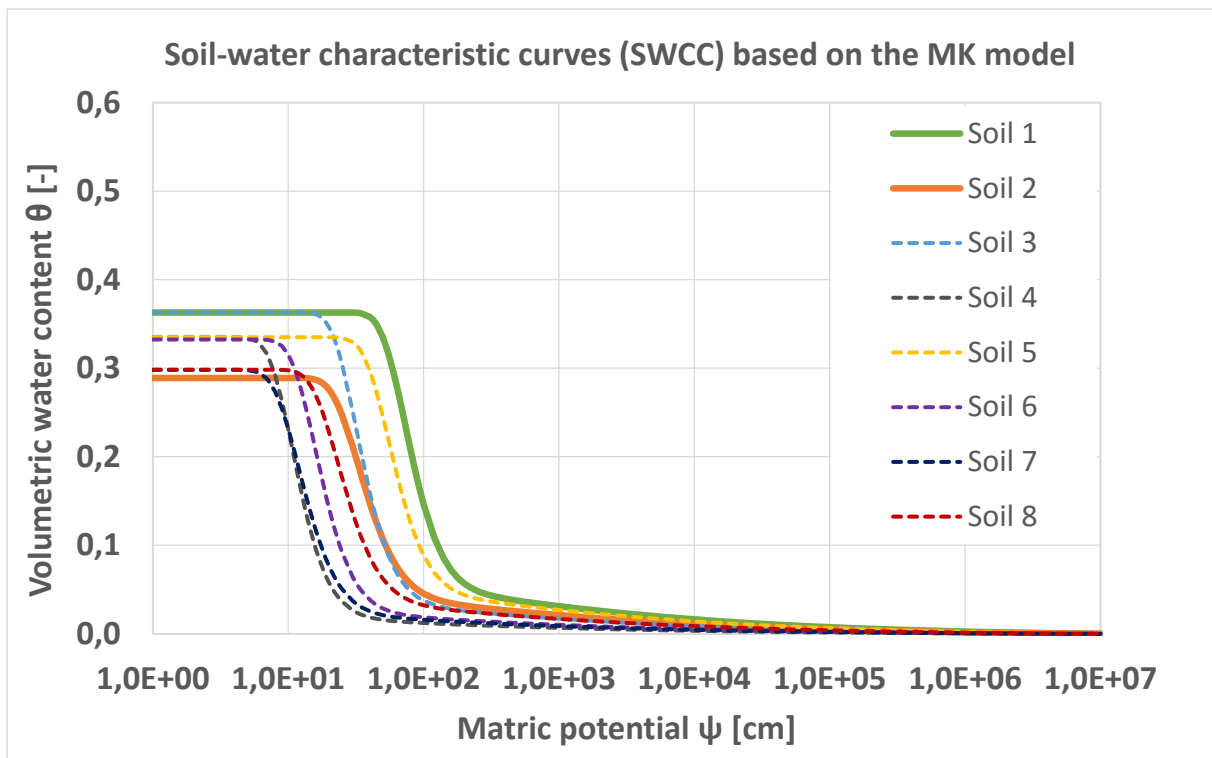
Figure A-9:   Water content-suction relationship determined with the MK model according to AUBERTIN ET AL. (2003) for all test soils

A.2.3.4 Development of water content considering foam penetration and residual water contents
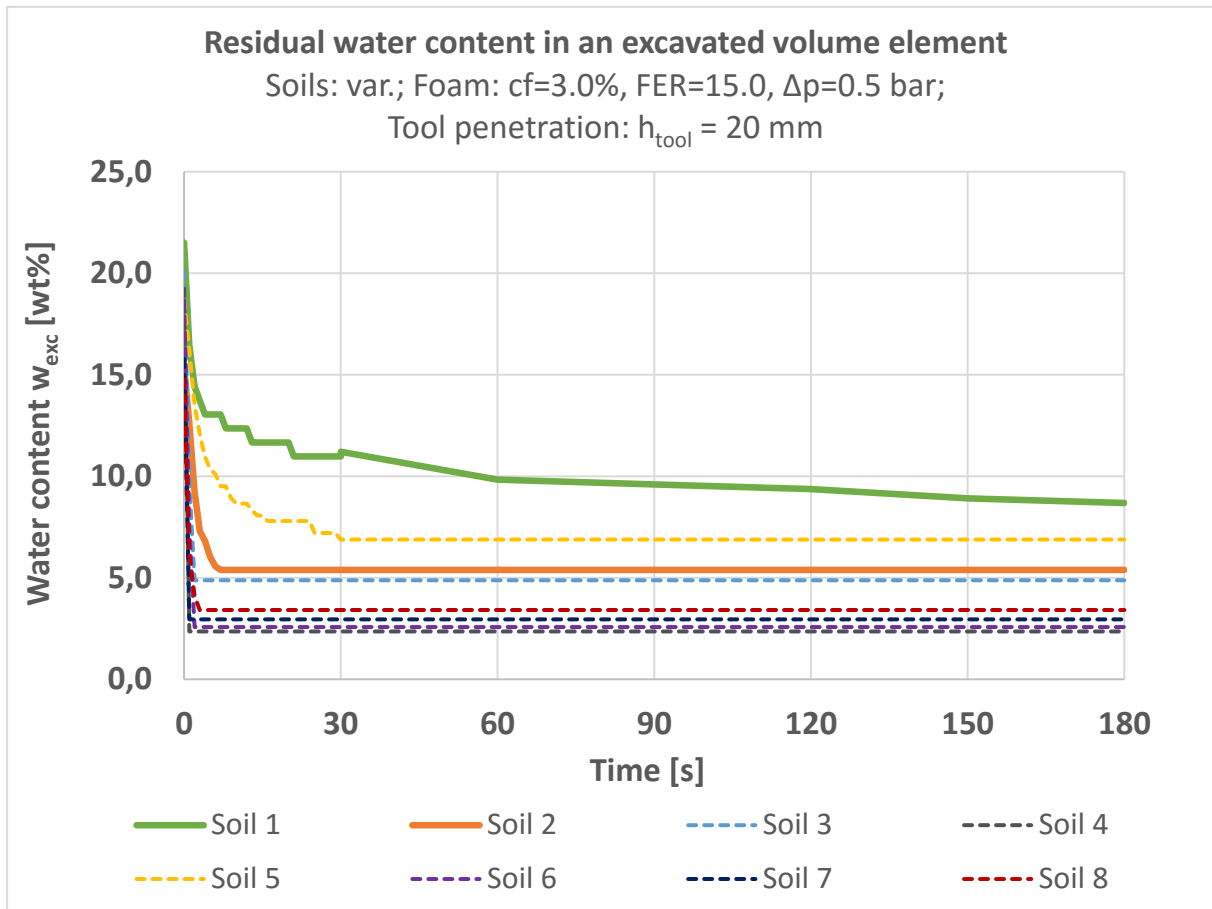
Figure A-10: Change in water content over time for volume elements composed of the different test soils 1 – 8 to be excavated by cutting tools with a penetration of 20 mm

A.3   Slump tests

A.3.1   Setup and testing procedure

<u>Test stand</u>
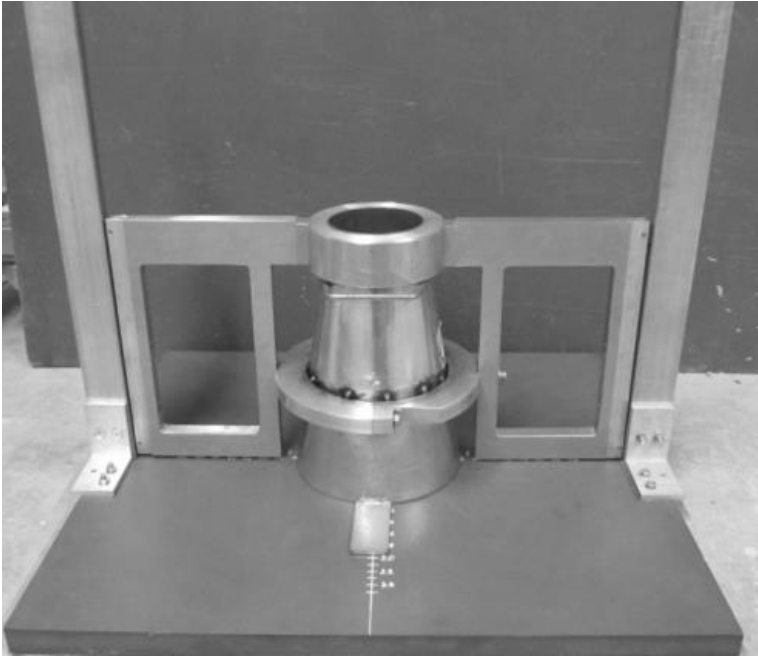
Figure A-11: Realised version of the modified slump test (GESING (2013))
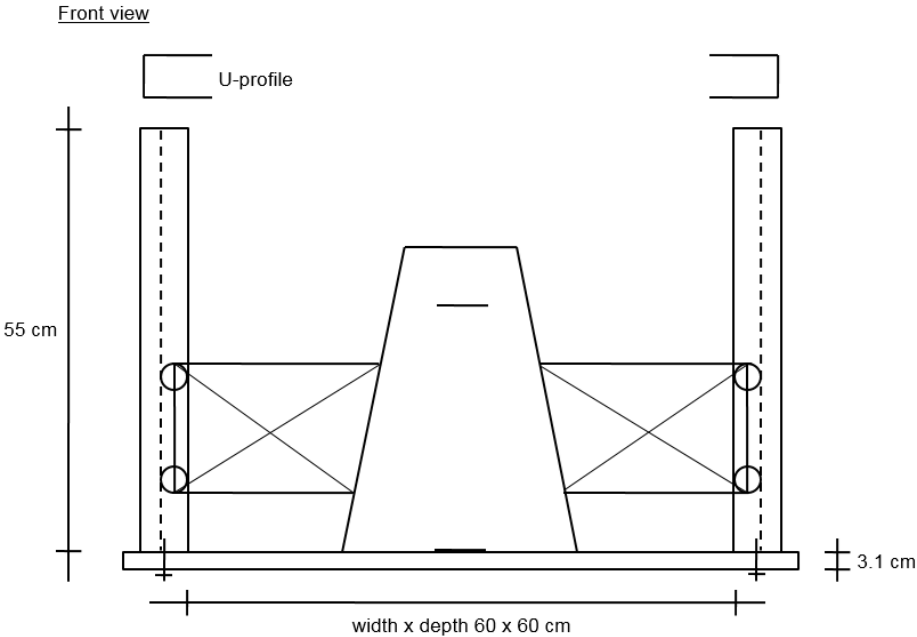
Figure A-12: Front view sketch of the modified slump test
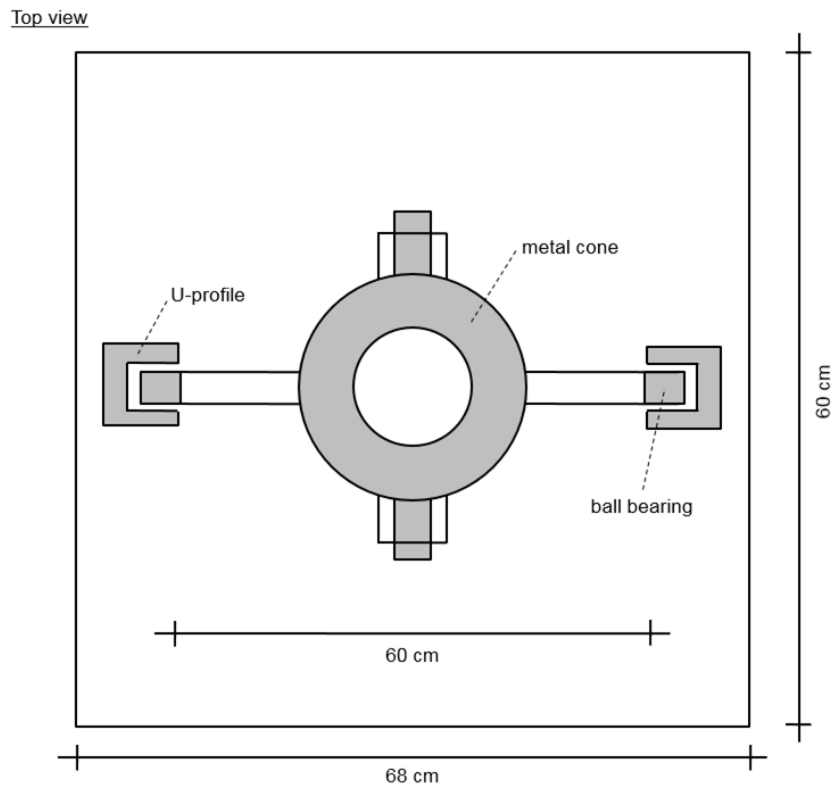
Figure A-13: Top view sketch of the modified slump test
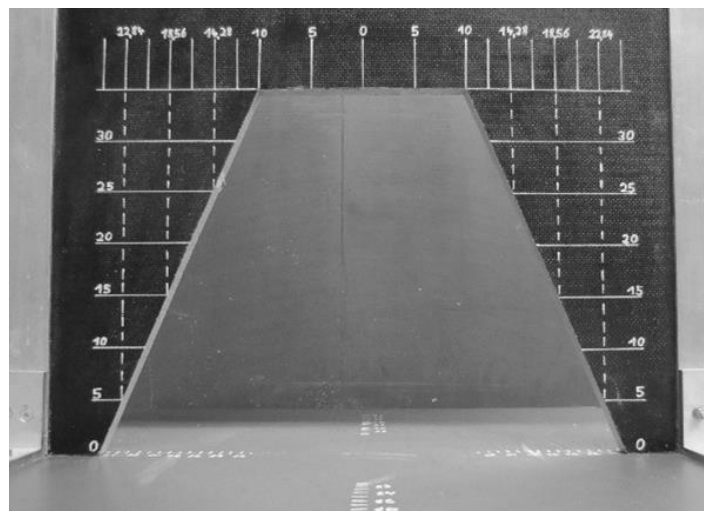
Figure A-14: Realised 2-d coordinate measuring plate for modified slump test
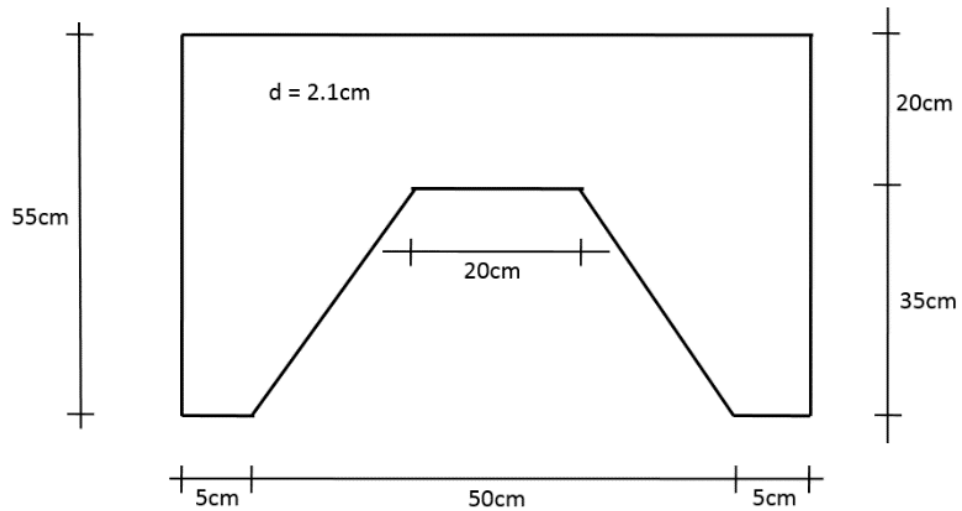
Figure A-15: Sketch of the 2-d coordinate plate

Equipment

- 1 Slump cone according to DIN EN 12350-2 (2009-08) or modified setup

- 1 Metal bar

- 1 Bottom plate (plane metal or plastic surface)

- 1 Bucket

- 1 Shovel

- 1 Rule

- 1 Ruler

- 1 Bucket with water and cloth

- 1 Digital camera with tripod

Preparations

1.   Place slump cone on bottom plate and load bottom ears with weights (standard test) or place slump cone in guide rails (modified test)

2.   Prepare soil-foam sample according to standard testing procedure (see section A.1) with 13 kg soil in a concrete bowl mixture (0:00 min)

3.   Mix for 15 seconds, then scrape adhering foam from mixer walls into the sample and mix again for 15 seconds

4.   Moist inner cone surfaces and bottom plate with water

5.   Fill sample into bucket and weigh sample mass

6.   Fill cone with sample material in 3 layers and compact each layer with metal bar by 25 hits within the layer

7.   Pull-off top surface with ruler to generate a planar sample surface which is flush with top cone edge

8.   Weigh remaining sample mass in the bucket, determine density in the cone

9.   Clean test stand from outside adhering material, start testing (8:30 min)

Procedure

10.   Pull slump cone at constant slow speed within 2 - 5 seconds (8:30 min)

11.   (Photograph from defined front position (8:50 min))

12.   Measure slump and slump flow values (9:20 - 9:50 min)

Remarks

Control time-steps sharply

A.3.2 Testing protocols

Date	Time	Test No.	Soil	Sample mass [g]	Density [g/cm³]	w [wt%]	FIR [%]	FER_{actual} [-]	Foam mass [g]	Slump [cm]	h_{01} [cm]	h_{02} [cm]	$h_{0,avg}$ [cm]	horizontal	vertical	Slump flow [cm]
04.02.2015	14:00	1	Fine sand	5898,4	1,07	12	100	14,7	463,9	24	0	0	0	44	44	44
04.02.2015	14:30	2	Fine sand	5987,3	1,09	12	100	15,1	451,7	24	0	0	0	40	44	42
18.02.2015	11:10	3	Fine sand	5699,9	1,04	12	100	14,4	487,2	24	0	0	0	44	46	45
09.02.2015	09:15	4	Fine sand	6335	1,15	12	90	15,1	408,8	24	0	0	0	38	40	39
18.02.2015	12:55	5	Fine sand	5969,7	1,09	12	90	14,5	435,4	24	0	0	0	42	41	41,5
18.02.2015	13:25	6	Fine sand	6098,3	1,11	12	90	15,1	419,6	23	0	0	0	40	43	41,5
09.02.2015	09:50	7	Fine sand	6787,3	1,23	12	80	14,1	386,8	19	0	0	0	33	36	34,5
18.02.2015	14:00	8	Fine sand	6274,5	1,14	12	80	14,8	380,5	22	0	0	0	38	41	39,5
18.02.2015	14:20	9	Fine sand	6270,6	1,14	12	80	15	373,9	22	0	0	0	39	41	40
09.02.2015	10:16	10	Fine sand	6795,9	1,24	12	80	14,4	355,2	19	0	0	0	31	32	31,5
19.02.2015	09:35	11	Fine sand	6475,8	1,18	12	75	14,9	354,8	20	0	0	0	35	38	36,5
19.02.2015	10:00	12	Fine sand	6547,6	1,19	12	75	14,8	355	20	0	0	0	33	36	34,5
09.02.2015	10:40	13	Fine sand	6764,3	1,23	12	70	15	318,5	19	0	0	0	33	34	33,5
09.02.2015	10:40	14	Fine sand	6564,1	1,19	12	70	14,8	331,7	20	0	0	0	32	35	33,5
19.02.2015	11:15	15	Fine sand	6549,3	1,19	12	70	14,7	333,9	20	0	0	0	33	34	33,5
09.02.2015	11:05	16	Fine sand	7104,1	1,29	12	60	15,4	266,5	13	2	3	2,5	26	28	27
19.02.2015	12:45	17	Fine sand	7007,4	1,27	12	60	14,9	283,3	14	3	2,5	2,75	25	28	26,5
13.02.2015	13:10	18	Fine sand	6904,1	1,26	12	60	15,2	278,2	14	4	4	4	27	29	28
09.02.2015	13:30	19	Fine sand	7115,6	1,29	12	55	15	250,7	13	4	2	3	24	28	26
19.02.2015	13:40	20	Fine sand	7095,6	1,29	12	55	14,8	260,6	11	6	6	6	23	26	24,5
19.02.2015	14:00	21	Fine sand	6962,9	1,27	12	55	15,2	254,5	13	6	3	4,5	26	29	27,5
09.02.2015	14:02	22	Fine sand	7552,7	1,37	12	50	14,9	229,2	6	6	7	6,5	22	20	21
19.02.2015	14:35	23	Fine sand	7152,8	1,30	12	50	15,2	231,8	9	8	7	7,5	24	26	25
20.02.2015	09:20	24	Fine sand	7271,9	1,32	12	50	15	233,8	6	6	7	6,5	21	23	22
09.02.2015	14:47	25	Fine sand	6204,7	1,13	10	100	14,4	474,7	23	0	0	0	38	40	39
20.02.2015	09:45	26	Fine sand	5639,9	1,03	10	100	15,3	459,7	23	0	0	0	43	44	43,5
20.02.2015	10:10	27	Fine sand	5782,9	1,05	10	100	15,3	458,8	23	0	0	0	40	41	40,5
10.02.2015	09:15	28	Fine sand	6476,4	1,18	10	90	14,5	424	20	0	0	0	32	35	33,5
10.02.2015	10:35	29	Fine sand	5992,9	1,09	10	90	15,3	412,2	23	0	0	0	38	41	39,5
20.02.2015	11:10	30	Fine sand	6048,5	1,10	10	90	15,3	412,9	23	0	0	0	39	39	39
10.02.2015	09:40	31	Fine sand	6601,1	1,20	10	80	14,8	369,6	19	0	0	0	30	33	31,5
14.01.2015		32	Fine sand		0,00	10	80	15,7	348,5	18	0	0	0	32	32	32
20.02.2015	11:45	33	Fine sand	6372,6	1,16	10	80	15,1	372,2	21	0	0	0	34	34	34
10.02.2015	10:20	34	Fine sand	6508	1,18	10	70	14,9	321,4	18	0	0	0	30	32	31
23.02.2015	10:55	35	Fine sand	6730,5	1,22	10	70	15,4	320,2	15	3	3	3	28	28	28
23.02.2015	11:15	36	Fine sand	6756,4	1,23	10	70	15,2	323	15	3	2	2,5	28	29	28,5
10.02.2015	10:45	37	Fine sand	6740,9	1,23	10	70	14,6	281,5	16	2	2	2	28	30	29
14.01.2015		38	Fine sand		0,00	10	60	15,7	260,7	10	6	6,5	6,25	25	26	25,5
19.01.2015		39	Fine sand		0,00	10	60	15,4	266,7	10	6	5	5,5	23	25	24
19.01.2015		zusätzlich	Fine sand		0,00	10	60	15,6	263,2	12	6	4	5	24	26	25
26.03.2015	09:40	39 b	Fine sand	6809,3	1,24	10	50	15	281,1	10	4,5	3	3,75	26	26	26
10.02.2015	11:15	40	Fine sand	7155,6	1,30	10	50	14,8	230,6	6	10	12	11	21	24	22,5
11.02.2015	11:40	41	Fine sand		0,00	10	50	15,3	229,8	3,5	9	11	10	20	21	20,5
23.02.2015	12:15	42	Fine sand	7171,8	1,30	10	50	15,3	229,8	4	12	12	12	21	22	21,5

Date	Time	Test No.	Soil	Sample mass [g]	Density [g/cm³]	w [wt%]	FIR [%]	FER_{actual} [-]	Foam mass [g]	Slump [cm]	h_{01} [cm]	h_{02} [cm]	$h_{0,avg}$ [cm]	Slump flow horizontal	Slump flow vertical	Slump flow [cm]
10.02.2015	11:55	43	Fine sand	5878,6	1,07	8	100	15,1	454,5	22	0	0	0	38	39	38,5
23.02.2015	13:50	44	Fine sand	5761,8	1,05	8		15,6	451,4	20	0	0	0	37	38	37,5
23.02.2015	14:30	45	Fine sand	5811,6	1,06	8		15,1	464,2	21	0	0	0	37	39	38
10.02.2015	13:40	46	Fine sand	5872	1,07	8	90	14	440,2	22	0	0	0	37	40	38,5
23.02.2015	15:10	47	Fine sand	6033,5	1,10	8		14,9	425,5	21	0	0	0	36	37	36,5
24.02.2015	09:15	48	Fine sand	6067,9	1,10	8		15,6	406	20	0	0	0	34	37	35,5
10.02.2015	14:05	49	Fine sand	6741,2	1,23	8	80	15,2	361,1	13	6	6	6	25	28	26,5
24.02.2015	09:45	50	Fine sand	6415,5	1,17	8		15,4	365,2	17	2	2,5	2,25	30	30	30
24.02.2015	10:05	51	Fine sand	6422,4	1,17	8		15,5	362,5	17	2	3	2,5	30	30	30
26.03.2015	09:05	51 b	Fine sand	6406,5	1,17	8		15	374,5	15	3,5	4	3,75	29	30	29,5
10.02.2015	14:30	52	Fine sand	6763,3	1,23	8	70	14,1	339,8	13	5	3	4	26	28	27
24.02.2015	10:25	53	Fine sand	6542,6	1,19	8		15,2	324,1	15	6	3	4,5	28	27	27,5
24.02.2015	10:55	54	Fine sand	6689,7	1,22	8		15,2	323,7	13	4	3	3,5	26	28	27
11.02.2015	09:00	55	Fine sand	7174,4	1,30	8	60	15,1	272,7	6	6	5	5,5	22	23	22,5
24.02.2015	11:20	56	Fine sand	6966,3	1,27	8		15,4	274,6	7	5	6	5,5	22	23	22,5
24.02.2015	11:40	57	Fine sand	6910,8	1,26	8		15,1	279	8	5	6	5,5	22	23	22,5
11.02.2015	09:50	58	Fine sand	7162,6	1,30	8	50	15,2	225,6	4	13	14	13,5	22	22	22
24.02.2015	12:00	59	Fine sand	7342,5	1,34	8		15,3	229	2	19	14	16,5	20	20	20
24.02.2015	13:55	60	Fine sand	7214,4	1,31	8		15,2	231,5	2,5	14,5	6,5	10,5	21	21	21
11.02.2015	10:30	61	Fine sand	5969,3	1,09	6	100	15,6	439,8	21	0	0	0	35	36	35,5
24.02.2015	14:35	62	Fine sand	5711	1,04	6		15	467	21	0	0	0	36	38	37
25.02.2015	09:20	63	Fine sand	5873,3	1,07	6		15,2	463,1	20	0	0	0	34	36	35
11.02.2015	11:00	64	Fine sand	6098,6	1,11	6	90	14,6	420,7	20	0	0	0	33	33	33
25.02.2015	09:50	65	Fine sand	6136,1	1,12	6		15,2	417	17	0	0	0	32	33	32,5
11.02.2015	10:10	66	Fine sand	6048,9	1,10	6		14,9	425,2	19	0	0	0	36	35	35,5
11.02.2015	11:25	67	Fine sand	6410,4	1,17	6	80	15,3	358	16	3	3	3	29	30	29,5
25.02.2015	10:30	68	Fine sand	6366,5	1,16	6		14,9	376,1	15	2,5	3	2,75	29	30	29,5
25.02.2015	10:55	69	Fine sand	6407,4	1,17	6		15,2	368,9	14	4	4	4	27	29	28
11.02.2015	13:40	70	Fine sand	6734	1,22	6	70	14,4	331,9	10	6	5	5,5	25	26	25,5
25.02.2015	11:15	71	Fine sand	6639,5	1,21	6		14,8	332,7	10	4	4	4	24	25	24,5
11.02.2015	11:40	72	Fine sand	6737,3	1,23	6		14,9	330,9	10	5	6	5,5	24	24	24
14.02.2015	14:05	73	Fine sand	6870,4	1,25	6	60	14,6	281	7	10	12	11	23	24	23,5
25.02.2015	12:05	74	Fine sand	7057,1	1,28	6		15,2	277,2	4	12	12	12	22	23	22,5
25.02.2015	14:20	75	Fine sand	6864,2	1,25	6		14,7	286,7	6	10	10	10	22	22	22
11.02.2015	14:30	76	Fine sand	7200,2	1,31	6	50	14,7	233,5	2	13	19	16	21	22	21,5
25.02.2015	14:55	77	Fine sand	7279,5	1,32	6		14,9	235,5	4	12	12	12	22	22	22
04.03.2015	14:40	78	Fine sand		0,00	6		14,7	238,8	2,5	15,5	16,5	16	20	20	20
12.02.2015	09:00	79	Fine sand	5889,6	1,07	4	100	15	457,2	21	2	2	2	34	34	34
05.03.2015	09:15	80	Fine sand	5891,8	1,07	4		14,5	483,5	18	1	1	1	31	34	32,5
05.03.2015	09:35	81	Fine sand	5727,9	1,04	4		14,6	479,8	19	0,5	0,5	0,5	32	33	32,5
12.02.2015	09:25	82	Fine sand	6112,2	1,11	4	90	14,5	426	18	4	3	3,5	31	31	31
05.03.2015	09:55	83	Fine sand	6153,5	1,12	4		15	421,4	14	2	0	1	27	30	28,5
05.03.2015	10:20	84	Fine sand	6059,6	1,10	4		14,8	428	16	4	4	4	30	30	30

Date	Time	Test No.	Soil	Sample mass [g]	Density [g/cm³]	w [wt%]	FIR [%]	FER_actual [-]	Foam mass [g]	Slump [cm]	h_{01} [cm]	h_{02} [cm]	h_{0,avg} [cm]	horizontal	vertical	Slump flow [cm]
12.02.2015	09:45	85	Fine sand	6537,5	1,19	4	80	14,8	370	11	7	7	7	25	26	25,5
05.03.2015	10:40	86	Fine sand	6480,3	1,18	4		14,8	379,1	9	8	7	7,5	24	25	24,5
05.03.2015	11:15	87	Fine sand	6454,8	1,17	4		14,8	380,7	10	6	6	6	25	26	25,5
12.02.2015	10:08	88	Fine sand	6849,3	1,25	4	70	15	318,3	8	11	12	11,5	25	26	25,5
05.03.2015	11:40	89	Fine sand	7041,1	1,28	4		14,8	332,1	1,5	28,5	10	19,25	20	21	20,5
05.03.2015	12:00	90	Fine sand	6848,8	1,25	4		14,7	334,7	5	10	8	9	22	22	22
26.03.2015	10:20	90 b	Fine sand	6836,9	1,24	4		15,3	322,4	2,5	13,5	13,5	13,5	21	21	21
12.02.2015	10:30	91	Fine sand	7210,3	1,31	4	60	14,7	280,2	1,5	28,5	20,5	24,5	20	20	20
05.03.2015	13:55	92	Fine sand	6990,2	1,27	4		14,8	284,3	1	17	18	17,5	20	20	20
05.03.2015	14:20	93	Fine sand	7232,2	1,32	4		14,9	282,4	1	22	21	21,5	20	20	20
26.03.2015	10:55	93 b	Fine sand	7107	1,29	4		15,3	275,1	0,5	28,5	28,5	28,5	20	20	20
12.02.2015	10:55	97	Fine sand	5967	1,09	2	100	14,8	462,8	17	4	3	3,5	29	31	30
05.03.2015	14:40	98	Fine sand	5970,9	1,09	2		14,7	476,7	15	5	4	4,5	29	30	29,5
06.03.2015	09:20	99	Fine sand	5965,5	1,09	2		14,5	48437	14	6	4	5	29	30	29,5
12.02.2015	11:25	100	Fine sand	6234,2	1,13	2	90	14,8	416,5	14	4	5	4,5	26	28	27
06.03.2015	09:45	101	Fine sand	6227,4	1,13	2		14,6	432,6	11	5	4	4,5	26	26	26
06.03.2015	10:10	102	Fine sand	6224,2	1,13	2		14,6	431,9	11	10	9	9,5	26	26	26
12.02.2015	13:20	103	Fine sand	6537,3	1,19	2	80	14,9	367,8	8	10	8	9	23	24	23,5
06.03.2015	10:25	104	Fine sand	6596,4	1,20	2		14,9	377,3	4	11	11	11	23	22	22,5
06.03.2015	10:50	105	Fine sand	6496,2	1,18	2		14,6	385,9	5	14	8	11	23	22	22,5
12.02.2015	13:55	106	Fine sand	7071,5	1,29	2	70	14,9	321	1	29	29	29	20	20	20
06.03.2015	11:15	107	Fine sand	6954,7	1,26	2		14,5	339,7	1	21	22	21,5	20	20	20
06.03.2015	11:40	108	Fine sand	7086,8	1,29	2		14,6	337,7	1	26	15	20,5	20	20	20
12.02.2015	14:25	112	Sand	7554,4	1,37	12	50	14,4	237,2	26	0	0	0	56	57	56,5
26.02.2015	10:15	113	Sand	7507,1	1,37	12		14,6	247	26	0	0	0	52	56	54
26.02.2015	10:55	114	Sand	7434,7	1,35	12		14,9	242,5	26	0	0	0	52	54	53
27.03.2015	09:40	114 b	Sand	7443,6	1,35	12		14,2	253,6	26	0	0	0	52	54	53
13.02.2015	09:45	115	Sand	8116,2	1,48	12	40	15,1	180,9	24	0	0	0	42	45	43,5
26.02.2015	14:45	116	Sand	7905,6	1,44	12		14,9	193,3	23	0	0	0	45	40	42,5
26.02.2015	13:05	117	Sand	7985,7	1,45	12		14,9	193,3	24	0	0	0	42	46	44
13.02.2015	10:10	118	Sand	8394,2	1,53	12	30	15,9	129	20	0	0	0	32	34	33
13.02.2015	13:30	119	Sand	8288,2	1,51	12		15,2	142,8	20	0	0	0	34	36	35
26.02.2015	14:10	120	Sand	8253,4	1,50	12		15	144,8	21	0	0	0	35	37	36
13.02.2015	10:30	121	Sand	8578,7	1,56	12	20	15,7	87,2	15	1	0	0,5	24	25	24,5
26.02.2015	14:40	122	Sand	8444,5	1,54	12		15,1	95,8	17	0	0	0	26	28	27
26.02.2015	14:55	123	Sand	8535,7	1,55	12		15,2	95,3	16	0	0	0	26	27	26,5
13.02.2015	10:50	124	Sand	8724,9	1,59	12	10	15,1	45,3	6	11,5	5	8,25	22	22	22
27.02.2015	09:25	125	Sand	8771,7	1,60	12		15	48,1	4	7	7	7	21	21	21
27.02.2015	09:45	126	Sand	8625,8	1,57	12		15,1	47,7	6	6	6	6	22	22	22
13.02.2015	11:15	127	Sand	7531,6	1,37	10	50	15,1	239,1	26	0	0	0	49	51	50
27.02.2015	10:10	128	Sand	7462,8	1,36	10		15,2	237,5	25	0	0	0	50	55	52,5
27.02.2015	10:35	129	Sand	7406,9	1,35	10		15	240,2	26	0	0	0	53	53	53
27.03.2015	10:10	129 b	Sand	7462,5	1,36	10		14,5	249,2	25	0	0	0	50	54	52

Date	Time	Test No.	Soil	Sample mass [g]	Density [g/cm³]	w [wt%]	FIR [%]	FER$_{actual}$ [-]	Foam mass [g]	Slump				Slump flow		
										Slump [cm]	h$_{o1}$ [cm]	h$_{o2}$ [cm]	h$_{0,avg}$ [cm]	horizontal	vertical	Slump flow [cm]
16.02.2015	09:05	130	Sand	7970,3	1,45	10	40	15,2	190,5	24	0	0	0	39	41	40
27.02.2015	11:00	131	Sand	7826,1	1,42	10		14,7	197,2	24	0	0	0	43	41	42
27.02.2015	11:40	132	Sand	7819,9	1,42	10		14,2	203,6	24	0	0	0	43	45	44
16.02.2015	09:30	133	Sand	8128,8	1,48	10		14,9	145,8	22	1	1	1	35	37	36
15.01.2015		134	Sand		0,00	10	30	15,9	128,8	20	2	0	1	31	32	31,5
29.01.2015		135	Sand		0,00	10		15,3	134,1	20	0	0	0	30	34	32
29.01.2015		zusätzlich	Sand		0,00	10		15	137,1	20	1	0	0,5	32	34	33
16.02.2015	09:50	136	Sand	8409	1,53	10	20	15,5	93	13	3	3	3	24	26	25
15.01.2015	12:05	137	Sand		0,00	10		15,7	87,4	14	3	4	3,5	24	26	25
02.03.2015	09:30	138	Sand	8353,8	1,52	10		15	96,5	13	3	3	3	24	26	25
16.02.2015	10:15	139	Sand	8695,4	1,58	10	10	15,2	47,4	2,5	15	12,5	13,75	22	22	22
15.01.2015	10:25	140	Sand		0,00	10		16,2	42,2	1	14	16	15	20	20	20
02.03.2015	09:55	141	Sand	8742,7	1,59	10		15,1	47,9	2	10	11	10,5	20	21	20,5
16.02.2015	10:45	142	Sand	7621	1,39	8	50	15,4	234,9	25	0	0	0	44	45	44,5
02.03.2015	10:15	143	Sand	7542,9	1,37	8		14,7	245	24	0	0	0	43	47	45
02.03.2015	10:40	144	Sand	7537,8	1,37	8		14,7	243,4	24	0	0	0	45	46	45,5
16.02.2015	11:10	145	Sand	7862,2	1,43	8	40	15,6	175,6	25	0	0	0	36	38	37
02.03.2015	11:00	146	Sand	7816	1,42	8		15	192,5	23	0	0	0	38	40	39
02.03.2015	11:20	147	Sand	7762,3	1,41	8		15,2	190,3	23	0	0	0	39	39	39
17.02.2015	09:40	148	Sand	8060,8	1,47	8	30	15	144,1	18	3	2,5	2,75	30	32	31
02.03.2015	11:45	149	Sand	7936,4	1,44	8		14,8	146,4	20	1	0,5	0,75	31	33	32
02.03.2015	13:40	150	Sand	7857,4	1,43	8		14,7	147,1	20	0	0	0	33	35	34
17.02.2015	10:00	151	Sand	8325,8	1,51	8	20	14,9	96,9	9	4	6	5	22	22	22
02.03.2015	14:15	152	Sand	8212,1	1,49	8		14,7	98,3	10	6	5	5,5	23	23	23
03.03.2015	09:15	153	Sand	8265,1	1,50	8		14,1	102,7	13	2,5	3	2,75	23	25	24
17.02.2015	10:30	154	Sand		0,00	8	10	14,9	48,6	0,5	17,5	21,5	19,5	20	20	20
03.03.2015	09:35	155	Sand	8756,7	1,59	8		14,5	49,9	0	30	30	30	20	20	20
03.03.2015	10:00	156	Sand	8532,2	1,55	8		14,7	49	0,5	21,5	21,5	21,5	20	20	20
17.02.2015	10:55	157	Sand	7644,9	1,39	6	50	15,1	239,4	24	0	0	0	39	40	39,5
03.03.2015	10:25	158	Sand	7477,2	1,36	6		14,7	245,9	24	0	0	0	42	44	43
03.03.2015	10:45	159	Sand	7426	1,35	6		14,8	243,5	24	0	0	0	42	44	43
28.01.2015	13:40	zusätzlich	Sand	7762,6	1,41	6	45	14,9	207,3	22	0	0	0	37	38	37,5
28.01.2015	14:05	zusätzlich	Sand	7799,4	1,42	6		14,8	208,6	21	2	1	1,5	36	36	36
04.02.2015	11:05	zusätzlich	Sand	7749,6	1,41	6		14,7	208,9	23	0	0	0	38	38	38
04.02.2015	11:35	160	Sand	7904,9	1,44	6	42	15,5	185,8	20	1	0,5	0,75	33	34	33,5
04.02.2015	11:55	161	Sand	7895	1,44	6		14,8	194,5	21	1,5	0,5	1	36	36	36
04.02.2015	12:15	162	Sand	7881,8	1,43	6		15,2	189,4	20	1	0,5	0,75	34	34	34
17.02.2015	12:25	163	Sand		0,00	6	40	15	192,2	21	0	0	0	34	36	35
15.01.2015	16:00	164	Sand		0,00	6		15,3	178,5	20	0	0	0	33	36	34,5
26.01.2015	11:15	165	Sand		0,00	6		15,7	174,5	15	3	1,5	2,25	31	31	31
26.01.2015	11:50	zusätzlich	Sand		0,00	6		15,4	177,4	15	4	3,5	3,75	30	30	30
27.03.2015	10:25	165 b	Sand	7858,7	1,43	6		14,9	194,2	21	0	0	0	34	35	34,5

Date	Time	Test No.	Soil	Sample mass [g]	Density [g/cm³]	w [wt%]	FIR [%]	FER$_{actual}$ [-]	Foam mass [g]	Slump [cm]	h$_{01}$ [cm]	h$_{02}$ [cm]	h$_{0,avg}$ [cm]	horizontal	vertical	Slump flow [cm]
28.01.2015	13:15	166	Sand	8134,2	1,48	6	30	15,2	134,8	10	3,5	4	3,75	24	27	25,5
26.01.2015	13:50	167	Sand		0,00	6		16,1	127,5	10	4	4	4	24	26	25
26.01.2015	13:00	168	Sand		0,00	6		16,7	122,7	12	4	3,5	3,75	26	27	26,5
15.01.2015	14:25	zusätzlich	Sand		0,00	6		15,9	128,8	12	3,5	3,5	3,5	26	27	26,5
27.03.2015	10:50	168 b	Sand	8009,1	1,46	6		15,3	141,6	14	3	2	2,5	27	29	28
17.02.2015	12:45	169	Sand	8358,7	1,52	6	20	15,2	94,9	4	10	10	10	21	22	21,5
03.03.2015	11:10	170	Sand	8254,3	1,50	6		14,8	97,6	6	8	6	7	22	22	22
03.03.2015	11:35	171	Sand	8226,7	1,50	6		14,7	98,5	7	6	6	6	21	22	21,5
17.02.2015	13:10	172	Sand	7672,8	1,40	4		15	241	21	0	0	0	35	37	36
03.03.2015	12:00	173	Sand	7548,8	1,37	4	50	14,6	247	23	0	0	0	39	39	39
03.03.2015	13:40	174	Sand	7593,4	1,38	4		15,1	239,4	23	0	0	0	38	39	38,5
17.02.2015	13:30	175	Sand	7772,7	1,41	4		14,7	196,4	18	3,5	2	2,75	31	34	32,5
03.03.2015	14:00	176	Sand	7835,8	1,43	4	40	15,1	191,5	17	1,5	1,5	1,5	31	32	31,5
03.03.2015	14:25	177	Sand	7730,2	1,41	4		14,6	197,9	19	1,5	1,5	1,5	33	34	33,5
17.02.2015	13:55	178	Sand	8069,4	1,47	4	30	15,3	141,8	9	6	7	6,5	25	24	24,5
03.03.2015	14:45	179	Sand	8013,2	1,46	4		14,7	147,2	10	6	6	6	24	26	25
04.03.2015	09:10	180	Sand	8030,8	1,46	4		14,7	147	12	5	5	5	25	26	25,5
17.02.2015	14:20	181	Sand		0,00	4	20	15	96,5	2	20	16	18	20	20	20
04.03.2015	09:40	182	Sand	8274,8	1,51	4		14,7	98,5	5	10	7	8,5	21	21	21
04.03.2015	10:00	183	Sand	8299,8	1,51	4		14,7	98,5	4	10	10	10	22	22	22
18.02.2015	09:30	184	Sand	7664,3	1,39	2	50	14,7	232,5	16	3	3	3	32	32	32
04.03.2015	10:30	185	Sand	7552,7	1,37	2		14,7	245,1	19	2	1,5	1,75	33	34	33,5
04.03.2015	10:55	186	Sand	7542,7	1,37	2		14,6	247,2	20	2	1	1,5	34	34	34
18.02.2015	09:55	187	Sand	7970,8	1,45	2	40	15,1	181	10	6	6	6	24	21	22,5
04.03.2015	12:50	188	Sand	7804,4	1,42	2		14,5	199	15	3,5	3	3,25	29	29	29
04.03.2015	13:10	189	Sand	7838	1,43	2		14,7	196,2	14	4	4	4	28	28	28
18.02.2015	10:15	190	Sand	8780,3	1,60	2	30	14,8	138,4	0,5	30	30	30	20	20	20
18.02.2015	10:50	191	Sand	8793,7	1,60	2		14,9	137,7	3,5	14,5	9,5	12	22	21	21,5
04.03.2015	13:45	192	Sand	8053,9	1,46	2		14,6	148,8	7	6	9	7,5	23	24	23,5
27.03.2015	11:10	192 b	Sand			2		14,7	147	4	13	12	12,5	21	21	21

A.3.3   Diagrams

A.3.3.1   *Slump data and analysis*
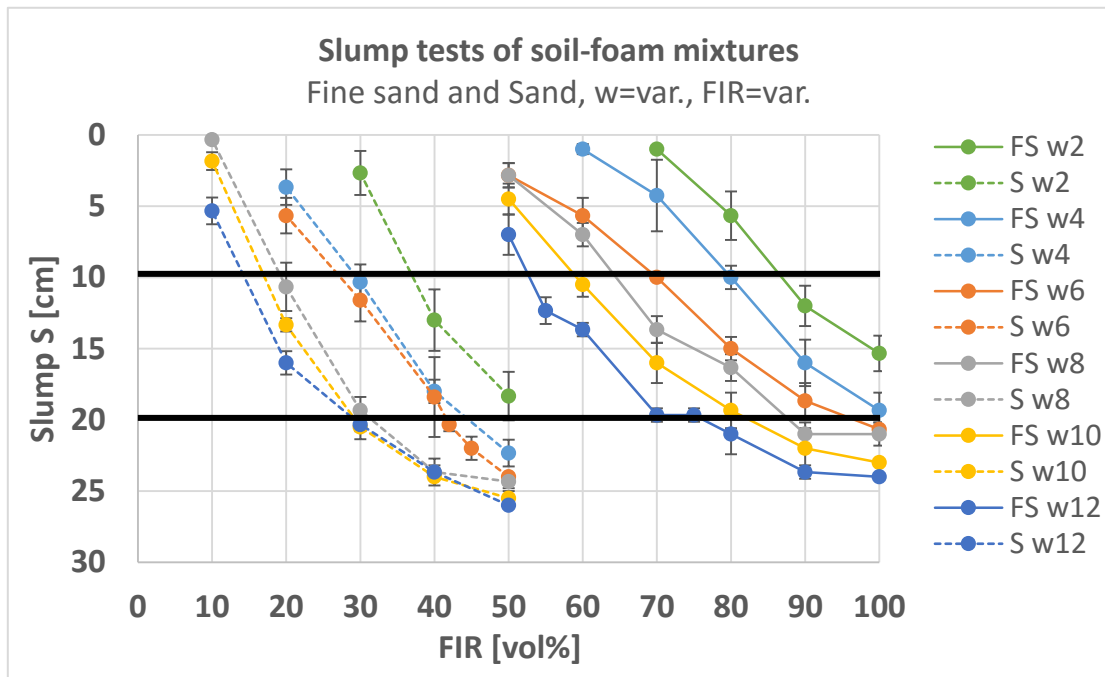
Figure A-16: Results from slump tests of different soil-foam mixtures depicted over FIR
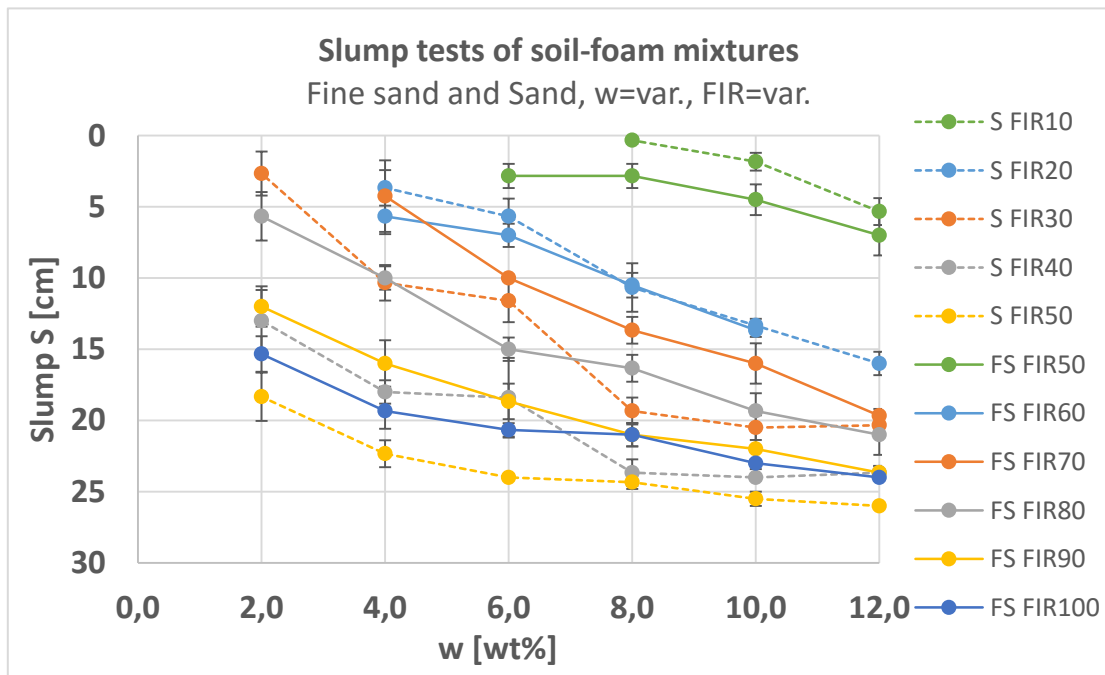
Figure A-17: Results from slump tests of different soil-foam mixtures depicted over w
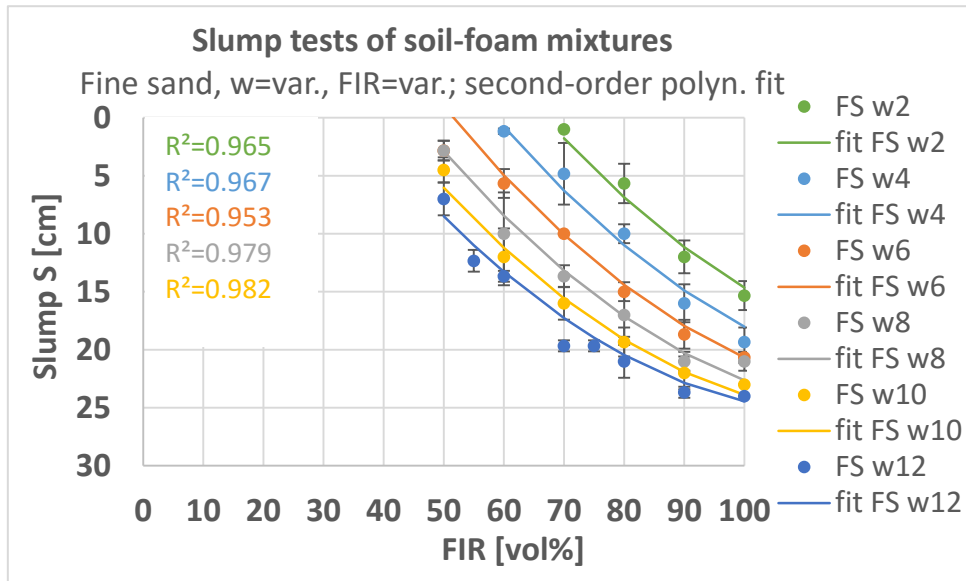
Figure A-18: Mean slump values S (dots) and standard deviations from experiments on fine sand-foam mixtures over foam injection ratio FIR fitted by a second-order polynomial equation (continuous lines)
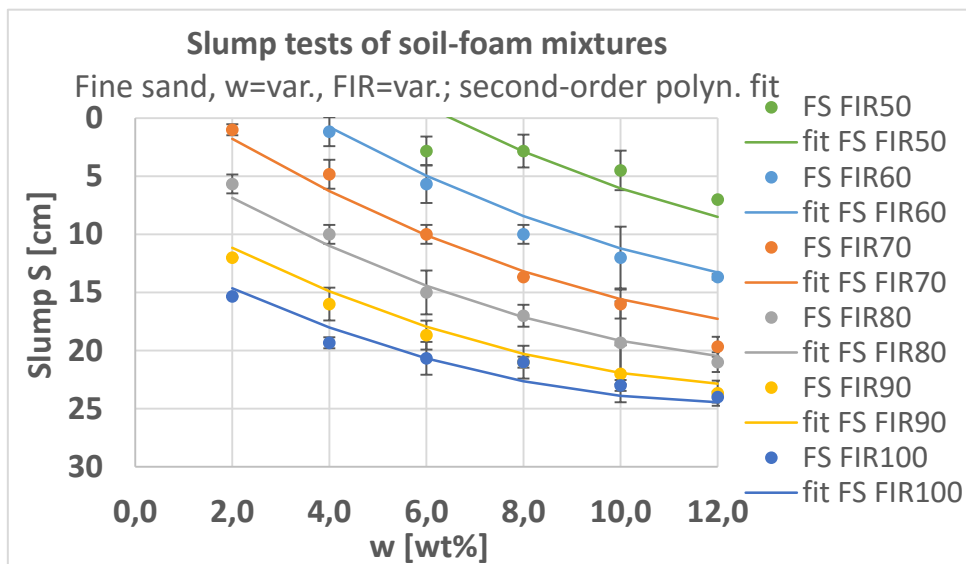
Figure A-19: Mean slump values S (dots) and standard deviations from experiments on fine sand-foam mixtures over water content w fitted by a second-order polynomial equation (continuous lines)
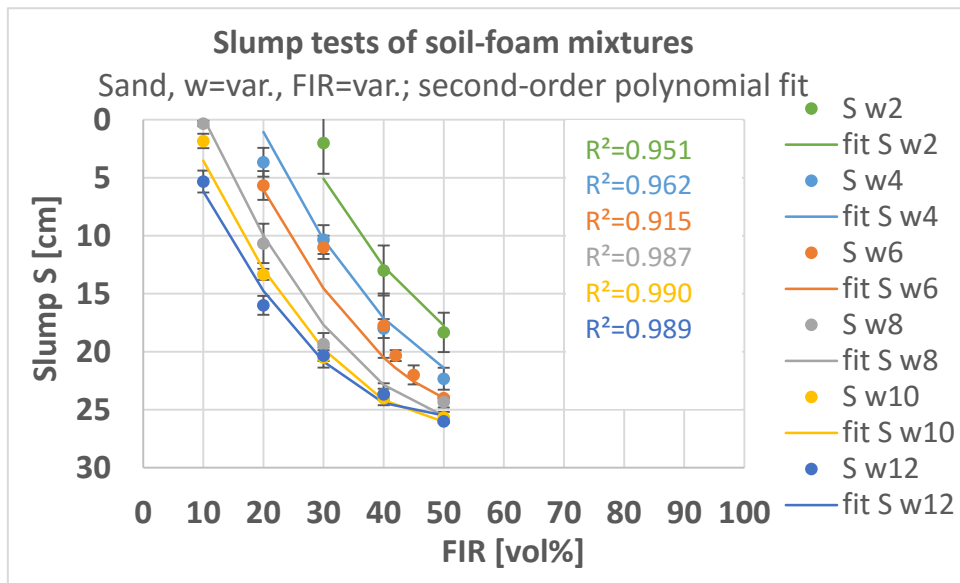
Figure A-20: Mean slump values S (dots) and standard deviations from experiments on sand-foam mixtures over foam injection ratio FIR fitted by a second-order polynomial equation (continuous lines)
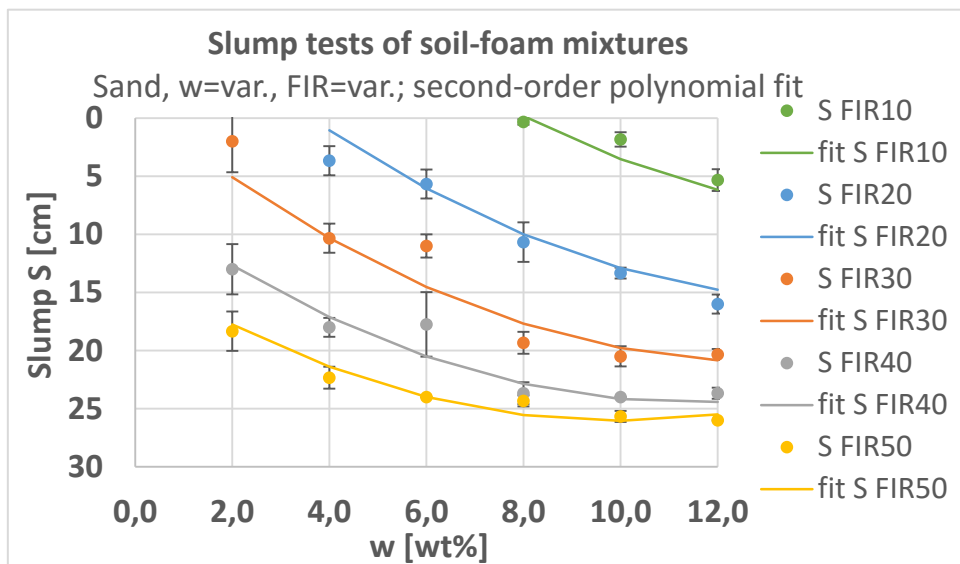
Figure A-21: Mean slump values S (dots) and standard deviations from experiments on sand-foam mixtures over water content w fitted by a second-order polynomial equation (continuous lines)
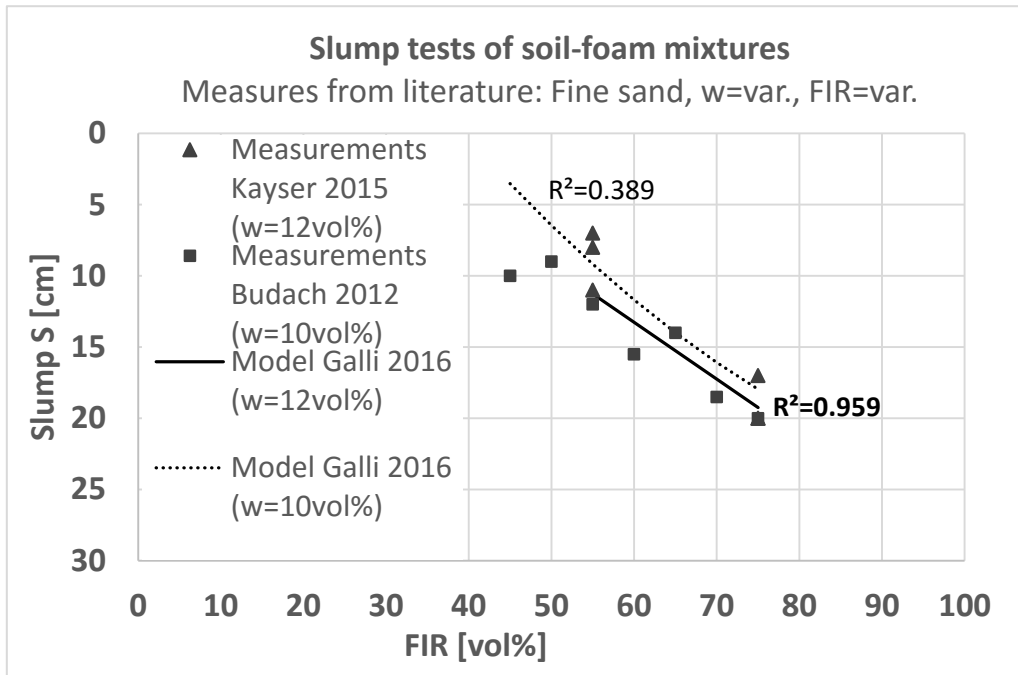
Figure A-22: Application of model function to slump measures on fine sand-foam mixtures from literature
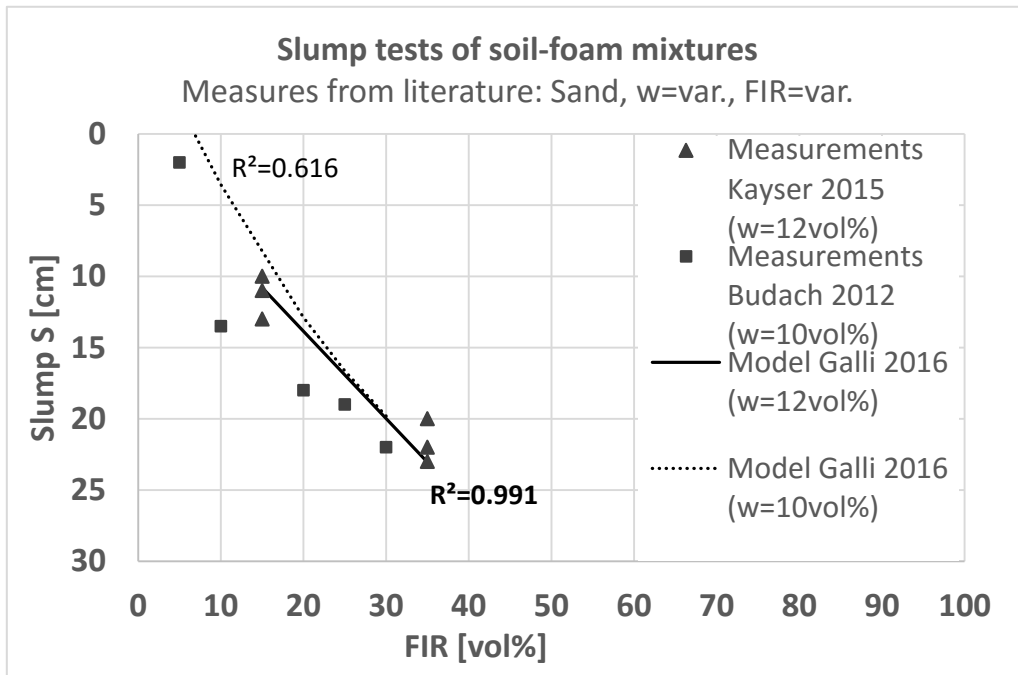
Figure A-23: Application of the model function to slump measures of sand-foam mixtures from literature

A.3.3.2   Slump flow data and analysis
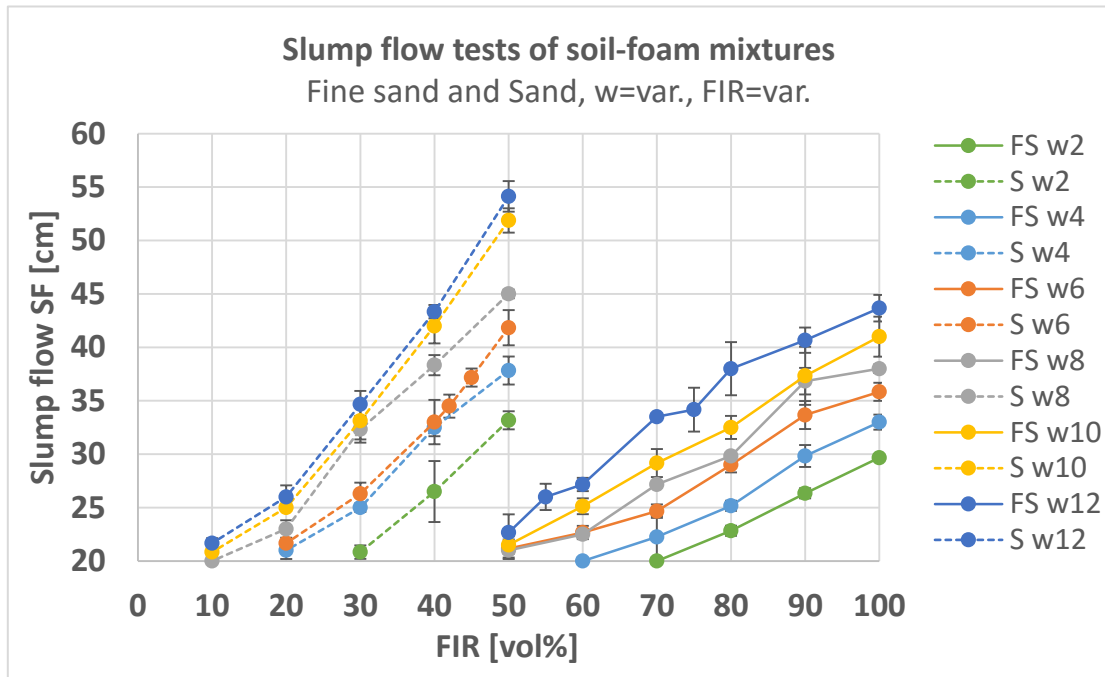
Figure A-24: Results from slump flow tests of different soil-foam mixtures depicted over FIR
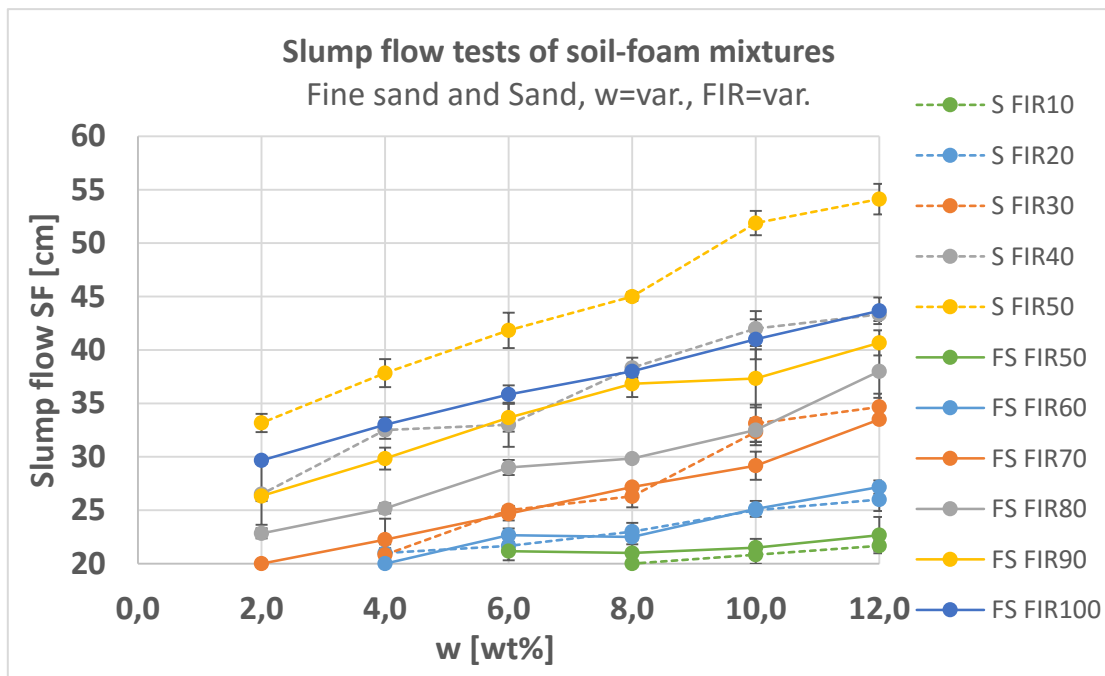
Figure A-25: Results from slump flow tests of different soil-foam mixtures depicted over w
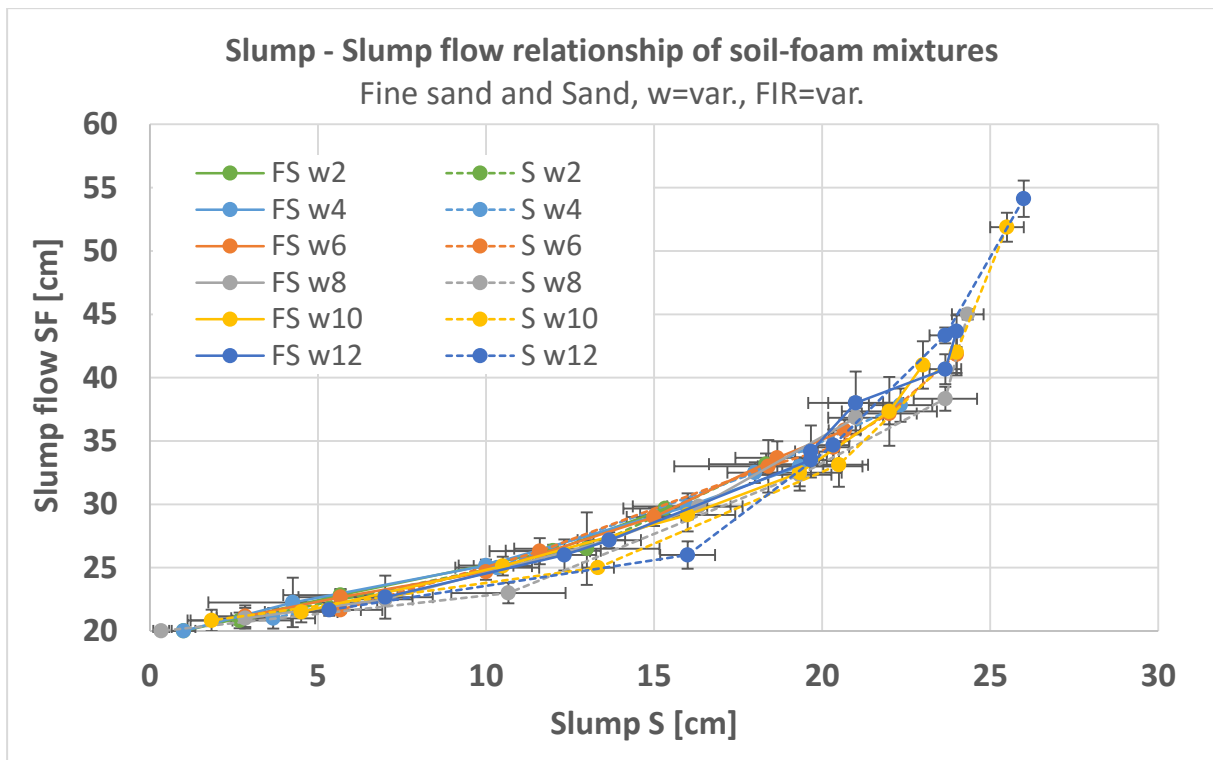
Figure A-26: Slumps and corresponding slump flow measures of different soil-foam mixtures
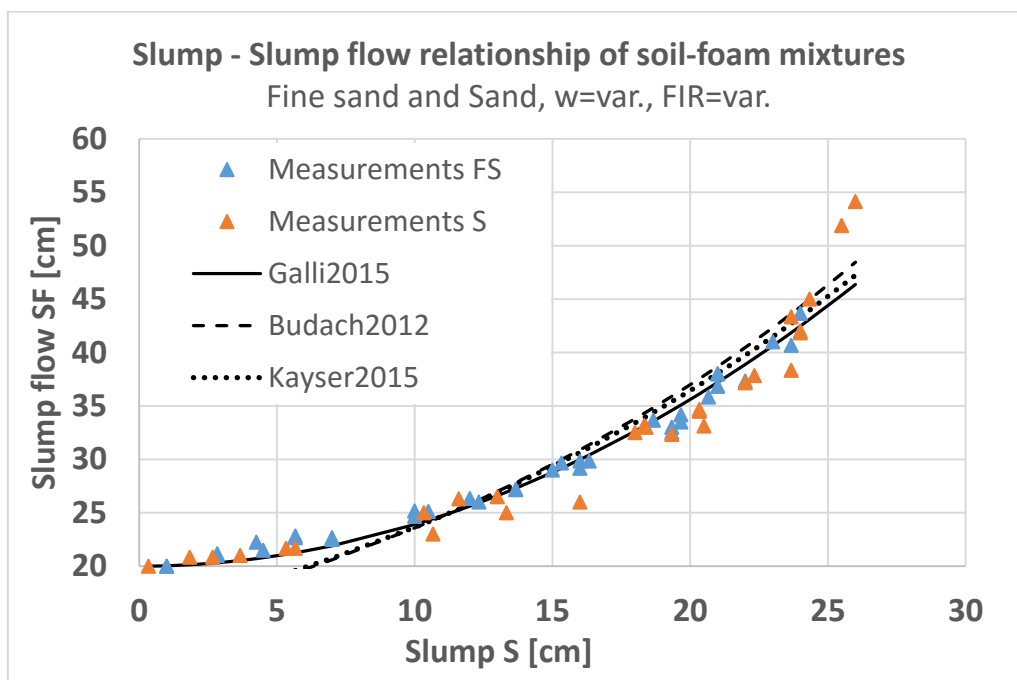
Figure A-27: Mean slump flow values SF over corresponding mean slump values S from experiments on different soil-foam mixtures (data points), regression models according to Galli (continuous line), BUDACH (2012) (dashed line) and KAYSER (2015) (dotted line)
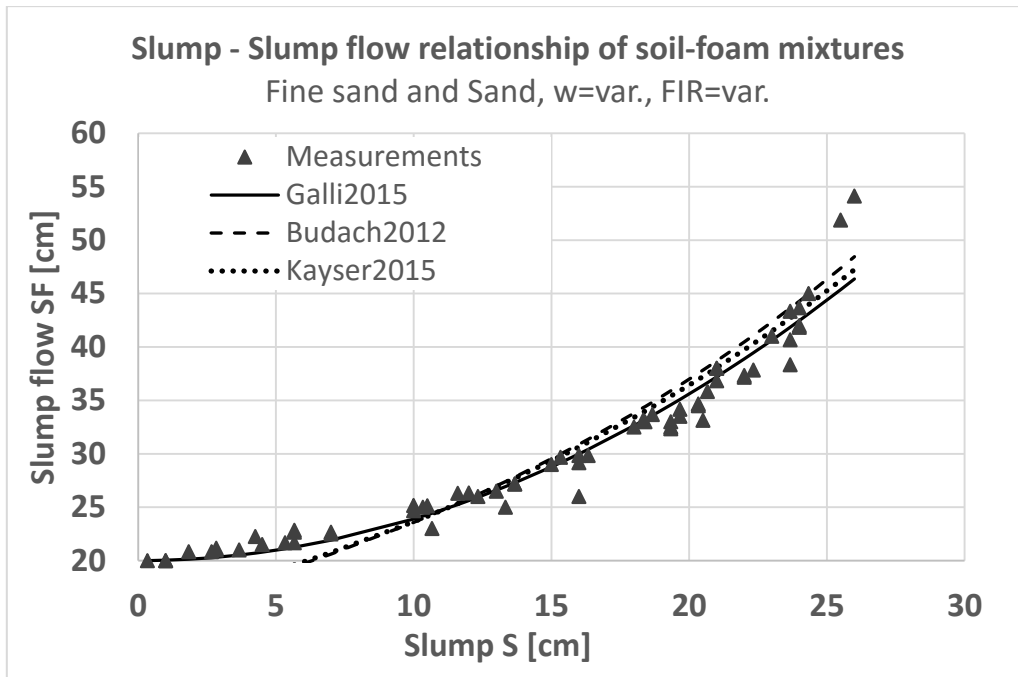
Figure A-28: Application of different models to slump test measurements of this study
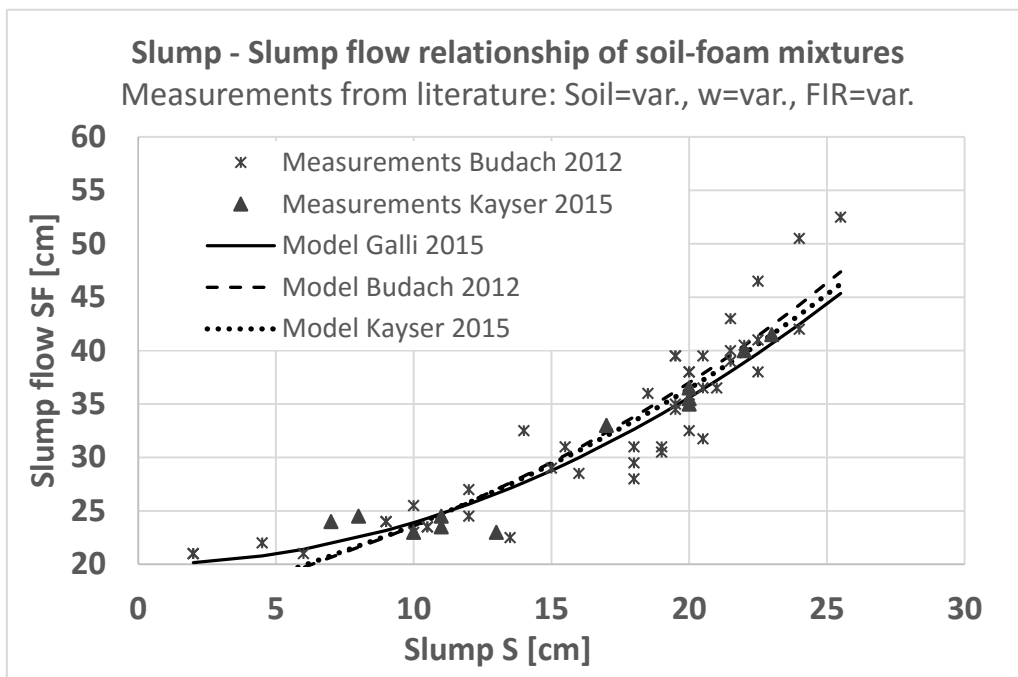
Figure A-29: Slump flow measures SF over corresponding slump values S from experiments on different soil-foam mixtures conducted by BUDACH (2012) (stars) and KAYSER (2015) (triangles), regression model according to Eq. 6.5 (continuous line)
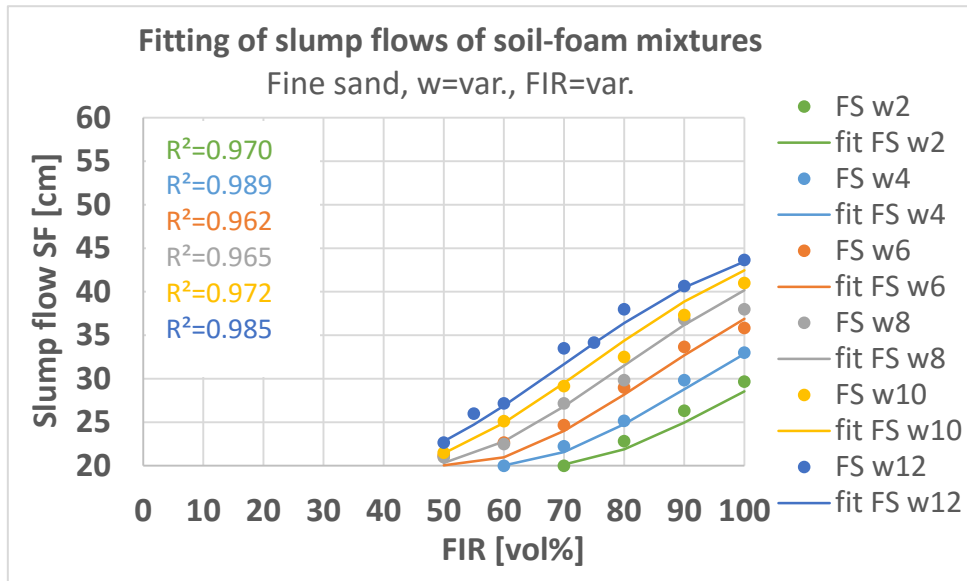
Figure A-30: Application of prognosis model to slump flow measurements for soil 1 (fine sand) in dependence of different water contents and FIRs
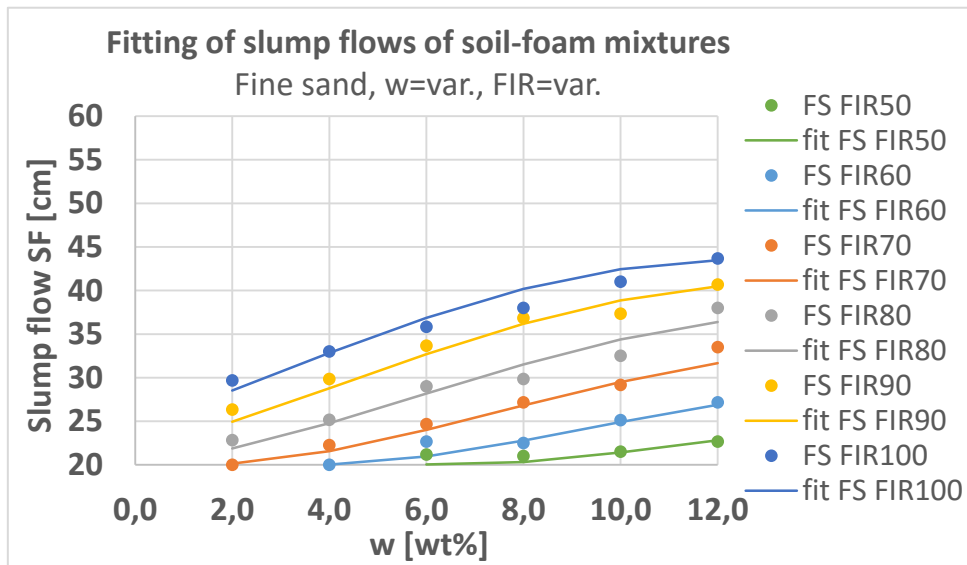
Figure A-31: Application of prognosis model to slump flow measurements for soil 1 (fine sand) in dependence of different water contents and FIRs
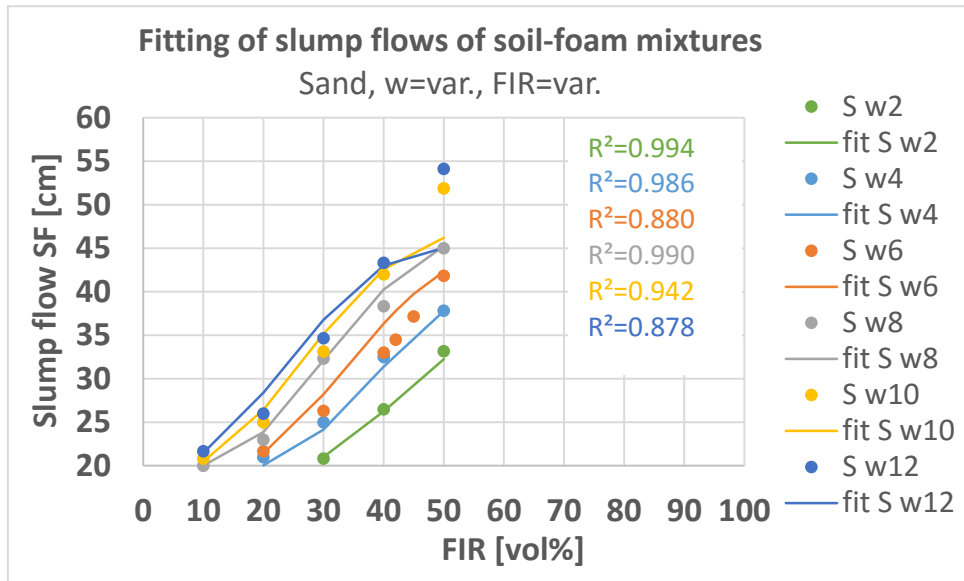
Figure A-32: Application of prognosis model to slump flow measurements for soil 2 (sand) in dependence of different water contents and FIRs
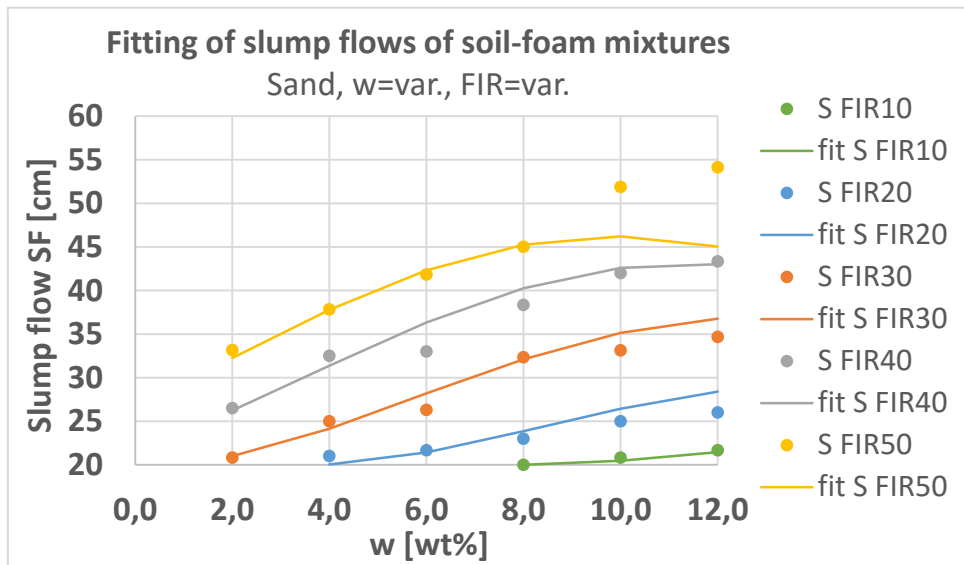
Figure A-33: Application of prognosis model to slump flow measurements for soil 2 (sand) in dependence of different water contents and FIRs

A.3.3.3   h0-data and analysis
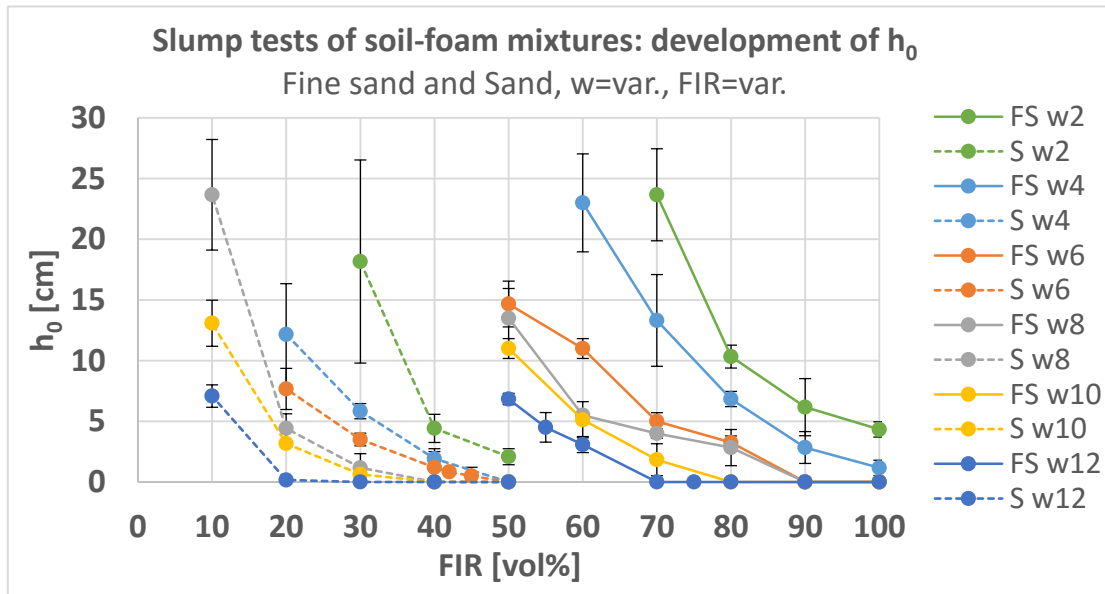
Figure A-34: Development of h_0 in slump tests of different soil-foam mixtures depicted over FIR
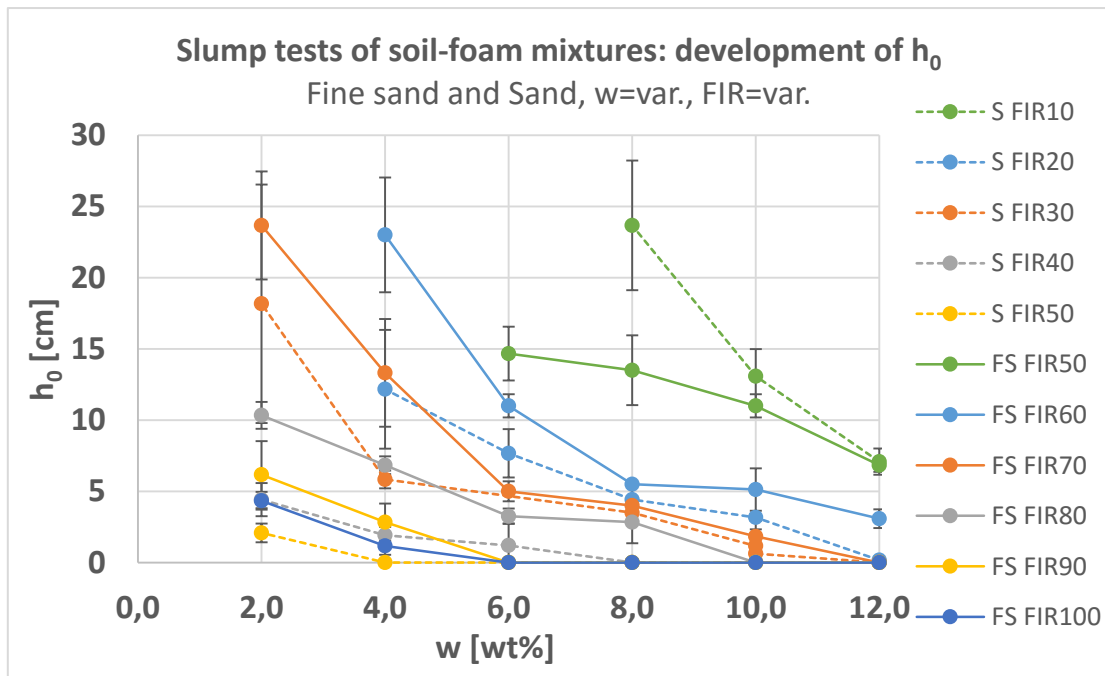
Figure A-35: Development of h_0 in slump tests of different soil-foam mixtures depicted over w

A.3.3.4   Application of analytical slump models and analysis
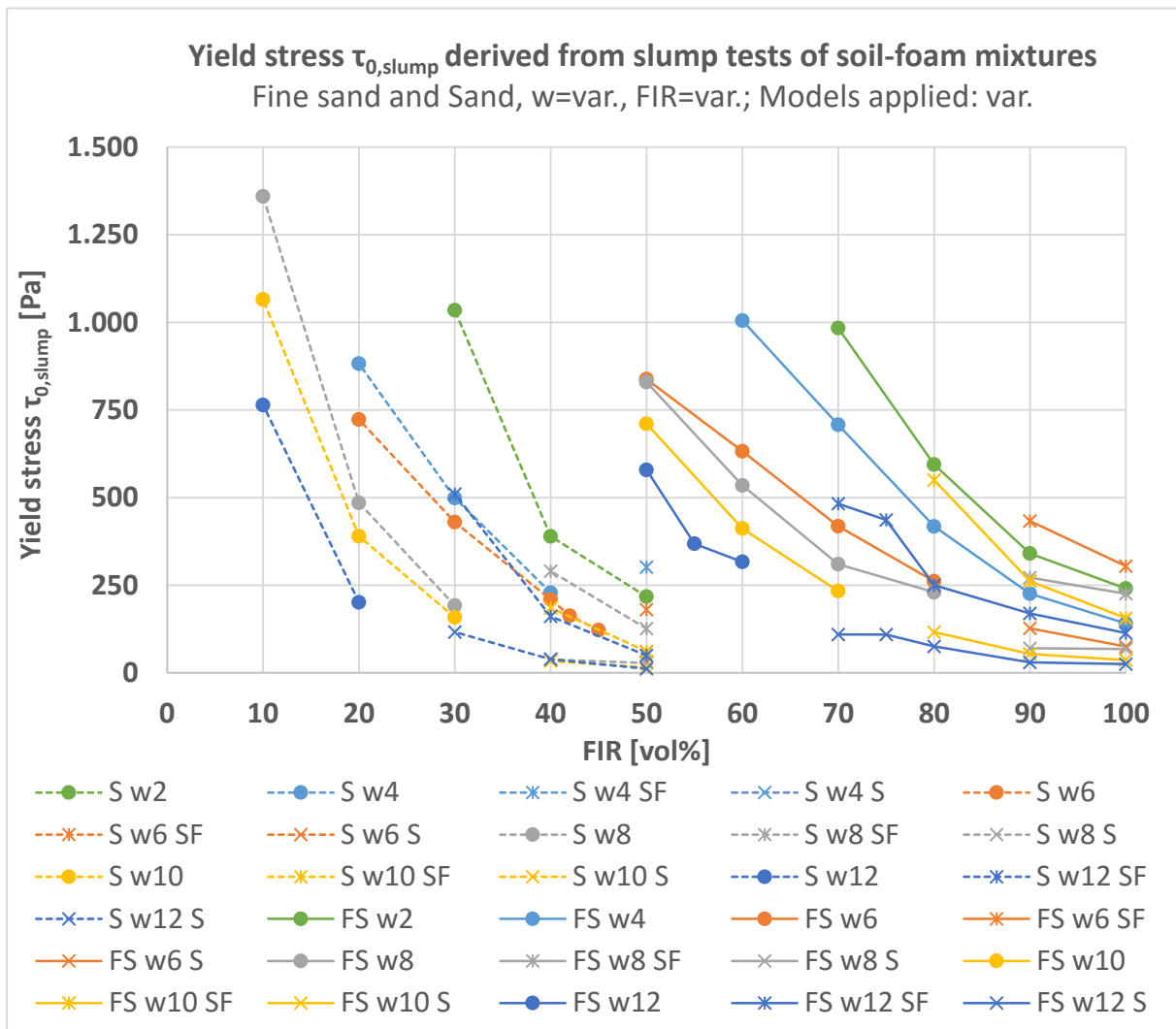
Figure A-36: Yield stresses τ$_{0,slump}$ derived from analytical slump models for different soil-foam-mixtures; no attribute: slump regime model (Eq. 6.19), attribute "SF": spread regime model based on slump flow measure (Eq. 6.25), attribute "S": spread regime model based on slump measure (Eq. 6.26)
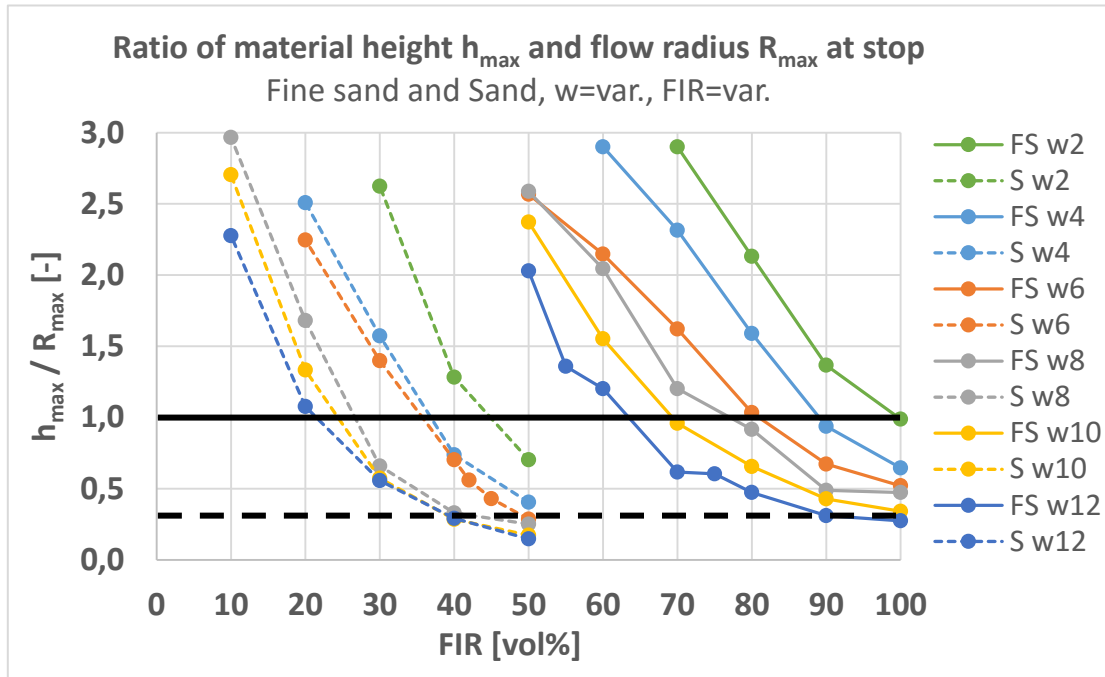
Figure A-37: Development of maximal material height h_{max} and maximum outflow radius R_{max} after slumping; continuous benchmark: ratio of 1.0, dashed benchmark: ratio of 0.33
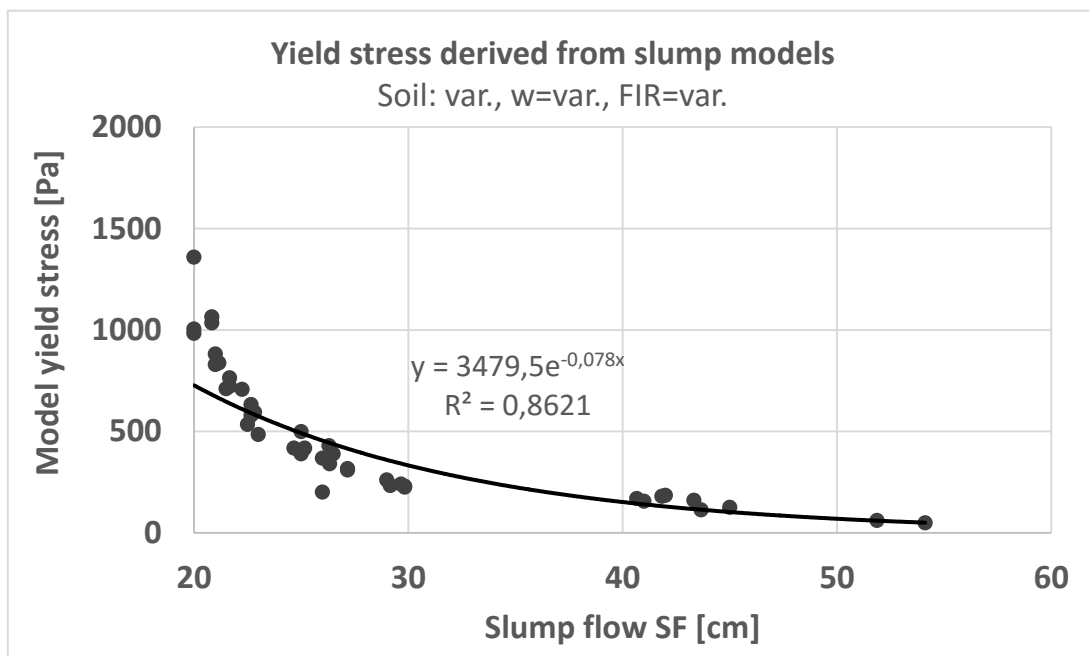
Figure A-38: Yield stresses derived from slump models and empirical approximation for closing the interim division outside the range of applicability ($h_0 = 0$ cm and $h_{max}/R_{max} \geq 0.34$) based on slump flow
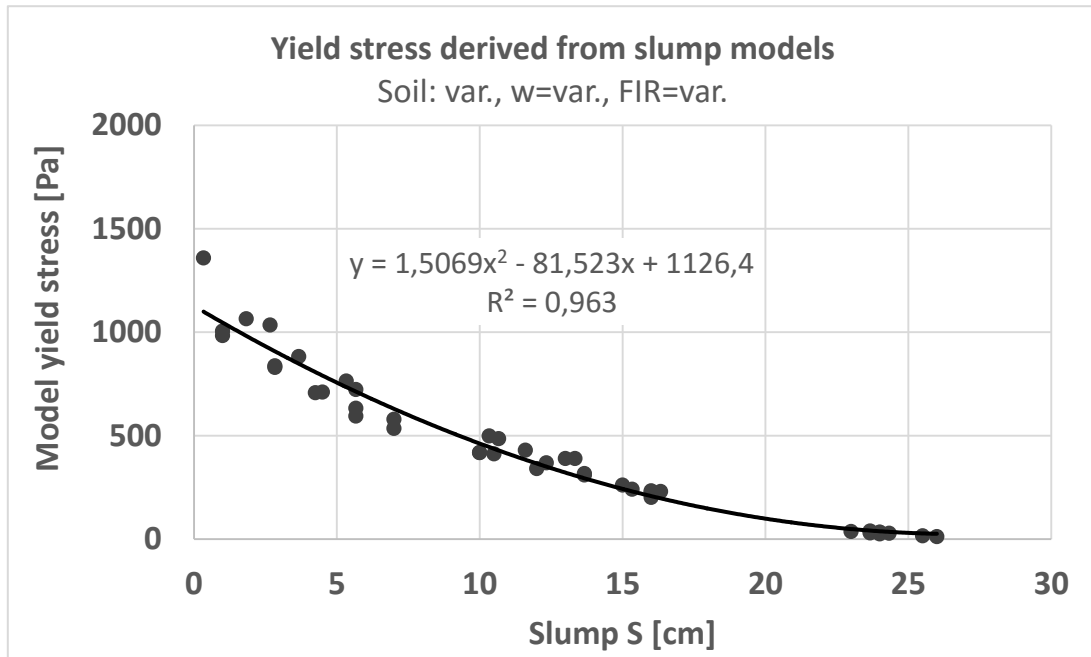
Figure A-39: **Yield stresses derived from slump models and empirical approximation for closing the interim division outside the range of applicability (h_0 = 0 cm and h_{max}/R_{max} ≥ 0.34) based on slump**

A.3.4   Output values from regression analysis

Table A-2:   Output values from multiple regression analysis of Eq. 6.1

Parameters		Soil 1 (Fine sand)			Soil 2 (Sand)		
		Reg. 1	*Confid. intervals*		Reg. 1	*Confid. intervals*	
			lower bound	*upper bound*		*lower bound*	*upper bound*
Regression coefficients	$b_0 =$	-64.126	*-79.334*	*-48.978*	-41.344	*-50.084*	*-32.615*
	$b_1 =$	4.122	*2.894*	*5.336*	4.609	*3.364*	*5.856*
	$b_2 =$	1.147	*0.811*	*1.483*	1.713	*1.374*	*2.053*
	$b_3 =$	-0.019	*-0.029*	*-0.009*	-0.040	*-0.057*	*-0.023*
	$b_4 =$	-0.088	*-0.138*	*-0.038*	-0.131	*-0.194*	*-0.068*
	$b_5 =$	-0.004	*-0.006*	*-0.002*	-0.013	*-0.017*	*-0.008*
t test	$t_{0.95} =$	2.052			2.086		
	$t_0 =$	8.669			9.873		
	$t_1 =$	6.910			7.716		
	$t_2 =$	7.000			10.536		
	$t_3 =$	3.897			4.978		
	$t_4 =$	3.608			4.352		
	$t_5 =$	4.079			6.494		
Coeff. of determ.	$\overline{R}^2 =$	0.968			0.970		
	$r =$	0.984			0.985		
F test	F_0	193.36			163.10		
	$f_{0.05}$	1.715			2.031		

A.3.5   Slump model considering relaxation

As mentioned in the discussion on the applicability of the slump models, one issue that was disregarded in the analysis was the compressibility of the soil-foam mix. The material slices in the lower section of the slump body actually experience relaxation due to a decreasing acting pressure on their top, which in turn results in a volume increase. Assuming that the sample expansion mainly takes place in horizontal / radial direction, the slump flow measure can be affected by consideration of relaxation. One exemplary calculation considering these relaxation effects expressed by Eq. 6.30 and Eq. 6.31 is shown in the following calculation sheets for a fine sand-foam mixture with w = 8 wt% and FIR = 80 vol%. The yield stress was taken from rheological investigations for this specific mixture. The volume increase ranges around 0.4 vol% affecting the material spread by 3 mm. Several calculations have been performed for different mixture compositions. Maximum volume increases range around this dimension, which is why relaxation was considered negligibly small in the present approach.

Prior to slumping

Density	rho =	1170	[kg/m³]		

No. of slices	n =	30	[-]		
Thickness of slice	dz =	1	[cm]		

Dead weight on slice	No.	rx(z) [cm] Eq 6-10	Axy(z) [cm²] see Eq 6-8	Wz [N] see Eq 6-8	pz(z) [Pa] Eq 6-11	tau_z(z) [Pa] Eq 6-12 (von Mises)
	1	5,1	81,2	0,458	56,453	32,593
	2	5,3	86,6	1,421	164,097	94,742
	3	5,4	92,2	2,447	265,436	153,250
	4	5,6	97,9	3,538	361,210	208,545
	5	5,8	103,9	4,695	452,056	260,995
	6	5,9	110,0	5,923	538,521	310,915
	7	6,1	116,3	7,221	621,079	358,580
	8	6,3	122,7	8,592	700,140	404,226
	9	6,4	129,4	10,038	776,063	448,060
	10	6,6	136,2	11,562	849,162	490,264
	11	6,8	143,1	13,165	919,712	530,996
	12	6,9	150,3	14,848	987,956	570,397
	13	7,1	157,6	16,615	1054,108	608,590
	14	7,3	165,1	18,467	1118,359	645,685
	15	7,4	172,8	20,407	1180,878	681,780
	16	7,6	180,7	22,435	1241,814	716,962
	17	7,8	188,7	24,555	1301,304	751,308
	18	7,9	196,9	26,767	1359,466	784,888
	19	8,1	205,3	29,075	1416,410	817,765
	20	8,3	213,8	31,480	1472,234	849,995
	21	8,4	222,6	33,984	1527,024	881,628
	22	8,6	231,5	36,589	1580,861	912,710
	23	8,8	240,5	39,298	1633,815	943,284
	24	8,9	249,8	42,111	1685,954	973,386
	25	9,1	259,2	45,032	1737,336	1003,051
	26	9,3	268,8	48,062	1788,014	1032,311
	27	9,4	278,6	51,203	1838,039	1061,193
	28	9,6	288,5	54,458	1887,456	1089,723
	29	9,8	298,6	57,827	1936,305	1117,926
	30	9,9	308,9	61,314	1984,625	1145,824

Actual total volume =			5497,569	[cm³]		
Theoretical total volume =			5497,787	[cm³]		

After slumping	**(without relaxation)**					
Slump measure	S =	16,33	[cm]			
Undeformed height	h_0 =	2,83	[cm]			
Yield stress	tau_0 =	230,576	[Pa]			
Calculated slump flow	SF_calc =	44,2	[cm]	=2*rx(z',n=30)		
Dead weight on slice	No.	rx(z') [cm]	dz' [cm]	Axy(z') [cm²]	Wz [N]	pz(z') [Pa]
		see Eq 6-13	Eq 6-13	= rx(z')^2*pi()	see Eq 6-8	=Wz/Axy
	1	5,1	1,00	81,2	0,458	56,453
	2	5,3	1,00	86,6	1,421	164,097
	3	5,4	1,00	92,2	2,447	265,436
	4	5,3	1,11	88,6	3,538	399,370
	5	6,1	0,88	117,6	4,695	399,370
	6	6,9	0,74	148,3	5,923	399,370
	7	7,6	0,64	180,8	7,221	399,370
	8	8,3	0,57	215,1	8,592	399,370
	9	8,9	0,51	251,4	10,038	399,370
	10	9,6	0,47	289,5	11,562	399,370
	11	10,2	0,43	329,6	13,165	399,370
	12	10,9	0,40	371,8	14,848	399,370
	13	11,5	0,38	416,0	16,615	399,370
	14	12,1	0,36	462,4	18,467	399,370
	15	12,8	0,34	511,0	20,407	399,370
	16	13,4	0,32	561,8	22,435	399,370
	17	14,0	0,31	614,8	24,555	399,370
	18	14,6	0,29	670,2	26,767	399,370
	19	15,2	0,28	728,0	29,075	399,370
	20	15,8	0,27	788,2	31,480	399,370
	21	16,5	0,26	850,9	33,984	399,370
	22	17,1	0,25	916,2	36,589	399,370
	23	17,7	0,24	984,0	39,298	399,370
	24	18,3	0,24	1054,4	42,111	399,370
	25	18,9	0,23	1127,6	45,032	399,370
	26	19,6	0,22	1203,5	48,062	399,370
	27	20,2	0,22	1282,1	51,203	399,370
	28	20,8	0,21	1363,6	54,458	399,370
	29	21,5	0,21	1448,0	57,827	399,370
	30	22,1	0,20	1535,3	61,314	399,370
				Total volume	5497,569	[cm³]

Relaxation

FER =	15	[-]	
FIR =	80	[vol%]	
alpha:	see Eq 6-31		

No.	(pz(z')-pz(z)) [Pa]	delta V [cm³] =Axy*dz/alpha	delta V [vol%] =delta V [cm³]/(Axy*dz)*100
1	0,00	0,00	0,00%
2	0,00	0,00	0,00%
3	0,00	0,00	0,00%
4	38,16	0,02	0,02%
5	-52,69	-0,02	-0,02%
6	-139,15	-0,06	-0,06%
7	-221,71	-0,11	-0,09%
8	-300,77	-0,15	-0,12%
9	-376,69	-0,20	-0,16%
10	-449,79	-0,25	-0,19%
11	-520,34	-0,31	-0,22%
12	-588,59	-0,37	-0,24%
13	-654,74	-0,43	-0,27%
14	-718,99	-0,49	-0,30%
15	-781,51	-0,56	-0,32%
16	-842,44	-0,63	-0,35%
17	-901,93	-0,71	-0,37%
18	-960,10	-0,78	-0,40%
19	-1017,04	-0,87	-0,42%
20	-1072,86	-0,95	-0,45%
21	-1127,65	-1,04	-0,47%
22	-1181,49	-1,13	-0,49%
23	-1234,45	-1,23	-0,51%
24	-1286,58	-1,33	-0,53%
25	-1337,97	-1,44	-0,56%
26	-1388,64	-1,55	-0,58%
27	-1438,67	-1,66	-0,60%
28	-1488,09	-1,78	-0,62%
29	-1536,94	-1,90	-0,64%
30	-1585,26	-2,03	-0,66%

	delta V_ges =	-22,0	[cm³]
	delta V_ges =	-0,40%	[vol%]

After slumping	(with relaxation)					
Calculated slump flow	SF_calc =	44,5	[cm]	=2*rx(z',n=30)		
Dead weight on slice	No.	rx(z') [cm]	dz' [cm]	Axy(z') [cm²]	Wz [N]	pz(z') [Pa]
		=rx(z',without relaxation)*(1-delta V [vol%])				
	1	5,1	1,00	81,2	0,458	56,453
	2	5,3	1,00	86,6	1,421	164,097
	3	5,4	1,00	92,2	2,447	265,436
	4	5,3	1,11	88,5	3,538	399,496
	5	6,1	0,88	117,6	4,695	399,195
	6	6,9	0,74	148,5	5,923	398,909
	7	7,6	0,64	181,1	7,221	398,636
	8	8,3	0,57	215,7	8,592	398,375
	9	9,0	0,51	252,1	10,038	398,124
	10	9,6	0,47	290,6	11,562	397,883
	11	10,3	0,43	331,1	13,165	397,651
	12	10,9	0,40	373,6	14,848	397,427
	13	11,5	0,38	418,3	16,615	397,209
	14	12,2	0,36	465,2	18,467	396,998
	15	12,8	0,34	514,3	20,407	396,793
	16	13,4	0,32	565,7	22,435	396,593
	17	14,0	0,31	619,4	24,555	396,398
	18	14,7	0,29	675,6	26,767	396,207
	19	15,3	0,28	734,2	29,075	396,021
	20	15,9	0,27	795,3	31,480	395,839
	21	16,5	0,26	858,9	33,984	395,659
	22	17,2	0,25	925,2	36,589	395,484
	23	17,8	0,24	994,1	39,298	395,311
	24	18,4	0,24	1065,7	42,111	395,141
	25	19,1	0,23	1140,1	45,032	394,973
	26	19,7	0,22	1217,4	48,062	394,808
	27	20,3	0,22	1297,5	51,203	394,645
	28	21,0	0,21	1380,5	54,458	394,484
	29	21,6	0,21	1466,5	57,827	394,326
	30	22,3	0,20	1555,5	61,314	394,169
			Total volume	5541,657	[cm³]	

A.4 Rheometry with BMS

A.4.1 Setup and testing procedure

Test stand
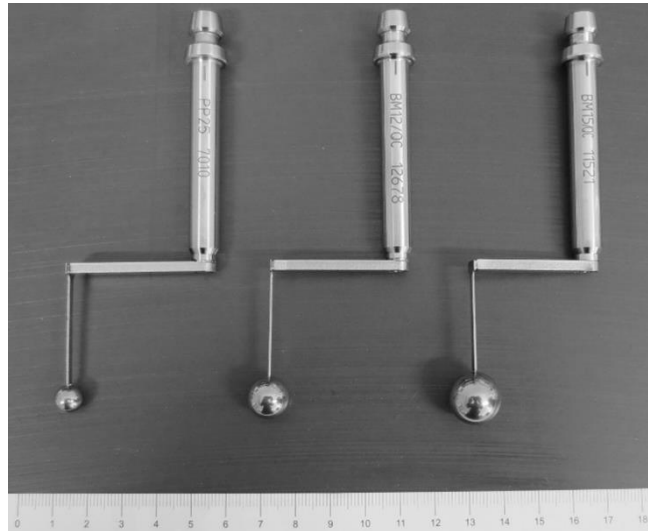
Figure A-40: **Rheometer with ball measuring system (BMS); right: BMS with different ball-sizes**

Equipment

- 1 Bucket

- 1 Shovel

- 1 Bowl

- 1 Ruler

- 1 Scraper

- Haegermann Table

Preparations

1. Connect BMS to rheometer, adjust height of the rheometer head and setup test routine in the control panel

2. Prepare soil-foam sample according to standard testing procedure (see section A.1) with 1,000 g soil in a bowl, mix it by hand with a scraper

3. Insert mixture into sample container and place on Haegermann Table (or similar)

4. Compact sample by 15 impacts with Haegermann Table (or 30 seconds e.g. on vibration table)

5. Pull-off surface with ruler to generate a planar sample surface which is flush with container top edge

6. Weigh sample mass, determine density

7. Place sample in rheometer and insert BMS into sample 30 seconds prior to test start

Procedure

8. Start testing by initialising test routine

Remarks

Control time-steps sharply

A.4.2   Testing protocols

test no. [-]	date [-]	BMS	soil [-]	m_{soil} [g]	w [V%]	m_{water} [g]	$m_{cup+foam}$ [g]	FER_{actual} [-]	FER_{target} [-]	FIR [%]	$m_{foam\,to\,add}$ [g]	m_{total} [g]	density [g/cm³]	Liquid m_{water}	$m_{surfactant}$	remarks
37	14.02.2015	8	fine sand	999,9	12	119,7	955,0	14,4	15,0	55	23,2	575,9	1,185	20.972,4	648,6	
38	14.02.2015	8	fine sand	1.000,1	12	119,8	954,0	14,4	15,0	55	23,1	585,5	1,204			
39	14.02.2015	8	fine sand	999,8	12	119,7	954,0	14,4	15,0	55	23,0	593,8	1,221			
40	15.02.2015	12	fine sand	1.000,0	12	120,1	951,8	14,6	15,0	55	22,8	585,4	1,204			
41	15.02.2015	12	fine sand	999,9	12	119,7	952,0	14,6	15,0	55	22,8	591,8	1,217			
42	15.02.2015	12	fine sand	1.000,1	12	119,7	951,4	14,7	15,0	55	22,7	595,7	1,225			
43	15.02.2015	12	fine sand	1.000,1	12	119,6	952,1	14,6	15,0	55	22,8	597,2	1,228			
44	15.02.2015	12	fine sand	1.000,2	12	120,3	950,8	14,7	15,0	55	22,6	597,4	1,229			
45	14.02.2015	15	fine sand	1.000,3	12	120,3	952,7	14,6	15,0	55	22,9	601,4	1,237			
46	14.02.2015	15	fine sand	999,4	12	120,0	954,1	14,4	15,0	55	23,1	585,8	1,205			
47	14.02.2015	15	fine sand	1.000,0	12	119,8	952,8	14,5	15,0	55	22,9	595,0	1,224			
48	14.02.2015	8	fine sand	1.000,0	12	120,0	953,5	14,5	15,0	75	31,3	534,7	1,100			
49	14.02.2015	8	fine sand	1.000,0	12	120,3	955,9	14,3	15,0	75	31,8	533,8	1,098			
50	14.02.2015	8	fine sand	1.000,0	12	120,0	956,9	14,2	15,0	75	32,0	530,6	1,091			
51	15.02.2015	12	fine sand	1.000,0	12	119,6	952,6	14,6	15,0	75	31,2	535,0	1,100			
52	15.02.2015	12	fine sand	1.000,1	12	120,3	952,5	14,6	15,0	75	31,2	528,8	1,088			
53	15.02.2015	12	fine sand	1.000,2	12	119,8	951,3	14,7	15,0	75	30,9	538,5	1,108			
54	15.02.2015	12	fine sand	999,8	12	120,2	950,8	14,7	15,0	75	30,8	539,6	1,110			
55	15.02.2015	12	fine sand	1.000,0	12	119,8	951,2	14,7	15,0	75	30,9	539,4	1,110			
56	14.02.2015	15	fine sand	1.000,1	12	120,3	953,6	14,5	15,0	75	31,4	537,1	1,105			
57	14.02.2015	15	fine sand	1.000,3	12	120,0	954,0	14,4	15,0	75	31,4	538,8	1,108			
58	14.02.2015	15	fine sand	999,9	12	119,9	955,0	14,4	15,0	75	31,6	535,9	1,102			
59	14.02.2015	8	sand	1.000,0	6	59,7	957,5	14,2	15,0	30	12,5	701,8	1,444			
60	14.02.2015	8	sand	1.000,1	6	60,0	955,6	14,3	15,0	30	12,3	702,7	1,445			
61		8	sand		6			-3,1	15,0	30	0,0		0,000			deckungsgleich mit V195, daher nicht durchgeführt
62	18.02.2015	12	sand	1.000,2	6	60,3	962,5	13,8	15,0	30	12,8	707,7	1,456			
63	18.02.2015	12	sand	1.000,4	6	59,8	962,5	13,8	15,0	30	12,8	707,8	1,456			
64	18.02.2015	12	sand	1.000,5	6	59,8	961,3	13,9	15,0	30	12,8	692,1	1,424			
65	18.02.2015	12	sand	1.000,0	6	59,7	960,5	13,9	15,0	30	12,7	714,3	1,469			
66		12	sand		6			-3,1	15,0	30	0,0		0,000			deckungsgleich mit V129, daher nicht durchgeführt
67	15.02.2015	15	sand	1.000,5	6	59,7	956,0	14,3	15,0	30	12,4	699,6	1,439	25.175,0	778,6	
68	15.02.2015	15	sand	1.000,0	6	60,2	955,2	14,3	15,0	30	12,3	698,6	1,437			
69	15.02.2015	15	sand	1.000,0	6	59,8	953,0	14,5	15,0	30	12,2	689,3	1,418			
70	14.02.2015	8	sand	1.000,5	6	60,0	954,2	14,4	15,0	42	17,2	684,4	1,408			
71	14.02.2015	8	sand	1.000,0	6	59,7	953,8	14,5	15,0	42	17,1	667,9	1,374			
72	14.02.2015	8	sand	1.000,4	6	59,7	956,0	14,3	15,0	42	17,3	687,6	1,414			
73	18.02.2015	12	sand	1.000,2	6	59,4	958,2	14,1	15,0	42	17,5	677,0	1,393	25.557,0	790,4	
74	18.02.2015	12	sand	1.000,0	6	59,7	957,2	14,2	15,0	42	17,4	684,9	1,409			
75	18.02.2015	12	sand	999,9	6	60,2	960,6	13,9	15,0	42	17,8	678,5	1,396			
76	18.02.2015	12	sand	1.000,0	6	60,3	959,6	14,0	15,0	42	17,7	677,7	1,394			
77	18.02.2015	12	sand	1.000,0	6	59,5	956,1	14,3	15,0	42	17,3	681,9	1,403			
78	15.02.2015	15	sand	1.000,2	6	59,7	955,0	14,4	15,0	42	17,2	681,1	1,360			
79	15.02.2015	15	sand	999,9	6	59,8	953,6	14,5	15,0	42	17,1	668,9	1,376			
80	15.02.2015	15	sand	1.000,1	6	60,1	954,5	14,4	15,0	42	17,2	678,1	1,395			

test no. [-]	date [-]	soil [-]	m_soil [g]	w [M%]	m_water [g]	m_cupfoam [g]	FER_actual [-]	FER_target [-]	FIR [%]	m_foam to add [g]	m_total [g]	density [g/cm³]	Liquid m_water	Liquid m_surfactant	remarks
81		fine sand		2			-3,1	15,0	50	0,0		0,000			
82		fine sand		2			-3,1	15,0	60	0,0		0,000			
83	08.01.2015	fine sand	1.000,0	2	20,3	960,0	14,0	15,0	70	27,7	596,6	1,227			
84	08.01.2015	fine sand	1.000,2	2	20,2	963,5	13,7	15,0	80	32,2	543,9	1,119			
85	08.01.2015	fine sand	1.000,1	2	19,9	961,5	13,8	15,0	90	35,9	516,8	1,063			
86	08.01.2015	fine sand	1.000,1	2	20,3	961,1	13,9	15,0	100	39,8	492,2	1,012			
87		fine sand		4			-3,1	15,0	50	0,0		0,000			
88	08.01.2015	fine sand	1.000,2	4	40,4	962,5	13,8	15,0	60	24,5	602,7	1,240			abgebrochen, nicht verwertbar
89	08.01.2015	fine sand	1.000,0	4	40,2	958,2	14,1	15,0	70	27,9	563,5	1,159	19.750,8	610,8	nur Runde 2-3 verwertbar
90	07.01.2015	fine sand	1.000,3	4	40,1	967,0	13,4	15,0	80	33,5	529,2	1,089			
91	07.01.2015	fine sand	1.000,2	4	40,1	968,2	13,3	15,0	90	38,0	498,5	1,025			
92	07.01.2015	fine sand	1.000,1	4	39,9	961,7	13,8	15,0	100	40,7	486,0	1,000			
93	07.01.2015	fine sand	1.000,2	6	60,0	964,9	13,6	15,0	50	21,1	608,4	1,251			abgebrochen, nicht verwertbar
94	07.01.2015	fine sand	1.000,0	6	60,2	965,3	13,5	15,0	60	25,4	586,1	1,206			
95	07.01.2015	fine sand	1.000,0	6	59,9	965,7	13,5	15,0	70	29,7	562,2	1,156			
96	07.01.2015	fine sand	1.000,1	6	60,1	961,5	13,8	15,0	80	33,1	545,1	1,121			
97	07.01.2015	fine sand	1.000,3	6	60,0	959,6	14,0	15,0	90	36,9	509,2	1,047			
98	07.01.2015	fine sand	1.000,0	6	60,1	968,0	13,3	15,0	100	42,9	491,1	1,010			
99	07.01.2015	fine sand	1.000,2	8	80,2	968,2	13,3	15,0	50	21,9	614,1	1,263			nur Runde 2-3 verwertbar
100	06.01.2015	fine sand	1.000,2	8	80,1	961,3	13,9	15,0	60	25,3	571,0	1,175			
101	06.01.2015	fine sand	1.000,0	8	80,0	965,7	13,5	15,0	70	30,2	548,8	1,129			
102	06.01.2015	fine sand	1.000,0	8	80,0	962,1	13,8	15,0	80	33,9	524,2	1,078			
103	06.01.2015	fine sand	1.000,0	8	79,9	962,7	13,7	15,0	90	38,2	517,6	1,065			
104	06.01.2015	fine sand	1.000,0	8	79,9	958,6	14,1	15,0	100	41,5	492,9	1,014	25.966,1	803,1	
105	11.12.2014	fine sand	1.000,2	10	100,2	963,6	13,7	15,0	50	21,7	612,8	1,261			
106	11.12.2014	fine sand	999,9	10	100,2	961,4	13,8	15,0	60	25,8	562,2	1,156	14.275,9	441,5	
107	09.12.2014	fine sand	1.000,0	10	100,3	968,7	13,3	15,0	70	31,3	533,9	1,098			
108	09.12.2014	fine sand	1.000,0	10	100,0	969,7	13,2	15,0	80	36,0	518,0	1,066			
109	09.12.2014	fine sand	1.000,1	10	100,1	973,0	13,0	15,0	90	41,2	489,7	1,007			
110	09.12.2014	fine sand	999,9	10	100,1	963,1	13,7	15,0	100	43,4	471,7	0,970			
111	09.12.2014	fine sand	999,9	12	120,2	970,3	13,2	15,0	50	23,0	590,1	1,214			
112	09.12.2014	fine sand	1.000,1	12	120,0	965,5	13,5	15,0	60	26,8	560,4	1,153			nicht kongruent zur Referenzversuchen
113	09.12.2014	fine sand	999,8	12	120,3	969,9	13,2	15,0	70	32,1	539,6	1,110			nicht kongruent zur Referenzversuchen
114	08.12.2014	fine sand	1.000,0	12	120,1	962,8	13,7	15,0	80	35,3	520,6	1,071			Zeit nicht aufgenommen, nicht kongruent zu
115	08.12.2014	fine sand	1.000,2	12	120,1	959,9	14,0	15,0	90	39,0	497,1	1,023			nicht kongruent zur Referenzversuchen
116	08.12.2014	fine sand	1.000,2	12	120,1	947,4	15,0	15,0	100	40,3	483,2	0,994	28.809,0	891,0	nicht kongruent zur Referenzversuchen

test no. [-]	date [-]	soil [-]	m_soil [g]	w [M%]	m_water [g]	m_cup+foam [g]	FER_actual [-]	FER_target [-]	FIR [%]	m_foam to add [g]	m_total [g]	density [g/cm³]	Liquid m_water	Liquid m_surfactant	remarks
117	21.01.2015	sand					-3,1	15,0	10	0,0		0,000			nicht durchgeführt
118	21.01.2015	sand	1.000,0	2	20,0	950,6	14,7	15,0	20	7,7	725,2	1,492			abgebrochen, nicht verwertbar
119	21.01.2015	sand	1.000,1	2	20,0	957,4	14,2	15,0	30	12,0	683,2	1,405			nicht verwertbar
120	21.01.2015	sand	999,9	2	19,9	957,2	14,2	15,0	40	16,0	656,8	1,351			
121	21.01.2015	sand	1.000,0	2	20,1	955,8	14,3	15,0	50	19,8	628,5	1,293			
122	21.01.2015	sand	999,6	4	40,0	958,2	14,1	15,0	10	4,1	740,0	1,522			abgebrochen, nicht verwertbar
123	21.01.2015	sand	999,9	4	39,9	959,3	14,0	15,0	20	8,2	704,4	1,449			
124	21.01.2015	sand	1.000,1	4	40,0	955,2	14,3	15,0	30	12,1	676,2	1,391			
125	21.01.2015	sand	1.000,1	4	40,0	959,6	14,0	15,0	40	16,5	644,5	1,326			
126	21.01.2015	sand	1.000,0	4	40,1	959,3	14,0	15,0	50	20,6	635,9	1,308			
127	21.01.2015	sand	999,9	6	60,0	952,4	14,6	15,0	10	4,0	744,4	1,531			abgebrochen, nicht verwertbar
128	21.01.2015	sand	1.000,0	6	60,0	956,2	14,3	15,0	20	8,3	681,3	1,401			Dichte niedriger als vorher
129	21.01.2015	sand	1.000,0	6	60,1	951,2	14,7	15,0	30	12,0	692,8	1,425	24.987,6	772,8	
130	15.01.2015	sand	1.000,0	6	60,0	957,0	14,2	15,0	40	16,6	653,3	1,344			
131	15.01.2015	sand	1.000,0	6	59,9	960,6	13,9	15,0	50	21,2	618,9	1,273			
132	15.01.2015	sand	1.000,0	8	79,9	956,5	14,2	15,0	10	4,2	711,7	1,464			abgebrochen, nicht verwertbar
133	15.01.2015	sand	1.000,0	8	79,9	959,5	14,0	15,0	20	8,6	687,3	1,414			
134	15.01.2015	sand	1.000,0	8	80,0	955,2	14,3	15,0	30	12,5	663,3	1,364			
135	15.01.2015	sand	999,6	8	80,0	955,0	14,4	15,0	40	16,7	628,6	1,293			
136	15.01.2015	sand	1.000,1	8	79,9	960,4	13,9	15,0	50	21,5	628,0	1,292			
137	15.01.2015	sand	1.000,1	10	100,2	954,3	14,4	15,0	10	4,2	718,7	1,478			
138	15.01.2015	sand	1.000,0	10	100,2	955,4	14,3	15,0	20	8,5	689,3	1,418			
139	15.01.2015	sand	1.000,2	10	100,1	960,4	13,9	15,0	30	13,2	665,4	1,369	19.981,1	618,0	
140	09.01.2015	sand	1.000,5	10	99,9	960,8	13,9	15,0	40	17,6	673,4	1,385			
141	09.01.2015	sand	1.000,2	10	100,2	962,7	13,7	15,0	50	22,2	641,7	1,320			
142	09.01.2015	sand	999,9	12	120,0	961,3	13,9	15,0	10	4,5	742,0	1,526			abgebrochen, nicht verwertbar
143	09.01.2015	sand	1.000,2	12	120,0	961,9	13,8	15,0	20	9,0	720,4	1,482	9.961,1	308,1	
144	08.01.2015	sand	1.000,6	12	119,9	961,5	13,8	15,0	30	13,5	700,8	1,442			
145	08.01.2015	sand	1.000,0	12	120,2	962,6	13,8	15,0	40	18,1	684,2	1,407			
146	08.01.2015	sand	1.000,6	12	119,8	962,4	13,8	15,0	50	22,6	637,1	1,311			

test no. [-]	date [-]	soil [-]	m_{soil} [g]	w [M%]	m_{water} [g]	$m_{cup+foam}$ [g]	FER_{actual} [-]	FER_{target} [-]	FIR [%]	$m_{foam\,to\,add}$ [g]	m_{total} [g]	density [g/cm³]	Liquid m_{water}	Liquid $m_{surfactant}$	remarks
147	27.01.2015	fine sand	1.000,0	2	20,0	965,3	13,5	15,0	50	20,3	603,3	1,241			ABORTED
148	27.01.2015	fine sand	999,9	2	20,0	964,5	13,6	15,0	60	24,3	584,0	1,201			nicht verwendbar
149	27.01.2015	fine sand	999,9	2	20,0	962,7	13,7	15,0	70	28,1	549,5	1,130			nur 2.-4. Runde verwendbar
150	27.01.2015	fine sand	1.000,0	2	20,0	964,4	13,6	15,0	80	32,4	533,8	1,098			
151	27.01.2015	fine sand	1.000,0	2	20,0	959,6	14,0	15,0	90	35,5	502,7	1,034			
152	27.01.2015	fine sand	1.000,1	2	20,0	966,2	13,5	15,0	100	40,9	488,3	1,004			
153	27.01.2015	fine sand	1.000,0	4	39,9	965,2	13,6	15,0	50	20,7	577,8	1,189			nur 2. und 3. Runde verwendbar
154	27.01.2015	fine sand	1.000,0	4	40,0	965,4	13,5	15,0	60	24,9	564,5	1,161			
155	27.01.2015	fine sand	1.000,0	4	40,0	959,4	14,0	15,0	70	28,1	536,9	1,104			
156	27.01.2015	fine sand	1.000,0	4	39,9	965,2	13,6	15,0	80	33,2	514,4	1,058			
157	27.01.2015	fine sand	1.000,1	4	40,1	964,5	13,6	15,0	90	37,2	503,9	1,037	19.921,4	616,1	
158	26.01.2015	fine sand	1.000,0	4	40,0	963,2	13,7	15,0	100	41,0	480,9	0,989			
159	22.12.2014	fine sand	999,9	6	59,4	960,0	14,0	15,0	50	20,5	603,3	1,241			
160	22.12.2014	fine sand	1.000,2	6	60,1	961,9	13,8	15,0	60	24,9	581,0	1,195			nicht verwendbar
161	22.12.2014	fine sand	999,7	6	60,2	963,0	13,7	15,0	70	29,2	535,8	1,102			
162	22.12.2014	fine sand	1.000,0	6	60,4	958,1	14,1	15,0	80	32,5	531,1	1,092			
163	22.12.2014	fine sand	999,6	6	59,9	960,5	13,9	15,0	90	37,0	512,7	1,055			
164	22.12.2014	fine sand	999,7	6	60,4	962,4	13,8	15,0	100	41,6		0,000			density measurement missing
165	21.12.2014	fine sand	999,6	8	80,0	965,2	13,6	15,0	50	21,5	582,4	1,198			density measurement missing, nicht verwendbar
166	21.12.2014	fine sand	1.000,3	8	79,6	970,2	13,2	15,0	60	26,5	534,9	1,100			
167	21.12.2014	fine sand	999,8	8	80,4	969,7	13,2	15,0	70	30,9	521,8	1,073			
168	21.12.2014	fine sand	999,7	8	79,6	967,5	13,4	15,0	80	34,9	501,3	1,031			
169	21.12.2014	fine sand	999,8	8	80,2	965,9	13,5	15,0	90	38,9	473,1	0,973			
170	21.12.2014	fine sand	1.000,1	8	79,8	966,4	13,7	15,0	100	43,3					
171	18.12.2014	fine sand	1.000,0	10	100,5	962,8	13,8	15,0	50	21,7	608,2	1,251			
172	18.12.2014	fine sand	999,7	10	99,3	961,8	13,7	15,0	60	25,8		0,000			density measurement missing
173	18.12.2014	fine sand	1.000,5	10	100,1	963,4	13,8	15,0	70	30,4	564,2	1,161			
174	18.12.2014	fine sand	1.000,3	10	100,8	962,5	13,8	15,0	80	34,6	521,0	1,072			
175	18.12.2014	fine sand	999,6	10	99,8	962,0	14,0	15,0	90	38,8	491,2	1,010			
176	18.12.2014	fine sand	1.000,0	10	100,5	960,0	14,0	15,0	100	42,6	478,9	0,985			
177	17.12.2014	fine sand	1.000,0	12	119,9	956,2	14,3	15,0	50	21,2	584,0	1,201	19.732,0	610,3	
178	17.12.2014	fine sand	1.000,0	12	120,1	961,4	13,8	15,0	60	26,2	567,6	1,168			
179	17.12.2014	fine sand	999,9	12	120,2	960,1	13,9	15,0	70	30,4	538,0	1,107			
180	17.12.2014	fine sand	1.000,0	12	120,2	956,7	14,2	15,0	80	34,1	507,6	1,044			
181	17.12.2014	fine sand	1.000,1	12	120,3	961,1	13,9	15,0	90	39,3	477,0	0,981			
182	17.12.2014	fine sand	1.000,0	12	120,1	959,7	14,0	15,0	100	43,3	451,5	0,929	25.091,2	776,0	

test no. [-]	date [-]	soil [-]	m_soil [g]	w [M%]	m_water [g]	m_cup+foam [g]	FER_actual [-]	FER_target [-]	FIR [%]	m_foam to add [g]	m_total [g]	density [g/cm³]	Liquid m_water	Liquid m_surfactant	remarks
183	26.01.2015	sand		2			-3,1	15,0	10	0,0		0,000			*nicht mehr durchgeführt
184	26.01.2015	sand	999,6	2	20,1	957,3	14,2	15,0	20	8,0	709,6	1,460			
185	26.01.2015	sand	1.000,0	2	19,9	957,4	14,2	15,0	30	12,0	681,8	1,402			nicht verwertbar
186	26.01.2015	sand	999,9	2	20,0	965,2	13,6	15,0	40	16,7	648,6	1,334			
187	26.01.2015	sand	1.000,0	2	20,0	961,8	13,8	15,0	50	20,5	623,5	1,283			
188	26.01.2015	sand	999,6	4	40,0	962,1	13,8	15,0	10	4,2	731,2	1,504	20.089,2	621,3	ABORTED
189	22.12.2014	sand	1.000,0	4	40,3	957,1	14,2	15,0	20	8,1	691,4	1,422			
190	22.12.2014	sand	999,8	4	40,1	959,4	14,0	15,0	30	12,4	689,8	1,419			
191	22.12.2014	sand	1.000,3	4	39,7	959,5	14,0	15,0	40	16,5	666,5	1,371			
192	22.12.2014	sand	999,8	4	39,9	960,8	13,9	15,0	50	20,8	618,3	1,272			
193	22.12.2014	sand	1.000,6	6	59,8	961,5	13,8	15,0	10	4,3	769,3	1,582			ABORTED
194	22.12.2014	sand	1.000,1	6	60,2	962,3	13,8	15,0	20	8,6	680,8	1,400			
195	22.12.2014	sand	1.000,0	6	60,4	964,1	13,6	15,0	30	13,0	684,7	1,408			
196	22.12.2014	sand	1.001,0	6	60,2	964,0	13,6	15,0	40	17,3	653,9	1,345			
197	22.12.2014	sand	999,9	6	60,2	964,3	13,6	15,0	50	21,6	624,1	1,284			
198	22.12.2014	sand	1.000,2	8	80,1	958,7	14,1	15,0	10	4,3	728,2	1,498			
199	22.12.2014	sand	1.000,1	8	79,2	955,7	14,3	15,0	20	8,4	717,0	1,475	25.187,6	779,0	
200	21.12.2014	sand	999,9	8	80,2	962,4	13,8	15,0	30	13,1	689,0	1,417			
201	21.12.2014	sand	999,8	8	80,6	961,9	13,8	15,0	40	17,4	661,2	1,360			
202	21.12.2014	sand	1.000,6	8	79,5	964,5	13,6	15,0	50	22,0	630,3	1,297			
203	21.12.2014	sand	1.000,3	10	100,1	965,1	13,6	15,0	10	4,5		0,000			density measurement missing
204	21.12.2014	sand	1.000,0	10	100,2	964,1	13,6	15,0	20	9,0	724,6	1,491			
205	21.12.2014	sand	1.000,5	10	99,5	963,5	13,7	15,0	30	13,4	697,4	1,435			
206	21.12.2014	sand	999,8	10	100,3	966,9	13,4	15,0	40	18,2	666,4	1,371	25.526,6	789,5	
207	18.12.2014	sand	1.000,2	10	100,1	959,4	14,0	15,0	50	21,8	619,9	1,275			
208	17.12.2014	sand	1.000,1	12	120,0	960,0	14,0	15,0	10	4,5	759,3	1,562			
209	17.12.2014	sand	999,9	12	119,9	959,2	14,0	15,0	20	8,9	722,1	1,485			
210	17.12.2014	sand	1.000,1	12	119,9	959,4	14,0	15,0	30	13,3	687,5	1,414			
211	17.12.2014	sand	999,9	12	120,0	958,8	14,0	15,0	40	17,7	666,5	1,371			
212	17.12.2014	sand	1.000,0	12	120,0	960,8	13,9	15,0	50	22,4	622,6	1,281			

test no.	date	soil	m_soil	w	m_water	m_cup+foam	FER_actual	FER_target	FIR	m_foam to add	m_total	density	Liquid		remarks
[-]	[-]	[-]	[g]	[M%]	[g]	[g]	[-]	[-]	[%]	[g]	[g]	[g/cm³]	m_water	m_surfactant	
213		fine sand		2			-3,1	15,0	50	0,0		0,000			
214		fine sand		2			-3,1	15,0	60	0,0		0,000			
215	16.02.2015	fine sand	1.000,0	2	20,1	954,1	14,4	15,0	70	26,7	604,4	1,243			abgebrochen, nicht verwertbar
216	13.02.2015	fine sand	1.000,1	2	20,0	966,8	13,4	15,0	80	32,8	545,3	1,122			
217	13.02.2015	fine sand	1.000,1	2	19,9	958,6	14,1	15,0	90	35,3	511,5	1,052			
218	13.02.2015	fine sand	1.000,0	2	20,0	956,1	14,3	15,0	100	38,6	501,6	1,032			
219		fine sand		4			-3,1	15,0	50	0,0		0,000			abgebrochen, nicht verwertbar
220	13.02.2015	fine sand	1.000,0	4	40,0	959,9	14,0	15,0	60	24,2	613,5	1,262			
221	13.02.2015	fine sand	1.000,0	4	40,1	959,8	14,0	15,0	70	28,2	567,2	1,167			
222	16.02.2015	fine sand	1.000,0	4	40,2	960,3	13,9	15,0	80	32,3	536,5	1,104	20.005,1	618,7	
223		fine sand	1.000,0	4	40,0	971,2	13,1	15,0	90	38,6	500,4	1,029			
224		fine sand	1.000,0	4	40,0	969,0	13,3	15,0	100	42,3	470,7	0,968			
225		fine sand	1.000,0	6	60,0	964,5	13,6	15,0	50	21,1	570,8	1,174			
226		fine sand	1.000,1	6	60,0	967,7	13,4	15,0	60	25,7	554,1	1,140	20.006,8	618,8	
227		fine sand	1.000,0	6	60,0	962,3	13,8	15,0	70	29,1	539,8	1,110			
228		fine sand	1.000,0	6	59,9	964,2	13,6	15,0	80	33,6	505,1	1,039			
229		fine sand	999,9	6	60,0	965,4	13,5	15,0	90	38,1	488,2	1,004			
230		fine sand	1.000,1	6	59,9	965,7	13,5	15,0	100	42,4	487,4	1,003			
231		fine sand	1.000,1	8	79,9	964,3	13,6	15,0	50	21,4	568,2	1,169			
232		fine sand	1.000,0	8	80,0	965,0	13,6	15,0	60	25,8	544,4	1,120			
233		fine sand	1.000,0	8	79,9	963,9	13,7	15,0	70	29,9	529,1	1,088	19.992,1	618,3	
234		fine sand	1.000,1	8	79,9	963,1	13,7	15,0	80	34,1	512,8	1,055			
235		fine sand	1.000,0	8	80,0	963,3	13,7	15,0	90	38,4	494,3	1,017			
236		fine sand	1.000,1	8	80,0	959,3	14,0	15,0	100	41,7	472,3	0,972			
237		fine sand	1.000,0	10	100,0	964,0	13,6	15,0	50	21,8	578,1	1,189			
238		fine sand	1.000,0	10	100,0	959,1	14,0	15,0	60	25,4	541,2	1,113	19.985,4	618,1	
239		fine sand	1.000,0	10	100,0	957,2	14,2	15,0	70	29,4	527,6	1,085			
240		fine sand	1.000,1	10	99,9	959,1	14,0	15,0	80	33,9	512,0	1,053			
241		fine sand	1.000,0	10	100,0	960,2	13,9	15,0	90	38,4	476,6	0,980			
242		fine sand	1.000,0	10	100,0	961,2	13,9	15,0	100	42,9	455,0	0,936			
243		fine sand	1.000,0	12	120,1	958,9	14,0	15,0	50	21,6	553,8	1,139			nicht kongruent zu Referenzversuchen
244		fine sand	1.000,0	12	120,0	962,1	13,8	15,0	60	26,3	541,7	1,114			nicht kongruent zu Referenzversuchen
245		fine sand	1.000,0	12	120,0	961,0	13,9	15,0	70	30,5	521,3	1,072			nicht kongruent zu Referenzversuchen
246		fine sand	1.000,0	12	120,0	957,0	14,2	15,0	80	34,1	476,7	0,981			nicht kongruent zu Referenzversuchen
247		fine sand	1.000,0	12	119,9	962,1	13,8	15,0	90	39,5	480,4	0,988			nicht kongruent zu Referenzversuchen
248		fine sand	1.000,0	12	120,1	959,1	14,0	15,0	100	43,2	457,3	0,941	20.056,2	620,3	nicht kongruent zu Referenzversuchen

test no.	date	soil	m_{soil}	w	m_{water}	$m_{Lup+foam}$	FER_{actual}	FER_{target}	FIR	$m_{foam\,to\,add}$	m_{total}	density	m_{water}	$m_{surfactant}$	remarks
[-]	[-]	[-]	[g]	[M%]	[g]	[g]	[-]	[-]	[%]	[g]	[g]	[g/cm³]			
249		sand		2			-3,1	15,0	10	0,0		0,000			
250		sand		2			-3,1	15,0	20	0,0		0,000			
251	20.02.2015	sand	1.000,2	2	20,2	956,8	14,2	15,0	30	12,0	701,2	1,442			
252	20.02.2015	sand	1.000,3	2	20,0	956,3	14,3	15,0	40	15,9	651,1	1,339			
253	20.02.2015	sand	1.000,3	2	19,9	958,5	14,1	15,0	50	20,1	645,7	1,328			
254		sand		4			-3,1	15,0	10	0,0		0,000			
255	20.02.2015	sand	1.000,1	4	40,0	955,8	14,3	15,0	20	8,1	716,2	1,473			abgebrochen, nicht verwertbar
256	19.02.2015	sand	1.000,4	4	40,1	960,5	13,9	15,0	30	12,5	682,7	1,404			
257	19.02.2015	sand	1.000,6	4	40,1	958,9	14,0	15,0	40	16,5	674,0	1,386			
258	19.02.2015	sand	1.000,2	4	40,0	957,3	14,2	15,0	50	20,4	636,4	1,309			
259		sand		6			-3,1	15,0	10	0,0		0,000			
260	19.02.2015	sand	1.000,1	6	59,9	962,0	13,8	15,0	20	8,5	704,5	1,449			
261		sand		6			-3,1	15,0	30	0,0		0,000			deckungsgleich mit V069, daher nicht durchgeführt
262	19.02.2015	sand	1.000,0	6	60,1	958,2	14,1	15,0	40	16,7	672,8	1,384			
263	19.02.2015	sand	1.000,0	6	60,0	959,5	14,0	15,0	50	21,0	654,1	1,345			
264	19.02.2015	sand	1.000,3	8	79,9	965,5	13,5	15,0	10	4,4	754,2	1,551			abgebrochen, nicht verwertbar
265	19.02.2015	sand	1.000,8	8	80,1	965,2	13,6	15,0	20	8,9	706,0	1,452			
266	19.02.2015	sand	1.000,4	8	80,0	949,4	14,8	15,0	30	12,1	700,3	1,441			
267	17.02.2015	sand	1.000,7	8	80,2	961,9	13,8	15,0	40	17,4	675,7	1,390			
268	17.02.2015	sand	1.000,5	8	80,1	960,3	13,9	15,0	50	21,5	653,3	1,344			
269	17.02.2015	sand	1.000,5	10	100,1	963,1	13,7	15,0	10	4,5	772,0	1,588			abgebrochen, nicht verwertbar
270	17.02.2015	sand	1.000,2	10	100,2	963,6	13,7	15,0	20	8,9	723,1	1,487			
271	17.02.2015	sand	1.000,5	10	100,0	961,5	13,8	15,0	30	13,3	703,4	1,447			
272	17.02.2015	sand	1.000,0	10	100,0	964,2	13,6	15,0	40	17,9	676,1	1,391			
273	17.02.2015	sand	1.000,0	10	100,1	962,3	13,8	15,0	50	22,2	644,2	1,325			
274	17.02.2015	sand	1.000,3	12	120,1	959,7	14,0	15,0	10	4,5	750,5	1,544	20.059,5	620,4	abgebrochen, nicht verwertbar
275	16.02.2015	sand	1.000,6	12	120,2	953,1	14,5	15,0	20	8,6	732,9	1,508			
276	16.02.2015	sand	1.000,1	12	119,9	955,0	14,4	15,0	30	13,0	705,8	1,452			
277	16.02.2015	sand	1.000,3	12	120,0	952,8	14,5	15,0	40	17,1	688,5	1,416			
278	16.02.2015	sand	1.000,0	12	120,0	953,1	14,5	15,0	50	21,4	641,4	1,319			

Repeated tests

test no.	date	BMS	soil	m_{soil}	w	m_{water}	$m_{cupfoam}$	FER_{actual}	FER_{target}	FIR	$m_{foam\,to\,add}$	m_{total}	density	Liquid		remarks
[-]	[-]	[-]	[-]	[g]	[Vol%]	[g]	[g]	[-]	[-]	[%]	[g]	[g]	[g/cm³]	m_{water}	$m_{surfactant}$	
89*	27.02.2015	12	Fine sand	1.000,2	4	40,0	954,6	14,4	15,0	70	27,3	573,0	1,179		0,0	nicht verwertbar
94	27.02.2015	12	Fine sand	1.000,1	6	60,0	957,5	14,2	15,0	60	24,3	599,8	1,234		0,0	nicht verwertbar
99	27.02.2015	12	Fine sand	1.000,0	8	80,0	959,0	14,0	15,0	50	20,8	625,3	1,286		0,0	abgebrochen, nicht verwertbar
102	27.02.2015	12	Fine sand	1.000,1	8	80,0	956,1	14,3	15,0	80	32,7	531,9	1,094		0,0	Mittelwert aus Haupt- und Wdh-Versuch bilden
103	27.02.2015	12	Fine sand	1.000,1	8	79,9	954,0	14,4	15,0	90	36,4	513,6	1,056		0,0	Mittelwert aus Haupt- und Wdh-Versuch bilden
105	27.02.2015	12	Fine sand	1.000,1	10	100,1	952,3	14,6	15,0	50	20,4	612,1	1,259		0,0	Mittelwert aus Haupt- und Wdh-Versuch bilden
112	27.02.2015	12	Fine sand	999,9	12	120,1	957,3	14,2	15,0	60	25,6	574,4	1,182		0,0	neuer Hauptversuch
113	27.02.2015	12	Fine sand	1.000,2	12	120,1	958,9	14,0	15,0	70	30,2	552,3	1,136		0,0	neuer Hauptversuch
114	27.02.2015	12	Fine sand	1.000,0	12	120,1	954,2	14,4	15,0	80	33,6	519,2	1,068		0,0	neuer Hauptversuch
115	27.02.2015	12	Fine sand	1.000,1	12	120,0	966,0	13,5	15,0	90	40,4	494,4	1,017		0,0	neuer Hauptversuch
116	27.02.2015	12	Fine sand	1.000,0	12	119,9	959,4	14,0	15,0	100	43,2	464,3	0,955	25.622,7	792,5	neuer Hauptversuch
119	26.02.2015	12	Sand	999,8	2	20,0	965,1	13,6	15,0	30	12,5	664,5	1,367		0,0	nur 2. Runde verwertbar
123	26.02.2015	12	Sand	1.000,0	4	40,0	966,1	13,5	15,0	20	8,6	697,9	1,436		0,0	nicht verwertbar
125	26.02.2015	12	Sand	1.000,0	4	40,0	963,3	13,7	15,0	40	16,9	641,2	1,319		0,0	Mittelwert aus Haupt- und Wdh-Versuch bilden
126	26.02.2015	12	Sand	1.000,0	4	40,0	963,8	13,7	15,0	50	21,1	627,5	1,291		0,0	Mittelwert aus Haupt- und Wdh-Versuch bilden
128	26.02.2015	12	Sand	1.000,0	6	60,0	960,9	13,9	15,0	20	8,5	697,9	1,436		0,0	Mittelwert aus Haupt- und Wdh-Versuch bilden
130	26.02.2015	12	Sand	1.000,0	6	60,0	964,4	13,6	15,0	40	17,3	647,2	1,331		0,0	Mittelwert aus Haupt- und Wdh-Versuch bilden
132	26.02.2015	12	Sand	1.000,0	8	80,0	962,6	13,8	15,0	10	4,4	710,7	1,462		0,0	nicht verwertbar
133	26.02.2015	12	Sand	999,9	8	80,0	961,6	13,8	15,0	20	8,7	684,7	1,408		0,0	nicht verwertbar
134	26.02.2015	12	Sand	1.000,0	8	80,0	968,1	13,3	15,0	30	13,5	665,1	1,368		0,0	Mittelwert aus Haupt- und Wdh-Versuch bilden
135	26.02.2015	12	Sand	1.000,0	8	80,1	963,2	13,7	15,0	40	17,5	631,9	1,300		0,0	Mittelwert aus Haupt- und Wdh-Versuch bilden
139	26.02.2015	12	Sand	999,8	10	100,0	963,9	13,7	15,0	30	13,4	670,2	1,379		0,0	Mittelwert aus Haupt- und Wdh-Versuch bilden
140	26.02.2015	12	Sand	1.000,0	10	100,0	961,2	13,9	15,0	40	17,6	652,5	1,342		0,0	Mittelwert aus Haupt- und Wdh-Versuch bilden
142	26.02.2015	12	Sand	1.000,0	12	120,1	960,2	13,9	15,0	10	4,5	743,9	1,530		0,0	neuer Hauptversuch
143	26.02.2015	12	Sand	1.000,0	12	120,1	962,0	13,8	15,0	20	9,0	718,8	1,479		0,0	Mittelwert aus Haupt- und Wdh-Versuch bilden
144	26.02.2015	12	Sand	1.000,0	12	119,9	965,4	13,5	15,0	30	13,8	687,3	1,414	20.018,2	619,1	Mittelwert aus Haupt- und Wdh-Versuch bilden

test no. [-]	date [-]	BMS [-]	soil [-]	m_soil [g]	w [V%]	m_water [g]	m_cup+foam [g]	FER_actual [-]	FER_target [-]	FIR [%]	m_foam to add [g]	m_total [g]	density [g/cm³]	Liquid m_water [g]	Liquid m_surfactant	remarks
148	04.03.2015	8	Fine sand	999,7	2	19,8	958,3	14,1	15,0	60	23,5	598,2	1,231	14.885,6	460,4	nicht verwendbar
149	04.03.2015	8	Fine sand	1.000,0	2	19,8	950,3	14,8	15,0	70	26,1	593,5	1,221		0,0	nicht verwendbar
153	04.03.2015	8	Fine sand	1.000,1	4	40,1	956,2	14,3	15,0	50	19,7	608,6	1,252		0,0	nicht verwendbar
160	04.03.2015	8	Fine sand	1.000,0	6	60,2	955,4	14,3	15,0	60	24,0	607,8	1,250		0,0	nicht verwendbar
161	04.03.2015	8	Fine sand	999,9	6	59,9	955,7	14,3	15,0	70	28,0	583,2	1,200		0,0	Mittelwert aus Haupt- und Wdh-Versuch bilden
165	04.03.2015	8	Fine sand	1.000,1	8	80,2	957,2	14,2	15,0	50	20,6	616,6	1,268		0,0	Mittelwert aus Haupt- und Wdh-Versuch bilden
173	04.03.2015	8	Fine sand	1.000,0	10	99,9	956,2	14,3	15,0	70	29,2	552,9	1,137		0,0	Mittelwert aus Haupt- und Wdh-Versuch bilden
176	04.03.2015	8	Fine sand	1.000,1	10	100,3	955,5	14,3	15,0	100	41,5	498,0	1,024		0,0	Mittelwert aus Haupt- und Wdh-Versuch bilden
184	04.03.2015	8	Sand	1.000,3	2	19,8	958,3	14,1	15,0	20	8,0	747,6	1,538		0,0	abgebrochen
185	04.03.2015	8	Sand	1.000,1	2	19,8	956,7	14,2	15,0	30	12,0	694,5	1,429		0,0	neuer Hauptversuch
189	04.03.2015	8	Sand	1.000,2	4	40,0	956,2	14,3	15,0	20	8,1	712,2	1,465		0,0	nicht verwendbar
194	04.03.2015	8	Sand	1.000,4	6	60,2	957,3	14,2	15,0	20	8,3	728,4	1,498		0,0	nicht verwendbar
196	04.03.2015	8	Sand	1.000,2	6	60,2	956,4	14,2	15,0	40	16,5	680,8	1,400		0,0	Mittelwert aus Haupt- und Wdh-Versuch bilden
198	04.03.2015	8	Sand	1.000,0	8	80,1	957,2	14,2	15,0	10	4,2	745,9	1,534		0,0	abgebrochen
203	04.03.2015	8	Sand	999,8	10	100,0	957,8	14,1	15,0	10	4,3	760,8	1,565		0,0	nicht verwertbar
208	04.03.2015	8	Sand	1.000,0	12	120,0	957,2	14,2	15,0	10	4,4	762,9	1,569		0,0	Mittelwert aus Haupt- und Wdh-Versuch bilden
217	03.03.2015	15	Fine sand	1.000,1	2	19,9	952,4	14,6	15,0	90	35,0	541,8	1,114		0,0	Mittelwert aus Haupt- und Wdh-Versuch bilden
218	03.03.2015	15	Fine sand	1.000,2	2	19,7	953,5	14,5	15,0	100	38,1	513,7	1,057		0,0	Mittelwert aus Haupt- und Wdh-Versuch bilden
229	03.03.2015	15	Fine sand	1.000,2	6	59,8	952,8	14,5	15,0	90	35,5	524,0	1,078		0,0	Mittelwert aus Haupt- und Wdh-Versuch bilden
230	03.03.2015	15	Fine sand	1.000,0	6	60,4	954,8	14,4	15,0	100	39,9	504,5	1,038		0,0	Mittelwert aus Haupt- und Wdh-Versuch bilden
243	03.03.2015	15	Fine sand	1.000,0	12	120,5	952,0	14,6	15,0	50	20,7	612,3	1,260		0,0	neuer Hauptversuch
244	03.03.2015	15	Fine sand	1.000,0	12	119,8	955,8	14,3	15,0	60	25,4	587,1	1,208		0,0	neuer Hauptversuch
245	03.03.2015	15	Fine sand	999,7	12	120,2	952,8	14,5	15,0	70	29,1	550,4	1,132		0,0	neuer Hauptversuch
246	03.03.2015	15	Fine sand	1.000,0	12	120,2	954,4	14,4	15,0	80	33,6	523,9	1,078		0,0	neuer Hauptversuch
247	03.03.2015	15	Fine sand	1.000,2	12	119,8	955,6	14,3	15,0	90	38,1	494,8	1,018		0,0	neuer Hauptversuch
248	03.03.2015	15	Fine sand	1.000,2	12	119,8	957,6	14,1	15,0	100	42,8	480,6	0,989		0,0	neuer Hauptversuch
260	03.03.2015	15	Sand	1.000,0	6	60,0	953,9	14,5	15,0	20	8,1	720,2	1,481		0,0	abgebrochen, nicht verwertbar
266	03.03.2015	15	Fine sand	1.000,2	8	80,2	953,5	14,5	15,0	30	12,4	715,1	1,471	25.411,0	785,9	Mittelwert aus Haupt- und Wdh-Versuch bilden
267c	27.02.2015	15	Sand	1.000,0	8	79,9	953,1	14,5	15,0	40	16,5	660,9	1,359		0,0	Mittelwert aus Haupt- und Wdh-Versuch bilden
267b	27.02.2015	15	Sand	1.000,0	8	80,0	951,7	14,6	15,0	40	16,4	674,2	1,387		0,0	nicht verwenden, mit BMS12 durchgeführt! --> gelöscht aus Rheoplus-Datei
228	03.03.2015	15	Fine sand	1.000,2	6	59,9	954,3	14,4	15,0	80	31,8	547,5	1,126		0,0	Mittelwert aus Haupt- und Wdh-Versuch bilden
149c	04.03.2015	8	Fine sand	1.000,2	2	20,1	955,9	14,3	15,0	70	27,0	592,4	1,219		0,0	nicht verwendbar
175	04.03.2015	8	Fine sand	1.000,2	10	100,0	958,3	14,1	15,0	90	38,0	508,5	1,046		0,0	Mittelwert aus Haupt- und Wdh-Versuch bilden
129	12.03.2015	12	Sand	1.000,0	6	60,0	962,5	13,8	15,0	30	12,8	692,9	1,425		0,0	neuer Hauptversuch

* alle Versuchsnr. mit Endung "b", wenn nicht anders angegeben

A.4.3 Diagrams and formulas

A.4.3.1 Average flow curves of main tests
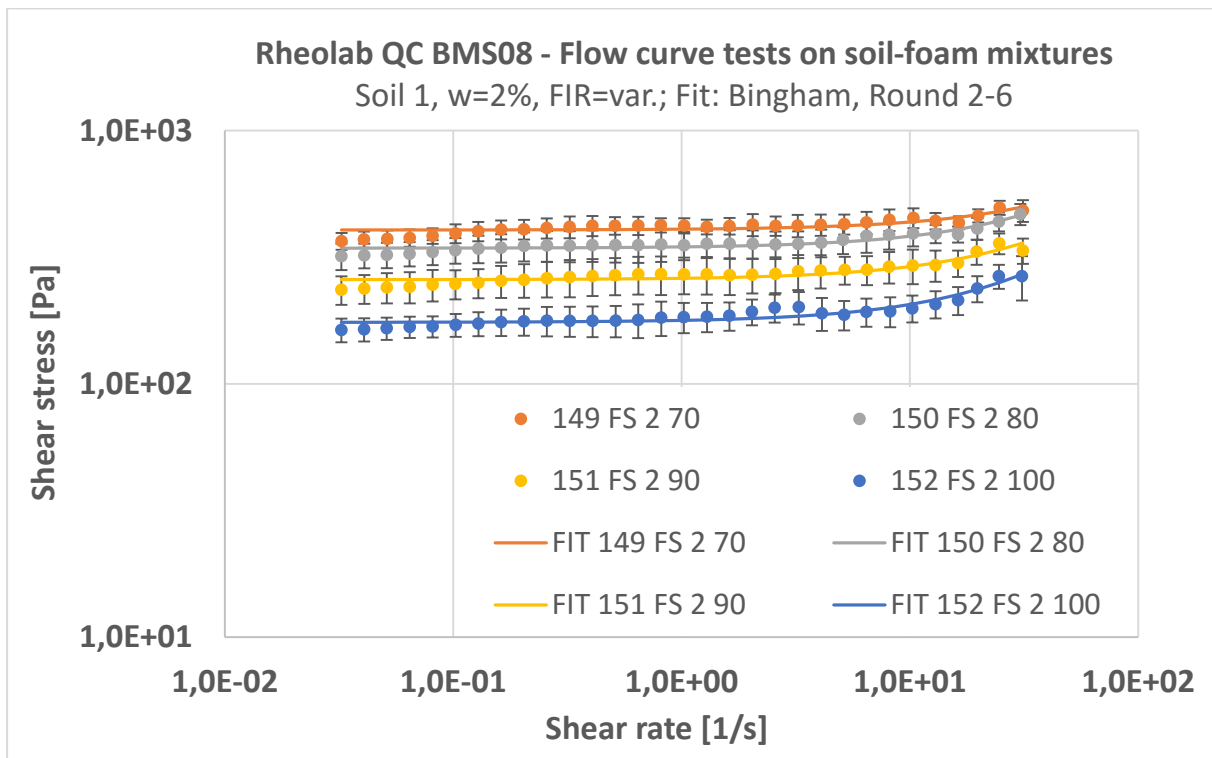
Figure A-41: **Average flow curve data of fine sand-foam mixtures with water content w = 2% and increasing foam content (BMS08, rounds 2 – 6); curve fitting with Bingham model**
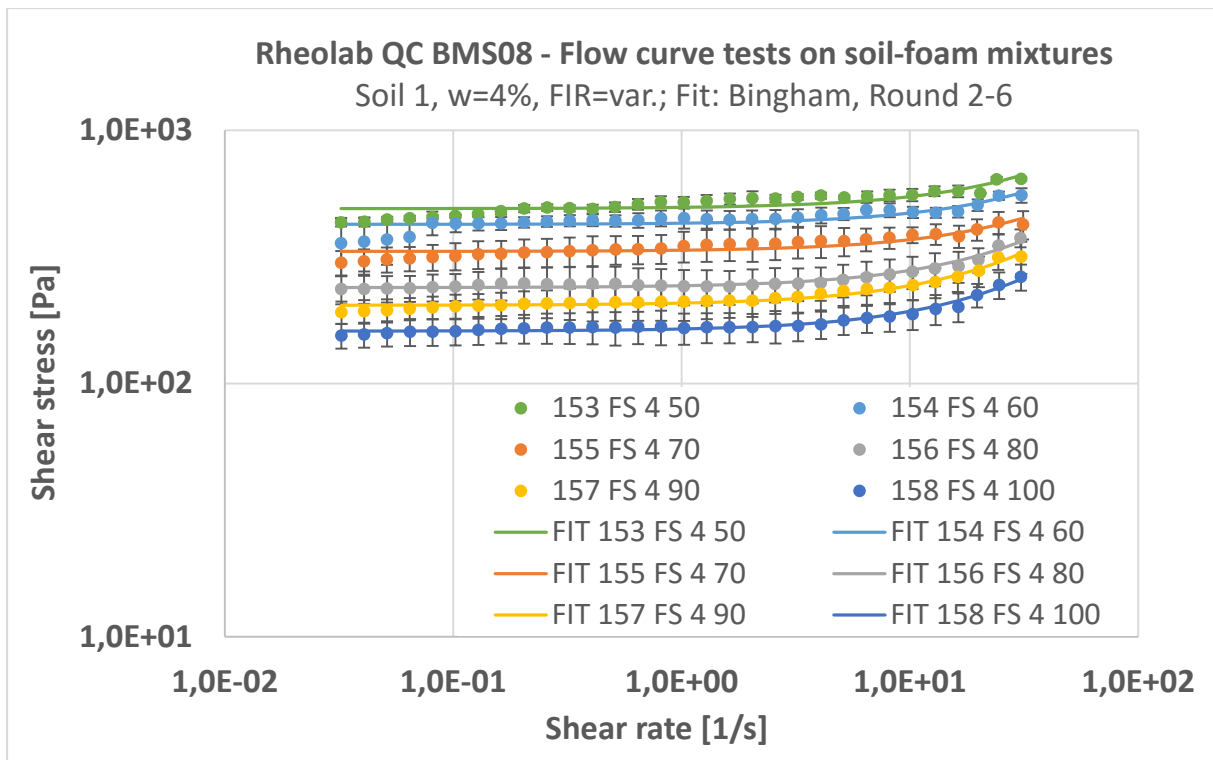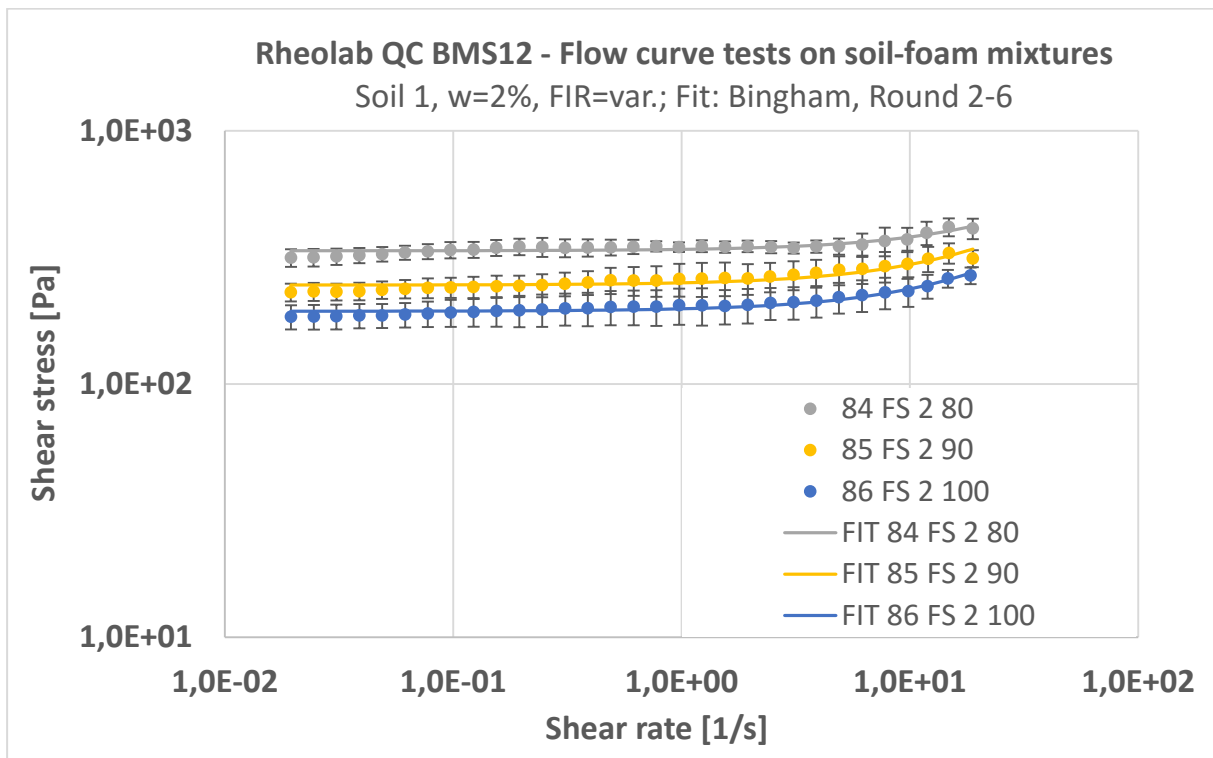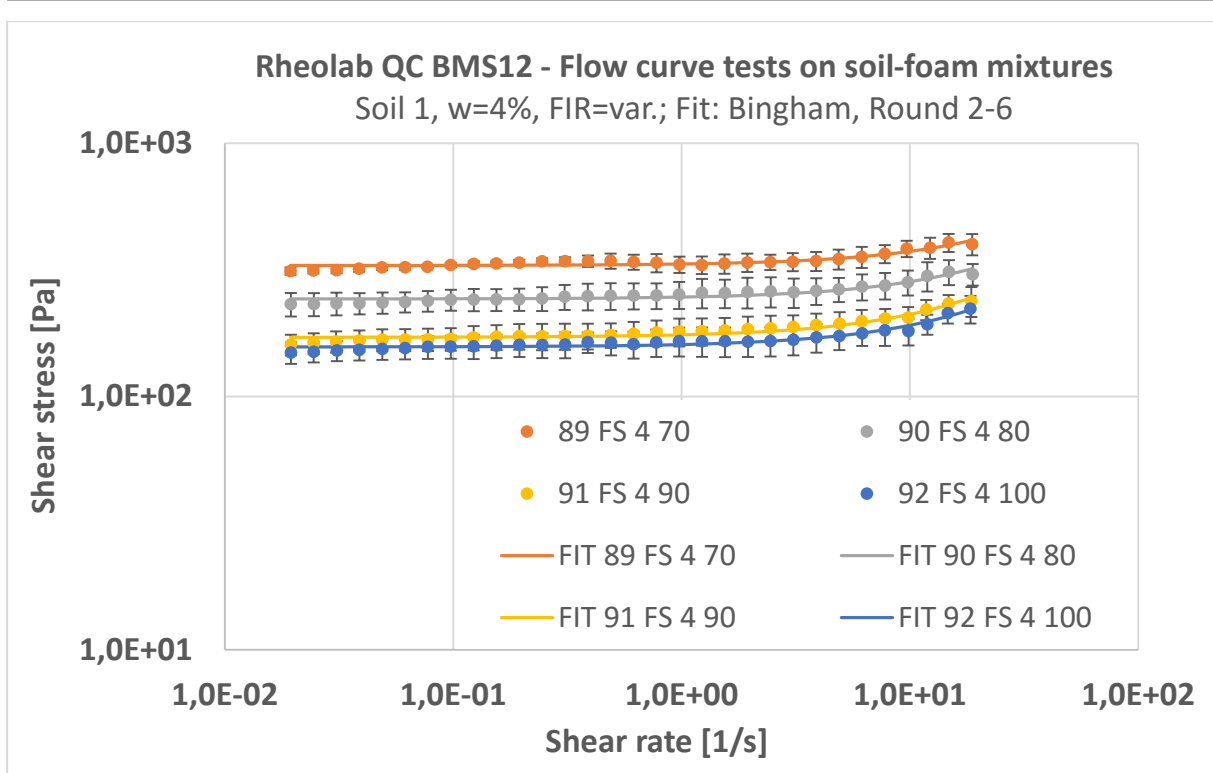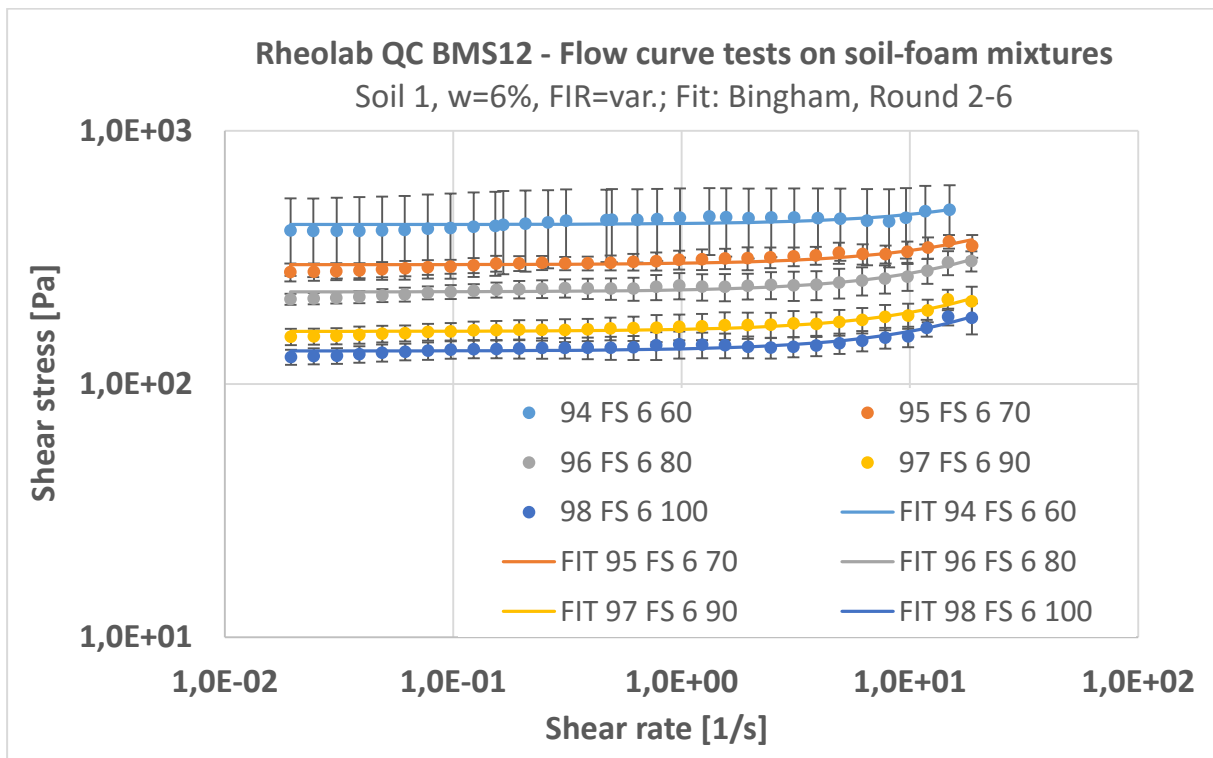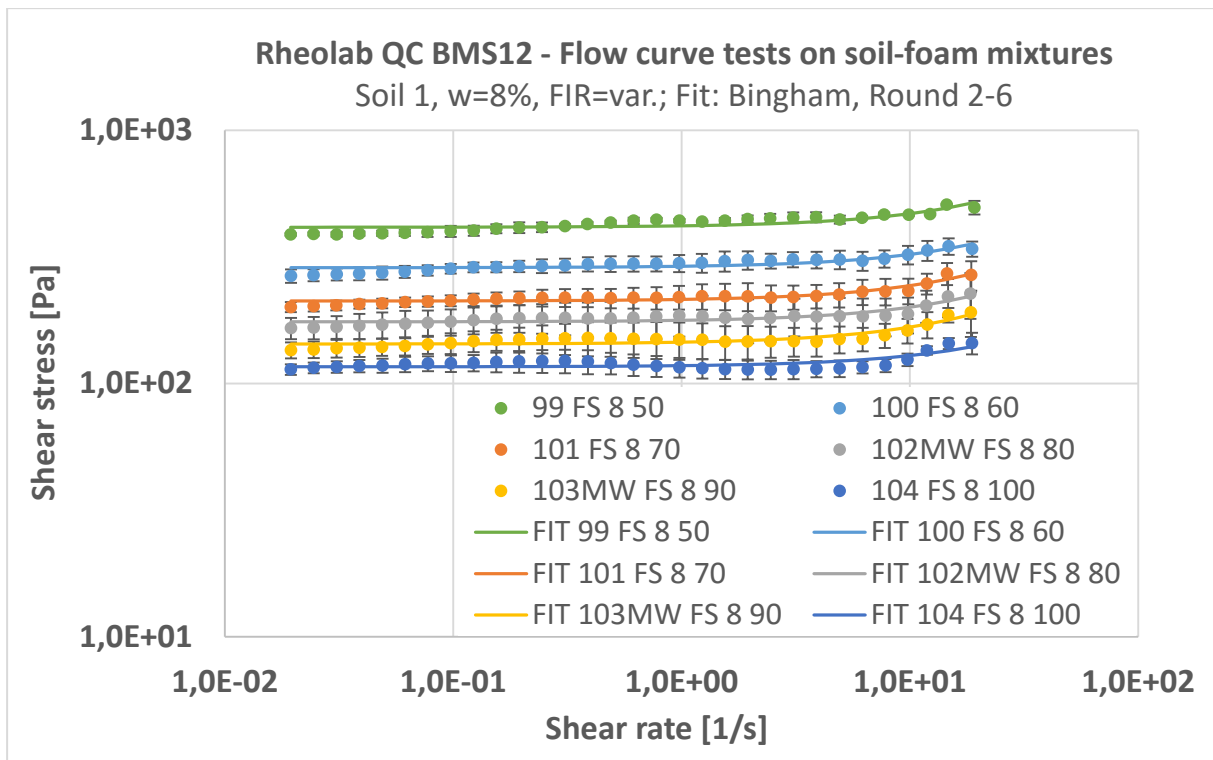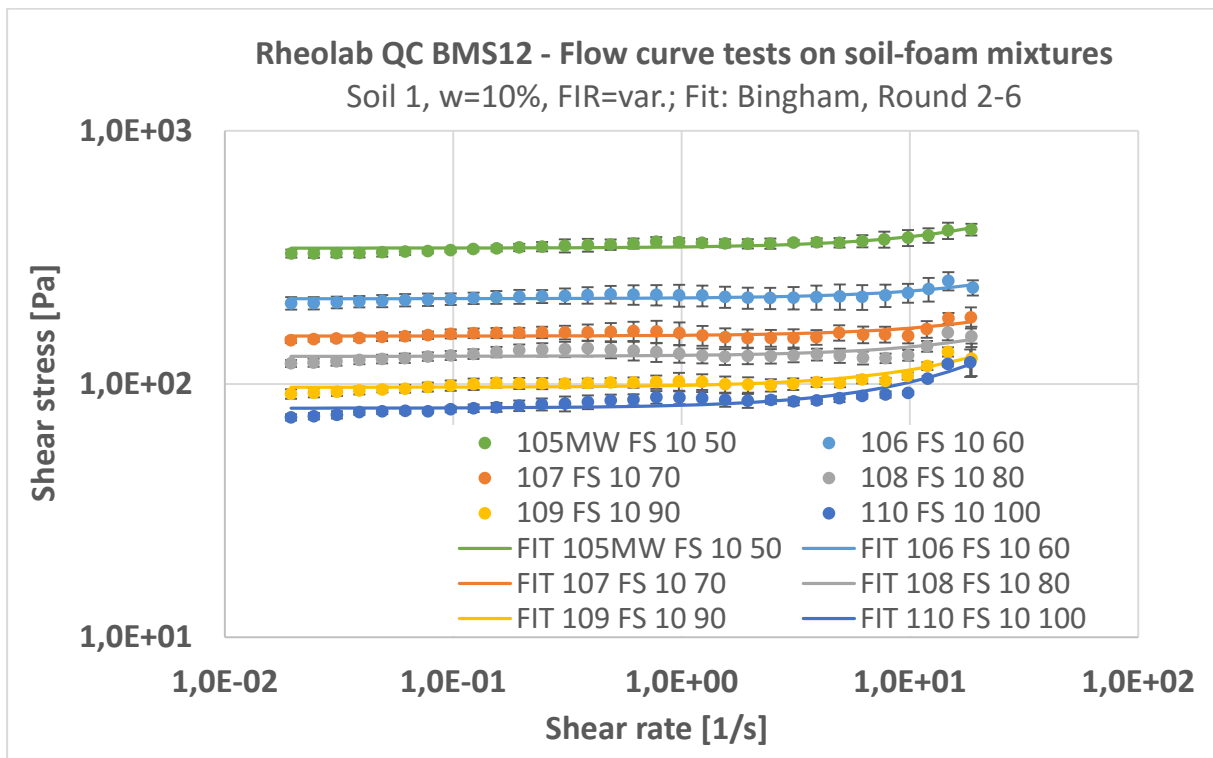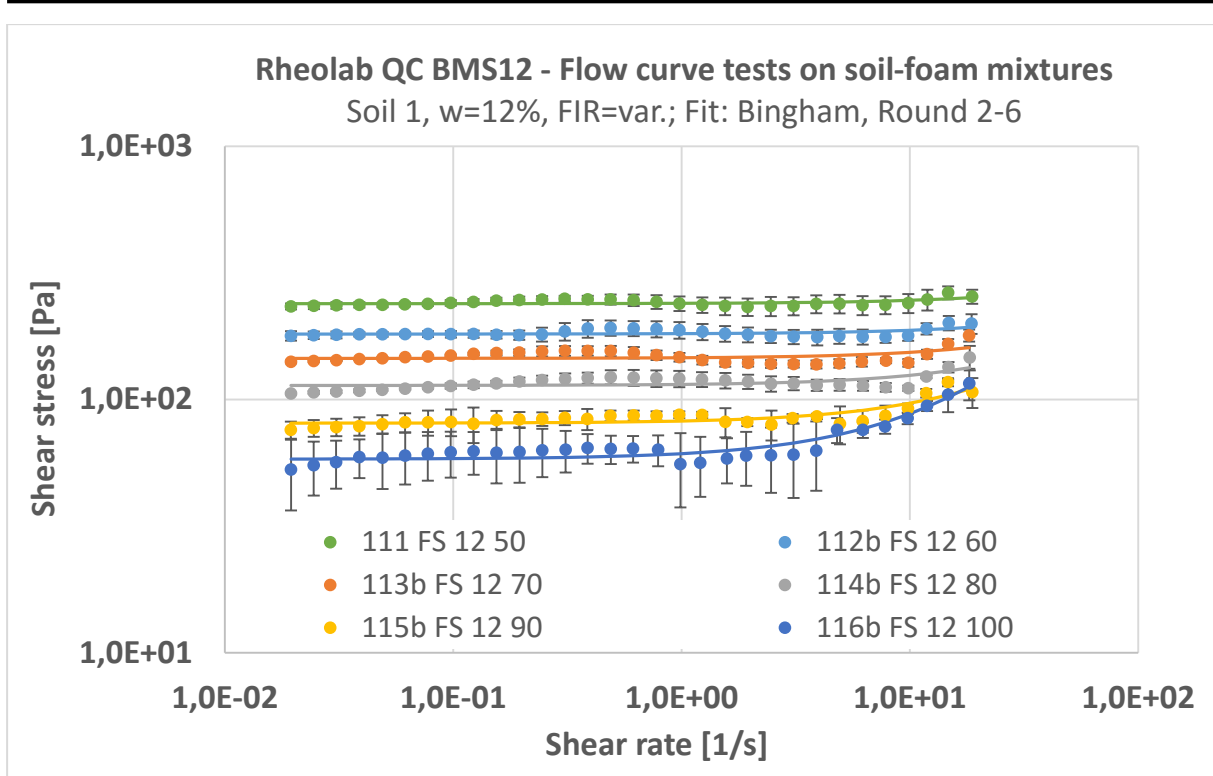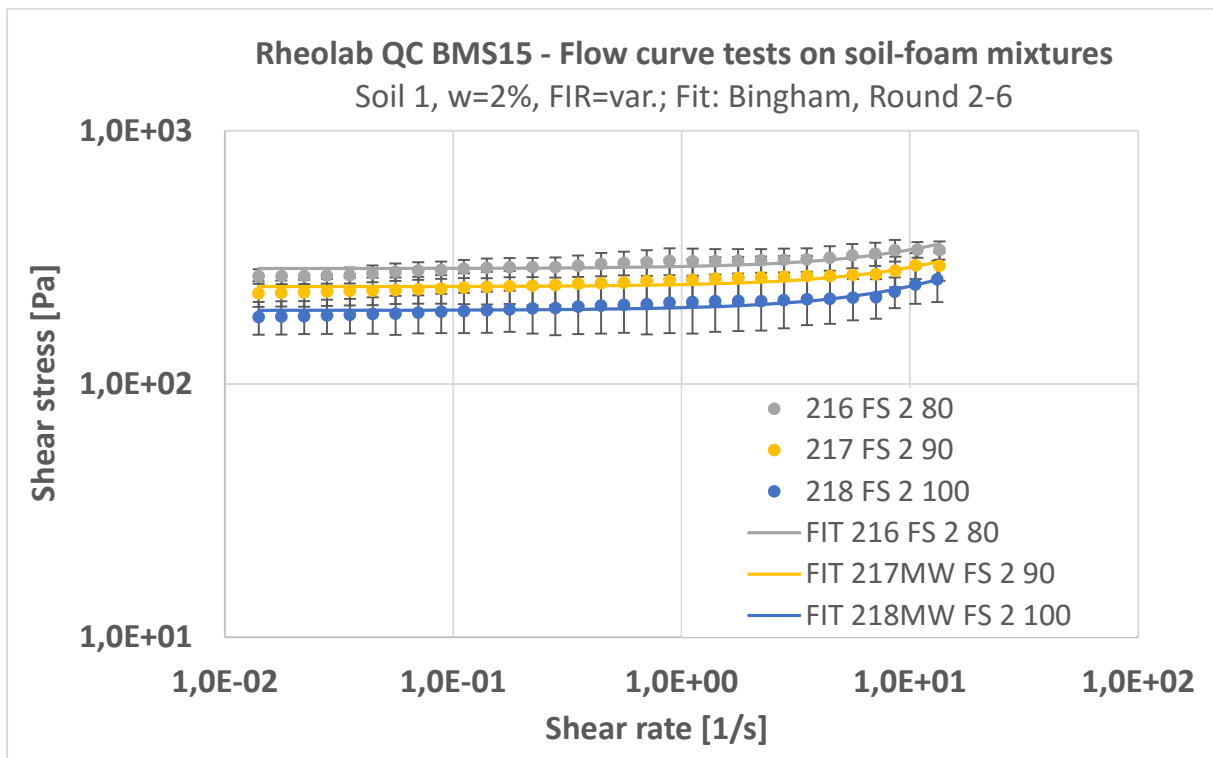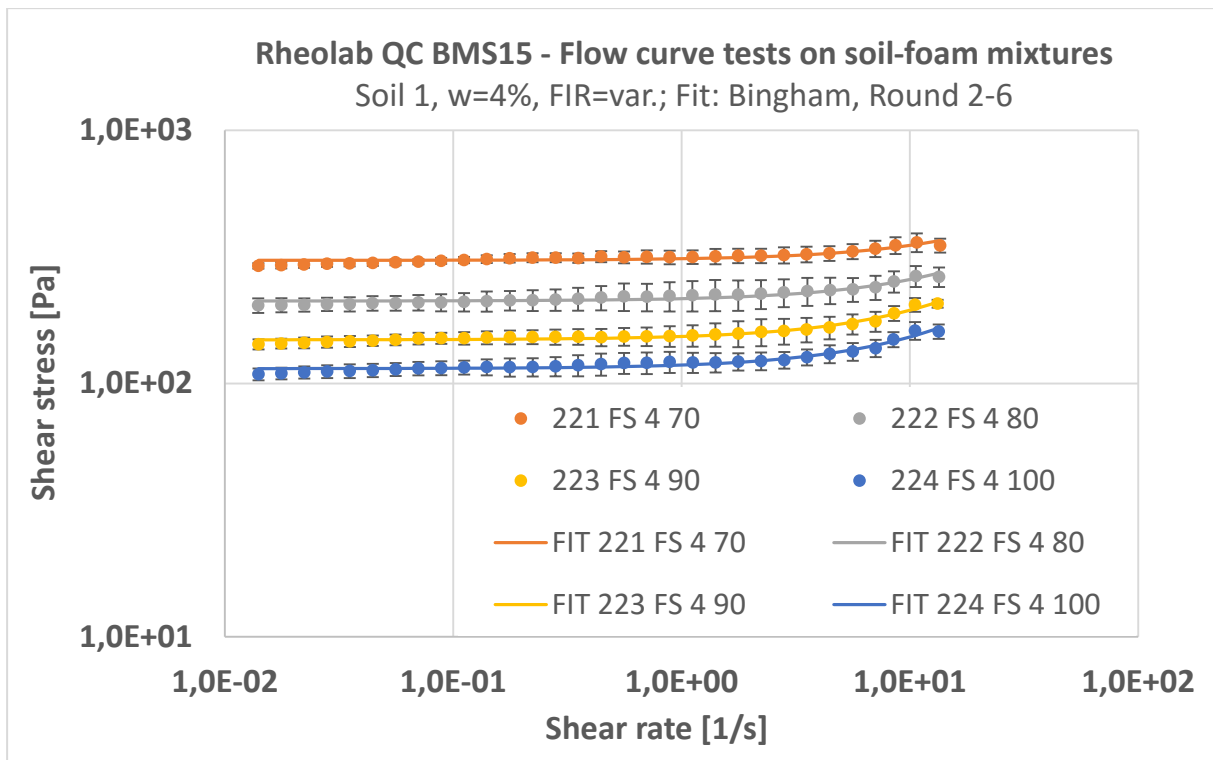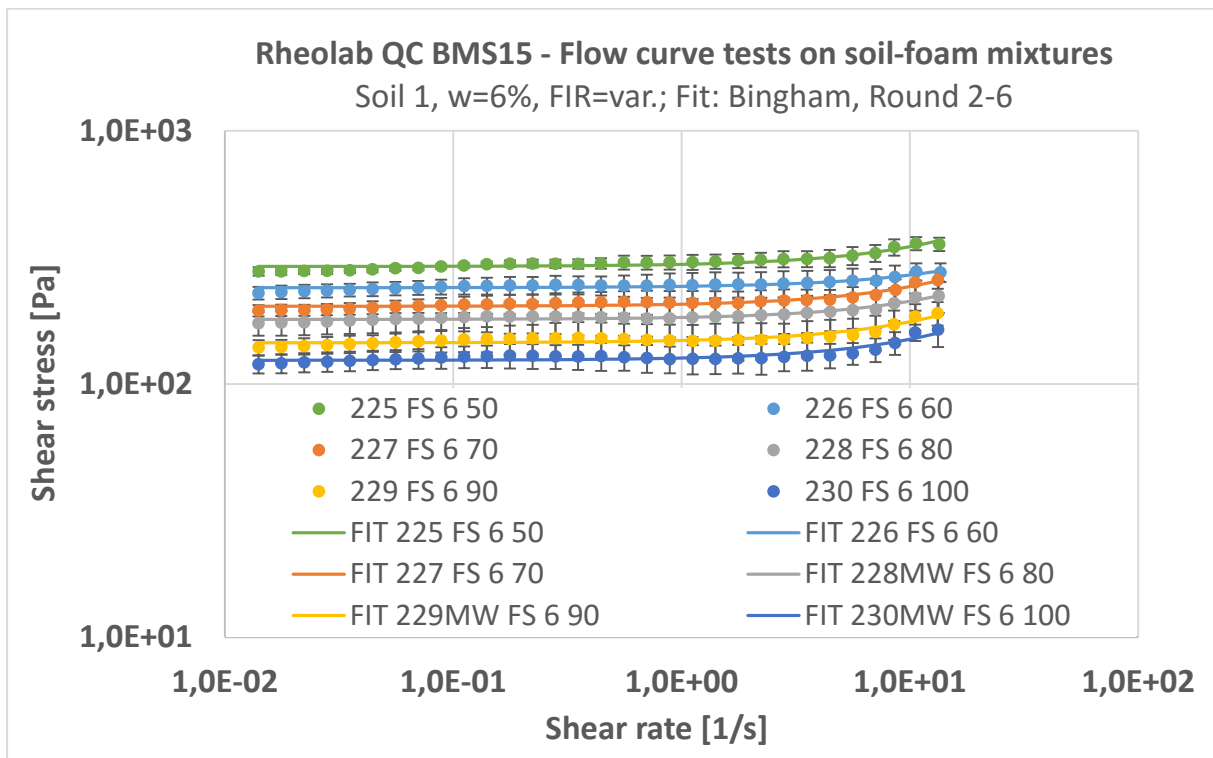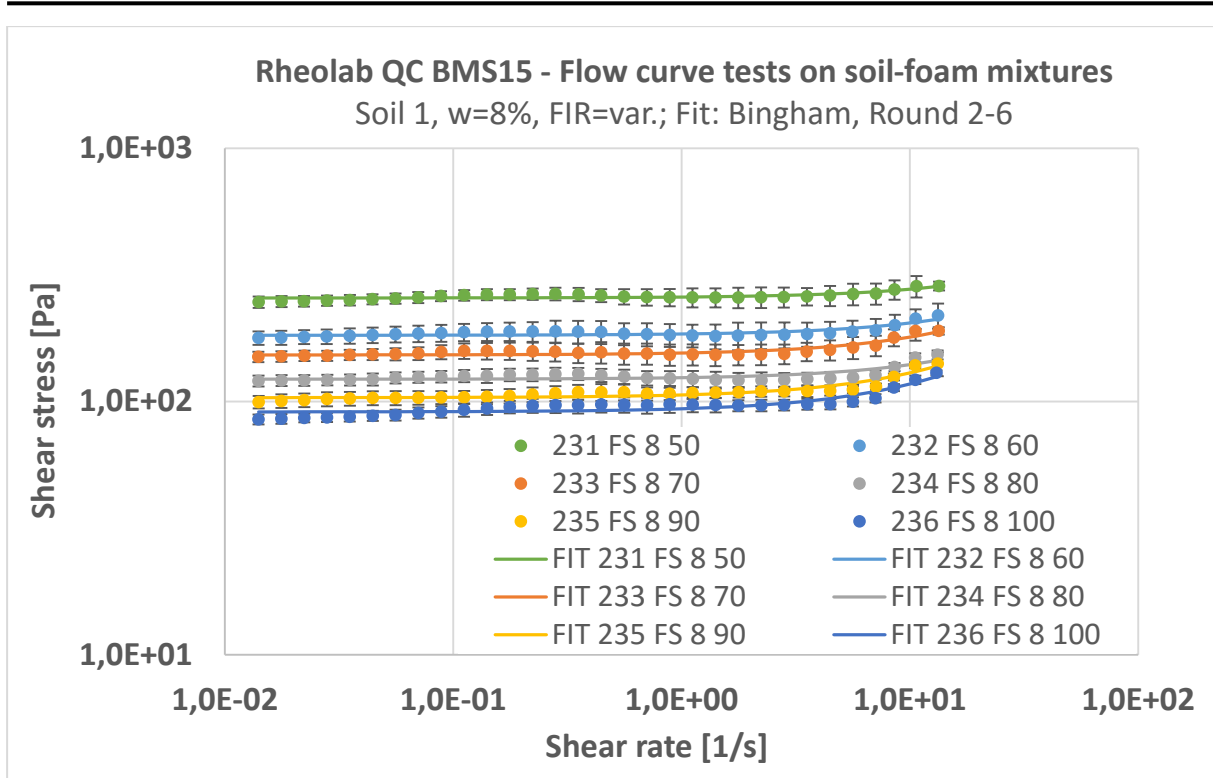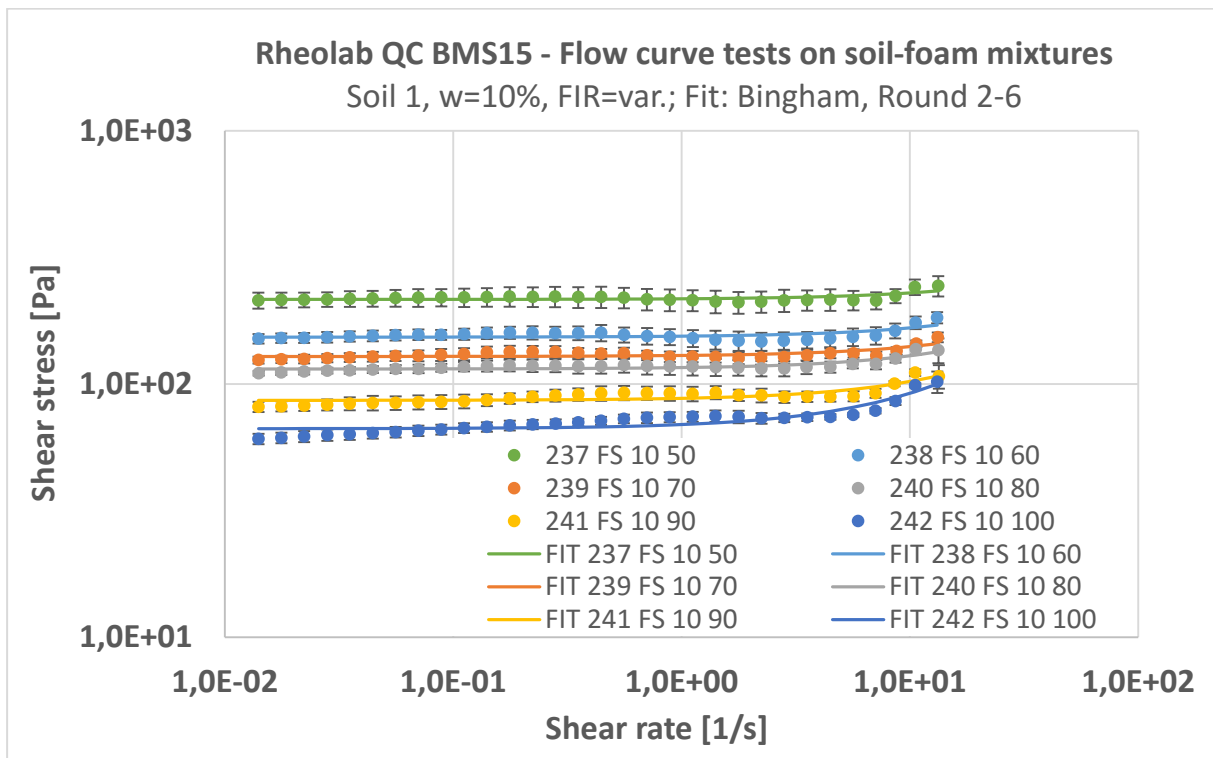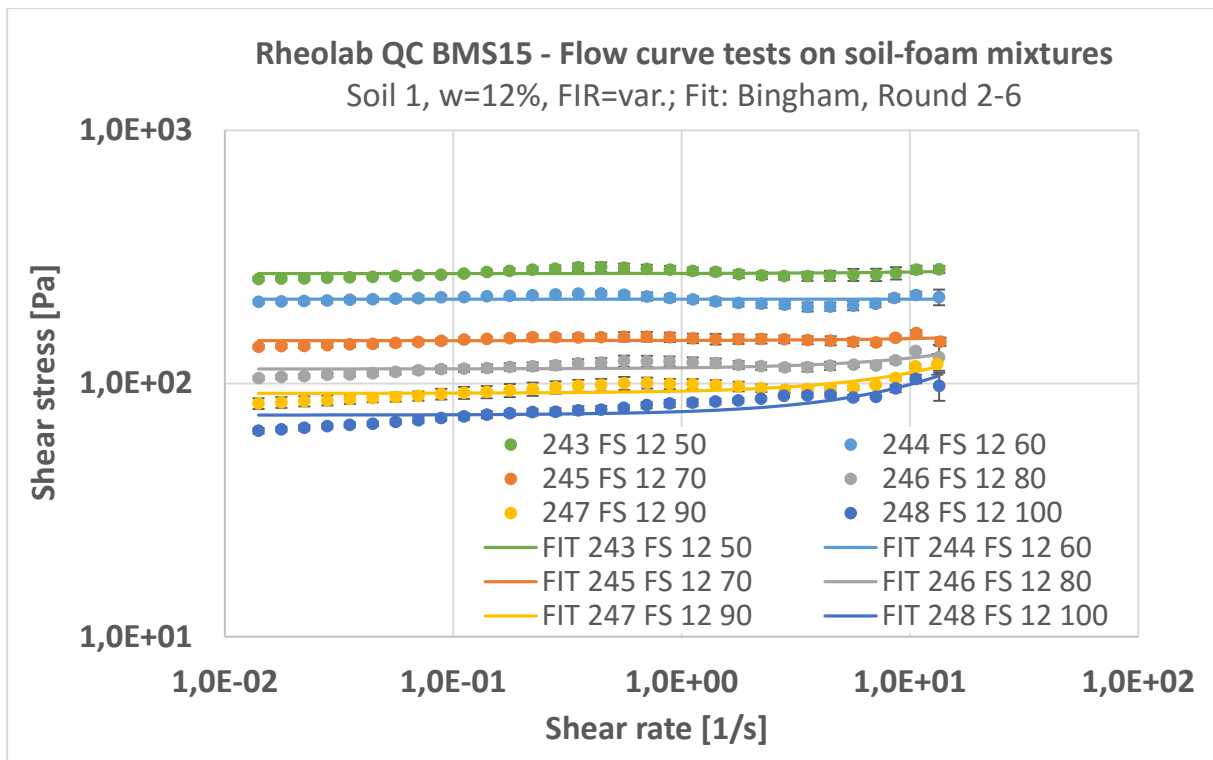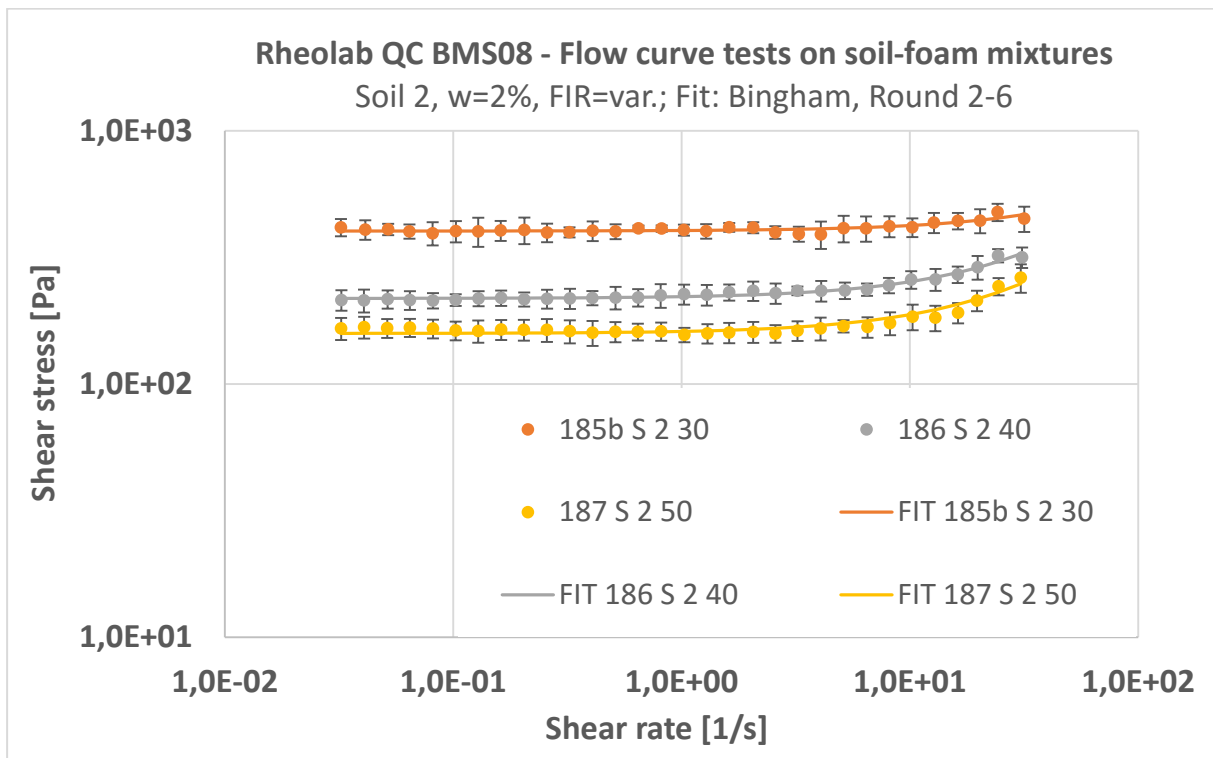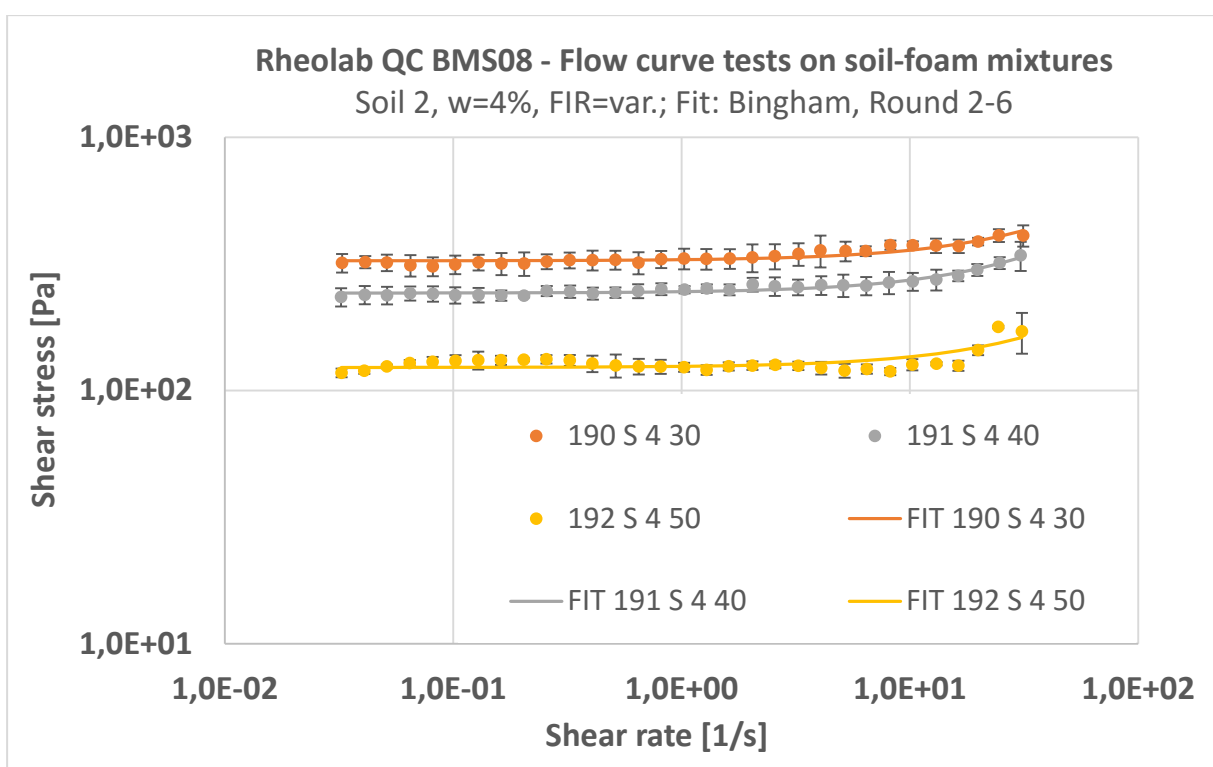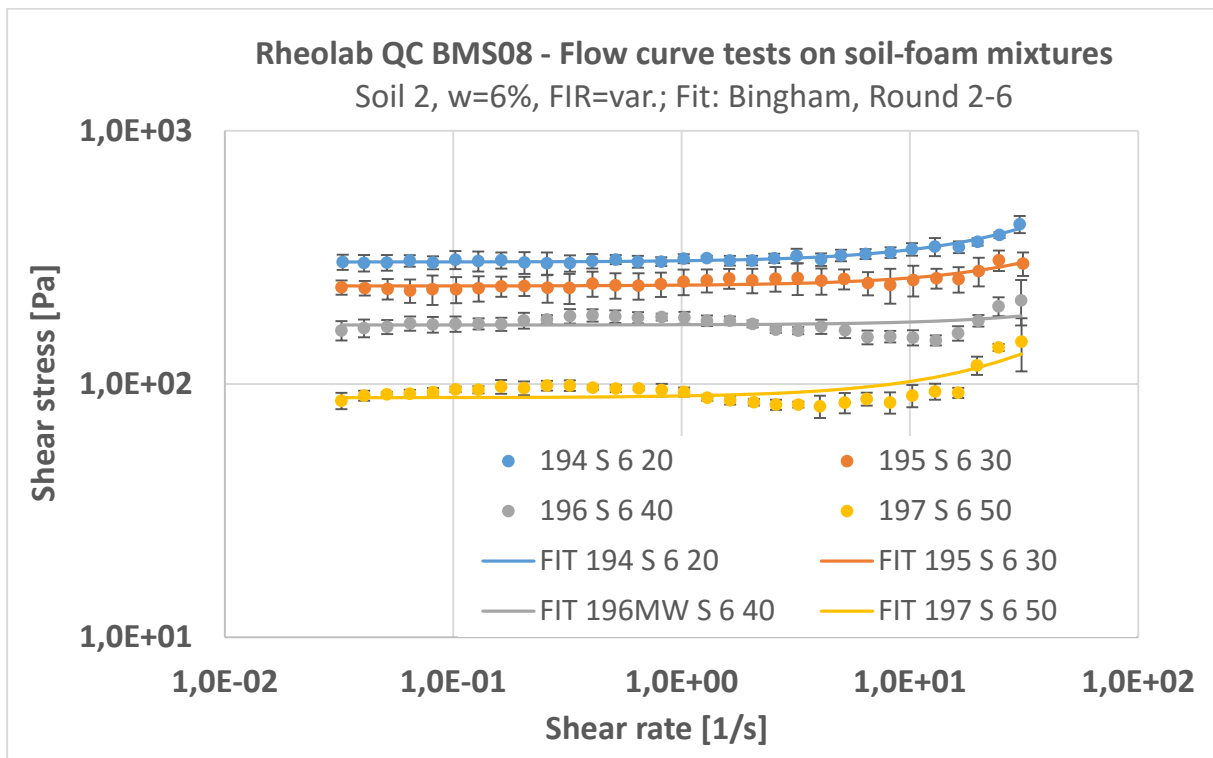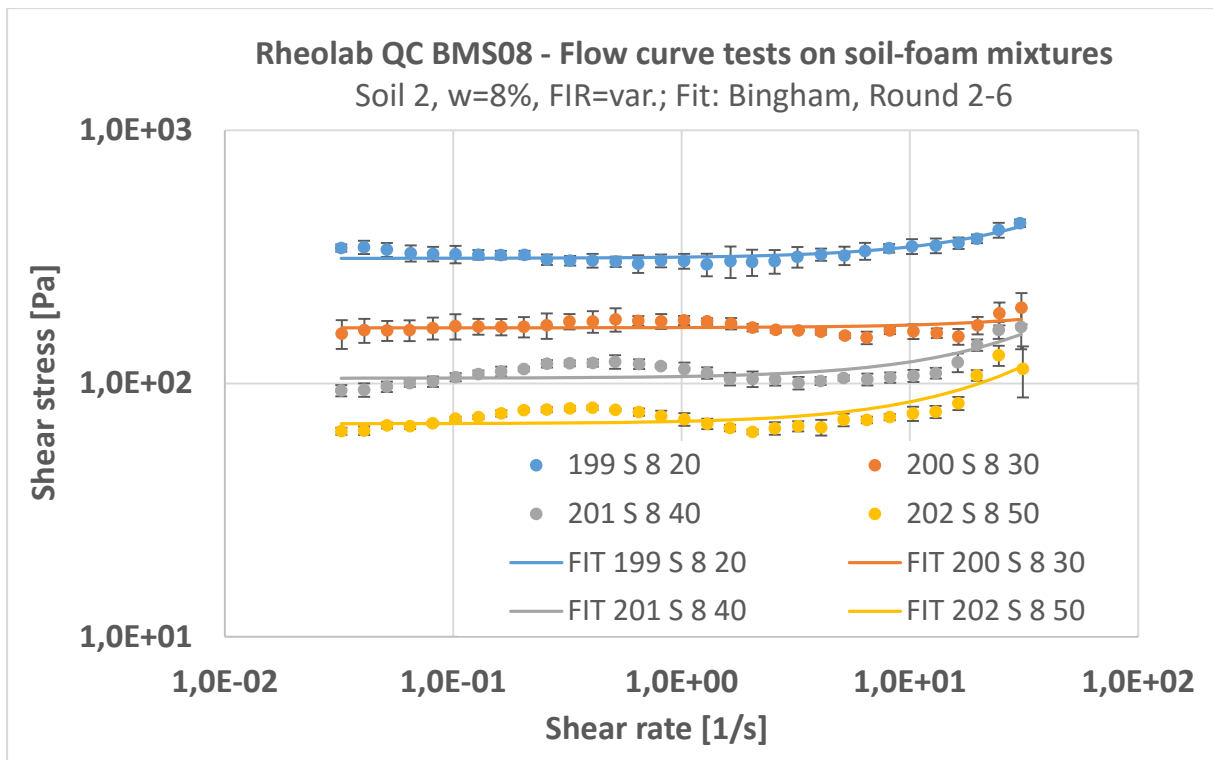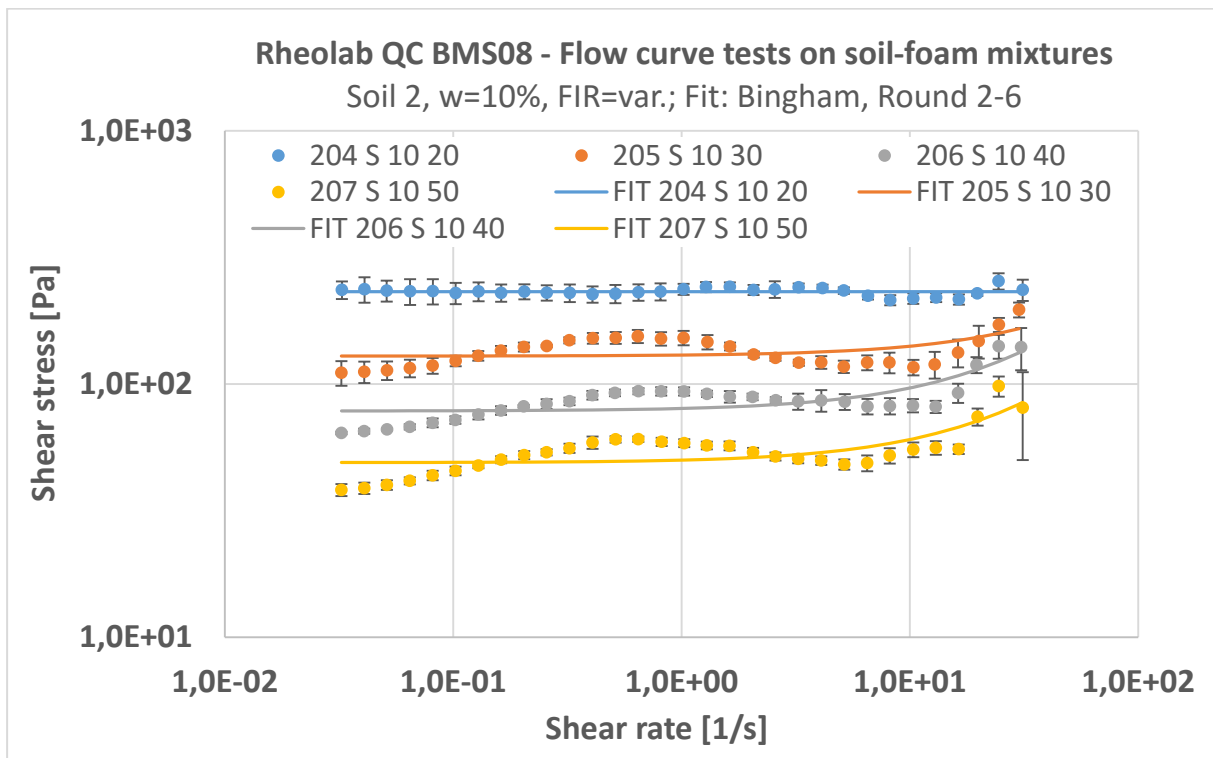
Figure A-42: Average flow curve data of fine sand-foam mixtures with water content w = 4% and increasing foam content (BMS08, rounds 2 – 6); curve fitting with Bingham model
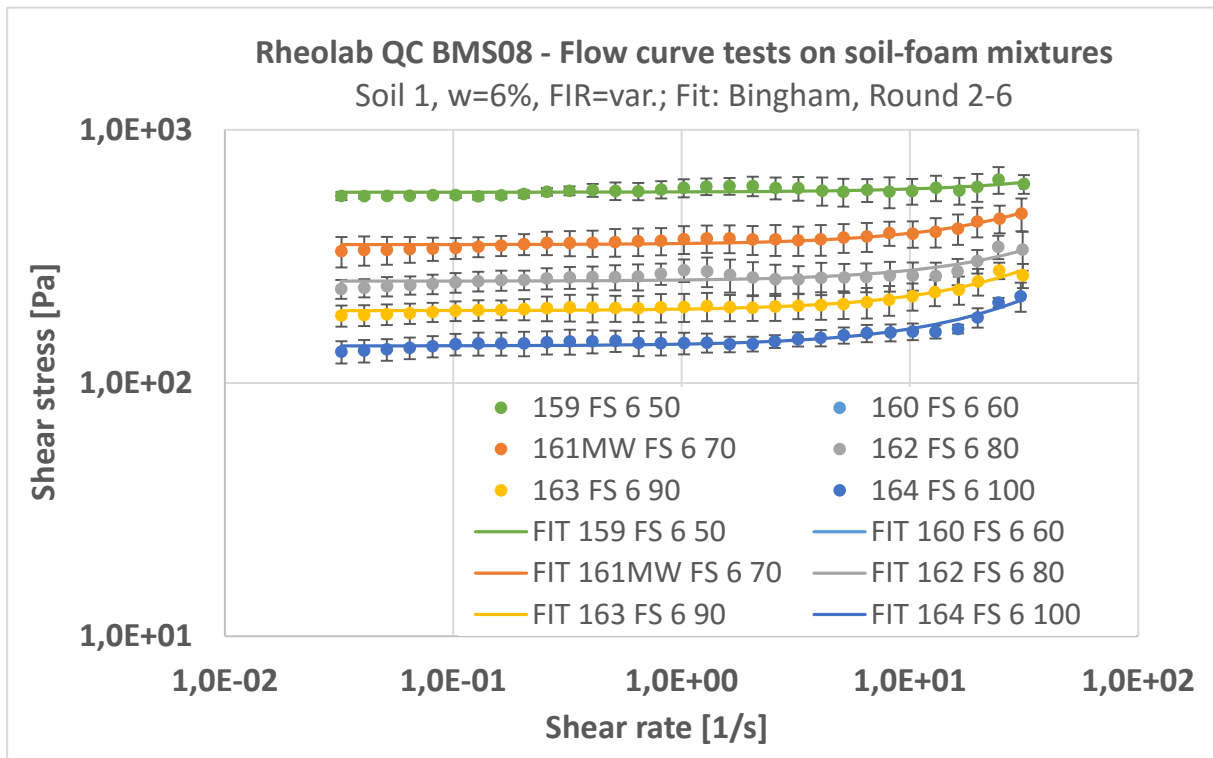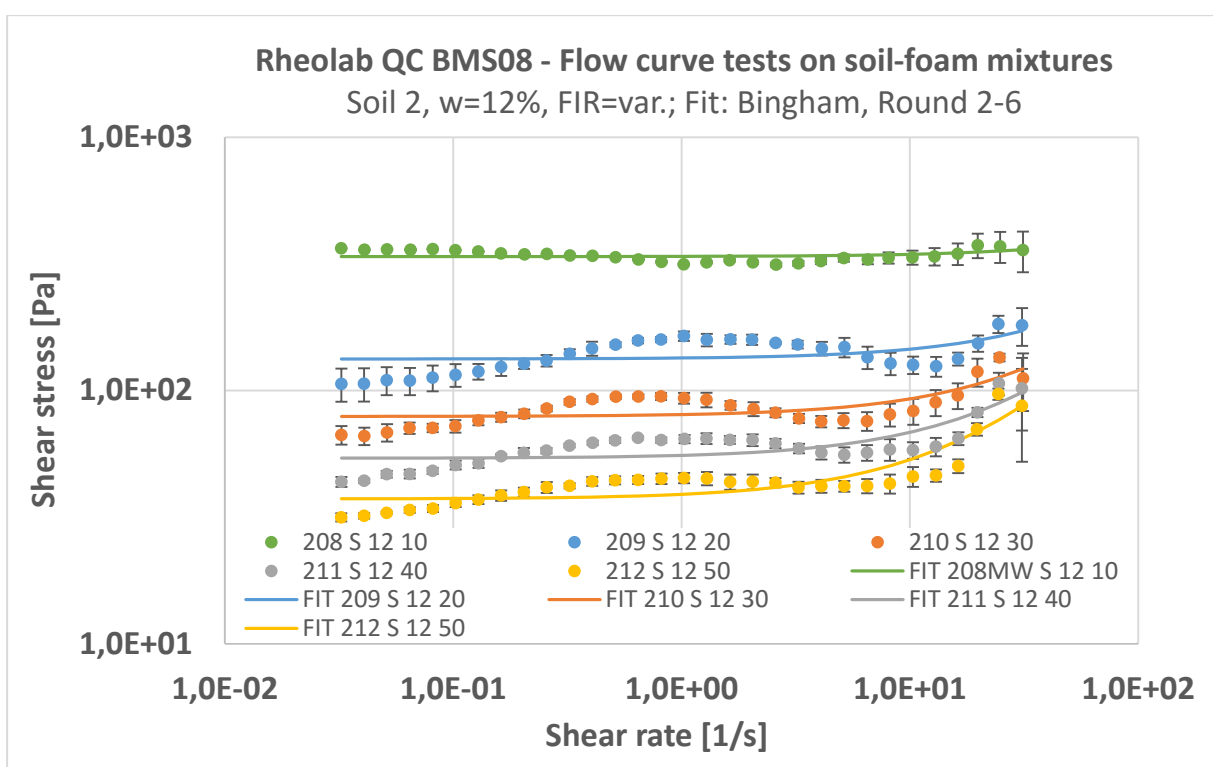

Figure A-43: Average flow curve data of fine sand-foam mixtures with water content w = 6% and increasing foam content (BMS08, rounds 2 – 6); curve fitting with Bingham model
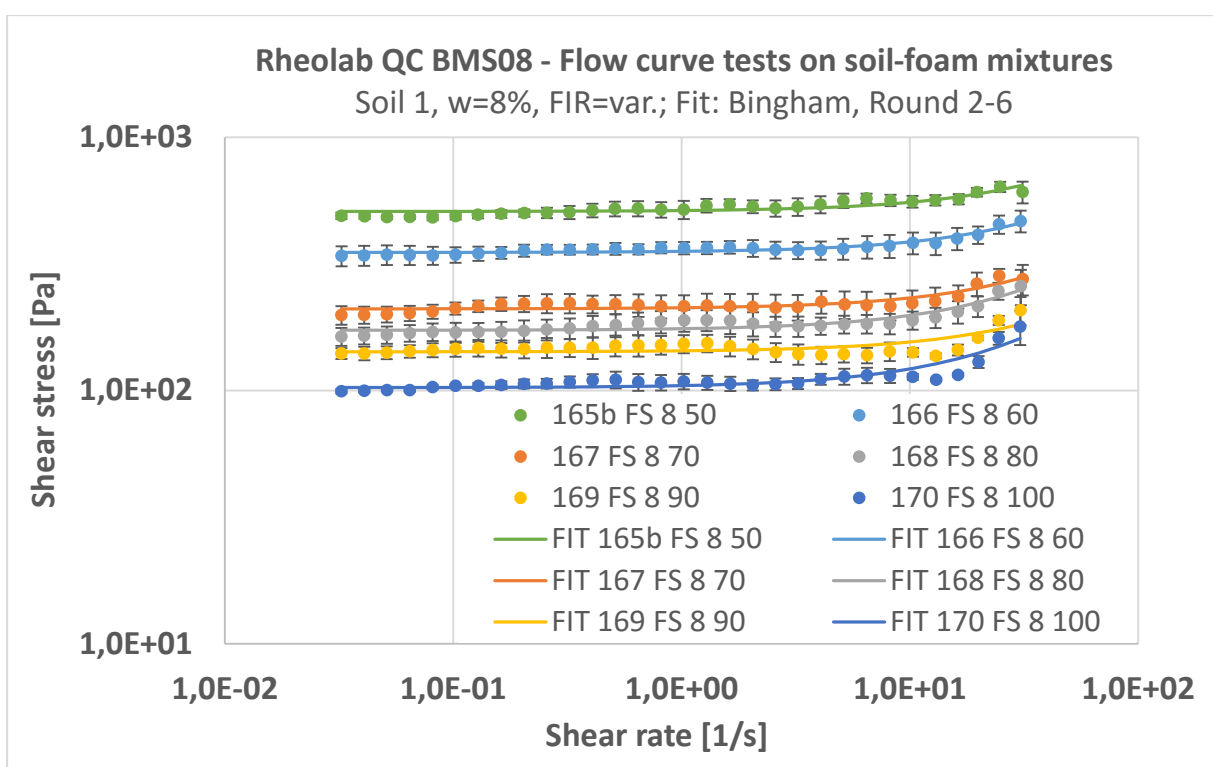
Figure A-44: Average flow curve data of fine sand-foam mixtures with water content w = 8% and increasing foam content (BMS08, rounds 2 – 6); curve fitting with Bingham model
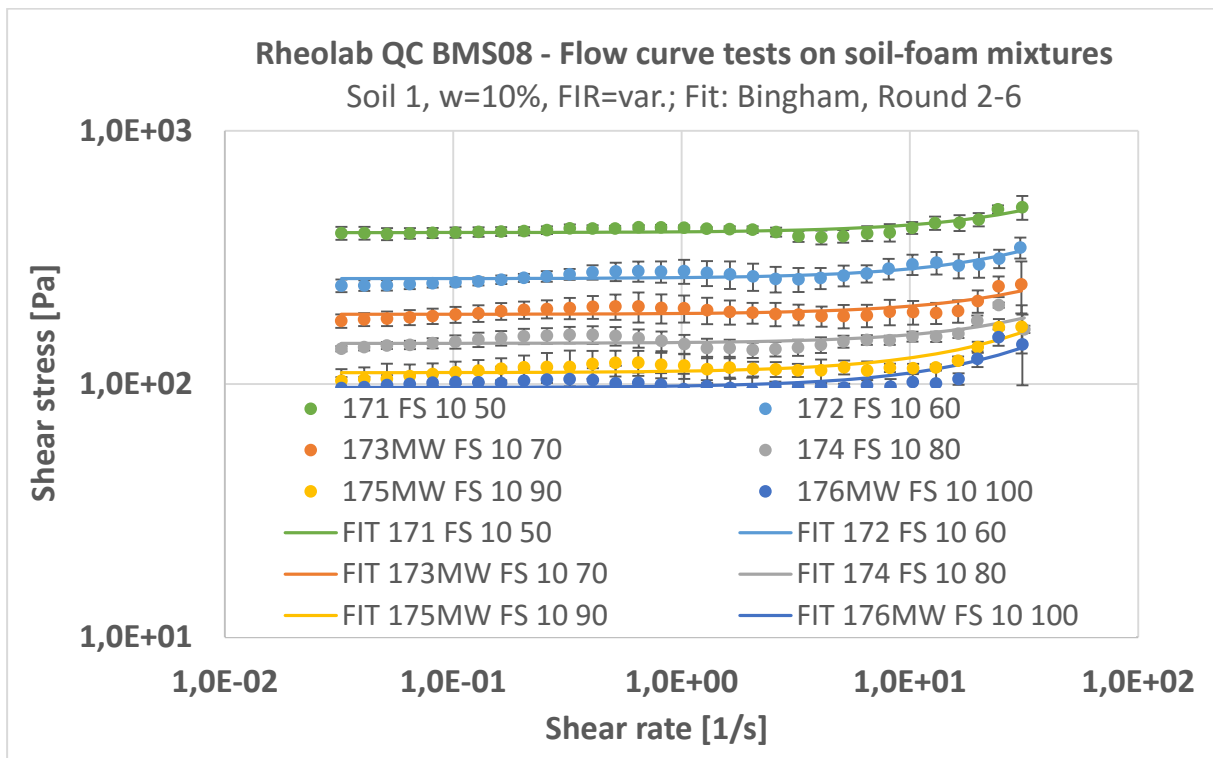
Figure A-45: Average flow curve data of fine sand-foam mixtures with water content w = 10% and increasing foam content (BMS08, rounds 2 – 6); curve fitting with Bingham model
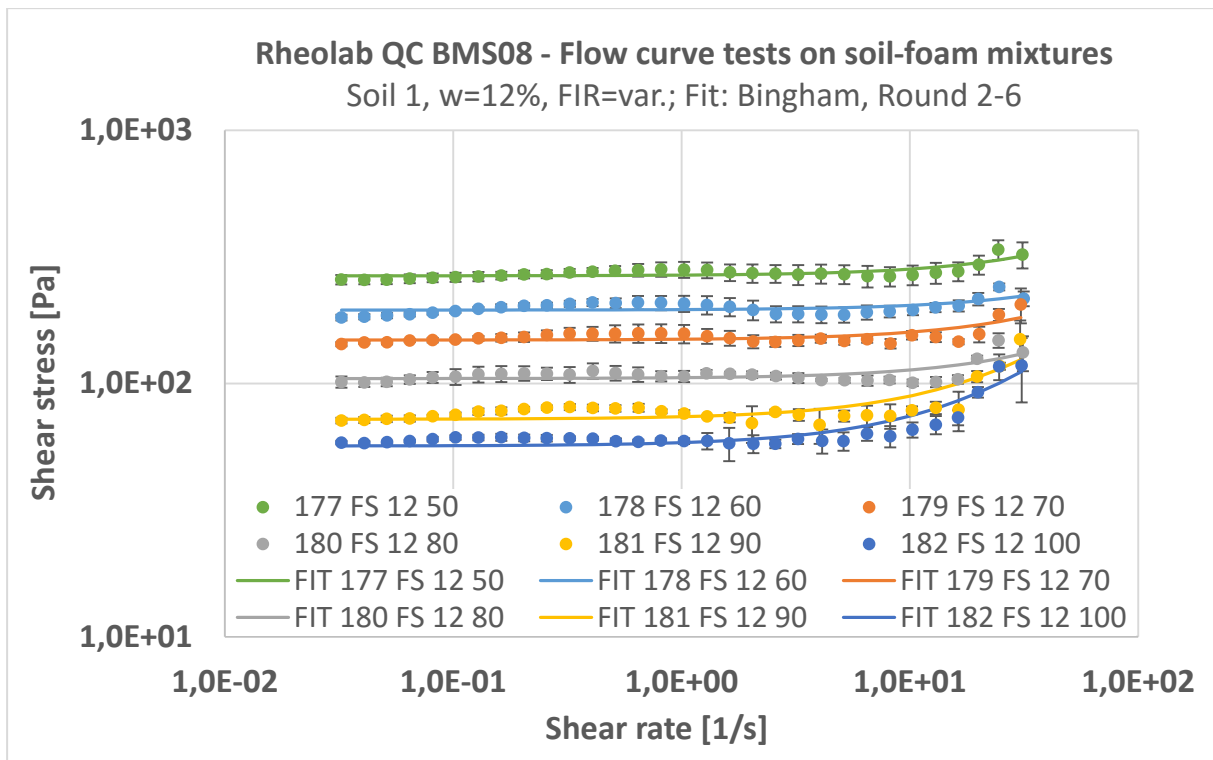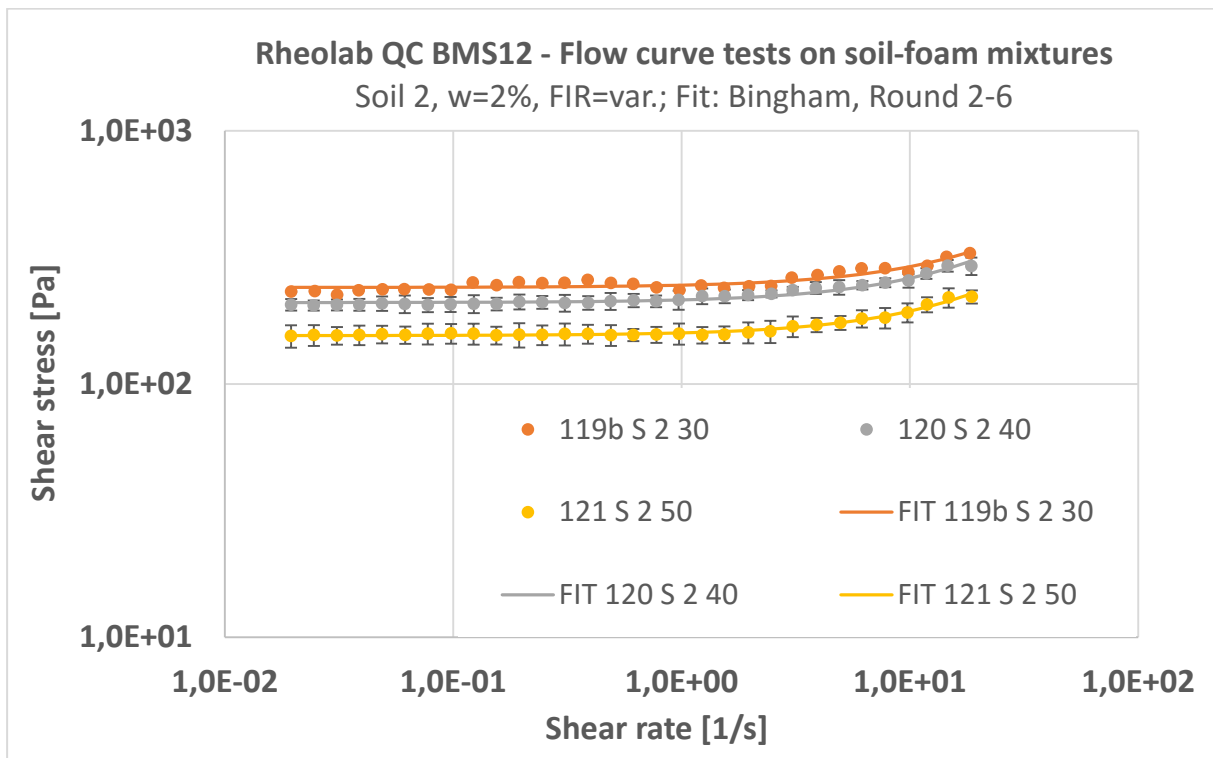
Figure A-46: Average flow curve data of fine sand-foam mixtures with water content w = 12% and increasing foam content (BMS12, rounds 2 – 6); curve fitting with Bingham model

Figure A-47: Average flow curve data of fine sand-foam mixtures with water content w = 2% and increasing foam content (BMS12, rounds 2 – 6); curve fitting with Bingham model
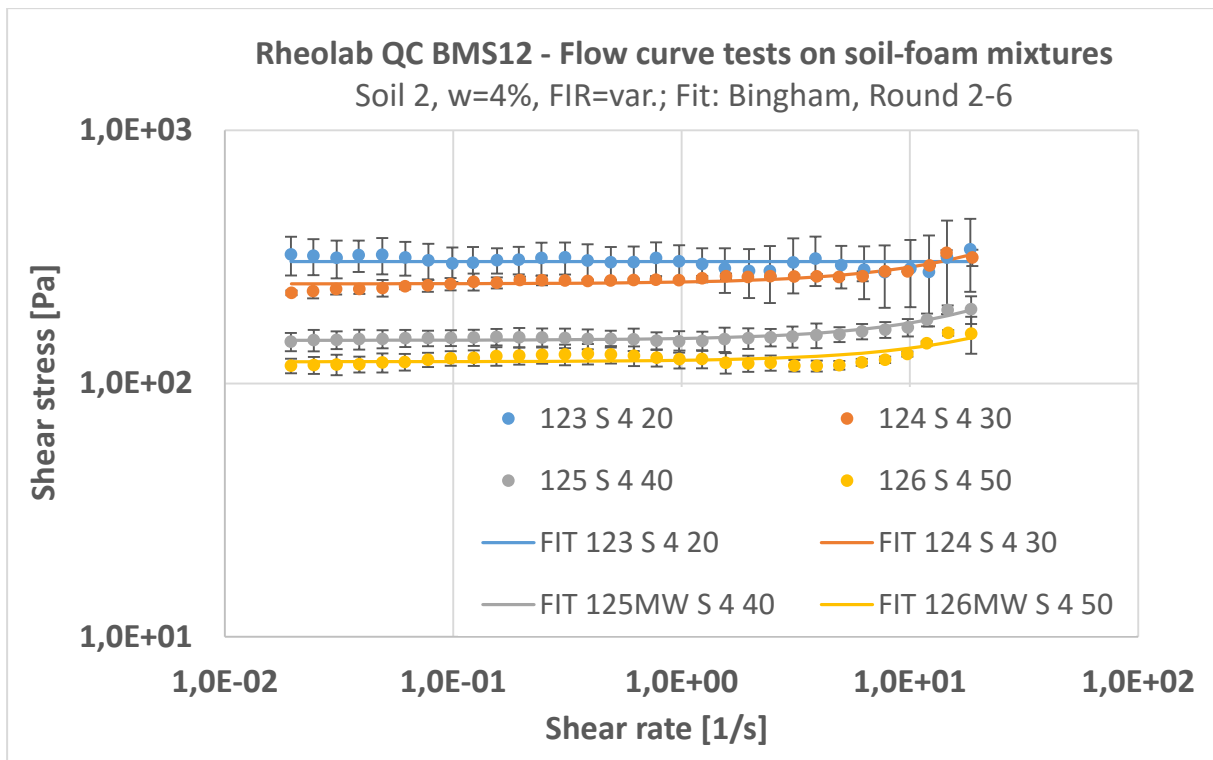
Figure A-48: Average flow curve data of fine sand-foam mixtures with water content w = 4% and increasing foam content (BMS12, rounds 2 – 6); curve fitting with Bingham model
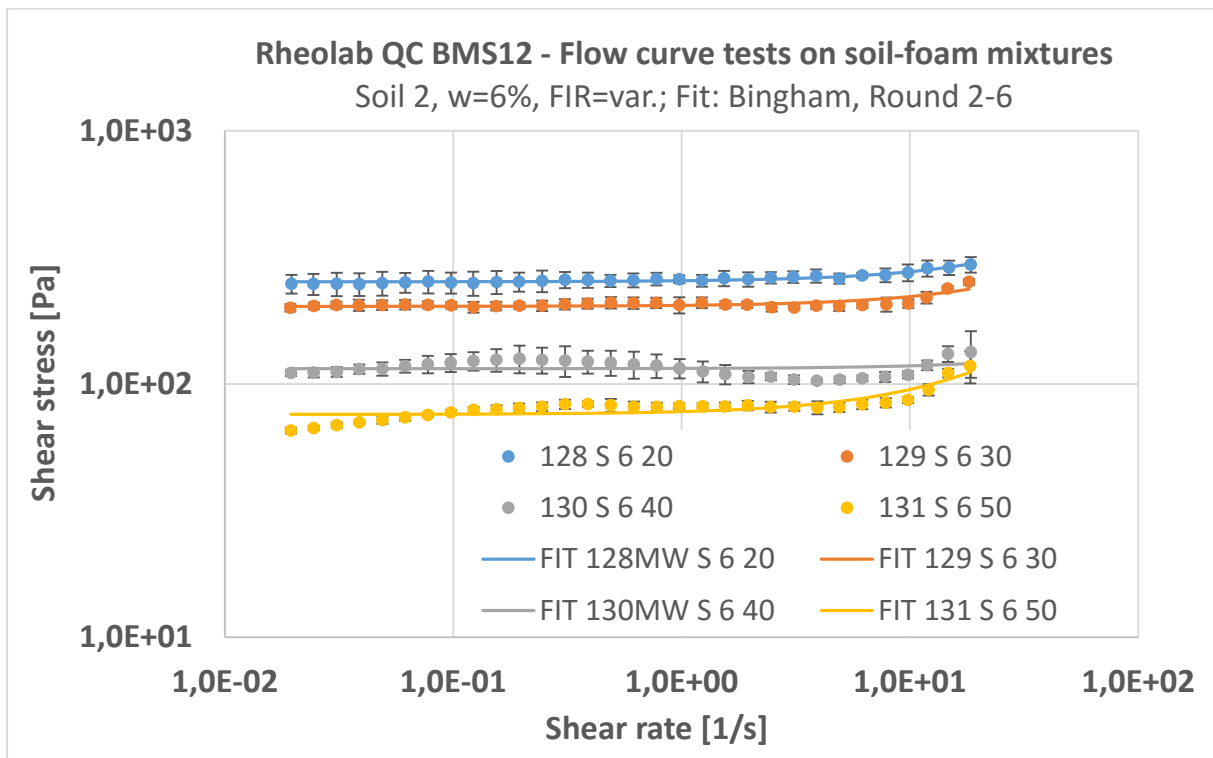

Figure A-49: Average flow curve data of fine sand-foam mixtures with water content w = 6% and increasing foam content (BMS12, rounds 2 – 6); curve fitting with Bingham model

Figure A-50: Average flow curve data of fine sand-foam mixtures with water content w = 8% and increasing foam content (BMS12, rounds 2 – 6); curve fitting with Bingham model
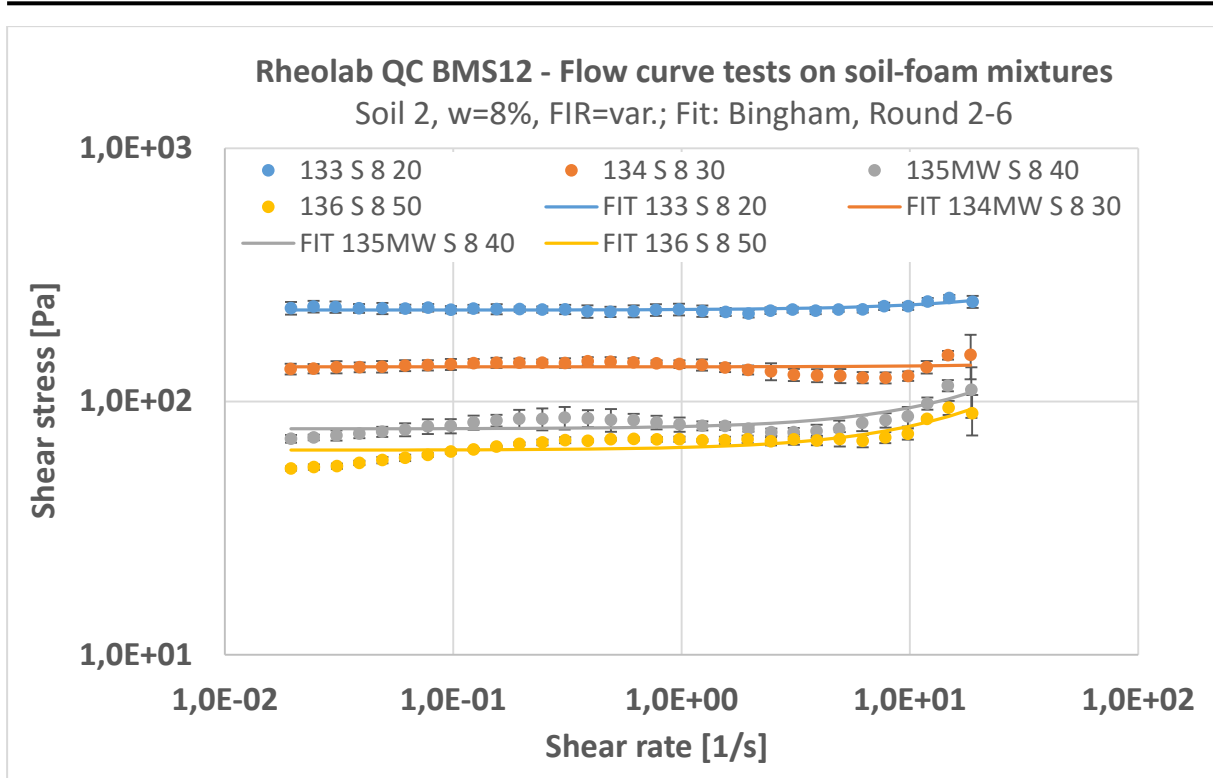

Figure A-51: Average flow curve data of fine sand-foam mixtures with water content w = 10% and increasing foam content (BMS12, rounds 2 – 6); curve fitting with Bingham model
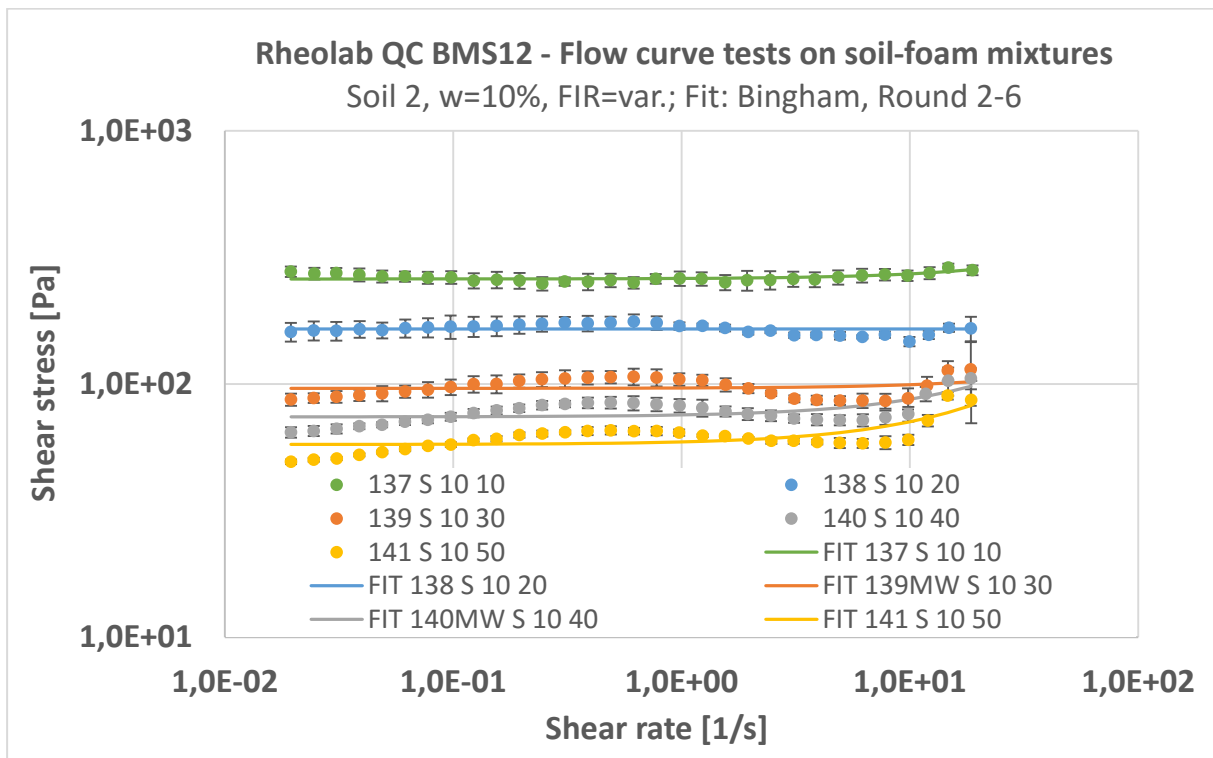
Figure A-52: Average flow curve data of fine sand-foam mixtures with water content w = 12% and increasing foam content (BMS12, rounds 2 – 6); curve fitting with Bingham model

Figure A-53: Average flow curve data of fine sand-foam mixtures with water content w = 2% and increasing foam content (BMS15, rounds 2 – 6); curve fitting with Bingham model

Figure A-54: Average flow curve data of fine sand-foam mixtures with water content w = 4% and increasing foam content (BMS15, rounds 2 – 6); curve fitting with Bingham model
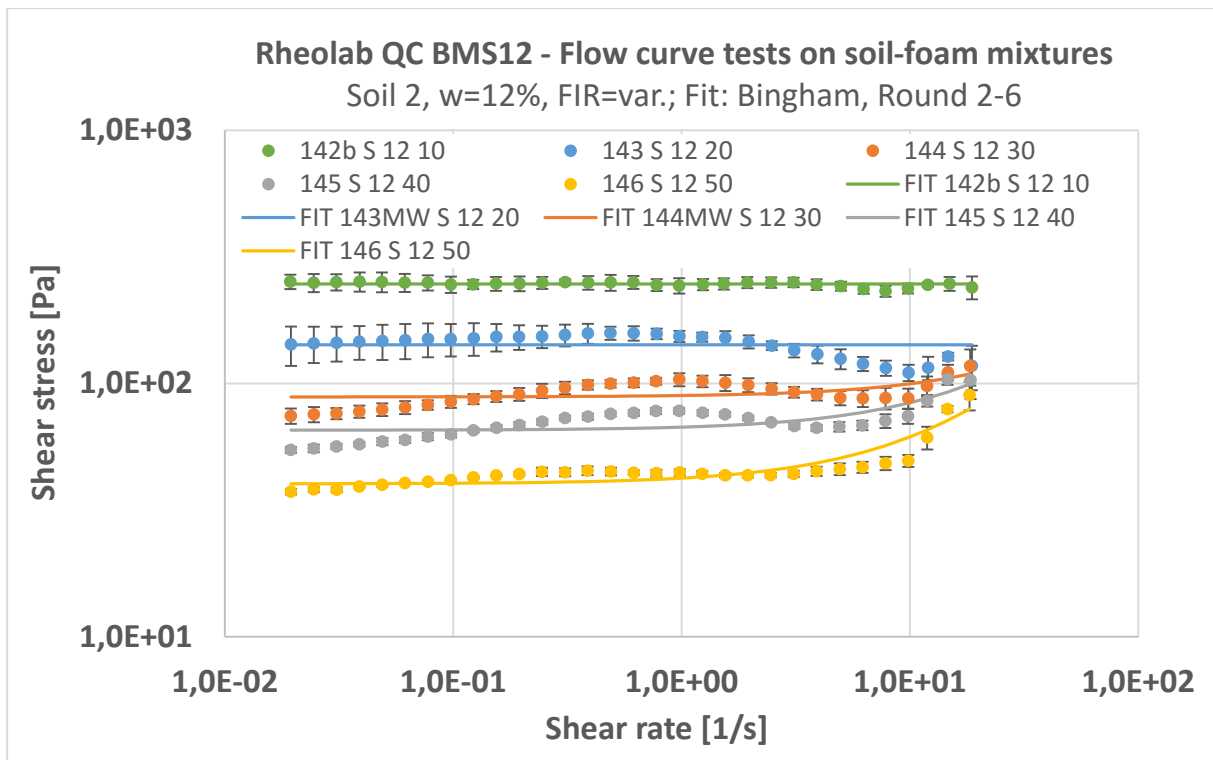

Figure A-55: Average flow curve data of fine sand-foam mixtures with water content w = 6% and increasing foam content (BMS15, rounds 2 – 6); curve fitting with Bingham model
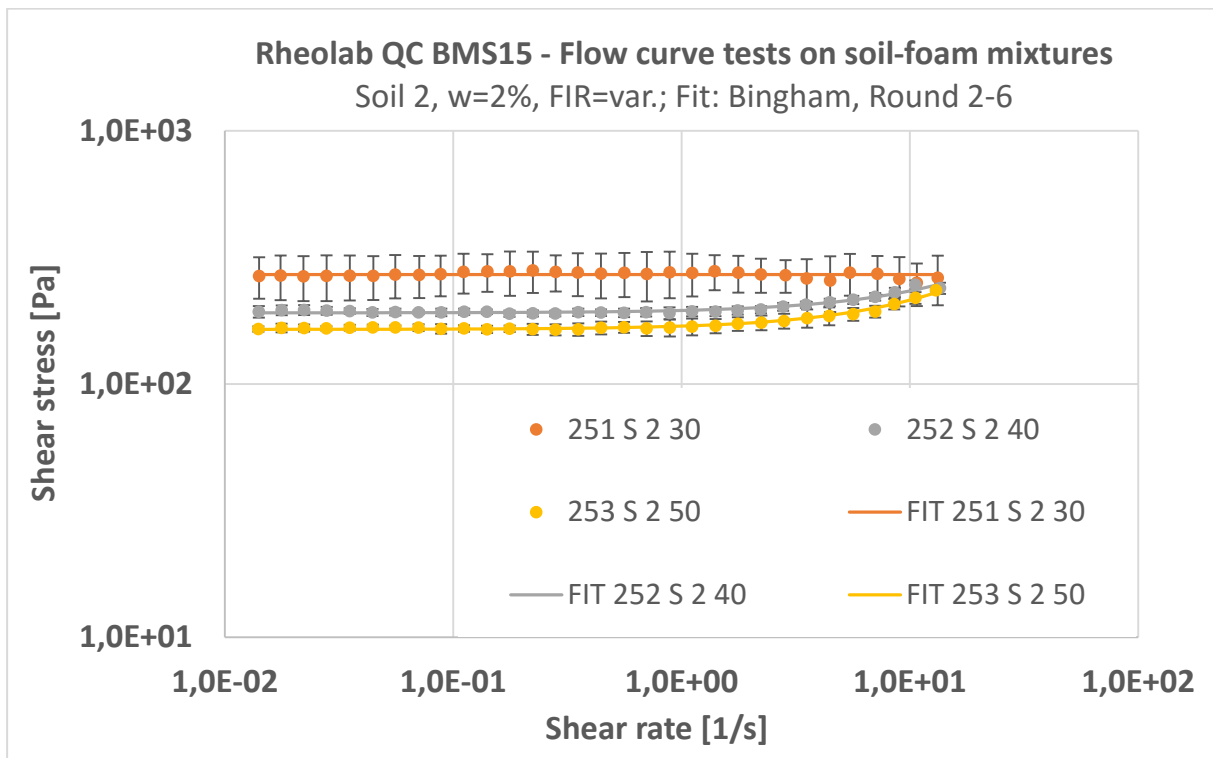
Figure A-56: Average flow curve data of fine sand-foam mixtures with water content w = 8% and increasing foam content (BMS15, rounds 2 – 6); curve fitting with Bingham model

Figure A-57: Average flow curve data of fine sand-foam mixtures with water content w = 10% and increasing foam content (BMS15, rounds 2 – 6); curve fitting with Bingham model

Figure A-58: Average flow curve data of fine sand-foam mixtures with water content w = 12% and increasing foam content (BMS15, rounds 2 – 6); curve fitting with Bingham model

Figure A-59: Average flow curve data of sand-foam mixtures with water content w = 2% and increasing foam content (BMS08, rounds 2 – 6); curve fitting with Bingham model
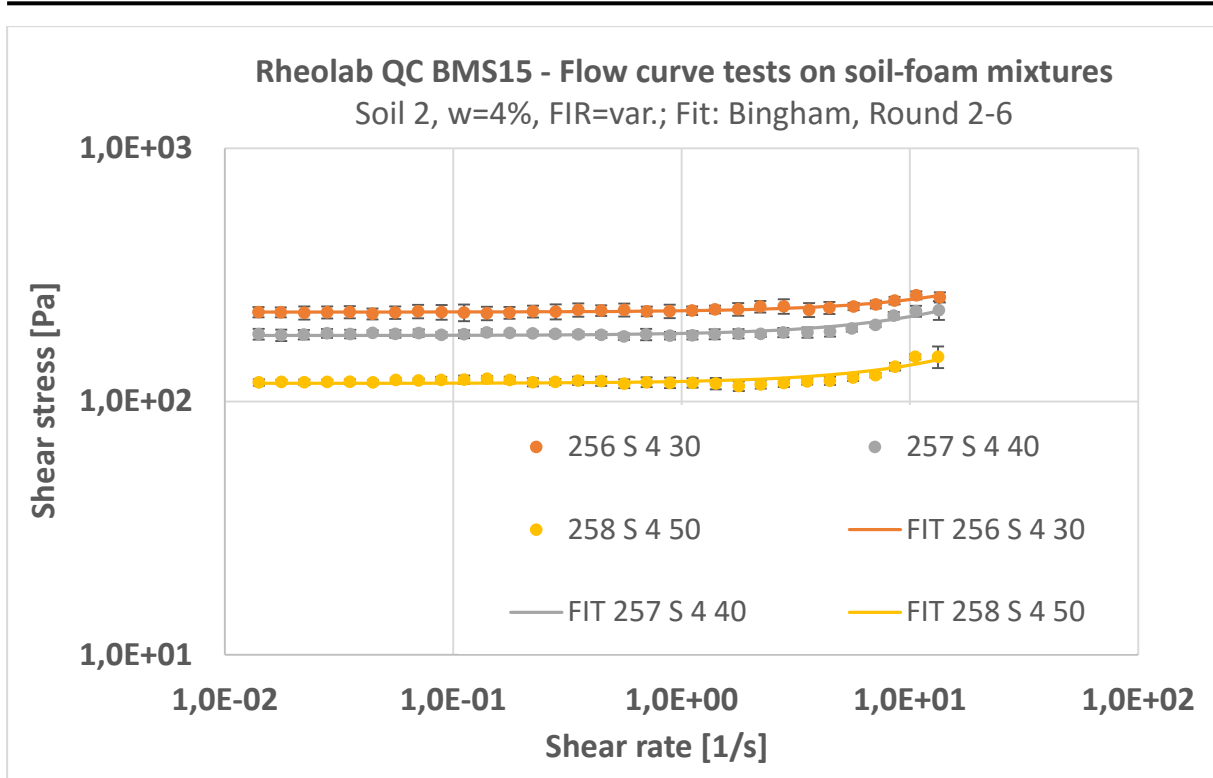
Figure A-60: Average flow curve data of sand-foam mixtures with water content w = 4% and increasing foam content (BMS08, rounds 2 – 6); curve fitting with Bingham model
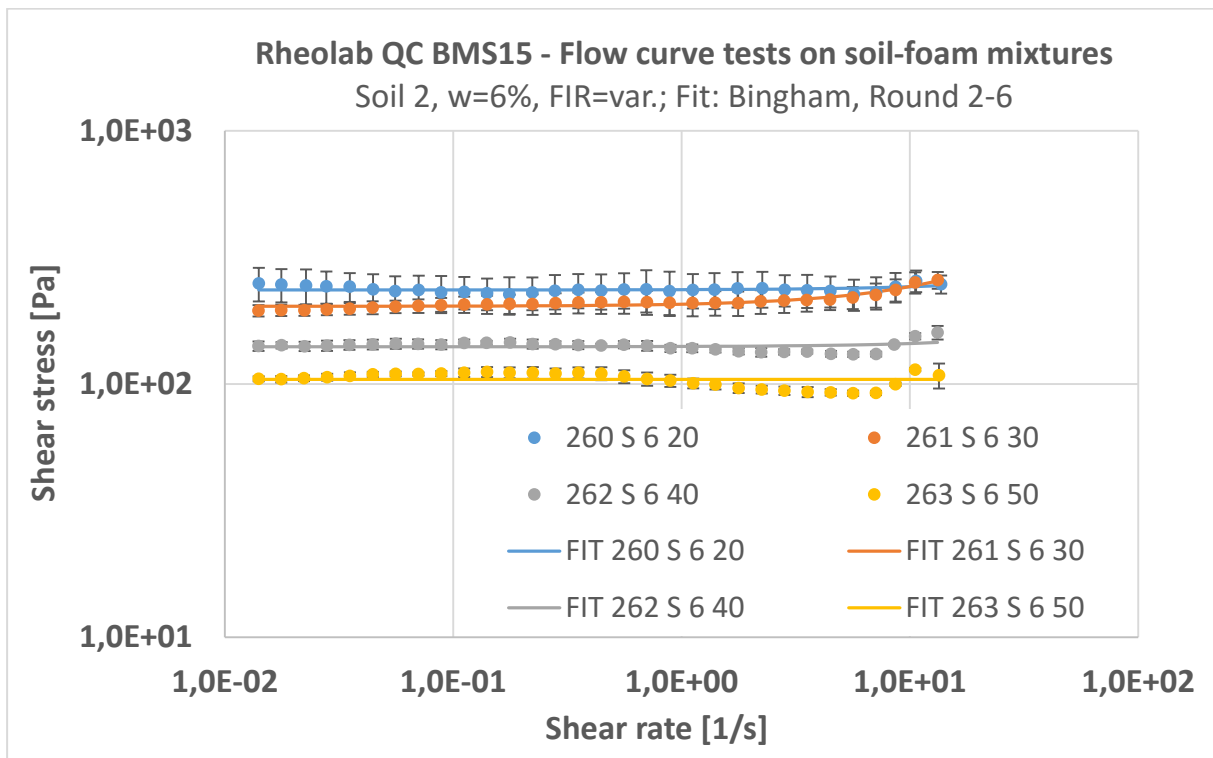

Figure A-61: Average flow curve data of sand-foam mixtures with water content w = 6% and increasing foam content (BMS08, rounds 2 – 6); curve fitting with Bingham model
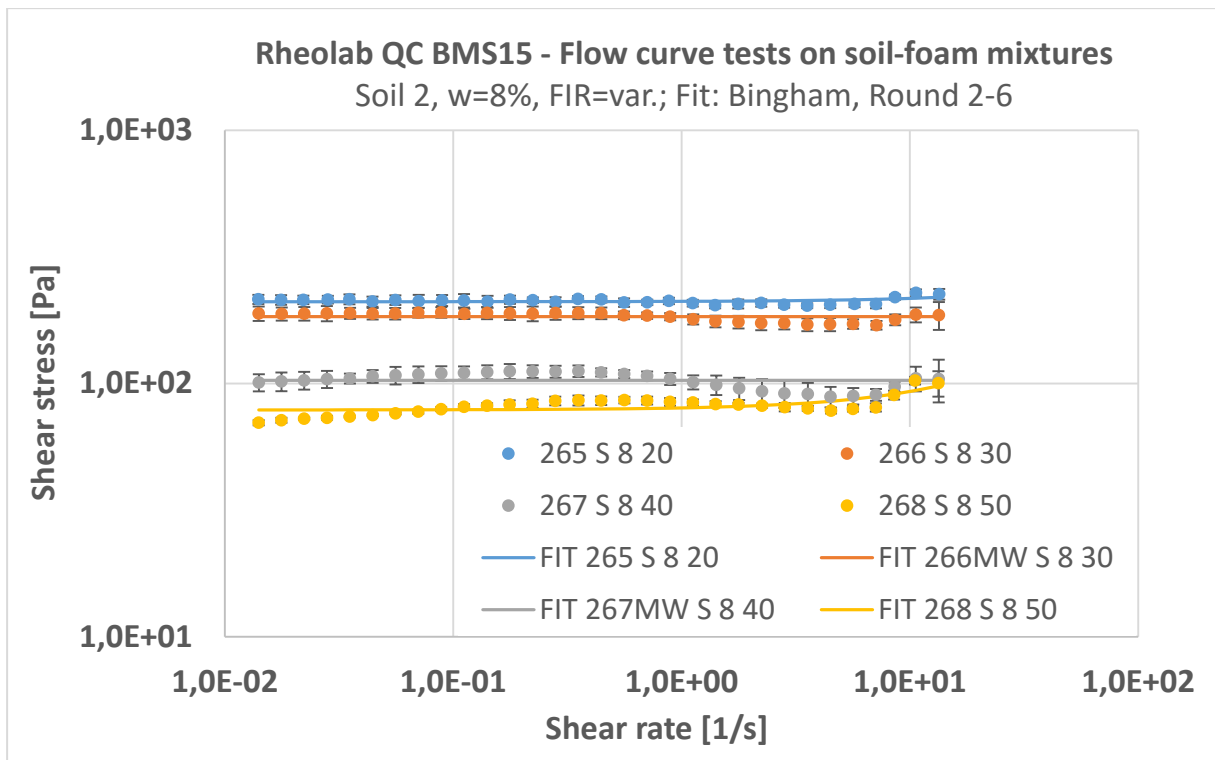
Figure A-62: Average flow curve data of sand-foam mixtures with water content w = 8% and increasing foam content (BMS08, rounds 2 – 6); curve fitting with Bingham model

Figure A-63: Average flow curve data of sand-foam mixtures with water content w = 10% and increasing foam content (BMS08, rounds 2 – 6); curve fitting with Bingham model

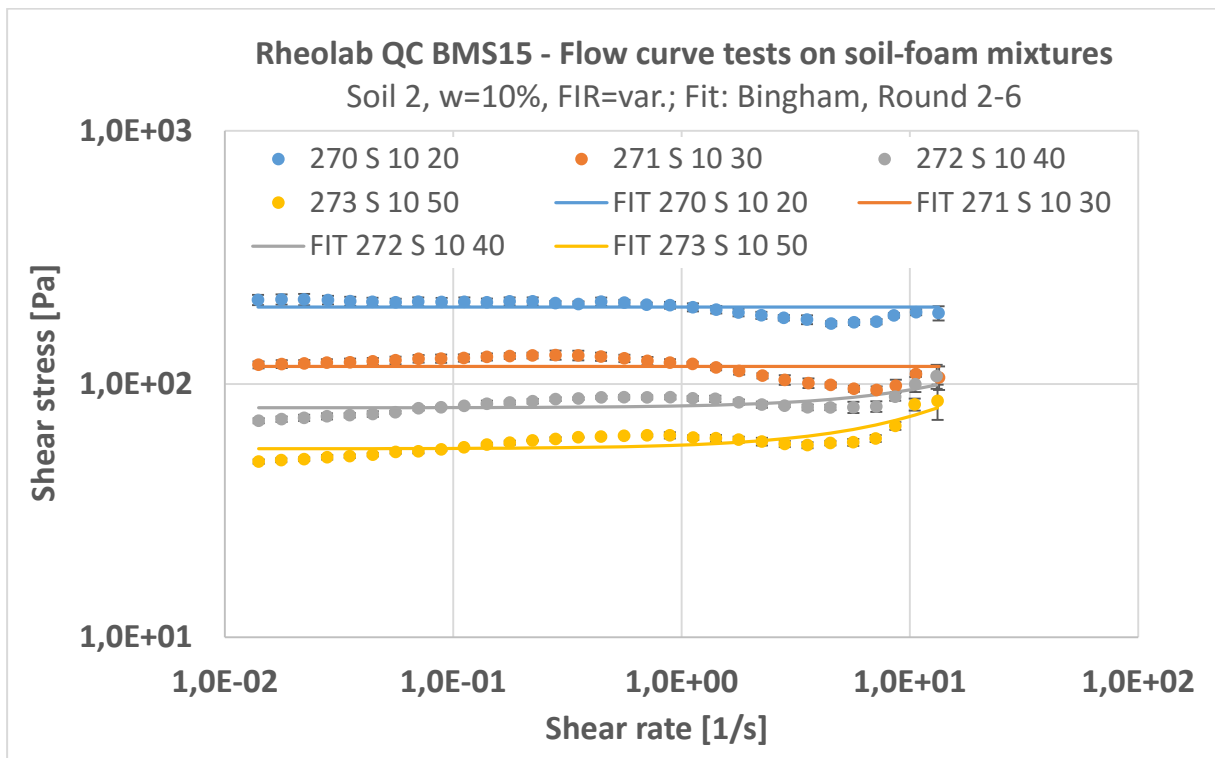**Figure A-64:** Average flow curve data of sand-foam mixtures with water content w = 12% and increasing foam content (BMS08, rounds 2 – 6); curve fitting with Bingham model

Figure A-65: Average flow curve data of sand-foam mixtures with water content w = 2% and increasing foam content (BMS12, rounds 2 – 6); curve fitting with Bingham model
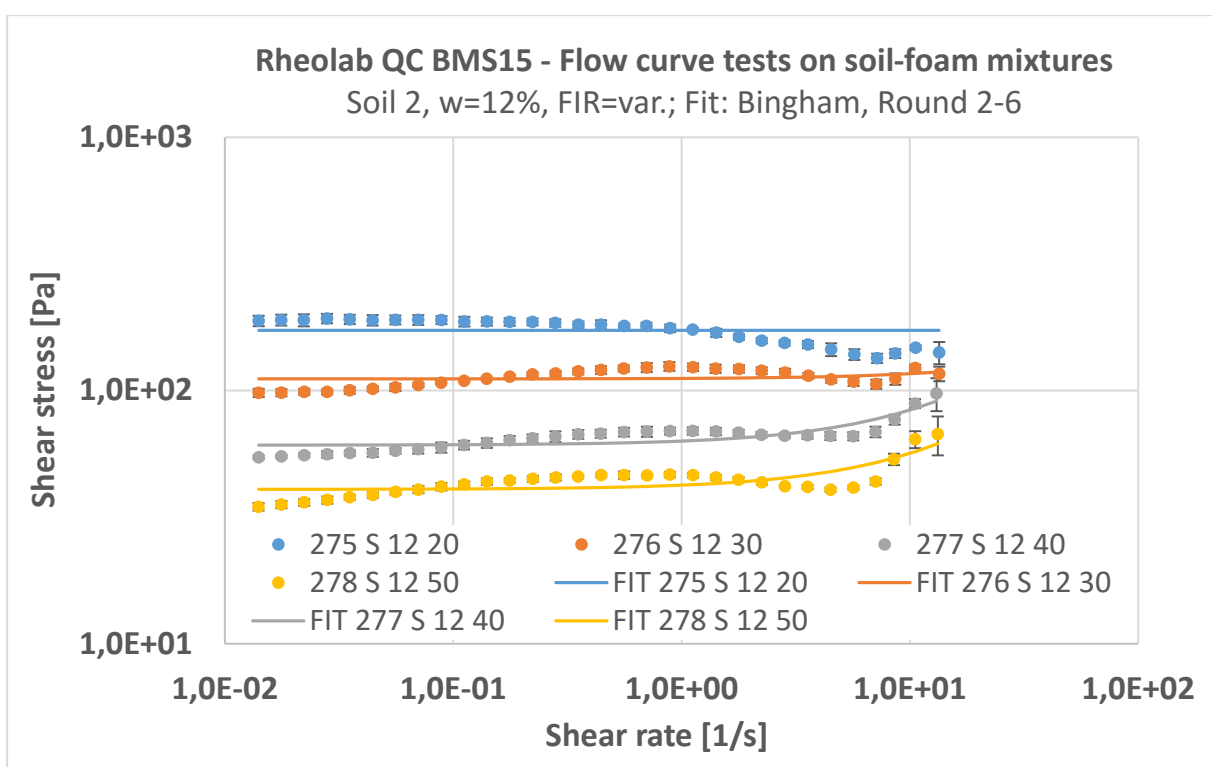
Figure A-66: Average flow curve data of sand-foam mixtures with water content w = 4% and increasing foam content (BMS12, rounds 2 – 6); curve fitting with Bingham model

Figure A-67: Average flow curve data of sand-foam mixtures with water content w = 6% and increasing foam content (BMS12, rounds 2 – 6); curve fitting with Bingham model

Figure A-68: Average flow curve data of sand-foam mixtures with water content w = 8% and increasing foam content (BMS12, rounds 2 – 6); curve fitting with Bingham model

Figure A-69: Average flow curve data of sand-foam mixtures with water content w = 10% and increasing foam content (BMS12, rounds 2 – 6); curve fitting with Bingham model

Figure A-70: Average flow curve data of sand-foam mixtures with water content w = 12% and increasing foam content (BMS12, rounds 2 – 6); curve fitting with Bingham model

Figure A-71: Average flow curve data of sand-foam mixtures with water content w = 2% and increasing foam content (BMS15, rounds 2 – 6); curve fitting with Bingham model

Figure A-72: Average flow curve data of sand-foam mixtures with water content w = 4% and increasing foam content (BMS15, rounds 2 – 6); curve fitting with Bingham model

Figure A-73: Average flow curve data of sand-foam mixtures with water content w = 6% and increasing foam content (BMS15, rounds 2 – 6); curve fitting with Bingham model

Figure A-74: Average flow curve data of sand-foam mixtures with water content w = 8% and increasing foam content (BMS15, rounds 2 – 6); curve fitting with Bingham model

Figure A-75: Average flow curve data of sand-foam mixtures with water content w = 10% and increasing foam content (BMS15, rounds 2 – 6); curve fitting with Bingham model

Figure A-76: **Average flow curve data of sand-foam mixtures with water content w = 12% and increasing foam content (BMS15, rounds 2 – 6); curve fitting with Bingham model**

A.4.3.2   *Formulas for the determination of BMS-yield stresses and diagrams*

$$\tau_{0,FS,BMS08} = 1686.632 - 53.398 \cdot w - 24.539 \cdot FIR \qquad \text{Eq. A-1}$$
$$+0.400 \cdot w \cdot FIR + 0.099 \cdot FIR^2 \qquad [Pa] \qquad R^2 = 0.945$$
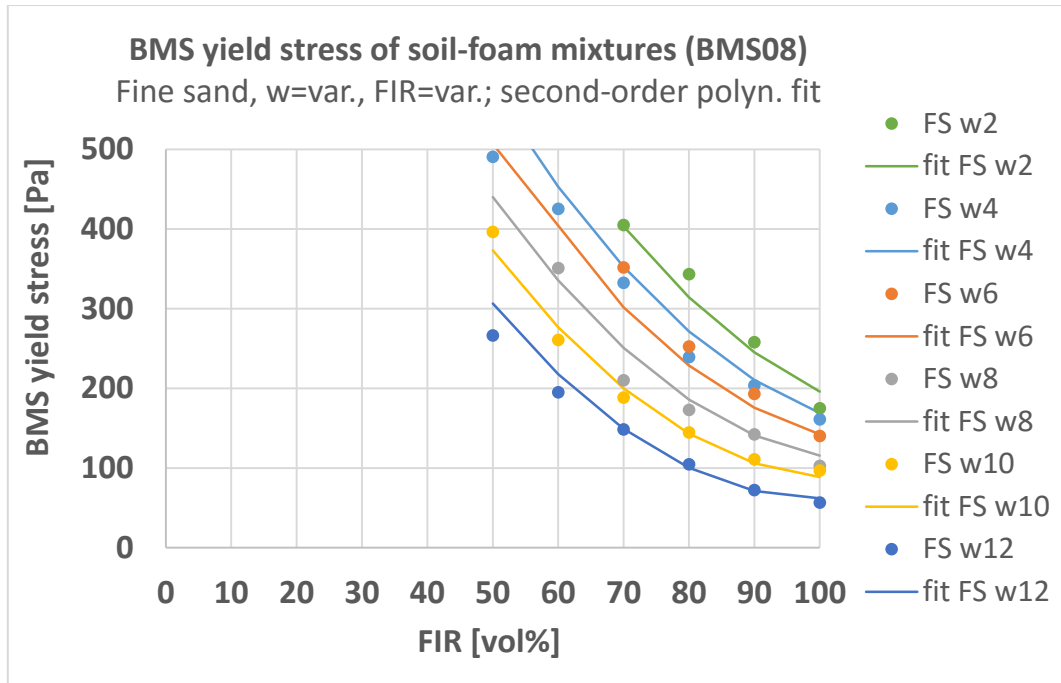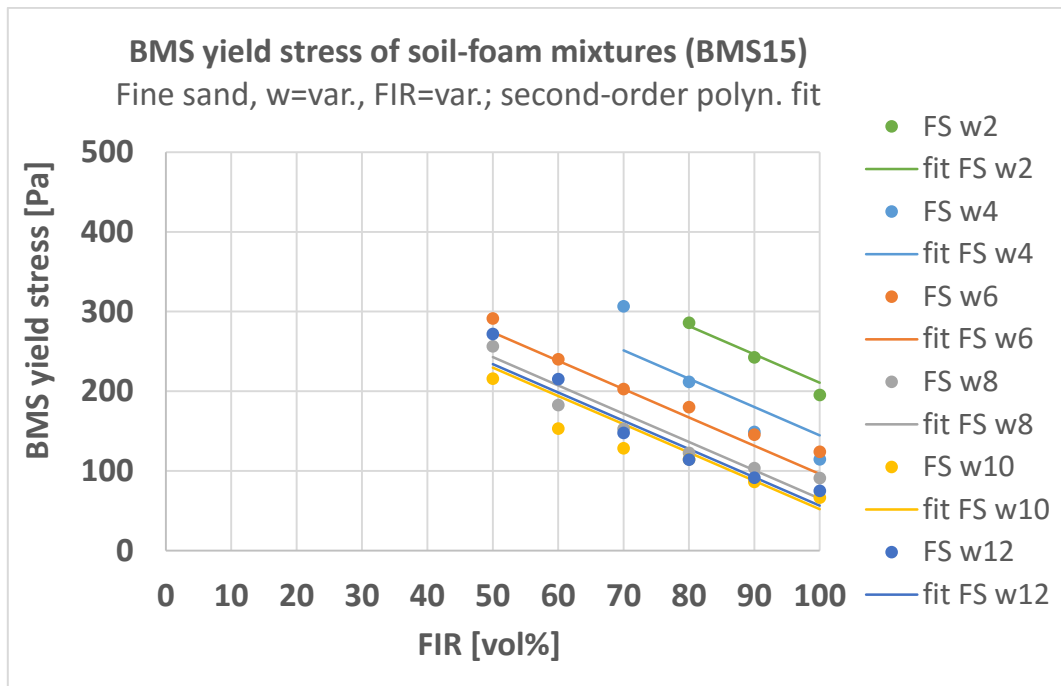

Figure A-77: Development of "BMS yield stresses" (Bingham) from flow curve tests on fine sand-foam mixtures (BMS08) depicted over FIR; data fitting with second-order polyn. function
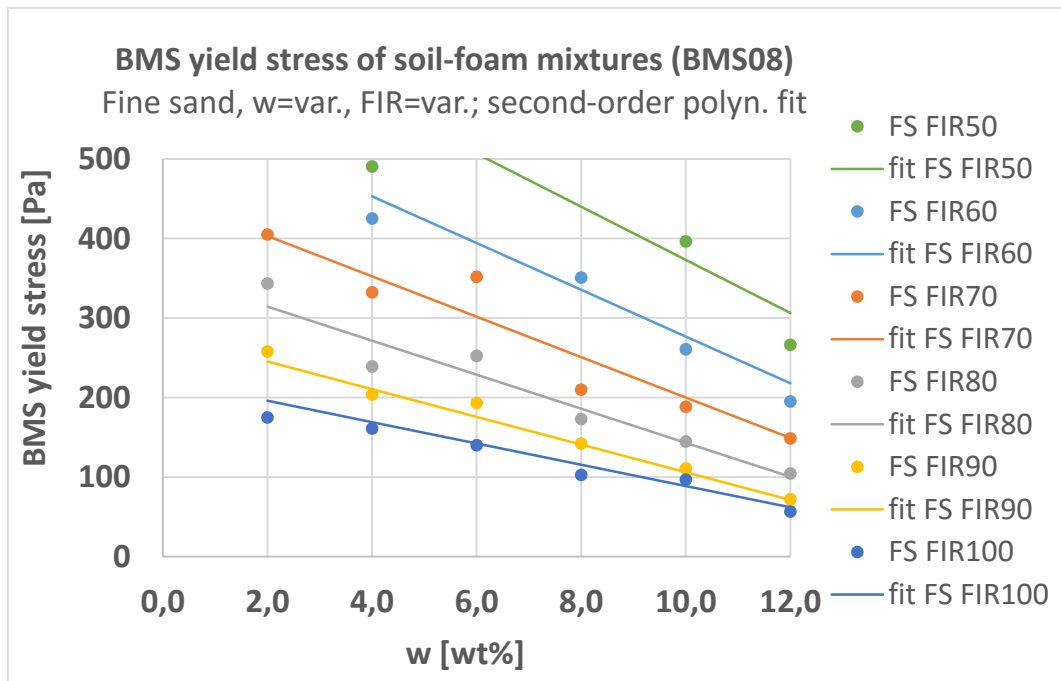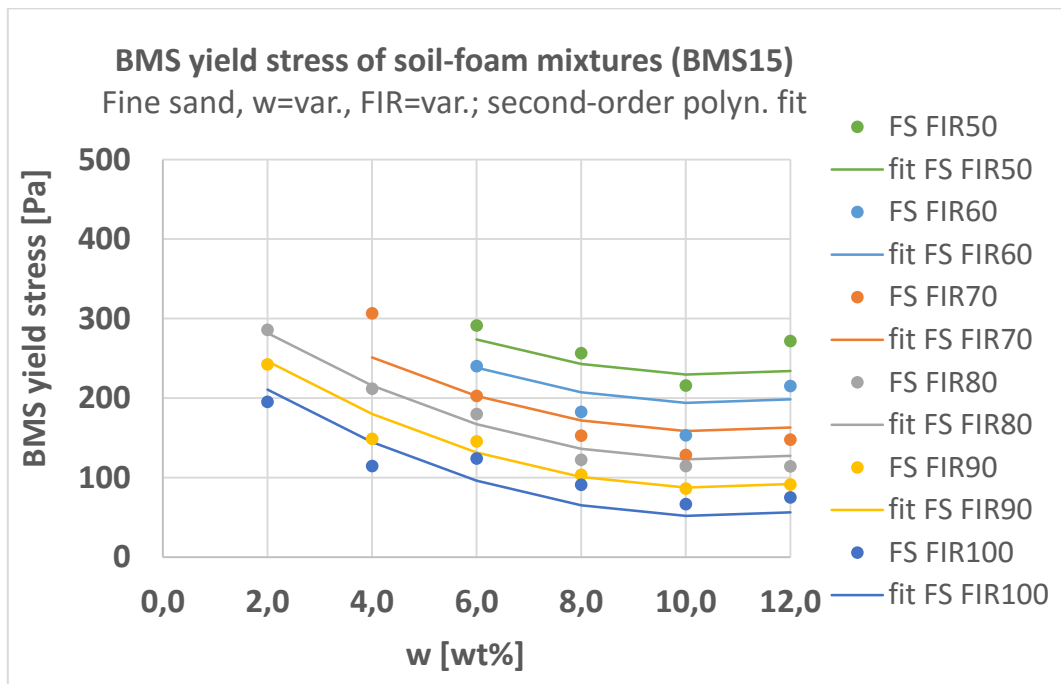

Figure A-78: Development of "BMS yield stresses" (Bingham) from flow curve tests on fine sand-foam mixtures (BMS08) depicted over w; data fitting with second-order polyn. function

$$\tau_{0,FS,BMS12} = 1732.975 - 68.934 \cdot w - 24.798 \cdot FIR$$

$$+0.578 \cdot w \cdot FIR + 0.095 \cdot FIR^2 \qquad \text{[Pa]} \qquad R^2 = 0.957$$

Eq. A-2
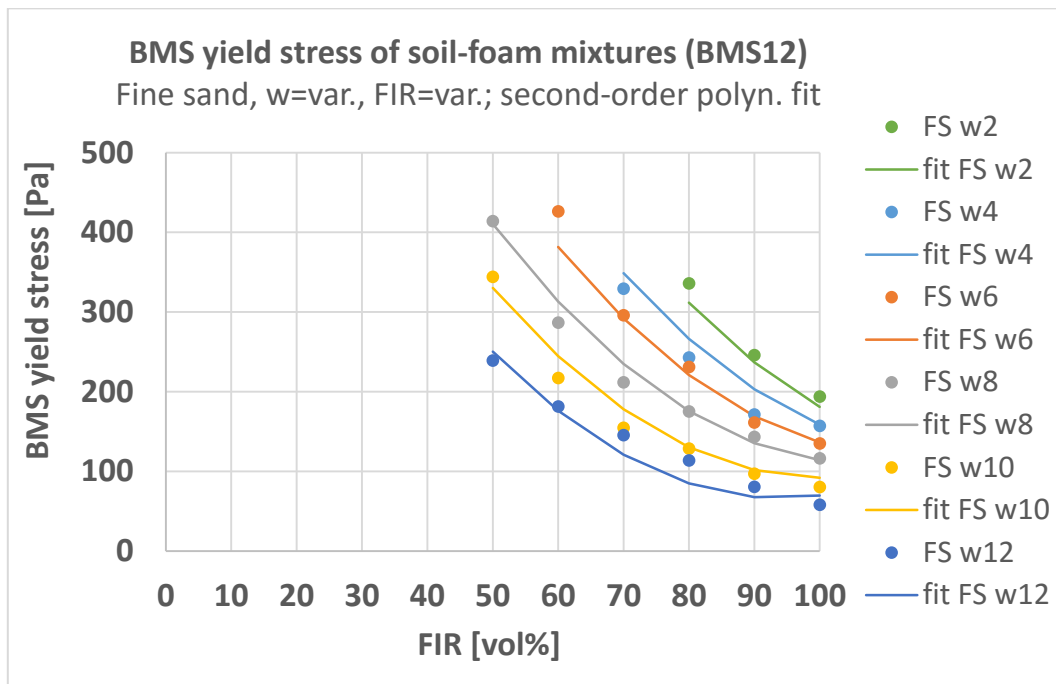
Figure A-79: Development of "BMS yield stresses" (Bingham) from flow curve tests on fine sand-foam mixtures (BMS12) depicted over FIR; data fitting with second-order polyn. function
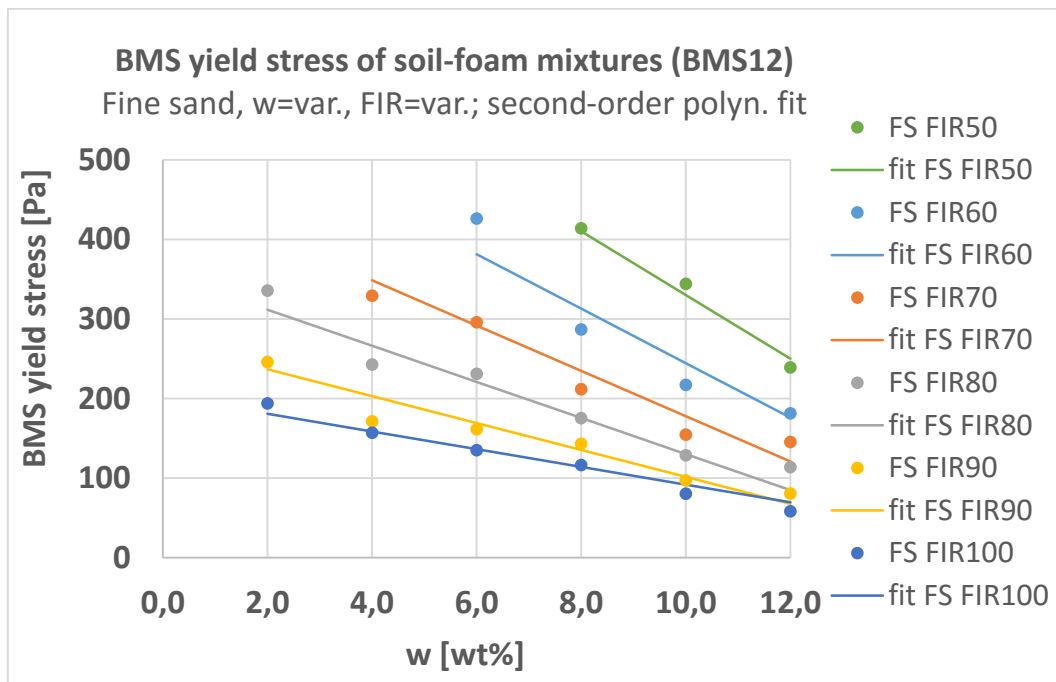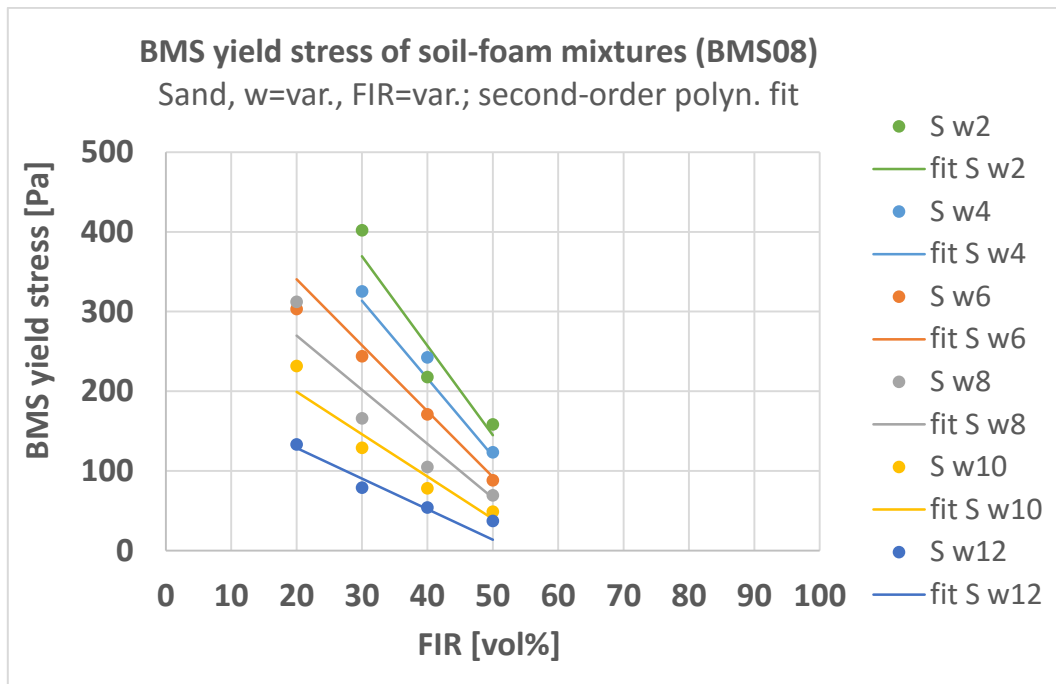

Figure A-80: Development of "BMS yield stresses" (Bingham) from flow curve tests on fine sand-foam mixtures (BMS12) depicted over w; data fitting with second-order polyn. function

$$\tau_{0,FS,BMS15} = 649.714 - 46.290 \cdot w - 3.552 \cdot FIR + 2.204 \cdot w^2 \qquad [Pa]$$

$$R^2 = 0.890 \qquad Eq. \; A\text{-}3$$

Figure A-81: Development of "BMS yield stresses" (Bingham) from flow curve tests on fine sand-foam mixtures (BMS15) depicted over FIR; data fitting with second-order polyn. function

Figure A-82: Development of "BMS yield stresses" (Bingham) from flow curve tests on fine sand-foam mixtures (BMS15) depicted over w; data fitting with second-order polyn. function

$$\tau_{0,S,BMS08} = 806.255 - 50.075 \cdot w - 12.704 \cdot FIR + 0.739 \cdot w \cdot FIR \quad [Pa]$$

$$R^2 = 0.939 \qquad \text{Eq. A-4}$$

Figure A-83: Development of "BMS yield stresses" (Bingham) from flow curve tests on sand-foam mixtures (BMS08) depicted over FIR; data fitting with second-order polynomial function
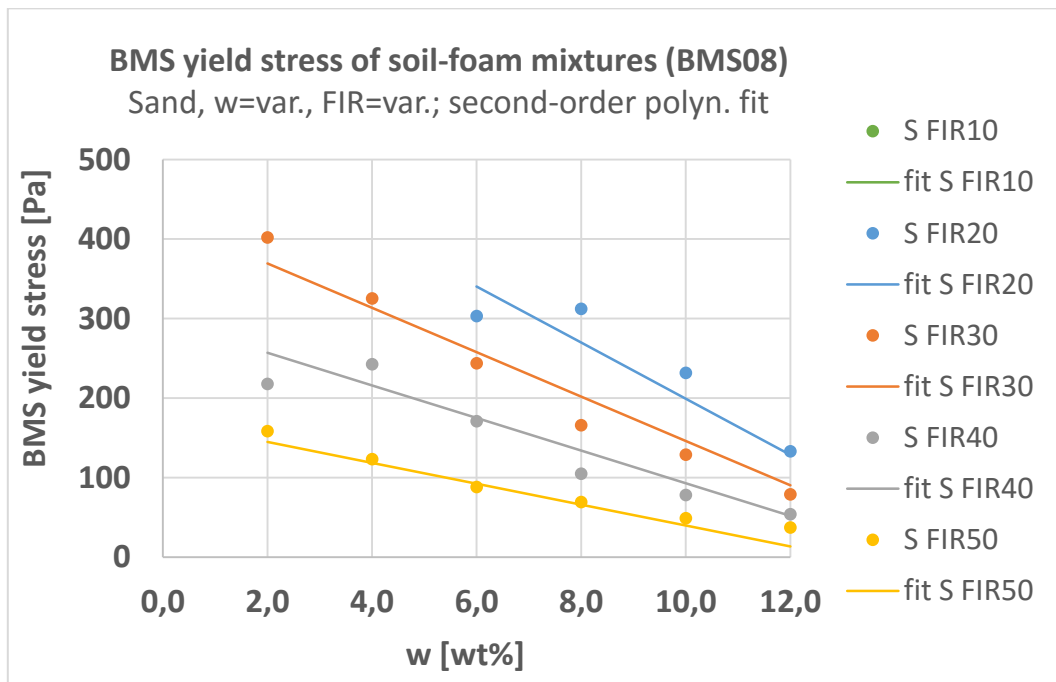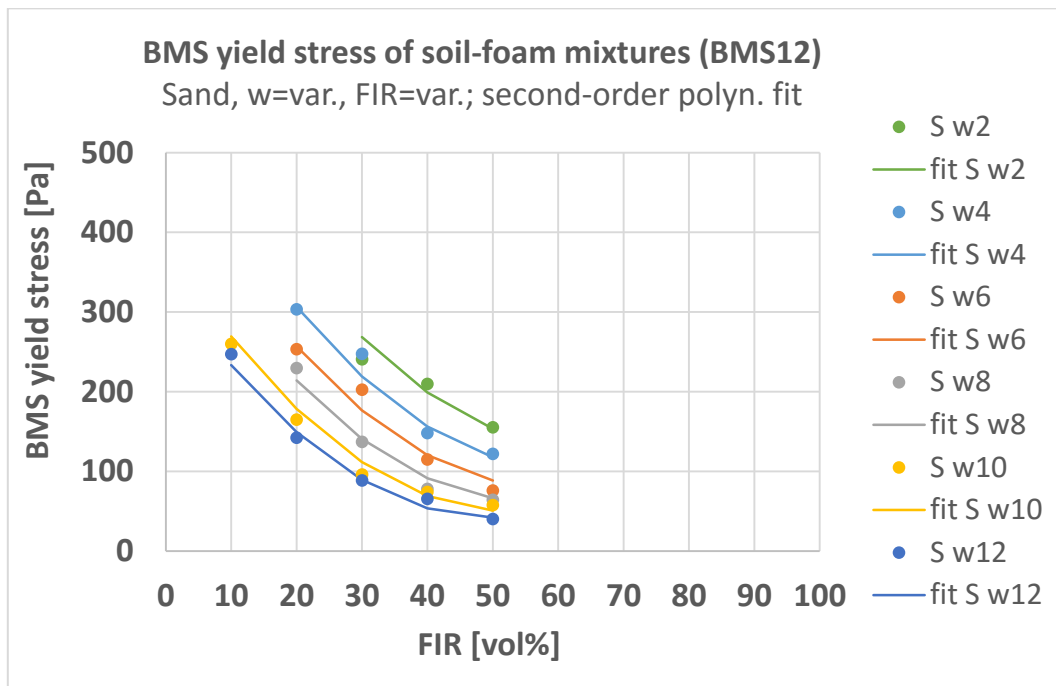

Figure A-84: Development of "BMS yield stresses" (Bingham) from flow curve tests on sand-foam mixtures (BMS08) depicted over w; data fitting with second-order polynomial function

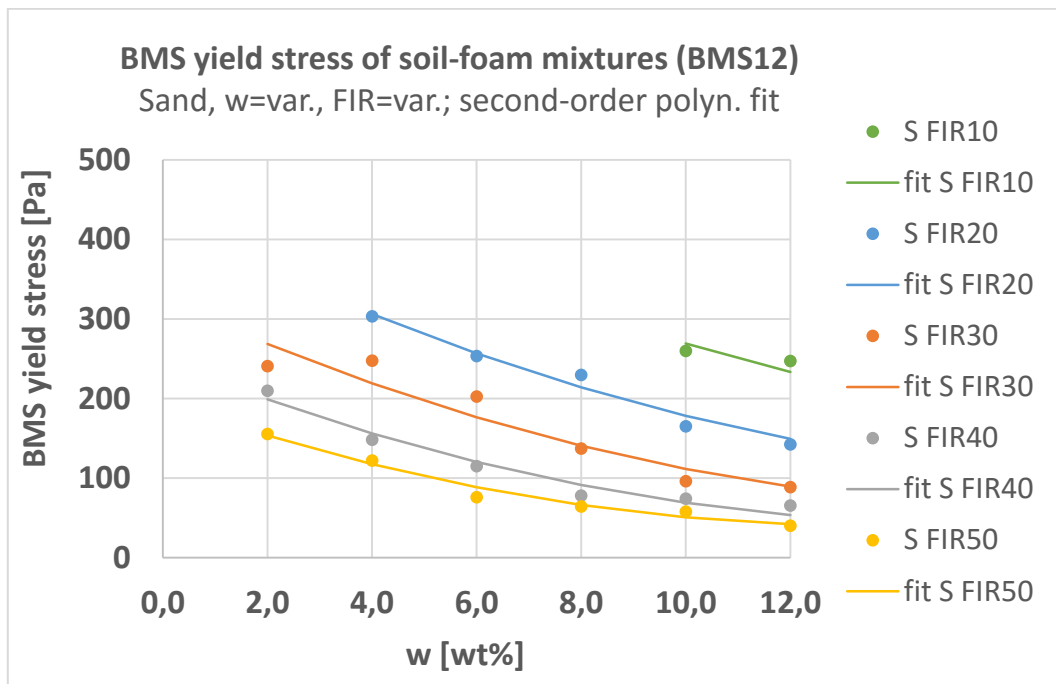$$\tau_{0,S,BMS12} = 699.385 - 40.012 \cdot w - 16.114 \cdot FIR \qquad \text{Eq. A-5}$$
$$+0.339 \cdot w \cdot FIR + 0.851 \cdot w^2 + 0.121 \cdot FIR^2 \qquad [Pa] \qquad R^2 = 0.965$$

Figure A-85: Development of "BMS yield stresses" (Bingham) from flow curve tests on sand-foam mixtures (BMS12) depicted over FIR; data fitting with second-order polynomial function
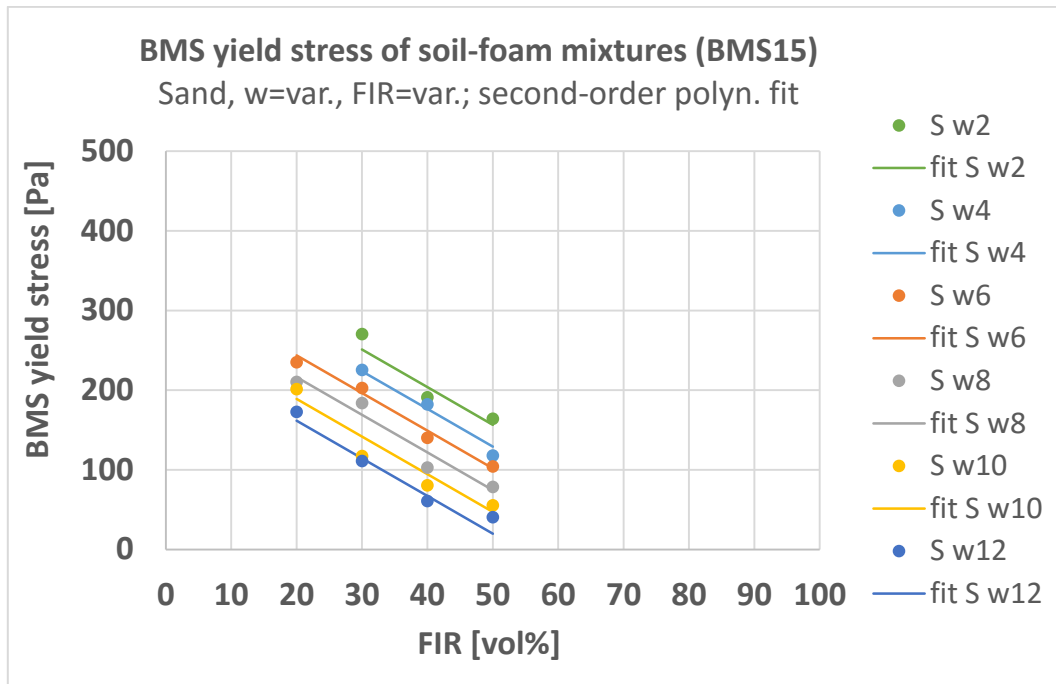

Figure A-86: Development of "BMS yield stresses" (Bingham) from flow curve tests on sand-foam mixtures (BMS12) depicted over w; data fitting with second-order polynomial function

$$\tau_{0,S,BMS15} = 420.304 - 13.664 \cdot w - 4.728 \cdot FIR \qquad [Pa] \qquad R^2 = 0.960 \qquad Eq. \text{ A-6}$$

Figure A-87: Development of "BMS yield stresses" (Bingham) from flow curve tests on sand-foam mixtures (BMS15) depicted over FIR; data fitting with second-order polynomial function
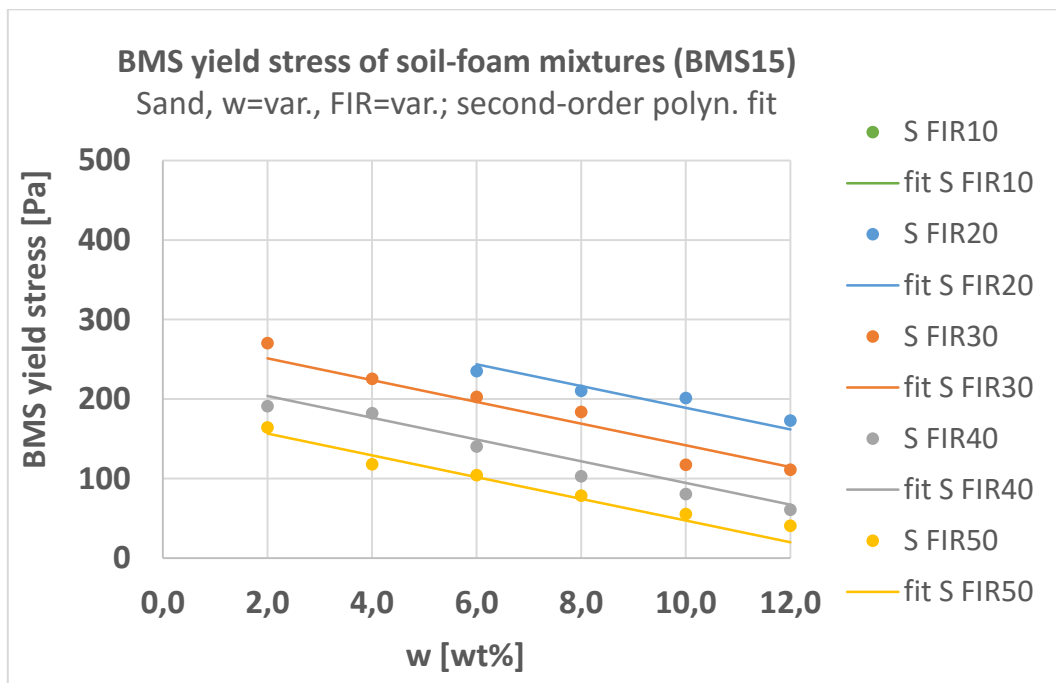

Figure A-88: Development of "BMS yield stresses" (Bingham) from flow curve tests on sand-foam mixtures (BMS15) depicted over w; data fitting with second-order polynomial function